Exploring Indirect Effects of MicroRNA-21 in Cardiac Fibrosis
A Proteomics Approach in Platelets

Barwari, Temo

Awarding institution:
King's College London

Exploring Indirect Effects of MicroRNA-21 in Cardiac Fibrosis: A Proteomics Approach in Platelets

PhD Thesis

Temo Barwari

School of Cardiovascular Medicine & Sciences

British Heart Foundation Centre of Research Excellence

August 2018

Submitted for the degree of Doctor of Philosophy from

King's College London

Supervisors: Professor Manuel Mayr & Professor Ajay M. Shah

Table of contents

‘Gutta cavat lapidem non vī sed saepe cadendo’

A droplet carves out a stone, not with force, but by persistently falling
(Latin translation from a fragment by Choerilus of Samos, 5th century BC)

Acknowledgements

The past few years have been an amazing journey! I am greatly indebted to several people along the way.

First of all, I would like to thank my supervisor Manuel Mayr. At first, I felt I had no idea what I was doing, but I realise in hindsight that you made me figure it out by myself and pushed me because I could and needed to be pushed. Never having seen a pipette before, this approach took me from frustration and sometimes misery, to excitement and a true fascination for science. I now see that you gave me the opportunity to figure it out for myself, which has shaped me into an independent researcher and an intrinsic scientist. This, I believe, is the actual objective of a PhD. The opportunities you then facilitated to enjoy the global world of science, through lab visits, collaborations and presentations at international meetings, have strengthened my desire to remain part of academia.

I am also grateful to the British Heart Foundation for their financial support and their increasing efforts to create a community of BHF alumni. Many thanks as well to my second supervisor, prof. Ajay Shah, for his support throughout my project. With the kind and patient guidance of my initial 'lab-moms' Seda Eminaga and Aitana Braza-Boïls, I quickly became more self-reliant in doing bench work by myself. Many thanks to the organisation of the Bruneck Study, in particularly Stefan Kiechl and Johan Willeit; it was great to be part of the amazing logistical operation during the study itself and to contribute to the wealth of scientific output that it continues to amass. Perhaps most importantly, the entire Proteomics Lab, past and current members, was an amazing group of people, right from the start and until the very end. The way I was welcomed into the group was an endless source of fun and support, which meant I never felt homesick. Equally so at more difficult times, be it at work or personal, you were true friends throughout.

Outside of London, I always felt the support, pride and love from 'home' in Amsterdam despite not being there. The distance has made me realise how blessed I am to have such loving people as a family and have made it an easy

decision to move back home. I look forward to spend more time with you and to be part of the little ones growing up. Kani, you were an amazing source of positivity and joy in the final stages of my PhD, which gave me an enormous amount of energy to push through the writing-up stage and viva. I am excited and look forward to building up a future together!

Abstract

Fibrosis is a major contributor to cardiac disease. No specific anti-fibrotic therapy is currently available. MicroRNA-21 (miR-21) has been implicated as a regulator of fibrosis and inhibitors of miR-21 are currently undergoing clinical trials. In this project, we used a proteomics approach to explore mechanisms of how miR-21 inhibition may attenuate fibrosis. First, primary murine cardiac fibroblasts were transfected with miR-21 mimics and inhibitors. Unexpectedly, proteomic analysis of their secretome showed limited changes in extracellular matrix (ECM) protein secretion despite a pro-proliferative effect of miR-21. Similarly, no significant differences were seen in the ECM of miR-21 *null* mouse hearts. In light of its ubiquitous expression, we searched for additional explanations as to how miR-21 might regulate fibrosis. In the year 2000 follow-up of the community-based Bruneck study (n=660), we compared circulating miR-21 with a proteomic panel of 229 proteins associated with cardiovascular disease. Several platelet-derived pro-fibrotic factors significantly correlated with plasma miR-21 levels, including the latency-associated peptide of TGF-β1. This correlation was confirmed by ELISA measurements of active TGF-β1 in platelet-poor plasma collected during the Bruneck 2015 follow-up (n=332). Immunohistological staining of murine bone marrow sections revealed marked co-localisation of TGF-β1 with megakaryocytes, whilst immune-mediated thrombocytopaenia in mice indicated platelet dependency of plasma TGF-β1 levels. When mice were treated with antagomiR-21, no differences were observed in the platelet count or their aggregation response. However, a proteomics analysis of the platelet releasate revealed TGF-β1 as differentially regulated. An attenuated TGF-β1 release after antagomiR-21 treatment was validated in platelets activated with collagen and a thrombin receptor-activating peptide. Mechanistically, Wiskott-Aldrich Syndrome protein, a negative regulator of platelet TGF-β1 secretion, was identified as a direct target of miR-21. In conclusion, this study reports a previously unrecognised effect of pharmacological miR-21 inhibition on platelet TGF-β1 release. Furthermore, we observed significantly lower platelet counts in blood from miR-21 *null* mice. This novel effect of miR-21 on platelets highlights the bone marrow as a potential key contributor to the anti-fibrotic effects of miR-21 inhibition.

Abbreviations

4E-BP1	eukaryotic translation initiation factor 4E-binding protein 1
α/δ-granule	alpha/dense granule
α-SMA	alpha smooth muscle actin (Acta2)
AA	arachidonic acid
AAV	adeno-associated virus
ACD	acid-citrate-dextrose
Ago	Argonaute
ANXA7	annexin A7
APC	allophycocyanin
CATL1	cathepsin L1 (Ctsl)
CD41	cluster of differentiation 41; integrin alpha-IIb (Itga2b)
CD45	protein tyrosine phosphatase, receptor type, C (Ptprc)
CF	cardiac fibroblast
Cq	quantification cycle
CTGF	connective tissue growth factor
CVD	cardiovascular disease
DAPI	4',6-diamidino-2-phenylindole
DGCR8	DiGeorge syndrome critical region gene-8
DKK1	Dickkopf-related protein 1
DNA	deoxyribonucleic acid
ECM	extracellular matrix
ECM1	extracellular matrix protein 1
EDTA	ethylenediaminetetraacetic acid
ELISA	enzyme-linked immunosorbent assay
FC	fold change
FDR	false discovery rate
FIBA/FIBB/FIBC	fibrinogen alpha/beta/gamma chain
FINC	fibronectin
G3P/GAPDH	glyceraldehyde-3-phosphate dehydrogenase
GFP	green fluorescent protein
GO	gene ontology
(HB-)EGF	(heparin-binding) epidermal growth factor
HEPES	4-(2-hydroxyethyl)-1-piperazineethanesulfonic acid
(HP)LC	(high-performance) liquid chromatography
I/R	ischaemia-reperfusion
IGF/I(GF)BP4	insulin-like growth factor/IGF-binding protein 4
IQR	interquartile range
LAP	latency-associated peptide (of TGF-β1)
LG3BP	galectin-3 binding protein (Lgals3bp)
LLC	large latency complex (of TGF-β1)

LNA	locked nucleic acid
LTBP	latent transforming growth factor beta-binding protein
MFAP5	microfibrillar-associated protein 5
MHC	myosin heavy chain
MI	myocardial infarction
mi(cro)RNA	microribonucleic acid
MMLV	Moloney murine leukaemia virus
MMP	matrix metalloproteinase
M_r	relative molecular mass
(MS/)MS	(tandem) mass spectrometry
NF-κB	nuclear factor κ-light-chain-enhancer of activated B-cells
NGS	next-generation sequencing
NSpC	normalised spectral count
P2Y12/P2ry12	P2Y purinoreceptor 12
PAR4 amide	proteinase-activated receptor-4 activating peptide AYPGKF amide
PBS	phosphate-buffered saline
PDGFβ	beta unit of platelet-derived growth factor
PEA	proximity extension assays
PF4	platelet factor 4
PPBP	pro-platelet basic protein
PPP	platelet-poor plasma
pri/pre-miRNA	primary transcript/precursor microribonucleic acid
PRP	platelet-rich plasma
PTEN	phosphatase and tensin homologue
qPCR	quantitative real-time polymerase chain reaction
RISC	ribonucleic acid-induced silencing complex
RNA(seq)	ribonucleic acid (sequencing)
RT	reverse-transcription
SDS	sodium dodecyl sulphate
SLC	small latency complex (of TGF-β1)
SLPI	secretory leukocyte protease inhibitor
TAC	transverse aortic constriction
TβRI/II/III	transforming growth factor beta receptor I/II/III
TGF-β1	transforming growth factor beta-1
TNFSF14	tumour necrosis factor superfamily 14
UTR	untranslated region
VAMP	vesicle-associated membrane protein
VCAM1	vascular cell adhesion molecule-1
VWF	von Willebrand factor
WAS(p)	Wiskott-Aldrich syndrome (protein)
WWP1	WW domain-containing protein 1

Figure list

Table list

Main tables:

Supplemental tables:

CHAPTER I

INTRODUCTION

1.1. The pathobiology of cardiac fibrosis

1.1.1 Heart failure and cardiac fibrosis: a clinical perspective

Despite major advances in the past decades, cardiovascular disease (CVD) continues to cause 3.9 million deaths in Europe each year, accounting for 45% of all mortality.[1] In addition, 85 million people are living with CVD, having a major impact on the loss of disability-adjusted life years. The longest CVD-related hospital stays are for patients suffering from heart failure. This clinical diagnosis is characterised by impairment of systemic perfusion, with the inability to meet the body's metabolic demands as a result of a structural and/or functional cardiac abnormality.[2] The aetiology of heart failure is diverse, but can roughly be divided in three categories: diseases of the myocardium, such as due to a genetic predisposition or ischaemic, toxic, inflammatory or metabolic damage; abnormal loading conditions, caused by hypertension, volume overload, or structural defects to the heart; and arrhythmias such as atrial fibrillation. Regardless of the aetiology, heart failure is characterised by the attempt of the heart to structurally compensate for functional impairment, generally referred to as ‘cardiac remodelling’. This process initially enables the heart to sustain the required demand of force. Over the long term, however, the cardiac pump function decreases, ultimately rendering the heart too weak to generate sufficient cardiac output to maintain homeostasis.

The cornerstone of current heart failure therapy mainly consists of symptom relief and delaying disease progression, with heart transplantation being the only cure. Heart failure therefore continues to be a major cause of morbidity and mortality. Several advances have been made with reducing the burden and slowing down progression of disease severity, such as the successful evaluation of a neprilysin inhibitor which has recently been added to the latest clinical guideline for heart failure treatment.[2] However, the 2-year mortality rate of 20% in the intervention arm of the neprilysin inhibitor trial highlights that there is still a need for a therapy that can prevent progression of pathological cardiac remodelling or even reverse it.[3]

1.1.2 The fibroblast as a key cell type in cardiac fibrosis

As mentioned previously, cardiac remodelling is key for the development of heart failure. Cardiac remodelling has been defined by the International Forum on Remodelling as 'genomic expression that results in molecular, cellular, and interstitial changes and is manifested clinically as changes in size, shape, and function of the heart resulting from cardiac load or injury'.[4] Cardiac remodelling can be either physiological or pathological, with the former progressing to the latter as the heart fails to compensate for loss of contractile function.

At the basis of cardiac remodelling lies a complex of structural and functional changes in different cell types and the extracellular matrix (ECM) that form the myocardium. Whilst cardiomyocytes respond to increased stretching by becoming hypertrophic[5], the tissue surrounding the cardiomyocytes changes both in composition and in volume. A main cellular constituent is the cardiac fibroblast (CF). Through producing a variety of matrix proteins and ECM-regulatory proteins, such as growth factors and proteases, CF play a major role in physiological maintenance of the ECM.[6] The ECM is a major determinant of the biomechanical and electrical properties of the heart.[7] CF produce the fibrillar collagens I and III that together comprise approximately 90% of all collagen in the heart, as well as many other less abundant structural and regulatory ECM molecules.[8]

Fibroblasts are also crucial in the development of cardiac fibrosis. As adult human cardiomyocytes lack the ability to regenerate, cardiac repair is dependent on the formation of scar tissue. This is characterised by accumulation and qualitative changes of the cardiac ECM that can lead to marked stiffening of the myocardium. Myocardial 'scarring' occurs in response to acute injury such as myocardial infarction (MI), but is also a common feature of non-ischaemic cardiomyopathies.[9] Interestingly, myocardial fibrosis shares mechanisms with scarring and wound healing in other tissues.[10] In general, tissue injury leads to a cascade of overlapping events that can be roughly divided in an inflammatory phase and a tissue remodelling phase.[7] The extent and pace of this sequence is dependent on the underlying cause, with

ischaemia resulting in massive cell necrosis and subsequent inflammation, whilst non-ischaemic fibrosis develops more gradually.

These two types of remodelling correspond to the two subtypes of fibrosis that are often distinguished histopathologically: *reactive* or *diffuse* fibrosis results from expansion of existing collagen fibres without marked cardiomyocyte loss and is often localised in perivascular areas of the myocardium; whereas *replacement* or *reparative* fibrosis is a more focal form of scar formation, characterised by deposition of newly produced ECM proteins.[11,12] In practice, there is often a mix of both fibrosis types at play. This is illustrated by the poorly understood phenomenon of reactive fibrosis at distant, non-infarcted areas that occurs in parallel with replacement fibrosis at the necrotic area after myocardial infarction.[13]

Upon tissue injury, infiltration of inflammatory cells such as neutrophils cause the release of several bioactive peptides and cytokines, both from local tissue and from infiltrating cells. These factors are thought to then drive the opsonisation of debris by macrophages as well as neovascularisation in and around the injured tissue. Furthermore, inflammatory signals stimulate the production of ECM proteins by activated fibroblasts, called myofibroblasts. Unlike in wound healing of skin injury, the cardiac scar remains relatively cell-rich[14], harbouring a combination of fibroblasts and myofibroblasts, surviving cardiomyocytes, endothelial cells, vascular smooth muscle cells, and inflammatory cells.

The phenotypic transition that fibroblasts undergo during this process is characterised by a more migratory phenotype, characterised by the expression of alpha-smooth muscle actin (α-SMA) and contractile bundles.[9] Furthermore, myofibroblasts are more proliferative and more sensitive to signalling molecules, whilst they also express more adhesion molecules and receptors. This differentiation is not absolute and the fibroblast morphology remains pleiomorphic.[15] Two main triggers determine the fibroblast transformation: feedback from the mechanical environment, and chemokines, with transforming growth factor beta-1 (TGF-β1) being most widely recognised.[16] The latter will be discussed in the following paragraphs.

In addition to resident CF, other cell types might also contribute to the myofibroblast pool in the injured heart. This may include endothelial and epithelial cells undergoing mesenchymal transition as well as bone marrow-derived cells.[17–20] In addition, circulating cells may also contribute to phenotypic switching by factors that they secrete, as was shown for circulating platelets and epithelial-to-mesenchymal transition in tumours.[21] The extent to which endothelium- and epithelium/epicardium-derived (myo)fibroblasts play a role in cardiac fibrosis remains a matter of debate.[9,22] Nevertheless, this paradigm shift highlights a growing appreciation of the interplay between tissue injury and systemic effects in the development of fibrosis.[12] The importance of the systemic context for the study of fibrosis will be further argued in this thesis.

1.1.3 TGF-β1 and pro-fibrotic signalling

1.1.3.1 TGF-β1 secretion in the heart

The most widely recognised factor in steering fibroblasts towards a pro-fibrotic state, and thereby a 'master switch' of fibrosis, is TGF-β1.[16,23] TGF-β1 expression increases during functional as well as fibrotic tissue repair.[24] Its activity appears to be key in the gradual shift from beneficial scar formation, compensating for tissue loss, towards adverse remodelling characterised by functional impairment of the tissue. Within the heart, its expression can be induced by an array of factors, including angiotensin II and mechanical stretch.[25] TGF-β1 is synthesised and secreted by cardiomyocytes[26] as well as fibroblasts.[27,28] In addition, immune cells and platelets may also be important contributors to myocardial TGF-β1 activity. In particular, extravasated platelets appear to be a key source in the early stages of infarct healing as well as during cardiac overload-induced fibrosis.[29,30]

Within the heart, TGF-β1 can also be found outside the cells, where it is stored in association with ECM proteins.[31] TGF-β1 is secreted in an inactive form, by non-covalent binding of TGF-β1 to the cleavage product of pro-TGF-β1, called the latency-associated peptide (LAP).[32] The complex between a TGF-β1 homodimer and LAP is referred to as the small latency complex (SLC).

This association prevents TGF-β1 from binding to cell receptors, therefore rendering it biologically inactive. Upon secretion into the extracellular space, the SLC is contained within the ECM through associating with other latency-associated proteins, in particular latent TGF-β1 binding protein-1 (LTBP1). Covalent binding of the SLC to LTBP1 and proteins with similar function constitutes the large latency complex (LLC). An illustration of the SLC and LLC is shown in **Figure 1**. Through this mechanism, TGF-β1 secretion and activity are uncoupled, requiring release from its latency complex rather than from a cell to activate signalling downstream of its receptors. Whilst there is constitutive secretion of TGF-β1 into the ECM in the healthy myocardium, TGF-β1 from other sources, with the circulation in particular, have also been implicated in cardiac remodelling.[29,33,34] The role of circulating and platelet-derived TGF-β1 in fibrosis are discussed in greater detail later.

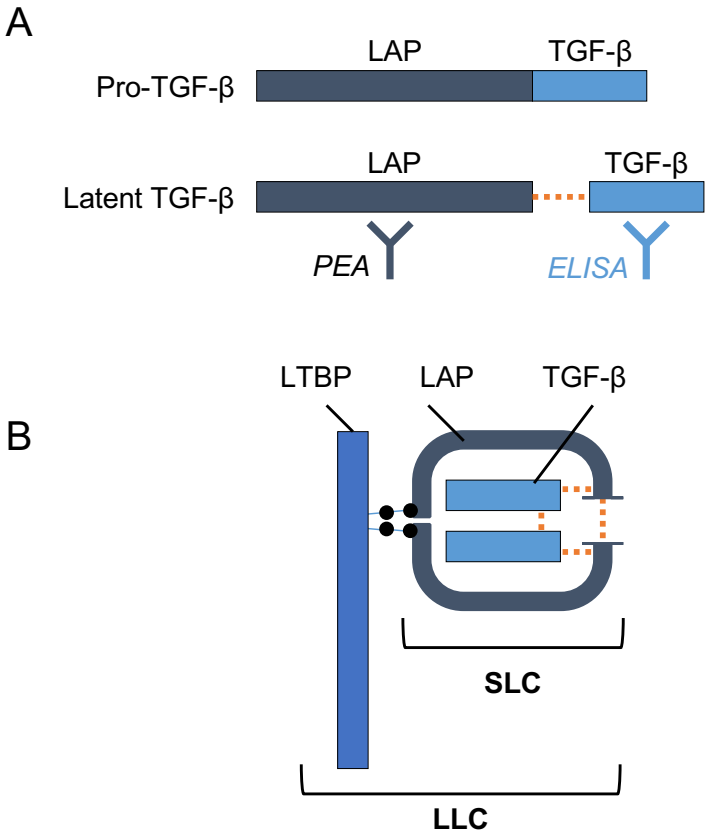

Figure 1. Transforming growth factor beta-1 (TGF-β1) and its latent forms. A: Following synthesis of pro-TGF-β1, this precursor is cleaved into the latency-associated peptide (LAP) and mature TGF-β1 by furin-like enzymes in the Golgi apparatus. Antibodies used in the proximity extension assay (PEA) panel (see **3.14**) and the ELISA (see **3.16**) that was used targeted different epitopes. **B:** Upon cleavage of the precursor, TGF-β1 dimers remain noncovalently bound to LAP, forming a small latency complex (SLC). A proportion of the SLC is by itself bound to latent-transforming growth factor beta-binding protein (LTBP) by disulfide bonds, forming a large latency complex (LLC).

1.1.3.2 Cardiac TGF-β as a potential therapeutic target

Activation of TGF-β1 occurs through disruption of the non-covalent binding within the SLC. Several factors are capable of causing this disruption, such as mechanical force[32], acidic pH levels[35], or several proteins, including integrins[36] and proteases such as matrix metalloproteinases[37], plasmin and thrombospondin-1.[38] After being released from its latency state, TGF-β1 can bind to the TGF-β type 2 receptor (TβRII) to activate the TGF-β type 1 receptor (TβRI), also known as activin receptor-like kinase 5, through phosphorylation. This subsequently leads to phosphorylation of intracellular Smad2/3. Phosphorylated Smad2/3 associates with Smad4 to enter the nucleus, where it can then affect transcription of an array of genes. In the heart, the phenotypical effects depend on the cell type, on one hand inducing cardiomyocyte hypertrophy, whilst driving the transition of fibroblasts to myofibroblast-like phenotypes with a concomitant increase in ECM protein deposition.[24]

Given its major role in the pathophysiology of fibrosis, TGF-β1 and its downstream signalling cascade have often been suggested as a therapeutic target. However, this approach is hampered by the involvement of TGF-β1 and its downstream signalling in many cellular processes. Targeting TGF-β signalling therefore inadvertently carries the risk for off-target effects. This is illustrated by the fact that TGF-β1 *null* mice die 3-4 weeks after birth due to excessive immune cell infiltration of heart, lungs and other organs.[39,40] Several studies have nevertheless evaluated pharmacological targeting of TGF-β signalling. *In vivo* inhibition of TGF-β1 in mice was shown to attenuate fibrosis and preserve cardiac function after transverse aortic constriction (TAC), a commonly used model of cardiac pressure overload.[41] However, as expected from the broad effects of TGF-β1, several studies have reported significant side effects or even increased mortality.[42,43] Interfering with downstream signalling of TGF-β1 may hold more promise for clinical utility, as this was shown to attenuate pulmonary fibrosis in mouse studies without concomitant side effects.[44–46] With either approach, interfering with TGF-β signalling would require meticulous timing for therapeutic intervention, given the apparent shift from being a beneficial to a detrimental contributor after injury. This is

illustrated by evidence that interfering with TGF-β signalling too early after acute injury results in inadequate resolution of inflammation, thereby worsening the outcome.[9]

In search for more specific effectors downstream of the TGF-β signalling cascade, Schafer *et al* recently reported interleukin-11 as a potential therapeutic target.[47] Primary human fibroblasts were isolated from atrial tissue and were then treated with recombinant TGF-β1. Subsequent RNA sequencing analysis of these cells identified interleukin-11 to be highly upregulated. Furthermore, the authors argue that interleukin-11 is highly specific to fibroblasts, using RNA sequencing data from the publicly available Genotype-Tissue Expression project and from a panel of primary cells. Using an inducible interleukin-11 knockout mouse model under the control of the collagen I α-2 gene, fibrosis formation upon angiotensin II treatment was markedly attenuated. Based on these findings, interleukin-11 targeting is proposed as a promising therapeutic strategy against fibrosis. The reported fibroblast specificity in this study is surprising in the context of exisiting literature, as interleukin-11 has previously been described as a key driver of megakaryopoiesis in the bone marrow.[48,49] Megakaryocytes and the bone marrow are not included in the RNA sequencing datasets used in this study. Furthermore, the authors do not assess whether the bone marrow or platelets were affected upon interleukin-11 targeting in mice. The suggested involvement of platelets in fibrosis, as described in the following paragraphs and as further argued by the findings of this thesis, warrant further evaluation of a platelet-mediated effect as an additional explanation of their findings.

1.1.3.3 TGF-β secretion and signalling beyond the heart

As mentioned earlier, TGF-β1 originating from other sources than cardiomyocytes or CF may also affect cardiac fibrosis and hypertrophy. The overlap between fibrogenesis, inflammation and tissue wound healing across tissues and organ systems, as well as the role of TGF-β signalling therein, further highlights that systemic inflammatory effects may orchestrate tissue remodelling. Plasma levels of TGF-β1 were significantly higher in patients with fibrotic liver disease.[50] In the context of autoimmune diseases, higher levels of

TGF-β1 were found in plasma[51] and inflamed synovial membranes[52] of patients with rheumatoid arthritis. Similar findings have been reported in inflammatory infiltrates in the gut of patients suffering from ulcerative colitis or Crohn's disease.[53] Across these inflammatory conditions, TGF-β1 can both worsen and improve disease outcomes, depending on the timing and the site of action. From a translational perspective, this underscores that interfering with TGF-β signalling requires a time- and site-targeted approach to avoid off-target effects.[54] Although the cellular origin of TGF-β1 is often unclear, it is interesting to note that an influx of immune cells during inflammation is often accompanied by platelet influx. Platelets in particular have been recognised as a major source of TGF-β1.[29,55]

1.2 Blood platelets and heart failure

1.2.1 Blood platelets beyond haemostasis

Blood platelets are primarily recognised for their function in thrombosis and haemostasis. In this role, platelets respond to endothelial damage, where exposure of sub-endothelial matrix proteins such as collagen induces platelet adhesion and activation through its surface receptors.[56] Being captured and bound together by von Willebrand factor (VWF)[57], the accumulation of activated platelets at a site of injury initiates the formation of a blood clot through the release of platelet granules. During this process of degranulation, platelet aggregation is further amplified through fibrinogen-mediated interactions with surface receptors on activated platelets and through the release of secondary platelet agonists adenosine diphosphate (ADP) and thromboxane A_2.[58] In addition, thrombin is generated at the platelet surface, acting as a strong platelet agonist whilst also converting fibrinogen into fibrin. The result of this orchestrated process is the formation of a platelet-fibrin clot, forming a plug to halt blood loss.

The function of platelets is not confined to haemostasis and thrombosis. Whilst the involvement of platelets in clot formation is well-recognised as a key event in coronary artery disease and stroke, their role in cardiovascular disease beyond thrombus formation has received less attention thus far. Nevertheless, there is increasing evidence for a role of activated platelets in the development and progression of heart failure and fibrosis.[59] Platelet granules, in particular alpha (α)-granules, contain not only mediators of haemostasis, but also an array of pro-inflammatory cytokines, growth factors and enzymes. This includes TGF-β1, as previously mentioned, which is expressed in many different cell types but is highly enriched in platelets.[60] Furthermore, platelets harbour several surface receptors that suggest their involvement in inflammatory processes. Although platelets are small in size, their high numbers in the blood support the concept that their total surface area and volume exceeds that of the total of all circulating leukocytes.[61] These observations are further supported by the role that platelets play in the wound healing response after haemostasis at a lesion site. As mentioned previously,

there is substantial overlap between the pathobiology of wound healing and the development of fibrosis across organs, rendering platelets an interesting potential source of mediators in the latter process as well.

1.2.2 Heart failure and antiplatelet therapy

Previous studies have indeed identified a role for platelets and platelet-derived proteins in heart failure. Heart failure patients were found to have higher plasma levels of soluble cluster of differentiation 40 ligand[62], pro-platelet basic protein (PPBP)[63], thrombospondin-1 and TGF-β1[64], all proteins released from platelets. These results imply increased platelet reactivity or activation in heart failure patients. Several explanations have been suggested for this finding, including increased platelet reactivity due to endothelial damage, disturbed nitric oxide production, increased oxidative stress or higher cytokine levels, which are all able to affect platelets.[65]

Based on the data implicating platelets in the pathophysiology of heart failure, antiplatelet therapy could be expected to delay its progression. Current therapy for heart failure consists of symptom relief with diuretics, combined with beta-adrenergic receptor blockers, angiotensin-converting enzyme inhibitors or angiotensin receptor blockers and aldosterone antagonists. These drugs do not treat the cause of heart failure but are aimed at inhibiting neurohumoral pathways that are thought to drive adverse cardiac remodelling.[66] There is currently no evidence for a benefit of antiplatelet therapy on survival in heart failure patients, unless there is an additional indication such as atrial fibrillation or coronary artery disease.[67] The survival benefit in these specific patients is likely due to the increased thromboembolic risk that these co-morbidities confer. Previous studies into antiplatelet therapy in heart failure did not evaluate whether there was a benefit on cardiac remodelling or the occurrence of fibrosis; outcome measures were solely based on all-cause mortality, major bleeding events and non-fatal cardiovascular events such as stroke, MI or embolisms. Nevertheless, current guidelines do not recommend routine prescription of antiplatelet drugs in heart failure patients.[2]

A potential explanation as to why platelet inhibition does not benefit heart failure patients is the increased bleeding risk that these drugs confer[66], possibly outweighing benefits of inhibition on the development of fibrosis. Distinguishing the antithrombotic effects from a potential benefit of decreased platelet release of pro-fibrotic mediators would require drugs that specifically act on either of these two mechanisms, which are currently not available.

1.2.3 Platelets in animal models of heart failure

Several studies have evaluated the role of platelets in heart failure using animal models of cardiac hypertrophy and fibrosis. Evaluating post-ischaemic cardiac remodelling, Kalkman *et al* found that aspirin treatment in rats undergoing MI did not change the extent of hypertrophy or replacement fibrosis in the infarcted area, but did reduce interstitial and perivascular fibrosis in the rest of the heart.[68] A study using a genetic model of cardiomyopathy in hamsters found that chronic aspirin treatment attenuated the development of hypertrophy and fibrosis.[69] Pharmacological platelet inhibition using clopidogrel attenuated the inflammatory and fibrotic response in mice undergoing hypertension-induced cardiac remodelling[70], whilst a similar benefit was seen for cardiac hypertrophy with the use of aspirin.[71] In mice, a similar model combined with transplantation of platelets that had been isolated from P-selectin *null* mice showed a similar benefit[72]; P-selectin is normally released from activated platelets and is an important mediator of inflammatory cell recruitment at injury sites. A more recent study also evaluated this effect by injecting antibodies against P-selectin into mice undergoing TAC-mediated cardiac remodelling. This led to a significant reduction in platelet-monocyte aggregate formation and markedly reduced the extent of fibrosis and hypertrophy.[73] In this same study, the effects of TAC in *P2ry12 null* mice were evaluated. This gene codes for the P2Y purinoreceptor 12 (P2Y12), a key platelet-activating receptor and the target of thienopyridine drugs such as clopidogrel and prasugrel. TAC was shown to increase platelet reactivity in wild-type mice, but this was reduced in the *P2ry12 null* mice. Consequently, fibrosis and hypertrophy were significantly reduced as well. This effect was reproduced by transplanting *P2ry12 null* bone marrow into wild-type mice, but abrogated when *P2ry12 null* mice received transfusions of wild-type platelets. Finally, inducing thrombocytopaenia with a CD41-targeting antibody also

alleviated TAC-mediated cardiac remodelling, abolishing the difference between *P2ry12 null* and wild-type mice. Altogether, these studies indicate that platelet activation contributes to cardiac remodelling in well-established animal models of heart failure.

Focusing on platelet TGF-β1, studies in megakaryocyte/platelet-specific TGF-β1 *null* mice had less extensive cardiac hypertrophy and fibrosis in response to TAC when compared to wild-type mice.[29] More recently, a study evaluating antiretroviral therapy-induced cardiomyopathy in mice found markedly higher levels of plasma TGF-β1, as well as a decrease in cardiac output with prominent fibrosis in wild-type mice. The same antiretroviral treatment in megakaryocyte-specific TGF-β1 *null* mice did not result in higher TGF-β1 plasma levels and these mice were protected from cardiac dysfunction and fibrosis.[74] Hence, platelet-derived TGF-β1 may indeed be a key contributor to cardiac remodelling.

As mentioned previously, platelets are known to be highly enriched in TGF-β1. Previous studies have shown that platelet TGF-β1 is synthesised in megakaryocytes in the spleen and bone marrow, where it is directly packaged into α-granules.[75] During platelet activation, these α-granules are released. There is a distinct pattern however for the release of TGF-β1 from platelets, which challenges the dogma of rapid degranulation upon platelet activation. Whilst translocation of P-selectin to the platelet membrane surface, a widely-used marker for platelet activation and α-granule secretion[76], occurs rapidly, TGF-β1 release appears more gradual.[77] This could be caused by a difference in solubility between the two proteins, but could also indicate that TGF-β1 is packaged in distinct particles, implying that there are different subtypes of α-granules. Within α-granules, TGF-β1 is stored in two different forms: 60-65% is bound within the LLC, whilst 30-35% is stored as part of the SLC. It has been reported that release dynamics differ for these two complexes: LLC is rapidly released upon platelet degranulation, whereas SLC is retained within the platelet/clot and is released during clot resorption by plasmin.[78]

In summary, heart failure and cardiac fibrosis are common features of CVD and there is great unmet demand for effective therapeutic strategies. Whilst locally resident CF are main contributors to the development of fibrosis, there is mounting evidence that systemic effects play an important role, with TGF-β1 being a major driver of pro-fibrotic signalling. The role of platelets as a source of TGF-β1 is still underappreciated in the context of HF despite previous animal studies showing that platelet-derived TGF-β1 can contribute to cardiac remodelling.

1.3 MicroRNAs in cardiovascular disease

1.3.1 The discovery of non-coding RNA

With completion of the Human Genome Project, it became apparent that only 1.5% of the human genome codes for genes that function in protein synthesis.[79] Except for the small proportion of the DNA that encodes 'infrastructural RNA' such as transfer and ribosomal RNA, the non-gene-coding regions of the DNA were initially considered 'junk DNA'. In the last two decades, there has been ongoing debate as to what proportion of the genome is functional. The ENCODE consortium claimed that 80% of the genome is "biochemically active", a statement which was based on DNA sequences being copied into RNA.[80] Others have however argued that the percentage of functional DNA is more likely to be around 10%, the main argument being that the genome needs 'decoy' DNA to cope with the relatively high rate of spontaneous mutations.[81] Whilst this discussion continues, many aspects of both normal development and pathology have in the meantime been ascribed to transcription products of the non-coding part of the genome, generally referred to as 'non-coding RNA'. Several categories of non-coding RNAs exist, comprising different subtypes of long non-coding RNAs and small non-coding RNAs. The subclass of functional non-coding RNA that has received most attention since their discovery in the early 1990's are the small noncoding RNAs called microRNAs (miRNAs).[82] In the following paragraphs, miRNA biosynthesis will be discussed briefly, followed by a summary of highlighted studies in the cardiovascular field and current analytical techniques as well as experimental applications.

1.3.2 MicroRNA biosynthesis, function and quantification

MiRNAs are short (~22 nucleotides) molecules that exert their function by binding to messenger RNA (mRNA), so-called 'miRNA targets', through sequence complementarity.[83,84] A graphical representation of miRNA biosynthesis and function is shown in **Figure 2**. Of particular interest within the miRNA sequence is the 'seed region', a section of six to eight nucleotides at the 5' end that is the critical determinant of miRNA-mRNA interaction. MiRNAs originate from primary transcripts (pri-miRNAs), derived from introns of protein

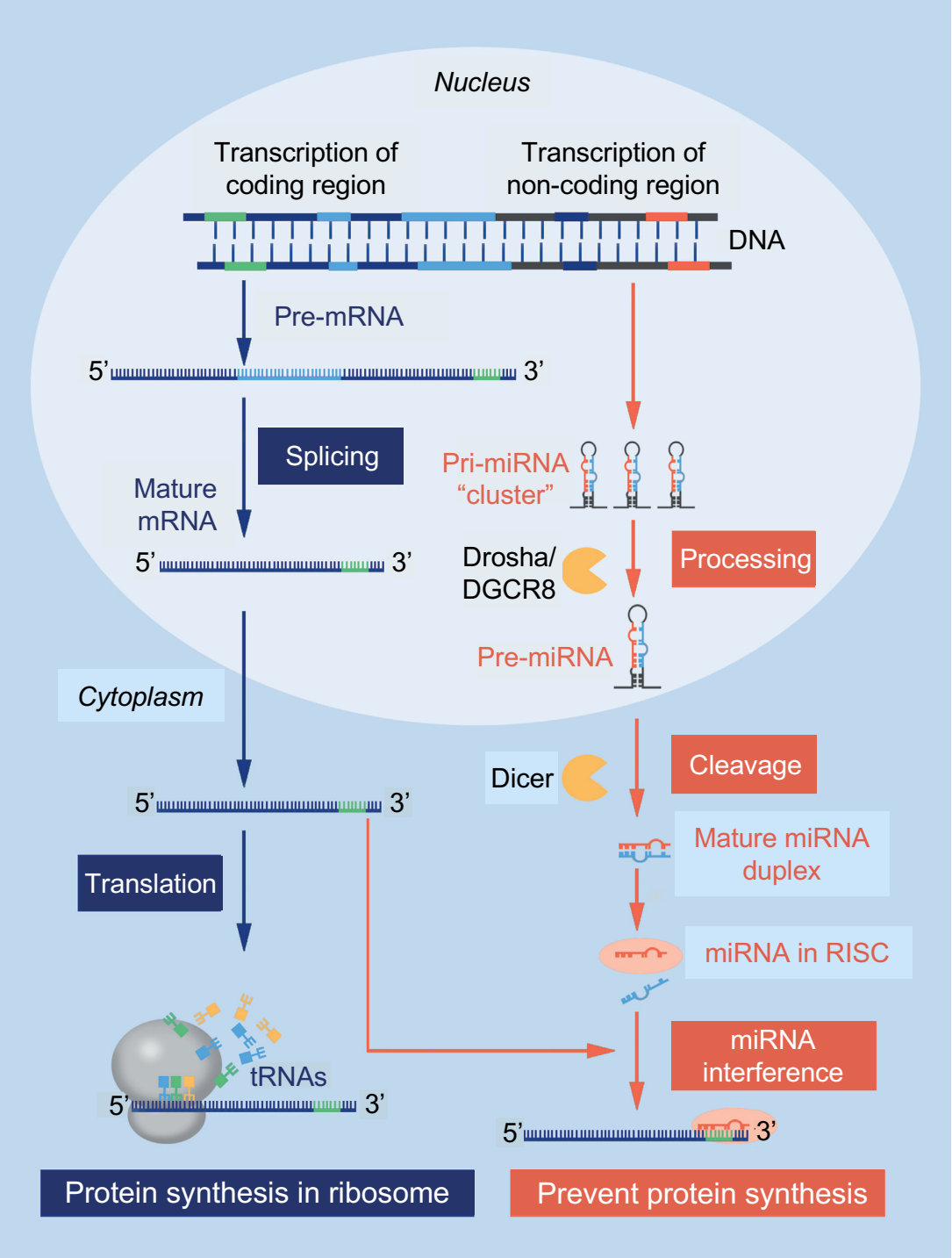

Figure 2. MicroRNA biosynthesis and function. MicroRNAs (miRNAs) originate from primary transcripts (pri-miRNAs) that are derived from introns (depicted in dark blue) of protein-coding genes or from intergenic regions within the genome. Primary transcripts are processed in the nucleus to a hairpin-shaped pre-miRNA by the Drosha/DiGeorge syndrome critical region 8 (DGCR8) complex, transported to the cytoplasm, and then processed to mature miRNA duplexes by the Dicer complex. To exert its function, the mature miRNA is incorporated into a ribonucleic acid-induced silencing complex (RISC). This leads to cleavage or translation repression of the mRNA, preventing a protein from being assembled. mRNA, messenger RNA; tRNA, transfer RNA. *(Previously published in Barwari et al. 2016, Journal of the American College of Cardiology, reprinted with permission; see* ***Appendix 2****)*

coding genes, introns/exons of noncoding genes, or intergenic regions within the genome.[85,86] Pri-miRNAs are processed by the Drosha/DiGeorge syndrome critical region gene-8 (DGCR8) complex in the nucleus, folding the transcript into a 60-100 nucleotide-long hairpin structure, called pre-miRNA.[87] Pre-miRNAs are then transported from the nucleus to the cytoplasm by exportin-5.[88] Here, pre-miRNAs are cleaved by the Dicer complex into duplexes consisting of two miRNA strands, designated guide strand and passenger strand, based on their subsequent relative levels.[89] Both strands can function as a mature miRNA.[90]

To exert their function, either one or both of the mature miRNA strands are incorporated into an RNA-induced silencing complex (RISC), consisting of a number of proteins including Argonaute. The miRNA within this complex serves as a guide to recognise target mRNAs. Depending on the base complementarity between the miRNA and its mRNA target, this can lead to cleavage or translation repression.[91] Single miRNAs can suppress more than one gene, and miRNAs with similar seed regions may suppress a similar, but non-identical set of genes and to differing degrees. Gene suppression is usually partial rather than total and a single gene can have binding sites for multiple miRNAs. This organisational complexity, illustrated by a high false-positive rate of target prediction algorithms[92], presents challenges in both understanding the functions of miRNAs and manipulating their effects.[93]

MiRNAs are relatively stable, and can be reliably measured in tissues, as well as in biofluids. Several techniques have been developed to identify and quantify miRNAs, each with benefits and disadvantages.[94] Quantitative real-time polymerase chain reaction (qPCR) is by far the most commonly used technique and can be regarded as the standard for miRNA quantification. Alternatively, methods with higher throughput include microarrays and RNA sequencing (RNAseq). Microarrays are suitable for relatively fast yet less accurate quantification of miRNAs, measuring hundreds of miRNAs in parallel. Similar to qPCR, microarrays rely on predefined primer sequences and are therefore not able to discover previously uncharacterised miRNAs. RNAseq provides “hypothesis-free” identification of RNA species, allowing for the discovery of new miRNAs and quantitative analysis of a comprehensive

miRNA transcriptome. The use of computational solutions to resolve reads into miRNAs suffers from the risk of reporting putative sequences which do not have real-world correlates.[95] We have recently discussed in greater detail the benefits and potential pitfalls with these techniques.[96]

To study the function of miRNAs across different cells and tissues, techniques have been developed to manipulate their expression levels. These methods include the conditional deletion of the gene encoding Dicer (see **Figure 2**), resulting in suppression of miRNA biosynthesis[97], but more commonly involve the overexpression or inhibition of a single miRNA.[98] When using isolated cells in culture, overexpression of a miRNA is most commonly achieved by binding synthetic miRNA mimics, identifical in sequence and chemistry to the naturally occurring single or duplex miRNA, to cationic molecules. MiRNA mimics bound to these reagents are then added to the medium, generally resulting in an efficient transfection of the mimics into the cytoplasm of the cultured cells. These mimics are naturally taken up by silencing complexes, resulting in a functional overexpression of the studied miRNA. Conversely, biological effects of a miRNA can be studied by inhibiting its expression, using anti-miRNA oligonucleotides, more commonly known as antimiRs.[99] For *in vitro* use, these antimiRs generally consist of an antisense oligonucleotide that is a perfect reverse complement to the targeted miRNA. These oligonucleotides contain several chemical modifications to enhance their binding affinity and their ability to resist nuclease activity, hence increasing their efficacy in binding their target miRNA. Upon transfection across the cell membrane using similar techniques as for miRNA mimics, antimiRs inhibit the functioning of targeted miRNAs by steric inhibition or by degradation, depending on the chemistry used. When using antimiRs *in vivo*, additional modifications are required to ensure stability. This is discussed further in paragraph **1.5**.

1.3.3 MicroRNAs: from discovery to cardiovascular applications

The first miRNA was identified in the *Caenorhabditis elegans* nematode. This molecule, called lin-4, was found during genetic screens aimed at developmental timing of gene expression. Lee *et al* showed that lin-4 was encoded by a sequence in the intron of a host gene and had sequence

complementarity to the 3' untranslated region (UTR) of lin-14 mRNA. The resulting duplex repressed the accumulation of LIN-14 protein, which had previously been implicated in the L1-to-L2 transition during *C. elegans* post-embryonic development.[82] The discovery of a second short non-coding RNA called let-7[100], which showed remarkable sequence conservation across species[101], paved the way for the rapid emergence of this field. In the following years, a range of other miRNAs were identified in what was previously considered 'transcriptional slop'.[102,103] The initial focus of research was on the developmental effects of miRNAs in smaller species. However, a study showing tissue-specific differences in miRNA expression levels[104] further sparked the interest in miRNAs.

The earliest reports in the cardiovascular field were published in 2005, identifying miR-1 as a regulator of cardiac differentiation.[105,106] Soon after, associations between miRNA levels and cardiovascular pathology were reported, including a landmark study by Van Rooij *et al*[107] that found several dysregulated miRNAs in failing hearts of humans and mice. Importantly, this study showed that upregulation of miRNAs caused phenotypic changes, indicating that miRNA dysregulation may be a cause or mediator of disease rather than just a readout. This study, as well as the successful development of pharmacological strategies to target miRNAs *in vivo*[108], ignited a surge of studies evaluating the effects of miRNAs in the cardiovascular field.

1.3.4 MiR-21 in cardiovascular disease

One of the most widely studied miRNAs is miR-21. Over the past decade, this miRNA has been at the forefront of proposed clinical utility, whilst also inciting controversy through reports with contradicting results. The gene coding for miR-21 in located on chromosome 11 (mouse) or 17 (human) within the penultimate intron of transmembrane protein 49, itself encoding a protein involved in vacuole formation and autophagy.[109] Transcription of miR-21 and this gene are independent and levels of the encoded protein are not altered in miR-21 *null* mice.[110] The earliest studies on miR-21 had an oncological focus, reporting it to be upregulated in glioblastoma cells where it had anti-apoptotic effects.[111] The overexpression was confirmed in six other solid tumour types[112], with another study identifying several targets that were implicated in

the observed effects on tumour growth and invasiveness.[113] One of the first reports on miR-21 in the cardiovascular field was the study by Van Rooij *et al*, evaluating miRNA expression levels in cardiac hypertrophy and heart failure.[107] Here, a substantial increase in miR-21 expression was found in hearts of mice undergoing TAC, as well as in transgenic mice expressing activated calcineurin A in the heart. Surprisingly, this study did not find increased miR-21 levels in human heart samples from idiopathic end-stage heart failure patients. Increased expression in hypertrophic rodent hearts[114–117] was however confirmed in several studies published soon after. These findings, combined with the association with apoptosis in several high-profile oncological studies, led miR-21 to become a major target of interest for potential therapeutic use.

1.3.4.1 MiR-21 and cardiac fibrosis

The first landmark study on miR-21 in heart failure and fibrosis was a study by Thum *et al.*[118] Whilst confirming the previously reported increased levels of miR-21 in failing hearts of human and rodent origin, this study attributed the increase to CF rather than cardiomyocytes. This was in line with a study published at the same time, where a cardiomyocyte-specific knockout of Dicer, disrupting miRNA biogenesis, had a relatively limited effect on cardiac miR-21 expression.[97] The findings by Thum *et al* were in line with previous reports on tumour cell apoptosis, concluding that miR-21 increased the survival of CF. As the responsible mechanism, targeting of Sprouty-1 was identified (see **Table 1** for a table of key miR-21 targets). This inhibitor of anti-apoptotic mitogen-activated protein kinase activity was found to be expressed only in the non-myocyte cell population of the heart. The authors argued that miR-21 and fibroblasts have a central role in the pathogenesis of heart failure, with miR-21 mediating enhanced CF survival and thus contributing to interstitial fibrosis and remodelling. Using antagomiR-21, a construct targeting miR-21 with a chemistry previously described for miR-122 inhibition[108], the authors showed an attenuation of TAC-induced cardiac dysfunction. This beneficial effect of pharmacological miR-21 inhibition was considered a major breakthrough in the cardiovascular miRNA field and consequently fuelled the interest in this topic.

Table 1. Major miR-21 targets in cardiac fibrosis.

Target	Effect of targeting	Cell type	Evidence	Citation
Sprouty-1	Decreases apoptosis through enhanced ERK-MAPK signalling	Fibroblast	Luciferase assay	Thum *et al*, Nature 2008[118]
PTEN	Increases MMP2 expression	Fibroblast	Luciferase assay	Roy *et al*, Cardiovasc Res 2009[119]
	Enhances Akt and NF-κB activity, inhibiting TGF-β1 expression and secretion	Bone marrow mesenchymal stem cell		Wu *et al*, Stem Cells 2015[120]
TGFBR3	Potentiates TGF-β signalling and myofibroblast differentiation	Fibroblast	Luciferase assay	Liang *et al*, IJBCB 2012[121]
WWP1	Decreases TβRI degradation and enhances TGF-β signalling	Fibroblast	qPCR and immunoblot	Tao *et al*, Heart, Lung & Circulation 2017[122]
SMAD7	Enhances ERK and Akt activity, increasing fibroblast survival and differentiation	Fibroblast	qPCR and immunoblot	Lorenzen *et al*, EHJ 2015[123]
WAS(p)	*Enhances release of TGF-β1 from platelets upon activation*	*Megakaryocyte /platelet*	*Luciferase assay*	*(current thesis)*

The results of Thum *et al,* however, were not reproduced in a subsequent study by Patrick *et al*.[110] Here, miR-21 *null* mice as well as a pharmacological inhibitor with a different design compared to antagomiRs were used. MiR-21 *null* mice as well as mice receiving this smaller miR-21 inhibitor had a normal baseline phenotype. Surprisingly, the extent of cardiac fibrosis in response to TAC and to angiotensin II, another common hypertension-based model of heart failure, was unaffected by miR-21 inhibition. In addition, MI was induced by ligation of the left anterior descending coronary artery in mice, whilst another approach included cross-breeding miR-21 *null* mice with mice expressing calcineurin A under the control of the myosin heavy chain (MHC) alpha isoform. None of these models showed a benefit of miR-21 inhibition or deletion. In contrast to the previous study by Thum *et al*, miR-21 inhibition was performed using Locked Nucleic Acid (LNA)-based octamers targeting the miR-21 seed sequence only. In response to the study by Patrick *et al*, Thum *et al* reported a side-by-side comparison of miR-21 inhibitors with different chemistry, confirming the lack of effect using the octamer whilst inhibition using

two types of 22-mer constructs did attenuate fibrosis.[124] A subsequent response from Patrick *et al* then mentioned the use of tamoxifen-inducible miR-21 *null* mice, where miR-21 inhibition directly prior to the TAC also failed to affect the phenotype.

Despite these inconsistent results, numerous studies have since consolidated the relation between miR-21 and cardiac fibrosis. Animal studies have found increased levels of miR-21 in the heart using TAC[125–131], a model of combined pulmonary valve insufficiency and stenosis[132], angiotensin II[123] or isoproterenol infusion[133–135] to induce cardiac remodelling, with only one report showing contradicting results.[136] Studies in human hearts were in line with these results, showing increased miR-21 in cardiac fibrosis due to aortic stenosis[137], chronic atrial fibrillation[138], arrhythmogenic right ventricular cardiomyopathy[139] and combined pulmonary valve insufficiency and stenosis.[132] *In vitro* studies have suggested that high glucose levels can increase miR-21 levels, inducing a myofibroblast-like phenotype in cultured rat CF.[140] Lastly, afterload enhancement in engineered heart tissue from neonatal rat ventricle caused fibrotic changes which could be attenuated by pre-treatment with a miR-21 inhibitor.[141]

Altogether, different *in vitro* and *in vivo* models of cardiac fibrosis as well as samples from human fibrotic hearts provide evidence for the involvement of miR-21 in cardiac fibrosis.

1.3.4.2 MiR-21 and myocardial ischaemia

Fibrosis and cardiac remodelling are a common feature after MI. Consequently, numerous studies have evaluated miR-21 in the context of myocardial ischaemia and ischaemic pre-conditioning. Whilst studies have reported inconsistent results regarding the effect of ischaemia on cardiac miR-21 levels[142–144], specific evaluation of the infarct area and remote area after ischaemia revealed that miR-21 was reduced in the former but increased in the latter region.[145–147] The miR-21 reduction could be prevented by subjecting the heart to ischaemia-reperfusion (I/R) prior to the infarct, whilst pre-treatment with a miR-21 mimic reduced the infarct size. A brief report by Yin *et al* showed that isolated miRNAs from *ex vivo* I/R-treated hearts contained high levels of

miR-21, whilst intra-cardiac injection of miR-21 mimic prior to MI resulted in a smaller infarct size.[148] These studies imply that in the acute phase of myocardial ischaemia, induction of miR-21 expression has a beneficial effect.

The hypothesis of miR-21 mediating the protective effect of I/R was supported by other studies. Beneficial effects of I/R were abolished by miR-21 inhibition[149] whilst transgenic miR-21 expression in cardiomyocytes[146] or intra-cardiac injection of miR-21 mimic[150] reduced myocardial damage of ischaemia. Intramyocardial injection of skeletal muscle cells that had been pharmacologically preconditioned to mimic I/R treatment, improved the outcome of MI in rat hearts; this effect was abolished by pre-treatment with miR-21 inhibitors.[151] Although most of these studies still focus on cardiomyocytes, Roy and colleagues reported that the miR-21 induction following I/R depended on CFs. Here, miR-21 targeting of phosphatase and tensin homologue (PTEN) resulted in increased expression of matrix metalloproteinase-2, a protease linked to cardiac dysfunction.[119]

Developing a method to regenerate cardiomyocytes after myocardial damage can be seen as a holy grail in cardiology.[152] Studying the potential involvement of miR-21 in this process, Xiao *et al* showed that cardiac progenitor cells secrete exosomes that contain miR-21. Both the release and the miR-21 content increased with hydrogen peroxide treatment and secreted exosomes were internalised by cardiomyocytes. Co-incubation with these exosomes restored hydrogen peroxide-induced downregulation of miR-21 and attenuated cardiomyocyte apoptosis.[153] A similar example of miR-21 acting as a paracrine mediator was shown in another study for the miR-21 passenger strand (miR-21-3p). Here, Bang and colleagues demonstrated that miR-21-3p was transferred to cardiomyocytes in CF-derived exosomes, where it exerted a pro-hypertrophic effect.[90]

In pursuit of a strategy to decrease the effect of micro-embolisation after percutaneous coronary interventions, Su *et al* used ultrasound-targeted microbubble destruction to deliver miR-21 in a pig model of coronary micro-embolisation.[154] Whilst miR-21 levels were not different after micro-embolisation, delivery of miR-21 showed a marked reduction of inflammation

and consequently attenuated cardiac dysfunction. Whether this was a direct effect on the myocardium or an effect on inflammatory cells or platelets was not assessed.

1.3.4.3 MiR-21 and atrial fibrillation

Evaluating the effect of miR-21 in fibrosis with a different aetiology, Adam *et al* focused on atrial fibrillation, showing higher miR-21 levels in left atrial appendages of patients suffering from this arrythmia.[155] MiR-21 levels correlated with the extent of fibrosis in a transgenic mouse model of atrial fibrillation[156] and systemic antagomiR-21 treatment in these mice decreased the extent of atrial fibrosis.[155] In line with these findings, Lavall *et al* showed that fibrosis due to chronic atrial fibrillation occurred through mineralocorticoid receptor stimulation and downstream miR-21 induction.[138] Adding a therapeutic angle, Cardin *et al* used intra-atrial injection of an LNA-based inhibitor of miR-21, which significantly decreased the extent of atrial fibrosis, cardiac dysfunction and susceptibility to arrhythmia.[157] Evaluating cardiac remodelling in response to ventricular tachypacing in dogs, Chen *et al* found miR-21 expression in the left atrium to increase with the development of fibrosis, whilst also showing that miR-21 was markedly enriched in CF compared to cardiomyocytes.[158] Similar studies confirmed the increase of miR-21 expression upon induction of atrial fibrillation and subsequent remodelling, with miR-21 inhibition attenuating adverse remodelling.[122,159,160] Interestingly however, atrial appendage biopsies from patients with chronic atrial fibrillation exhibited higher miR-21 levels in the isolated cardiomyocyte fraction[161], while another study found lower miR-21 levels in atrial biopsies and in plasma from atrial fibrillation patients.[162]

1.3.4.4 MiR-21 and TGF-β

As discussed previously, the TGF-β pathway is considered a major mediator in the development of fibrosis. Several studies have shown that miR-21 expression can be induced by TGF-β signalling, affecting various steps throughout the maturation process. This suggests considerable overlap between effects of miR-21 and TGF-β signalling. The main downstream mediators of TGF-β receptor activation, such as the Smad proteins, were

shown to induce transcription of pri-mir-21[163], the subsequent processing of pri-mir-21 to pre-mir-21 by Drosha[164] as well as Dicer-mediated cleavage of pre-mir-21 into mature miR-21.[129] In a murine MI model, both miR-21 and TGF-β1 were induced, whilst subsequent *in vitro* experiments in murine CFs identified TGF-β receptor III (TβRIII) as a direct target of miR-21.[121] As opposed to TGF-β receptor I and II, which together mediate TGF-β signal transduction, TGF-β receptor III acts as a reservoir for TGF-β receptor I/II ligands. Upregulation of this receptor appeared to prevent myocardial fibrosis from occurring in hypertensive rats.[165]

In the context of atrial fibrillation, Tao *et al* identified WW domain-containing protein 1 (WWP1) as a miR-21 target in CFs, causing decreased TβRI degradation and enhanced phosphorylation of Smad2.[122] Lorenzen *et al* reported that osteopontin, a downstream mediator of TGF-β signalling previously implicated in myofibroblast differentiation and cardiac fibrosis[166,167], contributed to miR-21 transcription in CF through inducing activator protein-1.[123] Inducing osteopontin through an adeno-associated virus serotype 9 (AAV9) vector aggravated angiotensin II-mediated fibrosis, whilst systemic miR-21 inhibition attenuated the adverse remodelling. Several other studies showed that TGF-β signalling could increase miR-21 levels.[132,168–171] Importantly however, there is little attention for cell specificity of observed effects across the *in vivo* analyses in these studies. For example, AAV9-mediated delivery implies cardiomyocyte-tropism rather than delivery to CF, whilst systemic miR-21 inhibition may also affect other cells within or beyond the heart. Nevertheless, miR-21 and TGF-β signalling seem to be tightly interwoven, with miR-21 levels in part depending on TGF-β activity whilst itself targeting inhibitors of the TGF-β signalling cascade. This suggests that miR-21 may be part of a feed-forward loop of the TGF-β pathway.

Conversely, miR-21 has also been shown to inhibit TGF-β signalling. One study found miR-21 to inhibit TGF-β1 expression and secretion in bone marrow stem cells.[120] Mechanistically, this effect was explained by miR-21-mediated targeting of PTEN which enhanced Akt and nuclear factor kappa-light-chain-enhancer of activated B cells (NF-κB) activity. Furthermore, miR-21 *null* stem

cells showed enhanced TGF-β1 secretion, which provided beneficial immunomodulatory effects when delivered to mice suffering from experimentally induced colitis. In a context of diabetic kidney disease, Lai *et al* found that miR-21 inhibited TGF-β signalling, with miR-21 inhibition aggravating TGF-β-induced glomerulosclerosis and podocyte apoptosis.[172] These studies seemingly oppose the previously mentioned observations that implied miR-21 to enhance TGF-β signalling. These observations highlight that the interaction between the two may be highly context- or cell-type dependent.

1.3.4.5 MiR-21 and systemic effects

Whilst the studies on miR-21, TGF-β and fibrosis focus on single cell types or organs, their results imply that an indirect or systemic effect of miR-21 and its inhibition may also be at play. A study by Toldo *et al* aimed to evaluate the role of miR-21 on the bridge between post-ischaemic remodelling and inflammation. Treatment with hydrogen sulphide and sodium sulphide, which have previously been reported to dampen inflammation after ischaemia, induced miR-21 in rat cardiomyocytes and in the entire myocardium. Sodium sulphide administration indeed dampened experimental inflammation and improved survival after MI in mice. This response was however not seen in miR-21 *null* mice, implicating miR-21 as a mediator of the observed anti-inflammatory effects. A study assessing miR-21 levels in obesity-induced cardiac hypertrophy using leptin receptor-deficient mice observed no effect on miR-21; nevertheless, systemic inhibition of miR-21 was able to decrease obesity and inflammation in white adipose tissue, highlighting the potential systemic and inflammatory effects of miR-21.[173]

Using a model relying on a systemic response, Gupta *et al* heterotopically transplanted allogenic or isogenic hearts in mice.[174] As allograft transplantation elicits a massive immune response, fibrosis develops very rapidly as part of the transplant rejection. Levels of miR-21 in these hearts significantly increased, an effect which was confirmed by elevated miR-21 levels in immune-rejected heart transplant specimens from humans. Interestingly, the authors observed that the increase in miR-21 levels was largely dependent on infiltrating $CD45^+$ cells. Influx of platelets was not evaluated. Although systemic

inhibition of miR-21 decreased fibrocyte and T-cell accumulation, but not infiltration of macrophages, the degree of fibrosis was significantly attenuated. In addition, transplanting a wild-type heart into a miR-21 *null* mouse resulted in significantly less fibrosis, indicating extra-cardiac miR-21 to be a major determinant of the pro-fibrotic effects. These findings are a key indication that systemic effects of miR-21 may be at play in the development of fibrosis.

Numerous studies have shown that in the heart, miR-21 is expressed not only in fibroblasts. Its presence in other cell types of the non-myocyte fraction of the cardiac cell population is highly relevant for the interpretation of previous and future studies, as well as for the application of miR-21 as a therapeutic

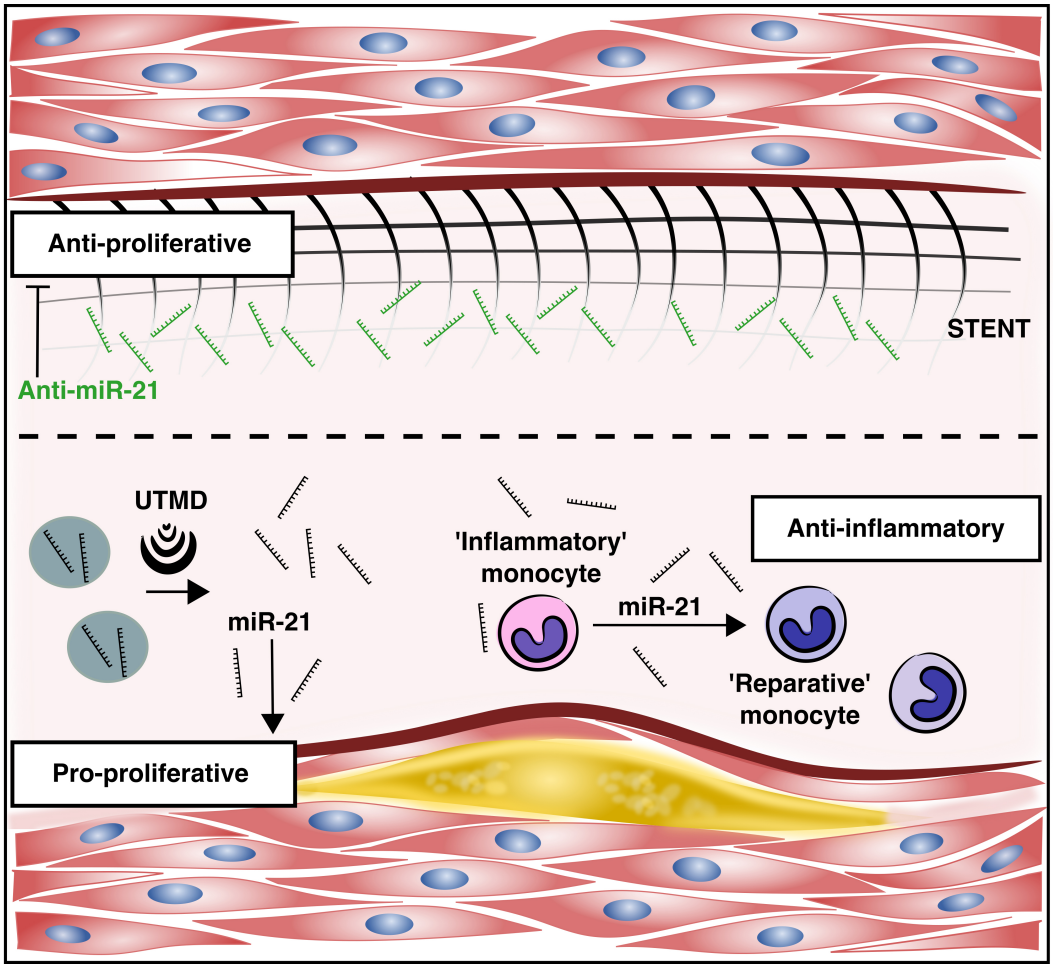

Figure 3. MicroRNA-21-based therapy for plaque vulnerability and in-stent restenosis. Delivery of miR-21 mimic to atherosclerotic plaques by ultrasound-targeted microbubble destruction (UTMD) enhanced smooth muscle cell proliferation, whilst also steering monocytes towards a reparative, anti-inflammatory phenotype. Conversely, stents coated with miR-21 inhibitor (anti-miR-21) prevented in-stent restenosis through their anti-proliferative effect on smooth muscle cells. This highlights the context dependency for the effects of miR-21. *(Courtesy of Dr. M. Rienks; see **Appendix 4**)*

target to treat fibrosis. In endothelial cells, miR-21 expression could be induced by TGF-β1 treatment, leading to endothelial-to-mesenchymal transition and thereby contributing to fibrosis formation.[170] This effect, observed during TAC-mediated cardiac pressure overload, could be inhibited by systemic administration of antagomiR-21. Brønnum *et al* reported that miR-21 was induced in epicardial cells after both TAC and MI, which subsequently induced epicardial-to-mesenchymal transition.[126]

In addition to its pro-fibrotic role, miR-21 enhanced neo-intimal growth through pro-proliferative and anti-apoptotic effects on vascular smooth muscle cells. Genetic, systemic and local inhibition of miR-21 reduced neo-intima formation and in-stent restenosis in different animal models.[175–178] However, whether the effects of miR-21 on smooth muscle cells are beneficial or detrimental is dependent on the context, as shown in **Figure 3**. We recently highlighted in an editorial commentary (see **Appendix 4**) two studies reporting miR-21 to enhance stability of atherosclerotic plaques.[179] One study focussed on the effects on macrophages, where miR-21 attenuated vascular inflammation and reduced plaque necrosis and instability.[180] The second study found a similar beneficial role for miR-21, yet with a greater emphasis on its effects in vascular smooth muscle cells.[181] Using a mouse model of atherosclerosis, local delivery of miR-21 mimic using ultrasound-targeted microbubble destruction enhanced plaque stability. As we highlighted in our commentary, it remains challenging to reliably attribute observed effects after manipulating miR-21 to a specific cell type for *in vivo* findings. Nevertheless, these studies support the suggested immunomodulatory function of miR-21 and its potential relation with cells in the circulation, whilst also adding to its potential as a therapeutic target.

1.3.5 MicroRNAs in cardiac fibrosis

In addition to miR-21, several other miRNAs have been implicated in fibrosis and CF biology. The most seminal findings will be highlighted in the following paragraphs and are summarised in **Table 2**.

Table 2. Key miRNAs implicated in cardiac fibrosis.

miRNA	Expression during fibrosis	Pro-/anti-fibrotic?	Effect *in vivo*
miR-15b	upregulated	anti-	- Systemic inhibition aggravated TAC-mediated fibrosis[182]
miR-21	upregulated	pro-	- Systemic pharmacological inhibition attenuated angiotensin II-[123], TAC-[118,124,127,131,170], cardiac allograft transplant-[174], and arryhtmia-induced[155,157,159] fibrosis; - Non-myocyte genetic inhibition attenuated TAC-induced fibrosis, yet myocyte inhibition aggravated TAC-induced fibrosis[131]; - Cardiac injection attenuated arrhythmia-induced fibrosis[160]; - Systemic pharmacological and genetic inhibition had no effect on TAC-, angiotensin II-, AMI-induced[110] or obesity-induced[173] fibrosis.
miR-24	downregulated	anti-	- Local lentiviral miR-24 delivery reduced fibrosis after MI.[183]
miR-29b	downregulated	anti-[184,185] or pro-[186,187]	- Systemic inhibition induced collagen expression[184]; - Systemic inhibition attenuated fibrosis.[187]
miR-101	downregulated (rodent)	anti-	- AAV9-mediated overexpression reduced fibrosis after MI in rats.[188]
miR-125b	upregulated	pro-	- Systemic inhibition attenuated angiotensin II-mediated fibrosis.[189]
miR-133	downregulated	anti-	- Transgenic miR-133 expression improved TAC-mediated fibrosis in mice.[190–192]

A study by Van Rooij *et al* found that expression of miR-29b was significantly reduced in hearts after MI, a change in opposite direction from that of miR-21.[184] Further experiments showed that miR-29b was mainly expressed in CF, where TGF-β signalling decreased its levels. *In silico* tools predicted several ECM proteins to be direct targets of miR-29b and collagen expression was indeed increased in hearts of mice after systemic miR-29b inhibition. A subsequent study from our group used a proteomic analysis of the CF secretome after miR-29 mimic and inhibitor transfections. This confirmed miR-29b to be anti-fibrotic by demonstrating a marked effect of miR-29b overexpression on ECM protein secretion by CF *in vitro*.[185] However, direct targeting of IGF1 and leukaemia inhibitory factor showed that miR-29b may

attenuate adverse remodelling not only through regulating ECM synthesis but also by modulating paracrine signalling of inflammatory mediators. The latter mechanism was illustrated by adding conditioned media from CF that had been transfected with miR-29b mimic to cardiomyocytes *in vitro*, which had an anti-hypertrophic effect. Whilst both these studies implicate miR-29b as an anti-fibrotic and anti-hypertrophic miRNA, other studies have shown opposite effects. A phenotypic screen to evaluate the effects of several miRNAs on cardiomyocytes showed miR-29b to induce hypertrophy.[186] More recently, Sassi *et al* showed that systemic inhibition of miR-29b attenuated cardiomyocyte hypertrophy and fibrosis using a TAC model in mice.[187] Interestingly, these observations were found to be the result of miR-29b on Wnt signalling in cardiomyocytes, putting these cells rather than CF at the centre of cardiac remodelling and suggesting miR-29b in cardiomyocytes to be pro-hypertrophic. These contradicting results for a single miRNA once more highlight the importance of the tissue and cell type context.

In addition to its role in cardiac hypertrophy, miR-133 is considered anti-fibrotic through targeting of connective tissue growth factor (CTGF), a key regulator of the fibrotic process downstream of the TGF-β signalling pathway [190], as well as collagen I α-1, a main constituent of the cardiac ECM.[191] miR-15b, which is upregulated in failing hearts in rats, mice and humans, was also shown to target multiple constituents of the TGF-β pathway. Its pharmacological inhibition showed an increase in hypertrophy and fibrosis.[182] Another miRNA interfering with this pathway, miR-101, was found to be downregulated in MI and treatment to increase its levels led to a reduction in fibrosis.[188] Using a similar MI model, lower miR-24 expression was found across the entire heart and intracardiac delivery of miR-24 using a lentiviral vector significantly reduced the infarct size. Mechanistically, direct targeting of furin was implicated as the mediator of this effect, in light of its function as a regulator of pro-TGF-β1 maturation.[183] More recently, miR-125b was shown to suppress several pathways involved in CF proliferation and activation, and its inhibition consequently ameliorated cardiac fibrosis.[189]

1.3.6 MicroRNAs and cardiomyocytes

Being the most prominent contributor to cardiac function, cardiomyocytes are key determinants of disease phenomena such as cardiac hypertrophy and reduced contractility. Furthermore, they constitute the majority of the myocardial cell volume. As mentioned in section **1.3.4.1**, intial studies considered myocardial miR-21 to be derived from these cells. More recent studies however indicate CF to be the major source, in particular in the context of injury. Nevertheless, several miRNAs have been implicated in cardiomyocyte biology and pathology, which will be discussed in the following paragraphs. Key myocardial miRNAs based on next-generation sequencing[193] are listed in **Table 3**, with their implication in cardiomyocyte biology and/or fibrosis highlighted. Interestingly, this indicates that miRNAs with reportedly pivotal roles in cardiac remodelling are not necessarily highly abundant within the non-failing myocardium.

In response to increased mechanical stretch caused by volume or pressure overload, several signal transduction pathways can be induced in cardiomyocytes, causing the cells to undergo significant transformation. This includes shifting towards expression of foetal gene programs.[194] In addition to changes in the ECM, for which CF are thought to be the main responsible cell type, impaired cardiomyocyte function forms the second hallmark of cardiomyopathy and heart failure.

In addition to its reported role in CF, miR-133 is highly abundant in cardiomyocytes. Its expression levels are reduced in animal models of hypertrophy[107] and in patients with hypertrophic cardiomyopathy or coronary artery disease-related heart failure.[195,196] *In vitro* and *in vivo* studies showed reactivation of foetal genes and increased hypertrophy upon miR-133 inhibition[195], whilst cardiac function was preserved upon miR-133 overexpression. Targeting of the beta-1 adrenergic receptor pathway, central to the progression and treatment of heart failure, was implicated as the underlying mechanism in the latter study.[197] A study inducing MI in rats after pre-treatment with the beta-1 adrenergic receptor blocker carvedilol, expected to preserve cardiac function, was associated with an increase in cardiac miR-133 levels.[198] MiR-133 is also expressed in skeletal muscle, albeit at lower

levels than in cardiomyocytes. Here, miR-133 inhibition again increased responsiveness to adrenergic stimuli and promoted differentiation to brown fat tissue.[199]

Table 3. Key miRNAs in the myocardium. Next-generation sequencing was performed using RNA from left ventricular myocardium biopsies from unused human donor hearts (n=4). MiRNA highlighted in the context of fibrosis (paragraph 1.3.5) and/or a role in cardiomyocytes (paragraph 1.3.6) are marked with a hash (#) and/or asterisk (*), respectively. Obtained from supplemental information of Leptidis *et al*.[193]

Rank	MicroRNA ID
1	miR-145
2	**miR-24 #**
3	miR-125a
4	miR-30d
5	**miR-1 ***
6	miR-23b
7	miR-1974
8	miR-99a
9	miR-30c
10	**miR-133 # ***
29	**miR-29b #**
31	**miR-125b #**
52	**miR-21 ***
108	**miR-15b #**
109	**miR-25 ***
165	**miR-208a ***
247	**miR-101 #**

MiR-1, part of a cluster together with miR-133 and highly abundant in the myocardium (see **Table 3**), showed a similar reduction in its expression levels in heart failure patients.[200] Both increased[201] and reduced[202] expression of miR-1 has been reported to cause electrophysiological abnormalities. Interestingly, miR-1 targets insulin-like growth factor-1 (IGF1), which itself represses processing of the pre-miR-1 transcript.[200] The IGF1 pathway is an important contributor to cardiac hypertrophy and arrhythmias, and increasing miR-1 levels seem to improve cardiac function.[203]

MiR-208 is also enriched in cardiomyocytes and regulates the balance between α- and β-MHC. Induction of the β-MHC isotype, the main isotype in the foetal heart, is a known maladaptive response to cardiac stress which

reduces contractility.[204] MiR-208 knockout mice, and rats treated systemically with anti-miR-208, had a preserved balance between both MHC isotypes in response to experimental cardiac stress, with better cardiac function.[205] These promising results suggested miR-208 inhibition could be a protective treatment in heart failure. However, β-MHC expression is not altered in normal hearts of miR-208 knockout mice, indicating that effects of this miRNA are either dependent on disease context or can be rescued by other miRNAs or other compensatory mechanisms.[206] Furthermore, deep sequencing data from human hearts suggest that miR-208 expression is relatively low compared with other cardiac miRNAs, such as miR-1 and miR-133 (see **Table 3**).[193,207] Pre-clinical trials using miR-208 inhibition in heart failure were announced in 2011, but have not progressed further.

In one study, miR-25 expression was repressed in failing human hearts[208], but its expression was increased in another study.[209] The former study described the targeting of deleterious embryonic gene programs that worsen cardiac function. The latter study however showed miR-25-mediated repression of sarcoplasmic/endoplasmic reticulum calcium adenosine triphosphatase, an important contributor to excitation–contraction coupling in cardiomyocytes. This subsequently improved cardiac function. Differences in timing and chemical properties of the anti-miR treatment, as well as the study duration, could explain these contradictory results.[210] This highlights the challenges for translational research, as different types of oligonucleotides targeting the same miRNA may not achieve the same therapeutic benefit.

1.4 Circulating microRNAs

A landmark study by Mitchell *et al* revealed that miRNAs are not just confined to the intracellular space of organ tissues, but are also present in the circulation.[211] Whilst circulating cells and platelets contain substantial amounts of miRNA, there is also a pool of miRNAs that exists in the blood plasma. The finding that miRNAs could be detected in cell-free serum and plasma was surprising, given the high levels of RNase activity in the blood. In contrast to mRNA, miRNAs remain relatively stable in the circulation through several protective mechanisms: association with RNA-binding proteins and lipoproteins, or housing in shed microvesicles, such as exosomes or microparticles.[212–214] These findings have opened another avenue for potential clinical application of miRNAs, where their circulating levels have potential to be used as biomarkers in cardiovascular disease and beyond. The relevance

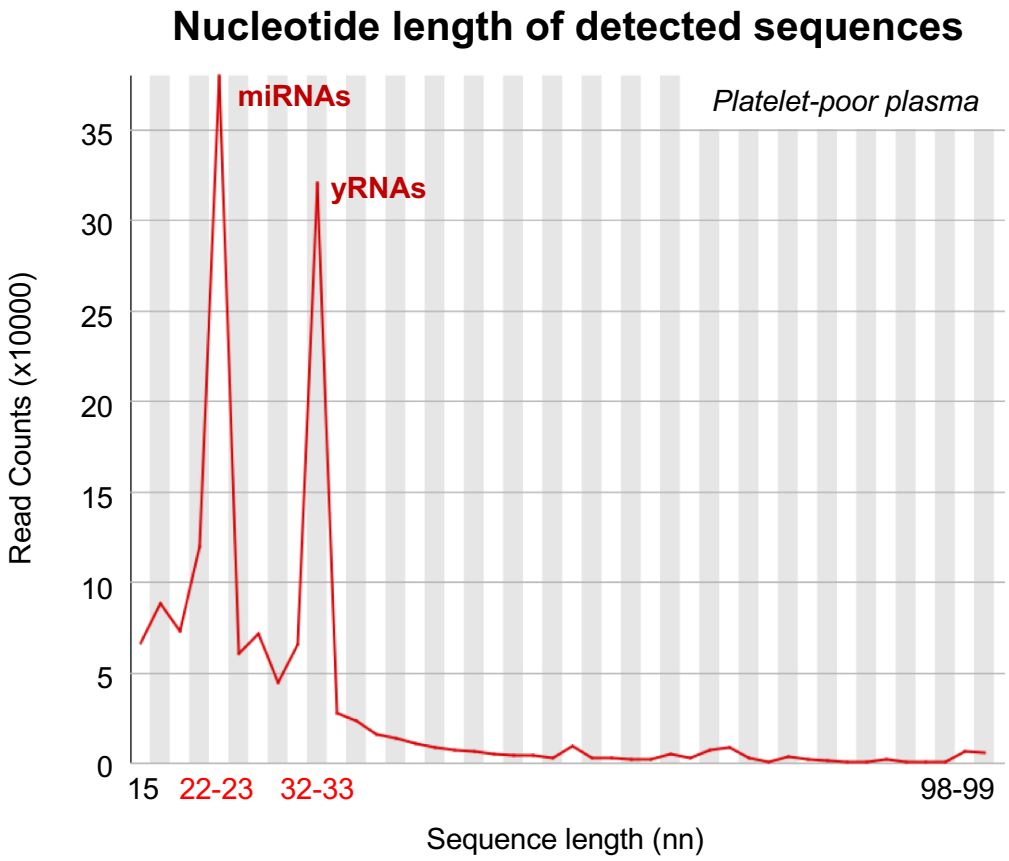

Figure 4. Next-generation sequencing of small RNAs in platelet-poor plasma. Representative histogram of sequence lengths for small RNAs identified in platelet-poor plasma. The two peaks correspond to miRNAs at 22-23 nucleotides (nn) in length, and yRNAs at 32-33 nn. (*Adapted from Sunderland et al, Circ Res 2017, see* ***Appendix 3***)

of extracellular miRNAs might however not be limited to their use as biomarkers, with several studies suggesting that miRNAs secreted from cells can act as mediators of paracrine or endocrine signalling.[96,215]

There are many more miRNAs encoded in the human genome than there are detectable in the circulation.[216] We previously detected >200 miRNAs using next-generation sequencing (NGS) in platelet-poor and platelet-rich plasma samples (see **Figure 4**).[217] Detectable miRNAs greatly vary in abundance. Not all miRNAs that are present in the circulation can be consistently detected with quantification cycle (Cq) values of <32 by qPCR, even after pre-amplification.

The subset of miRNAs that are detected in the circulation have been released from different organs as well as circulating cells. Importantly, this explains the profound pre-analytical effects of sample preparation on miRNA analysis in plasma and serum. This is true in particular for miRNAs that are present in blood cells, as activation or rupture of these cells and incomplete depletion during centrifugation masks measurements of genuine extracellular miRNAs.[96] Circulating miRNAs may be derived from several cell types, including bone marrow-derived cells and different organs. Interestingly however, our group has demonstrated that a sizeable subset of miRNAs that are detectable in the circulation show marked correlation, suggesting a shared cellular origin.[218] Further analysis of this subset has shown that their levels are affected by administration of antiplatelet drugs prior to blood sampling, implicating platelets as a major source of circulating miRNAs.[219]

1.4.1 Platelets and microRNAs

1.4.1.1 The profile of microRNAs in platelets

Due to their anucleate nature, platelets are incapable of transcribing new RNA. However, platelets do contain RNA, as well as the spliceosome machinery[220] and ribosomes.[221] Platelets are also believed to be capable of translating RNA into protein.[222] Furthermore, miRNAs are abundant in platelets, and platelets carry the required machinery for miRNA-induced silencing.[223,224] Over seven hundred different miRNAs have been identified in

platelets[225], with miRNA expression profiles in healthy individuals showing remarkable stability when repeatedly measured over a course of ten days.[226] However, miRNA expression ranks across different profiling studies greatly vary (see **Figure 5**).[96] This is likely not only due to inter-individual differences, but also because of differences in sample preparation and analysis.

The profile of platelet miRNAs was found to be altered in different disease states. RNAseq profiling and qPCR analysis of platelet miRNAs in patients suffering an acute MI identified several miRNAs to be present at lower levels.[227] *In vitro* analysis ascribed these changes to increased miRNA release from these platelets, as a result of a greater level of platelet activation. In another study, platelets from patients and mice with diabetes mellitus had lower levels of several miRNAs, which was found to be the result of hyperglycaemia on calpain-mediated cleavage of Dicer.[228]

There are several potential explanations for variation in the platelet miRNA profile. As platelets are anucleate, changes cannot be the result of transcriptional regulation in the platelet itself. Therefore, platelets are thought to inherit their miRNA content during the maturation and shedding process from megakaryocytes.[229] Consequently, the platelet miRNA profile may provide insights into megakaryocyte function in the bone marrow. There are however additional potential explanations for changes in miRNA levels: disease states that may affect miRNA precursor processing[228], differential shedding of microparticles from the platelets[227,230] and post-transcriptional modifications such as adenylation and uridylation.[224] Furthermore, it has been shown that platelets are able to take up mRNA from vascular cells, which may also be the case for miRNAs.[231]

In light of these observations, there is the opportunity to use platelet miRNAs as biomarkers as well as therapeutic targets. Our group has previously identified a loss of several miRNAs in the plasma of type 2 diabetes mellitus patients[232] and in response to antiplatelet therapy.[219] In addition, we found that a combination of plasma levels of three platelet-enriched miRNAs could predict future cardiovascular events[233], which was corroborated in a later

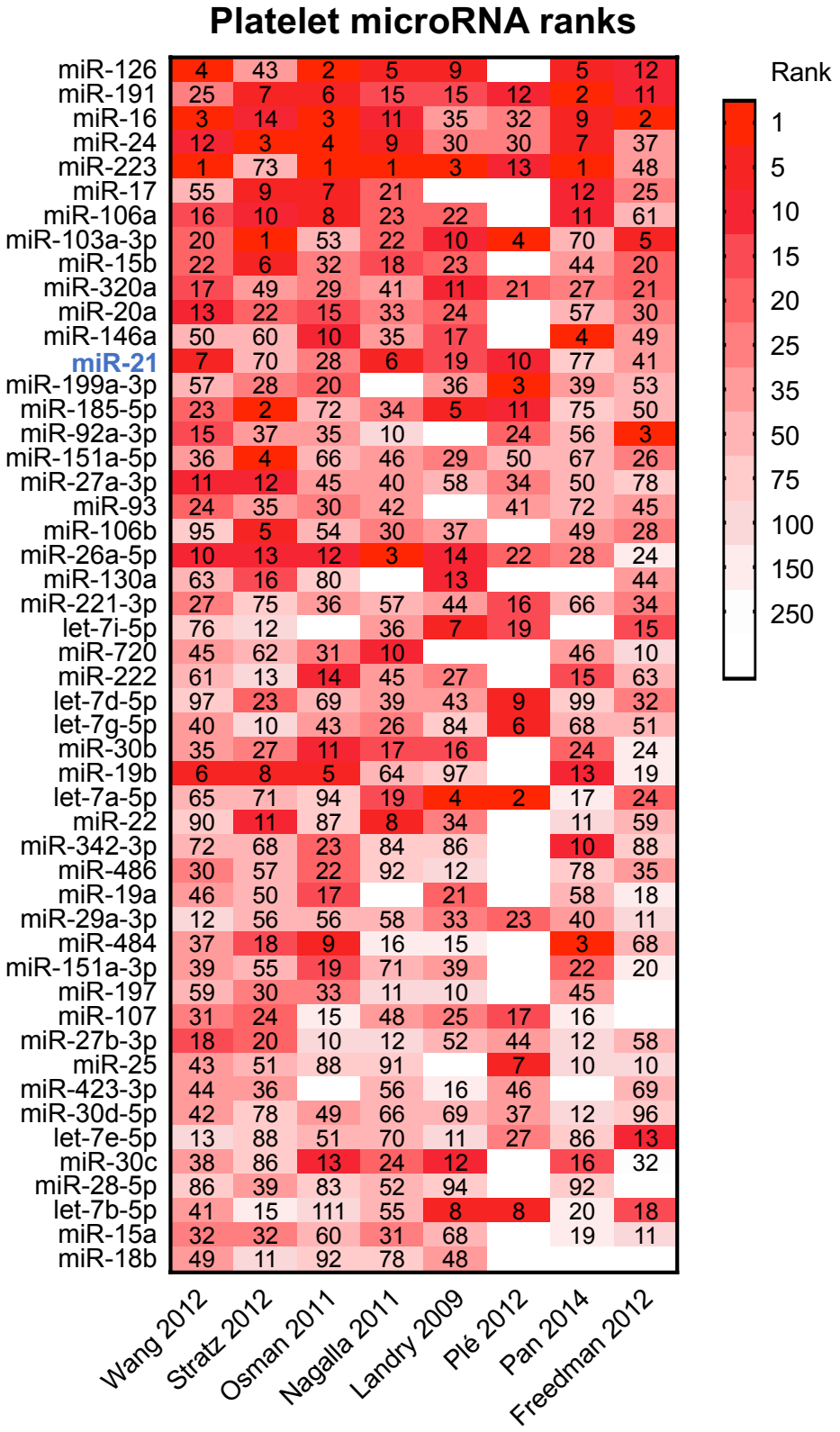

Figure 5. Platelet microRNA ranks across published studies. Relative abundance of miRNAs in platelets was reported in eight studies (indicated by first author and year of publication). The fifty highest ranking miRNAs on average are presented here, indicating marked variation between different studies for the miRNAs beyond the top ten. MiR-21 is ranked as the thirteenth most abundant miRNA in platelets. (*Adapted from Sunderland et al, Circ Res 2017; see* ***Appendix 3***)

study.[234] Plasma levels of platelet-enriched miR-126 were found to predict major adverse cardiac events in patients on dual antiplatelet therapy[235], a result particularly interesting in the context of our finding that plasma miR-126 significantly correlated with platelet activation markers.[217]

1.4.1.2 Platelet function and microRNAs

Platelet miRNAs might also reflect altered platelet function. Kondkar *et al.* isolated platelets from healthy volunteers and compared those from participants with relatively hyperreactive platelets to those with low reactivity. Transcriptomic analysis identified overexpression of vesicle-associated membrane protein 8 (*VAMP8*)/endobrevin in hyperreactive platelets, coding for a protein involved in α-granule secretion. MiR-96, harbouring a seed sequence predicted to target the 3' UTR of *VAMP8,* was found at lower levels in hyperreactive platelets, implicating it as a regulator of *VAMP8* translation.[236] In another study, racial disparity in survival of coronary heart disease was evaluated in the context of platelet function. Higher levels of phosphatidylcholine transfer protein-encoding mRNA were found in hyperreactive platelets. Subsequent miRNA profiling identified miR-376c as a regulator of this gene transcript.[237]

To date, only three studies have evaluated the effects of inhibiting a specific miRNA on platelet function. Using miR-223 *null* mice, one study failed to observe any differences in platelet count or their activity despite this miRNA being among the most abundant in platelets (see **Figure 5**).[238] A subsequent study however did observe modestly higher platelet activation in miR-223 *null* mice at low concentrations of agonists, resulting in increased thrombosis and embolisation after vascular injury. Proteomic analysis of platelets from these mice identified differences in protein abundance for coagulation factor XIII-A and kindlin-3, with the gene encoding the former being identified as a direct target of miR-223.[228] Our group in a recent study found miR-126 to strongly correlate with markers of platelet activation in the community-based Bruneck cohort. Using systemic pharmacological inhibition of miR-126 in mice, platelet aggregation in response to a thromboxane A_2 receptor agonist was significantly reduced. ADAM metallopeptidase domain 9 was identified as a direct target of miR-126.[217]

1.4.1.3 MiR-21 and platelets

A combined rank table of miRNA abundance in platelets based on eight different miRNA profiling studies (see **Figure 5**) includes miR-21 among the fifteen most abundant miRNAs in human platelets. In parallel with several platelet-enriched miRNAs, miR-21 was detected at significantly lower levels in the plasma of diabetic patients and in leptin-deficient hyperglycaemic mice.[232] Using a limb ischaemia-reperfusion injury model in healthy volunteers, plasma miR-21 was identified as part of a cluster with platelet-enriched miR-126, -223, -197 and -24. Interestingly, it was identified as the most significantly increasing miRNA over seven days after reperfusion.[233] Treating healthy volunteers with antiplatelet drugs prasugrel and acetylsalicylic acid over a period of three weeks significantly reduced plasma miR-21 levels.[219] In the previously mentioned study comparing platelet reactivity in the context of ethnicity, miR-21 was one of the miRNAs that was expressed significantly higher in blacks, which was associated with higher platelet reactivity.[237] In a recent study, we showed that a comparison between platelet-poor plasma (PPP) and platelet-rich plasma (PRP) using RNAseq identified markedly higher read counts of miR-21 in the latter. Furthermore, a platelet spike-in experiment, where we added increasing amounts of platelets to platelet-poor plasma, identified miR-21 levels to significantly increase. Analysis of plasma from the community-based Bruneck study showed significant correlation between miR-21 and platelet activity markers platelet factor 4 (PF4) and PPBP.[217]

Taken together, these studies provide strong evidence for miR-21 as a key platelet miRNA. To date however, no studies have evaluated the effects of miR-21 inhibition on platelet function.

1.4.2 Circulating microRNAs as biomarkers

The finding that miRNAs are stable in the circulation and in other body fluids has attracted much interest in their potential use as biomarkers.[211] Biomarkers are defined by the National Institutes of Health Biomarkers Definitions Working Group as "*a characteristic that is objectively measured and evaluated as an indicator of normal biological processes, pathogenic processes, or pharmacologic responses to a therapeutic intervention*".[239] MiRNAs harbour several features that make them well-suited for this purpose:

they can be measured noninvasively using commonly used techniques with high sensitivity and at relatively low cost. Furthermore, miRNAs display time-related changes during disease progression and are thought to have a long half-life.[83] On the other hand, however, there are several limitations that may explain why to date, miRNA biomarkers have not found their way to clinical application. Current quantification techniques require RNA isolation, followed by reverse-transcription (RT) and qPCR analysis, which is time-consuming and challenging to automate. Furthermore, these techniques generally rely on relative quantification, therefore complicating the identification of reference points for dysregulated levels. MiRNA quantification is therefore not well-suited for clinical use in an acute or sub-acute setting. In addition, as we will further argue in the discussion, pre-analytical factors can greatly interfere with levels of many miRNAs given their relative abundance in circulating cells compared to the freely circulating pool.[96]

In the cardiovascular field, several miRNAs have been suggested as potential biomarkers. Cardiac miRNAs are detectable in the circulation at high levels early after MI, which could be used to reduce time to diagnosis.[240] Evaluation of miRNA levels thus far did not show a benefit over the currently used high-sensitivity troponins.[241] Several studies have attempted to improve risk prediction models for MI using circulating miRNA levels. Karakas *et al* found a surprisingly strong correlation of single miRNAs with the risk of cardiovascular death, although this was in a highly selected population, and was not compared with traditional risk models.[242] In contrast, the combination of a miRNA panel with traditional Framingham risk models may benefit the predictive power for future acute MI, as was shown in two studies.[233,243] The miRNA panel in the study from our group[233] included miR-126 and miR-223, showing positive and negative association with incident MI, respectively. Mechanistic links between these two miRNAs and platelet function were described earlier in this chapter. In the context of heart failure, higher levels of miR-29a correlated with both hypertrophy and fibrosis as features of hypertrophic cardiomyopathy[244], but it is unclear whether this provides any clinical benefit over current diagnostic tools.

miR-21 was shown to be differentially expressed after MI, showing lower levels in the acute phase but increasing after a week.[245] This rise in miR-21 was later shown to be a predictor of poor neurological outcome.[246] These findings are in line with studies comparing patients with stable and unstable coronary artery disease, where serum and plasma miR-21 levels were higher in the latter. Furthermore, miR-21 levels correlated with markers of inflammation[247] and myocardial damage.[248] The relation of circulating miR-21 levels with cardiac damage was further evidenced by measuring serum levels after ablation of septal hypertrophy, which markedly increased its levels.[249] The increase persisted in a study with a follow-up of one year after a percutaneous coronary intervention.[250] Whether these findings reflect release of miR-21 from the myocardium, from bone marrow-derived cells, or a combination, was not investigated in these studies.

Looking at a patient group with more chronic clinical features, Villar *et al* showed that aortic stenosis patients had higher levels of miR-21 in the heart and plasma.[137] Levels correlated with collagen abundance in the heart, implying it as a potential marker of cardiac remodelling and fibrosis. A study in hypertrophic cardiomyopathy patients confirmed this increase in miR-21 levels, whilst also presenting it as part of a panel of eight miRNAs that were able to distinguish patients with diffuse fibrosis from those without signs of fibrosis based on plasma levels.[251] In a more recent study, plasma miR-21 was found to increase in the compensated stage of diastolic dysfunction, but decrease in the later stages of heart failure.[132] Altogether, these studies show that miR-21 is readily measured in the circulation and that its levels are affected in different disease states. None of these studies however determine the source of miR-21. Most studies infer that the observed changes in circulating miR-21 are reflecting changes in the miRNA content of the myocardium. However, circulating miR-21 changes could also be due to effects on other cellular sources such as leukocytes, the endothelium and platelets.

1.5 MicroRNAs: therapeutic manipulation

Several features of miRNAs have drawn the attention to evaluating their potential use as therapeutic targets. Whilst most traditional drugs rely on interfering with a single protein or receptor, miRNAs have been found to regulate the synthesis of several proteins that are biologically linked.[252] This is elegantly illustrated by miR-29b, described earlier in this chapter, simultaneously targeting an array of ECM protein-coding gene transcripts.

Furthermore, modified oligonucleotides were shown to potently reduce miRNA levels when administered locally or systemically.[108] These anti-miRs consist of synthetic single strands of modified nucleotides that are complementary to the endogenous miRNA. Various structural modifications have been designed to bypass degradation in tissues and to enhance intracellular delivery.[252] Importantly, despite being designed for the same purpose, the chemical properties of these different anti-miR agents may have a marked effect on its efficacy and side-effects. As will be pointed out in the discussion, contrasting outcomes between similar studies have been attributed to the differences in anti-miR designs.[253] A commonly used anti-miR design involving phosphorothioate backbone modifications was found to induce platelet aggregation due to interaction with the collagen receptor on the platelet surface.[254] In addition to miRNA inhibition strategies, cardiotropic adeno-associated viruses (AAV) achieve efficient cardiomyocyte-specific miRNA delivery.[131,255,256] As miRNA-based therapies approach clinical evaluation, there is increasing concern with regards to off-target effects, especially in light of the ubiquitous expression of most miRNAs. Hence, several methods have been proposed and evaluated to target miRNA mimics or inhibitors to a cell type or organ of interest.[257] Local delivery of a miR-21 inhibitor and mimic have been used by means of a coated stent or ultrasound-targeted microbubble destruction, respectively (see **Figure 3**).[177,179,181] Other techniques involve encapsulating molecules within nanoparticles or binding to polymers.[257] A more recently reported strategy used the binding of photolabile groups to an antimiR, rendering the agent inactive until its exposure to light at a specific wavelength.[258] Whilst these techniques all remain to be evaluated in a clinial

setting, the growing interest in their use implies a shift towards local therapeutic approaches rather than systemic miRNA inhibition. Currently, overexpressing a miRNA is generally considered less safe than inhibiting an endogenous miRNA.

Several miRNA-based therapies are under clinical evaluation. The most advanced anti-miR at present is “Miravirsen”, targeting miR-122 for treatment of hepatitis C.[108] A multicentre phase 2a trial[259] for this anti-miR has been completed and this drug is currently being evaluated in a phase 2b trial. The selection of miR-122 as the first to be clinically evaluated highlights the two main challenges that exist for miRNA-based therapy, in particular for CVD. Firstly, miR-122 shows exquisite tissue specificity, whilst most other miRNAs are ubiquitously expressed. Second, anti-miRs are predominantly taken up by the liver and kidneys when administered systemically. Consequently, tissue specificity of miR-122 inhibition can be achieved without requiring any additional steps to steer the agent towards the intended site of action.[259] Targeting the heart or vasculature with systemic anti-miRs would require significantly higher dosing and efficiency may be low.

Animal models have shown significant nephrotoxicity at higher doses of some anti-miRs, although the clinical trial of Miravirsen did not find significant renal injury in humans.[259] The human immune system has evolved to detect viral RNA. Toll-like receptors recognize both single- and double-stranded RNA.[260] High doses of synthetic oligonucleotides may elicit an immune response that could compromise efficacy and safety. Thus, cardiovascular applications will require solutions for local or cell type-specific delivery and clinically detectable, reliable read-outs to monitor successful target engagement.

1.5.1 MiR-21 as a therapeutic target

Anti-miR-21 therapy is currently being evaluated for the treatment of Alport syndrome, characterised by renal fibrosis.[261] Whilst miR-21 is ubiquitously expressed and thus lacks the tissue specificity of miR-122, targeting the kidney requires only low doses of systemically delivered anti-miR, similar to the liver.

Alport syndrome is an inherited disorder characterised by glomerulonephritis, associated with haematuria and proteinuria, that during young adulthood progresses into glomerular and tubulointerstitial fibrosis. This rapidly causes renal failure. Other characteristics of this syndrome are hearing loss and lens deformities in the eye.[262] Underlying these clinical features are mutations in the genes coding for three collagen type IV subunits that normally comprise a heterotrimer. This rare disorder almost inadvertently leads to renal failure that is only resolved by renal replacement therapy and transplantation of a donor kidney. In recent years, early start with angiotensin-converting enzyme inhibitors was found to delay progression towards renal failure, improving life expectancy of Alport syndrome patients.[263] Whilst benefits of this therapy can in part be explained by its antihypertensive effects, mouse studies have suggested that angiotensin-converting enzyme inhibitors prevent renal fibrosis irrespective of the antihypertensive effect, by reducing myofibroblast activation and TGF-β signalling.[264]

Evaluating Col4a3 *null* mice, a commonly used mouse model of Alport syndrome, miR-21 was found to be upregulated in the kidney at a young age.[261] This preceded the development of inflammation or renal dysfunction. Mice developed kidney failure by nine weeks, whilst biweekly systemic treatment with anti-miR-21 preserved renal function and extended the survival time. Histological evaluation revealed markedly reduced glomerulosclerosis compared to vehicle-treated mice, as well as a reduction in the number of macrophages and αSMA-expressing myofibroblasts. Transcriptomic analysis of renal RNA from Col4a3 *null* mice and wild-type littermate controls identified upregulation of several ECM genes and markers of fibroblast activation. Furthermore, this analysis implicated peroxisome proliferator-activated receptor alpha as a direct target that was de-repressed by anti-miR-21 treatment. This was shown to reduce mitochondrial ROS production as well as downstream effects of TGF-β signalling. Analysis of miR-21 *null* renal fibroblasts showed an increase in mitochondrial content and reduced ROS production, which persisted after TGF-β treatment.

First results from the evaluation of systemic anti-miR-21 treatment in Alport syndrome patients (ClinicalTrials.gov Identifier: NCT02855268) are expected this year. Whilst the aforementioned animal study implies a direct effect on renal fibroblasts, a systemic effect cannot be ruled out as a contributor to the observed effects. Furthermore, as these are the first results of miR-21 inhibition in humans, the outcome of this study will provide general insight into potential clinical use of anti-miR-21 agents in general.

CHAPTER II

AIMS & PROJECT DESIGN

There is an unmet clinical need for targeted therapeutic options against fibrosis. MiR-21 is widely described to be an important mediator of fibrosis in the heart and other organs. Pharmacological inhibition of miR-21 is currently undergoing clinical evaluation for renal fibrosis. Effects of miR-21 have mainly been seen after tissue injury and animal studies using miR-21 inhibition in the context of cardiac hypertrophy have been ambiguous. There is clear evidence for the involvement of circulating cells in tissue remodelling. MiR-21 is highly expressed in circulating cells, including monocytes and platelets. Thus, potential benefits of miR-21 inhibition may in part occur via indirect effects beyond the targeted organ.

In the current project, we aimed to gain more understanding of how miR-21 affects cardiac fibrosis. The following analyses were therefore performed:

1. To analyse the direct effects of miR-21 in CF with a comprehensive and unbiased approach, we used a proteomic analysis of the CF secretome after transfection of miR-21 mimics and inhibitors. Furthermore, transfected cells were analysed for differences in gene expression and their proliferation rate. Hearts from miR-21 *null* mice were analysed to determine changes in ECM gene expression and protein levels.

2. In a community-based cohort, we screened for associations of miR-21 with other mediators and cell types that may affect fibrosis. Using plasma samples, correlations were assessed between miR-21 and a panel of proteins previously associated with CVD and inflammation. This screening drew our attention to blood platelets as a major source of miR-21 and pro-fibrotic mediators such as TGF-β1. Using an *in vivo* model of thrombocytopaenia and a human megakaryoblastic cell line, we aimed to assert the contribution of blood platelets to circulating pro-fibrotic mediators and miR-21.

3. Next, we assessed effects of pharmacological miR-21 inhibition on platelet count, aggregation response and their releasate. These experiments identified a link between miR-21 and platelet TGF-β1, as

well as a novel direct miR-21 target that could explain these observations. In addition, analysis of blood and bone marrow from miR-21 *null* mice identified marked changes in leukocyte, platelet and megakaryocyte counts.

CHAPTER III

METHODS

3.1 Isolation of murine cardiac fibroblasts

Primary mouse CF were isolated from the hearts of male 8-10 week old C57BL/6 mice (Charles River) by collagenase II-based digestion as described previously.[185] Housing and animal care was in accordance with the UK Animals (Scientific Procedures) Act 1986. Cells from individual animals were maintained as separate cell lines. Mice were anaesthetised using an intraperitoneal injection of pentobarbital, followed by excision of the heart, which was then transferred to 'complete medium', comprised of Dulbecco's Modified Eagle's Medium (DMEM; Gibco, cat. no. 10938025) supplemented with L-Glutamine (Gibco, cat. no. 25030024), 1% penicillin/streptomycin (100 U/ml penicillin and 100 µg/ml streptomycin, Gibco, cat. no. 15140130) and 10% heat-inactivated Foetal Bovine Serum (FBS; Gibco, cat. no. 10270106). Atria and blood vessels were removed and the ventricular tissue was washed and cut into 1 mm^3 pieces, followed by pre-digestion in medium supplemented with 1% penicillin/streptomycin and 308.5 mg/L collagenase II (Worthington, cat. no. CLS-2) in a shaker-incubator for ten minutes at 37°C. The pre-digestion volume was then replaced with fresh digestion solution and incubated for 1 hour. Digested samples were then washed, resuspended and plated in complete medium and cultured on gelatine-coated 6-well plates. Culturing was performed in a humidified atmosphere of 95% air and 5% CO_2 at 37°C. 0.05% trypsin-ethylenediaminetetraacetic acid (EDTA) (Gibco, cat. no. 25300054) was used to detach cells for passaging. As previously shown by vimentin staining[185], the cell population after two passages predominantly consists of CFs. Cells at the third passage were used for transfections. Prior to transfection, cell viability was assessed by trypan blue (Sigma, cat. no. 93595; 0.22µm filtered) staining and subsequent counting using a Neubauer chamber under bright-field microscopy. A proportion of trypan blue-negative cells >90% was confirmed prior to plating for transfection.

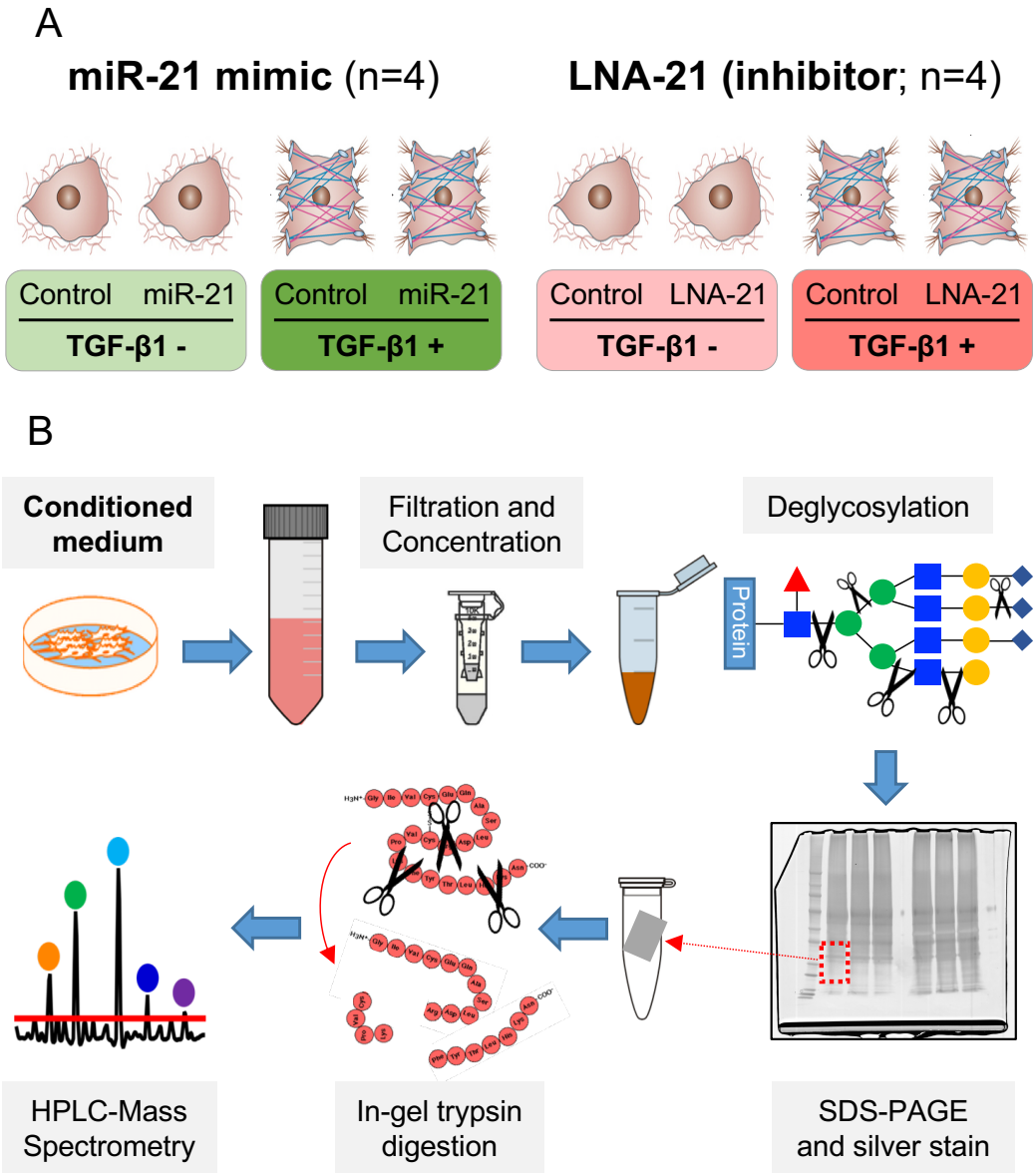

Figure 6. Workflow for the analysis of fibroblast conditioned media. A: Murine CFs were isolated from wild-type mice. Cells were transfected with miR-21 mimic or LNA-21 (inhibitor) and their respective controls. After 24 hours, cells were stimulated with TGF-β1 or control treatment to induce a myofibroblast-like phenotype. **B:** 48 hours after transfection and subsequent TGF-β1 treatment, conditioned media were collected. After removing cell debris by centrifugation, samples were filtered and concentrated using 3 kDa cut-off filter columns, removing contaminants such as amino acids and salts. As secreted proteins and ECM proteins in particular are heavily glycosylated, a sequential incubation with deglycosylating enzymes was performed. Samples were then reduced and denatured, followed by separation by sodium dodecyl sulphate polyacrylamide gel electrophoresis (SDS-PAGE). Proteins in the gel were visualised by silver staining to support subsequent gel cutting. Proteins inside the gel pieces were digested into peptides using trypsin. These peptides were then injected into a high-performance liquid chromatography (HPLC)-coupled mass spectrometer for identification and quantification of peptides.

3.2 MicroRNA transfection

A schematic representation of transfections is shown in **Figure 6, panel A**. Cells ($5x10^5$ cells/well) were plated at 60-70% confluency in a six-well plate coated with gelatine, with equal volumes of a cell suspension added to each well to obtain an equal number of cells per well. Attachment of cells was confirmed by microscopy prior to transfection. The following mimics (miRIDIAN microRNA mimic, Dharmacon, GE Healthcare) were used:
miR-21 (cat. no. C-300492-03-05): 5'-UAGCUUAUCAGACUGAUGUUGA-3'
Negative Control #1 (cat. no. CN-001000-01-05): sequence not specified

For miR-21 inhibition, Locked Nucleic Acid (LNA)-modified sequences were synthesised by Exiqon:
LNA-21 (cat.no. 339121, ID: YI04100689):
5'-CAACATCAGTCTGATAAGCT-3';
LNA-control (cat.no. 339126, ID: YI00199006):
5'-TAACACGTCTATACGCCCA-3'.

Transfections were carried out using Lipofectamine RNAiMAX (Life Technologies, cat. no. 13778075) in reduced serum medium (Opti-MEM; Gibco, cat. no. 31985070), according to manufacturer's instructions, at a final concentration of 50 nM for all four sequences. Efficiency of transfection was tested using a fluorescently labelled miRNA (miRIDIAN microRNA Mimic Transfection Control with Dy547, Dharmacon, GE Healthcare, cat. no. CP-004500-01-05) that was transfected in duplicate. 4',6-diamidino-2-phenylindole (DAPI; Sigma, cat. no. D9542) staining, based on binding to double-stranded DNA, was used to visualise the cell nuclei. Fluorescence microscopy was used after twenty-four hours, using a wavelength of 461 nm (blue) for DAPI and 570 nm (red) for the transfected mimic.

After 24 hours of incubation, cells were resuspended in serum-free medium after two washes. Cells were then stimulated with recombinant TGF-β1 (Peprotech, cat. no. 100-21) at a concentration of 10 ng/ml. After 48 hours, conditioned medium was collected from each well and cleaned from cell debris by centrifugation at 3000 x *g* for 10 minutes. The supernatant medium (approximately 1900 µl) was stored at -80°C until further processing. The CF

were washed in phosphate-buffered saline (PBS; Sigma, cat. no. D8537), followed by lysis in QIAzol lysis reagent (Qiagen, cat. no. 79306).

3.3 Conditioned media and cell processing for analysis

The processing of conditioned media for mass spectrometry analysis is schematically shown in **Figure 6, panel B**. Collected supernatant medium was desalted using Zeba Spin desalting columns (Thermo Scientific, cat. no. 89889), concentrated using concentration columns (Millipore, Amicon Ultra 0.5 ml 3 kDa, cat. no. UFC500324), precipitated with 100% ethanol (VWR, cat. no. 437433TDP), vacuum dried and then resuspended in 60 µL of deglycosylation buffer (50 mM sodium acetate, 50 mM Tris, pH 6.8, 25 mM EDTA), containing the following glycoprotein deglycosylation enzymes (Merck, cat. no. 362280): N-glycosidase F (1:200), β-1,4 galactosidase (1:200), β-N-acetylglucosaminidase (1:200), endo-α-N-acetylgalactosaminidase (1:200), recombinant α-2-3,6,8,9-neuraminidase (1:200), chondroitinase (1:100), heparanase (1:500) and endo-β-galactosidase (keratinase; 1:500). Samples were deglycosylated by incubation at 25°C for 2 hours, followed by 37°C for 48 hours in agitation. The deglycosylated samples were then used for sodium dodecyl sulphate (SDS)-polyacrylamide gel electrophoresis, followed by mass spectrometry (MS) or immunoblotting.

3.4 Gel electrophoresis and silver staining

Concentrated conditioned media samples were denatured, reduced and prepared for gel electrophoresis by adding sample loading buffer (100 mM Tris, 0.1% of 1 M SDS, 10% glycerol, 0.25% β-mercaptoethanol and 0.02% bromophenol blue). After incubation at 96°C for 5 minutes, gel-based separation was performed using Bis-Tris discontinuous 4-12% gradient polyacrylamide gels (NuPage, Invitrogen, cat. no. NP0315) in 3-(N-morpholino)propanesulfonic acid-SDS running buffer (MOPS-SDS, NuPage, Invitrogen, cat. no. NP0001-02), using a voltage of 120 mV. Protein profiles of the gels were visualised by silver staining. All steps were performed with gentle shaking. Gels were incubated in fixing solution (50% methanol, 5% acetic acid) for 30 minutes, followed by three brief washes in H_2O and an overnight rehydration step in H_2O at 4°C. Next, gels were incubated for 1 minute in

sensitising solution (0.8M sodium thiosulphate in H_2O), followed by three 1-minute washes in H_2O and silver staining for 30 minutes in 6 mM silver nitrate. After three brief washes in H_2O, developing solution (180 mM sodium carbonate, 0.04% formaldehyde) was added and the gels were gently shaken until proteins were sufficiently visualised. After three short washes in H_2O, stopping solution was added (5% acetic acid) for 10 minutes. Next, gels were washed three times for 5 minutes with H_2O and placed in clear plastic bags to be scanned using a calibrated scanner (GS-800, Bio-Rad).

3.5 Gel-based LC-MS/MS

Each gel lane was divided into twelve pieces, followed by destaining and in-gel tryptic digestion using an Investigator ProGest (Digilab) robotic digestion system. Eluted peptides were lyophilised under vacuum at -55°C for approximately 5 hours (Christ Alpha 1-2 LD Freeze Dryer) and resuspended in 40 µl of 2% acetonitrile, 0.05% trifluoroacetic acid in H_2O. Tryptic peptides were separated on a reversed-phase nano-flow high-performance liquid chromatography (HPLC) system (Dionex PepMap C18, 25 cm x 75 um, Dionex RSLC-nano) and eluted with a 70-minute gradient (0-3 min, 2-10% B; 3-37 min, 10-35% B; 37-40 min, 35-40% B; 40-50 min, 99% B; 50-70 min, 2% B; where A=0.1% formic acid in HPLC-grade H_2O and B=80% acetonitrile, 0.1% formic acid in HPLC-grade H_2O). The sequentially eluted peptides were directly analysed by an Orbitrap mass analyser (LTQ Orbitrap XL, Thermo Scientific) using full ion scan mode over the mass-to-charge (m/z) range of 400-1600, resolution 60000 (at m/z 400). Tandem MS (MS/MS) was performed using collision-induced dissociation in ion trap on the six most abundant ions in each full MS scan with dynamic exclusion. Raw files were searched against UniProt/SwissProt mouse and bovine databases (2015_02, 22689 protein entries), using Mascot software (version 2.3.01, Matrix Science). A mass tolerance of 10 ppm was selected for the precursor ions and at 0.8 Da for fragment ions. Carboxyamidomethylation of cysteine was set as a fixed modification and oxidation of methionine, proline and lysine (as hydroxylysine and hydroxyproline are common modifications on collagens) as variable modifications. Two missed cleavages were allowed. Search results were loaded into Scaffold (Proteome Software Inc., version 4.3.2) to validate the MS/MS-based peptide and subsequent protein identification and to calculate

the spectral count.[265,266] Peptide identifications were accepted if they could be established at a probability >95% as specified by the Peptide Prophet Algorithm.[265] Only tryptic peptides were included in the analysis. Protein identifications were accepted if they could be established at a probability >99% with at least two unique peptides.[266] Before statistical analysis, protein spectral counts were normalised by multiplying the number of spectra assigned to each protein with the ratio between the total spectral count of a sample and the average number of spectra across the experiment.

3.6 Cell proliferation assay

To determine the effects on proliferation upon miRNA transfections in cultured CF, a proliferation assay was performed using the xCELLigence RTCA DP Instrument (ACEA Biosciences). Cells were transfected using the same methods and concentrations as described in **3.2** (i.e. 50 nM for all four oligonucleotides). After 24 hours, cells were trypsinised in 0.05% Trypsin/EDTA and resuspended in complete medium (see **3.1**). Cells ($5x10^3$ cells/well in a volume of 200 µl/well) were then seeded in an E-Plate VIEW 16 (ACEA Biosciences, cat. no. 300600890) coated with 0.1% gelatine and allowed to attach whilst at room temperature for 30 minutes. Attachment of cells was confirmed by bright-field microscopy. Plates were then placed in the incubator at 37°C. Four biological replicates were run in duplicate for each transfection condition. Two wells per plate were loaded with media only to assess background levels. Cell index values were recorded by 150 sweeps per interval every 30 minutes until 75 hours after plating, using proprietary software. Data was analysed using the difference (Δ) in cell index and slope analysis functions according to manufacturer's instructions with the baseline recording reset at 4 hours.

3.7 RNA isolation

Total RNA was extracted using the miRNeasy Mini kit (Qiagen, cat. no. 217004) according to the manufacturer's recommendations, with some modifications. For RNA isolation from cultured or isolated cells, lysis was performed with 700 µl of QIAzol reagent. For isolation from heart, kidney and liver, a 1-2 mm piece was cut from the organ at anatomically consistent sites.

The tissue piece was directly placed into a tube containing Lysing Matrix D beads (MP Biomedicals, cat. no. 116913050) and 700 µl QIAzol reagent. Lysis was performed in a FastPrep-24 Homogeniser (MP Biomedicals) at 6000 rpm for two rounds of 20 seconds. Adequate lysis was macroscopically confirmed. Following brief incubation at room temperature, 140 µl of chloroform were added and the solution was mixed vigorously. Samples were then centrifuged at 12,000 x *g* for 15 minutes at 4°C. 280 µl of upper (aqueous) phase were carefully mixed with 420 µl of 100% ethanol and then applied to columns and washed according to the manufacturer's protocol. Total RNA was eluted in 35 µl of nuclease-free H_2O by centrifugation at 9000 x *g* for 1 minute at 4°C. Concentration of cellular or tissue RNA was determined by spectrophotometry based on absorbance at 260 nm using NanoDrop 2000c (Thermo Scientific). The ratio of absorbance at 260 and 280 nm was calculated to assess the extent of protein contamination.

For RNA isolation from plasma, a schematic representation is shown in **Figure 7**. Plasma samples were centrifuged for 10 minutes at 4000 x *g* at 4°C to pellet potential cell debris. 500 µl of QIAzol reagent were then combined with 100 µl of plasma and vigorously mixed. Following 5 minutes incubation at room temperature, 200 µl of spiking mixture were added. This mixture consisted of the following: 4 µl of diluted exogenous cel-miR-39-3p RNA

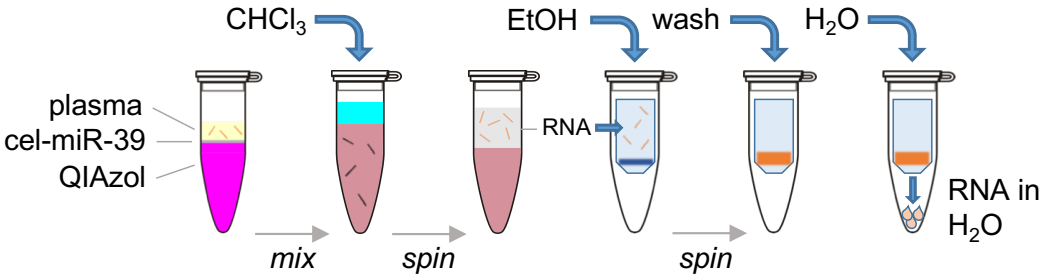

Figure 7. Plasma RNA extraction. For RNA isolation from plasma and other biofluids with low RNA content, an exogenous miRNA (cel-miR-39) was spiked into each sample to compensate for the lack of a suitable 'housekeeping' reference gene transcript. Analysis was performed using a per-volume approach, where the exogenous RNA allows for quality control and adjustment of variability introduced throughout the sample processing. Upon combining plasma with cel-miR-39 RNA and QIAzol lysis reagent, chloroform ($CHCl_3$) was added. After incubation, samples were centrifuged to obtain an aqueous (upper) phase enriched in RNA. This RNA was precipitated onto a column using 100% ethanol (EtOH), washed with a sequence of proprietary buffers, and then eluted with nuclease-free H_2O.

(Qiagen, cat. no. 219600; reconstituted in 100 µl and subsequently diluted 1:4000 in nuclease-free H_2O), 1.25 µl of carrier RNA from bacteriophage MS2 (Roche, cat. no. 10165948001) and 194.75 µl of QIAzol reagent. Samples were then vigorously mixed and incubated for 5 minutes at room temperature. Further RNA isolation was performed similar to the protocol for cell and tissue RNA, with the difference that no NanoDrop analysis was performed.

3.8 Reverse transcription and pre-amplification

For relative quantification of miRNA by qPCR, 100 ng of RNA (or 3 µl for plasma RNA) were used as input in each RT reaction. Reactions (and a pre-amplification step for plasma RNA) were set up according to the company's recommendations. Briefly, miRNAs were reverse-transcribed using the TaqMan MicroRNA Reverse Transcription Kit (Applied Biosystems, cat. no. 4366597), using 100 ng (or a fixed volume for plasma) RNA in 3 µl, 1 µl 10x RT buffer, 0.3 µl 100 mM deoxyribonucleotide triphosphate with deoxythymidine triphosphate, 1.2 µl 25 mM $MgCl_2$, 0.2 µl RNase inhibitor, 1 µl of 10x Megaplex RT primers (Rodent Pool A v2.0 [cat. no. 4399970] or Human Pool A v2.1 [cat. no. 4399966], Applied Biosystems), 2 µl Multiscribe Reverse Transcriptase and 0.8 µl of nuclease-free H_2O. The RT reaction was set up in a Veriti Thermal Cycler (Applied Biosystems) as follows: incubation at 16°C for 2 minutes, then forty cycles of 42°C for 1 minute and 50°C for 1 second, followed by reaction termination by incubation at 85°C for 5 minutes). For plasma miRNAs, pre-amplification was performed using Megaplex PreAmp Primers (Human Pool A v2.1, cat. no. 4399233; Rodent Pool A, cat. no. 4399203; Applied Biosystems), using 1 µl of undiluted RT product, 5 µl Pre-amplification Mastermix (Applied Biosystems, cat. no. 4488593), 3 µl nuclease-free H_2O and 1 µl of Megaplex PreAmp Primers. The pre-amplification reaction was performed by heating the samples at 95°C for 10 minutes, followed by twelve cycles of 95°C for 15 seconds and 60°C for 4 minutes. Finally, samples were heated at 95°C for 10 minutes to ensure enzyme inactivation. Pre-amplification reaction products were diluted 1:72 with nuclease-free H_2O before subsequent use in a qPCR reaction.

For RT of messenger RNA, the reaction was performed using the SuperScript VILO cDNA Synthesis Kit (Invitrogen, cat. no. 11755250). Per

sample, 2 µl of VILO RT Master Mix were combined with 8 µl of sample in a 25-100 ng/µl dilution. Thermal cycler stages were set as follows: incubation at 25°C for 10 minutes and 42°C for 2 hours, followed by termination of the reaction at 85°C for 5 minutes.

3.9 Real-time quantitative PCR

TaqMan hydrolysis assays were used to assess relative levels of miRNA or gene expression. 2.25 µl of diluted RT product or pre-amplification product were combined with 0.25 µl of Taqman miRNA Assay (20X) (Applied Biosystems; see **Table 4**) and 2.5 µl of the Taqman Universal PCR Master Mix No AmpErase UNG (Applied Biosystems, cat. no. 4324020) to a final volume of 5 µl. Reactions were loaded onto 384-well plates using a Bravo Automated Liquid Handling Platform (Agilent). The qPCR reaction was performed on a ViiA7 Real-Time PCR System (Applied Biosystems) at 95ºC for 10 minutes, followed by forty cycles of 95ºC for 15 seconds and 60ºC for 1 minute. Calculations of relative quantity were performed using the $2^{-\Delta\Delta Cq}$ method[267]: C_q values for each assay were substracted from the corresponding reference gene transcript C_q value for each sample, yielding ΔC_q values. For cellular and tissue RNA, the reference gene transcript was selected based on analysis of stability using the online RefFinder tool.[268] This platform combines four major algorithms designed to determine transcript stability, providing a ranking of analysed candidate reference transcripts. For plasma RNA, the exogenous cel-miR-39-3p spike-in was used as the reference transcript. To obtain $\Delta\Delta C_q$ values, ΔC_q values for each assay were then substracted from the average of the ΔC_q values within the prespecified control group (control mimic or control LNA transfection in TGF-β1-untreated cells; or antagomiR-control treatment); or from the average ΔC_q value of the calibrator sample in case of the Bruneck study samples. This calibrator sample consisted of a single RNA sample pool from a selection of samples of the cohort (separate sample pool for the Bruneck 2000 and 2015 evaluations). This calibrator was used throughout the entire analysis of each cohort evaluation and was run in duplicate on each qPCR plate. $\Delta\Delta C_q$ values were then inverted and converted to linear values using $2^{-\Delta\Delta Cq}$.

Table 4. TaqMan hydrolysis assays for use in qPCR.

Gene target	Corresponding protein ID	Assay ID	miRNA target	Assay ID
Acta2	ACTA_MOUSE	Mm01546133_m1	**cel-miR-39-3p**	000200
Actb	ACTB_MOUSE	Mm02619580_g1	**let-7d**	002283
Bgn	PGS1_MOUSE	Mm01191753_m1	**U6**	001973
Col11a1	COBA1_MOUSE	Mm00483387_m1	**RNU48**	001006
Col1a1	CO1A1_MOUSE	Mm00801666_g1	**miR-1**	002222
Col1a2	CO1A2_MOUSE	Mm00483888_m1	**miR-21**	000397
Col3a1	CO3A1_MOUSE	Mm00802300_m1	**miR-24**	000402
Col4a2	CO4A2_MOUSE	Mm00802386_m1	**miR-29a**	002112
Col5a2	CO5A2_MOUSE	Mm00483675_m1	**miR-29b**	000413
Col6a1	CO6A1_MOUSE	Mm00487160_m1	**miR-30b**	000602
Ctgf	CTGF_MOUSE	Mm01192933_g1	**miR-30c**	000419
Ctsl	CATL1_MOUSE	Mm00515597_m1	**miR-31**	002279
Dcn	PGS2_MOUSE	Mm00514535_m1	**miR-92a**	000431
Fbln2	FBLN2_MOUSE	Mm00484266_m1	**miR-93**	001090
Fbn1	FBN1_MOUSE	Mm00514908_m1	**miR-106a**	002169
Fn1	FINC_MOUSE	Mm01256744_m1	**miR-122**	002245
Fstl1	FSTL1_MOUSE	Mm00433371_m1	**miR-126**	002228
Gapdh	G3P_MOUSE	Mm99999915_g1	**miR-126***	000451
Grn	GRN_MOUSE	Mm00433848_m1	**miR-133**	002246
Hspg2	PGBM_MOUSE	Mm01181173_g1	**miR-143**	002249
Igfbp4	IBP4_MOUSE	Mm00494922_m1	**miR-145**	002278
Itga2b	ITA2B_MOUSE	Mm00439741_m1	**miR-146a**	000468
Lama4	LAMA4_MOUSE	Mm01193660_m1	**miR-150**	000473
Lamc1	LAMC1_MOUSE	Mm00711820_m1	**miR-191**	002299
Lgals3bp	LG3BP_MOUSE	Mm00478303_m1	**miR-199a-3p**	002304
Ltbp1	LTBP1_MOUSE	Mm00498234_m1	**miR-223**	002295
Nid1	NID1_MOUSE	Mm00477827_m1	**miR-320**	002277
Pf4	PLF4_MOUSE	Mm00451315_g1	**miR-486**	001278
Postn	POSTN_MOUSE	Mm01284919_m1	**miR-499**	001352
Ppbp	CXCL7_MOUSE	Mm00470163_m1		
Ppia	PPIA_MOUSE	Mm02342430_g1		
Ptprc	PTPRC_MOUSE	Mm01293577_m1		
Serpine1	PAI1_MOUSE	Mm00435858_m1		
Serpinf1	PEDF_MOUSE	Mm00441270_m1		
Sparc	SPRC_MOUSE	Mm00486332_m1		
Tgfb1	TGFB1_MOUSE	Mm01178820_m1		
Tgfb2	TGFB2_MOUSE	Mm00436955_m1		
Tgfb3	TGFB3_MOUSE	Mm00436960_m1		
Tgfbr1	TGFR1_MOUSE	Mm00436964_m1		
Tgfbr2	TGFR2_MOUSE	Mm03024091_m1		
Tgfbr3	TGFR3_MOUSE	Mm00803538_m1		
Vcam1	VCAM1_MOUSE	Mm01320970_m1		
Was	WASP_MOUSE	Mm00494167_m1		

3.10 Immunoblotting

Samples were prepared and separated on Bis-Tris discontinuous 4-12% polyacrylamide gradient gels as described earlier. For immunoblotting, proteins were transferred from the polyacrylamide gel to a nitrocellulose membrane in ice-cold transfer buffer (25 mM Tris base and 200 mM glycine dissolved in 20% methanol) for 2 hours at 350 mA. Proteins were then stained with Ponceau S solution (Sigma, cat. no. P7170) to confirm adequate transfer. For conditioned medium samples, blots were scanned after Ponceau S staining. After washing in PBS with 0.1% Tween-20 (Sigma, cat. no. 11332465001) (PBS-T), membranes were blocked with 5% fat-free milk in PBS-T for 1 hour at room temperature. Membranes were washed briefly in

Table 5. Antibodies used for various applications.

Target	Host species	Application	Company, catalogue number
Laminin-γ1	Rat	Immunoblotting (1:500)	Abcam, ab17792
Periostin	Rabbit	Immunoblotting (1:1000)	Novus Biologicals, NBP1-30042
Biglycan	Rabbit	Immunoblotting (1:500)	Abcam, ab94460
Decorin	Rabbit	Immunoblotting (1:130)	Santa Cruz, sc-22753
Argonaute2	Mouse	Immunoprecipitation	Abcam, ab57113
Anti-CD41	Rat	Flow cytometry, APC-labelled (1:10 to whole blood)	BioLegend, 133913
Anti-CD42b	Rat	Immunodepletion (4 mg/kg)	Emfret Analytics, R300
PF4	Rat	Immunohistochemistry; immunoblotting (1:500)	R&D Systems, MAB595
WASp	Rabbit	Immunoblotting (1:1000)	Cell Signaling, 4860
TGF-β1	Rabbit	Immunoblotting (1:1000); immunohistochemistry	Abcam, ab179695
β-actin	Mouse	Immunoblotting (1:10000)	Sigma, A1978
HRP-anti-rabbit	Mouse	Immunoblotting (secondary antibody, 1:5000)	Jackson ImmunoResearch, 211032171
HRP-anti-mouse	Goat	Immunoblotting (secondary antibody, 1:5000)	Jackson ImmunoResearch, 115035174
HRP-anti-rat	Goat	Immunoblotting (secondary antibody, 1:5000)	Jackson ImmunoResearch, 112055175

PBS-T and incubated overnight in primary antibody solution (see **Table 5**) at a 1:200-10000 dilution in 5% bovine serum albumin (BSA; Sigma, cat. no. A9418) in PBS-T at 4°C while shaking. Membranes were then washed three times for 15 minutes in PBS-T, followed by incubation with a light chain-specific horseradish peroxidase (HRP)-conjugated secondary antibody (Dako) to detect the primary antibody, in a 1:5000 dilution in 5% fat-free milk in PBS-T for 1 hour. After three washes in PBS-T (15 minutes each), membranes were developed using enhanced chemiluminescence (ECL; GE Healthcare, cat. no. RPN2109) using X-ray films (Fujifilm, cat. no. AUT-300-040D) and a Xograph processor with exposure time dependent on signal intensity. Densitometric analysis was performed using ImageJ software (v.1.48v, NIH, USA).

3.11 Three-step extraction for ECM protein enrichment

Hearts from miR-21 *null* mice were a kind gift from Prof. Grillari's laboratory at the University of Natural Resources and Life Sciences, Vienna, Austria. These mice were constructed as described by Patrick *et al*[110], by introducing loxP sites at both ends of pre-miR-21, located within the 3' UTR of the transmembrane protein 49 gene on chromosome 11. Cross-breeding the resulting homozygous floxed mice (miR-21$^{fl/fl}$) with homozygous CAG-Cre-expressing mice resulted in miR-21$^{-/-}$ mice at predicted Mendelian ratios. The removal of the miR-21-encoding locus did not affect the expression or protein levels of transmembrane protein 49 in the aorta, heart, kidney, liver, lung, spleen or skeletal muscle. Furthermore, no differences were observed in heart size and weight, or in cardiac function as determined by echocardiography.

To extract cardiac ECM proteins from miR-21$^{-/-}$ mice and wild-type littermates, 50 mg of ventricular heart tissue per sample were diced and immediately placed in ice-cold PBS to remove plasma contaminants. For all buffers in this protocol, protease inhibitor cocktail was included according to the manufacturer's instructions to inhibit a broad range of proteinase activity. To the PBS, 25 mM EDTA was added to ensure inhibition of metalloproteinases. Upon five washes in modified PBS, diced tissue pieces were incubated with 500 µl 0.5 M NaCl buffer (0.5 M NaCl, 10 mM Tris, 25 mM EDTA, pH 7.5). Samples were gently vortexed for one hour at room temperature. NaCl buffer was then removed and stored for later analysis.

Subsequently, tissue samples were incubated with 500 µl 0.1% SDS buffer (0.1% SDS, 25 mM EDTA) at room temperature for 16 hours with gentle vortexing to avoid mechanical disruption of the ECM. SDS solution was then removed and stored for later use. Finally, the samples were briefly washed in SDS buffer and then placed in 250 µl guanidine hydrochloride (GuHCl) buffer (4 M GuHCl, 50 mM sodium acetate, 20 mM EDTA, pH 5.8). Incubation was performed for 48 hours at room temperature and vortexed vigorously to enhance mechanical disruption of the ECM structure. GuHCl extracts were then collected and stored until later analysis. Protein concentrations in all three fractions were then determined by Bradford assay (BioRad, cat. no. 5000006) according to manufacturer's instructions using bovine serum albumin standard curves prepared in corresponding buffers for each fraction. Proteins in the NaCl and GuHCl fractions were then prepared for MS analysis as follows: 15 µg of protein was precipitated by adding a ten-fold volume of 100% ethanol to GuHCl samples and 100% acetone to NaCl samples. Samples were vortexed and stored at -20°C overnight. Proteins were further precipitated with centrifugation at 16000 x *g* for 40 minutes at 0°C. Supernatant volume was removed up to a residual volume of approximately 50 µl. Protein precipitates were fully dried using a SpeedVac Concentrator (ThermoFisher Scientific, Savant SPD131DDA) for approximately 20 minutes. Protein pellets were then resuspended in 20 µl deglycosylation solution as described earlier, but without N-glycosidase F. Samples were briefly vortexed and centrifuged, followed by incubation at 25°C for 2 hours and 37°C for 24 hours. Samples were then centrifuged and dried using the SpeedVac Concentrator for approximately 30 minutes. Protein pellets were then resuspended in 20 µl of 1:100 N-glycosidase F in H_2O^{18}. Samples were briefly vortexed and centrifuged, followed by incubation at 37°C for 48 hours. Samples were then stored at -20°C until processing for MS. Following HPLC-MS/MS analysis, identified proteins were annotated using the Matrisome database.[269]

3.12 In-solution digestion and HPLC-MS/MS analysis

Deglycosylated GuHCl/NaCl extracts were denatured by the addition of 9 M urea, 3 M thiourea in a 1:2 ratio (final concentration 6 M urea, 2 M thiourea). Samples were then reduced by adding 100 mM dithiothreitol (final concentration 10 mM) followed by incubation at 37°C for 1 hour. The samples

were then cooled down to room temperature before alkylation of proteins using iodoacetamide (final concentration 50 mM) followed by incubation in the dark for 1 hour at room temperature. Proteins were then precipitated using pre-chilled (-20°C) acetone in a 6:1 volume ratio. Samples were briefly vortexed and centrifuged, followed by storage at -20°C overnight. Dried protein pellets were obtained as described in the previous section. For protein digestion, samples were resuspended in 30 µl trypsin solution, containing 0.01 µg/µl trypsin in 0.1 M triethylammonium bicarbonate, pH 8.2. Proteins were digested overnight at 37°C under agitation (240 rpm). The digestion was stopped by acidification of the samples with 10% v/v trifluoroacetic acid (final concentration 1%). Peptide samples were purified using a 96-well C18 spin plate (MicroSpin, Harvard Apparatus, cat. no. 745617). The resin was activated using 200 µl methanol and centrifuged at 1000 x *g* for 1 minute. Wash steps included 200 µl of 80% acetonitrile, 0.1% trifluoroacetic acid in H_2O, and three equilibration steps using 200µl of 1% acetonitrile, 0.1% trifluoroacetic acid in H_2O with centrifugation (1000 x *g* for 1 minute) after each step. Samples were loaded onto the resin and centrifuged at 2250 x *g* for 1 minute; the flow through was reloaded onto the resin a second time and centrifugation repeated. The resin was then washed three times with 200 µl 1% acetonitrile, 0.1% trifluoroacetic acid in H_2O (centrifugation at 2250 x *g* for 1 minute). Finally, the samples were eluted with 170 µl of 50% acetonitrile, 0.1% trifluoroacetic acid in H_2O (centrifugation at 1000 x *g* for 1 minute); this step was repeated, combining the collected eluate. Samples were then dried down using the SpeedVac Concentrator for approximately 5 hours. Dried peptide samples were then resuspended in 0.05% trifluoroacetic acid in 2% acetonitrile and separated on a nano-flow LC system (Dionex UltiMate 3000 RSLC-nano). Samples were injected onto a nano-trap column (Acclaim® PepMap100 C18 Trap, 5mm x 300um, 5um, 100Å), at a flow rate of 25 µL/min for three minutes, using 2% acetonitrile, 0.1% formic acid in H_2O. The following nano-LC gradient was then used to separate the peptides at 0.3 µL/min: 0−10 min, 2-10% B; 10−200min, 10-30% B; 200−210min, 30−40% B; 210-220min, 99%B, 220-240min 2%B, where A=0.1% formic acid in H_2O, B=80% acetonitrile, 0.1% formic acid in H_2O. The nano column (Acclaim® PepMap100 C18, 50 cm x 75 µm, 3µm, 100 Å) was set at 40°C and coupled to a nanospray source (Picoview, New Objective, US). Spectra were collected from a Q Exactive Plus

(Thermo Fisher Scientific) using full MS mode (resolution of 70,000 at 200 m/z) over the mass-to-charge (m/z) range 350–1600. Data-dependent MS2 scan was performed using the top fifteen ions in each full MS scan (resolution of 17,500 at 200 m/z) with dynamic exclusion enabled. Thermo Scientific Proteome Discoverer software (version 1.4.0.288) was used to search raw data files against the human database (UniProtKB/Swiss-Prot version 2017_02, 17,511 protein entries) using Mascot (version 2.6.0, Matrix Science). The mass tolerance was set at 10 ppm for precursor ions and 20 mmu for fragment ions. Trypsin was used as the enzyme with up to two missed cleavages being allowed. Carbamidomethylation of cysteine was chosen as a fixed modification; oxidation of methionine, lysine and proline, and deamidation of asparagine in the presence of O^{18} water were chosen as variable modifications. Scaffold (version 4.3.2, Proteome Software Inc., Portland, OR) was used to validate MS/MS-based peptide and protein identifications with the following filters; a peptide probability of greater than 95.0% (as specified by the Peptide Prophet algorithm), a protein probability of greater than 99.0%, and at least two independent peptides per protein. The normalised total precursor intensity was used for quantification.

3.13 Bruneck study

The Bruneck study is a community-based, prospective survey of the epidemiology and pathogenesis of atherosclerosis and cardiovascular disease.[233,270] The study protocol was reviewed and approved by the Ethics Committees of Verona and Bolzano, and all participants provided their written informed consent before entering the study. At the 1990 baseline evaluation, the study population comprised an age- and sex- stratified random sample of all inhabitants of Bruneck aged 40-79 years (125 men and 125 women from each of the fifth through eighth decades of age, all white). Samples from the year 2000 (n=660) and 2015 (n=332) follow-up were used for the present study. Participant characteristics for both study evaluations are shown in **Table 6**. Citrate plasma samples were drawn after an overnight fast and twelve hours of abstinence from smoking. During the 2000 follow-up, plasma was prepared within two hours from blood drawing by single centrifugation at 4000 x *g* for 15 minutes at room temperature and aliquots were immediately stored at -80°C. Our work on circulating miRNAs and their relation with platelets[96,217] drew

attention to the importance of platelets as a potential source of contamination. This had been reported by others, both in the context of protein measurements[271–273] and miRNAs.[274,275] As TGF-β1 became a focus of attention within this project, in part due to our observations from the Bruneck study 2000 follow-up, the importance of preanalytical variables became increasingly pertinent. Several studies have previously highlighted the importance of platelet activation as a major confounder of circulating TGF-β1 measurements.[29,64,276,277] We therefore devised a tailored protocol for platelet-poor plasma preparation during the 2015 follow-up, based on previous studies[29,64] and protocols previously devised for specific haematological analyses.[278,279] First, PRP was isolated by centrifugation at 175 x *g* for 15 minutes with slow brake. An aliquot of PRP was then supplemented with prostacyclin (PGI_2, 2 µg/mL; Tocris Bioscience, cat. no. 2989) and centrifuged at 1000 x *g* for 10 minutes to obtain PPP. Samples were divided into aliquots and immediately stored at -80°C.

Table 6. Clinical characteristics of Bruneck study participants during the 2000 and 2015 evaluations.

	Bruneck study	
Follow-up year	**2000**	**2015**
Participants, n	660	332
Age, mean (SD)	66.0 (10.3)	75.2 (7.2)
Male sex, n (%)	324 (49.1)	168 (50.6)
Diabetes, n (%)	70 (10.6)	24 (7.2)
Antiplatelet therapy, n (%)	79 (12.0)	101 (30.4)

3.14 Plasma proximity extension assays

Low-abundant plasma proteins were analysed using Olink Proseek Proximity Extension Assays (PEA; CVD I [cat. no. 91201] and Inflammation I [cat. no. 91301] panels). Plasma samples were centrifuged for 1 minute at room temperature at 400 x *g*. All following centrifugations were performed using these settings. 1 µl of sample, interplate control or negative control was combined with 3 µl of incubation mix (prepared by combining 280 µl incubation solution and 40 µl of incubation stabiliser, A-probes and B-probes each) on a 96-well plate. The plate was centrifuged and incubated overnight at 4°C. The

next day, 96 µl of extension mix was added to each well, made up of 9385 µl H_2O, 1100 µl PEA solution, 55 µl PEA enzyme and 22 µl PCR polymerase. The plate was then vortexed and centrifuged. Samples were placed in a thermal cycler (Veriti, Applied Biosystems, cat. no. 4375786) and run with the following protocol: extension for 20 minutes at 50°C and a hot start of 5 minutes at 95°C, followed by seventeen PCR cycles of 30 seconds at 95°C, 1 minute at 54°C and 1 minute at 60°C. In a new plate, 2.8 µl of these samples were combined with 7.2 µl of detection mix (consisting of 550 µl detection solution, 230 µl H_2O, 7.8 µl detection enzyme and 3.1 µl PCR polymerase). Next, the primer plate was thawed and vortexed and both plates were then centrifuged. A 96.96 dynamic array integrated fluidics circuit (IFC; Fluidigm, cat. no. BMK-M-96.96) was primed by emptying one 150 µl syringe of control line fluid (Fluidigm, cat. no. 89000021) into the accumulator. 5 µl of primer and 5 µl of sample were added to the inlets on respective sides of the fluidics circuit. The fluidics circuit was then run in an IFC Controller HX (Fluidigm, cat. no. BMK-IFC-HX) to combine the primers with samples. Finally, the fluidics circuit was loaded in a Biomark HD system (Fluidigm, cat. no. BMKHD) and analysed using the following programme: thermal mixing by incubation at 50°C for 2 minutes, 70°C for 30 minutes and 25°C for 10 minutes, followed by a hot start at 95°C for 5 minutes, followed by forty cycles at 95°C for 15 seconds and 60°C for 1 minute. Results were analysed using NPX Manager Software (Olink).

3.15 Plasma protein quantification by mass spectrometry

For the mass spectrometry-based PlasmaDive kit (Biognosys AG, cat. no. Ki-3004), plasma samples were processed according to the manufacturer's instructions with one exception: peptide standards were spiked in before and not after tryptic digestion and C18 clean-up. 10 µl of plasma samples were denatured, reduced and alkylated as described above. 20 µg of proteins were spiked with one hundred authentic heavy peptide standards. Seven proteins were below the limit of detection. An in-solution digestion was performed as described in **paragraph 3.12**. After solid phase extraction with 96-well C18 spin columns, the eluted peptides were dried using a SpeedVac Concentrator and resuspended in 40 µl of LC solution. The samples were analysed on an Agilent 1290 LC system interfaced to an Agilent 6495 Triple Quadrupole MS.

10 µl samples were directly injected onto a 25 cm column (AdvanceBio Peptide Map 2.1 x 250 mm, Agilent, cat. no. 651750-902) and separated over a 23-minute gradient at 300 µl/min. The data were analysed using Skyline software version 3.1 (MacCross Lab) and protein concentrations were calculated using the heavy/light ratio.

3.16 Enzyme-linked immunosorbent assays (ELISA)

Levels of TGF-β1 (R&D Systems, cat. no. DY1679 for mouse; DY240 for human) and PF4 (cat. no. DY595) were measured using DuoSet ELISA Development kits and DuoSet Ancillary Reagent Kits 1 and 2 (cat. no. DY007 and DY008, respectively). Plates were coated with 100 µl capture antibody reconstituted in plate coating buffer and incubated at room temperature overnight. All incubations in the protocol were carried out at room temperature. Plates were washed three times with 300 µl washing buffer; all following washes throughout the protocol were carried out in a similar manner. Plates were then blocked with the appropriate block buffer for at least 1 hour. For mouse TGF-β1, 5 µl of sample were treated with 1.25 µl of 1 M HCl for 10 minutes and then neutralised with 1.25 µl 1.2 M NaOH/0.5 M 4-(2-hydroxyethyl)-1-piperazineethanesulfonic acid (HEPES). Samples were then diluted with reagent diluent to a final dilution of 45x. For human TGF-β1, plasma was pre-diluted by adding 6.6 µl of sample to 81.4 µl reagent diluent, followed by adding 22 µl 1 M HCl. After mixing and 10 minutes incubation, 22 µl of 1 M NaOH/0.5 M HEPES were added to neutralise the samples. The resulting final dilution was 20x. For PF4, 1 µl of sample was diluted in 999 µl of reagent diluent to obtain a 1000x dilution. The ELISA plates were washed and 100 µl of diluted sample or the appropriate standard were loaded. Plates were incubated for two hours while gently shaking. Detection antibody was diluted in reagent diluent and 100 µl were added after washing. After two hours of incubation, plates were washed and 100 µl of streptavidin-HRP diluted in reagent diluent were added. After incubation in the dark for twenty minutes, plates were washed and 100 µl of substrate solution were added. After twenty minutes of incubation, 50 µl of stop solution were added to each well. Absorbance at 450 nm was then measured on a plate reader (Tecan Infinite 200 Pro) using 570 nm as a reference wavelength. Results were calculated

using a four-parameter logistic fit for a 7-point standard curve consisting of serial twice-diluted recombinant protein in sample dilution buffer, analysed in duplicate. Furthermore, for each matrix and assay, a spike-recovery protocol was performed to assess linearity for serial dilutions of the neat and spiked matrix. For this purpose, a sample pool was generated for each assayed matrix (supernatant of activated PRP from antagomiR-treated mice; human PPP from the Bruneck study 2015 evaluation). A representative example of this analysis is shown in **Figure 8**. For the analysis of the Bruneck study 2015 PPP samples, the sample pool was run in triplicate on each ELISA plate. A ratio of the average measurement for this pool on each plate was calculated towards the

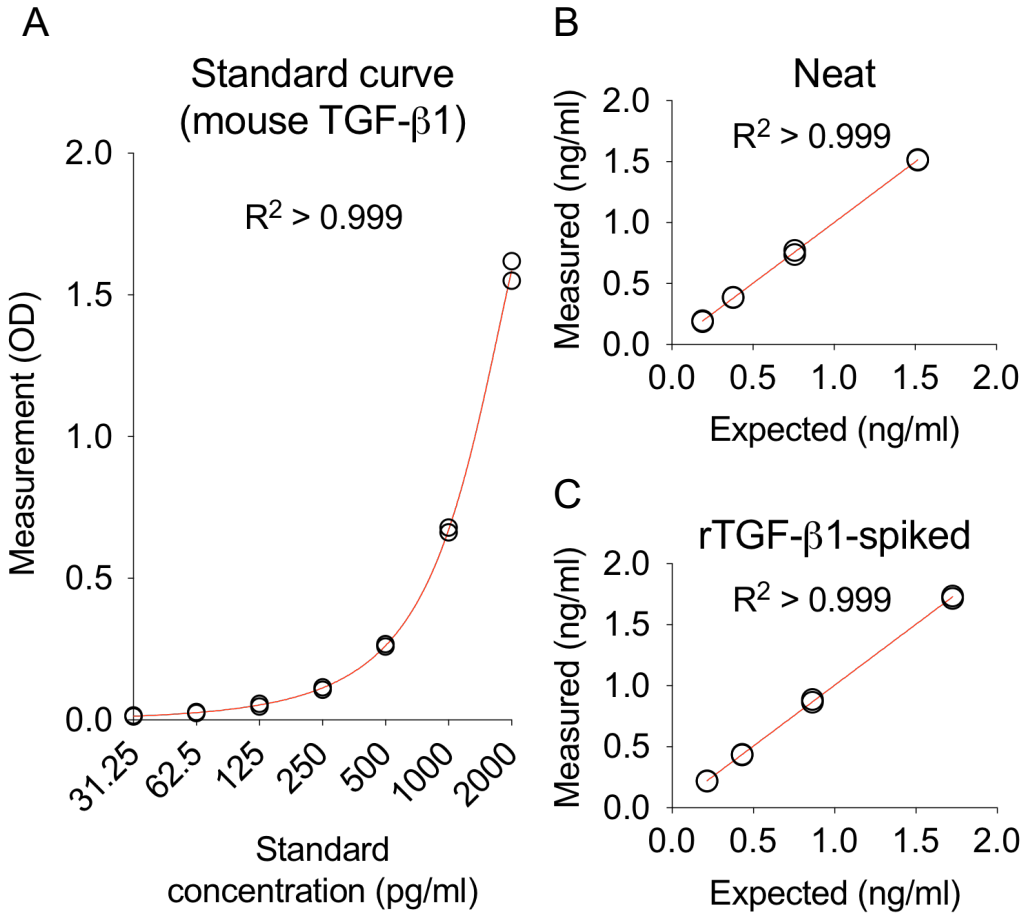

Figure 8. ELISA standard curve and linearity measurements for murine plasma. **A:** A 7-point standard curve was generated using serial dilution of recombinant murine TGF-β1 in sample dilution buffer. Samples loaded in duplicate. X-axis showing expected concentration, with the background-corrected absorbance (optical density, OD) shown on the Y-axis. R^2 indicates goodness of fit for the shown 4-parameter logistic equation curve. **B,C:** A pool consisting of equal amounts of each analysed plasma sample was generated to assess linearity of the measurements using this matrix. A serial dilution of neat sample pool (**B**) and sample pool spiked with recombinant murine TGF-β1 (rTGF-β1) was generated and analysed, showing linearity of the measurement for both analyses. Samples analysed in duplicate; R^2 indicates goodness of fit for the shown linear regression curve.

average of all sample pool measurements across the plates. This ratio (<20% deviation from the average) was used as an adjustment factor for obtained sample measurements.

3.17 Human plasma isolation from human blood

Preparation of conventional plasma and PPP in the Bruneck cohort is described in the methods section of the Bruneck study. A schematic representation is shown in **Figure 9, panel A**. For preparation of PRP and PPP for PEA and NGS analysis, blood was drawn into syringes pre-filled with acid-citrate-dextrose buffer (ACD; 85 mM trisodium citrate dehydrate, 66.6 mM citric acid monohydrate, 111 mM anhydrous D-glucose, Sigma) in a ratio of 1:6 of

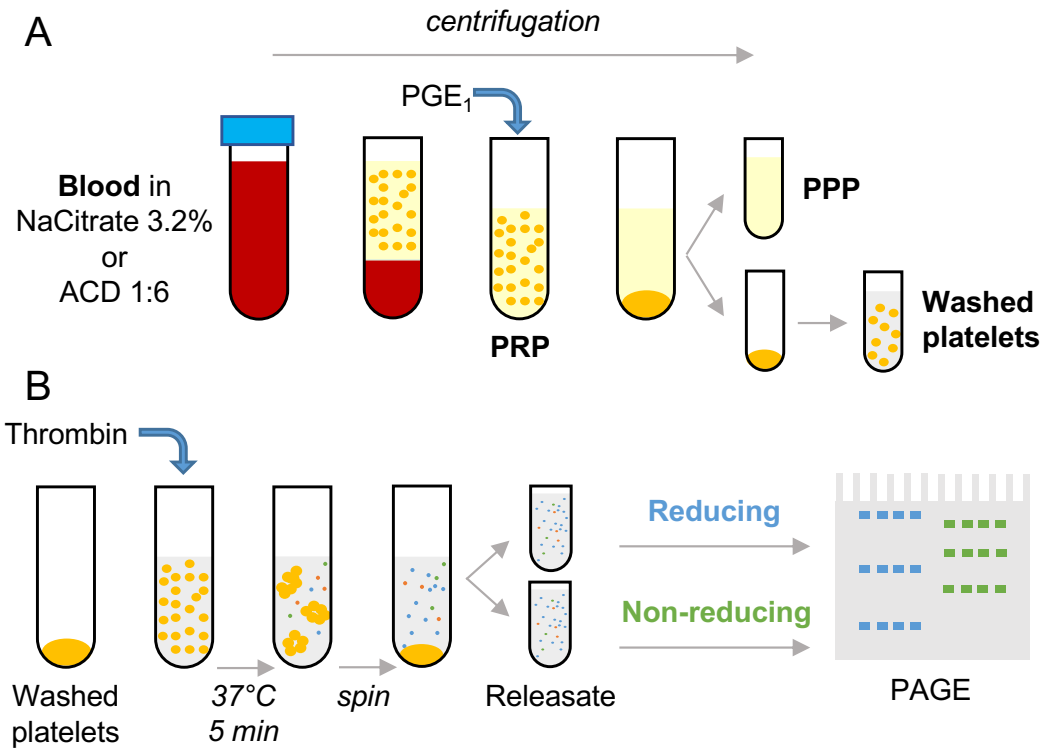

Figure 9. Plasma and platelet releasate isolation. A: For isolation of plasma and platelets, blood was drawn into sodium citrate (NaCitrate) or acid-citrate-dextrose (ACD) buffer with a final dilution of 3.2% or a blood:ACD ratio of 6:1, respectively. Initial centrifugation was performed at low speed to obtain an upper phase of platelet-rich plasma (PRP) which was carefully collected. For subsequent faster centrifugation to obtain platelet-poor plasma (PPP) and the platelet pellet, prostaglandin E_1 (PGE_1) was added to reduce platelet activation. **B:** For platelet releasate isolation, the platelet pellet was washed twice, followed by platelet activation with thrombin. The releasate was then isolated by centrifugation. Human releasate samples were treated with either reducing or non-reducing conditions with subsequent analysis by polyacrylamide gel electrophoresis (PAGE). Separated proteins were then isolated from the gel after silver staining and digested for mass spectrometric analysis.

ACD:blood. All centrifugations were carried out at room temperature. PRP was first isolated by centrifugation at 190 x *g* for 30 minutes without brake. The top two-thirds of the upper phase was collected to stay clear of the buffy coat interphase. An aliquot of PRP was stored at -80°C for later analysis. The remainder of collected PRP was then further centrifuged at 280 x *g* to remove leukocytes after adding 1 µg/ml PGE_1 (Sigma, cat. no. P5515) and 10 µM indomethacin (Sigma, cat. no. I7378) to inhibit platelet aggregation. The supernatant PRP was then centrifuged at 1180 x *g* for 10 minutes to pellet down platelets. Supernatant PPP was collected and stored at -80°C for later analysis.

3.18 Human platelet releasate isolation and gel electrophoresis

For the human platelet releasate analysis, platelets were isolated as described in the previous paragraph. Isolation of the releasate is graphically shown in **Figure 9, panel B.** Pellets were washed twice in modified Tyrode-HEPES buffer (NaCl 134 mM, KCl 2.9 mM, Na_2HPO_4 0.34 mM, $NaHCO_3$ 12 mM, HEPES 20 mM, $MgCl_2$ 1 mM, Glucose 5 mM), supplemented with 1 µg/ml PGE_1 and 10 µM indomethacin, with centrifugation at 1180 x *g* for ten minutes in between. The platelet pellet was then resuspended in modified Tyrode-HEPES buffer without inhibitors and left to rest for 30 minutes. Platelet suspensions were then transferred to glass cuvettes. These were placed in an aggregometer (ChronoLog, cat. no. 490) that was pre-warmed to 37°C. 1 U/ml thrombin from human plasma (Sigma, cat. no. T7009) was then added, followed by incubation for 5 minutes at 37°C under constant stirring. Next, ice-cold protease inhibitor cocktail was added. Subsequent centrifugation for 5 minutes at 1000 x *g* and 1 hour at 20000 x *g*, both at 4°C, were performed to deplete the platelet releasate from any cellular material. Samples were then cleaned and concentrated to a 25 µl volume using Amicon 3 kDa concentration columns as described earlier. Protein concentrations were determined using the 3-(4-carboxybenzoyl)quinoline-2-carboxaldehyde protein quantitation kit (CBQCA, ThermoFisher, cat. no. C6667) according to the manufacturer's instructions. Equal amounts of protein were aliquoted and adjusted to equal volumes with PBS. Samples were then separated in two equal parts, followed by addition of reducing sample loading buffer as described in **paragraph 3.4** or by adding non-reducing sample buffer that was free of β-mercaptoethanol

but was supplemented with 100 µM maleimide (Sigma, cat. no. 129585). Samples with reducing buffer subsequently underwent heating at 95°C for 5 minutes. A 5-15% polyacrylamide 20x25 cm gel was casted using a 2-DEoptimiser (Nextgen) and a Dalt six gel casting tank (GE Healthcare). After allowing the gels to set overnight at 4°C, a 5% stacking gel was casted on top using an 18-well gel comb. After setting overnight at 4°C, samples were reduced and non-reduced samples were separated by electrophoresis at 2W for 15 minutes, 3W for 30 minutes and 30W for 200 minutes. Protein profiles of the gels were visualised by silver staining using the PlusOne Silver Staining Kit (GE Healthcare, cat. no. 17-1150-01) protocol. All steps were performed with gentle shaking. After electrophoresis, the gel was washed in H_2O incubated in fixing solution (10% acetic acid, 40% v/v methanol) at room temperature for 60 hours. Next, the gel was washed in H_2O three times and then incubated in sensitising solution (30% v/v methanol, 0.2% w/v sodium thiosulphate and 0.5 M sodium acetate) for 30 minutes at room temperature. After three 5-minute washes in H_2O, protein bands were silver stained by incubation in 0.25% w/v $AgNO_3$. After 20 minutes, the gel was washed twice for 1 minute in H_2O, and then developed (2.5% w/v sodium carbonate, 0.0148% w/v formaldehyde) for 3 minutes. Stopping solution (1.46% w/v EDTA-Na_2•H_2O) was then added for 10 minutes, followed by three 5-minute washes in H_2O. The gel was then transferred to a clear plastic bag to allow for scanning (GS-800, Bio-Rad). Each gel lane (i.e. sample) was divided in forty-eight gel pieces, that were subsequently processed using the ProGest system as described in **paragraph 3.5**.

3.19 Platelet depletion

Male C57BL/6J mice (Harlan) were treated with a rat anti-mouse glycoprotein Ibα (GPIbα) antibody (4 mg/kg, Emfret Analytics, cat. no. R300) or sterile PBS via intraperitoneal injection. After 48 hours, blood was collected by cardiac puncture into ACD in a ratio of 6:1 for blood:ACD. 50 µl of whole blood were added to QIAzol reagent for RNA isolation. Within 1 hour, the remaining blood was centrifuged at 1000 x *g* at room temperature for 10 minutes to obtain PPP. A second centrifugation was performed at 10000 x *g* for 10 minutes at room temperature with addition of 1 µM PGE_1 to reduce

potential activation of residual platelets. Supernatant PPP was collected and stored at -80°C until further analysis.

3.20 Argonaute2 immunoprecipitation

Cells from a megakaryoblastic leukaemia cell line (MEG-01, ATCC) were cultured in RPMI-1640 medium (Life Technologies, cat. no. 52400) supplemented with 10% FBS, 100 U/ml penicillin and 100 µg/ml streptomycin at 37ºC in a humidified atmosphere of 5% CO_2. Immunoprecipitation of ribonucleoprotein was carried out in 50-100 million MEG-01 cells after lysis in 500 µl ice cold polysome lysis buffer (5 mM $MgCl_2$, 100 mM KCl, 10 mM HEPES, pH 7.0, 0.5% Nonidet P-40) with freshly added 1 mM DTT, 100 U/ml RNase inhibitor (Life Technologies) and protease inhibitor cocktail for 15 minutes. Centrifugation was performed at 14,000 × *g* at 4°C for 10 minutes. The supernatant was mixed with 500 µl of ice-cold NT2 buffer (50 mM Tris, pH 7.4, 150 mM NaCl, 1 mM $MgCl_2$, 0.05% Nonidet P-40) containing freshly added 200 U/ml RNase inhibitor, 0.5% vanadyl ribonucleoside, 1 mM DTT, 15 mM EDTA and 50 µl mouse anti-human Ago2 (see **Table 5**) antibody-coated sepharose G beads (Dynabeads™ Protein G, ThermoFisher, cat. no. 10004D). Incubation was carried out overnight at 4°C on a rocking platform. The following day, beads were washed five times with ice-cold NT2 buffer and used for RNA isolation, RT and qPCR as described above. RNA was isolated from washed beads coated with anti-Ago2-antibody or isotype control antibody, and from sample not incubated with beads (input). C_q values from qPCR analysis were inverted and normalised to each corresponding isotype control sample ($-\Delta C_q$).

3.21 Platelet aggregometry with oligonucleotides

To assess whether different miRNA-targeting oligonucleotide constructs induced platelet aggregation, light transmission aggregometry was performed using blood from healthy volunteers. Prior to the blood sample being taken, all healthy volunteers had abstained from aspirin, NSAIDs and any other anti-platelet therapy for a minimum of fourteen days. Blood was drawn by venepuncture from the antecubital vein using a 19G butterfly needle into a syringe pre-filled with tri-sodium citrate (0.32% w/v final; Sigma, cat. no.

S1804). After transferring blood to 15 ml conical tubes, samples were centrifuged at 175 x g for 15 minutes at room temperature without brake. The top two-thirds of supernatant PRP was transferred and kept at 37 ºC until use. A PPP sample to serve as background reading was prepared by centrifugation at 15000 x *g* for 2 minutes of remaining upper phase and interphase blood from the initial centrifugation. Aggregation in response to different agonists was measured in a PAP-8E turbidimetric aggregometer (1200 rev/min, 37 °C; Bio/Data, cat. no. 106075), using adenosine diphosphate (ADP, 5 µM; Labmedics, cat. no. Chrono-Par 384) or Horm collagen (1 µg/ml) as agonists. Oligonucleotides were all reconstituted and diluted to 10 µM in sterile PBS. Blank PBS served as a negative control. 200 µl of PRP was placed in a glass cuvette containing a stir bar. After brief incubation, 25 µl of agonist, oligonucleotide (final concentration 1 µM) or PBS were added, followed by immediate initiation of aggregometry reading. Registration was performed for 40 minutes, recoding maximal and final percent aggregation values.

3.22 Systemic inhibition of miR-21

Male C57BL/6J mice (Harlan) were treated with cholesterol-conjugated antagomiR constructs (Fidelity Systems, custom-made). Sequences were designed to target miR-21 (5'-U*C*AACAUCAGUCUGAUAAG*C*U*A*-Chol*T-3') or to serve as non-targeting control (5`-A*A*GGCAAGCUGACCCUGAA*G*U*U*-Chol*T-3'), using a similar design as previously used for other miRNAs in our laboratory[217,280,281] and in other studies.[108,118] Constructs were reconstituted in sterile PBS at 37ºC and intraperitoneal injections were performed on three consecutive days in a dose of 25 mg/kg for the platelet releasate isolation, and 40 mg/kg for the aggregometry experiments, the ELISA measurements in plasma and the platelet isolation. Seven days after treatment initiation, mice were anaesthetised using pentobarbital for blood and tissue collection. Following blood collection (see **3.25 and 3.26**), heart, kidney and liver were excised and washed in sterile PBS, followed by immediate freezing on solid carbon dioxide.

3.23 Mouse bone marrow analysis

Femora were excised, washed, and stored in sterile PBS at 4ºC until processing. To isolate bone marrow cells, bones were cleaned of soft tissue and briefly washed in 70% ethanol, followed by washing in sterile PBS. Bones were then cut at the epiphysis at either end of the bone, exposing the bone marrow. Using a syringe pre-filled with sterile PBS and carrying a 25G needle, bone marrow cells were flushed out of the bone onto a 100 µm cell strainer (Corning, cat. no. 08-771-19) placed onto a 50 ml conical tube. Samples were centrifuged for 5 minutes at 350 x *g* at 4ºC. The supernatant was discarded and samples were resuspended in sterile PBS, followed by centrifugation at similar conditions. Supernatant was again removed and cells were resuspended in sterile PBS and centrifuged. After removal of supernatant PBS, cells were lysed in 700 µl QIAzol reagent for RNA isolation.

3.24 Bone marrow immunohistochemistry

Excised and washed femora were placed in 4% formaldehyde and stored at 4°C for three days. Bones were then washed in PBS twice and transferred to 0.38M EDTA in H_2O, pH 7.0, and incubated at 4°C for three weeks, refreshing the EDTA solution twice per week. Following washing with PBS, bone tissues were dehydrated through a series of graded ethanol baths and then infiltrated with paraffin wax. Bone tissues were then embedded in paraffin for subsequent microtome sectioning (5 µm). After placing on glass slides, sections were baked at 60°C for 2 hours. Epitope unmasking was achieved using hot sodium citrate buffer incubation for 20 minutes. Sections were washed three times with PBS-T and incubated with primary antibodies of TGF-β1 and PF4 or species-matched isotopes overnight at 4°C after blocking with 10% FBS in PBS-T for 1 hour. Following three 5-minute washes in PBS-T, sections were incubated for 1 hour at room temperature with secondary antibody (Alexa Fluor 594 and 633, Life Technologies) in 10% FBS/PBS-T, according to the source of the primary antibody. Nuclei were stained with DAPI (1:1000 dilution) for 10 minutes. Sections were then mounted on a Vecta Mount (Vector Laboratories, cat. no. H-5000). Sections were visualised with a 20X objective using an inverted Nikon NI-E microscope equipped with a Yokogawa CSU-X1 spinning disk confocal unit and an Andor iXon 3 EM-CCD

camera. Images were acquired using NIS-elements 4.0 software. Megakaryocyte counting was performed after blinding of immunostained sections using Fiji ImageJ software, version 2.0.0-rc-65/1.51w.

3.25 Murine platelet and leukocyte count

For flow cytometry-based platelet counting, blood was collected into ACD by cardiac puncture. Whole blood was diluted 25x with modified Tyrode-HEPES buffer at 37ºC. To label platelets, samples were incubated with 5 µl of 0.2 mg/ml allophycocyanin (APC)-labelled anti-mouse CD41 antibody in the dark for 15 minutes at room temperature. Unstained control samples were prepared by treatment with an equal amount of modified Tyrode-HEPES buffer. After incubation, samples were further diluted to a final dilution of 1:1000 using the same buffer. Samples were then analysed using an Accuri C6 flow cytometer (BD Biosciences) with slow flow. A set volume of each sample was analysed to allow for absolute concentration calculation. Events corresponding to platelets were identified according to forward and side scatter as well as by identification of APC-positive events. Subsequent quantification of events was performed post-acquisition using FlowJo v7.4 (Tree Star). For miR-21 *null* mice and littermates, blood cell counting was performed using a Hemavet 950FS (Drew Scientific) using proprietary software according to manufacturer's instructions.

3.26 Murine platelet isolation

For the isolation of washed platelets and the platelet releasate, blood was collected into ACD by cardiac puncture. ACD-blood was diluted 1:1 with filtered Tyrode-HEPES buffer, supplemented with 1 g/L bovine serum albumin. PRP was obtained by centrifugation at 100 x *g* for 8 minutes at room temperature without brake. The top two-third of supernatant was transferred and supplemented with 1 µl/mg PGE_1, immediately followed by centrifugation at 800 x *g* for 10 minutes at room temperature without brake. Supernatant PPP was transferred and the platelet pellet was washed twice by resuspending in modified Tyrode-HEPES buffer supplemented with 1 µl/mg PGE_1, each time followed by centrifugation at 800 x *g* for 10 minutes at room temperature without brake. Platelets were then lysed by a freeze-thaw and by subsequent

lysis in ice-cold cell lysis buffer (Cell Signaling, cat. no. 9803) supplemented with protease inhibitor cocktail and phosphatase inhibitor (PhosSTOP, Roche, cat. no. 04906845001). Samples were then incubated on ice for 20 minutes, followed by centrifugation at 15000 x *g* for twenty minutes at 4ºC. The supernatant of this lysate was collected and the protein concentration was analysed using the BCA protein assay kit.

3.27 Murine platelet releasate isolation

For isolation of the platelet releasate from murine blood, ACD-blood was pooled per four mice, followed by centrifugation at 150 x *g* for 10 minutes at room temperature. The top two-thirds of the supernatant PRP was carefully transferred and combined with 10 µM indomethacin and 1 µM PGE_1. Platelet pellets were obtained by centrifugation of PRP at 500 x *g* for 10 minutes at room temperature without brake. Supernatant PPP was collected, and the platelet pellet was washed twice with modified Tyrode-HEPES buffer, supplemented with 1 µM PGE_1 and 10 µM indomethacin, with centrifugation at 500 x *g* for 10 minutes at room temperature in between. The platelet pellet was then resuspended in 200 µl of modified Tyrode-HEPES buffer without PGE_1 and indomethacin, and platelets were activated with 1U/ml thrombin, followed by incubation for 5 minutes at 37°C under constant shaking. After 5 minutes, ice-cold protease inhibitor cocktail was added. Subsequent centrifugation for 5 minutes at 1000 x *g* and 1 hour at 20000 x *g*, both at 4°C, were performed to isolate the platelet releasate. Samples were concentrated using Amicon 3kDa concentration columns. Protein concentration was measured using the CBQCA Protein Quantitation Kit. Equal protein amounts were then separated by gel electrophoresis and processed for LC-MS/MS analysis as described in earlier in this chapter. Injection volumes for each sample were further adjusted based on quantitative densitometry of the silver-stained gel. Mass spectrometry analysis of the peptides was performed as described in paragraph **3.5**, with the following differences: raw files were searched against UniProt/SwissProt mouse database (2015_02); only oxidation of methionine was set as a variable modification; peptide identifications were accepted if they could be established at a probability > 85% and protein identifications were accepted if they could be established at a probability > 99.9% with at least two unique peptides. Proteins with less than five identified spectra in both

treatment conditions were excluded from analysis. Gene ontology (GO) annotation was performed using the α-granule (GO:0031091), α-granule lumen (GO: 0031093) and dense (δ) granule lumen (GO:0031089) terms. To enhance visualisation, key plasma, cytoskeletal and mitochondrial contaminants were removed unless previous detection in the human releasate, in previous literature[282,283] or by GO annotation. For further illustration of effects on TGF-β1, peptide identifications were accepted if they could be established at a probability >95% and protein identifications were accepted if they could be established at a probability >80% with at least one unique peptide.

3.28 Murine platelet aggregometry

For platelet aggregometry from antagomiR-treated mice, blood was collected from the inferior vena cava using syringes containing lepirudin (Refludan, 25 µg/ml; Celgene/Bachem, cat. no. H-6618) for aggregometry experiments and ELISA measurements. Whole blood was diluted 1:1 with modified HEPES-Tyrode's buffer supplemented with 1 g/l bovine serum albumin before centrifugation at 100 x *g* for 8 minutes at room temperature without brake. Half-area 96-well microtiter plates (Greiner Bio-One, cat. no. M8060) were pre-coated with hydrogenated gelatine (0.75% w/v; Sigma, cat. no. G1393) in PBS to block non-specific activation of blood. 4 µl of vehicle or agonist solution was then added to each well: arachidonic acid (AA; 0.03-0.6 mM; Sigma, cat. no. A8798), Horm collagen (0.1–3 µg/ml; Nycomed, cat. no. 2067474) and the PAR-4 activating peptide AYPGKF amide (PAR4 amide, 30–100 µM; Bachem, cat. no. H-6046). To each well, 35 µl of PRP was added and the plate was then placed onto a heated plate shaker (Bioshake IQ, Q Instruments, cat. no. 1808-1021) at 37°C for 5 minutes mixing at 1200 rpm. Light transmission of each well was determined using a 96-well plate reader (Sunrise Absorbance Reader, Tecan, cat. no. 30825) at 595 nm.

3.29 *In silico* target prediction

Initial target prediction for the human and mouse *WAS/Was* gene by miR-21 was performed using mirWalk 2.0[284], which combines twelve algorithms to identify putative miRNA binding sites within a selected region of a gene. The

miRWalk score indicates the number of algorithms that identified putative targeting for a specific gene. The 3'UTR was selected for analysis to screen for canonical miRNA-mRNA interaction. Predicted targets from this analysis were combined with genes that are annotated to be experimentally validated targets of miR-21, using the manually curated amiGO database.[285] Results are presented in **Supplemental table 5**. As the RNAhybrid platform[286] was found to identify putative interaction for miR-21, this was further analysed in detail. Interaction sites were searched within the entire 3'UTR of the *Was* gene using a minimum energy threshold of -20 kcal/mol.

3.30 Luciferase reporter assays

The 3'-UTR of the mouse Was gene was cloned into the XhoI and PmeI linkers of the dual-luciferase reporter vector psiCHECK-2 (Promega, cat. no. C8021; see **Figure 44A**). The following primer set was used:
WAS F: AGTCATCTTCCTTCCAGCAA;
WAS R: TCTCTGTATAGCCCTGGCTG.
The reporter constructs (200 ng) were transfected together with miR-21 mimic (5 nmol/L) or mimic control using Lipofectamine RNAiMAX as described in 3.2. Transfections were performed in quadruplicate into HEK293T cells, 12 hours after plating $2x10^5$ cells/well in twelve-well plates. After two days, cells were harvested in 200 µL Glo Lysis Buffer (Promega, cat. no. E2661) and the activities of both Renilla and firefly were measured. Each lysate (20 µl) was analysed using Dual-Glo Luciferase reagents (Promega, cat. no. E1910). First, Luciferase Reagent II was added to the lysate and luciferase activity was measured for 10 seconds. Then, Stop and Glo reagent was added to stop firefly luciferase activity and catalyse the Renilla firefly activity. Samples were incubated for 2 seconds and then Renilla activity was measured for 10 seconds. Firefly luciferase activity was normalised to constitutive Renilla luciferase activity for each well. Three independent experiments were performed.

3.31 Statistical analysis

MS data were quantified using normalised spectral counts. Qspec[287] was used to detect differential expression in the fibroblast secretome analysis.

Qspec utilizes a hierarchical Bayes estimation of generalised linear mixed effects model (GLMM) to share information across proteins, which increases the power to detect differential expression. The false discovery rate (FDR) was calculated using an Empirical Bayes method and FDR <5% was considered significant. All other statistical analyses were performed with Microsoft Excel (version 15.41) and GraphPad Prism (version 7.0d). Distribution of data was analysed using the Shapiro-Wilk normality test, where a p-value >0.05 was considered to indicate normal distribution. When at least one sample group within an experiment showed non-normal distribution, non-parametric tests were used for the analysis. To reduce the risk of type II statistical error in the context of the limited sample size, parametric tests were used to analyse the gene expression and immunoblotting data of the transfected CF and their secretome. For unpaired data, a t-test with Welch's correction or Mann-Whitney ranks test was performed for parametric and non-parametric distribution, respectively. For paired data, a paired t-test or Wilcoxon's matched-pairs signed ranks test were used, depending on the normality of data distribution. For comparison in more than one dimension, a two-way analysis of variance (ANOVA) was used, with *post-hoc* analysis of individual effects by Šidák's test. Time course data of the CF proliferation assay was analysed using the non-parametric Friedman test with *post-hoc* analysis of differences between each targeting and non-targeting transfection type using Dunn's multiple comparisons test. Comparison of gene expression and ECM protein abundance between miR-21 *null* or wild-type mice was performed using an FDR approach with the two-stage step-up method of Benjamini, Krieger and Yekutieli, with an FDR for significant discovery set to 5%. Relationships between the concentrations of plasma proteins and the relative quantities of miRNAs were investigated using Pearson correlations with p-value adjustment (producing q-values) using FDR adjustment according to Benjamini, Krieger and Yekutieli. Data are shown as mean ± standard error of the mean (SEM) unless stated otherwise. ANOVA results are shown as F ([degrees of freedom numerator],[degrees of freedom denominator]): [F distribution]. P-values or q-values <0.05 were considered significant, with * indicating $p<0.05$, ** $p<0.01$ and *** $p<0.001$.

CHAPTER IV

RESULTS

4.1 MiR-21 and cardiac fibroblasts

4.1.1 *In vitro* transfection of cardiac fibroblasts

Primary CFs were isolated from the ventricles of eight mouse hearts, followed by transfections with miR-21 mimic or inhibitor (LNA), as well as their respective controls.[185] To visualise adequate delivery, a fluorescently labelled oligonucleotide was transfected using similar reagents and conditions. After 24 hours, localisation of the labelled miRNA was observed by fluorescence microscopy, as shown in **Figure 10**. The transfected Cy3-labelled miRNA was visible outside the nuclei of the CFs, suggesting cytoplasmic localisation.

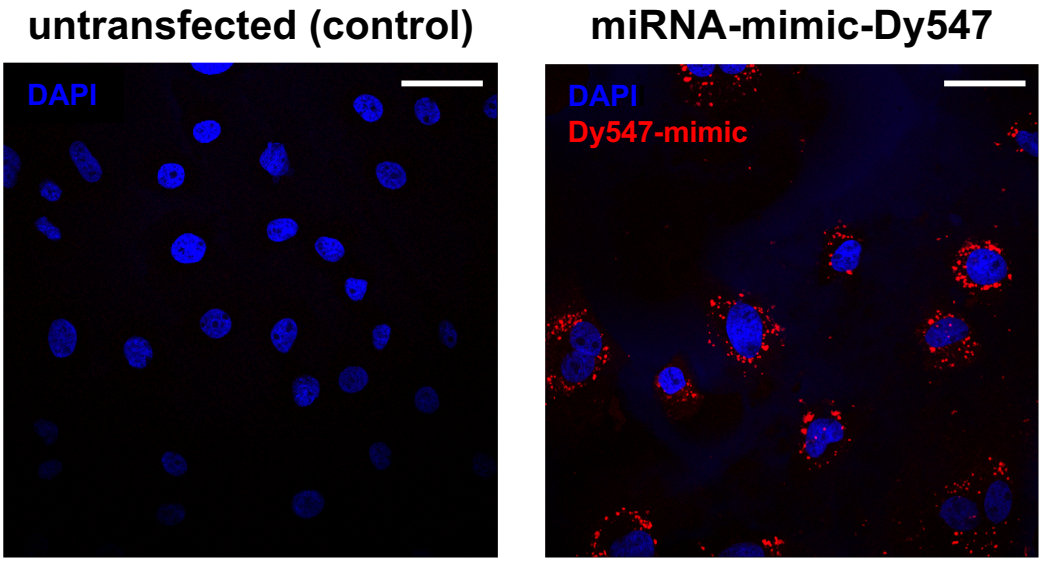

Figure 10. Transfection of cardiac fibroblasts. Isolated murine CFs were transfected with a microRNA labelled with red fluorescent dye (Dy547-mimic) to confirm transfection efficiency by microscopy. Nuclei were visualised by 4′,6-diamidino-2-phenylindole (DAPI) staining. Transfected cells displayed signal around the nuclei, indicating cytoplasmic localisation. Shown images are representative of the n=2 vs. 2 for this transfection. Scale bar denotes 50 µm.

4.1.2 Proliferation assay

Previous literature suggests that miR-21 may have an effect on CF apoptosis or survival. We therefore pursued an *in vitro* strategy to determine the effects of miR-21 mimic and inhibitor transfection on their proliferation rate. To analyse the effect of miR-21 manipulation, we used an electrical impedance-based assay (xCELLigence). This system measures the impedance of a low-voltage current between two gold electrodes in the well of an adapted cell culture plate, where the magnitude of impedance (represented as ‘cell index’) is dependent on cell number and size as well as their attachment.

Primary CFs were isolated from wild-type mice and transfected with miR-21 mimic or LNA-21 and their respective controls. The cell index was recorded every 30 minutes up to 25 hours and the slope was recorded between 4 and 15, 20 or 25 hours (see **Figure 11, panel A and B**). Normal distribution of these measurements was confirmed using a Shapiro-Wilk normality test ($p=0.29$ and 0.86 for miR-21 mimic and LNA-21, respectively). Two-way ANOVA analysis of the three slope recordings over time after miR-21 mimic transfections identified a significant effect of time ($F(2,12)=13.7$, $p=0.0008$), transfection type ($F(1,6)=63.0$, $p=0.0002$) and an interaction between these two variables ($F(2,12)=13.7$, $p=0.0008$). *Post-hoc* simple main effects analysis using Šidák's multiple comparisons test showed significantly higher slopes in miR-21 mimic-transfected cells compared to control transfections at 15 hours ($p<0.001$), 20 hours ($p<0.001$) and 25 hours ($p=0.0027$). Similar analysis in LNA-transfected cells identified a significant effect of time ($F(2,12)=15.4$, $p=0.0005$) but not for transfection type ($F(1,6)=3.4$, $p=0.11$). A significant interaction between both variables was observed ($F(2,12)=15.4$, $p=0.0005$), with main effects analysis showing significant difference in slope only at 15 hours ($p=0.0262$), but not at 20 hours ($p=0.21$) or 25 hours ($p=0.93$).

30-minute readings of cell index, normalised to background readings, are represented in **Figure 11, panel C and D**. Cell confluence was reached after 25 hours, limiting the ability to proliferate. Recordings beyond this point are therefore not included in the analysis. As the cell index data were not normally distributed, analysis of these readings was performed using the non-parametric Friedman test with subsequent comparisons between the respective transfection types using Dunn's multiple comparisons test. The Friedman test identified statistically significant differences across groups ($p<0.0001$) and subsequent comparison between control mimic and miR-21 mimic transfection and LNA-control and LNA-21 identified significant differences for both ($p=0.0095$ and $p<0.0001$, respectively). Visual inspection of both graphs highlights in both mimic and LNA transfections that the difference in proliferation rate is most pronounced between 15 and 20 hours,

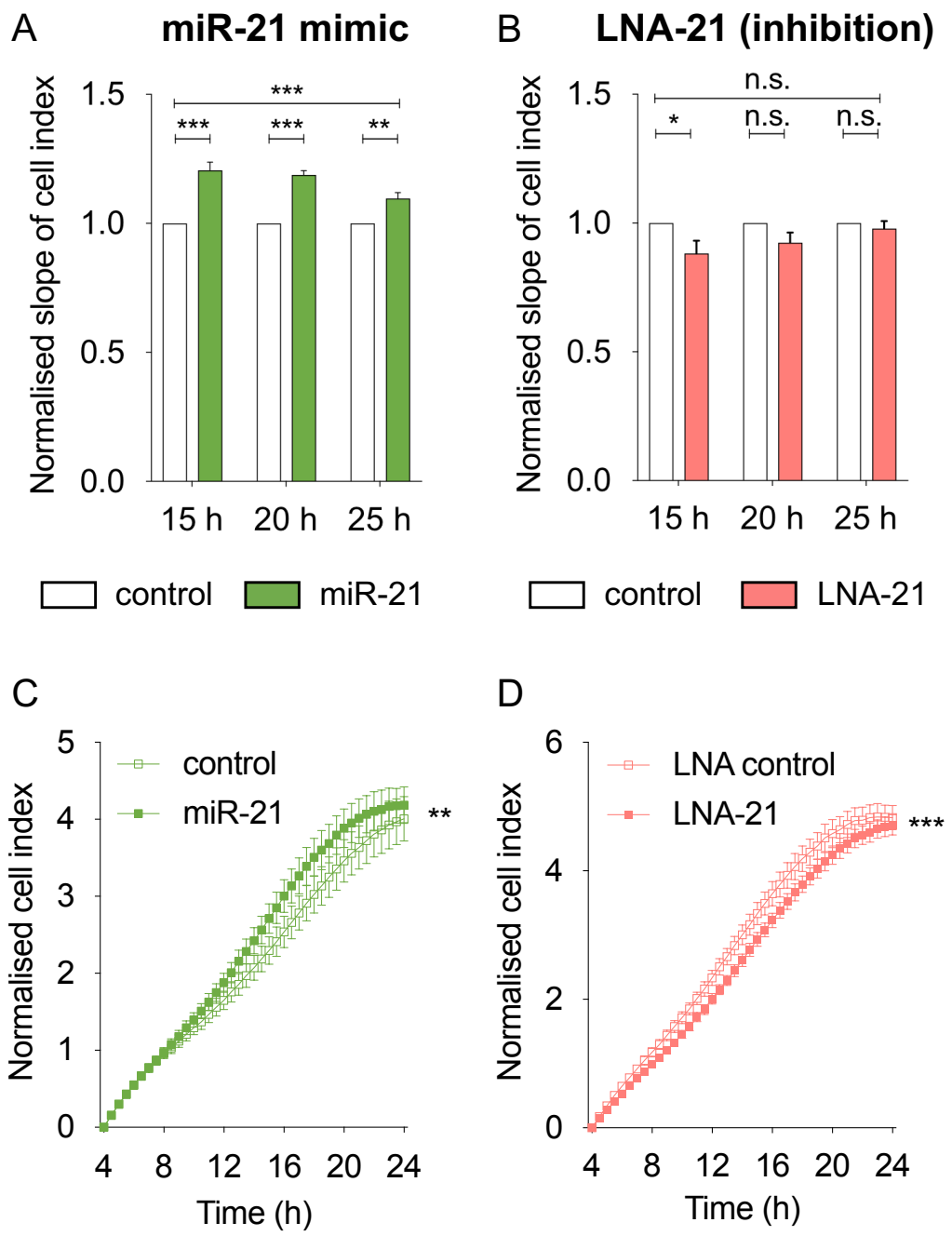

Figure 11. Cardiac fibroblast proliferation after transfections. Murine cardiac fibroblasts were transfected with miR-21 mimic or inhibitor (LNA-21) and plated in a impedance-based proliferation assay plate (xCELLigence) for 25 hours. This method records a cell index value that is considered a readout of cell number, size and attachment. The slope of the cell index over time, normalised to the slope of the control transfection for each biological replicate, is shown in **A** and **B** for miR-21 mimic and inhibitor, respectively. Two-way ANOVA and post-hoc testing for the slope during analysis over 15, 20 and 25 hours identified a significantly higher slope after miR-21 mimic transfection at all three time points, whilst miR-21 inhibitor showed a significantly reduced proliferation only after 15 hours. Normalised cell index readings over time, recorded each 30 minutes, showed significantly increased and reduced proliferation with miR-21 mimic and inhibitor transfection, respectively (**C** and **D**; Friedman test with *post-hoc* Dunn's multiple comparisons test). Four biological replicates were analysed for each condition.

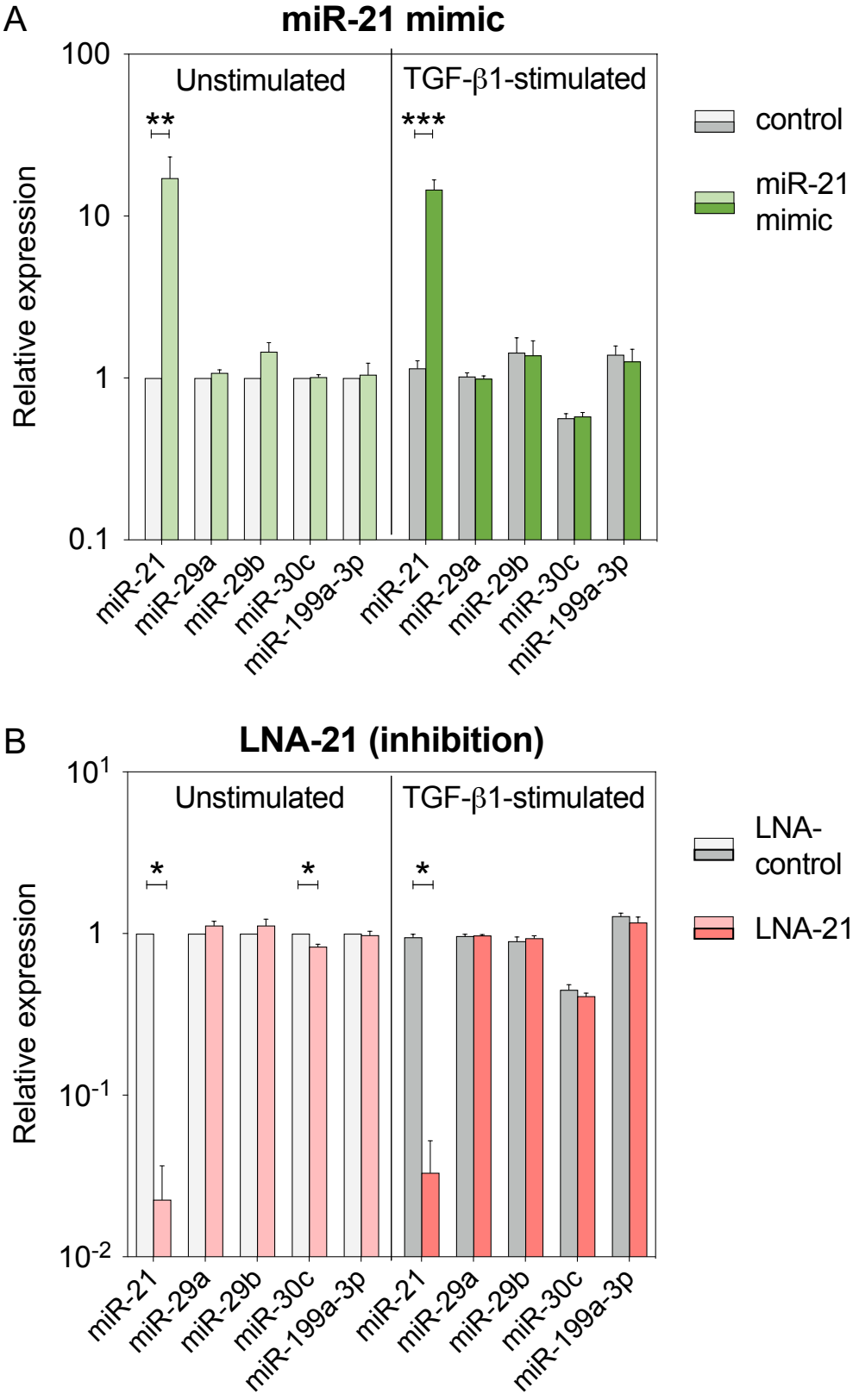

Figure 12. MicroRNA levels after cardiac fibroblast transfections. RNA was isolated from CFs, transfected with miR-21 mimic or control (**A**) and LNA-21 or LNA-control (**B**), and harvested 48 hours after TGF-β1 or vehicle control (unstimulated) treatment. MicroRNA levels were determined by qPCR, using *sno202* as a reference gene. Statistical analysis was performed using paired t-tests, n=4 for each condition.

as also identified by the analysis of the slope coefficients. As the slope decreases, differences in normalised cell indices between both groups decrease as well. In conclusion, these data indicate that miR-21 significantly increases the proliferation rate of CF *in vitro* within a 24-hour time period.

4.1.3 Validation of in vitro transfection and TGF-β1-treatment

To determine effects of miR-21 on CF gene expression and protein secretion, miR-21 mimic, inhibitor or their respective controls were transfected into CFs, followed by treatment with recombinant TGF-β1 or a vehicle control (see **Figure 6, panel A**). Four biological replicates were used for each condition. Cells and their conditioned media were harvested after 48 hours of incubation. At this time, TGF-β1-treated CFs appeared larger and more elongated, suggesting induction of a myofibroblast-like phenotype.

To determine the level of overexpression or knockdown after oligonucleotide transfection, miRNA levels were determined by qPCR in RNA isolated from CFs (see **Figure 12**). Transfection of miR-21 mimic resulted in increased expression levels compared to the control mimic (average paired fold change (FC) 17.2 and 12.8; paired t-test $p=0.003$ and $p<0.001$ for TGF-β1-untreated and treated cells, respectively), whilst inhibition of miR-21 by transfection of inhibitor (LNA-21) reduced the expression of miR-21 in comparison to transfection of a non-targeting LNA sequence (FC 0.02 and 0.03; $p=0.042$ and $p=0.036$). Levels of other fibroblast miRNAs did not show major differences between miR-21 overexpression or inhibition and their respective controls.

In addition to the observed phenotypical changes upon TGF-β1 treatment, several gene expression changes indicated the induction of a myofibroblast-like phenotype. At the transcriptional level, significant induction of miR-199a-3p could be observed (FC 1.34; $p=0.004$), whereas a marked reduction was found for expression levels of miR-30c (FC 0.51; $p<0.0001$). Levels of miR-21 were not significantly different between TGF-β1-treated and -untreated cells after control transfection (FC 1.05; $p=0.59$). Increased transcript levels were observed for genes commonly used as markers of the

myofibroblast-like phenotype (see **Figure 13**), such as α-SMA (Acta2; FC 1.62; paired t-test p=0.005) and periostin (Postn; FC 3.20; p=0.014), as well as for the TGF-β signalling marker CTGF (FC 1.32; p=0.026) and for the gene transcript of TGF-β1 itself (FC 1.23; p=0.017).[288,289] Conversely, transcript levels of the *Igfbp4* gene, coding for insulin-like growth factor-binding protein 4 (IBP4), were markedly lower in TGF-β1-treated cells (FC 0.25; p<0.0001). This downstream effect of TGF-β1 was previously reported in periosteal connective tissue.[290] Gene expression for interleukin-11 was assessed in light of the recent identification as a downstream mediator of TGF-β signalling (see section **1.1.3.2**); its expression levels in presence and absence of TGF-β1 treatment remained below the limit of detection (average C_q 35).

4.1.4 Differential regulation of proteins following transfection

To determine effects of miR-21 on production of ECM proteins, the conditioned media of CFs were collected 48h after transfections, as mentioned before. Secreted proteins were prepared for analysis by mass spectrometry (see **Figure 6, panel B**). Overall, 144 ECM proteins were identified (see **Supplemental table 1**). Amongst the most abundantly secreted proteins were collagen I and III, fibronectin and fibulin-2, all common core constituents of the extracellular matrix.[8] In line with the previously described induction of periostin gene expression, markedly higher spectral counts were identified in the conditioned media of TGF-β1-treated cells compared to control-treated cells for this protein after normalisation to total spectral counts (**Figure 14**). Strikingly, in comparison to previous analysis of murine CF secretome changes upon mimic or inhibitor transfection for a different miRNA[185], there were relatively few differences after transfection of miR-21 mimic or LNA-21 (see **Figure 15**). This apparent lack of miR-21 effects on ECM secretion was observed in both TGF-β1-stimulated and –unstimulated cells.

Upon miR-21 mimic transfection, granulin (GRN; log2 FC 1.08; FDR=0.0003) and IBP4 (log2 FC 1.25; FDR<0.001) were more abundant in media from unstimulated CF (see **Figure 15 and 16**). In TGF-β1-stimulated CFs, granulin showed an increased abundance as well (log2 FC 0.89; FDR<0.0001), yet with a less than two-fold change. Similarly, cathepsin L1

(CATL1; log2 FC 0.59; FDR=0.0106) and the α1 chain of collagen XI (COBA1; log2 FC 0.44; FDR=0.0240) increased significantly but less than two-fold.

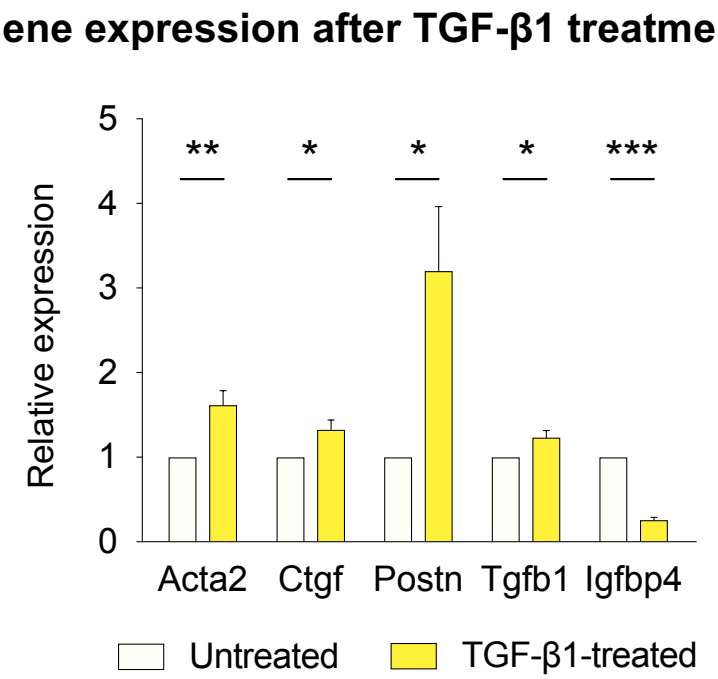

Figure 13. Gene expression after TGF-β1 treatment. In RNA isolated from CFs, gene expression levels for several markers of TGF-β signalling and a myofibroblast-like phenotype were significantly induced. *Ppia* was used as reference gene transcript. Analysis by paired t-tests, n=8 for each treatment type.

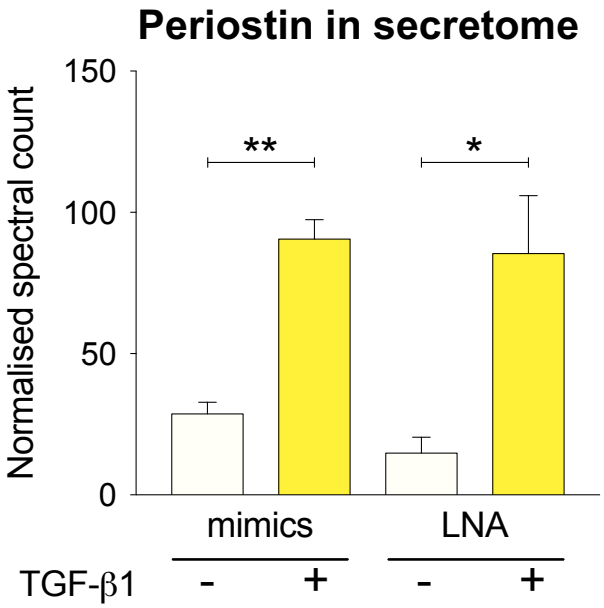

Figure 14. Periostin levels in the fibroblast secretome after TGF-β1 treatment. Mass spectrometric analysis of periostin showed markedly higher levels after TGF-β1 treatment. Spectral counts were normalised to the total spectral count for each sample. Analysis by Wilcoxon matched-pairs signed ranks test, n=8 per condition.

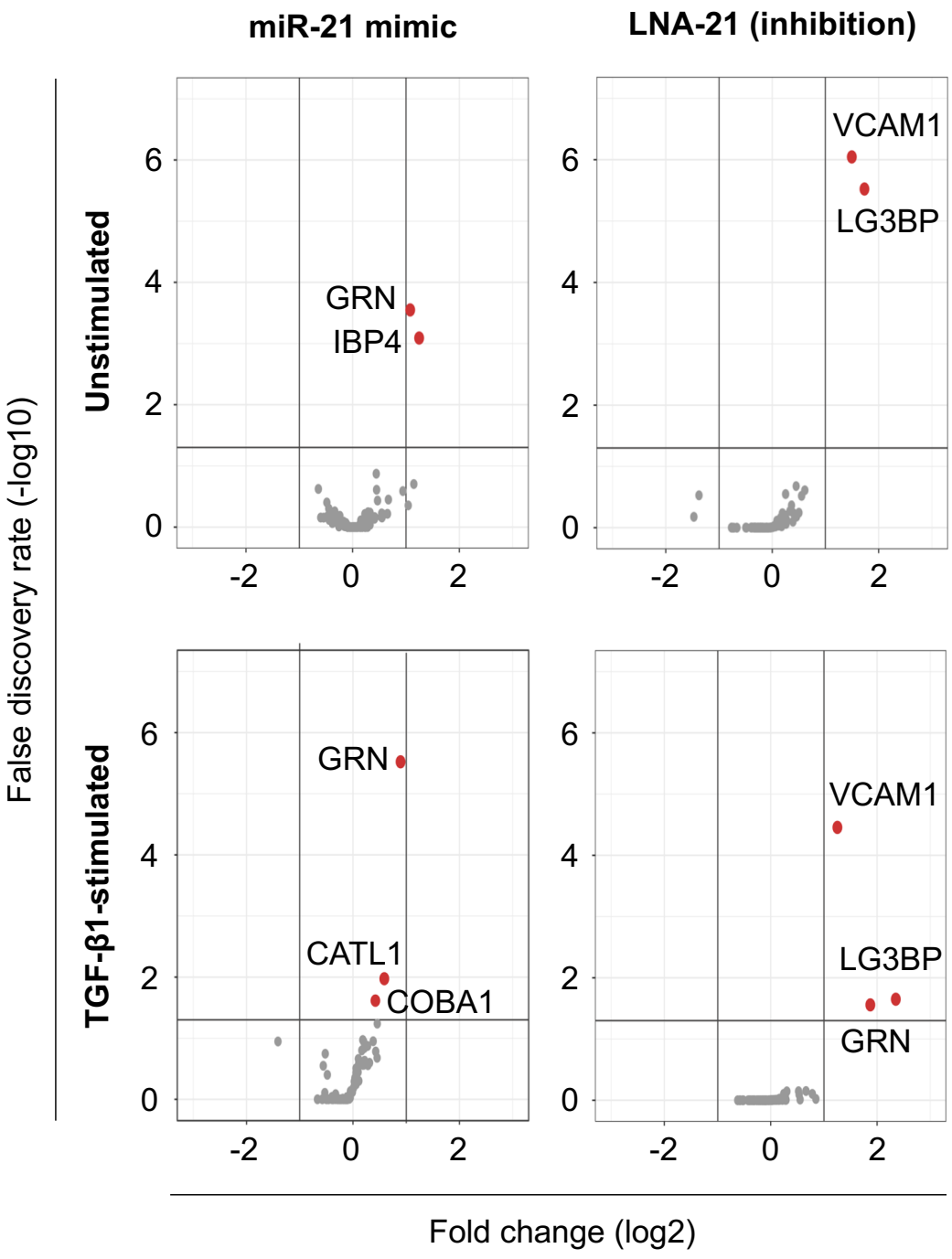

Figure 15. Murine cardiac fibroblast secretome after miR-21 transfections. Volcano plots show proteins identified in the secretome of unstimulated and TGF-β1-stimulated cells after transfection of miR-21 mimic or LNA-21 (miR-21 inhibitor). Fold changes constitute the ratios after miR-21 overexpression or inhibition compared with a corresponding control transfection. FDR was calculated using an Empirical Bayes method and an FDR< 0.05 was considered significant; n=4 for each comparison. GRN, granulin; IBP4, insulin-like growth factor-binding protein 4; VCAM1, vascular cell adhesion molecule-1; LG3BP, galectin-3 binding protein; CATL1, cathepsin L1; COBA1, collagen XI, α1 chain.

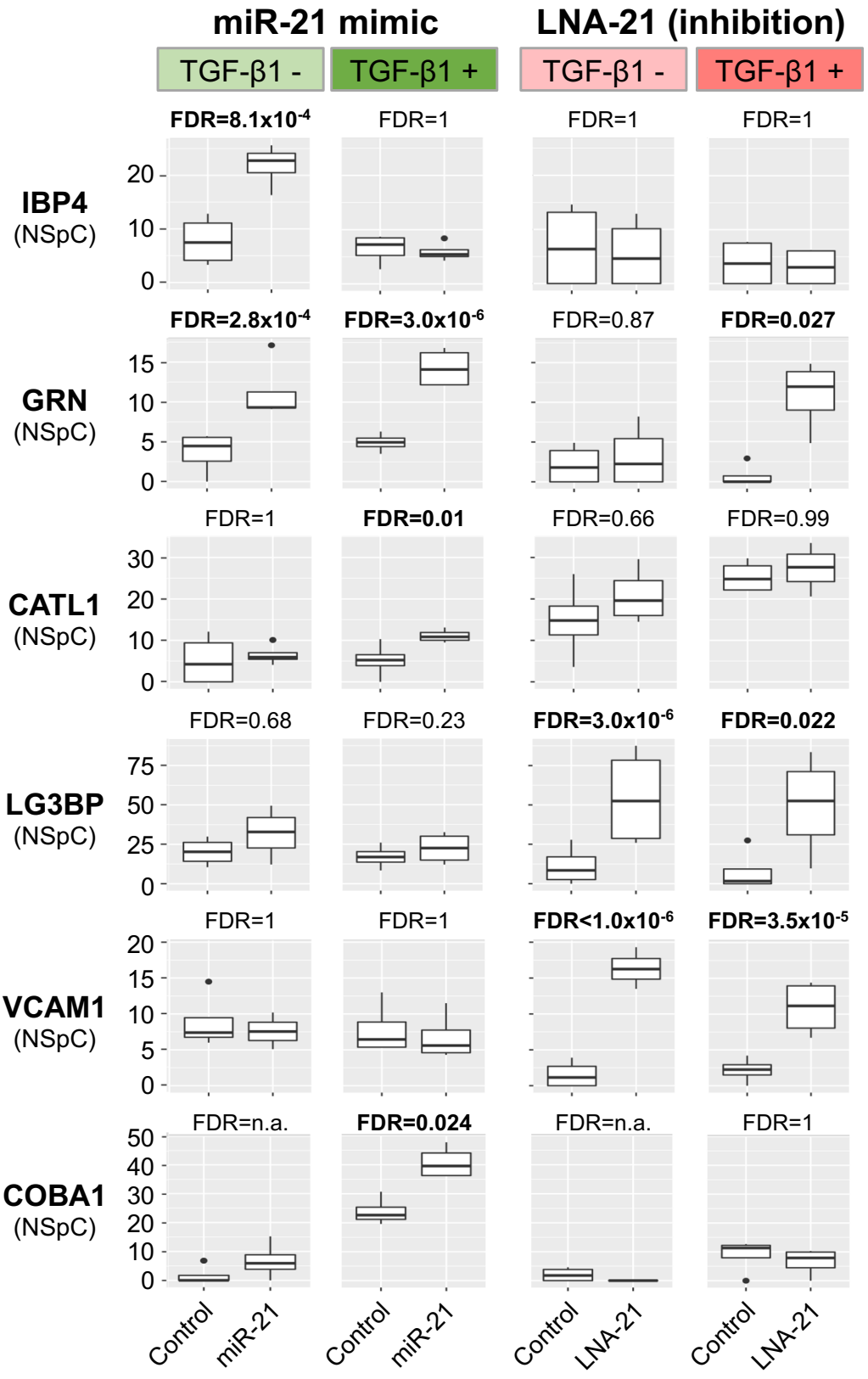

Figure 16. Differentially expressed proteins in the cardiac fibroblast secretome after miR-21 overexpression or inhibition. Box plots are shown for proteins that were identified as differentially regulated in at least one of the studied conditions. The Y-axis represents the normalised spectral count (NSpC). The false discovery rate (FDR) was calculated using an Empirical Bayes method, with an FDR <0.05 considered statistically significant; n=4 for each condition. TGF-β1 - and + corresponds with unstimulated and TGF-β1-stimulated cells, respectively.

Upon miR-21 inhibition, two consistently affected proteins were vascular cell adhesion molecule-1 (VCAM1) and galectin-3 binding protein (LG3BP), both increased by more than two-fold in the secretome of unstimulated (VCAM1: log2 FC 1.50; FDR<0.0001; LG3BP: log2 FC 1.73; FDR<0.0001) and TGF-β-stimulated CFs (VCAM: log2 FC 1.25; FDR<0.0001; LG3BP: log2 FC 1.73; FDR<0.0001). There was no detectable change for these proteins upon miR-21 mimic transfection. Conversely, granulin abundance was increased in the secretome of TGF-β1-stimulated CFs after miR-21 inhibitor transfection, in a

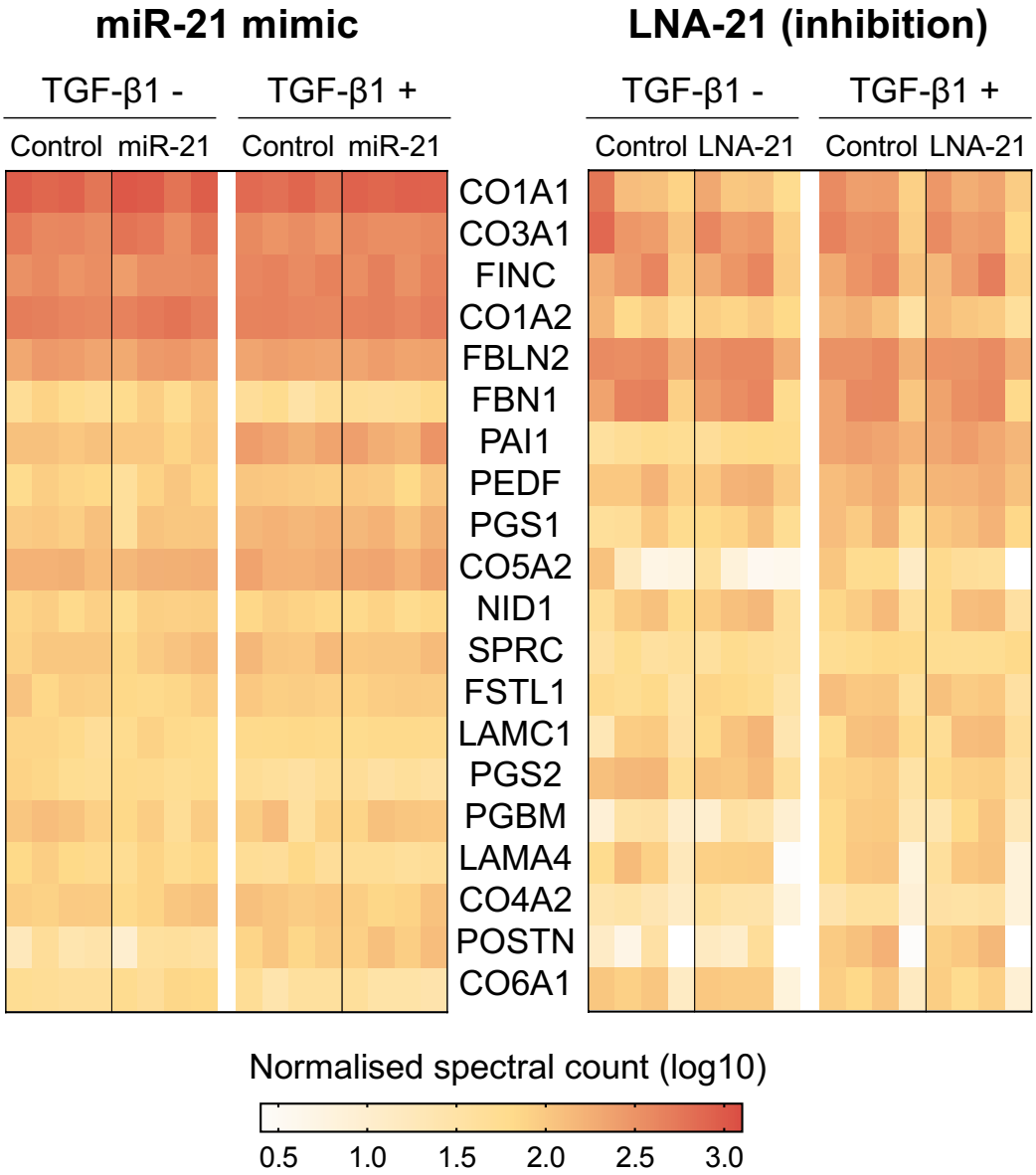

Figure 17. Twenty most abundant proteins in the cardiac fibroblast secretome. Mass spectrometric identification of proteins in the conditioned media showed major overlap with other studies using a similar approach. Interestingly, no differences were observed between miR-21 overexpression or inhibition and their respective controls (four biological replicates for each condition). This was equally the case in TGF-β1-unstimulated (TGF-β1 -) and -stimulated (TGF-β1 +) cells. See Supplemental table 1 for abbreviations and for a list of identified proteins.

similar direction as for miR-21 mimic transfection (log2 FC: 1.87; FDR<0.0001).

Consistent with previous analyses in our own group as well as by others[185,291], the most abundant proteins that were detected across the different samples included several subtypes of collagens, with collagen I and III having the highest average spectral counts, as well as fibronectin. In addition, as shown in **Figure 17**, several proteins associated with crosslinking these core proteins were also highly abundant amongst the identified spectra. These included several basement membrane proteins such as collagen type IV, laminin and perlecan (PGBM/Hspg2). Strikingly, no significant difference was observed for any of these proteins after miR-21 overexpression or inhibition.

In conclusion, miR-21 mimic and inhibitor transfections in murine CF resulted in increased secretion of IBP4 and granulin, and LG3BP, VCAM1 and granulin respectively. These transfections did not significantly alter the secretion of major extracellular matrix proteins.

4.1.5 Validation of proteomics data by immunoblotting

To assess differences in protein abundance in the CF secretome using an additional technique, immunoblotting was performed with concentrated and deglycosylated conditioned medium samples. Analysing four different proteins showed stable detection across all samples, with most striking differences appearing between TGF-β1-treated and -untreated samples (see **Figure 18**). Densitometry was performed to evaluate relative differences in intensity on the blots (see **Figure 19**).

Consistent with our gene expression and proteomics data, increased periostin secretion in response to TGF-β1 treatment was also observed using immunoblotting of concentrated conditioned media (FC: 4.51 and 10.26; p=0.0004 and p<0.0001 for mimic- and LNA-transfected samples, respectively). A similar increase was observed for the small leucine-rich repeat proteoglycan biglycan (Bgn/PGS1; FC: 3.46 and 6.96; p=0.0020 and 0.0015), which has previously been reported[292], whilst no significant effect was

observed for basement membrane protein laminin γ1 (Lamc1; FC: 0.80 and 0.97; p=0.11 and 0.55) or another small leucine-rich repeat proteoglycan, decorin (Dcn/PGS2; FC: 1.13 and 0.89; p=0.38 and 0.11).

In line with our proteomics findings, immunoblotting did not show major changes in protein levels after miR-21 mimic or inhibitor transfections in the secretome of either TGF-β1-treated and -untreated cells. Whilst the γ1 chain of laminin showed a significant increase after miR-21 overexpression in untreated CF (FC: 1.70; p=0.0500), this was not seen after TGF-β1 stimulation (FC: 0.91; p=0.32). Furthermore, miR-21 inhibition, both in TGF-β1-untreated and -treated cells, did not show an opposite effect for this protein (FC: 1.36 and 1.22; p=0.15 and 0.14, respectively), suggesting non-specific changes. No significant changes were seen for any of the other analysed proteins. Altogether, these results indicate a marked effect of TGF-β1 on the induction of a myofibroblast-like phenotype but no modulation by either the miR-21 mimic or miR-21 inhibitor transfection.

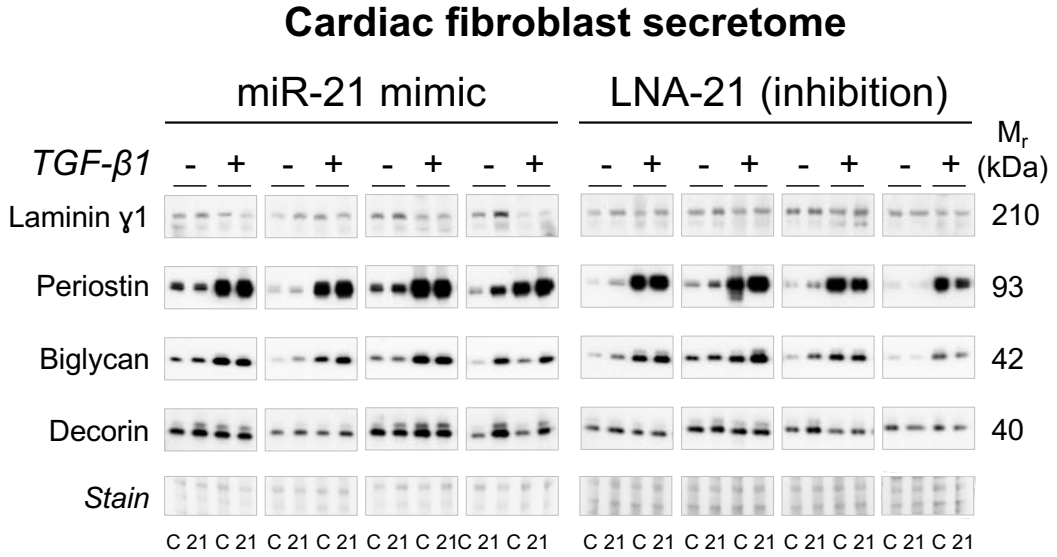

Figure 18. Immunoblots of cardiac fibroblast secretome after transfections. Immunoblotting was performed with concentrated and deglycosylated conditioned media for several ECM proteins. Concomitant Ponceau S stain is shown at the bottom. Four biological replicates were analysed for each condition. C = control mimic / LNA; 21 = miR-21 mimic / LNA-21. TGF-β1 + / - indicates treatment 48 hours prior to conditioned media collection. M_r, relative mass.

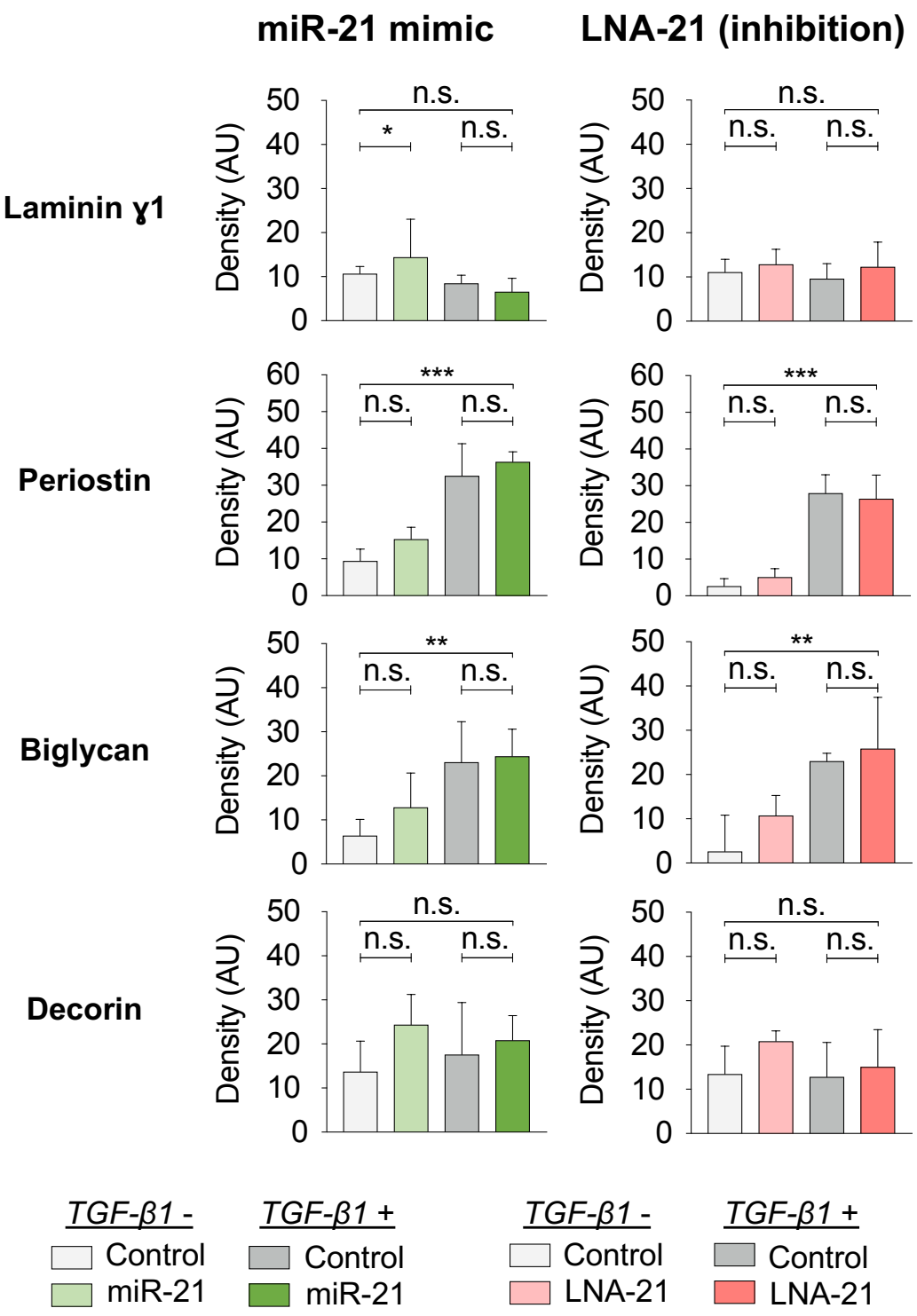

Figure 19. Densitometry of cardiac fibroblast secretome immunoblots. Relative differences in optical density were determined in the immunoblot analysis of the fibroblast secretome. Whereas a marked effect of TGF-β1 treatment was seen for periostin and biglycan, no significant differences were found between miR-21/LNA-21 and their respective controls. Statistical analysis was performed using paired t-tests, with n=4 for transfection comparisons and n=8 for effects of TGF-β1 treatment. TGF-β1 + / - indicates treatment 48 hours prior to conditioned media collection. AU, artificial units; n.s., not significant.

4.1.6 Differential expression of genes after transfections

MiRNAs can repress the expression of genes by direct targeting, leading to either translational repression or degradation of mRNA strands (see **Figure 2**).[93] Our previously mentioned study, also using miRNA transfections in CF, showed a marked effect on gene expression levels of several ECM proteins upon miR-29 overexpression.[185] To validate the findings of our current secretome analysis, we studied corresponding gene expression of the most abundantly secreted proteins, as well as those that showed differential regulation in the conditioned media upon transfection.

In general, a similar pattern was seen for gene expression changes as was observed for protein abundance: there were profound effects of TGF-β1 treatment, but few changes with miR-21 overexpression or inhibition. Induction of α-SMA, periostin, CTGF and TGF-β1 expression by TGF-β1 treatment have been described earlier in this chapter (**Figure 13**). To determine expression levels of genes encoding proteins that significantly changed in the secretome analysis after miR-21 manipulation, further qPCR analysis was performed. Resulting fold changes of gene expression levels are shown in the context of protein changes in **Figure 20**. The largest fold change was observed for the expression level of LG3BP (*Lgals3bp*) after LNA-21 transfection, both in TGF-β1-treated and –untreated cells, in line with the proteomics analysis (FC: 2.63 and 2.64; p=0.0091 and 0.0033, respectively). Concomitant reduction of *Lgals3bp* expression after miR-21 mimic transfections however failed to reach statistical significance (FC: 0.92 and 0.85; p=0.52 and 0.35). A similar pattern was seen for expression of granulin, significantly decreasing after miR-21 overexpression in TGF-β1-treated cells (*Grn*; FC: 0.86; p=0.0247), whereas the concomitant upregulation fell short of statistical significance (FC: 1.29 and 1.18; p=0.20 and 0.21). Expression of cathepsin L1 showed a minor but significant induction after miR-21 inhibition in TGF-β1-treated cells (FC: 1.11; p=0.0191), in contrast with the proteomics analysis where significantly higher protein levels of cathepsin L1 were seen after miR-21 mimic transfection.

In addition to genes encoding differentially regulated proteins, we also performed qPCR analysis for expression levels of the twenty most abundantly identified proteins, comprising a panel of key ECM constituents (see **Figure**

21). In general, greater effects were observed with miR-21 mimic transfections than with LNA-21. Of these, the most striking induction was seen for periostin after miR-21 overexpression in both stimulated and unstimulated cells (FC: 4.86 and 5.60; $p<0.0001$ and $p<0.0001$). Expression after LNA-21 transfection was not affected. The α1 chain of collagen I (*Col1a1*; FC: 1.27 and 1.51; p=0.0.0150 and 0.0015), the α2 chain of collagen V (*Col5a2*; FC: 1.57 and 1.68; p=0.0058 and 0.0005), fibronectin (*Fn1*; FC: 1.24 and 1.43; p=0.0448 and 0.0013) and fibrillin-1 (*Fbn1*; FC: 1.22 and 1.32; p=0.0219 and 0.0036) all showed expression changes in a similar direction, yet to a lesser extent. No corresponding reduction was seen for their expression levels after miR-21 inhibition. The greatest decrease after miR-21 mimic transfection was observed for decorin (*Dcn*; FC: 0.53 and 0.48; $p<0.0001$ and p=0.0011) and biglycan (*Bgn*; FC: 0.81 and 0.85; p=0.0199 and 0.0122), with no concomitant induction after miR-21 inhibition.

In summary, gene expression in CF showed major changes upon treatment with TGF-β1. Overexpression of miR-21 induced expression for a number of ECM genes, whilst the effect on periostin was most striking. These changes did not result in a concomitant change of protein levels as analysed in the CF secretome. No major effect on gene expression was seen after miR-21 inhibition.

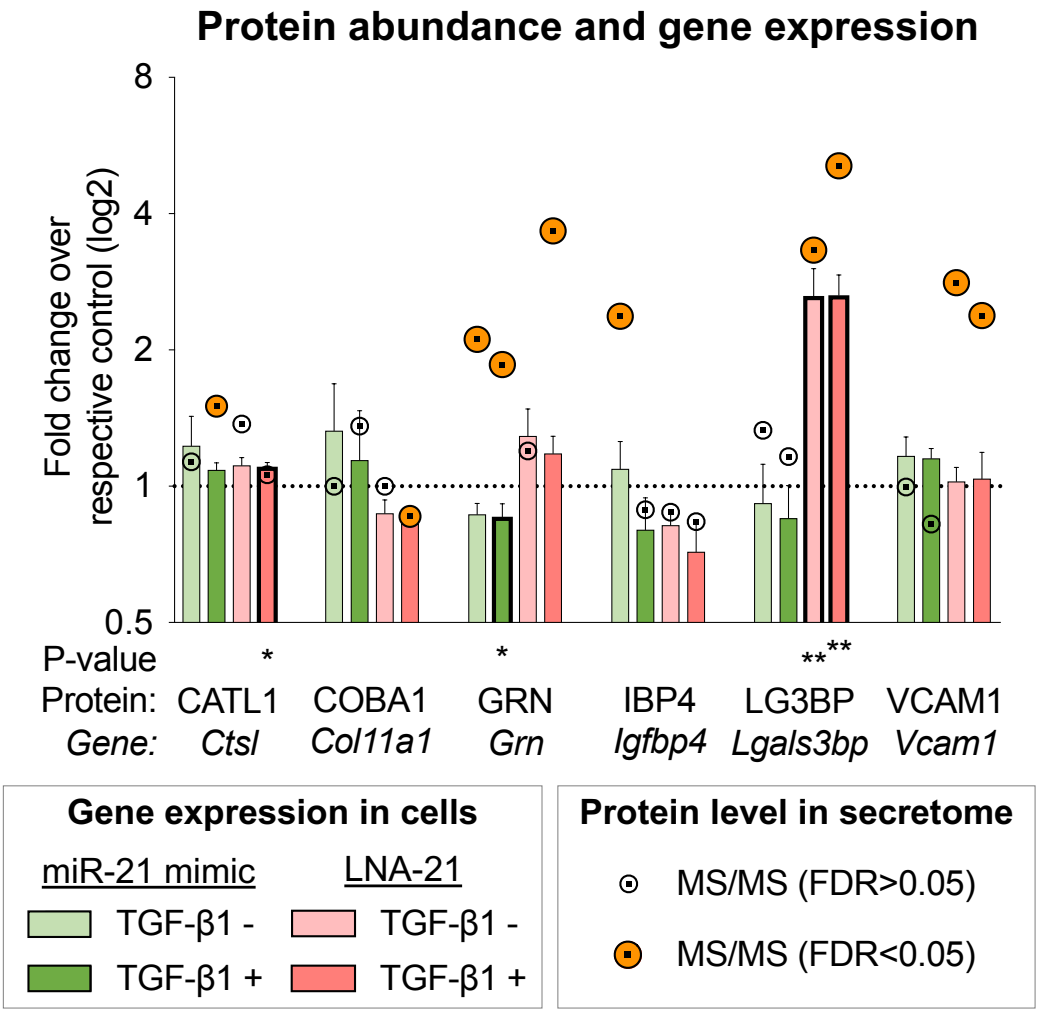

Figure 20. Fibroblast gene expression changes after transfection and their corresponding secretome protein levels. Fibroblast expression was determined for genes encoding proteins that showed a significant change in the secretome analysis. Gene expression levels (bars) represent paired fold changes over the respective controls as analysed in the lysed fibroblasts, using *Ppia* as the reference gene transcript. Four biological replicates were analysed for each condition. Asterisk below bars denote p-values for the comparisons with the respective controls, with * <0.05 and ** <0.01. Protein levels (nodes) indicate fold changes over respective controls as determined by mass spectrometric analysis of the fibroblast secretome after transfection. An FDR<0.05 is indicated by an orange-coloured node.

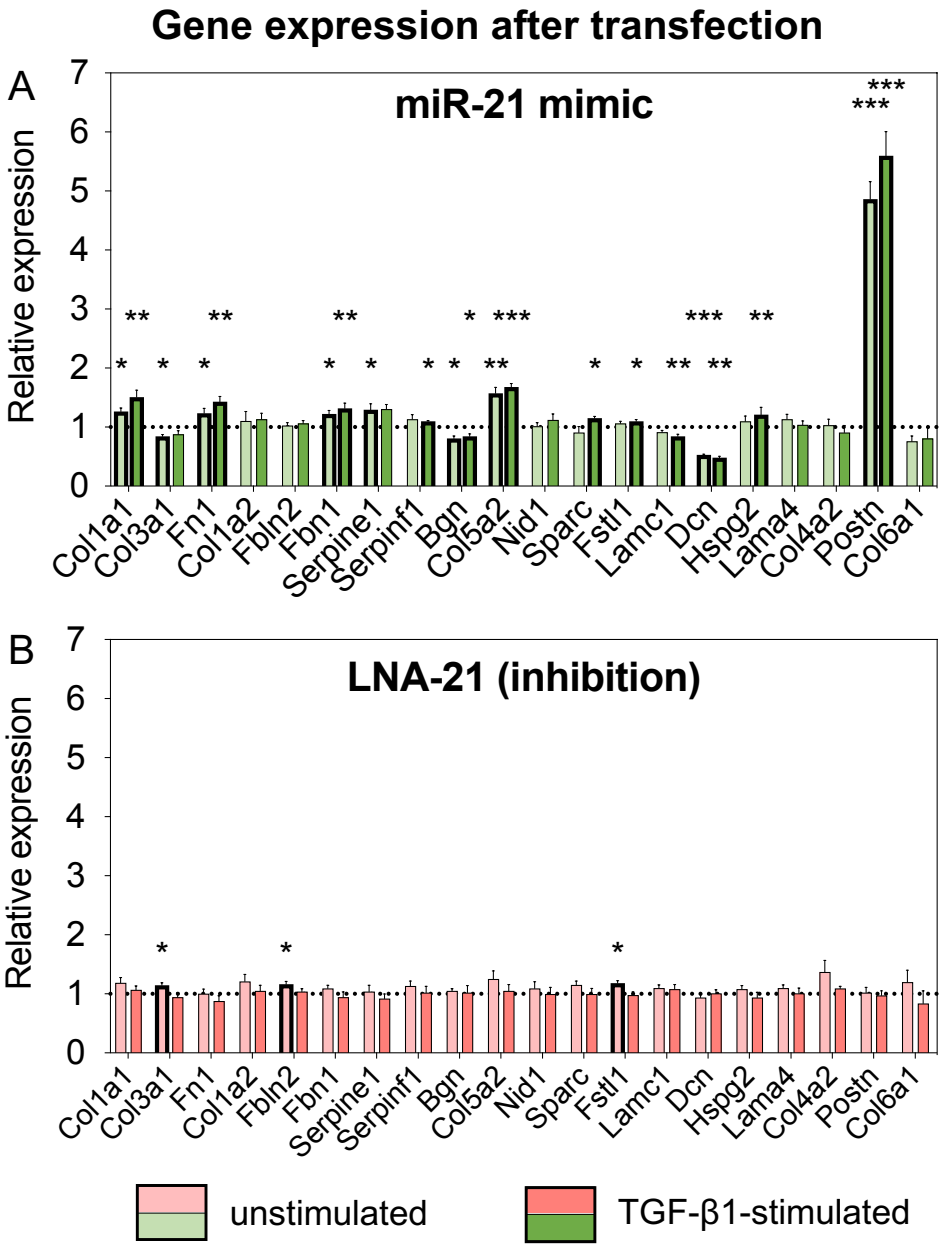

Figure 21. Gene expression after miR-21 transfections in cardiac fibroblasts. Gene expression levels in CFs were determined by qPCR to evaluate effects of miR-21 overexpression (**A**) or inhibition (**B**). Gene transcripts corresponding to the twenty most abundantly detected proteins in the secretome were assessed. Expression is represented as the fold change between miR-21 mimic and control mimic transfection (**A**), or between LNA-21 and LNA-control transfection (**B**). The analysis was performed separately for TGF-β1-untreated and -treated cells. *Ppia* was used as reference gene transcript. Statistical analysis was performed using a paired t-test, n=4 for each condition.

4.1.7 Cardiac extracellular matrix in miR-21 *null* mice

As described in previous paragraphs, pharmacological manipulation of CF *in vitro* showed an effect on their proliferation but did not result in any major effects on ECM protein secretion, as would be expected based on previous *in vivo* studies on miR-21 and on our own previous work using this approach for other miRNAs associated with fibrosis. Therefore, we aimed to further study the effects of miR-21 ablation on the cardiac ECM using miR-21 *null* hearts (see **Figure 22**), collected from six miR-21 *null* mice and six wild-type littermates. To determine whether there was an effect on miRNA and gene expression in these hearts, RNA was isolated from the apex and analysed by RT-qPCR. Furthermore, to evaluate changes in the composition of the ECM in these hearts, we performed mass spectrometry analysis of ECM proteins extracted using our 3-step method that has been developed for this purpose.[8,293,294]

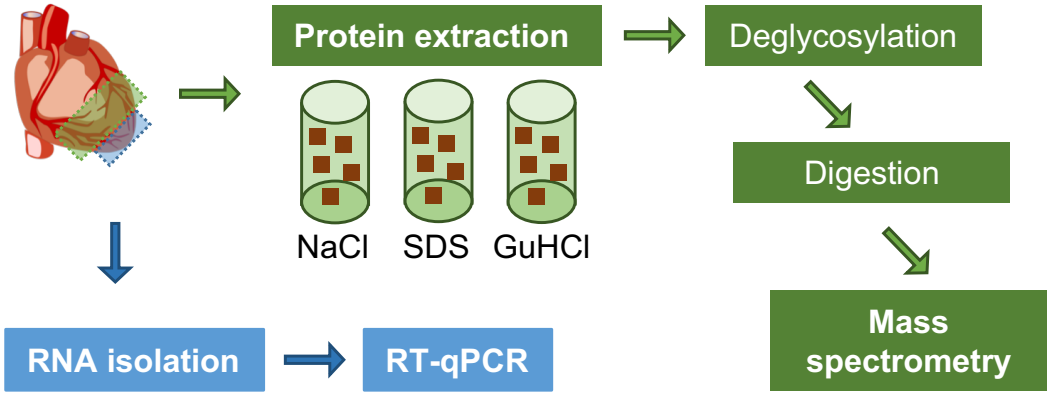

Figure 22. MicroRNAs, gene expression and the cardiac ECM in miR-21 *null* mice. Hearts were dissected for RNA isolation and subsequent RT-qPCR analysis for gene and miRNA expression. For three-step ECM protein enrichment, another tissue piece from the ventricles was dissected, followed by sequential incubation in sodium chloride (NaCl), sodium dodecyl sulphate (SDS) and guanidine hydrochloride (GuHCl) buffers. Isolated proteins were then deglycosylated, digested and analysed by mass spectrometry.

As shown in **Figure 23 (panel A)**, several abundant miRNAs were analysed. Whilst absence of miR-21 was confirmed, none of the other analysed miRNAs were significantly dysregulated when compared to wild-type hearts. To evaluate potential changes in expression of genes that were studied in the CF analysis, we performed qPCR analysis for the twenty most abundantly secreted proteins in the CF secretome. In addition, genes coding

for the proteins that showed a significant change in any of the transfection conditions were assessed. To account for multiple testing, an FDR approach was used to determine statistical significance of differences in gene expression, with the Q set to 5% (see **Supplemental table 2**). Fold changes across proteins were limited, with the greatest changes observed for the α4 chain of laminin (*Lama4*; FC: 1.14; q=0.1100) and for secreted protein acidic and rich in cysteine (*Sparc*; FC: 1.27; q=0.2983). However, none of the comparisons yielded a significant result.

To determine changes at protein level, analysis of the cardiac ECM was performed. In brief, ventricular tissue was sequentially incubated in 0.5M NaCl buffer, 0.1% SDS buffer and 4M GuHCl buffer. Proteins in the NaCl and GuHCl fractions were then deglycosylated, followed by analysis by LC-MS/MS. Identified proteins were annotated using the Matrisome database for murine ECM proteins.[269] In total, twenty-three and thirty-two proteins showed consistent detection across samples in the NaCl and GuHCl extracts, respectively (see **Figure 23, panel B**). Of these fifty-five proteins, significant overlap was seen with the twenty most highly identified proteins secreted by CF *in vitro*, as described earlier in this chapter. To determine differences between wild-type and miR-21 *null* extracts, a similar FDR approach was used as for the gene expression analysis. No significant protein changes were observed for the fifty-five analysed proteins (see **Supplemental table 3**).

In summary, combined analysis of gene expression and the ECM of the miR-21 *null* heart did not reveal significant changes. These findings are in line with previous findings that reported no phenotypical or functional differences in miR-21$^{-/-}$ mice without presence of tissue damage or a systemic effect otherwise.

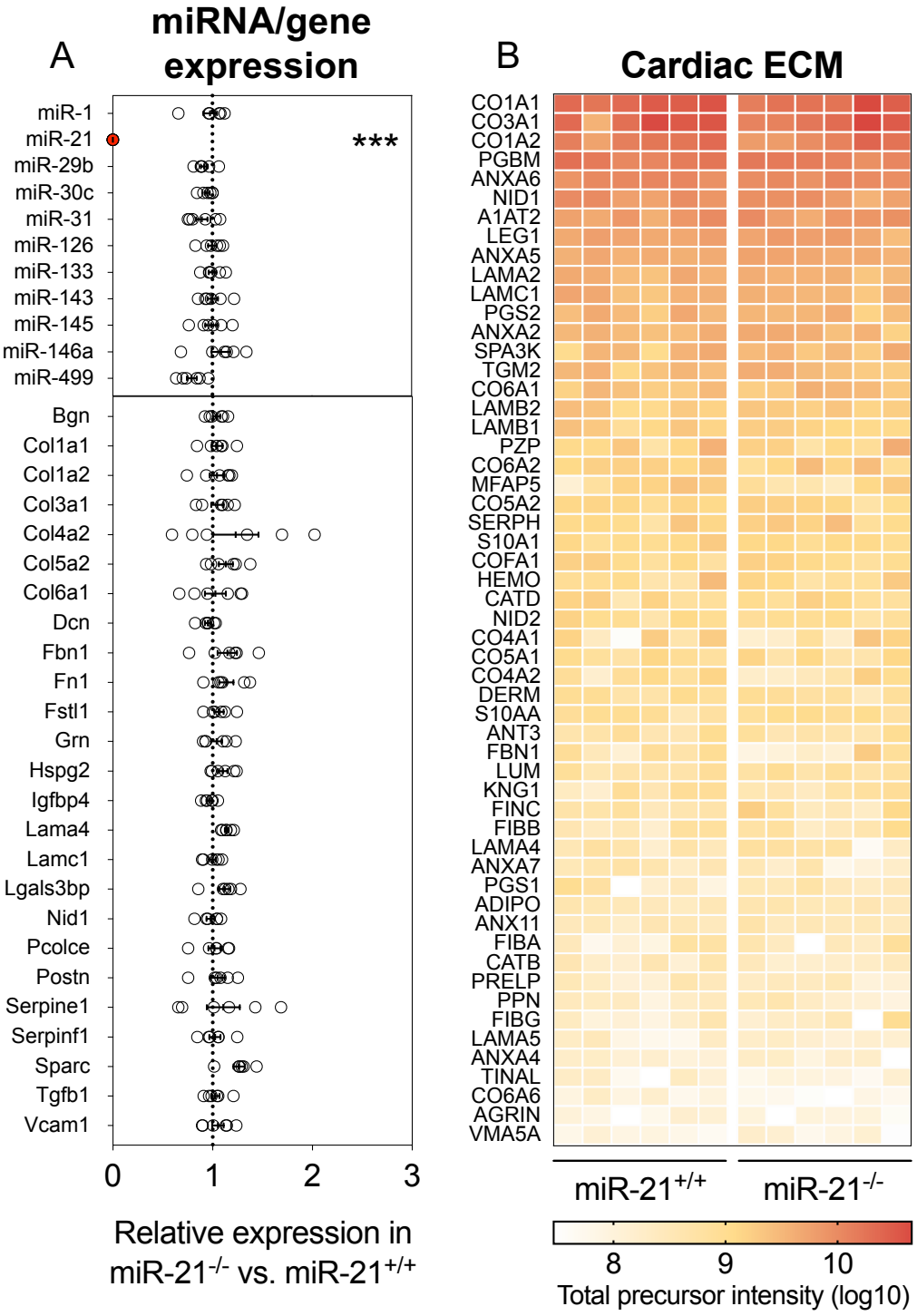

Figure 23. Comparison of microRNA and gene expression and ECM protein abundance in miR-21 *null* hearts. A: MiR-21 levels were undetectable in the heart, whilst other cardiac miRNAs did not show a significant difference in expression. Similarly, expression of selected genes based on CF transfection experiments were unaltered. *U6* and *Actb* were used as reference transcripts, respectively. **B:** Levels of fifty-five ECM proteins identified in the NaCl and GuHCl buffer extracts were not significantly different between hearts from miR-21 *null* mice and littermate controls. There was marked overlap in identified proteins when compared with the CF secretome analysis. An FDR-based approach was used for all three analyses with $q<0.05$ deemed statistically significant. n=6 vs. 6 for both genotypes in both analyses. See **Supplemental table 2 and 3** for abbreviations.

4.2 Circulating miR-21 and associated proteins in the Bruneck study

Given the results of previous publications and our own analysis in CF, we proceeded to evaluate potential indirect effects of miR-21 in the context of cardiac fibrosis. MiR-21 is ubiquitously expressed across tissues and abundant in the circulation. Furthermore, as discussed in the introduction, previous studies of miR-21 consistently show that there is a pronounced effect of miR-21 manipulation only in a context of injury, where systemic effects are likely to be at play. Therefore, we hypothesised that there are potential indirect effects that may affect the outcome of pharmacological inhibition of miR-21. Several past studies in our group have assessed circulating miRNAs in samples from the Bruneck study. To investigate potential systemic effects of miR-21, additional analyses were performed in the Bruneck 2000 follow-up and new samples were collected during the 2015 evaluation to facilitate the study of miR-21 in the circulation.

4.2.1 Plasma proteome screening for correlation with miR-21

We first analysed correlations of miR-21 with circulating proteins previously associated with CVD and inflammation. In plasma samples from the Bruneck study year 2000 follow-up (n=660), levels of miR-21 were measured by qPCR, whilst proteins were analysed using a combination of predefined PEA panels, LC-MS/MS and ELISA (for PF4 and PPBP).

Of the PEA panels, 132 proteins were in the stable detection range. When combined with measurements of the mass spectrometry-based PlasmaDive panel, a total of 229 proteins were quantified across the cohort. A graphical representation of the individual correlation coefficient and their statistical significance is shown in **Figure 24**, with proteins of potential interest highlighted. Interestingly, there was remarkable correlation between levels of miR-21 and two markers of platelet activation, PF4 (Pearson *r*: 0.73, $q=3.0x10^{-109}$) and PPBP (Pearson *r*: 0.69, $q=4.3x10^{-94}$). Furthermore, the correlating proteins included several pro-fibrotic factors: high levels of correlation with miR-21 were found for the β unit of platelet-derived growth factor (PDGFβ; Pearson *r*: 0.73, $q=1.0x10^{-110}$) and epidermal growth factor (EGF; *r*: 0.72,

q=2.2x10^{-104}). A striking correlation with miR-21 was also seen for the LAP of TGF-β1 (LAP-TGF-β1; *r*: 0.65, q=2.4x10^{-79}), as well as other factors that have previously been linked to fibrosis, including eukaryotic translation initiation factor 4E-binding protein 1 (4E-BP1; *r*: 0.63; q=5.6x10^{-74}) and tumour necrosis factor superfamily 14 (TNFSF14; *r*: 0.56; q=1.7x10^{-55}).[295,296]

As previously discussed in the introduction and as also implied by our observations in CF, TGF-β1 is widely described as a master regulator of fibrosis. Therefore, the correlation between TGF-β1 and miR-21 in the circulation (see **Figure 25, panel A**) warranted further investigation, in particular in relation to its release by platelets.

4.2.2 Effects of plasma preparation on biomarkers

As described in the paragraphs above, analysis in the Bruneck 2000 follow-up showed a significant correlation between plasma levels of miR-21 and LAP-TGF-β1. Furthermore, both were strongly correlated to markers of platelet reactivity. To further validate this association, new plasma samples were collected during the 2015 evaluation of the Bruneck cohort (see **Appendix 1**). Given the importance of plasma sample preparation, as we recently summarised in a review article (see **Appendix 3**), we used a tailored protocol to prepare PPP samples for additional analysis of miR-21 and associated proteins (see **Figure 9, panel A**).[96]

To screen for differences between conventional plasma and PPP, the same two panels of PEA were analysed for low-abundant proteins in the collected PPP (n=332). Measurements of miR-21 levels were performed by qPCR. Pearson correlations and concomitant FDR-adjusted p-values (q-values) were calculated between miR-21 and all proteins that were measured by PEA, as shown in **Figure 24, panel B**. All nineteen significantly correlating proteins in PPP had also been returned as such in the analysis using conventional plasma from the year 2000 follow-up. The opposite was however not the case; several proteins that showed high correlations in conventional plasma did not show the same in PPP (**Figure 26**). Among them, LAP-TGF-β1 showed a striking difference in correlation with miR-21, with a Pearson *r* of

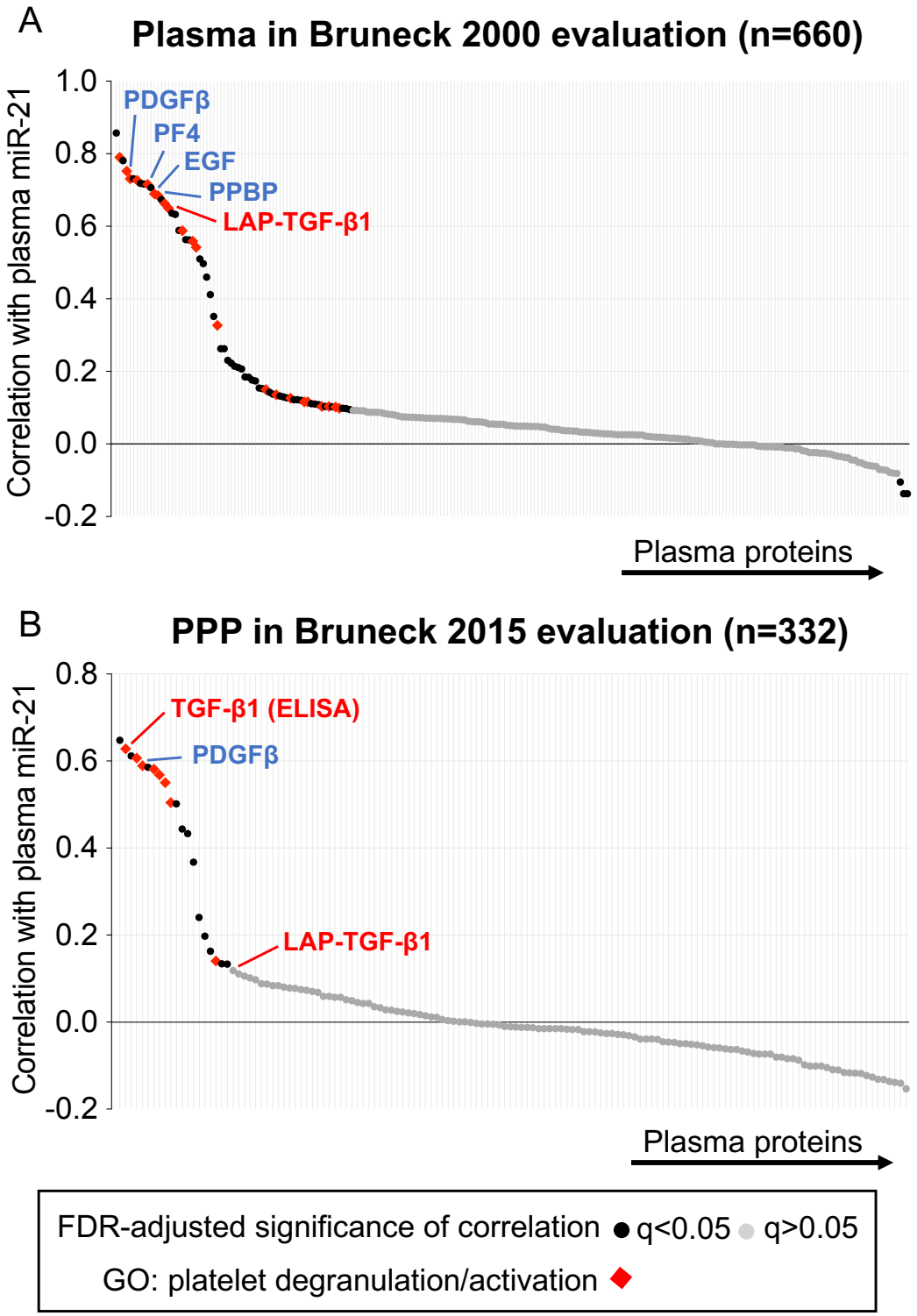

Figure 24. Correlation of miR-21 with pro-fibrotic factors and markers of platelet activation in the Bruneck study cohort. Using a proteomics screen, Pearson coefficients for the correlation of miR-21 with platelet activation markers (PF4, PPBP) and LAP-TGF-β1, as well as other circulating proteins associated with cardiovascular disease, inflammation and fibrosis were determined. Individual proteins are listed on the X-axis, with the corresponding Pearson correlation to miR-21 shown on the Y-axis. Analysis was performed using conventional plasma samples from the year 2000 (A; n=660 in conventional plasma) and 2015 (B; n=332 in PPP) evaluation of the community-based Bruneck study. Black points indicate a FDR-adjusted significance <0.05, with red points indicating annotation for platelet degranulation/activation gene ontology (GO) terms.

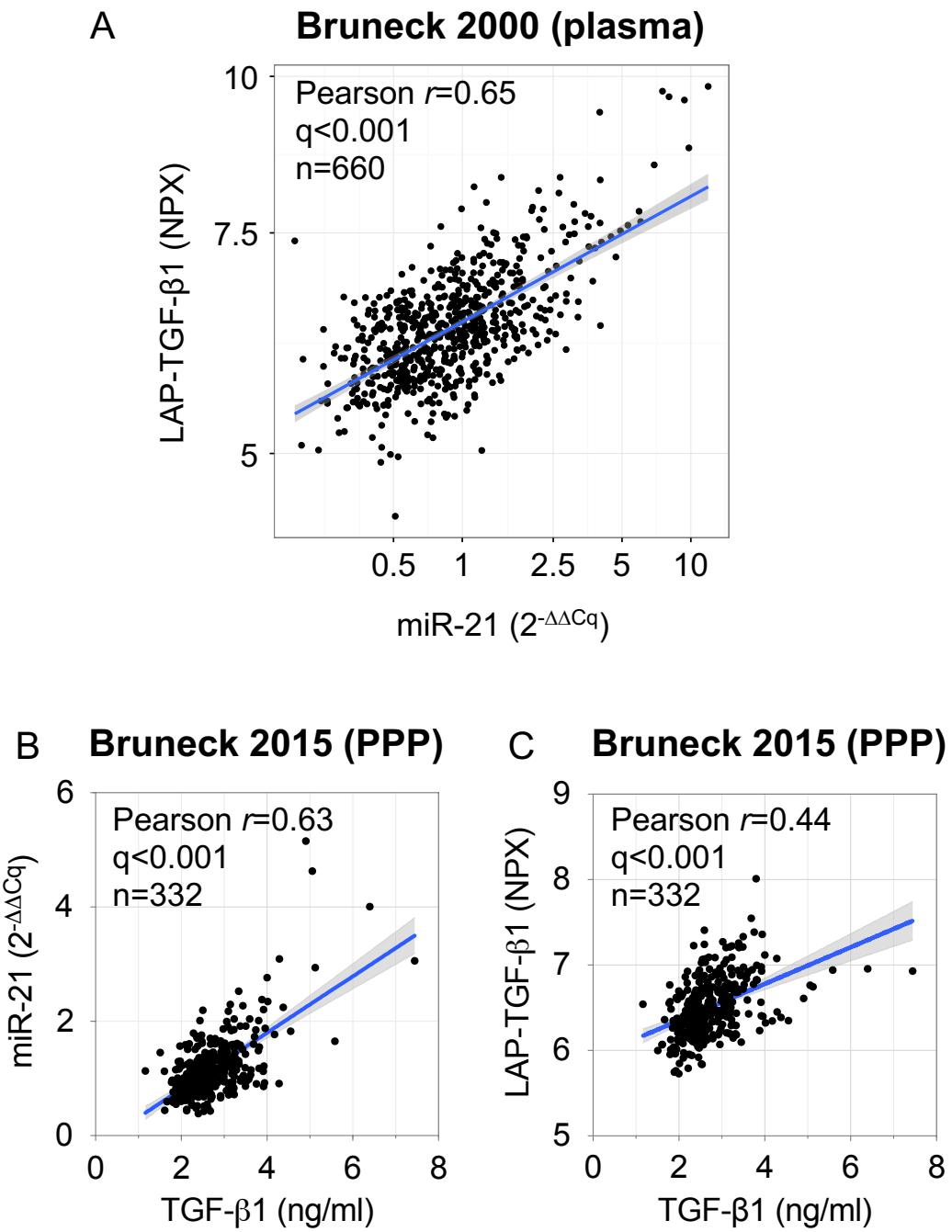

Figure 25. Correlation of plasma miR-21 and TGF-β1 in the Bruneck study cohort. A: Scatter plot for relative plasma levels of miR-21 (provided as relative quantity as measured by qPCR, using the $2^{-\Delta\Delta Cq}$ formula with exogenous cel-miR-39 and a sample pool serving as reference for the ΔC_q and $\Delta\Delta C_q$ quantification, respectively) and LAP-TGF-β1 (as determined by PEA) as measured in the Bruneck year 2000 evaluation, indicating a marked correlation. **B:** ELISA and qPCR measurements of mature TGF-β1 and miR-21, respectively, showed a marked correlation in PPP collected during the Bruneck 2015 evaluation. **C:** Correlation between PEA-based measurements of LAP-TGF-β1 and mature TGF-β1 as measured by ELISA. NPX, normalised protein expression.

0.65 ($q=2.4x10^{-79}$) in conventional plasma but an *r* of 0.12 (q=0.22) in PPP. Similarly, strong correlations had been found for several other proteins, including 4E-BP1 and proteinase-activated receptor 1 (PAR-1; *r*: 0.66; $q=2.6x10^{-84}$), whereas no significant correlation with miR-21 was found for these proteins in PPP (4E-BP1; *r*: 0.08; q=0.44; PAR-1; *r*: 0.14; q=0.14). For EGF, significant correlation was found in both conventional plasma and PPP (*r*: 0.58; $q<1.0x10^{-15}$), whereas for heparin-binding EGF (HB-EGF), significant correlation was found only in conventional plasma (*r*: 0.56; $q=7.1x10^{-56}$, versus *r*: 0.07; q=0.51 in PPP).

To further explore this interference of residual platelets or other cell types during analysis of circulating proteins or RNA, an experiment was performed using PRP and PPP (see **Figure 9, panel A**). Both sample types were prepared from blood from two healthy volunteers. These were then separately analysed using the same PEA panels. For each individual, a ratio of the relative abundance between PRP and PPP was calculated for each analysed protein. The average of this ratio is shown for the proteins in **Figure 26.**

In this analysis, most proteins that showed a correlation with miR-21 in conventional plasma and/or PPP, showed a FC (ratio) greater than one. As expected, LAP-TGF-β1 showed a PRP/PPP ratio of 1.2, implying its presence in platelets. For HSP-27 however, despite strong correlations with miR-21 in both plasma preparations (*r*: 0.79 and 0.51; $q=3.7x10^{-141}$ and $<1.0x10^{-15}$ in conventional plasma and PPP, respectively), no difference in abundance was seen between PPP and PRP (ratio 1.0). A similar trend, yet to a lesser extent, was seen for PDGFβ, with similarly strong correlations (r: 0.73 and 0.59; $q=1.0x10^{-110}$ and $<1.0x10^{-15}$) in both plasma types but a PRP/PPP ratio of 1.1. Finally, for PAR-1, Dickkopf-related protein 1 (DKK1) and HB-EGF, significant correlations were seen in conventional plasma (*r*: 0.66, 0.59 and 0.56; $q=2.6x10^{-84}$, $2.1x10^{-62}$ and $7.1x10^{-56}$), with no significant correlation with miR-21 in PPP (*r*: 0.14, 0.13 and 0.07; q=0.14, 0.15 and 0.51) despite PRP/PPP ratios of 1.1, 1.1 and 1.2, respectively. Altogether, these results warrant further investigation of the identified correlation between LAP-TGF-β1 and miR-21 in PPP.

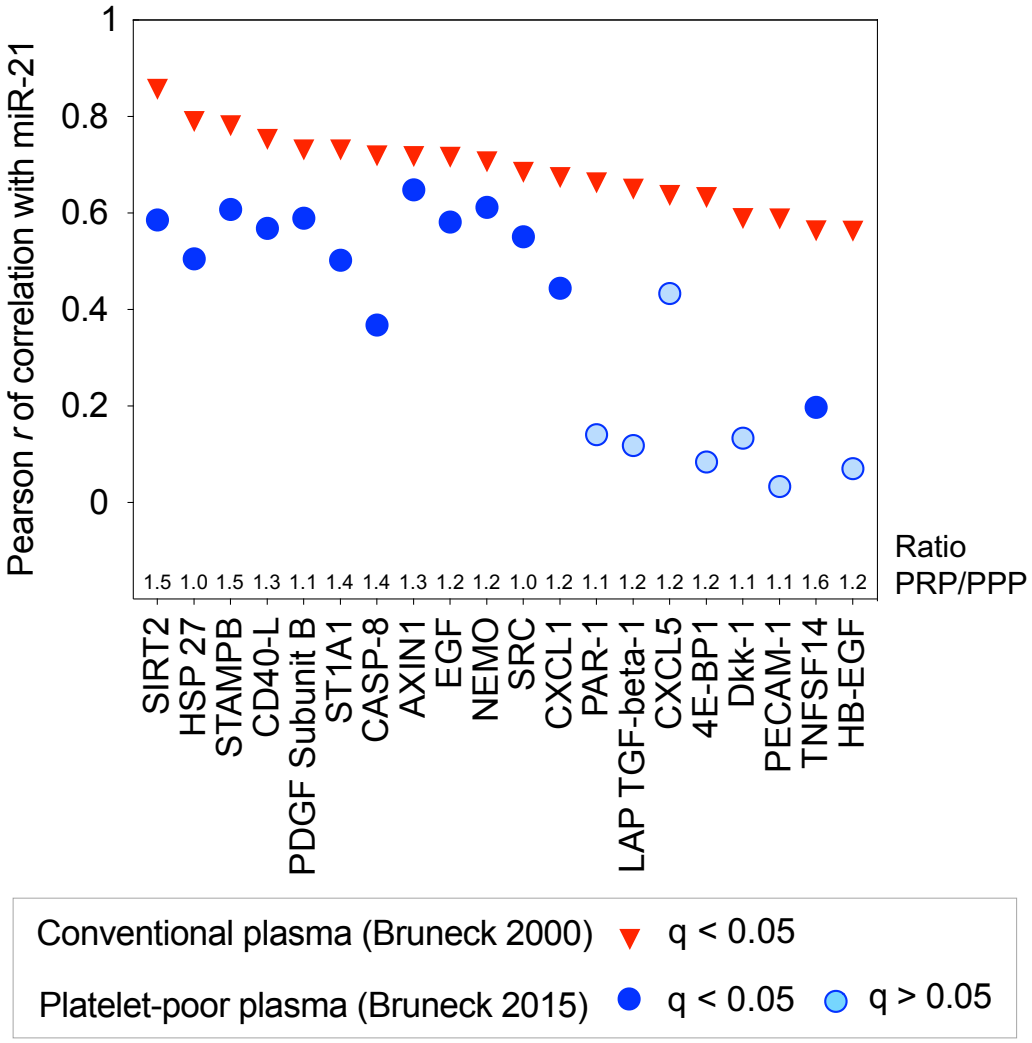

Figure 26. Comparison of conventional and platelet-poor plasma for correlates of miR-21. Measurements of miR-21 and plasma proteins in the 2000 (n=660) and 2015 (n=332) evaluation of the Bruneck study were compared, constituting conventional plasma and PPP, respectively. Whilst there is a degree of overlap between both analyses, several proteins, including LAP-TGF-β1, failed to be significantly correlated to miR-21 in PPP. Additionally, a direct comparison between PRP and PPP was performed to determine potential enrichment in platelets for individual proteins. The presented ratio represents the average change between PRP-PPP sample pair (n=2 vs. 2).

4.2.3 Analysis of non-reduced human platelet releasate

To gain more insight in the release profile of platelets upon their activation, in particular with regards to TGF-β1, we performed a proteomics analysis of platelet releasate samples from healthy human volunteers (see **Figure 9, panel B**). Proteins were treated with either reducing or non-reducing conditions, followed by separation by gel electrophoresis. Each sample lane was then divided in forty-eight gel pieces that were separately analysed by LC-

MS/MS. This allowed for inference of the relative molecular mass of the protein or protein-complex from which each identified peptide was derived.

Results for fibronectin, the β-chain of fibrinogen, TGF-β1 and LTBP1 are shown in **Figure 27**. For each protein, spectral counts for identified proteotypic peptides are shown in the corresponding location of the polyacrylamide gel where these were detected by the mass spectrometer. With reducing conditions, all proteotypic peptides for fibronectin were detected near its predicted relative molecular mass (M_r) of 263 kDa. Using non-reducing conditions however, a larger proportion of identified peptides were found in gel bands higher up in the gel, which may be in accordance with its homodimeric structure, consisting of two fibronectin monomers that are linked by disulphide bonds at their C-terminus.[297] A similar result can be seen for the beta chain of fibrinogen. Here, reducing conditions led to identification of all peptides just below its predicted M_r of 57 kDa, potentially indicating cleavage at amino acid residue 44-45 by thrombin which produces a 50 kDa cleavage product.[298] The secreted fibrinogen glycoprotein consists of two trimers, each consisting of three polypeptide chains (α, β and γ) and with a relative molecular mass of approximately 340 kDa.[299] Peptides of all three fibrinogen chains (only β is shown in **Figure 27**) were detected in segments derived from the top of the gel, above the protein marker of 260 kDa, consistent with its multimeric structure that is supported by disulphide bonds between the different chains.

For TGF-β1, a different distribution of peptides was also seen between reducing and non-reducing sample preparation. As described in the introduction (see **Figure 1, panel A**), pro-TGF-β1 (predicted M_r 41.3 kDa, containing three glycosylation sites) is proteolytically cleaved into a LAP (predicted M_r 28.6 kDa, containing three glycosylation sites) and mature TGF-β1 (predicted M_r 12.7 kDa). As shown in **Figure 1** (**panel B**), TGF-β1 forms a non-covalent homodimer (predicted M_r 25.4 kDa) that is contained in the small latency complex (SLC) by two LAP. This SLC can be bound to a latency-binding protein such as LTBP1 to form a large latency complex (LLC). As shown in **Figure 27** (**panel C**), reducing conditions resulted in identification of peptides belonging to LAP and to mature TGF-β1 in two distinct parts of the gel, indicating a molecular mass of approximately 38 kDa and 12.5 kDa,

respectively. This is in accordance with monomeric conformation at the time of gel electrophoresis, with the M_r of 38 kDa for LAP being consistent with glycosylation at its three predicted glycosylation sites. These results, combined with the absence of simultaneous detection of LAP and TGF-β1 peptides in the 50 kDa region, indicate that none of the detected peptides in the releasate were derived from uncleaved pro-TGF-β1.

Analysis of the platelet releasate using non-reducing conditions yielded detection of LAP and TGF-β1 peptides in distinct regions as well, yet at different locations in the gel compared to reducing conditions. TGF-β1 peptides were all detected in the gel region relating to a relative molecular mass just above 20 kDa, suggesting a homodimer of TGF-β1. Again, no TGF-β1 peptides were detected in the same region as LAP peptides, further supporting the absence of uncleaved pro-TGF-β1. LAP peptides were detected in gel pieces derived from the high end of the gel, above the 260 kDa protein marker. This suggests that LAP could be part of a complex with other proteins or has a conformation that hampers further migration of the protein through the gel. Identification of LAP in non-reduced samples occurred in the same gel pieces as the identification of LTBP1 peptides (see **Figure 27, panel D**), the major protein involved in the LLC (see **Figure 1, panel B**).[32] The co-detection in gel pieces above 260 kDa implies that the identified LTBP1 and LAP were part of a multimer. Additionally, LTBP1 peptides were detected at a lower molecular weight segment of the gel (estimated at 180-240 kDa) in the non-reduced samples, whereas for the reduced samples, all detected LTBP1 peptides were found in the latter gel segment. This region is in accordance with the predicted molecular mass of LTBP1, which equates to 186.8 kDa without considering the seven potential glycosylation sites within this protein.

Altogether, this analysis of the human platelet releasate using reducing and non-reducing conditions indicates that platelets release mature TGF-β1 in a cleaved homodimer form. Therefore, measurement of LAP and mature TGF-β1 may not reflect the same biologically active component. These findings warrant further investigation of the previously identified correlation between plasma miR-21 and LAP-TGF-β1 by evaluating plasma levels of mature TGF-β1.

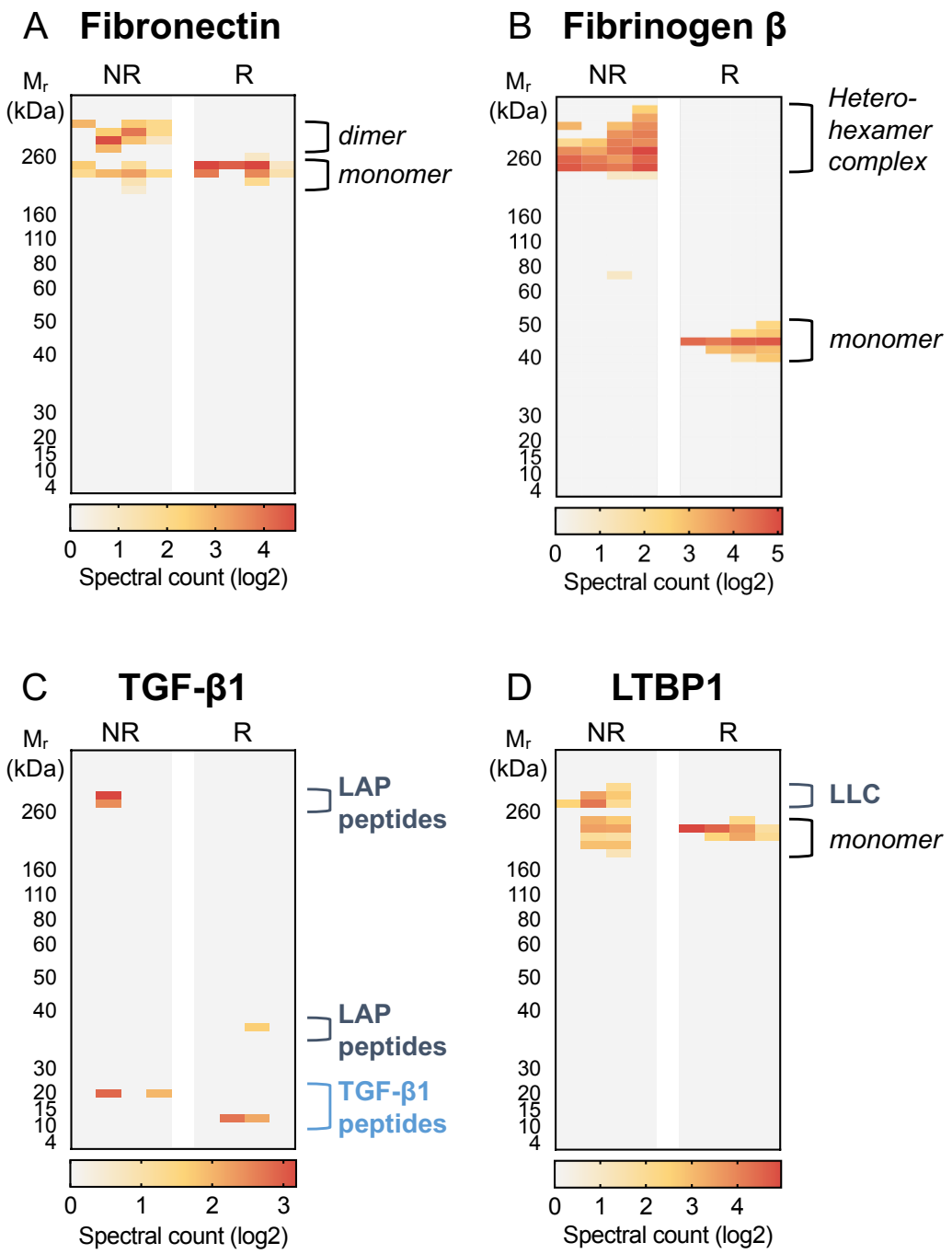

Figure 27. Human platelet releasate proteins under reducing and non-reducing conditions. Releasate was isolated from platelets of healthy human volunteers (n=4) by thrombin-induced activation, followed by gel-based LC-MS/MS analysis using reducing (R) and non-reducing (NR) conditions. **A:** For fibronectin, non-reducing conditions indicated the presence of a monomer and dimer. **B:** Fibrinogen β chain peptides were detected at a relative molecular mass (M_r) corresponding to 50 kDa, whilst non-reducing conditions corresponded to the presence of the fibrinogen hetero-hexamer complex. **C:** Reducing conditions identified LAP and TGF-β1 peptides in distinct gel regions that corresponded with their individual M_r, indicating a post-cleavage status of pro-TGF-β1. Non-reducing conditions identified the TGF-β1 peptides at a region corresponding to a dimeric form, whilst LAP peptides were identified at a much higher gel region that also contained peptides of LTBP1 (**D**). This indicates platelet secretion of LAP as part of a large latency complex (LLC).

4.2.4 Correlation of miR-21 and TGF-β1 in the Bruneck study

As shown in **Figure 1**, **panel A**, the epitope that is recognised as part of the PEA panel is part of the LAP and will hence recognise LAP-TGF-β1 and pro-TGF-β1. However, as shown by the comparison of reduced and non-reduced human platelet releasate samples, TGF-β1 is released from platelets in a post-cleavage state. Quantification of TGF-β1 using an antibody that recognised the LAP and its correlation with plasma levels of miR-21 was shown to be affected by the plasma sample preparation method. Therefore, we set out to quantify TGF-β1 using an epitope that lies within the sequence of 'mature' TGF-β1. For this purpose, an ELISA was performed on PPP from the 2015 follow-up of the Bruneck study.

Results for the ELISA measurements and their correlation with miR-21 levels as well as LAP are shown in **Figure 25, panel B and C**. In contrast to the results of the PEA measurement of LAP, the TGF-β1-targeted ELISA showed a highly significant correlation with miR-21 (r: 0.63, $p<0.0001$). The latter correlation is also included in **Figure 24, panel B**, to highlight this major discrepancy. Both being derived from cleaved pro-TGF-β1, a correlation between TGF-β1 and LAP was indeed found (r: 0.44, $q<0.0001$), yet this correlation was less pronounced than the correlation with miR-21.

4.3 *In vivo* study of miR-21 and platelets

4.3.1 Antibody-mediated platelet depletion in mice

To determine the effect of a reduced platelet count on circulating levels of TGF-β1 as well as miR-21, a mouse model of immune-mediated thrombocytopaenia was used. Male wild-type mice were injected intraperitoneally with a single dose of anti-CD42b antibody (see **Figure 28, panel A**) or an equal volume of PBS as a control. At the dose of 4 mg/kg antibody, the platelet count is reduced for several days.[300] After 48 hours, animals were sacrificed and blood was prepared for RNA isolation and protein analysis, using whole blood as well as PPP.

Analysis of RNA isolated from whole blood showed a significant decrease in levels of the platelet-specific gene transcripts for integrin α-IIb (*Itga2b*; FC: 0.05; p<0.0001), *Pf4* (FC: 0.06; p<0.0001) and *Ppbp* (FC: 0.03; p<0.0001), indicating a severe reduction in platelet numbers (see **Figure 28, panel B**). Consistent with the hypothesis of platelets being a major source of circulating TGF-β1, transcript levels of *Tgfb1* were significantly reduced as well, yet not to the same extent as aforementioned platelet-specific transcripts (FC: 0.43; p<0.0001). To determine effects on other circulating cells, gene transcripts of protein tyrosine phosphatase, receptor type, C (*Ptprc*; encoding the CD45 antigen) were measured. In contrast with the platelet-specific or platelet-enriched transcripts, *Ptprc* transcript levels were not significantly affected by the anti-CD42b treatment (FC: 1.17; p=0.70).

Next, circulating levels of miRNAs were analysed. PPP was prepared for this purpose by sequential centrifugation of blood. In contrast with the whole blood mRNA analysis, miRNA changes showed a trend towards higher levels after platelet depletion (see **Figure 29, panel A**), suggesting a possible release during immune-mediated thrombocytopenia either from platelets or other cell types. The only significant change after 48 hours was observed for miR-320 (FC: 1.37; p=0.0177). Some platelet-enriched miRNAs such as miR-24 (FC:1.33; p=0.11) showed a trend in the same direction. No change was observed for miR-106a (FC: 1.31; p=0.34), miR-126 (FC: 1.27; p=0.34), miR-

21 (FC: 1.12; p=0.76), miR-146a (FC: 0.98; p>0.99) and miR-223 (FC: 0.97; p>0.99).

Using PPP, protein levels were analysed by ELISA. First, levels of the platelet-specific PF4 were analysed. As shown in **Figure 29, panel B**, PF4 concentrations were markedly reduced after anti-CD42b treatment (median [IQR] 1.6 [1.6-1.6] ng/ml) compared to the control group (median [IQR] 106.6 [82.4-128.7] ng/ml), showing a statistically significant difference when analysed by the Mann-Whitney test (p=0.0013). A similar effect was seen for levels of TGF-β1, yet to a lesser extent (see **Figure 29**, **panel B**): levels in control-treated animals had a median [IQR] of 1.9 [1.6-2.1] ng/ml, whilst levels after platelet depletion were significantly reduced (p=0.0025), with a median [IQR] of 0.78 [0.73-0.84] ng/ml. These results further highlight platelets as a major source of circulating TGF-β1.

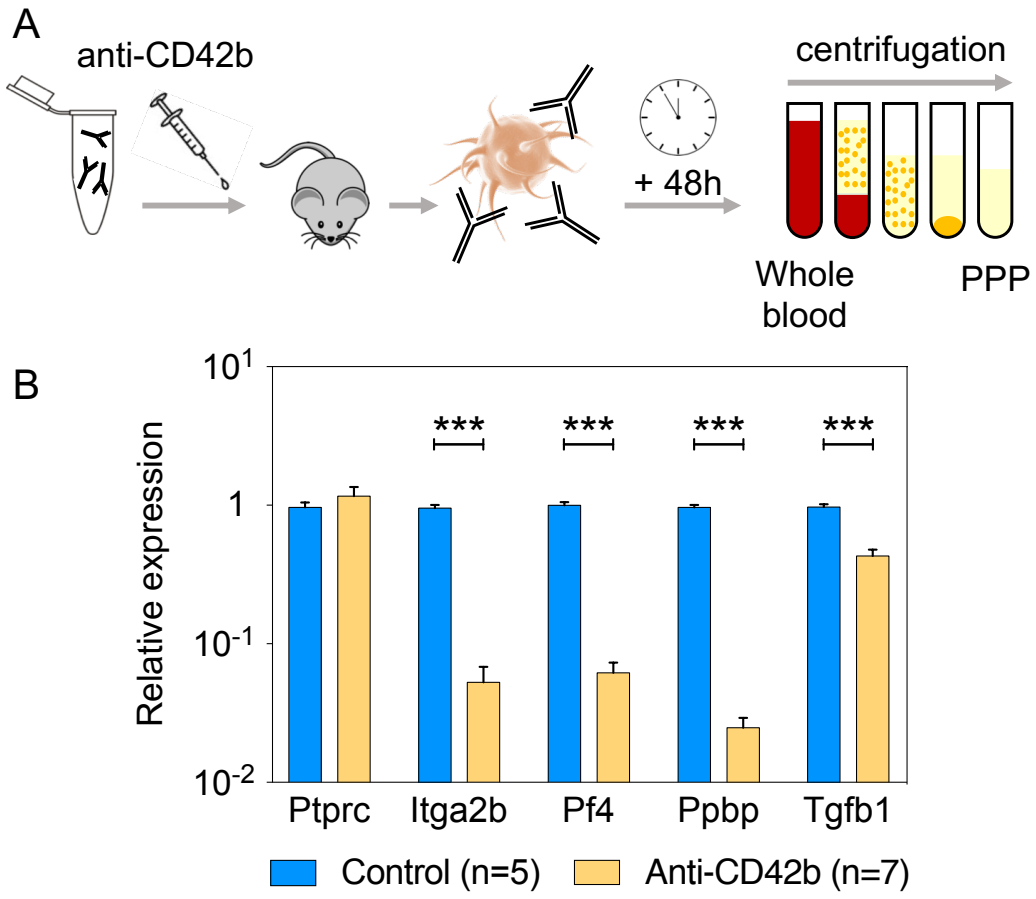

Figure 28. Immune-mediated platelet depletion in mice. A: Wild-type mice were treated with a monoclonal antibody directed against GPIbα (anti-CD42b; 4 mg/kg intraperitoneally; n=7) or PBS (control; n=5). Whole blood and PPP were collected 48 hours after injection. **B:** Expression levels of several platelet genes, as well as *Tgfb1*, were significantly lower in whole blood after platelet depletion. Expression of *Ptprc*, widely expressed in leukocytes, was not altered. *Gapdh* was used as reference gene transcript. Statistical analysis was performed with Welch's t-test.

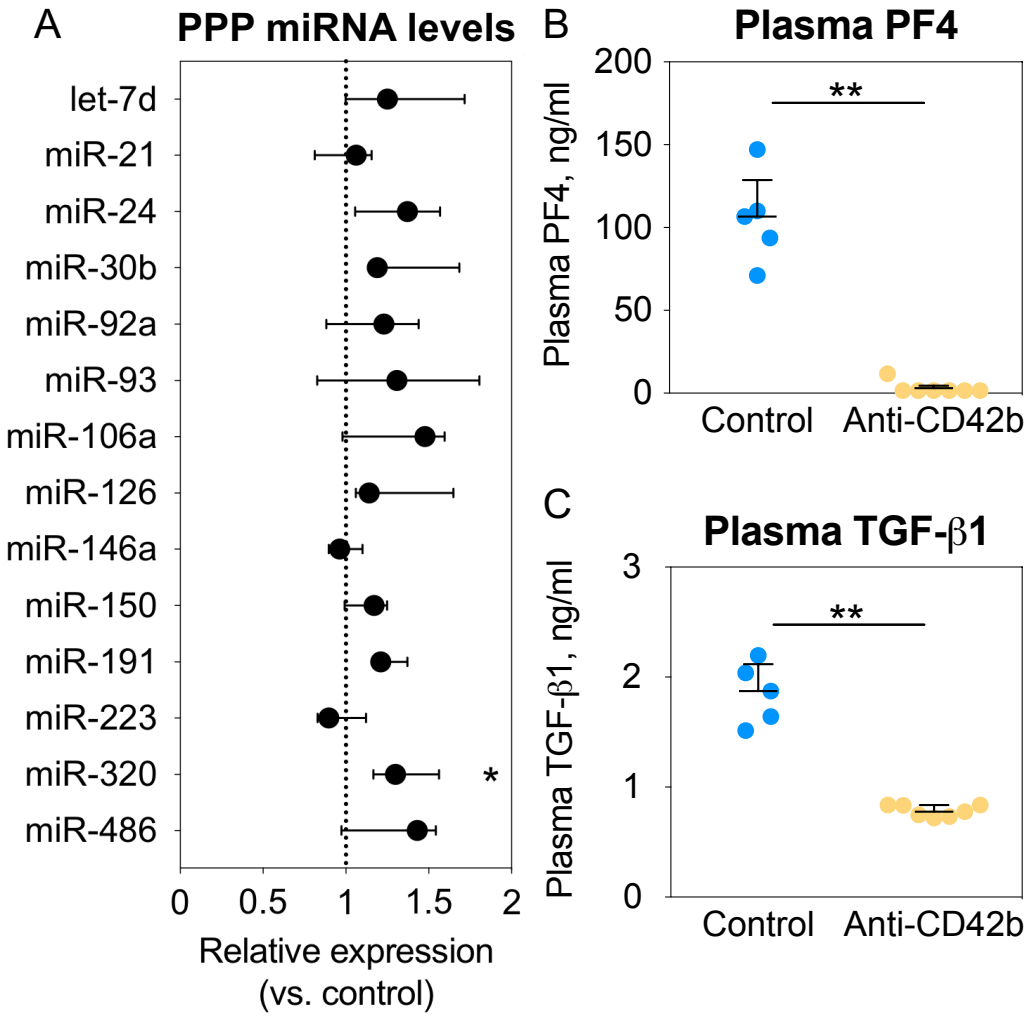

Figure 29. Effects of platelet depletion in mice on plasma TGF-β1 and microRNA levels. A: Platelet depletion did not significantly alter miR-21 levels in PPP, whilst other miRNAs showed a trend towards higher levels after platelet depletion. Exogenous cel-miR-39 was used as reference. **B,C:** Plasma levels of PF4 were below the limit of detection for the majority of samples from anti-CD42b-treated mice. TGF-β1 was detectable in both treatment groups, yet its levels were significantly reduced after platelet depletion. Both proteins were measured using an ELISA. Data shown as median (IQR). qPCR and ELISA measurements were analysed using the Mann-Whitney test, with n=5 (control) vs. 7 (anti-CD42b).

4.3.2 Argonaute-2 immunoprecipitation in megakaryoblastic cells

As shown in **Figure 2**, miRNAs regulate translation of mRNA through their inclusion in the RISC, which subsequently mediates the targeting of mRNA in the cytoplasm. Therefore, analysing miRNAs that are co-precipitated when using an antibody targeting Argonaute2 (Ago2), a main component of the miRNA processing machinery and the RISC, can provide additional information on functional miRNAs within a cell type. To study this in the context of platelets, a human oncological megakaryoblastic cell line (MEG-01) was used. Sepharose beads coated with anti-Ago2 antibody were incubated with

MEG-01 cell lysate (see **Figure 30, panel A**). Beads were then washed and RNA was isolated from the bound complexes. A non-specific IgG was used as control. Analysis by qPCR showed marked enrichment of miR-21 (average C_q 17.1, 24.7 and 24.5 for anti-Ago2, IgG control and input sample), whilst this was not observed for small RNAs *U6* and *RNU48* (see **Figure 30, panel B**). Enrichment of miR-126 and -223 was shown as a positive control, as we previously found these miRNAs to be highly enriched in the RISC of MEG-01 cells and in platelets.[217]

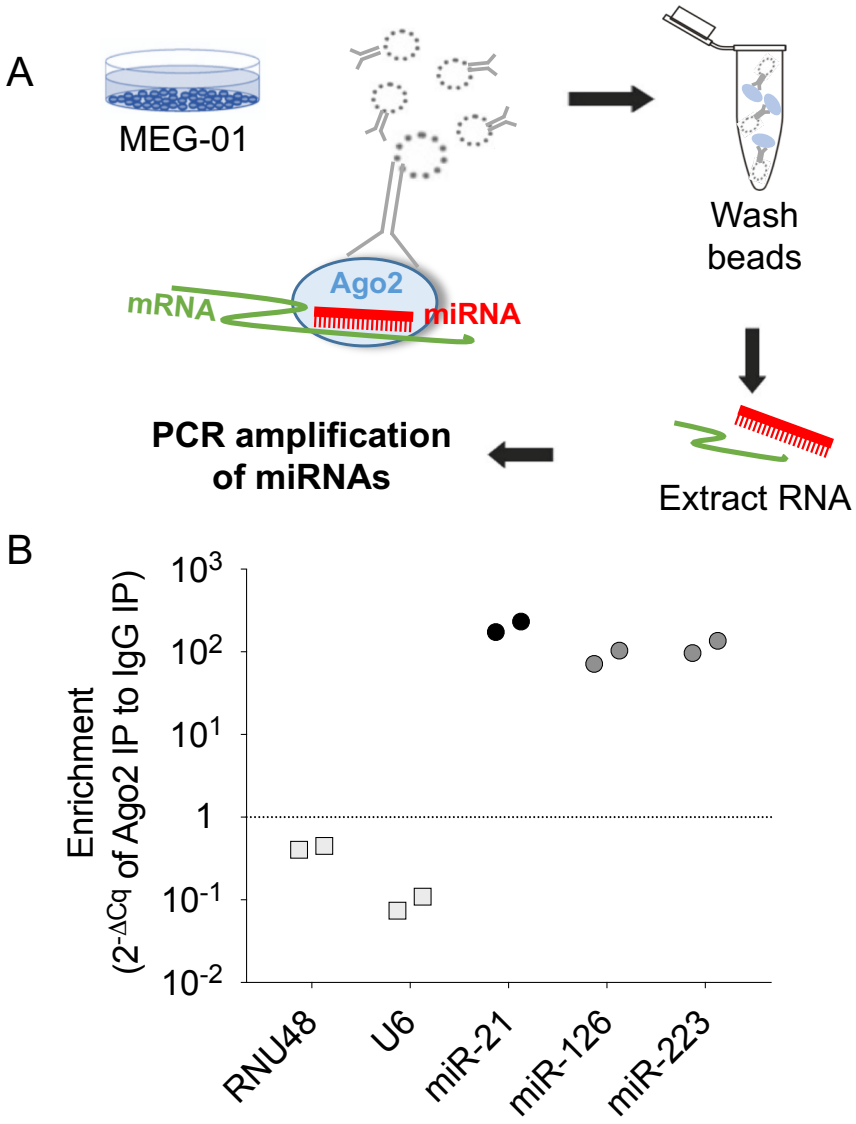

Figure 30. Argonaute2 immunoprecipitation in megakaryoblastic cells. A: Cells from a megakaryoblastic tumour cell line (MEG-01) were used to determine enrichment of miRNAs in argonaute2 (Ago2) complexes. Lysed MEG01 cells were incubated with anti-AGO2 antibody-coated beads. Co-precipitated RNA was isolated from antibody-bound complexes and analysed by qPCR. **B:** qPCR measurements are expressed as the difference in C_q value when anti-AGO2 mediated pull-down was compared with a control IgG antibody. Marked enrichment was observed for miR-21, as was previously shown for miR-126 and miR-223. Two replicates from different passages were used. *U6* and *RNU48* were used as control RNAs.

4.3.3 *In vitro* effect of oligonucleotides on platelet activation

Next, we set out to determine effects of *in vivo* inhibition of miR-21 to identify mechanisms that might be at play in the context of fibrosis and anti-fibrotic treatment using miR-21 inhibitors. As described in the introduction, several strategies have been conceived to systemically target specific miRNAs using modified oligo(deoxy)nucleotides. Importantly, a report by Flierl *et al* showed the ability of oligonucleotides with a length of 18 nucleotides or greater and with PS backbone modifications to activate platelets by interaction with platelet surface glycoprotein VI, the receptor for collagen.[254] To evaluate whether we could confirm this for the oligonucleotides that we intended to use for systemic miR-21 inhibition in mice, we performed light transmission aggregometry experiments using PRP from human volunteers incubated with different designs of miRNA-targeting oligonucleotides (see **Figure 31, panel A**) as agonist.

PRP was isolated from citrate-anticoagulated blood from healthy human volunteers by centrifugation. Using a light transmission aggregometer, various preparations of oligonucleotides were added, alongside with saline as negative control and collagen and ADP as positive controls for receptor-mediated platelet aggregation. Maximum aggregation was recorded for a period of 40 minutes after adding saline, oligonucleotide or platelet aggregation agonist. PRP was placed in a glass cuvette in the aggregometer at 37°C whilst stirring, followed by adding of fully phosphorothioate-modified oligonucleotides using an LNA backbone, with lengths varying from 15-23 nucleotides. Furthermore, an antagomiR consisting of 22 nucleotides was used, harbouring two and four PS backbone modifications at the 5' and 3' end, respectively. Apart from the 15-nucleotide LNA, all oligonucleotides were cholesterol-conjugated. Whilst ADP and collagen consistently induced platelet aggregation, none of the oligonucleotides tested showed an effect (see **Figure 31, panel B**).

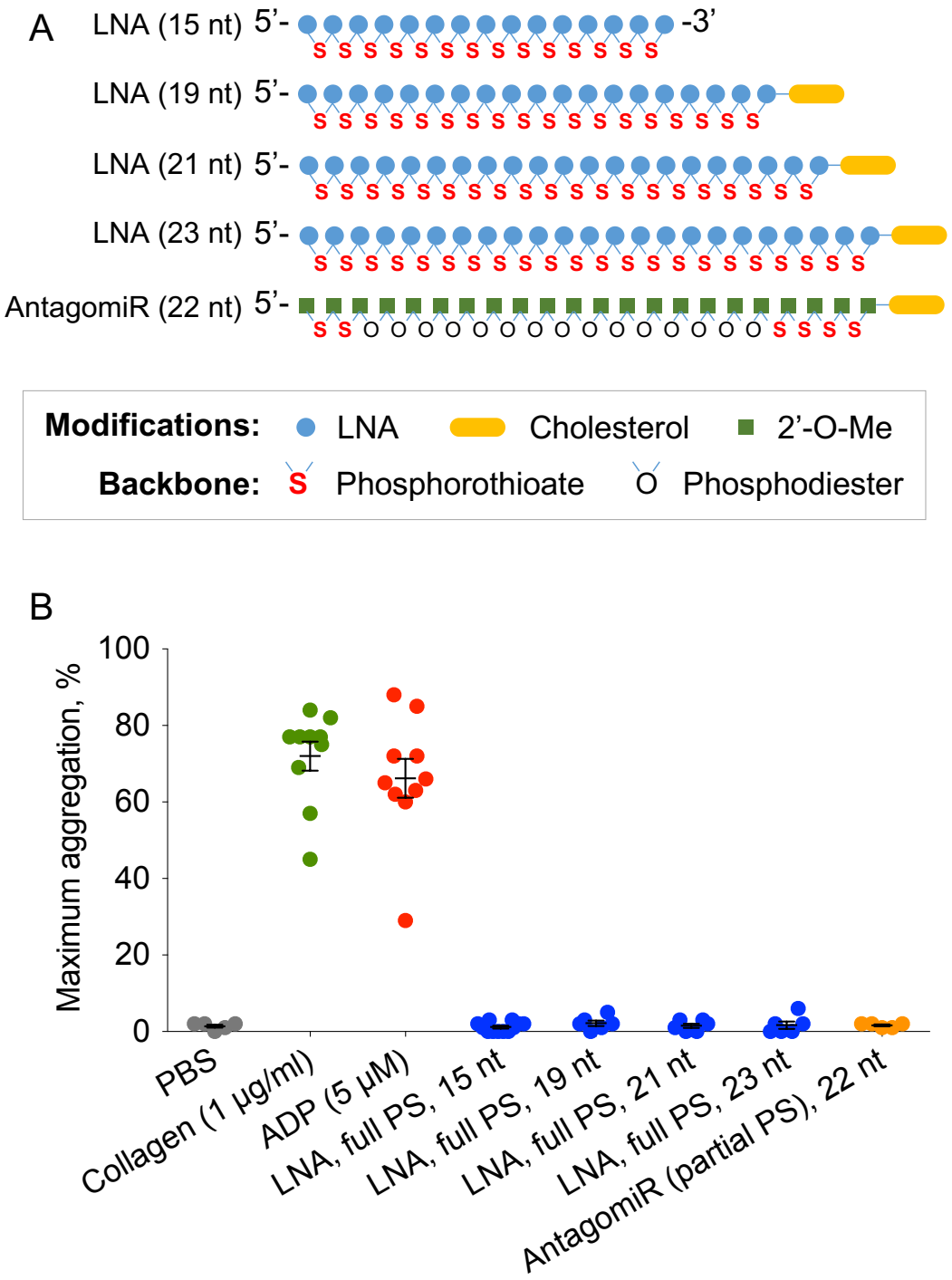

Figure 31. Effect of anti-miRs on platelet aggregation *in vitro*. A: Human PRP was incubated with several anti-miR constructs. All LNA-based anti-miRs had phosphorothioate (PS) backbone modifications in the entire molecule, whereas antagomiR constructs had such modifications only at two and four nucleotides on the 5' and 3' end, respectively. AntagomiR nucleosides were modified by adding a methyl group to the 2' hydroxyl of the ribose moiety (2'-O-Me) across the molecule, whereas LNA constructs harboured a methylene group connecting the 2' oxygen and 4' carbon of the ribose moiety in each nucleoside. Cholesterol conjugation was used in all tested oligonucleotides except for the 15-nucleotide LNA. **B:** Maximum aggregation within 40 minutes was measured using conventional light transmission aggregometry in response to PBS, collagen, ADP, and the anti-miR constructs in PRP from 8-10 individuals.

4.3.4 Systemic miR-21 inhibition using antagomiR

Based on the results from the Bruneck study and subsequent experiments, we aimed to study the effects of miR-21 inhibition on platelets using an *in vivo* approach. Inhibition was achieved through delivering intraperitoneal injections of antagomiR-21 or a non-targeting sequence (control) antagomiR, on three consecutive days. This approach was chosen due to previous experience in our laboratory for other miRNAs, resulting in stable and efficacious inhibition.[217,280,281] Collection of blood and tissues was performed on the seventh day after therapy initiation.

Efficacy of miR-21 inhibition by the antagomiR was evaluated in several tissues. RNA was isolated from bone marrow, heart, liver and kidney samples, followed by qPCR analysis of miR-21 and several other miRNAs. It is well established that penetrance and targeting efficacy varies between different tissues, with liver and kidney generally taking up the greatest amount after systemic delivery.[108] As shown in **Figure 32**, significant downregulation was achieved in bone marrow, heart, liver and kidney. In bone marrow, miR-21

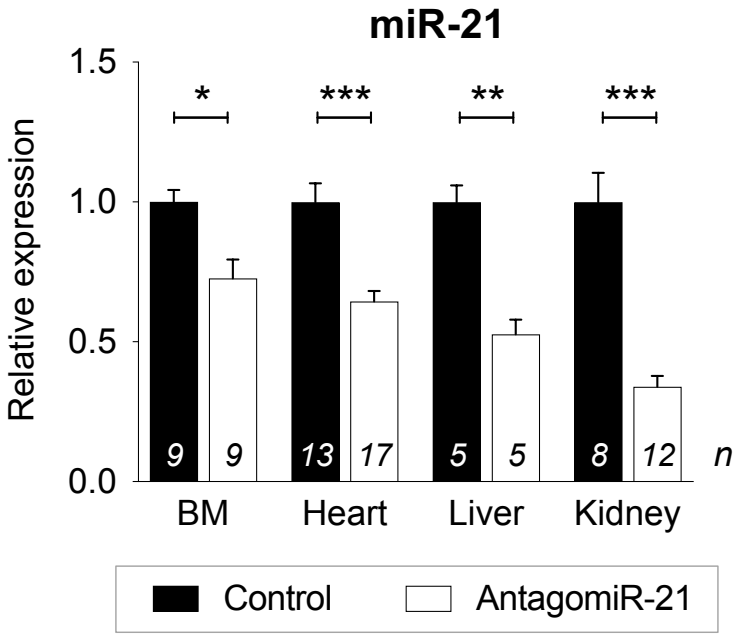

Figure 32. Effect of antagomiR-21 across tissues. Analysis of miR-21 levels by qPCR in RNA from bone marrow (BM), heart, liver and kidney showed a significant downregulation after antagomiR-21 treatment when compared to antagomiR-control. The effect on liver and kidney miR-21 was most pronounced. *U6* (BM) and *sno202* (heart, liver and kidney) were used as reference transcripts based on the comprehensive Ref Finder score within each tissue type. Statistical analysis was performed using Mann-Whitney tests; n-numbers are shown on each bar.

levels were 73% of those detected after control treatment (FC: 0.73; Mann-Whitney test p=0.0137), whilst in heart samples, miR-21 levels were down to 64% (FC: 0.64, p<0.0001). As expected, the liver and kidney showed a more pronounced inhibition, with levels being reduced to 53% (FC: 0.53; p=0.0079) and 34% (FC: 0.34; p<0.0001) of that detected after control antagomiR treatment, respectively.

In addition to quantifying the inhibition of the targeted miRNA, we evaluated effects on other miRNAs in these tissues. AntagomiR treatment can have off-target effects due to non-specific inhibition, as well as through secondary effects that occur as a result of the intended miRNA inhibition. In the heart (see **Figure 33, panel A**), miR-1 was significantly inhibited (FC: 0.90; p=0.0150), although the relative change was much lower than that of miR-21. In the bone marrow (see **Figure 33, panel B**), no significant differences in expression levels were found for the five miRNAs that were quantified in addition to miR-21. In the liver and kidney (see **Figure 33, panels C and D**), no significant effects were seen for the analysed miRNAs, although the liver showed a downward trend for the liver-specific miR-122 (FC: 0.87, p=0.056).

4.3.5 Platelet count after antagomiR-21 treatment

To evaluate the effect of systemic miR-21 inhibition on platelets, we first assessed the platelet count. Whole blood was drawn into ACD buffer and incubated with APC-conjugated anti-CD41 antibody, targeting the platelet- and megakaryocyte-specific transmembrane glycoprotein IIb. Samples were diluted for flow cytometry, with analysis performed by quantification of detected events in a predefined volume. Gating windows, based on forward and side scatter, were selected for platelets and for RBC/WBC, as shown in **Figure 34**, **panel A**. Platelets constituted 26.0% (22.6-28.3; median [IRQ]) of the total number of recorded events. Subsequent analysis of the platelet scatter population showed a median (IQR) of 64.8% (58.9-75.8) of events to be positive for CD41-APC signal (**Figure 34, panel B**).

Comparison of control-treated and antagomiR-21-treated animals showed similar platelet counts. Using gated platelets based on scatter (see **Figure 34, panel C**), a median (IQR) platelet count of 2.2 (1.9-2.3) $x10^9$/ml

blood was observed in control animal samples, whilst this was 2.3 (1.5-2.7) x10^9/ml blood in samples from antagomiR-21-treated animals. Analysis of

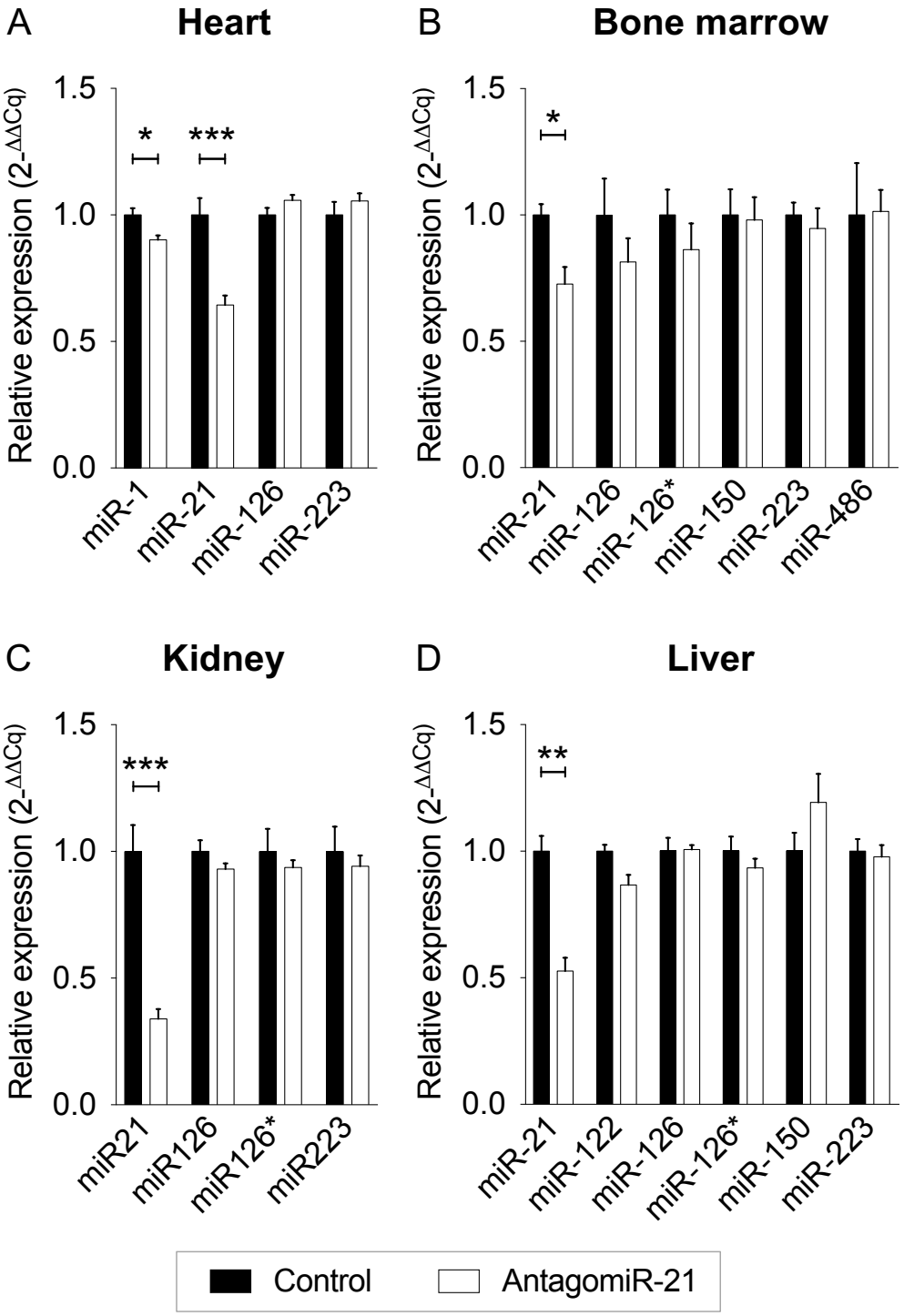

Figure 33. Effect of antagomiR-21 on other microRNAs. Levels of abundant miRNA in different tissues were analysed to assess secondary or off-target effects of systemic antagomiR-21 treatment. **A:** In heart tissue, a significant yet slight reduction of the miR-1 was observed, yet with a fold change much lower than that of miR-21. *Sno202* was used as reference transcript; n=13 vs. 17. **B, C, D:** In bone marrow (n=9 vs. 9), liver (n=5 vs. 5) and kidney (n=8 vs. 12), no significant changes were seen for the assessed miRNAs. *U6* was used as a reference transcript for bone marrow, whilst *sno202* was used for liver and kidney. Statistical analysis was performed using Mann-Whitney tests.

CD41+ events showed a similar result (see **Figure 34, panel D**), with median (IQR) concentrations of 0.81 (0.57-0.91) x10^9 and 0.61 (0.57-0.87) x10^9 events per ml of blood from control- and antagomiR-21-treated mice, respectively. Both these parameters were not significantly different when tested by the Mann-Whitney test (p>0.99 for gated platelets, p=0.55 for $CD41^+$ events).

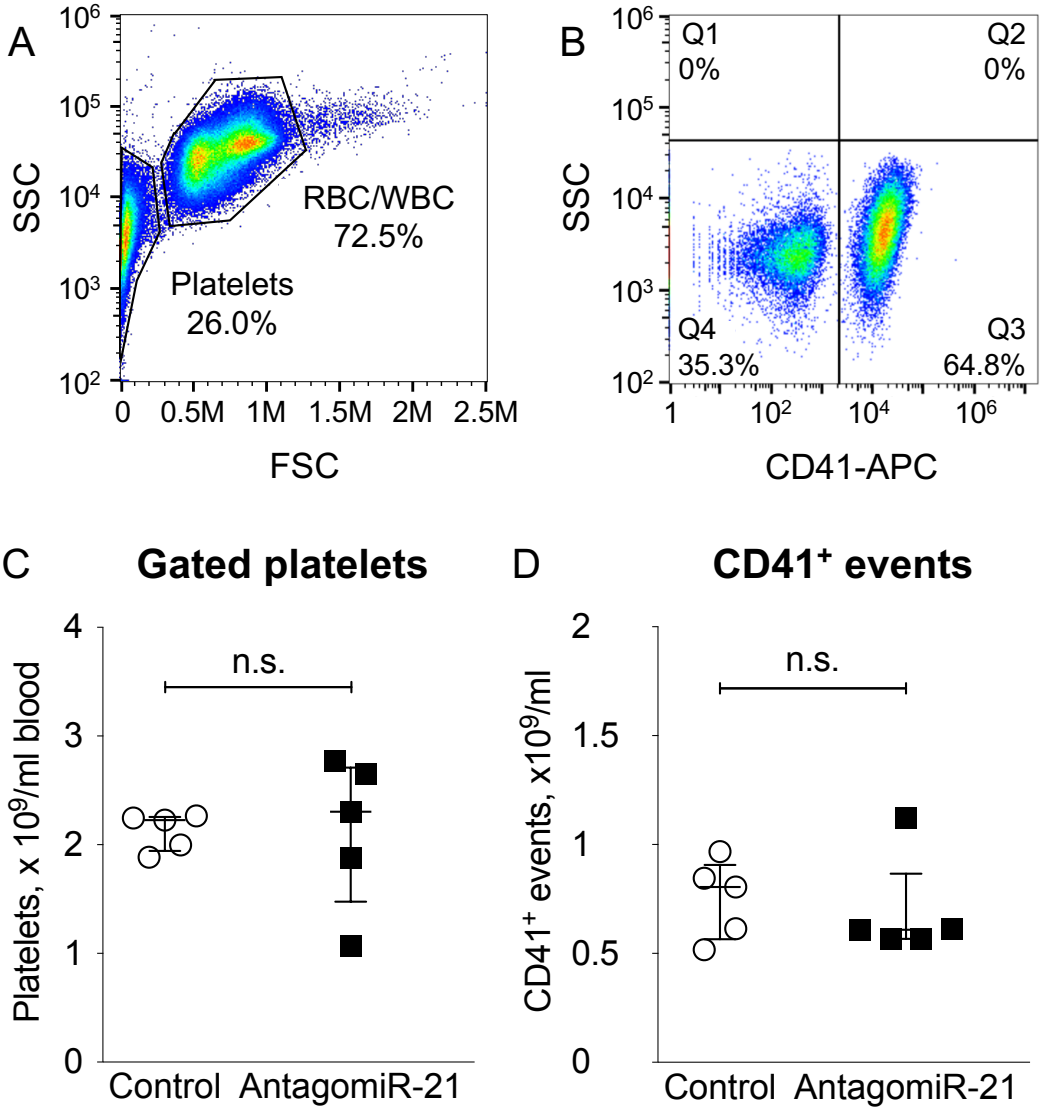

Figure 34. Platelet count after pharmacological miR-21 inhibition. Blood was taken from mice after antagomiR-21 or antagomiR-control treatment (n=5 vs. 5). Whole blood was incubated with APC-conjugated anti-CD41 antibody (CD41-APC) prior to dilution for flow cytometry. **A:** A representative image of the selected gating window for platelets and for red and white blood cells (RBC/WBC) based on forward (FSC) and side scatter (SSC). Median percentages are shown to indicate the proportion of gated events in relation to the total events. **B:** Gated platelets were analysed for CD41-APC intensity, with quadrant 3 and 4 (Q3 and Q4) corresponding to stained and unstained platelets, respectively. Median percentages relating to the total gated platelet population are shown in each quadrant. **C,D:** The concentration of gated platelets and of CD41-positive events was not significantly different between control- and antagomiR-21-treated mice. Lines and error bars indicate median (IQR). Mann-Whitney tests were used for statistical comparisons. n.s., not significant.

4.3.6 Platelet aggregation after antagomiR-21 treatment

In addition to platelet counts, an important assessment in the context of platelet function is the evaluation of their aggregation response to different agonists. This technique depends on changes in light transmission over time upon inducing platelet aggregation in PRP (see **Figure 35, panel A**). For the evaluation of mouse platelets after antagomiR treatment, we have previously used a method based on light transmission of diluted PRP on a 96-well plate that had been pre-coated with platelet agonists in varying concentrations.[217,301] Using a similar approach, we assessed whether there were any differences in the platelet aggregation response after miR-21 inhibition.

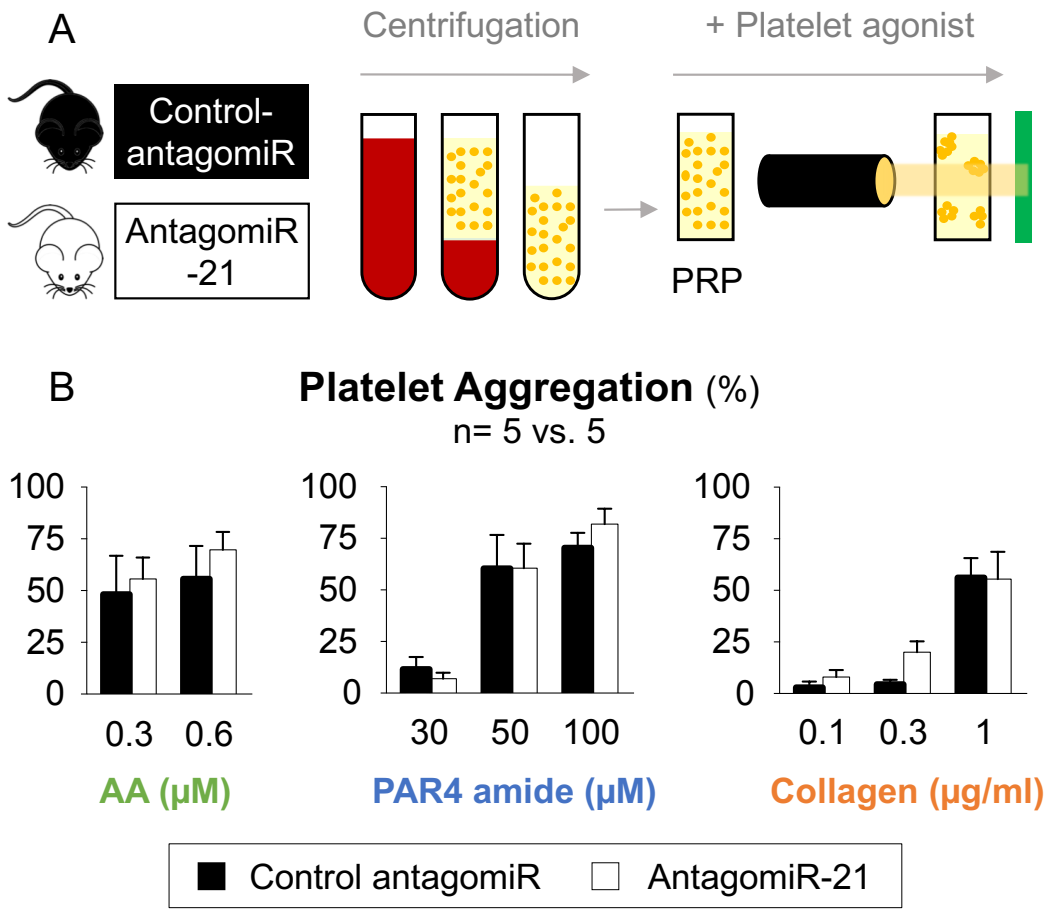

Figure 35. Platelet aggregation after pharmacological miR-21 inhibition. A: Blood was taken from mice after systemic treatment with antagomiR-21 or -control (n =5 vs. 5). Using sequential centrifugation, PRP was isolated. This was then added to wells of a 96-well plate containing platelet agonists in varying concentrations. Light transmission was measured after 5 minutes, with simultaneous readings in untreated PPP and PRP samples serving as positive and negative reference. **B:** Platelet aggregation was assessed in response to increasing concentrations of arachidonic acid (AA), protease activated receptor 4-activating peptide (PAR4 amide) or collagen. Whilst increasing concentrations of PAR4 amide and collagen caused increasing platelet aggregation, this response was not different between control- and antagomiR-21-treated mice.

Results of the platelet aggregation analysis are shown in **Figure 35, panel B**. Untreated PRP and PPP prepared from each blood sample served as the references for 0% and 100% aggregation, respectively. PRP was incubated on the plate for 5 minutes, followed by measurement of light transmission. AA induced aggregation up to 52.0±10.1% when using 0.3 µM and 62.8±8.8% with 0.6 µM. Two-way ANOVA analysis did not show a significant effect of agonist concentration ($F(1,16)$: 0.60; $p=0.45$) or antagomiR treatment type ($F(1,16)$: 0.59; $p=0.45$). However, for PAR4 amide, a thrombin receptor-activating peptide, a significant effect of the concentration was seen ($F(2,24)$: 26; $p<0.0001$), with aggregation measuring 9.3±3.2%, 60.5±9.5% and 76.2±5.3% for 30, 50 and 100 µM of this agonist, respectively. This aggregation-inducing effect was not different between control and antagomiR-21-treated mice ($F(1,24)$: 0.090; $p=0.77$). Using collagen as an agonist showed a similar response, with a significant effect of the agonist concentration ($F(2,23)$: 28; $p<0.0001$), inducing 5.5±2.3%, 11.5±3.6% and 55.9±7.7% aggregation with 0.1, 0.3 and 1 µg/ml of collagen, respectively. Here, too, no difference was seen between the two antagomiR types ($F(1,23)$: 1.2; $p=0.28$).

4.3.7 Murine platelet releasate proteome after antagomiR-21 treatment

Having analysed the platelet count and their aggregation response after systemic antagomiR-21 treatment, we then evaluated effects on the proteins that platelets secrete upon activation. To screen for differences in this context, platelets were isolated and washed after treatment with antagomiR-21 or control, followed by activation with thrombin, a potent platelet agonist. The supernatant of the aggregated and activated platelets, i.e. their releasate, was then analysed by gel-based LC-MS/MS (see **Figure 36, panel A**).

Identified proteins with at least five identified spectra in at least one of the two compared groups were included in the analysis. As shown in **Supplemental table 4**, proteins that were identified in the murine releasate showed major overlap with the previously analysed human platelet releasate. Abundant proteins included thrombospondin-1, with a normalised spectral count (NSpC) of 421.9±54.4 and 289.4±31.2 in control and antagomiR-21 (log

2 FC: -0.54, p=0.12), and the three chains of fibrinogen: α-chain (FIBA: NSpC 154.7±44.1 vs. 55.4±14.3), β-chain (FIBB: NSpC 111.5±35.5 vs. 44.2±14.3) and γ-chain (FIBG: NSpC 110.0±36.5 vs. 25.8±8.9) for control vs. antagomiR-21, respectively. Differences between the two treatment types did not reach statistical significance for any of these three chains (log2 FC: -1.48, -1.34 and -2.09; p=0.14, 0.19 and 0.14, respectively).

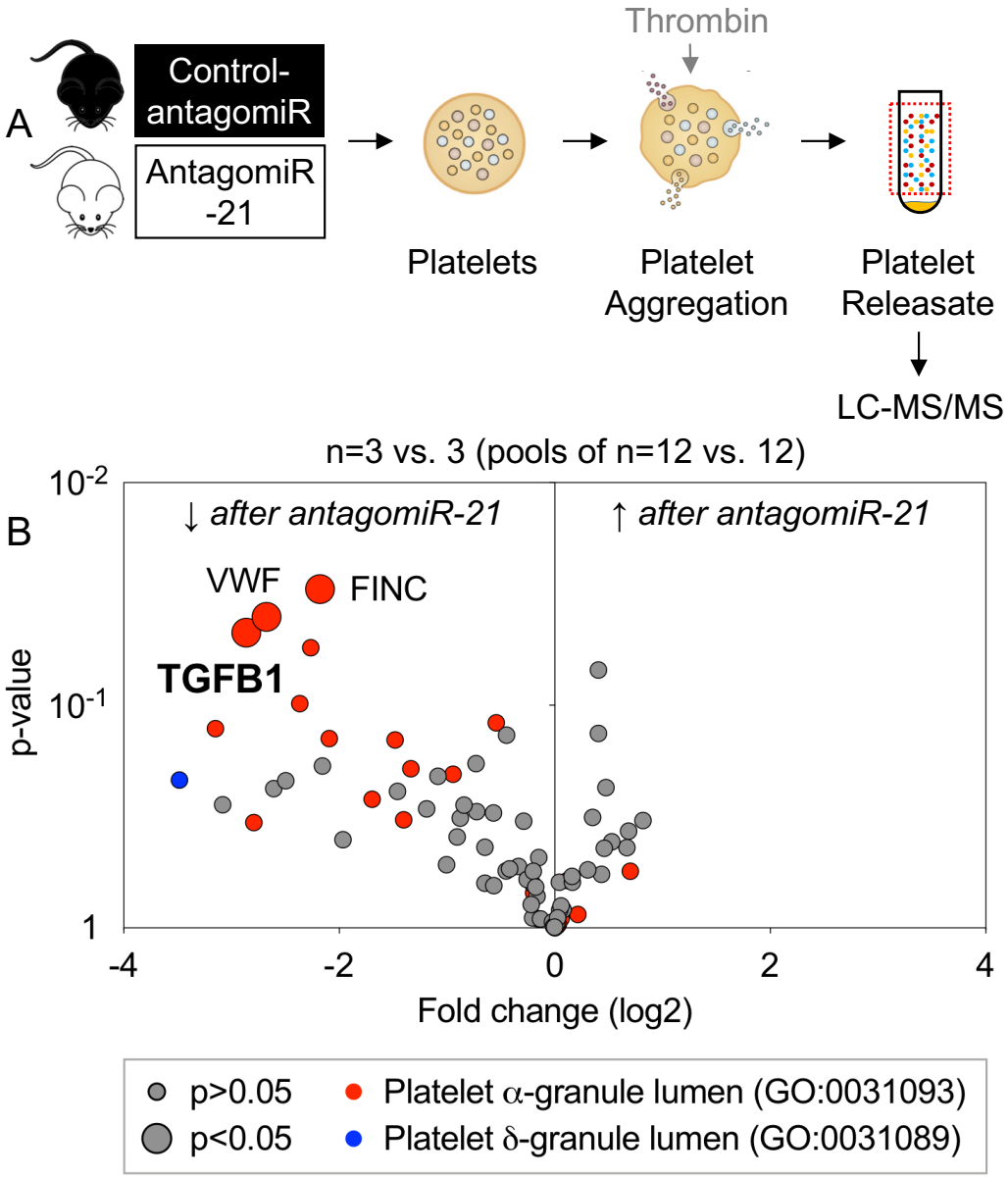

Figure 36. Murine platelet releasate after pharmacological miR-21 inhibition. A: Blood from antagomiR-treated mice was pooled per four mice, followed by isolation and washing of platelets (final n=3 vs. 3 for antagomiR-21 and control). The platelet releasate was obtained by thrombin-induced aggregation, which was then processed for gel-based LC-MS/MS analysis. **B:** Significantly decreased release was seen for TGF-β1 (TGFB1), as well as for von Willebrand factor (VWF) and fibronectin (FINC). Gene ontology (GO) annotation of identified proteins showed that in addition to these three proteins, several other α-granule showed a trend towards lower levels in the releasate of antagomiR-21-treated mice. One identified protein was annotated with presence in the dense (δ) granule lumen. Statistical analysis was performed using Welch's t-test.

As shown in **Figure 36, panel B**, three proteins were identified at significantly lower levels in the releasate from antagomiR-21 treated mice: fibronectin (FINC, log2 FC: -2.18; p=0.0300), von Willebrand factor (VWF, log2 FC: -2.67; p=0.0400) and TGF-β1 (TGFB1, log 2 FC: -2.86; p=0.0472). As indicated by the colour-coding of the individual items on the Volcano plot, GO annotation of the releasate proteins identified these three as present in the platelet α-granule lumen (GO: 0031093). Whilst not reaching statistical significance, a large proportion of the proteins that were detected at lower levels after antagomiR-21 carried this same annotation. These include the three fibrinogen chains and thrombospondin-1, as mentioned above, as well as PF4 (log2 FC: -1.69; p=0.2638), commonly used as a marker of α-granule release. Extracellular matrix protein 1 (ECM1) was the only identified protein annotated with the GO term of the platelet δ-granule lumen (GO: 0031089).

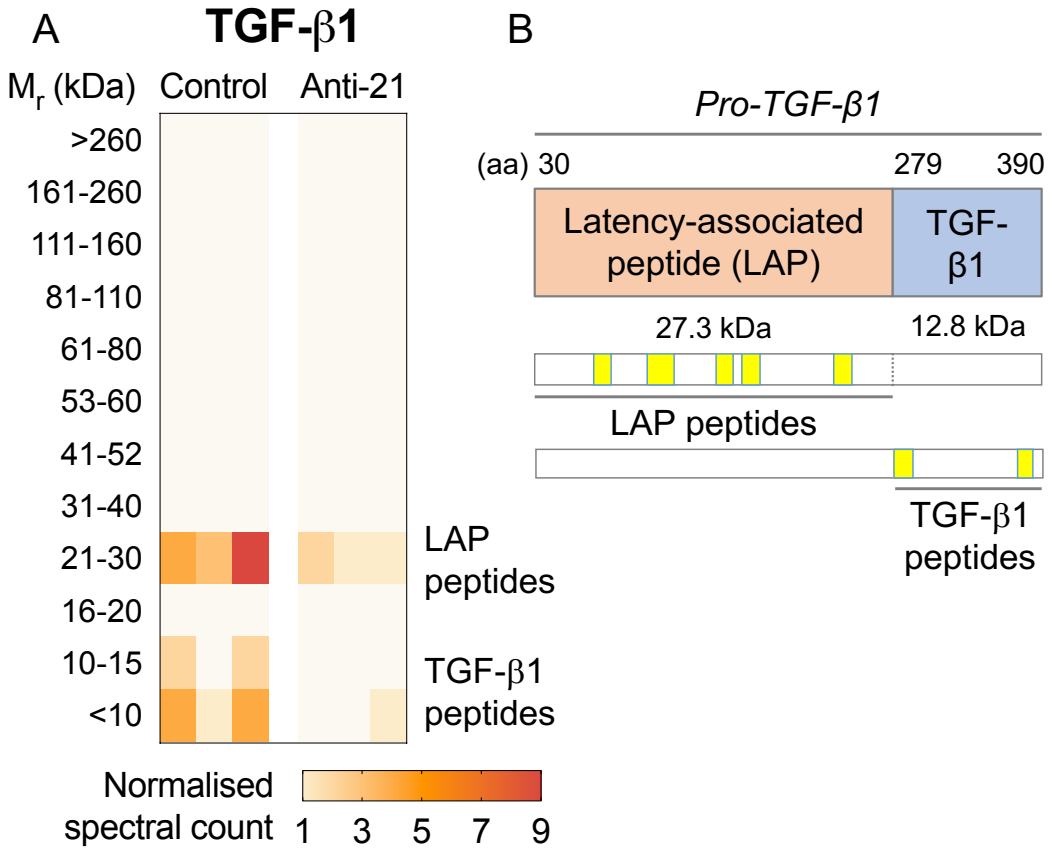

Figure 37. Platelet TGF-β1 release after pharmacological miR-21 inhibition. Using gel-based LC-MS/MS analysis allowed for identification of specific peptides in relation to their migration level during gel electrophoresis. Using lower threshold settings to enhance identification of low-abundant peptides, the gel representation showed a reduced identification of both LAP and TGF-β1 peptides in the releasate from antagomiR-21-treated mice (**A**). Sequence coverage across the pro-TGF-β1 sequence is shown in **B**. M_r, relative molecular mass; aa, amino acid residues.

When looking at the decreased release of TGF-β1 more closely, peptide-specific analysis is in line with the results from the human platelet releasate. This is illustrated more clearly when comparing the antagomiR-21 and control platelet releasate using a lowered protein and peptide threshold setting to enhance detectability of low abundant peptides. As shown in **Figure 37, panel A**, identification of peptides occurred in two distinct regions of the gel, for both control and antagomiR-21 releasate samples. Decreased levels in the latter samples appeared to be consistent across both gel regions. Individual peptide identification showed that LAP peptides and TGF-β1 peptides were identified in the higher and lower segment, both in agreement with the corresponding relative molecular mass (see **Figure 37, panel B**).

4.3.8 Platelet releasate analysis by ELISA

The importance of TGF-β1 and its release from platelets in tissue repair and the pro-fibrotic response was discussed in the introduction. We therefore aimed to validate the observation of reduced TGF-β1 platelet release after systemic antagomiR-21 treatment. For this purpose, measurement of TGF-β1 was performed by ELISA in the supernatant of platelets after activation with different agonists in several dosages, as described in the aggregometry experiment (see **Figure 38, panel A**).

As shown in **Figure 38, panel B**, TGF-β1 levels in PPP after antagomiR-21 treatment did not differ from controls. Adding increasing concentrations of agonists to PRP significantly increased TGF-β1 release for PAR4 amide ($F_{(2,24)}$: 8.6, $p=0.0015$) and collagen ($F_{(2,23)}$: 7.0, $p=0.0043$), but not for AA ($F_{(1,16)}$: 1.9, $p=0.18$). In line with the proteomics analysis of the thrombin releasate, TGF-β1 release after PAR4 ($F_{(1,24)}$: 11.0, $p=0.0029$) and collagen ($F_{(1,23)}$: 6.1, $p=0.0210$) receptor activation was attenuated after antagomiR-21 treatment when using a high dosage of either agonist. This effect was not observed for AA ($F_{(1,16)}$: 1.7, $p=0.21$). *Post-hoc* analysis of the individual comparisons at different dosages, using Šidák's test, confirmed the significant difference at 100 µM PAR4 amide (adjusted $p=0.0002$) and 1 µg/ml collagen (adjusted $p=0.0022$).

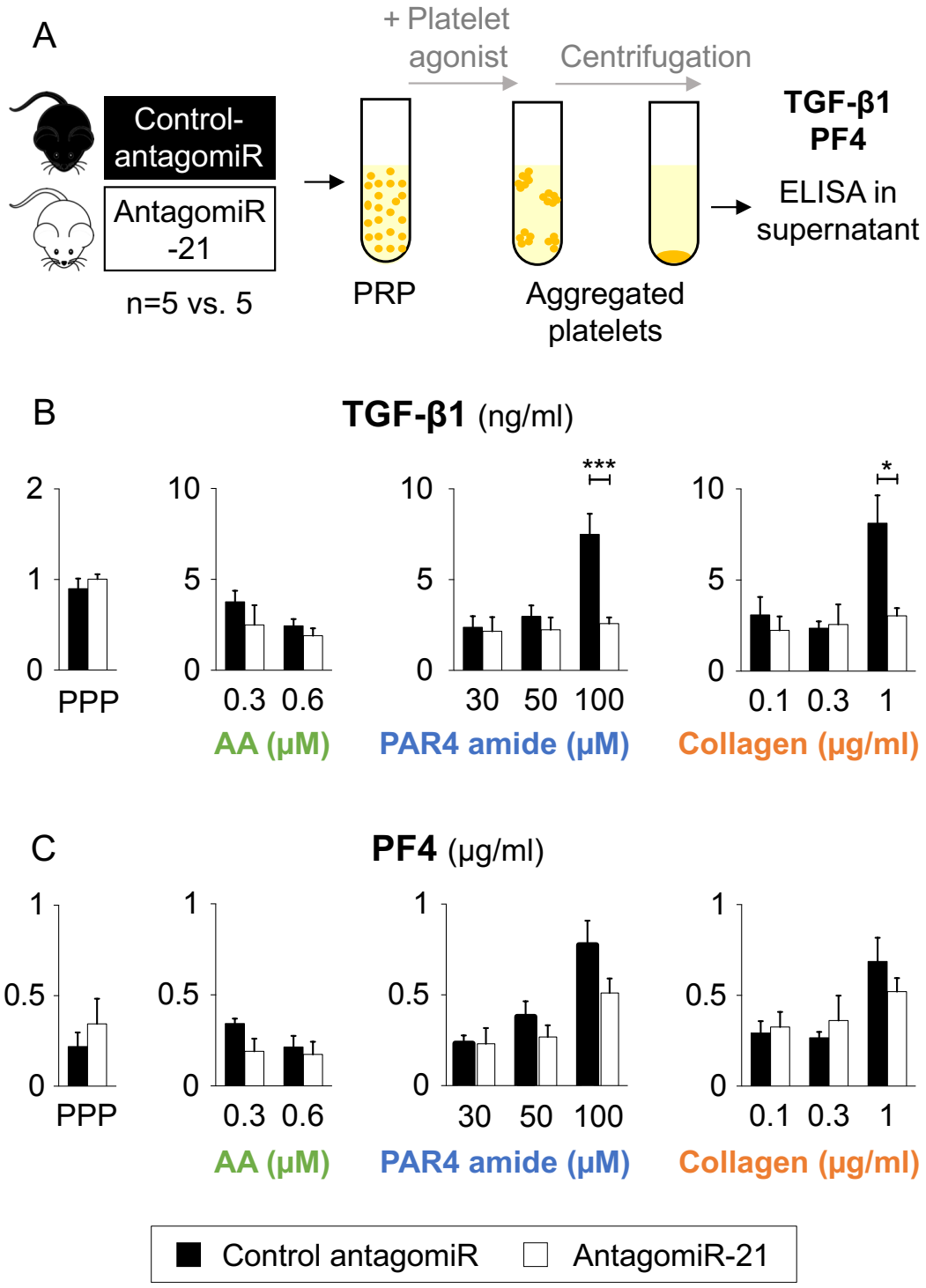

Figure 38. ELISA measurements in activated platelet supernatant after pharmacological miR-21 inhibition. A: Blood from antagomiR-21 or -control mice (n=5 vs. 5) was centrifuged to obtain PRP. Platelets were activated with different agonists, followed by centrifugation of samples to obtain the supernatant. **B:** Levels of TGF-β1 in PPP did not differ between both antagomiR types. Conversely, supernatant from PRP treated with PAR4 amide and collagen showed a dose-dependent increase of TGF-β1 levels, which was significantly less pronounced in PRP from antagomiR-21-treated mice. **C:** For PF4, a similar dose-dependent increase was seen for PAR4 amide and collagen, which was however not significantly affected by antagomiR-21 treatment. Statistical analysis was performed using a two-way ANOVA with *post-hoc* analysis using Šidák's test.

To assess whether the observed effect of antagomiR-21 treatment was part of a general effect on α-granule release, levels of PF4 were quantified by ELISA in the same samples (see **Figure 38, panel C**). Whilst a significant effect on PF4 release was seen with increasing concentrations of PAR4 amide ($F(2,24)$: 12.4, $p=0.0002$) and collagen ($F(2,23)$:7.0, $p=0.0043$), no effect was seen for AA ($F(1,16)$: 1.5, $p=0.24$). This is in line with the observations for TGF-β1. In contrast to TGF-β1, despite showing a trend towards lower PF4 release, individual comparisons between antagomiR-21 and control for the high-dose PAR4 amide ($p=0.12$) and collagen ($p=0.49$) did not reveal a significant difference.

4.3.9 TGF-β1 gene expression after antagomiR-21 treatment

The observation of decreased TGF-β1 release from platelets after antagomiR-21 treatment could imply two effects: lower platelet TGF-β1 content, or an effect on its release. We first evaluated whether there was a difference in expression of TGF-β1 and related genes. Megakaryocytes comprise <0.1% of the total cell population in the bone marrow, limiting the ability to isolate these cells from the total bone marrow. We therefore evaluated expression levels in the isolated whole bone marrow. As shown in **Figure 39**, **panel A**, no significant difference was seen for *Tgfb1* expression between bone marrow from antagomiR-21- and control-treated mice (FC: 1.11, $p=0.23$ for Welch's t-test). Similarly, no differences were observed for any of the TGF-β receptors (FC: 1.09, 1.02, 1.18 for *Tgfbr1*, *Tgfbr2* and *Tgfbr3*, with $p=0.37$, 0.99 and 0.34, respectively) or for *Ltbp1* (FC:1.06; $p=0.35$). Expression of *Tgfb2* and *Tgfb3* was below the threshold of reliable detection (average Cq 37.5 and 34.1, respectively). This is markedly lower compared to expression of *Tgfb1* (average Cq 25).

Potential effects of antagomiR-21 on *Tgfb1* gene expression in tissues were also evaluated. As shown in **Figure 39, panel B**, expression levels in the heart, liver and kidney were not significantly affected by systemic antagomiR-21 treatment (FC: 0.99, 1.12 and 0.94, with $p=0.96$, 0.45 and 0.60, respectively), despite significant inhibition of miR-21 levels as shown in **Figure 32**.

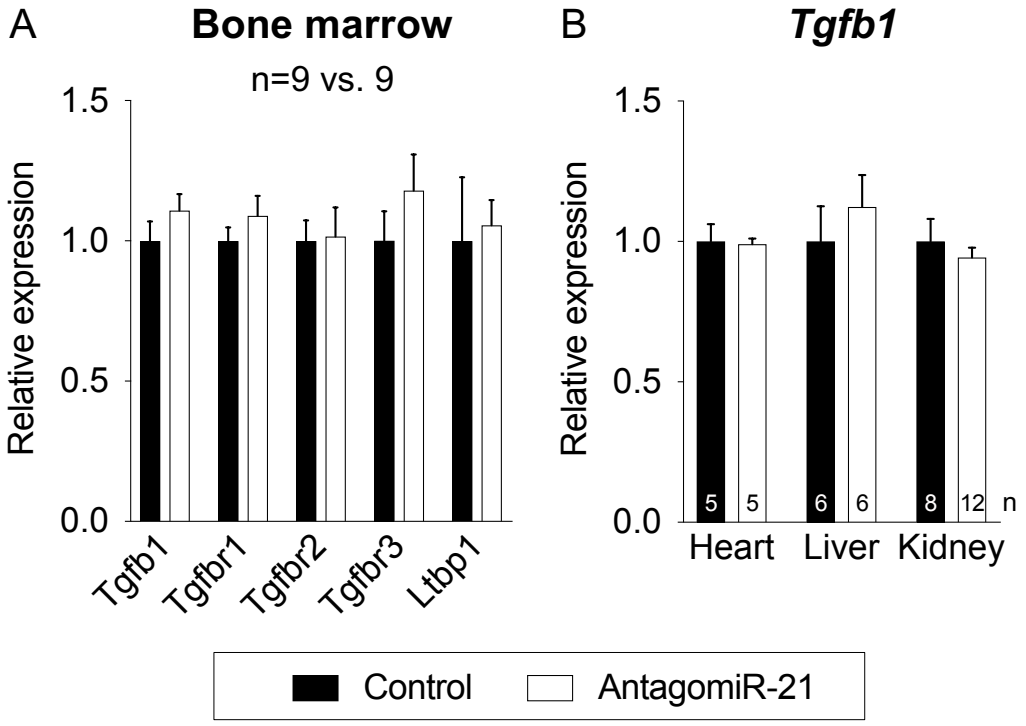

Figure 39. Gene expression after pharmacological miR-21 inhibition. A: To determine effects of systemic antagomiR-21 treatment on gene expression, qPCR analysis was performed in isolated bone marrow cells. Expression levels of *Tgfb1*, the three TGF-β receptors and *Ltbp1* were not significantly different between control- and antagomiR-21-treated mice (n=9 vs. 9). *Gapdh* was used as reference transcript. **B:** Transcript levels of *Tgfb1* were analysed in other tissues after antagomiR-21 treatment, showing no significant difference after miR-21 inhibition. Gene transcripts of *Actb*, *B2m* and *Ppia* were used as reference in heart (n=5 vs. 5 for control vs. antagomiR-21), liver (n=6 vs. 6) and kidney (n=8 vs. 12), respectively, based on RefFinder stability ranking within each tissue. Numbers on bars reflect the sample size of each group. Statistical analyses were performed using Welch's t-test.

4.3.10 Bone marrow histology after antagomiR-21 treatment

We were not able to analyse *Tgfb1* expression in isolated megakaryocytes due to their low abundance within the bone marrow population. Therefore, we aimed to determine TGF-β1 protein levels in the megakaryocytes resident in the bone marrow. Femora from antagomiR-21-treated mice and respective controls were harvested, fixed and decalcified to allow for histological sectioning and immunofluorescent staining (see **Figure 40, panel A**). In addition to using an anti-TGF-β1 antibody, megakaryocytes were stained using an anti-PF4 antibody. DAPI was used to visualise nuclei.

Representative images are shown in **Figure 40, panel B and C**. Localisation of TGF-β1 and PF4 were both equally distributed, with punctate enrichment appearing throughout the section. The species-specific control IgG staining showed low background signal for both stainings. As can be seen from the yellow signal in the overlay image, there was remarkable co-localisation of the antibodies targeting these two proteins. Magnification at 60x showed large

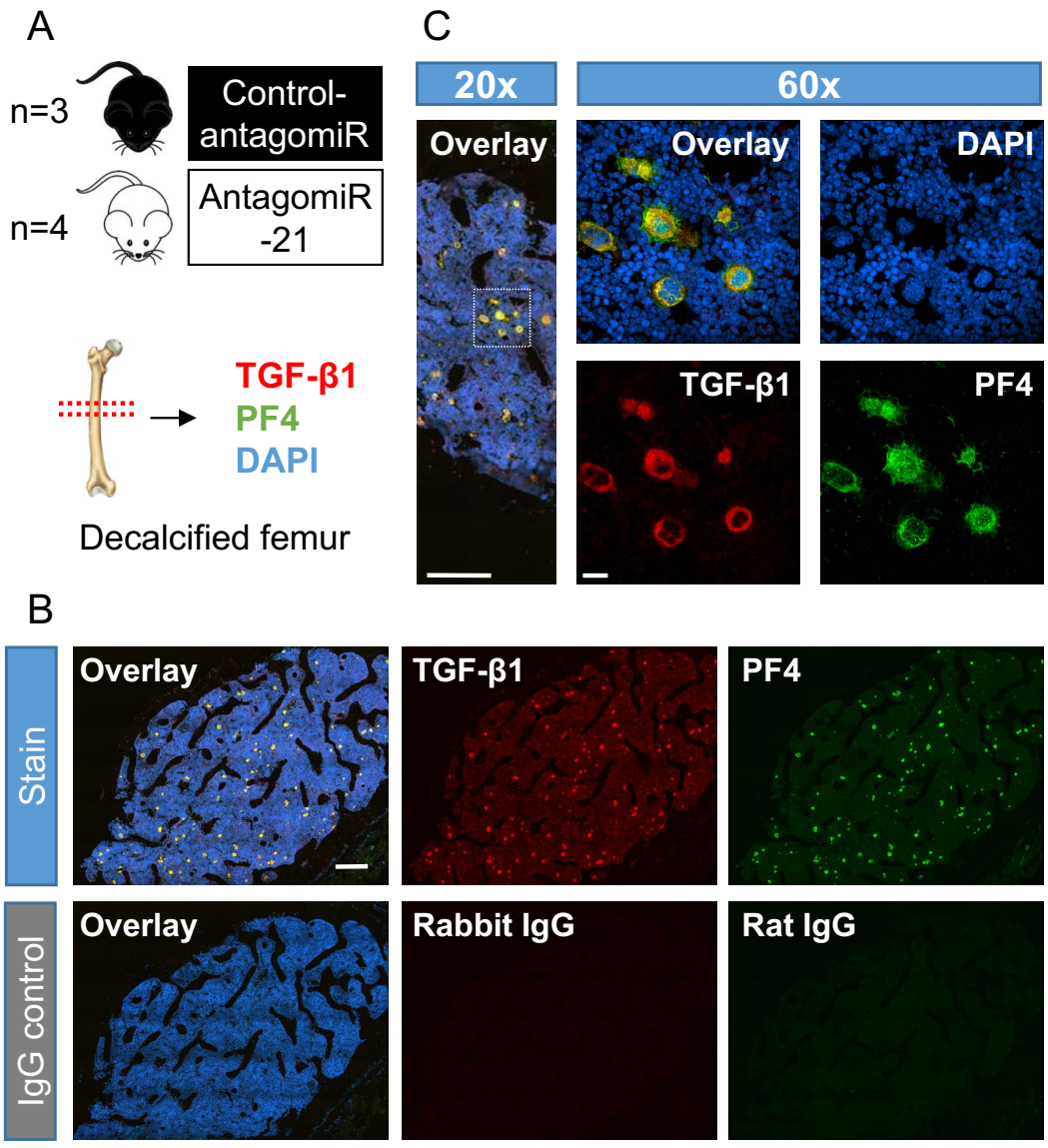

Figure 40. Immunohistochemistry in the murine bone marrow. A: After systemic treatment with antagomiR-21 or -control, mouse femora were processed for histological analysis by fixation and decalcification (n=3 vs. 4 for control and antagomiR-21-treated mice). Transverse sections were stained for TGF-β1 (red), PF4 (green) and a nuclear counterstain (DAPI, blue). **B:** Punctate localisation of TGF-β1 as well as PF4 was seen throughout the sections. Overlay of both channels showed remarkable overlap as indicated by yellow signal. Scale bar denotes 200 µm. **C:** Analysis at 60x magnification allowed for a more detailed appreciation of overlapping TGF-β1 and PF4 signal, identifying the cellular and lobulated nuclear morphology characteristic of megakaryocytes. Scale bars denote 200 µm and 20 µm for 20x and 60x panels, respectively.

and lobulated nuclei in the cells that stained positive for both proteins, a key characteristic of the morphology of megakaryocytes.[302] In addition, signal intensity beyond the areas of co-localisation was negligible. Images of sections

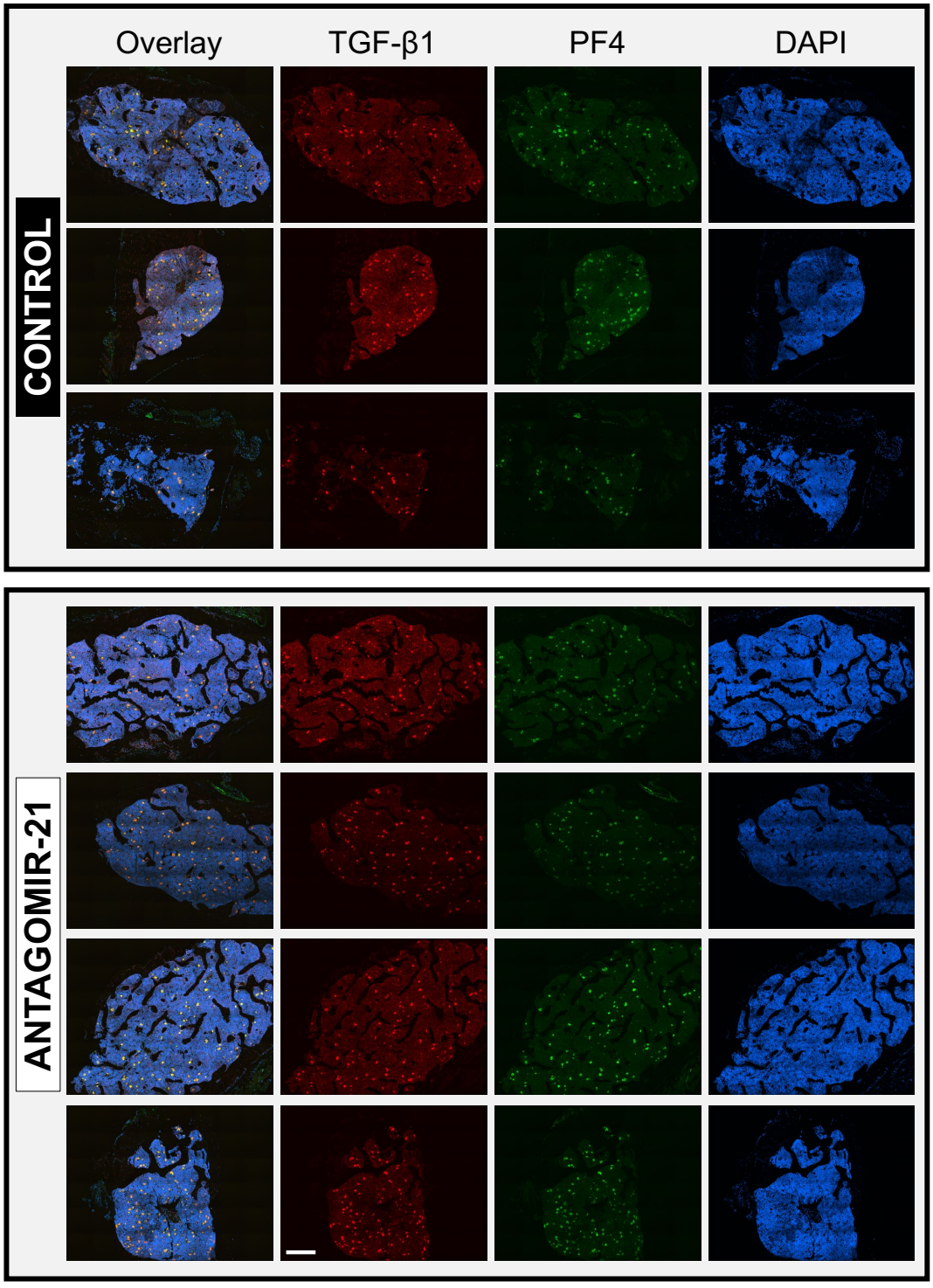

Figure 41. Bone marrow immunohistochemistry after pharmacological miR-21 inhibition. Immunohistological analysis was performed for bone marrow samples of mice treated with antagomiR-21 (n=4) or -control (n=3). Distribution of PF4-positive cells, as well as the intensity of TGF-β1, did not show a difference between both treatment types. Scale bar denotes 200 µm.

from all animals are shown in **Figure 41**. Whilst co-localisation of TGF-β1 and PF4 was seen consistently across the samples, the levels of TGF-β1 did not seem to differ between sections from antagomiR-21-treated animals and those treated with control antagomiR.

4.3.11 Immunoblot analysis of platelets after antagomiR-21 treatment

As the quantitative accuracy of immunohistochemistry is limited, we also determined TGF-β1 levels in platelets that were isolated after systemic antagomiR treatment (see **Figure 42, panel A**). In addition to TGF-β1, we determined levels of Wiskott-Aldrich Syndrome protein (WASp), encoded by the *Was* gene. Whilst playing an important role in actin polymerisation in leukocytes, this protein had previously been reported to control the release of TGF-β1 from platelets.[77] Interestingly, this protein is exclusively expressed in haematopoietic cells. Therefore, we investigated whether decreased platelet TGF-β1 release after systemic inhibition of miR-21 could have been explained by regulation of this protein.

Immunoblot analysis of isolated platelets confirmed our previous observations of TGF-β1 levels in megakaryocytes, with no significant difference being observed between platelets from antagomiR-21- and control-treated mice (see **Figure 42, panel B and C**). No differences were observed for PF4 levels (see **Figure 42, panel B and E**). Interestingly however, a difference was indeed observed for levels of WASp, with significantly higher levels in the platelets of antagomiR-21-treated mice. This difference was confirmed by relative densitometry (see **Figure 42, panel B and D**).

4.3.12 Identification of *Was* as a direct target of miR-21

Regulation of the *Was* gene by miR-21 was further studied in the bone marrow by qPCR. In contrast to the expression levels of *Tgfb1* (**Figure 39**), *Was* levels in the bone marrow were significantly higher after antagomiR-21 treatment (FC: 1.29; p=0.0323), as shown in **Figure 43**, **panel A**.

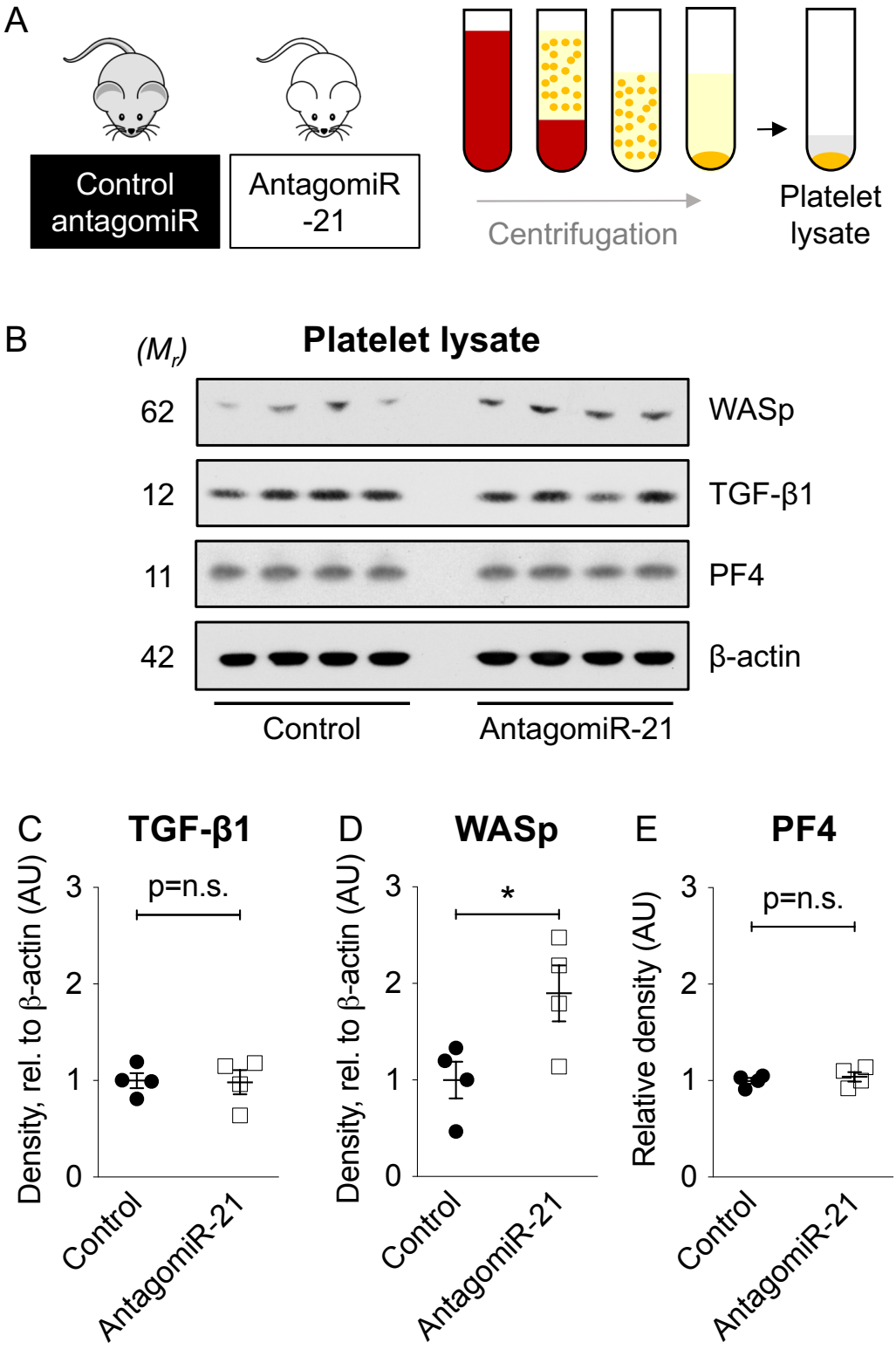

Figure 42. Immunoblot of lysed platelets isolated after pharmacological miR-21 inhibition. A: After systemic treatment with antagomiR-21 or -control (n=4 vs. 4), blood platelets isolated by sequential centrifugation were washed and lysed. **B:** Immunoblotting was performed to determine levels of WASp, TGF-β1 and PF4, whilst levels of β-actin served as a loading control. **C,D:** Densitometric analysis showed significantly higher levels of WASp in platelets from antagomiR-21-treated mice, whilst no difference was found for TGF-β1 and PF4. Signal intensity was normalised to the signal of β-actin for C and D. Statistical testing was performed using Welch's t test. M_r, relative molecular mass; AU, arbitrary units; n.s., non-significant.

In silico analysis for target prediction was performed next using the miRWalk algorithm, which combines the algorithms of twelve individual prediction tools.[284] Results of this analysis were combined with manually curated GO annotation of genes that were experimentally validated miR-21 targets (see **Supplemental table 5**). One prediction algorithm, RNAhybrid[286], predicted base pairing between the miR-21 seed sequence and the 3' UTR of the *Was* transcript (see **Figure 43, panel B**). As antagomiR-21 treatment had a significant effect on *Was*/WASp levels in mouse platelets and bone marrow, we used a luciferase reporter assay to determine direct targeting of *Was* by miR-21. Given that the *in silico* prediction was based on one algorithm and target prediction is known to suffer from false-positive findings (as shown in

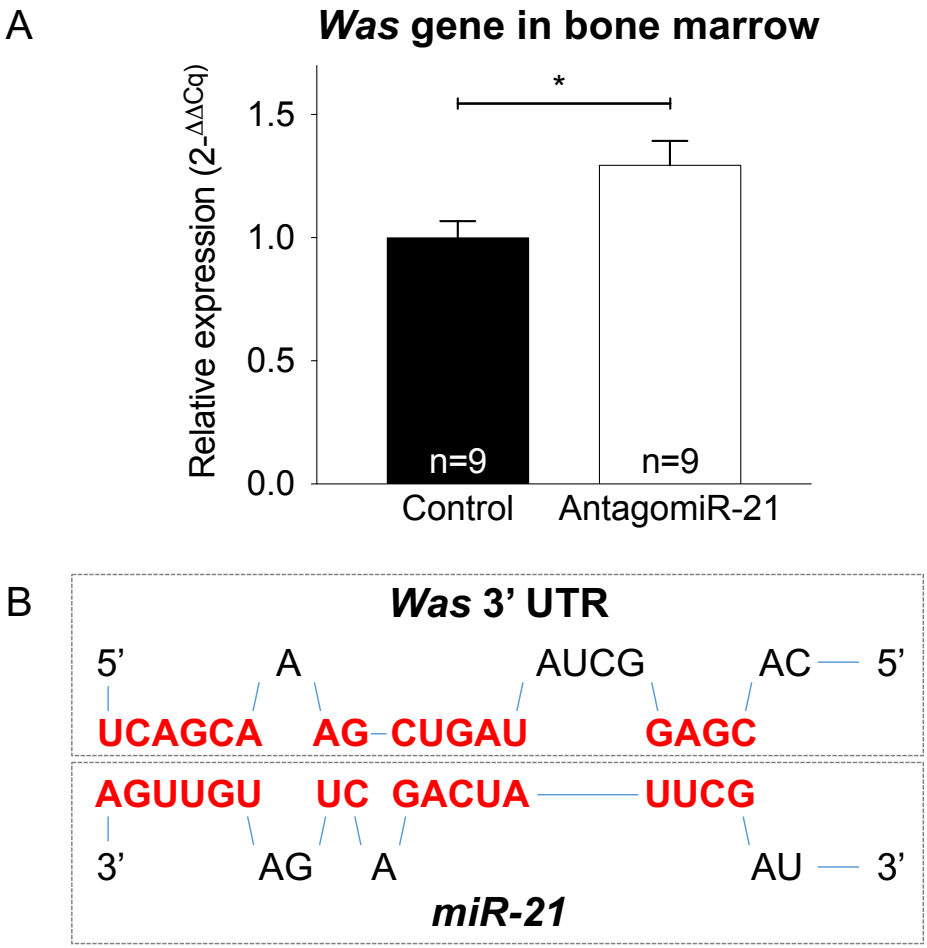

Figure 43. Bone marrow *Was* expression and predicted targeting by miR-21. A: An increased expression of *Was* in bone marrow cells after control (n=9) or antagomiR-21 treatment (n=9) corroborated the immunoblotting findings in lysed platelets. Transcript levels of *Gapdh* were used as reference and statistical comparisons were performed using Welch's t-test. **B:** *In silico* prediction algorithms identified a potential interaction between the 3' UTR of the *Was* gene transcript by miR-21, suggesting canonical targeting. Predicted targeting according to the RNAhybrid algorithm[265] is shown.

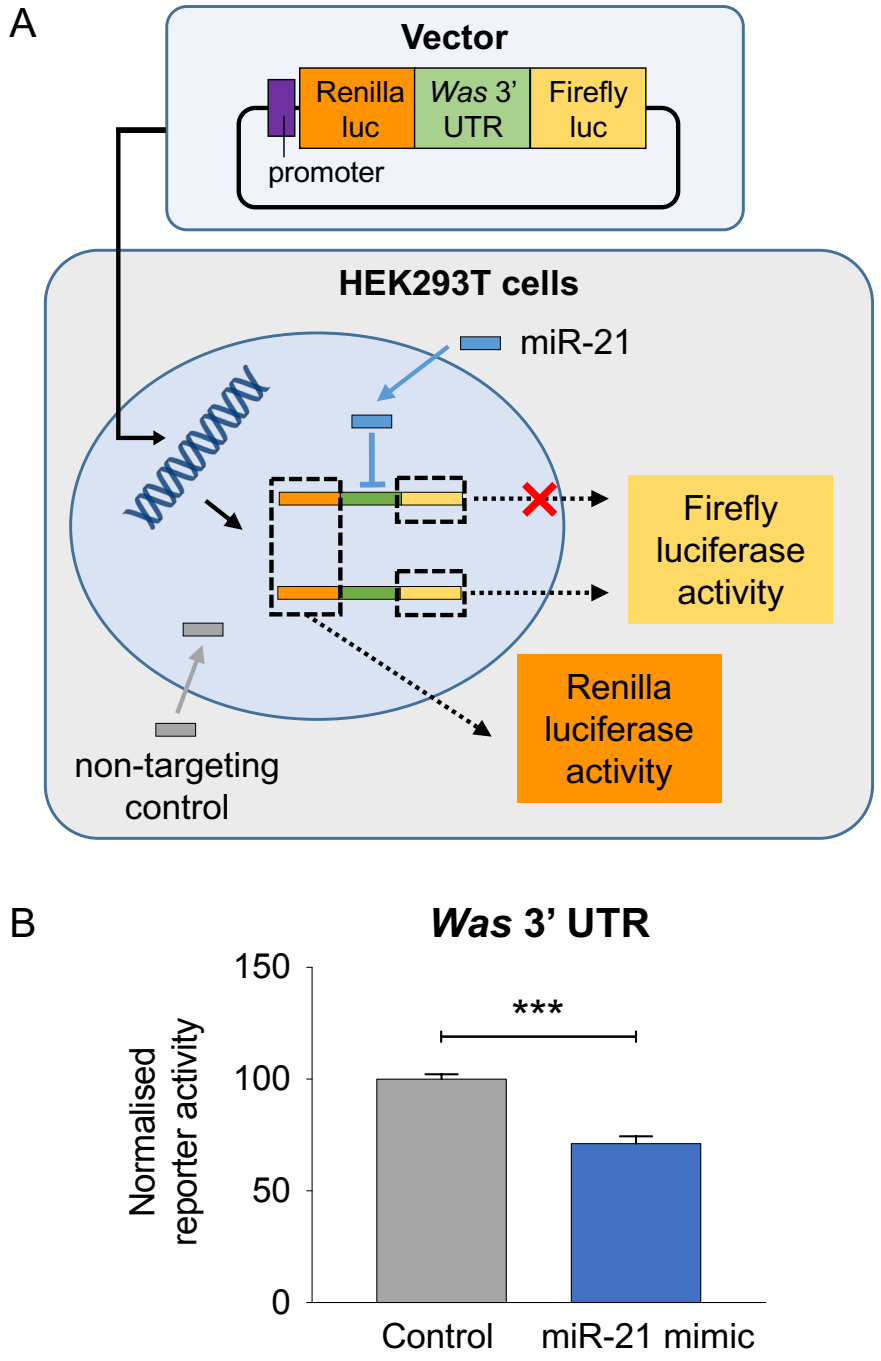

Figure 44. Luciferase reporter assay for targeting of *Was* by miR-21. A: The 3' UTR of the *Was* gene transcript was cloned into a vector, between the Renilla and firefly luciferase reporter genes. This construct was transfected into HEK293T cells together with miR-21 mimic or a non-targeting control. Targeting of the 3' UTR would result in a reduced Firefly reporter activity, whilst Renilla reporter activity would not be affected. **B:** Three independent experiments were performed, each time using triplicates and quadruplicates for control and miR-21 transfection, respectively. Firefly reporter activity, normalised to constitutive Renilla reporter activity, was significantly reduced after miR-21 mimic transfection in all three experiments. This indicates direct targeting of the cloned *Was* 3' UTR sequence by miR-21. Statistical analysis was performed using a paired t-test.

Supplemental table 5), we cloned the entire 3' UTR sequence of *Was* into a dual-luciferase (Renilla and firefly) reporter vector. These constructs were transfected into HEK293T cells together with miR-21 mimic or a non-targeting control sequence (see **Figure 44, panel A**). After 48 hours, normalised firefly luciferase activity was significantly reduced in miR-21-transfected cells (FC: 0.71; p=0.0010), indicating direct targeting of the *Was* 3' UTR by miR-21 (see **Figure 44, panel B**).

4.3.13 Analysis of blood and bone marrow from miR-21 *null* mice

Previous studies into miR-21 and cardiac fibrosis have highlighted a discrepancy between pharmacological and genetic inhibition of this miRNA.[110,118] In line with the observations by others[110], the size, weight and behaviour did not differ between miR-21 *null* mice and their littermate controls. Survival over several months was not different between both genotypes and there were no signs of spontaneous bleeding. To assess potential changes in platelets in miR-21 *null* mice, we first performed a whole-blood platelet count using a Hemavet haematology analyser (see **Figure 45**). In contrast to short-term pharmacological inhibition of miR-21, blood from miR-21 *null* mice showed significantly lower concentrations of platelets, with a mean (SEM) count of 647 (48) $x10^9$/L and 527 (27) $x10^9$/L for miR-21 *null* and wild-type blood, respectively (p=0.0333). Numbers of leukocyte subtypes were also significantly lower in miR-21 *null* mice, with mean (SEM) counts of 3.3 (0.4) $x10^9$/L and 1.5 (0.3) $x10^9$/L for lymphocytes (p=0.0020) and 132 (34) $x10^6$/L and 37 (10) $x10^6$/L for monocytes (p=0.0055), respectively. For the latter two cell types, average counts for the miR-21 *null* mice still fell within the normal reference range.

To determine whether these changes in the blood were accompanied by changes in the bone marrow, immunohistological staining was performed in decalcified femoral sections. As shown in **Figure 46, panel A and B**, a significant increase in megakaryocyte numbers was seen in miR-21 *null* bone marrow, with a median (interquartile range) count per mm^2 of 84.7 (78.0-90.0) and 106.3 (99.5-121.2) for wild-type and miR-21 *null* mice, respectively (p=0.003 for Mann-Whitney test). We next studied gene expression levels in the bone marrow of these mice (see **Figure 46, panel C**). No significant

difference was seen for expression of *Tgfb1* or *Ptprc* (CD45). However, transcript levels of several megakaryocyte-specific genes were significantly induced (FC: 1.70 [p=0.005] for *Itga2b*, 1.72 [p=0.026] for *Pf4,* 1.90 [p=0.030] for *Ppbp*). Altogether, platelet and megakaryocyte numbers were significantly altered in miR-21 *null* mice.

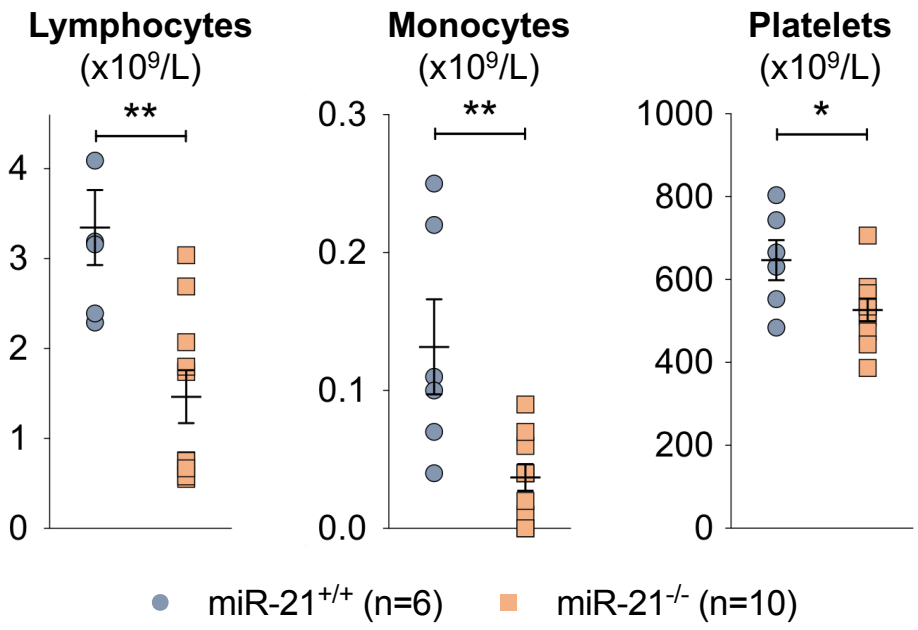

Figure 45. Hemavet blood count in miR-21 *null* mice. Automated blood cell counting identified significantly lower numbers of platelets, lymphocytes and monocytes in miR-21 *null* mice (n=10) compared to wild-type littermates (n=6). Welch's t-test was used for statistical comparison.

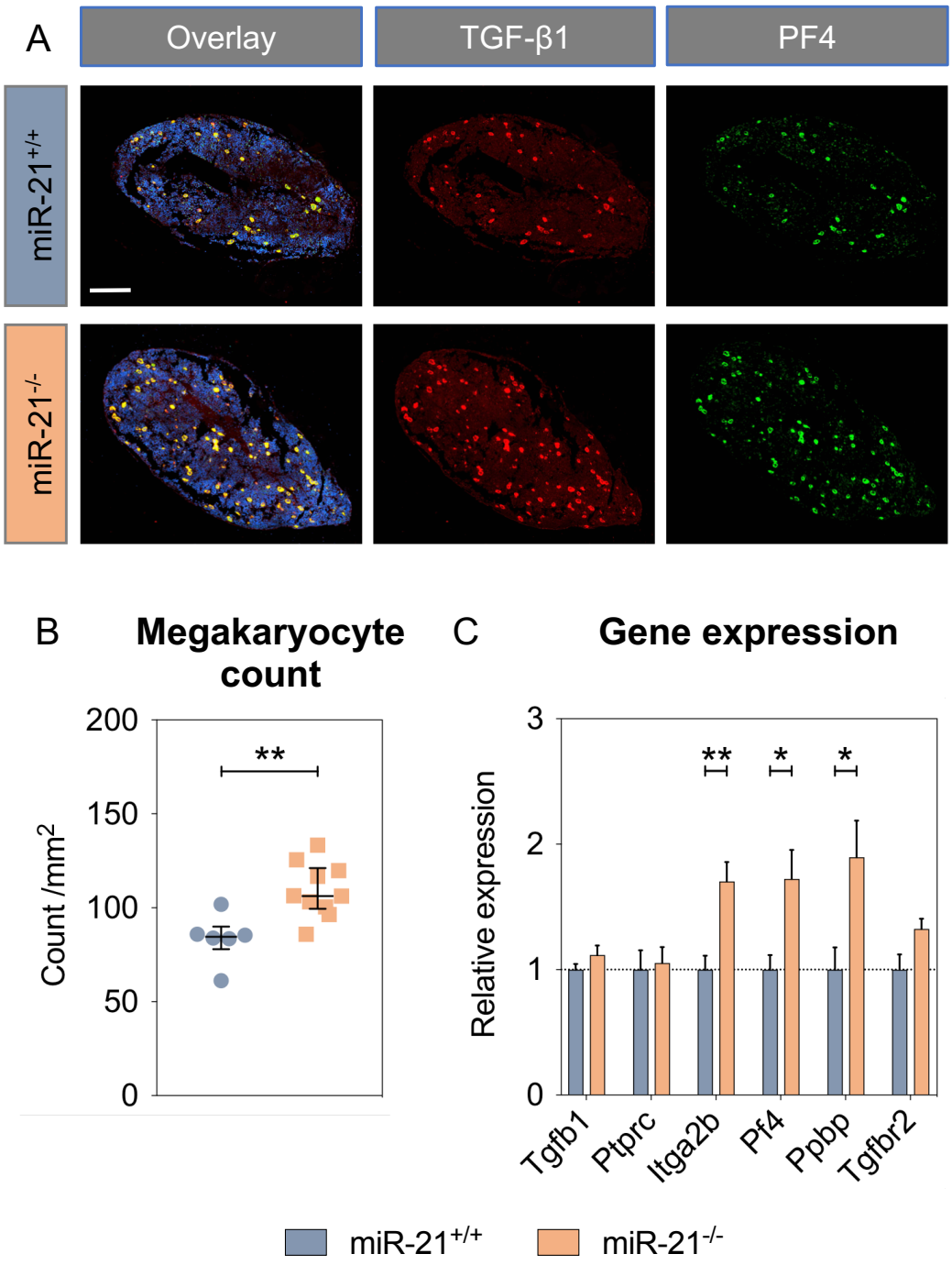

Figure 46. Bone marrow analysis in miR-21 *null* mice. A: Representative image of immunohistochemical analysis for TGF-β1 (red), PF4 (green) and a nuclear counterstain (DAPI, blue) in femoral bone marrow sections of miR-21 *null* mice (n=10) and littermate controls (n=6), identifying a higher number of PF4-positive cells. Scale bar denotes 200 µm. **B:** Blinded counting of megakaryocytes, identified as PF4-positive cells, showed significantly higher numbers in bone marrow from miR-21 *null* mice. Counting was performed using Fiji ImageJ software, with statistical comparison using the Mann-Whitney test. **C:** Expression levels of megakaryocyte-specific genes in isolated bone marrow cells, including *Pf4*, were significantly higher in miR-21 *null* mice. Transcript levels of *Tgfb1* and *Ptprc* (CD45) were not affected. Statistical comparisons were performed using Welch's t-test; n=6 vs. 6.

CHAPTER V

DISCUSSION

5.1 Direct effects of miR-21 in the heart

To this day, there is an unmet clinical need for treatment options of heart failure. Therefore, there is much interest in disentangling the underlying molecular processes that cause or worsen this clinical syndrome. MiR-21 has been widely implicated in the development and progression of fibrosis, a key feature of heart failure. Contradicting results from studies using different strategies to target miR-21 highlight the need for a better understanding of mechanisms that are at play. As the main source of ECM proteins, fibroblasts are widely regarded to be the main drivers of fibrosis. The scientific emphasis has therefore primarily been on the effects of miR-21 in these cells. This has indeed identified several potential mechanisms. However, there are limitations with the experimental approach that has been used so far. This includes the use of relatively crude methods to determine cell specificity of findings, as well as selection bias due to evaluation of pre-selected proteins rather than those identified through a wider screening approach. We therefore used a proteomic screening approach to analyse miR-21-mediated changes in the CF secretome. In addition, we validated results using immunoblotting for selected proteins and performed gene expression analysis for abundant and dysregulated proteins. In light of previous reports, we analysed the CF proliferation rate after transfection of miR-21 mimics and -inhibitors. To complement these strategies, we screened for differences in gene expression and protein levels in miR-21 *null* hearts.

5.1.1 The cardiac fibroblast secretome after transfections

Myocardial cells are generally subdivided into either cardiomyocytes or non-myocytes. Whilst this dichotomy is widely accepted, the latter population is often presumed to predominantly consist of fibroblasts. We will discuss the consequences of this assumption in **paragraph 5.1.5**. To enhance the confidence that an effect or observation indeed occurred in fibroblasts, several cell markers have been proposed. Despite an array of markers being in use, their specificity is contested, as pointed out in a recent study.[303] However, it can be argued that ECM production is primarily a readout of fibroblasts within the non-myocyte fraction of the heart.[12] Therefore, the ECM secretome

analysis of CF may to a certain extent bypass the discussion of fibroblast specificity in the non-myocyte cell population.

Most techniques determine changes in protein levels using antibodies. Though offering a straightforward method for protein quantification, there is bias towards selection of what proteins are analysed and for which ones appropriate and technically suitable antibodies are found. In contrast, the use of MS allows for a comprehensive identification and quantification of proteins. Although MS has many advantages, there is an extent of bias as well: untargeted MS favours detection of larger and more abundant proteins, which are more readily identified, whilst smaller and less abundant proteins can remain undetected in complex protein mixtures. Furthermore, without authentic reference standards MS data cannot be used to accurately compare quantities across different proteins. Using the CF secretome for MS analysis offers the opportunity to analyse an accumulation of ECM changes over a longer time course, for a wide range of proteins. This markedly increases the sensitivity. As miRNAs fine-tune protein synthesis, changes upon manipulating miRNA levels can be small and therefore challenging to detect. Previous studies using the same approach were indeed able to identify a marked effect of miRNA manipulation[185] and hypoxia[291] on CF protein secretion. We therefore used a similar approach to study effects of miR-21.

Significant changes of miR-21 levels were seen in transfected CF, indicating successful overexpression and inhibition. Furthermore, a marked effect of TGF-β1 treatment was seen at the transcriptional and protein level. A significant induction was seen for expression and secretion of periostin, as well as other commonly used markers of a myofibroblast-like phenotype. Despite the identification of 144 different proteins, there was a surprising lack of changes in the CF secretome after miR-21 overexpression and inhibition. Strikingly, no significant effect was observed on any of the key structural ECM proteins, as will be discussed in **paragraph 5.1.1.5**.

Despite having no major effect on ECM protein secretion, the secretome analysis did identify some proteins of potential interest. Upon miR-21 inhibition, VCAM1 and LG3BP levels increased in the secretome, whilst overexpression

had no effect. Gene expression analysis for LG3BP was in line with these findings. For IBP4 and granulin, higher levels were observed after miR-21 overexpression, although granulin levels also increased after miR-21 inhibition. Whilst these changes are unlikely to explain the reported effects of miR-21 inhibition in cardiac fibrosis, potential significance of these findings will be discussed.

5.1.1.1 Vascular cell adhesion protein 1

VCAM1 is a cell adhesion molecule that has been described extensively for its function in tissue inflammation[304] and CVD, such as atherosclerosis.[305] Expression of VCAM1 in endothelial cells is stimulated by inflammation, facilitating the adhesion of leukocytes to the vascular endothelium. Binding to VCAM1 has downstream signalling effects that enhances leukocyte transmigration into the underlying stroma. Pharmacological disruption of the VCAM1-leukocyte interaction is currently being used in the treatment of multiple sclerosis, indicating a pivotal role for this protein in inflammation.[306]

Expression of VCAM1 in endothelial cells has been widely described, yet its presence has also been reported in other cell types. These include vascular smooth muscle cells[307] and CF, where its expression could be induced through phosphorylation of p38 MAP kinase, one of the signalling pathways downstream of TGF-β activity.[308] A more recent report studied the role of VCAM1 in pulmonary fibrosis.[309] Here, VCAM1 levels were increased in plasma and in pulmonary fibroblasts from patients with idiopathic pulmonary fibrosis, as well as in bleomycin-induced fibrotic lungs in mice. This study confirmed induction downstream of TGF-β, using *in vitro* TGF-β1 treatment of human lung fibroblasts. Silencing VCAM1 in fibroblasts had an anti-proliferative effect, implicating its expression in pro-fibrotic signalling. It remains unanswered what the *in vivo* effect of fibroblast VCAM1 is in the context of inflammation and fibrosis.

Increased secretome levels of VCAM1 after miR-21 inhibition could also be derived from residual endothelial cells. These cells are thought to succumb when cultured in fibroblast media, which is indeed supported by both microscopic and qPCR analysis after our CF isolation and subculture protocol.

Nevertheless, some residual endothelial cell presence in the non-myocyte culture cannot be ruled out. Transfection of miR-21 inhibitor promoted proliferation of endothelial cells that had been treated with rapamycin, a known inhibitor of endothelial cell proliferation and migration.[310] Other studies have shown that miR-21 enhances endothelial cell differentiation[311] and proliferation.[312] The latter supports the hypothesis that transfection of miR-21 inhibitor into residual endothelial cells may have enhanced their survival, causing an increased level of endothelial cell-derived VCAM1. Of note, miR-21 in endothelial cells also increased VCAM1 expression, through targeting peroxisome proliferator-activated receptor-α. This implies an effect directly opposite to our observation.[313] Altogether, these findings suggest that VCAM1 identified in the secretome is unlikely to have been endothelial cell-derived.

5.1.1.2 Galectin-3-binding protein

The second protein that showed significantly increased levels after miR-21 inhibition was LG3BP. This member of the macrophage scavenger receptor cysteine-rich domain superfamily[314] has previously been implicated in modulating cell-cell and cell-matrix adhesion during inflammation.[315,316] Fibroblasts were shown to secrete LG3BP. Binding studies revealed interactions with fibronectin and several collagens, but secretion levels were found to be much lower than e.g. fibronectin, implicating it as an ECM component without being a major structural component.[315] We recently identified LG3BP as part of a four-biomarker signature of high-risk atherosclerotic plaques, implicating it as a circulating marker of plaque instability that is derived from the vascular ECM.[317]

To our knowledge, there have been no reports on the role of LG3BP in cardiac fibrosis. However, its secretion from a breast cancer cell line had anti-fibrotic effects through inhibiting monocyte-derived fibrocyte differentiation.[318] LG3BP and its binding partner galectin-3[316], previously shown to be pro-fibrotic in response to MI[319] and cardiac inflammation[320], were shown to compete in their anti- and pro-fibrotic effects, respectively.[318] In light of this, increased CF secretion of LG3BP upon miR-21 inhibition could imply that miR-21 has a pro-fibrotic effect through targeting LG3BP, enhancing galectin-3-induced fibrocyte and fibroblast differentiation and consequently fibrosis.

Increased expression and secretion of LG3BP upon miR-21 inhibition could imply de-repression of a direct target. However, we did not find a decrease in its secretion or gene expression upon miR-21 mimic transfection, as would be expected in the case of direct targeting. We also did not find a supposed anti-fibrotic effect reflected in decreased secretion of other ECM proteins. Nevertheless, our *in vitro* analysis does not allow for detection of potential paracrine effects of LG3BP. Further study would be required to determine if increased LG3BP secretion upon miR-21 inhibition could attenuate cardiac fibrosis.

5.1.1.3 Insulin-like growth factor binding-protein 4

Increased secretome levels of IBP4 were found after miR-21 mimic transfection in unstimulated CF. IBP4 expression and secretion has previously been reported in human fibroblasts[321] and in rat lung fibroblasts, where it was shown to control IGF-mediated cell proliferation. Accumulation in the conditioned media of lung fibroblasts occurred in response to treatment with various growth factors, including PDGF and fibroblast growth factor 2.[322,323] IGFs regulate an array of biological processes, mainly related to growth hormone signalling. In the circulation, they are bound to a set of binding proteins (IGFBP; IBP) [324] that on one hand regulate IGF activity, but act independently of their IGF ligand. The mechanisms and actions of both IGF-regulating and IGF-independent activity vary for the different IBP subtypes.[325]

Focusing on IBP4, *in vitro* and mouse studies showed its ability to block IGF activity in bone formation[326] and muscle growth.[327] Endothelial overexpression inhibited IGF-induced angiogenesis[328] and adipose tissue expansion in adipocytes.[329] In the heart, IBP4 enhances cardiomyocyte differentiation. Furthermore, it is required for cardiomyogenesis through a mechanism independent of IGF.[330,331] These observations corroborate the suggested mode of action for IBPs, regulating the bioavailability and activity of IGF. However, in contrast with these observations, systemic administration of IBP4 increased bone formation and serum IGF levels, suggesting its ability to enhance IGF signalling through impeding IGF clearance.[326,332] A similar mechanism has been suggested for storage of IBP-bound IGF in the ECM,

which could play a part in wound healing[325] and may therefore be involved in fibrosis formation.

Increased levels of IBP4 in the CF secretome after miR-21 mimic transfection could have several explanations. First, pro-proliferative effects of miR-21 may result in increased IBP4 synthesis and secretion. Alternatively, decreased cleavage due to lower levels of IGF or other proteolytic enzymes could have caused a relative increase of IBP4. IGF, reported to be the main determinant of IBP4 cleavage[323], fell below the threshold of reliable detection in the secretome samples and was therefore excluded from analysis. Regardless, the absence of an effect in TGF-β1-stimulated CF or upon miR-21 inhibition on IBP4 levels in the secretome challenges the relevance of our finding in the context of myocardial fibrosis.

5.1.1.4 Granulins

Granulins showed increased levels in media from both unstimulated cells transfected with miR-21 mimic and in TGF-β1-stimulated cells transfected with miR-21 inhibitor. In addition, a significant increase, yet with less than a two-fold change, was seen after transfection of miR-21 mimic in TGF-β1-stimulated CF.

The recent discovery that mutations in the progranulin gene give rise to frontotemporal dementia has resulted in an increased interest in this protein.[333] The progranulin protein is a secreted glycoprotein that can be cleaved into seven complete and one half mutually homologous peptides by metalloproteinases such as matrix metalloproteinase 9.[334] In addition to the brain, granulins are widely expressed across tissues and cell types, including fibroblasts, where they are induced upon tissue injury.[335] Interestingly, a later study, focussing on inflammation and wound repair, found that uncleaved progranulin and cleaved granulins have opposing effects.[336] Cleavage is regulated by two molecules, with elastase digesting progranulin into the individual granulins, whilst the binding of secretory leukocyte protease inhibitor (SLPI) to progranulin protects it from elastase-mediated cleavage. Elastase is released from neutrophils during inflammation, while SLPI is released from the epithelium as well as macrophages and neutrophils. Thus, the balance

between elastase and SLPI and the concomitant balance between progranulin and its cleavage products is under control of different but overlapping sources of inflammatory mediators.

Functionally, progranulin was shown to stimulate cell proliferation through activating MAP kinase and phosphoinositide 3-kinase[337], whilst cleaved granulins inhibited growth of epithelial cells.[336] In contrast, granulins, but not progranulin, were shown to attract neutrophils through triggering epithelial release of interleukin-8, whilst progranulin inhibited neutrophil activation and spreading. Furthermore, progranulin has a rate-limiting effect on wound healing in SLPI-deficient mice where progranulin cleavage is impaired. This implies that granulins promote inflammation, whilst progranulin enhances re-epithelialisation and wound healing. In light of the pathophysiology of fibrosis, uninjured tissue is abundant in SLPI and consequently progranulin, preventing inflammation from occurring. Upon injury, infiltrating leukocytes release elastase, cleaving resident progranulin into granulins that impede tissue regeneration and promote further activation of the inflammation response.[336,338]

Increased secretion of granulin upon miR-21 mimic transfection is in line with the previously described induction of both miR-21 and granulin in fibroblasts upon tissue injury. The simultaneous increase in granulin release upon miR-21 inhibition may at first seem inconsistent. However, activity of progranulin and its cleavage products is highly dependent on the context of inflammatory cells. Consequently, the observed increase is unlikely to have a functional effect on cardiac fibrosis by itself. Despite having received little attention outside of the field of neuroinflammation, the progranulin/SLPI/elastase system may be of importance in the context of cardiac injury. Further study of this axis, as well as the effect of miR-21 inhibition *in vivo*, is warranted to assess its relevance for the pathophysiology of cardiac fibrosis.

In summary, we found no significant effect of miR-21 mimic or inhibitor transfection on fibroblast secretion of ECM proteins, in contrast to a previous report using a similar technique for a different miRNA.[185] Upon miR-21

inhibition, we did observe an increased secretion of VCAM1, a leukocyte cell adhesion molecule that may be involved in pro-fibrotic signalling but could also have been derived from residual endothelial cells; and for LG3BP, which may have anti-fibrotic effects through inhibiting fibroblast differentiation. None of the changes upon miR-21 mimic transfection in TGF-β1-stimulated cells reached statistical significance whilst showing a greater than two-fold change. In unstimulated cells, the observed increase in IBP4 secretion may have occurred as a downstream effect of miR-21 signalling, where its presence in the ECM may enhance pro-proliferative signalling by IGF through inhibiting IGF clearance. The changes that were seen for progranulin appear unspecific and are unlikely to be of significance without the context of the leukocyte-derived factors that determine its signalling effects.

5.1.1.5 Major ECM proteins

As expected in the secretome of fibroblasts, the majority of identified proteins were key structural proteins such as collagens and major glycoproteins, as illustrated by **Figure 17**. A relatively large proportion of the total identified spectra consisted of peptides from type I and type III collagen. These fibrillar collagens are the most abundant collagens in the myocardium, accounting for approximately 80% and 10% of total myocardial collagen content, respectively.[11,339] Fibronectin was identified as third most abundant protein. This glycoprotein mediates the attachment of collagen fibrils to the sarcolemma together with basement proteins such as collagen type IV and laminin, both being linked together by perlecan.[340] High levels of all these proteins were identified in the CF secretome.

There is striking similarity regarding identified proteins between this analysis and those previously reported by our own group[185] and recently by others.[291] However, in contrast to both other studies, no significant changes were observed upon miR-21 manipulation, regardless of the presence or absence of TGF-β1 stimulation. In contrast, marked effects were seen with TGF-β1 stimulation itself. Whilst this is not surprising, it does indicate the ability of the used experimental setup to identify changes in gene expression and protein secretion. This further supports the conclusion that direct effects of miR-21 on ECM secretion by CF are limited.

5.1.2 Cardiac fibroblast proliferation after transfections

In contrast to the lack of changes on ECM secretion, a significant effect of miR-21 was seen on CF proliferation. This is consistent with the observed induction of periostin gene expression after miR-21 overexpression, which is a key marker of fibroblast proliferation and differentiation.[289] Upon miR-21 mimic transfection, a 24-hour follow-up identified a significantly higher proliferation rate, whereas transfection of miR-21 inhibitor showed the opposite effect when compared to its respective control. This finding is in line with previous observations from one of the first studies on miR-21 and cardiac fibrosis; here, miR-21 transfection increased CF survival *in vitro* as assessed by annexin V expression.[118] This effect was confirmed in a smaller report published recently, using a 3-(4,5-dimethylthiazolyl-2)-2,5-diphenyltetrazolium bromide (MTT) assay.[135]

As described in the Methods chapter (**paragraphs 3.3-3.5**), proteomic analysis of the CF secretome was performed using equal volumes of media and equal cell numbers for each sample at the start of the experiment. Therefore, an effect on proliferation would have also affected protein levels in the secretome. This was however not observed, for which several explanations can be given. Firstly, the difference in proliferation rate was relatively modest, both after miR-21 overexpression and inhibition, which could mean that the effect is insufficient to cause significant changes in protein secretion over a 48-hour period. Second, to reduce the contamination of conditioned media with bovine serum, secretome analysis was performed using culture in serum-free medium. This may have suppressed proliferation overall, potentially compromising the ability to observe an effect of miR-21 manipulation. Previous analyses however were able to detect marked and extensive changes in gene expression and protein secretion by CF using a similar serum-free culture protocol.[185,291] Lastly, secretome analysis was performed using conditioned media containing proteins that accumulated over a 48-hour period. The CF proliferation assay implied a trend towards decreasing differences after 24 hours, implying contact inhibition as cells reach a state of confluence within the well (see **Figure 11**). It cannot be ruled out that a similar effect limited the

sensitivity of the CF secretome analysis to detect proliferation-driven differences.

5.1.3 Analysis of miR-21 *null* mouse hearts

Previous studies on miR-21 and cardiac fibrosis have used both pharmacological and genetic inhibition in mice, combined with different pathological scenarios. Results from two main studies on miR-21 and cardiac fibrosis were diametrically opposed. The first study showed a profound benefit of systemic antagomiR-21 treatment[118], whilst the second study found no difference, neither after pharmacological inhibition using an octamer-based LNA inhibitor specifically targeting the miR-21 seed sequence, nor in miR-21 *null* mice.[110] The latter study also reported a normal phenotype of miR-21 *null* mice at baseline. This evaluation included the relative heart weight, fractional shortening as determined by echocardiography and protein levels of previously reported miR-21 targets. However, no analysis of gene expression or protein levels for ECM proteins was provided. Therefore, we used a proteomics approach focussed on the ECM, using a three-step protein extraction protocol as extensively used in previous work from our group.[8,294] In addition, we performed gene expression analysis for several cardiac miRNAs and for transcripts encoding the most highly abundant proteins in the secretome analysis, as well as the significantly changing ones.

Apart from the absence of miR-21, no significant differences were found for levels of the other analysed miRNAs, nor for the gene transcripts that were quantified. For the ECM protein analysis, there was remarkable overlap between the proteins that were detected at high levels and those that were found at the highest levels in the CF secretome. Despite the stable detection of fifty-five ECM proteins, no significant differences were observed between the miR-21 *null* and wild-type mouse hearts. Proteins that showed the greatest trends towards differences, although none reaching statistical significance, were microfibrillar-associated protein 5 (MFAP5), an ECM glycoprotein that has been reported to be a target of anti-fibrotic miR-29 and is involved in myofibroblast differentiation[341]; annexin A7 (ANXA7), a protein involved in calcium handing and electrical conduction in the heart[342]; and the collagen VI α6 chain. MFAP5 and collagen VI have both been reported to induce

myofibroblast differentiation in the heart.[343] Whilst these could be interesting proteins to study further, validation of these findings would be required, in particular given the lack of significant changes for any of these proteins. Furthermore, as the used mouse model is a global miR-21 *null* mouse, it cannot be ruled out that these findings are an indirect effect due to the lack of miR-21 in other tissues or cell types. Importantly, the analysis of miR-21 *null* hearts underlines that miR-21 confers pro-fibrotic effects only in presence of tissue injury and a concomitant systemic response.

5.1.4 Contradicting results in previous studies

Whilst a remarkable benefit of systemic miR-21 inhibition has been widely reported, studies with opposing outcomes have disputed this conclusion. Several studies and commentaries have attributed disparate results to differences in the miR-21-targeting strategy. The first major study that failed to observe a benefit of miR-21 used both miR-21 *null* mice and short LNA octamers targeting miR-21.[110] The lack of effect in miR-21 *null* mice could be due to compensatory mechanisms that occur due to embryological absence of miR-21[253], or due to effects in other tissues that indirectly affect the fibrotic phenotype upon myocardial injury. Our observation of reduced platelet and leukocyte counts are an example of an extracardiac factor that may have affected the outcome. A head-to-head comparison of different anti-miRs indeed highlighted the disparity between pharmacological strategies.[124] Furthermore, phosphorothioate backbone modifications, a commonly used feature in anti-miRs, may induce platelet activation[254], which may have had a marked effect on the outcomes of different studies. Besides, these findings may impede their clinical application if platelet aggregation is indeed induced. As reported in **paragraph 4.3.3**, we were unable to detect a platelet aggregation-inducing effect using light transmission aggregometry. Further safety studies specifically addressing this point are crucial prior to clinical evaluation.

Differences in oligonucleotide design also affects their penetrance and retention across various tissues.[344] A particular oligonucleotide design may target a certain cell type more efficiently. Contradicting results between studies using anti-miRs could therefore be explained by different pharmacodynamics.

The findings from our study, implicating miR-21 in systemic effects that may affect fibrosis, emphasises the importance of this aspect. Varying levels of penetrance in tissues beyond the targeted organ may be a relevant contributor that is insufficiently appreciated.

5.1.5 Contributing cell types in cardiac fibrosis

As pointed out in the introduction, the landmark study by Thum *et al*[118] concluded that the differential expression of miR-21, as well as the supposed therapeutic mechanism of miR-21 inhibition, depended on CF. The conclusion that miR-21 was primarily a fibroblast miRNA in the heart was subsequently confirmed in other studies.[97,119,127,132,158] However, its expression in other cell types within and beyond the heart, such as endothelial cells and skeletal muscle cells, was also shown soon after. Expression in those cell types was linked to angiogenesis dysfunction[345] and cell survival.[151] The ubiquitous expression of miR-21 is of importance for the interpretation of previous and future studies.

Conclusions about miR-21 expression within the cardiac cell population requires a critical appraisal of the experiments that underlie the attribution to fibroblasts. In most studies that determine cell type-specific changes and effects of miR-21 in the heart, a dichotomous approach is used. This means that cells are classified as either cardiomyocytes or 'fibroblasts'. Detection of miR-21 is either carried out using *in situ* hybridisation in diseased tissues[119,127], or by qPCR analysis or Northern blotting of isolated cells. Cell isolation techniques depend on differential attachment to a cell culture dish or differential sedimentation of cardiac cells obtained by enzymatic tissue digestion.[118,132,158] These commonly used techniques separate cardiomyocytes from other cell types, yet the composition of the latter is not limited to fibroblasts. Several studies have aimed to characterise the non-myocyte fraction, however this has so far been limited to fibroblasts, vascular cells such as smooth muscle cells and endothelial cells, and leukocytes.[14,131] Interestingly, a recent report in rat hearts identified miR-21 specifically in inflammatory cell infiltrates after myocardial injury using histopathological analysis.[346]

In an attempt to clarify some of the controversy regarding the responsible cell types for miR-21 induction in injured hearts and the therapeutic benefit, Ramanujam *et al* aimed to distinguish effects in different cell types.[131] To do so, viral vectors with different tissue tropism were used. Whilst AAV9 was highly selective for cardiomyocytes, Moloney murine leukaemia virus (MMLV) targeted the non-myocyte cells but not cardiomyocytes. A further analysis of the composition of the non-myocyte fraction was in line with previous literature[14], showing endothelial cells, fibroblasts and immune cells. MiR-21 expression was found to be highest in the fibroblasts. Using an MMLV-green fluorescent protein (GFP) vector for visualisation, 60% of endothelial cells and fibroblasts appeared infected, whereas $CD45^{+}$ immune cells did not acquire a detectable GFP signal. Similar results were found when treating miR-$21^{fl/fl}$ mice with AAV9 and MMLV vectors harbouring codon-improved Cre recombinase (iCre). Successful infection with this vector should result in iCre-mediated miR-21 knockdown. MMLV-iCre significantly reduced miR-21 expression in CF, but not in cardiomyocytes or in the kidney, liver, lung or spleen. AAV9 on the other hand reduced miR-21 expression in cardiomyocytes as well as in the liver.

When inducing cardiac remodelling using TAC, inhibiting miR-21 in cardiomyocytes worsened fibrosis, potentially by inducing apoptosis. Non-myocyte inhibition however showed a strong attenuation of fibrosis and cardiomyocyte hypertrophy. From the seemingly opposing roles of miR-21 inhibition depending on which cell type is targeted, and the lack of disease attenuation in global miR-21 *null* mice, the authors argue that miR-21 may act systemically as a modulator of inflammation. In this context, it is striking that effects of pharmacological inhibition of miR-21 on the fibrotic phenotype are only observed in presence of tissue damage. As this is likely to be accompanied by a systemic response, an indirect effect of miR-21 becomes a more likely hypothesis. This is supported by high expression levels of miR-21 in cells of hematopoietic origin.

Although these results highlight the importance of both fibroblasts and other systemic effects in the development of cardiac fibrosis, platelets were not included in the analysis despite previous evidence for their involvement.[29,34,70,347–349] In addition to immune cells, platelets have also been

shown to infiltrate the diseased heart tissue.[350] The link between platelets and tissue fibrosis has been suggested in other tissues such as the liver.[351,352] Although these studies imply platelet activation and/or sequestration within injured tissue, it is challenging to experimentally differentiate between blood contaminants and 'resident' cells. The sequence of washing and enzymatic digestion steps that is used during isolation of the different cardiac cell fractions is likely to lyse the platelets that were present within the tissue. Whilst the potential effects of the isolation methods on leukocytes has been determined, there is no mention of potential effects on cells that may have been lost during this process.[14]

5.2 Systemic effects of miR-21

In addition to being expressed in a wide range of somatic cells, miR-21 has also consistently been found in cells of hematopoietic origin.[353] Whilst its expression in bone marrow progenitor cells is relatively low, this increases as the different progenitors progress through the differentiation stages towards mature cells.[354–356] The involvement of an immune response during tissue remodelling may therefore contribute to the reported functions of miR-21. Expression and processing of the miR-21 precursor is enhanced by TGF-β signalling. Increased tissue expression might therefore reflect changes secondary to the inflammatory response.

Furthermore, increased cardiac levels of miR-21 may also reflect the influx of immune cells rather than induction of miR-21 expression in resident tissue cells.[346] Transfer of miRNAs from circulating cells to infiltrated tissue may modulate the translation of proteins in the inflamed organ.[353,357] Thus far, most studies have attributed changes in miR-21 expression to resident cell types only. The contribution of circulating cells may therefore have been overlooked. As we have recently pointed out however, it is debatable how plausible miRNA transfer is as a modulator of mRNA translation in a recipient cell, given the several orders of magnitude difference in abundance between circulating and cellular miRNA levels.[96]

5.2.1 Inflammatory cells and miR-21

Whilst miR-21 induction in inflammatory cells is widely described, it appears that it acts as an 'emergency brake' on inflammation.[179] Expression of miR-21 increases in endotoxin-treated macrophages upon the engulfment of apoptotic cells, resulting in an attenuation of the inflammatory response.[358] During macrophage polarisation *in vitro*, changes in miR-21 expression are not as pronounced[359], suggesting that miR-21 induction only occurs in the presence of tissue damage. In macrophages, miR-21 directly targets the pro-inflammatory programmed cell death protein 4, thereby increasing the secretion of anti-inflammatory interleukin-10.[358,360] In addition, targeting of PTEN steers macrophages towards a reparative phenotype[361], promoting

resolution of inflammation and tissue recovery.[362] Altogether, miR-21 activation appears to modulate the inflammatory response, in part through steering monocyte differentiation towards a more reparative macrophage phenotype.

Canfrán-Duque *et al* showed that miR-21 is the most abundant miRNA in macrophages.[180] Studying its effects on atherosclerosis, miR-21 accumulated in murine atherosclerotic plaques, along with the macrophage marker CD68. Using a combination of double miR-21$^{-/-}$/LDLr$^{-/-}$ mice, macrophage deficiency of miR-21 promoted vascular inflammation and plaque necrosis. Deficiency of miR-21 in bone marrow cells in LDLr$^{-/-}$ mice resulted in larger and less stable atherosclerotic plaques due to increased vessel wall infiltration. Furthermore, miR-21$^{-/-}$ macrophages produced higher levels of cytokines upon endotoxin stimulation and cleared less apoptotic material *in vitro* but were more susceptible to apoptosis and lipid accumulation. These results are in line with the previously mentioned immunomodulatory effects of miR-21 in macrophages. A recent study by Jin *et a*l found more advanced plaque formation at an early age in *Apoe*$^{-/-}$*miR21*$^{-/-}$ mice, with a concomitant increase of macrophage infiltration and foam cell formation. Factors that are secreted from *Apoe*$^{-/-}$*miR21*$^{-/-}$ macrophages could suppress vascular smooth muscle cell proliferation *in vitro*.[181]

The suggested role of miR-21 as an 'emergency brake' on the inflammatory response is not limited to monocytes and macrophages. Through targeting interleukin-12p35, miR-21 steers T-cells towards a Th_2 response[363,364], which is considered a mechanism to counterbalance the pro-inflammatory Th_1 cells. Consequently, higher levels of miR-21 are associated with auto-immune diseases such as allergic airway inflammation[365] and psoriasis[366], pathologies believed to be mediated by Th_2 cells. These findings have led to landmark papers on leukocyte miR-21 as a therapeutic target, where miR-21 inhibition in mice improved psoriasis[366] and lupus erythematosus.[367] From an oncological perspective, miR-21 is considered an 'oncomiR' for its effects on tumour cell proliferation, but also because of its inhibitory effect on the immune response to tumour cells.[112] These results underline the potential side effects of systemic or local miR-21-targeting

therapy, whilst also supporting the notion that systemic miR-21 inhibition may act through circulating cells. Our findings of miR-21 inhibition affecting TGF-β1 release may indeed be an example of this hypothesis, where increased release of this pleiotropic cytokine can have widespread effects on inflammation depending on the timing after injury.[368]

In our study, we have identified WASp as a direct miR-21 target in megakaryocytes and platelets. Whilst this protein plays a key role in inflammatory cells (see **5.3.6.2**), it remains to be determined whether this targeting and potential downstream consequences upon miR-21 inhibition also occur in leukocytes. We have discussed in the introduction that miRNA targeting can be highly dependent on tissue or cell-type.[369] Our analysis of blood cells in miR-21 *null* mice identified differences in the number of circulating platelets and leukocyte subtypes. Whilst this finding has not been reported previously, to our knowledge, it emphasises that miR-21 inhibition has key effects on the bone marrow and bone marrow-derived cells. Whether the effects on platelet WASp levels and blood cell counts contribute to the role of miR-21 on inflammation remains to be studied.

5.2.2 miR-21 and associated proteins in the circulation

Circulating miRNAs and other non-coding RNAs have been studied extensively in the context of cardiovascular disease. Initial studies focussed mainly on their biomarker potential. More recent studies however implicate circulating miRNAs as functional or pathological mediators, either in leukocytes and platelets or by transfer to cells in the vessel wall.[96,227] In this study, we used a proteomics approach to screen for associations of circulating miR-21 with proteins involved in CVD and inflammation.

Given the complexity and large dynamic range of the plasma proteome, a hybrid strategy was used to quantify proteins. MS can provide quantification for relatively high-abundant proteins using heavy-labelled peptide standards that are added to the samples during sample preparation.[370] To quantify smaller and less abundant proteins, proximity extension assays were used. This technique relies on amplification of annealed DNA tags that are attached to antibody pairs targeting neighbouring epitopes within a single protein.[371]

With previous studies linking several miRNAs, including miR-21, to platelets as a major source, conventional sandwich ELISAs were used to complement measurements with markers of platelet activation. This strategy allowed us to quantify a broad panel of proteins in the plasma samples collected as part of the Bruneck study.

In line with previous findings, this analysis showed marked overlap between proteins correlating with miR-21 and those indicating platelet activation. This suggests that a distinct proportion of the protein panel shared its source with miR-21. Interestingly, miR-21 showed pronounced correlation with several proteins implicated in wound repair and fibrosis. This is not surprising in light of the established role of platelets in tissue injury. Of the highly correlating proteins, one of major interest from the perspective of fibrosis was LAP-TGF-β1. TGF-β1 has previously been reported to be abundant in platelets[55] with its release being implicated in cardiac disease[29,34] but also in other disease processes such as cancer metastasis.[21] These findings prompted the hypothesis that miR-21 inhibition may affect fibrosis through modulating the role of platelets in tissue remodelling.

5.2.3 Cellular contaminants of circulating biomarkers

Platelets contain a vast range of proteins inside their granules, many of which are released upon their activation. During preparation of blood plasma or serum for experimental or clinical analysis purposes, centrifugation is applied to separate blood cells from the cell-free fraction. The use of blood tubes containing anticoagulants such as citrate, heparin or EDTA is aimed at obtaining cell-free plasma whilst preventing activation or lysis of blood cells prior to or during sample preparation. The preparation of serum depends on clot formation inside the blood container after venepuncture, either spontaneously or enhanced with clot-activating factors. Whilst serum is often described as ‘plasma minus fibrinogen and clotting factors’, this statement overlooks the fact that platelet activation during clotting causes degranulation with a concomitant increase in platelet-derived protein levels. This is reflected in the significantly higher levels of PF4 in serum samples when compared with plasma[271] as well as a markedly different proteome.[372] For proteins that are

abundant in platelets, this consequently means that serum measurements do not reflect protein levels of the cell-free fraction of the circulating volume.

Previous work has shown that protein analysis using plasma is profoundly affected by pre-analytical variables. Several factors can perturb sample quality, such as pre-centrifugation delay, freeze-thaw cycles and haemolysis. A recent study determined effects of such variables on plasma proteins measured by the same two proximity extension assay panels as used in our study.[373] Whilst freeze-thaw cycles had no major impact, the time and storage temperature between venepuncture and centrifugation was found to have a significant effect on protein levels. This is in line with findings from previous studies.[372]

Another potential contaminant during plasma preparation is the unintended activation or residual presence of blood platelets. This introduces significant variation in the plasma composition, with regards to both proteins[271–273] and miRNAs (see **Figure 47**).[274,275] We have recently published a set of recommendations regarding sample preparation for the measurement of circulating miRNAs, most of which equally apply for proteins (see **Appendix 3**).[96] Samples should be handled carefully to avoid haemolysis. To avoid platelet activation, samples should be handled at room temperature and centrifugation should be performed in two steps at a consecutive lower and higher speed and in presence of platelet activation inhibitors.

Focussing on the observed correlation between plasma miR-21 and LAP-TGF-β1, there have been several reports that indicate the importance of sample preparation for this protein specifically. Wakefield *et al* in 1995 highlighted the importance of platelet activation when measuring its plasma levels[276], arguing that plasma rather than serum needs to be used for the measurement of TGF-β1. More recent studies emphasise the confounding effects of residual platelet content and platelet activation on TGF-β1 measurements.[29,64,277] Despite evidence for its importance in preclinical models, effects of circulating TGF-β1 on organ fibrosis and in oncology are

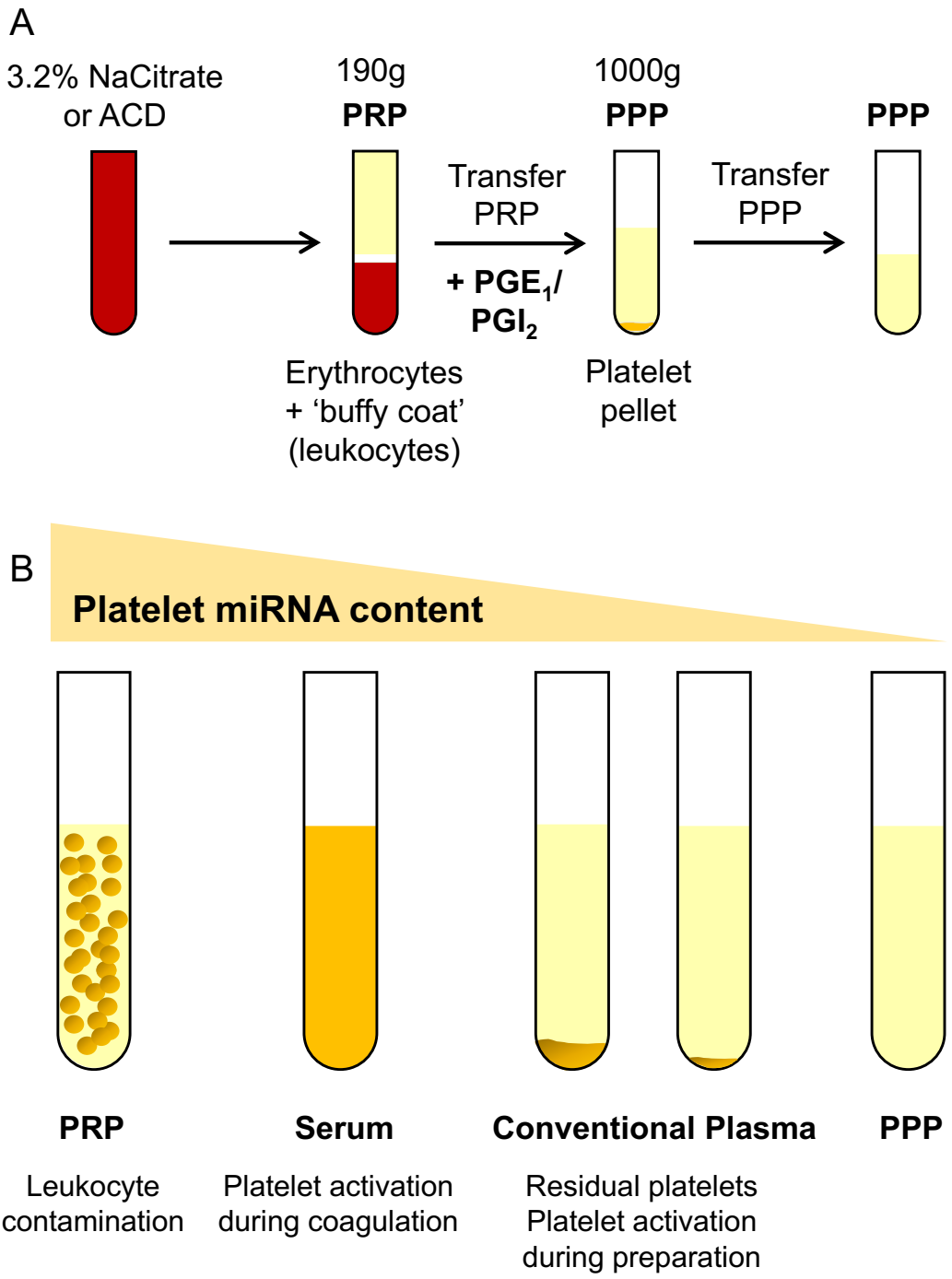

Figure 47. The platelet contamination continuum in blood samples. A: Workflow for the preparation of PPP from PRP by two-step centrifugation. Addition of prostaglandin such as PGE_1 or PGI_2 inhibits platelet activation during centrifugation. **B:** Concerns with regards to miRNA and protein measurements in the different samples range from contamination with leukocytes in PRP and proteolytic activity in serum to residual platelets in plasma. PRP and serum should reflect a combination of plasma and platelet content; PPP should reflect in vivo platelet release; plasma samples reflects extracellular miRNA and protein content but may additionally reflect either cell content or release. This continuum is dependent on the number of residual platelets in the plasma samples and platelet activation during plasma preparation, in particular during centrifugation.

hampered by inadequate pre-analytical procedures. The highly variable baseline measurements for TGF-β1 appear to have prevented further research from being taken forward. Altogether, this context underscores a more tailored analysis of plasma and platelet samples to study the interaction between miR-21 and platelet TGF-β1.

5.2.4 Circulating and platelet-derived TGF-β1

Previous studies have shown that large pools of TGF-β1 are stored within platelets, mainly in its latency-associated form.[60,78] In addition to carrying substantial amounts of TGF-β1, platelets are also the only cell type known to constitutively express the surface-docking leucine-rich repeat-containing protein 32.[374] Through this receptor, platelets do not only carry TGF-β1 secreted from its own granules, but can also capture TGF-β1 that is secreted from other cell types.[375] A recent study by Rachidi *et al* found that through this receptor, platelets are a key determinant of the activation of circulating TGF-β1.[368] This is functionally in line with a previous study that showed activation factors being co-released with latent TGF-β1 upon activation.[376] Altogether, these studies indicate that platelets play a crucial role in delivering active TGF-β1 during their activation.

5.2.4.1 Protein complexes in the human platelet releasate

To provide further insight into platelet-released TGF-β1, we performed a comprehensive analysis of the human platelet releasate by MS analysis, comparing reduced and non-reduced supernatant from thrombin-activated washed platelets. The ability of this approach to differentiate between biologically relevant multimeric complexes was shown for several proteins; as examples, fibrinogen and fibronectin were presented in the results section. Analysis of TGF-β1 in the releasate using this approach highlighted two key aspects. Firstly, reducing conditions showed that all detected TGF-β1 and LAP peptides were found separate from each other, indicating that there was no detectable presence of uncleaved pro-TGF-β1. Second, comparison of reducing and non-reducing conditions indicated that all TGF-β1 peptides were detected at a part of the gel that implies a homodimer not bound to LAP. On the other hand, LAP peptides were detected much higher than the predicted

molecular mass of LAP itself or the SLC, indicating binding to other proteins. Co-localisation in the gel with peptides derived from LTBP1 indicate the presence of the canonical LLC.

These findings indicate that within five minutes of thrombin-mediated activation, the platelet releasate contains TGF-β1 in its active form, either as a result of rapid activation by co-released factors or due to active TGF-β1 release per se. As protease inhibitors were added 5 minutes after thrombin activation, pro-TGF-β1 cleavage or SLC/LLC dissociation is unlikely to have occurred beyond this time point. In the context of plasma measurements for TGF-β1, these results indicate that an approach using antibodies that target the LAP rather than the active segment of this protein might provide a suboptimal readout for TGF-β1. This was highlighted by our analysis in PPP using separate measurements for LAP and active TGF-β1, as discussed in the following paragraph.

5.2.4.2 Correlations after optimised sample preparation

For the 2015 Bruneck study follow-up, we collected samples taking into account the concerns described in the literature as well as our own analysis of the platelet releasate. To minimise platelet contamination, we optimised a protocol that involved similar features as recently reported by Mancini *et al* to be the optimal conditions for the analysis of plasma TGF-β1.[64] Using PPP, measurement of miR-21 by qPCR and a plasma protein panel by PEA allowed us to compare their correlations and assess their dependence on sample preparation. Additionally, the analysis in PPP provided a readout more likely to reflect the *in vivo* situation in the circulation.

In PPP, several proteins were also found to strongly correlate with miR-21, overlapping with those identified in conventional plasma from the Bruneck study 2000 follow-up. Conversely however, there was a marked proportion of proteins that did not show any correlation in PPP whilst doing so in the previous analysis using conventional plasma. Interestingly, one of the proteins that showed a markedly lower correlation with miR-21 in PPP compared to that in conventional plasma, was LAP-TGF-β1. A comparison of PRP and PPP

confirmed platelet dependency but is unable to differentiate between platelet content and release. Our PPP preparation method is aimed at decreasing both *ex vivo* platelet activation as well as reducing the number of residual platelets in the plasma. The previously mentioned study by Rachidi *et al* showed that TGF-β1 is released from its latency complex whilst being retained on the GARP receptor at the platelet surface.[368] Although this study does not provide any details as to what happens to LAP after TGF-β1 is released from the latency complex that is captured by GARP, their findings could suggest that LAP stays behind within this receptor on the platelet membrane. Consequently, this would result in a disproportionately high amount of LAP to be detected with higher levels of residual platelets in plasma.

To bypass the dependency on measurements that measure LAP as a readout for TGF-β1, we performed ELISA measurements that selectively detect active TGF-β1, as shown in **Figure 1**. In contrast to the PEA-based measurement of LAP-TGF-β1, a strong correlation was indeed found between miR-21 and the ELISA-based TGF-β1 measurement. Correlation between LAP-TGF-β1 and active TGF-β1 was relatively moderate however. In the context of studies aimed at optimising plasma TGF-β1 measurements, the average concentration found in the Bruneck 2015 PPP was in a similar range as those reported by both Mancini *et al* and Wakefield *et al*.[64,276] Despite specific measures to reduce *ex vivo* platelet activation and residual platelet content, the strong correlation between miR-21 and TGF-β1 persisted. This strengthens the hypothesis that platelets are the mutual source of extracellularly circulating miR-21 and TGF-β1.

5.3 Platelets and miR-21

The study of human plasma from the Bruneck cohort identified a link between miR-21 and TGF-β1 in platelets. In light of the literature, this may play an important role in the pathophysiology of fibrosis. We therefore went on to further analyse the effects of miR-21 on platelets using *in vivo* models.

5.3.1 Immunodepletion of platelets in mice

To study the correlation between miR-21, TGF-β1 and platelets, we first used an interventional model in mice. Through antibody-mediated platelet depletion in wild-type mice, we determined the consequence of reduced platelet counts on levels of both miR-21 and TGF-β1 after 48 hours. Our hypothesis of platelets being a major source for both, suggests that their levels would be reduced after platelet depletion. In the murine PPP, a significant reduction was indeed found for TGF-β1, along with platelet activation marker PF4, which is in line with previous literature.[29] However, this decrease was not observed for miR-21 or for any of the other miRNAs that were measured, with miR-320 showing increased levels after platelet depletion despite it being described as platelet-enriched.

Several reasons could explain why no effect of platelet depletion was seen for miR-21. Firstly, the half-life of miR-21 may exceed the 48-hour time frame that was used in this experiment. Studies have reported markedly varying half-life values for plasma miRNAs, ranging from several hours[377] to weeks.[378] This half-life can be expected to show a wide range across the circulating miRNA pool, as there is variation in the mechanisms that protect different miRNAs from degradation in the circulation.[212] For miR-21, a previous study evaluated the effect of antiplatelet therapy on plasma levels. In patients on aspirin, evaluation of miR-21 levels 48 hours after initiation with additional antiplatelet drugs (clopidogrel or dipyridamole) showed no effect, whereas single or dual antiplatelet treatment initiation in therapy-naïve healthy volunteers did show a significant decrease of plasma miR-21 after one week.[219]

Upon platelet depletion, we did find higher levels of miR-320 in plasma, whilst a trend in a similar direction was seen for several other miRNAs that are considered platelet-enriched. Rapid platelet aggregate formation and a drop in their count are seen upon administration of the anti-CD42b antibody.[379] This may imply that platelet miRNAs are released into the circulation upon platelet aggregation. Platelet activation 48 hours prior to isolation of plasma may indeed explain why levels of platelet miRNAs are increased, in particular in the context of a relatively long half-life. Alternatively, circulating levels of miR-21 may to a significant extent be dependent on non-platelet sources such as leukocytes, dampening the effect that is seen for miRNAs such as miR-320. Furthermore, to our knowledge it is currently unknown whether systemically delivered anti-CD42b antibody affects megakaryocytes and whether these constitute a potential source of circulating miRNAs upon activation or rupture. Further study into the half-life of miR-21 and circulating miRNAs in general are needed to characterise their dynamic profile upon secretion into the blood.

5.3.2 Immunoprecipitation in megakaryoblastic cells

Whilst we have so far shown dependency of miR-21 on platelets in the circulation, there is ongoing debate as to what extent platelet RNA has functional relevance.[380,381] Generally, platelet RNA is considered to be a readout of the RNA signature in the megakaryocytes from which they are derived. Therefore, we used a cell line model of megakaryocytes to study miR-21 levels.

Megakaryocytes constitute a relatively small fraction of the bone marrow cell population and are therefore challenging to isolate in substantial amounts. Thus, megakaryoblastic cell lines are commonly used as a surrogate, in particular the human leukaemic cell line MEG-01. To study whether miR-21 was actively processed and part of the silencing complex that mediates the function of miRNAs, we performed an immunoprecipitation in these cells using an Ago2-targeting antibody. In the co-precipitated RNA, we found marked enrichment of miR-21, along with miR-126 and miR-223 which are also commonly described platelet-enriched miRNAs.[217] Conversely, *U6* and *RNU48* were used as non-miRNA controls, with, as expected, no enrichment being found. The fact that MEG-01 cells are oncological cells requires careful

interpretation from a translational perspective. However, in light of our other findings on miR-21 as an abundant platelet miRNA in both humans and mice, Ago2 immunoprecipitation in MEG-01 cells supports the hypothesis that miR-21 has a functional role in megakaryocytes. This suggests that miR-21 may regulate protein synthesis within megakaryocytes as well as in platelets.

5.3.3 Systemic inhibition of miR-21 in mice

5.3.3.1 Oligonucleotide constructs and platelet aggregation

We aimed to further study the effects of miR-21 in platelets by using *in vivo* miR-21 inhibition. As specific types of oligonucleotides were reported to induce platelet aggregation by interacting with the collagen receptor[254], we first evaluated several anti-miR constructs ourselves. For this purpose, we isolated PRP from healthy volunteers and incubated the platelet suspensions with different types of oligonucleotides using similar concentrations as described in the report by Flierl *et al*. For our *in vivo* miR-21 inhibition studies, we selected a cholesterol-conjugated antisense antagomiR-21 construct with similar chemical properties as the inhibitors previously used in our group to systemically inhibit miR-29b[185], miR-195[281], miR-126[217] and miR-122.[280] None of the tested oligonucleotides showed an effect on platelet aggregation within 40 minutes.

Interestingly, our panel of oligonucleotides included several subtypes that met with the criteria to affect platelets as described by Flierl *et al* but failed to see induction of aggregation. A recent study further investigated the effect of oligonucleotide modifications on platelets.[382] Here, platelet aggregation was induced by oligonucleotides with at least twelve consecutive phosphorothioate backbone modifications. However, LNA modification of the ribose moiety of the backbone, as also used for the majority of oligonucleotides that we tested, markedly reduced this pro-aggregation effect. The antagomiR construct that we tested contained two and four phosphorothioate modifications on either end, falling well below the reported minimum threshold to affect platelets. In summary, these studies and our results suggest that extensive phosphorothioate backbone modifications can induce platelet aggregation but this effect can be mitigated by additional modifications to the backbone. Given

the results from these studies as well as our own analysis, we proceeded to use the cholesterol-conjugated antagomiR-21 and a chemically corresponding non-targeting control-antagomiR for *in vivo* inhibition of miR-21.

5.3.3.2 Effects of antagomiR-21 across tissues

Systemically delivered antagomiRs remain stable for over 2 weeks after delivery. A different extent of downregulation is seen across tissues, depending on the bioavailability and the endogenous miRNA levels in each tissue.[108] To achieve sustained inhibition, repeated injections are often used. In order to determine the efficacy of miR-21 inhibition across different tissues, we used qPCR analysis of isolated RNA. As a positive control for adequate antagomiR preparation and efficacy, RNA extracted from the liver is often used, being the organ that is most readily targeted after antagomiR injection. In our experiments, marked inhibition was indeed observed in the liver, as well as in the kidney. Major tissue penetrance has previously been reported in the latter organ as well, which is highlighted by selection of the kidney for the first clinical trial of miR-21 inhibition. Significant downregulation was also observed in the bone marrow and heart, although to a lesser extent.

To evaluate off-target or secondary effects of antagomiR-21 treatment, we evaluated several key miRNAs in each of the above-mentioned tissues. Effects that are observed can be due to non-specific binding of the antagomiR to other miRNAs but is more likely to be the effect of the interference with transcription, processing or degradation of other miRNAs through various factors. In our analysis, a significant effect was observed for miR-1 in the heart, although the change in expression of less than 10% is unlikely to have a major impact on this highly abundant cardiac miRNA.

Most studies using miRNA inhibition provide little information regarding the effects beyond the organ and miRNA of interest. One of the exceptions is the previously mentioned study by Ramanujam *et al* (see **paragraph 5.1.5**), using AAV9- and MMLV-mediated miR-21 inhibition in specific cell types within the heart.[131] In this study, AAV9-mediated inhibition reduced miR-21 levels in cardiomyocytes as well as in the liver. Conversely, intra-pericardially delivered MMLV specifically targeted non-myocytes in the heart, with evaluation of miR-

21 in kidney, liver, lung and spleen showing no effect. MiR-21 levels in the bone marrow were not reported. However, their supplemental information showed a minor effect of intra-pericardial MMLV-GFP injections on isolated bone marrow cells. Of note, cells were isolated using an anti-CD45 antibody, thereby excluding megakaryocytes and platelets.

In the following paragraphs, we will discuss effects of systemic miR-21 inhibition that could affect cardiac disease. Our findings highlight the need within the miRNA research field to evaluate effects beyond the organ and miRNA that are the focus of a specific study. This is increasingly the case as studies progress towards application of local miRNA targeting strategies. With this trend, the focus will be increasingly narrowed down to the area of interest without guarantees that the effect is actually occurring solely at this site. We have recently pointed out this note of caution in a commentary that accompanied a study using local miR-21 delivery to prevent atherothrombotic events.[179,181]

5.3.4 Platelet count and aggregation after miR-21 inhibition

Upon systemic treatment with antagomiR-21 by three intraperitoneal injections on consecutive days, the animals were kept for four days until collection of blood and other tissues. Mouse platelets are known to have a life span of approximately 5 days.[383] By collecting samples 7 days after therapy initiation, it can be assumed that the vast majority of platelets in the circulation were synthesised by megakaryocytes that had been exposed to antagomiR-21. Flow cytometry-based counting was performed using the forward and side scatter characteristic of platelets, as well as APC-labelled anti-CD41 antibody positivity. Neither of these measurements showed a significant difference in platelet count. To our knowledge, none of the previous studies have reported platelet counts after systemic inhibition of miR-21.

In contrast to its pharmacological inhibition, genetic ablation of miR-21 resulted in lower circulating platelet and leukocyte counts, as determined by automated cell counting. Whilst the monocyte and lymphocyte concentrations in miR-21 *null* mice did still fall within the normal range, these findings warrant further investigation as to whether the inflammatory response is affected (see

5.2.1). The contradicting findings between pharmacological and genetic inhibition of miR-21 on platelet counts puts further emphasis on the discrepancy between these two strategies. The increase in megakaryocyte numbers in miR-21 *null* mice may suggest compensatory upregulation of megakaryocyte proliferation in response to lower platelet counts. Alternatively, lower platelet counts in combination with higher megakaryocyte numbers may indicate a failure of megakaryocytes to mature towards the platelet-releasing differentiation stage. Further study is required to elucidate the underlying mechanisms for our observations.

As pharmacological miR-21 inhibition did not affect platelet counts, we next assessed effects on the platelet aggregation response to different agonists. Being a key feature of the platelet response to surface receptor-mediated activation, measurement of aggregation is widely used as a platelet function test. The most commonly used method in humans for this purpose is light transmission aggregometry. This method involves the isolation of PRP, which is then placed in a glass cuvette inside an aggregometer. This device detects transmission of light in real-time through the PRP-containing cuvette, where platelets in the suspension absorb light. Under continuous stirring and heating to 37°C, different platelet agonists are added. As platelets aggregate, transmission of light through the cuvette increases.

As this method requires a volume of approximately 200 µl for each cuvette, it is not well-suited for the study of murine platelets. To address this issue, a low-volume adaptation of the aggregometry method has been designed, allowing for the assessment of aggregation response to a range of agonists whilst requiring markedly lower amounts of blood.[384] We recently applied this method to determine the platelet aggregation response in mice after systemic inhibition of miR-126 (see **Appendix 3**).[217] Here, this method identified significantly reduced aggregation to several platelet agonists. These findings highlighted both the ability of systemic inhibition of a miRNA to affect platelet function, as well as the ability of plate-based aggregometry measurements to detect such differences. Furthermore, we confirmed in this study that there was no difference between PBS-treated mice compared to

antagomiR-control, corroborating our *in vitro* findings that the antagomiR construct does not induce platelet aggregation.

We used the same method to determine the platelet aggregation response after systemic miR-21 inhibition. Aggregation was seen in response to both concentrations of AA, as well as to the higher concentrations of PAR4 amide and collagen. There was no significant difference across the different agonists between PRP from antagomiR-21-treated mice and controls, suggesting that miR-21 does not affect platelet activation.

There are however several limitations of this approach. Firstly, subtle differences may not be identified as only a selected panel of agonists is used in the assay. MiR-21 may affect the response to secondary mediators of platelet activation that were not evaluated. Furthermore, as miRNAs fine-tune protein levels and effects are therefore often subtle, this assay may lack sensitivity to detect changes that occur *in vivo*. Our previous findings for miR-126, however, do highlight that this method is capable of detecting miRNA-related changes; a similar dosing regimen was used for miR-21 as for our previous analysis of miR-126. Moreover, plate-based light transmission aggregometry has been proven a valuable tool for the evaluation of platelet reactivity in humans.[385]

5.3.5 The platelet releasate after antagomiR-21 treatment

In addition to the platelet count and their reactivity to different agonists, we analysed the effect of systemic antagomiR-21 treatment on the platelet releasate. In terms of platelet function, it can be argued that the proteins released upon activation confer a major share. With regards to the role of platelets in haemostasis, the initial activation by external agonists such as sub-endothelial collagen is rapidly followed by the release of factors that recruit and activate other platelets. The ‘snowball effect’ of secondary platelet activation is therefore highly dependent on the platelet releasate. Furthermore, as discussed in the introduction, proteins released by platelets are widely implicated in functions related to inflammation and tissue repair. Therefore, an effect of miR-21 on proteins in the platelet releasate may affect the pathophysiology of fibrosis.

5.3.5.1 Proteomic screen of the platelet releasate

Although several pro-fibrotic proteins are known to be secreted from platelets, we pursued an unbiased proteomics approach to determine the effects of miR-21 inhibition. To do so, the releasate was isolated from platelets of mice upon pharmacological antagomiR-21 treatment, and was then analysed by untargeted gel-based MS. This method was similar to the one used to analyse the conditioned media of CF as well the human platelet releasate. Comparing human and murine platelet releasates revealed a major overlap, highlighting both the consistency of this method as well as the translational potential of findings in the murine releasate.

Comparison of the releasate from antagomiR-21-treated mice with respective controls identified three proteins that were released at lower levels after systemic miR-21 inhibition, including TGF-β1. TGF-β1 is generally considered to be an α-granule constituent, as described in the introduction. Both other proteins that showed significantly lower levels in the antagomiR-21 releasate are also found in these granules. As indicated by the GO analysis of the releasate, this comparison could suggest that reduced release was seen for several α-granule proteins. However, recent studies have contested the platelet granule classification, suggesting that here is heterogeneity in α-granule content and release. This will be discussed later in this chapter.

Of the proteins that showed higher levels in the platelet releasate of antagomiR-21-treated mice, none reached statistical significance. However, it can be noted that the majority of these proteins have been identified outside of the α-granule, highlighting the contrast with those that were found at lower levels in these releasates. For example, approximately 90% of platelet GAPDH has been reported to reside in the cytosol.[386] Similarly, Src, a key mediator in platelet receptor-downstream signalling, is found in the cytosol where it is closely associated with the tails of membrane-bound receptors.[387] Enrichment of this kinase in platelets is further indicated by the high correlation with miR-21 in PPP, as we found in our analysis in the Bruneck study cohort (see **Figure 26**). Catalase, involved in the decomposition of hydrogen peroxide, has been found in small amounts in peroxisomes, an organelle distinct from the other

platelet granules.[388] Equal amounts of protein from each platelet releasate sample were injected into the mass spectrometer. Hence, the inhibited release of α-granule proteins from antagomiR-21-treated mouse platelets may have resulted in a relatively higher detection of proteins that reside outside of these granules.

5.3.5.2 Validation by ELISA using different agonists

We used MS analysis of the releasate as a screening tool for potentially affected proteins. No correction for multiple testing was performed, necessitating independent validation of findings using an alternative technique. Given its high sensitivity and specificity, we used ELISA measurements in the supernatant of platelets activated with different agonists. This allowed for the assessment of potential agonist-specific and dose-specific effects. Given the interest in TGF-β1 in the context of fibrosis, we focussed on this protein in particular. To determine a general effect on α-granules, PF4 was selected, being a widely used marker of release from these granules.

First, TGF-β1 and PF4 levels were measured in PPP. No difference was found for either protein between antagomiR-21-treated mice and controls. For TGF-β1, this implies that pharmacological miR-21 inhibition does not lower TGF-β1 systemically. Furthermore, it discredits the possibility that lower TGF-β1 levels found by MS analysis of the releasate can be attributed to plasma contamination. PPP levels of PF4 can be interpreted as a marker of *in vivo* platelet activation, due to its platelet specificity. As PF4 levels in PPP were not different after miR-21 inhibition *in vivo*, it can be inferred that there is no difference in platelet activation upon this treatment. This is in line with our findings for the aggregation response.

In contrast, changes were observed when analysing the releasate in response to platelet agonists. For PF4, a significant increase was seen in response to increasing dosage of platelet agonist, indicating its correlation with platelet activation. Expectedly, this increase paralleled the aggregometry results that have been discussed previously. A similar response was seen for TGF-β1 levels in control-antagomiR samples, which increased with higher

concentrations of collagen and PAR4 amide. Strikingly however, antagomiR-21 treatment attenuated the increase in TGF-β1 release from platelets at a high dosage of either agonist. Although a similar pattern could be discerned for PF4 release, this did not reach statistical significance.

5.3.5.3 Changes in platelet or megakaryocyte TGF-β1 levels

Decreased TGF-β1 levels in the platelet releasate after pharmacological miR-21 inhibition could depend on either lower levels in platelets or an inhibitory effect on its release. To assess its protein levels, platelets were isolated from mice upon antagomiR treatment and lysed for protein extraction. Using immunoblotting, no significant difference was seen between platelets isolated from antagomiR-control- and antagomiR-21-treated mice. To determine whether a difference could be observed in gene expression, bone marrow extracts from the same mice were assessed. Here, too, no significant difference was seen for *Tgfb1* expression. Although TGF-β1 is enriched in platelets, other sources of this protein could in theory also affect platelet levels, given the ability of platelets to engulf proteins. However, *Tgfb1* expression in the heart, kidney and liver was also unaltered, despite significant miR-21 inhibition. This is supported by similar PPP levels after antagomiR-21 treatment.

As megakaryocytes form a small proportion of the bone marrow cell population, we determined TGF-β1 levels in this cell type by histological analysis. Megakaryocytes were identified by staining with a PF4 antibody and DAPI, revealing the characteristically large and lobulated nuclei. Strikingly, TGF-β1 levels were highly enriched in megakaryocytes, whereas there was very little signal beyond PF4-positive cells. This is in line with earlier observations by others, where the localisation of TGF-β1 was specifically ascribed to α-granules in porcine bone marrow sections.[75] Although somewhat circumstantial, these findings suggest that the gene expression signal of whole bone marrow extracts should to a large extent reflect megakaryocyte expression levels. Furthermore, comparison between bone marrow from antagomiR-21-treated mice and respective controls appeared to show a similar number of PF4- and TGF-β1-positive cells. Intensity of TGF-β1 signal

did not markedly differ between both treatments, in line with immunoblot findings in platelets as well as the gene expression levels in bone marrow cells.

5.3.6 Mechanisms affecting platelet degranulation

Analysis of TGF-β1 levels in isolated platelets and bone marrow indicated that decreased releasate levels may reflect reduced TGF-β1 secretion rather than content. We have discussed in the introduction that TGF-β1 is generally considered to be contained within platelet α-granules. Although several other α-granule proteins also showed a trend towards lower release after systemic antagomiR-21 treatment, most did not reach statistical significance. This may be explained by the relatively small sample size, which is limited due to the number of animals that are required to isolate sufficient platelets for proteomic releasate analysis. Alternatively, these findings could imply that platelet release of TGF-β1 and other granule proteins does not always occur simultaneously.

Platelets contain two distinct channel systems[389]: the open canalicular system, consisting of tortuous, tubular invaginations of the plasma membrane, and the dense tubular system. The latter system can be considered the platelet equivalent of the endoplasmatic reticulum. With regards to granule content, platelets carry lysosomes, and platelet-specific granule types generally referred to as α- and δ- granules. α-granules contain and release a vast number of proteins[282], with often opposing function. It has therefore been suggested that multiple subtypes of α-granules must exist.[390] Resolution of current imaging techniques limits the ability to test this hypothesis adequately.[391] The granule content is thought to be released upon fusing with the membrane, without being consumed by the membrane.

There have been several reports suggesting differential release of proteins from α-granules.[392] Italiano *et al* used immunofluorescence and immunoelectron microscopy to show that pro- and anti-angiogenic factors were stored in different subtypes of α-granules. These were released by activation of different thrombin receptors.[393] A subsequent study from the same group showed that this could differentially affect angiogenesis and that

aspirin treatment could attenuate the pro-angiogenic effect of platelets.[394] A similar differential packaging was seen for VWF and fibrinogen, which was attributed to VWF being megakaryocyte-derived whilst fibrinogen is acquired through endocytosis.[395] Interestingly, the proteomics analysis in our study showed a significant decrease in VWF release, whilst lower release of all three fibrinogen chains did not reach statistical significance. It remains to be elucidated what the mechanisms are that regulate fusion with the membrane for specific subtypes of granules. As potential mediators of this differential release, members of the soluble N-ethylmaleimide-sensitive factor attachment protein receptor (SNARE) family have been suggested. Platelets carry at least four subtypes of vesicular SNAREs (VAMP-2,-3,-7 and -8), and differential kinetics upon platelet activation for granules carrying these proteins have previously been reported.[396] Altogether, this indicates that a specific effect on TGF-β1 release is indeed plausible, although the known mechanisms to explain such an effect are currently limited.

5.3.6.1 Control of platelet TGF-β1 release by WASp

With the focus of our analysis on TGF-β1 due to its role in wound healing and fibrosis, we aimed to identify specific mechanisms that control its release from platelets. Kim *et al*[77] reported that the secretion of TGF-β1 from platelets in both humans and mice is curtailed by WASp as well as by actin polymerisation.

WASp has extensively been described as a regulator of actin polymerisation in neutrophils, macrophages and lymphocytes[397], being expressed solely in hematopoietic cells.[398] WASp itself has no catalytic activity, but functions as a scaffold that brings together the actin-related protein 2/3 complex with monomeric globular actin, which then acts as a starting point for actin 'nucleation' (i.e., filamentous actin polymerisation onto existing filamentous actin). Most WASp in the cytoplasm is present in an auto-inhibited form, conferred by non-covalent interaction of the verprolin homology, cofilin homology and acidic region domain with the GTPase-binding domain. Cell division control protein 42 homolog has been described as the main mediator

for the release of this auto-inhibition. In addition, phosphorylation is a key requirement for WASp activity, for which the mechanism is described below.

Whilst WASp is present in platelets, it is not required for platelet spreading, despite the importance of cytoskeletal filamentous actin polymerisation and doubling in this process.[399] This was confirmed by observing normal actin assembly upon thrombin-receptor activation in murine *Was null* platelets and human platelets treated with a WASp inhibitor.[77] This suggests a redundancy in the regulation mechanisms of actin polymerisation. From a translational point of view, this could indicate that potential side effects are limited when using platelet WASp as a therapeutic target.

In order to confer its effect on TGF-β1 release, WASp requires phosphorylation at Tyrosine-291 (or Tyrosine-293 in mice) by Fyn and hematopoietic cell kinase, both Src family kinases.[400] This phosphorylation occurs within minutes from platelet activation through collagen receptor glycoprotein VI[401,402] as well as the thrombin-activated receptors.[403] Kim *et al* further showed that upon thrombin-mediated platelet activation, phosphorylated WASp preferentially localises with TGF-β1-containing granules inside the platelets.[77] Pharmacological blocking of Src kinases prior to platelet activation increased the release of TGF-β1 from both humans and wild-type mice platelets, but not from Was *null* mice. These results indicate that the modulating effect of platelet TGF-β1 is Src family kinase-dependent and occurs in response to both thrombin- and collagen-mediated activation. Strikingly, this is in line with our findings in platelets from antagomiR-21-treated mice; a significantly lower release of TGF-β1 was seen for thrombin and collagen receptor-mediated activation but not for arachidonic acid.

5.3.6.2 Identification of WASp as a direct miR-21 target

To determine whether systemic miR-21 inhibition affected WASp levels, we performed immunoblot analysis in isolated platelets. This analysis confirmed higher levels of WASp in platelets from antagomiR-21-treated mice. With platelet TGF-β1 levels previously identified to be unaffected, increased WASp levels may have indeed resulted in a restriction of TGF-β1 release,

resulting in our observations by MS and ELISA quantification. Direct targeting of the *Was* gene was further implied by the significant increase of transcript levels in bone marrow cells. Although the change in platelet WASp abundance and bone marrow *Was* expression is relatively modest, this is not unexpected when interpreted in the context of miRNAs as 'fine tuners' of protein levels.

In silico target prediction for miR-21 is notorious for being affected by a high false-positive rate (see **Supplemental table 5**). The vast number of predicted targets for miR-21 is in line with this perception. Similarly, the large number of experimentally validated miR-21 targets that are only predicted by one out of twelve algorithms suggests that this method suffers from a high false-negative rate as well. Both limitations of current prediction algorithms is commonly described in the literature but as of yet, no methods with higher specificity are available.[92] Our analysis of the effects of systemic miR-21 inhibition revealed a phenomenon for which a mechanism had already been unveiled, therefore bypassing the need for miR-21 target prediction as a starting point for analysis. *In silico* prediction did however reveal the *Was* gene as a potential target, supporting further analysis by luciferase reporter assay.

Despite the identification of a specific interaction between miR-21 and the 3' UTR of the *Was* gene transcript using target prediction, we evaluated the entire 3'UTR in the reporter assay in light of the false-positive risk of *in silico* findings. The use of a dual reporter assay to assess miRNA interaction with a transcript 3' UTR can be seen as the gold standard to confirm canonical miRNA targeting.[404] In three independent experiments, a significant reduction of *Was* reporter activity was seen. This finding in itself merely indicates the ability for miR-21 and the 3' UTR of *Was* to interact. However, in combination with the immunoblot and gene expression analysis in platelets and bone marrow, respectively, as well as the observed effect on platelet TGF-β1 release, these findings imply *Was* as a *bona fide* direct target of miR-21.

5.4 Study limitations

In this study, we have used an *in vitro* approach to study effects on CF. This approach disrupts potential interaction with other cell types in the myocardium as well as potential endocrine effects that may alter fibroblast biology. It has been reported that cultured fibroblasts are more representative of a myofibroblast-like phenotype, implying that *in vitro* study does not adequately reflect mechanisms that may be at play in quiescent cells. Results obtained from miR-21 *null* hearts are more likely to reflect the ECM in presence of resting fibroblasts. The use of serum-free conditions during culture may have repressed the secretory effects of cultured cells, potentially masking effects of miR-21. This is discussed in **paragraph 5.1.2.** Furthermore, the use of a relatively small sample size decreases the power to detect potential changes. As pointed out earlier, HPLC-MS/MS detection is biased towards abundant and large proteins, implying that smaller ECM or regulatory proteins may have fallen below the detection threshold. However, previous studies have been able to detect marked differences in ECM secretion using similar conditions.[185,291]

The data obtained from human plasma samples is based on associations. It is therefore not valid to assume a causative link between platelet activation and levels of miRNAs and proteins. Observed associations should only be interpreted as an indication for their shared source. Furthermore, we have discussed the challenges regarding sample preparation in light of platelet and leukocyte contamination of plasma. We have used specific methods to minimise the level of carryover or activation of cells. Nonetheless, we cannot assume that the observed protein or miRNA signal solely reflects their extracellular levels. Similarly, platelet isolation methods confer a risk of co-isolating leukocytes. Results from experiments with isolated platelets or PRP may therefore be partially derived from leukocytes. Study of TGF-β1 and proteins used as markers of platelet activation are likely to be platelet-derived, in light of their high enrichment in platelets and megakaryocytes. Levels of WASp, however, are more likely to be susceptible to the risk of leukocyte contamination. We have not assessed leukocyte

numbers after pharmacological miR-21 inhibition and whether changes in cell counts may have contributed to observed differences.

We have shown that miR-21 may affect fibroblasts directly but may also affect fibrosis in the heart and other organs by interfering with systemic contributors. Whether the observed effect of miR-21 on platelet TGF-β1 release could affect cardiac fibrosis in presence of cardiac stress, remains speculative. Although previous studies imply that disrupting platelet TGF-β1 release can benefit the cardiac morphology and function, it is currently unclear whether the effect of miR-21 inhibition on TGF-β1 levels could confer similar results. As our interventional data is based on mouse experiments, it remains to be studied whether the observed interactions are also present in humans.

Whilst our findings imply that pharmacological miR-21 inhibition may affect fibrosis via megakaryocytes and platelets, we do not have direct evidence to support this hypothesis. If further experiments confirm this hypothesis and the fibrotic response in the heart can indeed be attenuated through a mechanism targeting the release of pro-fibrotic factors by platelets, this would be an interesting new strategy for potential therapeutic use. Shifting the therapeutic focus from the heart to the bone marrow would be beneficial in the context of anti-miR pharmacokinetics, as a relatively low dose treatment may suffice when targeting the bone marrow.

5.5 Future plans and outlook

5.5.1 Further experimental plans

Systemic treatment with a miR-21 inhibitor revealed a decrease in platelet TGF-β1 release, identifying a potential additional mechanistic explanation for previously observed anti-fibrotic effects. As mentioned in the previous section, the link between reduced platelet TGF-β1 release and fibrosis remains speculative, as we have not evaluated this directly. Other studies have however shown that platelet depletion and inhibition[68–73], as well as the specific inhibition of platelet TGF-β1 release[29,74], can attenuate cardiac hypertrophy and fibrosis. Whether this beneficial effect does indeed contribute to the overall effect of miR-21 inhibition requires further experimental evaluation.

To investigate this direct link, several additional experiments could be performed. Firstly, an *in vitro* assessment of primary CF proliferation can be carried out in presence of the platelet releasate from mice treated with antagomiR-21 or control-antagomiR. In light of the established effects of TGF-β1 on proliferation, this may provide a functional angle to the altered releasate content from antagomiR-21-treated mice. Furthermore, antagomiR-21 treatment appeared to affect the release of other α-granule proteins as well. This experimental approach would provide an opportunity to disentangle the relative contribution of TGF-β1, through combining the platelet releasate with recombinant TGF-β1 or TGF-β1-neutralising antibody when added to CF in culture.

Using an *in vivo* approach, much insight would be provided by establishing a megakaryocyte- and platelet-specific miR-21 knockout mouse, through cross-breeding miR-21$^{fl/fl}$ with PF4-Cre mice. These mice could then be evaluated in terms of their bone marrow and platelet phenotype, as well as in their response to cardiac overload and injury. The latter could be induced by commonly used models, such as infusion of angiotensin II, TAC, or the induction of MI by coronary artery ligation. Furthermore, an evaluation of the

bone marrow and circulating platelets would provide additional insights into the altered megakaryocyte and platelet numbers in total miR-21 *null* mice.

An additional strategy would involve transplantation of miR-21 *null* bone marrow into irradiated wild-type mice and vice versa, followed by evaluation of fibrosis and remodelling in response to injury. Whilst this approach is less time-consuming, it is also less specific, in particular given the abundance of miR-21 in other bone marrow cells. Observations from these mice would determine the effect of miR-21 in megakaryocytes/platelets or the bone marrow, respectively. However, the potential discrepancy between genetic models and pharmacological inhibition remains (see section **5.3.4**). Lastly, antagomiR-21 treatment could be combined with antiplatelet therapy or platelet depletion in mice undergoing cardiac injury. A reduced benefit of miR-21 inhibition in absence of platelet activation would imply that platelets indeed play a role in the reported attenuation of fibrosis after antagomiR-21 treatment.

In addition to experimental models, there are several insights that could be gained from patients. We observed in mice that platelets are a major determinant of circulating levels of TGF-β1. This link could be evaluated in patients with altered platelet numbers or function. Whilst patients suffering from immune-mediated idiopathic thrombocytopaenic purpura may form a human equivalent of our platelet depletion experiment in mice, blood from patients with essential or reactive thrombocythemia could provide the other end of the spectrum. Furthermore, a more specific assessment of α-granule release in relation to circulating TGF-β1 as well as the occurrence and progression of cardiac fibrosis could be performed in Gray Platelet Syndrome patients. This rare, inherited disorder is characterised by a strong reduction of α-granules within platelets.[405]

From a pharmacological perspective, the outcome of the clinical trial that is currently evaluating systemic miR-21 inhibition will directly answer whether there is a benefit on renal fibrosis. The potential role of platelets warrants a subset analysis of patients on antiplatelet therapy and of patients with altered platelet counts or reactivity. This could provide further insight as to whether platelets alter the efficacy of miR-21 inhibition. An effect of

antiplatelet therapy would have major implications for the clinical use of miR-21-targeting therapy. This would be particularly relevant when prescribed for the treatment of cardiac fibrosis, given the common use of antiplatelet therapy in heart failure patients.

5.5.2 Scientific outlook

Our results are a timely contribution given that miR-21-based therapies are progressing to clinical trials for Alport Syndrome. In recent years, there has been an emerging interest in local application of miRNA-based therapy. The current assumption is that miR-21 inhibition attenuates fibrosis predominantly through direct effects on CF. Whilst local therapy aims to decrease off-target effects, our findings emphasise the need to ensure that observed benefits are indeed occurring at the suggested site of delivery. In the context of our findings, local delivery of an anti-miR may in fact limit therapeutic efficacy if the beneficial effects occur indirectly. This is particularly relevant for miR-21, which is abundantly expressed in a range of tissues, including circulating cells that are implicated in inflammation, haemostasis and tissue repair. These features emphasise the importance of the systemic context of miR-21 targeting and of miRNA-based therapeutics in general. Further study would need to determine the relative contribution of miR-21 inhibition in different tissues.

The observed effect of miR-21 may provide a method to selectively interfere with TGF-β1 activity. Previous studies have evaluated TGF-β1 as a therapeutic target, but its broad involvement in various biological mechanisms precludes a systemic approach. Selectively targeting the release of TGF-β1 from platelets upon their activation could prove to be a more tailored approach where the effect is naturally directed to a site of injury. Targeting of miR-21 in this context could thereby provide an interesting strategy. In general, a broad appraisal of the multifaceted systemic response of targeting ubiquitously expressed miRNAs will aid the success of miRNA-based therapeutics in clinical trials.

5.6 Conclusions

In this project, we have identified a novel mechanism through which pharmacological inhibition of miR-21 may affect the development and progression of cardiac fibrosis. As miR-21 has been implicated in the development and progression of fibrosis, it has been suggested as a potential drug target for this largely untreated feature of heart failure. Clinical trials are currently ongoing to evaluate its safety and benefits in the context of renal fibrosis. This highlights the need to thoroughly investigate the effects of miR-21 inhibition.

Using a combination of *in vitro* studies and the analysis of miR-21 *null* hearts, we observed a surprisingly limited direct effect of miR-21 on the cardiac ECM. In line with previous studies, miR-21 did show a pro-proliferative effect on CF *in vitro*. Notably, we found circulating miR-21 to be enriched in platelets. Here, pharmacological miR-21 inhibition attenuated the release of TGF-β1 through de-repressing WASp, a newly identified direct miR-21 target. In miR-21 *null* mice, we observed changes in circulating platelet and leukocyte numbers with concomitant bone marrow changes. These findings (see **Figure 48, panel A**) may have implications for miR-21-based therapeutics, in particular for suggested use of locally delivered anti-miRs.

Fibroblasts have been widely implicated as the main culprit in cardiac fibrosis. We have discussed the limitations of ascribing effects to this cell type within the myocardium, where the expression of miR-21 in resting resident fibroblasts may be overestimated. Cell type and organ specificity is of particular relevance in light of anti-miR therapy. Variation between miR-21 targeting strategies has been suggested to explain conflicting study results. As miR-21 is particularly abundant in hematopoietic cells, effects of its inhibition may, at least in part, depend on circulating cells. A platelet contribution may explain why miR-21 inhibition has no effect on fibrosis in the absence of tissue injury, as tissue injury induces platelet activation. The emerging literature implicating inflammatory cells and platelets in the development and

progression of fibrosis emphasises the need to broaden the evaluation beyond the heart.

Whilst effects of miR-21 on inflammation have been widely studied, its role in platelets remains to be largely unknown. In miR-21 *null* mice, we found significantly lower platelet counts. Translational relevance and implications of this finding remain to be explored. Upon pharmacological miR-21 inhibition, we did not find an effect on platelet numbers or their reactivity, but did observe miR-21 to affect the release of TGF-β1. The TGF-β pathway plays a central role in fibroblast activation and miR-21 can modulate TGF-β downstream signalling. Platelets are a major source of TGF-β1 and its release has previously been implicated in heart failure. Our observation of miR-21 affecting platelet TGF-β1 release suggests a feed-forward mechanism, where TGF-β1 induces miR-21 expression in megakaryocytes, which subsequently enhances platelet TGF-β1 release through inhibiting WASp. Consequently, miR-21-mediated release of platelet TGF-β1 may affect cardiac fibrosis (see **Figure 48, panel B**).

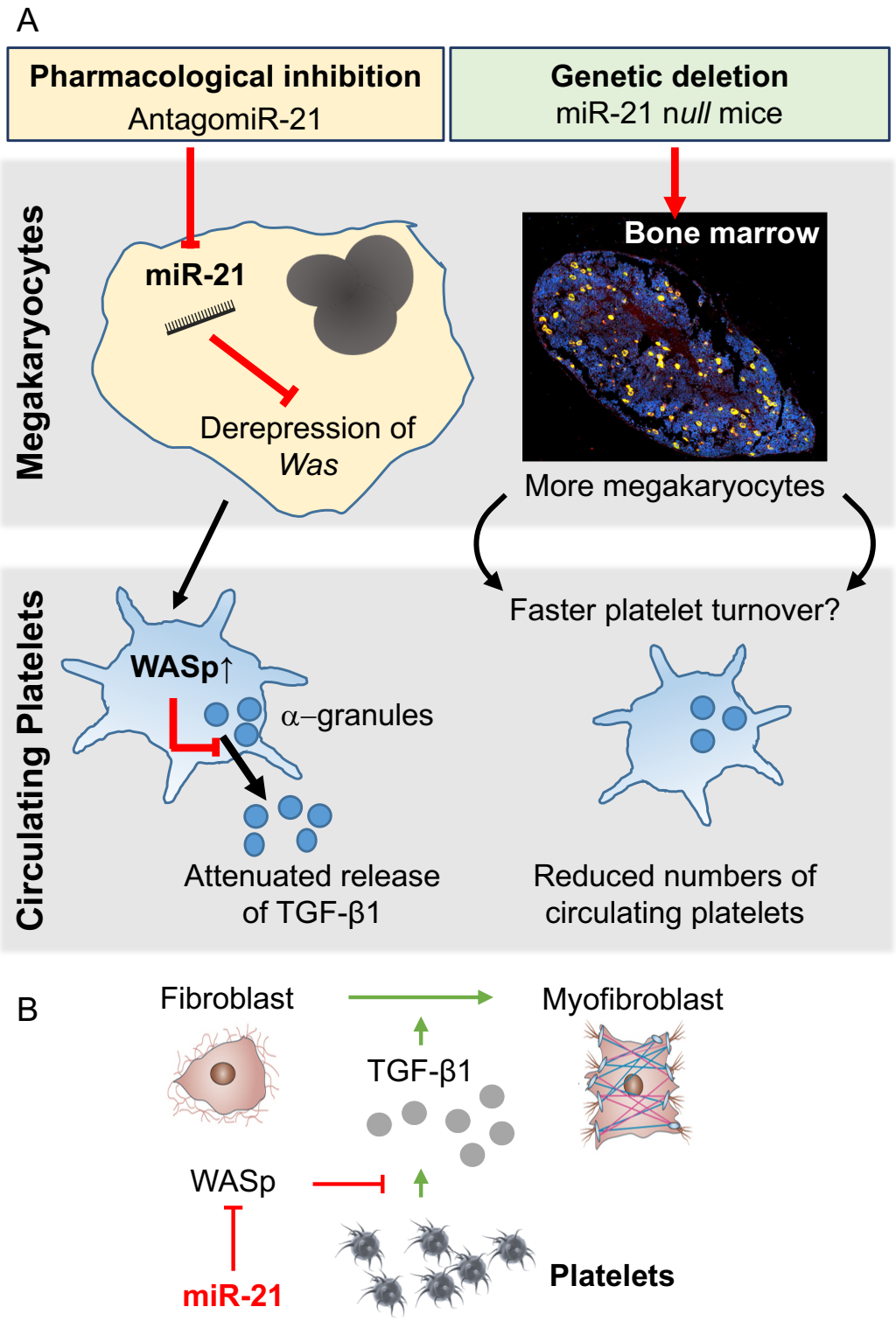

Figure 48. Summary: miR-21 may affect cardiac fibrosis through effects on megakaryocytes and platelets. A. Pharmacological inhibition of miR-21 in mice increases megakaryocyte expression levels of *Was*, a direct target of miR-21. Higher levels of the corresponding WASp protein suppress the release of TGF-β1 from platelets. Genetic deletion of miR-21 in mice results in decreased platelet counts but higher megakaryocyte numbers. **B:** Platelet-derived TGF-β1 was previously shown to enhance cardiac fibrosis in response to pressure overload. TGF-β1 is a key mediator of fibroblast proliferation and differentiation. Thus, observed protective effects of miR-21 inhibition in different fibrosis models might, at least in part, be dependent on bone marrow and bone-marrow derived cells.

References

1. Wilkins E, Wilson L, Wickramasinghe K, Bhatnagar P, Leal J, Luengo-Fernandez R, Burns R, Rayner M, Townsend N. *European Cardiovascular Disease Statistics 2017*. Brussels; 2017.
2. Ponikowski P, Voors AA, Anker SD, et al. 2016 ESC Guidelines for the diagnosis and treatment of acute and chronic heart failure: The Task Force for the diagnosis and treatment of acute and chronic heart failure of the European Society of Cardiology (ESC). *Eur Heart J*. 2016;37(27):2129–2200.
3. McMurray JJ, Packer M, Desai AS, Gong J, Lefkowitz MP, Rizkala AR, Rouleau JL, Shi VC, Solomon SD, Swedberg K, Zile MR, PARADIGM-HF Investigators and Committees. Angiotensin-neprilysin inhibition versus enalapril in heart failure. *N Engl J Med*. 2014;371(11):993–1004.
4. Cohn JN, Ferrari R, Sharpe N. Cardiac remodeling--concepts and clinical implications: a consensus paper from an international forum on cardiac remodeling. *J Am Coll Cardiol*. 2000;35(3):569–582.
5. Burchfield JS, Xie M, Hill JA. Pathological ventricular remodeling: mechanisms: part 1 of 2. *Circulation*. 2013;128(4):388–400.
6. Souders CA, Bowers SLK, Baudino TA. Cardiac fibroblast: the renaissance cell. *Circ Res*. 2009;105(12):1164–1176.
7. Spinale FG. Myocardial matrix remodeling and the matrix metalloproteinases: influence on cardiac form and function. *Physiol Rev*. 2007;87(4):1285–1342.
8. Barallobre-Barreiro J, Lynch M, Yin X, Mayr M. Systems biology-opportunities and challenges: the application of proteomics to study the cardiovascular extracellular matrix. *Cardiovasc Res*. 2016;112(3):626–636.
9. Rog-Zielinska EA, Norris RA, Kohl P, Markwald R. The Living Scar--Cardiac Fibroblasts and the Injured Heart. *Trends Mol Med*. 2016;22(2):99–114.
10. Wernig G, Chen S-Y, Cui L, Van Neste C, Tsai JM, Kambham N, Vogel H, Natkunam Y, Gilliland DG, Nolan G, Weissman IL. Unifying mechanism for different fibrotic diseases. *Proc Natl Acad Sci U S A*. 2017;114(18):4757–4762.
11. Horn MA, Trafford AW. Aging and the cardiac collagen matrix: Novel mediators of fibrotic remodelling. *J Mol Cell Cardiol*. 2016;93:175–185.
12. Rockey DC, Bell PD, Hill JA. Fibrosis--a common pathway to organ injury and failure. *N Engl J Med*. 2015;372(12):1138–1149.
13. Czubryt MP. Common threads in cardiac fibrosis, infarct scar formation, and wound healing. *Fibrogenesis Tissue Repair*. 2012;5(1):19.
14. Bönner F, Borg N, Burghoff S, Schrader J. Resident cardiac immune cells and expression of the ectonucleotidase enzymes CD39 and CD73 after ischemic injury. *PLoS One*. 2012;7(4):e34730.
15. Ma Y, Iyer RP, Jung M, Czubryt MP, Lindsey ML. Cardiac Fibroblast Activation Post-Myocardial Infarction: Current Knowledge Gaps. *Trends Pharmacol Sci*. 2017;38(5):448–458.
16. Desmoulière A, Geinoz A, Gabbiani F, Gabbiani G. Transforming growth factor-beta 1 induces alpha-smooth muscle actin expression in granulation tissue myofibroblasts and in quiescent and growing

cultured fibroblasts. *J Cell Biol*. 1993;122(1):103–111.
17. Krenning G, Zeisberg EM, Kalluri R. The origin of fibroblasts and mechanism of cardiac fibrosis. *J Cell Physiol*. 2010;225(3):631–637.
18. Zeisberg EM, Tarnavski O, Zeisberg M, Dorfman AL, McMullen JR, Gustafsson E, Chandraker A, Yuan X, Pu WT, Roberts AB, Neilson EG, Sayegh MH, Izumo S, Kalluri R. Endothelial-to-mesenchymal transition contributes to cardiac fibrosis. *Nat Med*. 2007;13(8):952–961.
19. Zhou B, Honor LB, He H, et al. Adult mouse epicardium modulates myocardial injury by secreting paracrine factors. *J Clin Invest*. 2011;121(5):1894–1904.
20. Ruiz-Villalba A, Simón AM, Pogontke C, Castillo MI, Abizanda G, Pelacho B, Sánchez-Domínguez R, Segovia JC, Prósper F, Pérez-Pomares JM. Interacting resident epicardium-derived fibroblasts and recruited bone marrow cells form myocardial infarction scar. *J Am Coll Cardiol*. 2015;65(19):2057–2066.
21. Labelle M, Begum S, Hynes RO. Direct signaling between platelets and cancer cells induces an epithelial-mesenchymal-like transition and promotes metastasis. *Cancer Cell*. 2011;20(5):576–590.
22. Moore-Morris T, Guimarães-Camboa N, Banerjee I, et al. Resident fibroblast lineages mediate pressure overload-induced cardiac fibrosis. *J Clin Invest*. 2014;124(7):2921–2934.
23. Sime PJ, Xing Z, Graham FL, Csaky KG, Gauldie J. Adenovector-mediated gene transfer of active transforming growth factor-beta1 induces prolonged severe fibrosis in rat lung. *J Clin Invest*. 1997;100(4):768–776.
24. Leask A. Getting to the heart of the matter: new insights into cardiac fibrosis. *Circ Res*. 2015;116(7):1269–1276.
25. Rosenkranz S. TGF-beta1 and angiotensin networking in cardiac remodeling. *Cardiovasc Res*. 2004;63(3):423–432.
26. Flevaris P, Khan SS, Eren M, Schuldt AJT, Shah SJ, Lee DC, Gupta S, Shapiro AD, Burridge PW, Ghosh AK, Vaughan DE. Plasminogen Activator Inhibitor Type I Controls Cardiomyocyte Transforming Growth Factor-β and Cardiac Fibrosis. *Circulation*. 2017;136(7):664–679.
27. Gray MO, Long CS, Kalinyak JE, Li HT, Karliner JS. Angiotensin II stimulates cardiac myocyte hypertrophy via paracrine release of TGF-beta 1 and endothelin-1 from fibroblasts. *Cardiovasc Res*. 1998;40(2):352–363.
28. Campbell SE, Katwa LC. Angiotensin II stimulated expression of transforming growth factor-beta1 in cardiac fibroblasts and myofibroblasts. *J Mol Cell Cardiol*. 1997;29(7):1947–1958.
29. Meyer A, Wang W, Qu J, Croft L, Degen JL, Coller BS, Ahamed J. Platelet TGF-β1 contributions to plasma TGF-β1, cardiac fibrosis, and systolic dysfunction in a mouse model of pressure overload. *Blood*. 2012;119(4):1064–1074.
30. Bujak M, Frangogiannis NG. The role of TGF-beta signaling in myocardial infarction and cardiac remodeling. *Cardiovasc Res*. 2007;74(2):184–195.
31. Hinz B. The extracellular matrix and transforming growth factor-β1: Tale of a strained relationship. *Matrix Biol*. 2015;47:54–65.
32. Shi M, Zhu J, Wang R, Chen X, Mi L, Walz T, Springer TA. Latent TGF-β structure and activation. *Nature*. 2011;474(7351):343–349.
33. Villar A V, Cobo M, Llano M, Montalvo C, González-Vílchez F, Martín-

Durán R, Hurlé MA, Nistal JF. Plasma levels of transforming growth factor-beta1 reflect left ventricular remodeling in aortic stenosis. *PLoS One*. 2009;4(12):e8476.
34. Ahamed J, Terry H, Choi ME, Laurence J. Transforming growth factor-β1-mediated cardiac fibrosis: potential role in HIV and HIV/antiretroviral therapy-linked cardiovascular disease. *AIDS*. 2016;30(4):535–542.
35. Lyons RM, Keski-Oja J, Moses HL. Proteolytic activation of latent transforming growth factor-beta from fibroblast-conditioned medium. *J Cell Biol*. 1988;106(5):1659–1665.
36. Henderson NC, Arnold TD, Katamura Y, et al. Targeting of αv integrin identifies a core molecular pathway that regulates fibrosis in several organs. *Nat Med*. 2013;19(12):1617–1624.
37. Yu Q, Stamenkovic I. Cell surface-localized matrix metalloproteinase-9 proteolytically activates TGF-beta and promotes tumor invasion and angiogenesis. *Genes Dev*. 2000;14(2):163–176.
38. Murphy-Ullrich JE, Poczatek M. Activation of latent TGF-beta by thrombospondin-1: mechanisms and physiology. *Cytokine Growth Factor Rev*. 2000;11(1–2):59–69.
39. Kulkarni AB, Huh CG, Becker D, Geiser A, Lyght M, Flanders KC, Roberts AB, Sporn MB, Ward JM, Karlsson S. Transforming growth factor beta 1 null mutation in mice causes excessive inflammatory response and early death. *Proc Natl Acad Sci U S A*. 1993;90(2):770–774.
40. Shull MM, Ormsby I, Kier AB, Pawlowski S, Diebold RJ, Yin M, Allen R, Sidman C, Proetzel G, Calvin D. Targeted disruption of the mouse transforming growth factor-beta 1 gene results in multifocal inflammatory disease. *Nature*. 1992;359(6397):693–699.
41. Kuwahara F, Kai H, Tokuda K, Kai M, Takeshita A, Egashira K, Imaizumi T. Transforming growth factor-beta function blocking prevents myocardial fibrosis and diastolic dysfunction in pressure-overloaded rats. *Circulation*. 2002;106(1):130–135.
42. Engebretsen KVT, Skårdal K, Bjørnstad S, Marstein HS, Skrbic B, Sjaastad I, Christensen G, Bjørnstad JL, Tønnessen T. Attenuated development of cardiac fibrosis in left ventricular pressure overload by SM16, an orally active inhibitor of ALK5. *J Mol Cell Cardiol*. 2014;76:148–157.
43. Frantz S, Hu K, Adamek A, Wolf J, Sallam A, Maier SKG, Lonning S, Ling H, Ertl G, Bauersachs J. Transforming growth factor beta inhibition increases mortality and left ventricular dilatation after myocardial infarction. *Basic Res Cardiol*. 2008;103(5):485–492.
44. Kang J-H, Jung M-Y, Yin X, Andrianifahanana M, Hernandez DM, Leof EB. Cell-penetrating peptides selectively targeting SMAD3 inhibit profibrotic TGF-β signaling. *J Clin Invest*. 2017;127(7):2541–2554.
45. Kunamalla A, Ng J, Parini V, et al. Constitutive Expression of a Dominant-Negative TGF-β Type II Receptor in the Posterior Left Atrium Leads to Beneficial Remodeling of Atrial Fibrillation Substrate. *Circ Res*. 2016;119(1):69–82.
46. Okada H, Takemura G, Kosai K, Li Y, Takahashi T, Esaki M, Yuge K, Miyata S, Maruyama R, Mikami A, Minatoguchi S, Fujiwara T, Fujiwara H. Postinfarction gene therapy against transforming growth factor-beta signal modulates infarct tissue dynamics and attenuates left ventricular remodeling and heart failure. *Circulation*. 2005;111(19):2430–2437.

47. Schafer S, Viswanathan S, Widjaja AA, et al. IL-11 is a crucial determinant of cardiovascular fibrosis. *Nature*. 2017;552(7683):110–115.
48. Permyakov EA, Uversky VN, Permyakov SE. Interleukin-11: A Multifunctional Cytokine with Intrinsically Disordered Regions. *Cell Biochem Biophys*. 2016;74(3):285–96.
49. Tepler I, Elias L, Smith JW, Hussein M, Rosen G, Chang AY, Moore JO, Gordon MS, Kuca B, Beach KJ, Loewy JW, Garnick MB, Kaye JA. A randomized placebo-controlled trial of recombinant human interleukin-11 in cancer patients with severe thrombocytopenia due to chemotherapy. *Blood*. 1996;87(9):3607–14.
50. Flisiak R, Prokopowicz D. Transforming growth factor-beta1 as a surrogate marker of hepatic dysfunction in chronic liver diseases. *Clin Chem Lab Med*. 2000;38(11):1129–1131.
51. Rico MC, Manns JM, Driban JB, Uknis AB, Kunapuli SP, Dela Cadena RA. Thrombospondin-1 and transforming growth factor beta are pro-inflammatory molecules in rheumatoid arthritis. *Transl Res*. 2008;152(2):95–98.
52. Szekanecz Z, Haines GK, Harlow LA, Shah MR, Fong TW, Fu R, Lin SJW, Rayan G, Koch AE. Increased synovial expression of transforming growth factor (TGF)-beta receptor endoglin and TGF-beta 1 in rheumatoid arthritis: possible interactions in the pathogenesis of the disease. *Clin Immunol Immunopathol*. 1995;76(2):187–194.
53. Lawrance IC, Maxwell L, Doe W. Inflammation location, but not type, determines the increase in TGF-beta1 and IGF-1 expression and collagen deposition in IBD intestine. *Inflamm Bowel Dis*. 2001;7(1):16–26.
54. Pohlers D, Brenmoehl J, Löffler I, Müller CK, Leipner C, Schultze-Mosgau S, Stallmach A, Kinne RW, Wolf G. TGF-beta and fibrosis in different organs - molecular pathway imprints. *Biochim Biophys Acta*. 2009;1792(8):746–756.
55. Assoian RK, Sporn MB. Type beta transforming growth factor in human platelets: release during platelet degranulation and action on vascular smooth muscle cells. *J Cell Biol*. 1986;102(4):1217–1223.
56. Massberg S, Gawaz M, Grüner S, Schulte V, Konrad I, Zohlnhöfer D, Heinzmann U, Nieswandt B. A crucial role of glycoprotein VI for platelet recruitment to the injured arterial wall in vivo. *J Exp Med*. 2003;197(1):41–49.
57. Savage B, Saldívar E, Ruggeri ZM. Initiation of platelet adhesion by arrest onto fibrinogen or translocation on von Willebrand factor. *Cell*. 1996;84(2):289–297.
58. Gurbel PA, Jeong Y-H, Navarese EP, Tantry US. Platelet-Mediated Thrombosis: From Bench to Bedside. *Circ Res*. 2016;118(9):1380–1391.
59. Chung I, Lip GYH. Platelets and heart failure. *Eur Heart J*. 2006;27(22):2623–2631.
60. Assoian RK, Komoriya A, Meyers CA, Miller DM, Sporn MB. Transforming growth factor-beta in human platelets. Identification of a major storage site, purification, and characterization. *J Biol Chem*. 1983;258(11):7155–7160.
61. von Hundelshausen P, Weber C. Platelets as immune cells: bridging inflammation and cardiovascular disease. *Circ Res*. 2007;100(1):27–

40.
62. Pignatelli P, Cangemi R, Celestini A, Carnevale R, Polimeni L, Martini A, Ferro D, Loffredo L, Violi F. Tumour necrosis factor alpha upregulates platelet CD40L in patients with heart failure. *Cardiovasc Res*. 2008;78(3):515–522.
63. Shah A, Passacquale G, Gkaliagkousi E, Ritter J, Ferro A. Platelet nitric oxide signalling in heart failure: role of oxidative stress. *Cardiovasc Res*. 2011;91(4):625–631.
64. Mancini D, Monteagudo J, Suárez-Fariñas M, Bander J, Varshney R, Gonzalez J, Coller BS, Ahamed J. New methodologies to accurately assess circulating active transforming growth factor-β1 levels: implications for evaluating heart failure and the impact of left ventricular assist devices. *Transl Res*. 2017:1–14.
65. Mentz RJ, Lazzarini V, Fiuzat M, Metra M, O'Connor CM, Felker GM. Is there a rationale for antiplatelet therapy in acute heart failure? *Circ Heart Fail*. 2013;6(4):869–876.
66. Carazo M, Berger JS, Reyentovich A, Katz SD. Role of Antiplatelet Therapy and Anticoagulation in Nonischemic Cardiomyopathy. *Cardiol Rev*. 2016;24(5):211–217.
67. Lip GYH, Wrigley BJ, Pisters R. Antiplatelet agents versus control or anticoagulation for heart failure in sinus rhythm. *Cochrane database Syst Rev*. 2016;(5):CD003333.
68. Kalkman EAJ, van Suylen RJ, van Dijk JP, Saxena PR, Schoemaker RG. Chronic aspirin treatment affects collagen deposition in non-infarcted myocardium during remodeling after coronary artery ligation in the rat. *J Mol Cell Cardiol*. 1995;27(11):2483–2494.
69. Wu R, Yin D, Sadekova N, Deschepper CF, de Champlain J, Girouard H. Protective effects of aspirin from cardiac hypertrophy and oxidative stress in cardiomyopathic hamsters. *Oxid Med Cell Longev*. 2012;2012:761710.
70. Jia L-X, Qi G-M, Liu O, Li T-T, Yang M, Cui W, Zhang W-M, Qi Y-F, Du J. Inhibition of platelet activation by clopidogrel prevents hypertension-induced cardiac inflammation and fibrosis. *Cardiovasc Drugs Ther*. 2013;27(6):521–530.
71. Yin Z, Wang X, Zhang L, Zhou H, Wei L, Dong X. Aspirin Attenuates Angiotensin II-induced Cardiomyocyte Hypertrophy by Inhibiting the Ca(2+)/Calcineurin-NFAT Signaling Pathway. *Cardiovasc Ther*. 2016;34(1):21–29.
72. Liu G, Liang B, Song X, Bai R, Qin W, Sun X, Lu Y, Bian Y, Xiao C. P-selectin increases angiotensin II-induced cardiac inflammation and fibrosis via platelet activation. *Mol Med Rep*. 2016;13(6):5021–5028.
73. Wu L, Zhao F, Dai M, Li H, Chen C, Nie J, Wang P, Wang DW. P2y12 receptor promotes pressure overload-induced cardiac remodeling via platelet-driven inflammation in mice. *Hypertension*. 2017;70(4):759–769.
74. Laurence J, Elhadad S, Robison T, Terry H, Varshney R, Woolington S, Ghafoory S, Choi ME, Ahamed J. HIV protease inhibitor-induced cardiac dysfunction and fibrosis is mediated by platelet-derived TGF-β1 and can be suppressed by exogenous carbon monoxide. *PLoS One*. 2017;12(10):e0187185.
75. Fava RA, Casey TT, Wilcox J, Pelton RW, Moses HL, Nanney LB. Synthesis of transforming growth factor-beta 1 by megakaryocytes and

its localization to megakaryocyte and platelet alpha-granules. *Blood*. 1990;76(10):1946–1955.
76. Larsen E, Celi A, Gilbert GE, Furie BC, Erban JK, Bonfanti R, Wagner DD, Furie B. PADGEM protein: a receptor that mediates the interaction of activated platelets with neutrophils and monocytes. *Cell*. 1989;59(2):305–312.
77. Kim H, Falet H, Hoffmeister KM, Hartwig JH. Wiskott-Aldrich syndrome protein (WASp) controls the delivery of platelet transforming growth factor-β1. *J Biol Chem*. 2013;288(48):34352–34363.
78. Grainger DJ, Wakefield L, Bethell HW, Farndale RW, Metcalfe JC. Release and activation of platelet latent TGF-beta in blood clots during dissolution with plasmin. *Nat Med*. 1995;1:932–937.
79. Venter JC, Adams MD, Myers EW, et al. The sequence of the human genome. *Science*. 2001;291(5507):1304–1351.
80. ENCODE Project Consortium. An integrated encyclopedia of DNA elements in the human genome. *Nature*. 2012;489(7414):57–74.
81. Graur D. An Upper Limit on the Functional Fraction of the Human Genome. *Genome Biol Evol*. 2017;9(7):1880–1885.
82. Lee RC, Feinbaum RL, Ambros V. The C. elegans heterochronic gene lin-4 encodes small RNAs with antisense complementarity to lin-14. *Cell*. 1993;75(5):843–854.
83. Condorelli G, Latronico MV, Cavarretta E. microRNAs in cardiovascular diseases: current knowledge and the road ahead. *J Am Coll Cardiol*. 2014;63(21):2177–2187.
84. Jonas S, Izaurralde E. Towards a molecular understanding of microRNA-mediated gene silencing. *Nat Rev Genet*. 2015;16(7):421–433.
85. Cai X, Hagedorn CH, Cullen BR. Human microRNAs are processed from capped, polyadenylated transcripts that can also function as mRNAs. *RNA*. 2004;10(12):1957–1966.
86. Lee Y, Kim M, Han J, Yeom K-H, Lee S, Baek SH, Kim VN. MicroRNA genes are transcribed by RNA polymerase II. *EMBO J*. 2004;23(20):4051–4060.
87. Denli AM, Tops BBJ, Plasterk RHA, Ketting RF, Hannon GJ. Processing of primary microRNAs by the Microprocessor complex. *Nature*. 2004;432(7014):231–235.
88. Yi R, Qin Y, Macara IG, Cullen BR. Exportin-5 mediates the nuclear export of pre-microRNAs and short hairpin RNAs. *Genes Dev*. 2003;17(24):3011–3016.
89. Chendrimada TP, Gregory RI, Kumaraswamy E, Norman J, Cooch N, Nishikura K, Shiekhattar R. TRBP recruits the Dicer complex to Ago2 for microRNA processing and gene silencing. *Nature*. 2005;436(7051):740–744.
90. Bang C, Batkai S, Dangwal S, et al. Cardiac fibroblast-derived microRNA passenger strand-enriched exosomes mediate cardiomyocyte hypertrophy. *J Clin Invest*. 2014;124(5):2136–2146.
91. Rana TM. Illuminating the silence: understanding the structure and function of small RNAs. *Nat Rev cell Biol*. 2007;8(1):23–36.
92. Zampetaki A, Mayr M. MicroRNAs in vascular and metabolic disease. *Circ Res*. 2012;110(3):508–522.
93. Barwari T, Joshi A, Mayr M. MicroRNAs in cardiovascular disease. *J Am Coll Cardiol*. 2016;68(23):2577–2584.

94. Pritchard CC, Cheng HH, Tewari M. MicroRNA profiling: approaches and considerations. *Nat Rev Genet*. 2012;13(5):358–369.
95. Wang Z, Gerstein M, Snyder M. RNA-Seq: a revolutionary tool for transcriptomics. *Nat Rev Genet*. 2009;10(1):57–63.
96. Sunderland N, Skroblin P, Barwari T, Huntley RP, Lu R, Joshi A, Lovering RC, Mayr M. MicroRNA biomarkers and platelet reactivity: the clot thickens. *Circ Res*. 2017;120(2):418–435.
97. da Costa Martins PA, Bourajjaj M, Gladka M, Kortland M, van Oort RJ, Pinto YM, Molkentin JD, De Windt LJ. Conditional dicer gene deletion in the postnatal myocardium provokes spontaneous cardiac remodeling. *Circulation*. 2008;118(15):1567–1576.
98. Lim LP, Lau NC, Garrett-Engele P, Grimson A, Schelter JM, Castle J, Bartel DP, Linsley PS, Johnson JM. Microarray analysis shows that some microRNAs downregulate large numbers of target mRNAs. *Nature*. 2005;433(7027):769–73.
99. Lennox K a, Behlke M a. Chemical modification and design of anti-miRNA oligonucleotides. *Gene Ther*. 2011;18(12):1111–20.
100. Reinhart BJ, Slack FJ, Basson M, Pasquinelli AE, Bettinger JC, Rougvie AE, Horvitz HR, Ruvkun G. The 21-nucleotide let-7 RNA regulates developmental timing in Caenorhabditis elegans. *Nature*. 2000;403(6772):901–906.
101. Pasquinelli AE, Reinhart BJ, Slack F, et al. Conservation of the sequence and temporal expression of let-7 heterochronic regulatory RNA. *Nature*. 2000;408(6808):86–89.
102. Lau NC, Lim LP, Weinstein EG, Bartel DP. An abundant class of tiny RNAs with probable regulatory roles in Caenorhabditis elegans. *Science*. 2001;294(5543):858–862.
103. Lee RC, Ambros V, Erdmann VA, et al. An extensive class of small RNAs in Caenorhabditis elegans. *Science*. 2001;294(5543):862–864.
104. Lagos-Quintana M, Rauhut R, Yalcin A, Meyer J, Lendeckel W, Tuschl T. Identification of Tissue-Specific MicroRNAs from Mouse. *Curr Biol*. 2002;12:735–739.
105. Kwon C, Han Z, Olson EN, Srivastava D. MicroRNA1 influences cardiac differentiation in Drosophila and regulates Notch signaling. *Proc Natl Acad Sci U S A*. 2005;102(52):18986–18991.
106. Zhao Y, Samal E, Srivastava D. Serum response factor regulates a muscle-specific microRNA that targets Hand2 during cardiogenesis. *Nature*. 2005;436(7048):214–220.
107. van Rooij E, Sutherland LB, Liu N, Williams AH, McAnally J, Gerard RD, Richardson JA, Olson EN. A signature pattern of stress-responsive microRNAs that can evoke cardiac hypertrophy and heart failure. *Proc Natl Acad Sci U S A*. 2006;103(48):18255–18260.
108. Krützfeldt J, Rajewsky N, Braich R, Rajeev KG, Tuschl T, Manoharan M, Stoffel M. Silencing of microRNAs in vivo with “antagomirs”. *Nature*. 2005;438(7068):685–689.
109. Calvo-Garrido J, Carilla-Latorre S, Lázaro-Diéguez F, Egea G, Escalante R. Vacuole membrane protein 1 is an endoplasmic reticulum protein required for organelle biogenesis, protein secretion, and development. *Mol Biol Cell*. 2008;19(8):3442–53.
110. Patrick DM, Montgomery RL, Qi X, Obad S, Kauppinen S, Hill JA, van Rooij E, Olson EN. Stress-dependent cardiac remodeling occurs in the absence of microRNA-21 in mice. *J Clin Invest*. 2010;120(11):3912–

3916.
111. Chan JA, Krichevsky AM, Kosik KS. MicroRNA-21 is an antiapoptotic factor in human glioblastoma cells. *Cancer Res*. 2005;65(14):6029–6033.
112. Volinia S, Calin GA, Liu C-G, et al. A microRNA expression signature of human solid tumors defines cancer gene targets. *Proc Natl Acad Sci U S A*. 2006;103(7):2257–2261.
113. Zhu S, Wu H, Wu F, Nie D, Sheng S, Mo Y-Y. MicroRNA-21 targets tumor suppressor genes in invasion and metastasis. *Cell Res*. 2008;18(3):350–359.
114. Sayed D, Hong C, Chen I-Y, Lypowy J, Abdellatif M. MicroRNAs play an essential role in the development of cardiac hypertrophy. *Circ Res*. 2007;100(3):416–424.
115. Sayed D, Rane S, Lypowy J, He M, Chen I-Y, Vashistha H, Yan L, Malhotra A, Vatner D, Abdellatif M. MicroRNA-21 targets Sprouty2 and promotes cellular outgrowths. *Mol Biol Cell*. 2008;19(8):3272–3282.
116. Tatsuguchi M, Seok HY, Callis TE, Thomson JM, Chen J-F, Newman M, Rojas M, Hammond SM, Wang D-Z. Expression of microRNAs is dynamically regulated during cardiomyocyte hypertrophy. *J Mol Cell Cardiol*. 2007;42(6):1137–1141.
117. Cheng Y, Ji R, Yue J, Yang J, Liu X, Chen H, Dean DB, Zhang C. MicroRNAs are aberrantly expressed in hypertrophic heart: do they play a role in cardiac hypertrophy? *Am J Pathol*. 2007;170(6):1831–1840.
118. Thum T, Gross C, Fiedler J, et al. MicroRNA-21 contributes to myocardial disease by stimulating MAP kinase signalling in fibroblasts. *Nature*. 2008;456:980–984.
119. Roy S, Khanna S, Hussain S-RA, Biswas S, Azad A, Rink C, Gnyawali S, Shilo S, Nuovo GJ, Sen CK. MicroRNA expression in response to murine myocardial infarction: miR-21 regulates fibroblast metalloprotease-2 via phosphatase and tensin homologue. *Cardiovasc Res*. 2009;82(1):21–29.
120. Wu T, Liu Y, Fan Z, Xu J, Jin L, Gao Z, Wu Z, Hu L, Wang J, Zhang C, Chen W, Wang S. miR-21 Modulates the Immunoregulatory Function of Bone Marrow Mesenchymal Stem Cells Through the PTEN/Akt/TGF-β1 Pathway. *Stem Cells*. 2015;33(11):3281–3290.
121. Liang H, Zhang C, Ban T, Liu Y, Mei L, Piao X, Zhao D, Lu Y, Chu W, Yang B. A novel reciprocal loop between microRNA-21 and TGFβRIII is involved in cardiac fibrosis. *Int J Biochem Cell Biol*. 2012;44(12):2152–2160.
122. Tao H, Zhang M, Yang J, Shi K-H. MicroRNA-21 via Dysregulation of WW Domain-Containing Protein 1 Regulate Atrial Fibrosis in Atrial Fibrillation. *Heart Lung Circ*. 2017:1–10.
123. Lorenzen JM, Schauerte C, Hübner A, et al. Osteopontin is indispensible for AP1-mediated angiotensin II-related miR-21 transcription during cardiac fibrosis. *Eur Heart J*. 2015;36(32):2184–2196.
124. Thum T, Chau N, Bhat B, Gupta SK, Linsley PS, Bauersachs J, Engelhardt S. Comparison of different miR-21 inhibitor chemistries in a cardiac disease model. *J Clin Invest*. 2011;121(2):461-462; author reply 462-463.
125. Yang K-CC, Ku Y-CC, Lovett M, Nerbonne JM. Combined deep

microRNA and mRNA sequencing identifies protective transcriptomal signature of enhanced PI3Kα signaling in cardiac hypertrophy. *J Mol Cell Cardiol*. 2012;53(1):101–112.
126. Brønnum H, Andersen DC, Schneider M, Sandberg MB, Eskildsen T, Nielsen SB, Kalluri R, Sheikh SP. miR-21 promotes fibrogenic epithelial-to-mesenchymal transition of epicardial mesothelial cells involving Programmed Cell Death 4 and Sprouty-1. *PLoS One*. 2013;8(2):e56280.
127. Dong S, Ma W, Hao B, Hu F, Yan L, Yan X, Wang Y, Chen Z, Wang Z. microRNA-21 promotes cardiac fibrosis and development of heart failure with preserved left ventricular ejection fraction by up-regulating Bcl-2. *Int J Clin Exp Pathol*. 2014;7(2):565–574.
128. Dong X, Liu S, Zhang L, Yu S, Huo L, Qile M, Liu L, Yang B, Yu J. Downregulation of miR-21 is Involved in Direct Actions of Ursolic Acid on the Heart: Implications for Cardiac Fibrosis and Hypertrophy. *Cardiovasc Ther*. 2015;33(4):161–167.
129. García R, Nistal JF, Merino D, Price NL, Fernández-Hernando C, Beaumont J, González A, Hurlé MA, Villar A V. p-SMAD2/3 and DICER promote pre-miR-21 processing during pressure overload-associated myocardial remodeling. *Biochim Biophys Acta*. 2015;1852(7):1520–1530.
130. Cheng M, Wu G, Song Y, Wang L, Tu L, Zhang L, Zhang C. Celastrol-Induced Suppression of the MiR-21/ERK Signalling Pathway Attenuates Cardiac Fibrosis and Dysfunction. *Cell Physiol Biochem*. 2016;38(5):1928–1938.
131. Ramanujam D, Sassi Y, Laggerbauer B, Engelhardt S. Viral vector-based targeting of miR-21 in cardiac nonmyocyte cells reduces pathologic remodeling of the heart. *Mol Ther*. 2016;24(11):1939–1948.
132. Reddy S, Hu D, Zhao M, Blay E, Sandeep N, Ong S, Jung G, Kooiker KB, Coronado M, Fajardo G, Bernstein D. miR-21 is associated with fibrosis and right ventricular failure. *JCI insight*. 2017;2(9):1–14.
133. Ning B, Zhang Y, Wu D, Cui J, Liu L, Wang P-W, Wang W, Zhu W, Chen Y, Zhang T. Luteolin-7-diglucuronide attenuates isoproterenol-induced myocardial injury and fibrosis in mice. *Acta Pharmacol Sin*. 2017;38(3):331–341.
134. Tao H, Zhang J-G, Qin R-H, Dai C, Shi P, Yang J-J, Deng Z-Y, Shi K-H. LncRNA GAS5 controls cardiac fibroblast activation and fibrosis by targeting miR-21 via PTEN/MMP-2 signaling pathway. *Toxicology*. 2017;386(May):11–18.
135. Cao W, Shi P, Ge J-J. miR-21 enhances cardiac fibrotic remodeling and fibroblast proliferation via CADM1/STAT3 pathway. *BMC Cardiovasc Disord*. 2017;17(1):88.
136. de Melo BL, Vieira SS, Antônio EL, Dos Santos LFN, Portes LA, Feliciano RS, de Oliveira HA, Silva JA, de Carvalho P de TC, Tucci PJF, Serra AJ. Exercise Training Attenuates Right Ventricular Remodeling in Rats with Pulmonary Arterial Stenosis. *Front Physiol*. 2016;7:541.
137. Villar A, García R, Merino D, Llano M, Cobo M, Montalvo C, Martín-Durán R, Hurlé MA, Nistal JF. Myocardial and circulating levels of microRNA-21 reflect left ventricular fibrosis in aortic stenosis patients. *Int J Cardiol*. 2013;167(6):2875–2881.
138. Lavall D, Selzer C, Schuster P, Lenski M, Adam O, Schäfers H-J,

Böhm M, Laufs U. The mineralocorticoid receptor promotes fibrotic remodeling in atrial fibrillation. *J Biol Chem*. 2014;289(10):6656–6668.
139. Zhang H, Liu S, Dong T, Yang J, Xie Y, Wu Y, Kang K, Hu S, Gou D, Wei Y. Profiling of differentially expressed microRNAs in arrhythmogenic right ventricular cardiomyopathy. *Sci Rep*. 2016;6:28101.
140. Liu S, Li W, Xu M, Huang H, Wang J, Chen X. Micro-RNA 21Targets Dual Specific Phosphatase 8 to Promote Collagen Synthesis in High Glucose-Treated Primary Cardiac Fibroblasts. *Can J Cardiol*. 2014;30(12):1689–1699.
141. Hirt MN, Werner T, Indenbirken D, Alawi M, Demin P, Kunze A-CC, Stenzig J, Starbatty J, Hansen A, Fiedler J, Thum T, Eschenhagen T. Deciphering the microRNA signature of pathological cardiac hypertrophy by engineered heart tissue- and sequencing-technology. *J Mol Cell Cardiol*. 2015;81:1–9.
142. Gu G-L, Xu X-L, Sun X-T, Zhang J, Guo C-F, Wang C-S, Sun B, Guo G-L, Ma K, Huang Y-Y, Sun L-Q, Wang Y-Q. Cardioprotective Effect of MicroRNA-21 in Murine Myocardial Infarction. *Cardiovasc Ther*. 2015;33(3):109–117.
143. Rana I, Kompa AR, Skommer J, Wang BH, Lekawanvijit S, Kelly DJ, Krum H, Charchar FJ. Contribution of microRNA to pathological fibrosis in cardio-renal syndrome: impact of uremic toxins. *Physiol Rep*. 2015;3(4):e12371.
144. Huang W, Tian S-S, Hang P-Z, Sun C, Guo J, Du Z-M. Combination of microRNA-21 and microRNA-146a Attenuates Cardiac Dysfunction and Apoptosis During Acute Myocardial Infarction in Mice. *Mol Ther Nucleic Acids*. 2016;5(March):e296.
145. Dong S, Cheng Y, Yang J, Li J, Liu X, Wang X, Wang D, Krall TJ, Delphin ES, Zhang C. MicroRNA expression signature and the role of microRNA-21 in the early phase of acute myocardial infarction. *J Biol Chem*. 2009;284(43):29514–29525.
146. Sayed D, He M, Hong C, Gao S, Rane S, Yang Z, Abdellatif M. MicroRNA-21 is a downstream effector of AKT that mediates its antiapoptotic effects via suppression of Fas ligand. *J Biol Chem*. 2010;285(26):20281–20290.
147. Yang Q, Yang K, Li A. microRNA-21 protects against ischemia-reperfusion and hypoxia-reperfusion-induced cardiocyte apoptosis via the phosphatase and tensin homolog/Akt-dependent mechanism. *Mol Med Rep*. 2014;9(6):2213–2220.
148. Yin C, Salloum FN, Kukreja RC. A novel role of microRNA in late preconditioning: upregulation of endothelial nitric oxide synthase and heat shock protein 70. *Circ Res*. 2009;104(5):572–575.
149. Cheng Y, Zhu P, Yang J, Liu X, Dong S, Wang X, Chun B, Zhuang J, Zhang C. Ischaemic preconditioning-regulated miR-21 protects heart against ischaemia/reperfusion injury via anti-apoptosis through its target PDCD4. *Cardiovasc Res*. 2010;87(3):431–439.
150. Qin Y, Yu Y, Dong H, Bian X, Guo X, Dong S. MicroRNA 21 inhibits left ventricular remodeling in the early phase of rat model with ischemia-reperfusion injury by suppressing cell apoptosis. *Int J Med Sci*. 2012;9(6):413–423.
151. Haider KH, Idris NM, Kim HW, Ahmed RPH, Shujia J, Ashraf M. MicroRNA-21 is a key determinant in IL-11/Stat3 anti-apoptotic

signalling pathway in preconditioning of skeletal myoblasts. *Cardiovasc Res*. 2010;88(1):168–178.
152. Eschenhagen T, Bolli R, Braun T, et al. Cardiomyocyte Regeneration: A Consensus Statement. *Circulation*. 2017;136(7):680–686.
153. Xiao J, Pan Y, Li XH, Yang XY, Feng YL, Tan HH, Jiang L, Feng J, Yu XY. Cardiac progenitor cell-derived exosomes prevent cardiomyocytes apoptosis through exosomal miR-21 by targeting PDCD4. *Cell Death Dis*. 2016;7(6):e2277.
154. Su Q, Li L, Liu Y, Zhou Y, Wang J, Wen W. Ultrasound-targeted microbubble destruction-mediated microRNA-21 transfection regulated PDCD4/NF-κB/TNF-α pathway to prevent coronary microembolization-induced cardiac dysfunction. *Gene Ther*. 2015;22(12):1000–1006.
155. Adam O, Löhfelm B, Thum T, Gupta SK, Puhl S-L, Schäfers H-J, Böhm M, Laufs U. Role of miR-21 in the pathogenesis of atrial fibrosis. *Basic Res Cardiol*. 2012;107(5):278.
156. Adam O, Zimmer C, Hanke N, Hartmann RW, Klemmer B, Böhm M, Laufs U. Inhibition of aldosterone synthase (CYP11B2) by torasemide prevents atrial fibrosis and atrial fibrillation in mice. *J Mol Cell Cardiol*. 2015;85:140–150.
157. Cardin S, Guasch E, Luo X, Naud P, Le Quang K, Shi Y, Tardif J-C, Comtois P, Nattel S. Role for MicroRNA-21 in atrial profibrillatory fibrotic remodeling associated with experimental postinfarction heart failure. *Circ Arrhythm Electrophysiol*. 2012;5(5):1027–1035.
158. Chen Y, Wakili R, Xiao J, Wu C-T, Luo X, Clauss S, Dawson K, Qi X, Naud P, Shi Y-F, Tardif J-C, Kääb S, Dobrev D, Nattel S. Detailed characterization of microRNA changes in a canine heart failure model: Relationship to arrhythmogenic structural remodeling. *J Mol Cell Cardiol*. 2014;77:113–124.
159. He X, Zhang K, Gao X, Li L, Tan H, Chen J, Zhou Y. Rapid atrial pacing induces myocardial fibrosis by down-regulating Smad7 via microRNA-21 in rabbit. *Heart Vessels*. 2016;31(10):1696–1708.
160. Huang Z, Chen X-J, Qian C, Dong Q, Ding D, Wu Q-F, Li J, Wang H-F, Li W-H, Xie Q, Cheng X, Zhao N, Du Y-M, Liao Y-H. Signal Transducer and Activator of Transcription 3/MicroRNA-21 Feedback Loop Contributes to Atrial Fibrillation by Promoting Atrial Fibrosis in a Rat Sterile Pericarditis Model. *Circ Arrhythm Electrophysiol*. 2016;9(7):e003396.
161. Barana A, Matamoros M, Dolz-Gaitón P, Pérez-Hernández M, Amorós I, Núñez M, Sacristán S, Pedraz Á, Pinto Á, Fernández-Avilés F, Tamargo J, Delpón E, Caballero R. Chronic atrial fibrillation increases microRNA-21 in human atrial myocytes decreasing L-type calcium current. *Circ Arrhythm Electrophysiol*. 2014;7(5):861–868.
162. McManus DD, Tanriverdi K, Lin H, Esa N, Kinno M, Mandapati D, Tam S, Okike ON, Ellinor PT, Keaney JF, Donahue JK, Benjamin EJ, Freedman JE. Plasma microRNAs are associated with atrial fibrillation and change after catheter ablation (the miRhythm study). *Hear Rhythm*. 2015;12(1):3–10.
163. Zhong X, Chung ACK, Chen H-Y, Meng X-M, Lan HY. Smad3-mediated upregulation of miR-21 promotes renal fibrosis. *J Am Soc Nephrol*. 2011;22(9):1668–1681.
164. Davis BN, Hilyard AC, Lagna G, Hata A. SMAD proteins control DROSHA-mediated microRNA maturation. *Nature*.

2008;454(7200):56–61.
165. Hermida N, López B, González A, Dotor J, Lasarte JJ, Sarobe P, Borrás-Cuesta F, Díez J. A synthetic peptide from transforming growth factor-beta1 type III receptor prevents myocardial fibrosis in spontaneously hypertensive rats. *Cardiovasc Res*. 2009;81(3):601–609.
166. Lenga Y, Koh A, Perera AS, McCulloch CA, Sodek J, Zohar R. Osteopontin expression is required for myofibroblast differentiation. *Circ Res*. 2008;102(3):319–327.
167. Collins AR, Schnee J, Wang W, Kim S, Fishbein MC, Bruemmer D, Law RE, Nicholas S, Ross RS, Hsueh WA. Osteopontin modulates angiotensin II-induced fibrosis in the intact murine heart. *J Am Coll Cardiol*. 2004;43(9):1698–1705.
168. Denby L, Ramdas V, McBride MW, Wang J, Robinson H, McClure J, Crawford W, Lu R, Hillyard DZ, Khanin R, Agami R, Dominiczak AF, Sharpe CC, Baker AH. miR-21 and miR-214 are consistently modulated during renal injury in rodent models. *Am J Pathol*. 2011;179(2):661–672.
169. Ardite E, Perdiguero E, Vidal B, Gutarra S, Serrano AL, Muñoz-Cánoves P. PAI-1-regulated miR-21 defines a novel age-associated fibrogenic pathway in muscular dystrophy. *J Cell Biol*. 2012;196(1):163–175.
170. Kumarswamy R, Volkmann I, Jazbutyte V, Dangwal S, Park D-H, Thum T. Transforming growth factor-β-induced endothelial-to-mesenchymal transition is partly mediated by microRNA-21. *Arterioscler Thromb Vasc Biol*. 2012;32(2):361–369.
171. Bhagat TD, Zhou L, Sokol L, et al. miR-21 mediates hematopoietic suppression in MDS by activating TGF-β signaling. *Blood*. 2013;121(15):2875–2881.
172. Lai JY, Luo J, O'Connor C, et al. MicroRNA-21 in glomerular injury. *J Am Soc Nephrol*. 2015;26(4):805–816.
173. Seeger T, Fischer A, Muhly-Reinholz M, Zeiher AM, Dimmeler S. Long-Term inhibition of miR-21 leads to reduction of obesity in db/db mice. *Obesity*. 2014;22(11):2352–2360.
174. Gupta SK, Itagaki R, Zheng X, et al. miR-21 promotes fibrosis in an acute cardiac allograft transplantation model. *Cardiovasc Res*. 2016;110(2):215–226.
175. Ji R, Cheng Y, Yue J, Yang J, Liu X, Chen H, Dean DB, Zhang C. MicroRNA expression signature and antisense-mediated depletion reveal an essential role of MicroRNA in vascular neointimal lesion formation. *Circ Res*. 2007;100(11):1579–1588.
176. McDonald RA, Halliday CA, Miller AM, Diver LA, Dakin RS, Montgomery J, McBride MW, Kennedy S, McClure JD, Robertson KE, Douglas G, Channon KM, Oldroyd KG, Baker AH. Reducing in-stent restenosis: therapeutic manipulation of miRNA in vascular remodeling and inflammation. *J Am Coll Cardiol*. 2015;65(21):2314–2327.
177. Wang D, Deuse T, Stubbendorff M, et al. Local microRNA modulation using a novel anti-miR-21-eluting stent effectively prevents experimental in-stent restenosis. *Arterioscler Thromb Vasc Biol*. 2015;35(9):1945–1953.
178. McDonald RA, White KM, Wu J, Cooley BC, Robertson KE, Halliday CA, McClure JD, Francis S, Lu R, Kennedy S, George SJ, Wan S, van

Rooij E, Baker AH. miRNA-21 is dysregulated in response to vein grafting in multiple models and genetic ablation in mice attenuates neointima formation. *Eur Heart J*. 2013;34(22):1636–1643.
179. Barwari T, Rienks M, Mayr M. MicroRNA-21 and the vulnerability of atherosclerotic plaques. *Mol Ther*. 2018;26(4):938–940.
180. Canfrán-Duque A, Rotllan N, Zhang X, Fernández-Fuertes M, Ramírez-Hidalgo C, Araldi E, Daimiel L, Busto R, Fernández-Hernando C, Suárez Y. Macrophage deficiency of miR-21 promotes apoptosis, plaque necrosis, and vascular inflammation during atherogenesis. *EMBO Mol Med*. 2017;9(9):1244–1262.
181. Jin H, Li Y, Chernogubova E, et al. Local delivery of miR-21 stabilizes fibrous caps in vulnerable atherosclerotic lesions. *Mol Ther*. 2018:492–500.
182. Tijsen AJ, van der Made I, van den Hoogenhof MM, Wijnen WJ, van Deel ED, de Groot NE, Alekseev S, Fluiter K, Schroen B, Goumans M-J, van der Velden J, Duncker DJ, Pinto YM, Creemers EE. The microRNA-15 family inhibits the TGFβ-pathway in the heart. *Cardiovasc Res*. 2014;104(1):61–71.
183. Wang J, Huang W, Xu R, Nie Y, Cao X, Meng J, Xu X, Hu S, Zheng Z. MicroRNA-24 regulates cardiac fibrosis after myocardial infarction. *J Cell Mol Med*. 2012;16(9):2150–2160.
184. van Rooij E, Sutherland LB, Thatcher JE, DiMaio JM, Naseem RH, Marshall WS, Hill JA, Olson EN. Dysregulation of microRNAs after myocardial infarction reveals a role of miR-29 in cardiac fibrosis. *Proc Natl Acad Sci U S A*. 2008;105(35):13027–13032.
185. Abonnenc M, Nabeebaccus AA, Mayr U, et al. Extracellular matrix secretion by cardiac fibroblasts: role of microRNA-29b and microRNA-30c. *Circ Res*. 2013;113(10):1138–1147.
186. Jentzsch C, Leierseder S, Loyer X, Flohrschütz I, Sassi Y, Hartmann D, Thum T, Laggerbauer B, Engelhardt S. A phenotypic screen to identify hypertrophy-modulating microRNAs in primary cardiomyocytes. *J Mol Cell Cardiol*. 2012;52(1):13–20.
187. Sassi Y, Avramopoulos P, Ramanujam D, et al. Cardiac myocyte miR-29 promotes pathological remodeling of the heart by activating Wnt signaling. *Nat Commun*. 2017;8(1):1614.
188. Pan Z, Sun X, Shan H, Wang N, Wang J, Ren J, Feng S, Xie L, Lu C, Yuan Y, Zhang Y, Wang Y, Lu Y, Yang B. MicroRNA-101 inhibited postinfarct cardiac fibrosis and improved left ventricular compliance via the FBJ osteosarcoma oncogene/transforming growth factor-β1 pathway. *Circulation*. 2012;126(7):840–850.
189. Nagpal V, Rai R, Place AT, Murphy SB, Verma SK, Ghosh AK, Vaughan DE. MiR-125b Is Critical for Fibroblast-to-Myofibroblast Transition and Cardiac Fibrosis. *Circulation*. 2016;133(3):291–301.
190. Duisters RF, Tijsen AJ, Schroen B, Leenders JJ, Lentink V, van der Made I, Herias V, van Leeuwen RE, Schellings MW, Barenbrug P, Maessen JG, Heymans S, Pinto YM, Creemers EE. miR-133 and miR-30 regulate connective tissue growth factor: implications for a role of microRNAs in myocardial matrix remodeling. *Circ Res*. 2009;104(2):170–178.
191. Castoldi G, di Gioia CRT, Bombardi C, Catalucci D, Corradi B, Gualazzi MG, Leopizzi M, Mancini M, Zerbini G, Condorelli G, Stella A. MiR-133a regulates collagen 1A1: Potential role of miR-133a in

myocardial fibrosis in angiotensin II-dependent hypertension. *J Cell Physiol*. 2012;227(2):850–856.
192. Matkovich SJ, Wang W, Tu Y, Eschenbacher WH, Dorn LE, Condorelli G, Diwan A, Nerbonne JM, Dorn GW. MicroRNA-133a protects against myocardial fibrosis and modulates electrical repolarization without affecting hypertrophy in pressure-overloaded adult hearts. *Circ Res*. 2010;106(1):166–75.
193. Leptidis S, El Azzouzi H, Lok SI, de Weger R, Olieslagers S, Olieslagers S, Kisters N, Silva GJ, Heymans S, Cuppen E, Berezikov E, De Windt LJ, da Costa Martins P. A deep sequencing approach to uncover the miRNOME in the human heart. *PLoS One*. 2013;8(2):e57800.
194. McKinsey TA, Olson EN. Toward transcriptional therapies for the failing heart: chemical screens to modulate genes. *J Clin Invest*. 2005;115(3):538–546.
195. Carè A, Catalucci D, Felicetti F, et al. MicroRNA-133 controls cardiac hypertrophy. *Nat Med*. 2007;13(5):613–618.
196. Danowski N, Manthey I, Jakob HG, Siffert W, Peters J, Frey UH. Decreased expression of miR-133a but not of miR-1 is associated with signs of heart failure in patients undergoing coronary bypass surgery. *Cardiology*. 2013;125(2):125–130.
197. Castaldi A, Zaglia T, Di Mauro V, et al. MicroRNA-133 modulates the β1-adrenergic receptor transduction cascade. *Circ Res*. 2014;115(2):273–283.
198. Xu C, Hu Y, Hou L, et al. β-Blocker carvedilol protects cardiomyocytes against oxidative stress-induced apoptosis by up-regulating miR-133 expression. *J Mol Cell Cardiol*. 2014;75:111–121.
199. Trajkovski M, Ahmed K, Esau CC, Stoffel M. MyomiR-133 regulates brown fat differentiation through Prdm16. *Nat Cell Biol*. 2012;14(12):1330–1335.
200. Elia L, Contu R, Quintavalle M, Varrone F, Chimenti C, Russo MA, Cimino V, De Marinis L, Frustaci A, Catalucci D, Condorelli G. Reciprocal regulation of microrna-1 and insulin-like growth factor-1 signal transduction cascade in cardiac and skeletal muscle in physiological and pathological conditions. *Circulation*. 2009;120(23):2377–2385.
201. Yang B, Lin H, Xiao J, Lu Y, Luo X, Li B, Zhang Y, Xu C, Bai Y, Wang H, Chen G, Wang Z. The muscle-specific microRNA miR-1 regulates cardiac arrhythmogenic potential by targeting GJA1 and KCNJ2. *Nat Med*. 2007;13(4):486–491.
202. Zhao Y, Ransom JF, Li A, Vedantham V, von Drehle M, Muth AN, Tsuchihashi T, McManus MT, Schwartz RJ, Srivastava D. Dysregulation of Cardiogenesis, Cardiac Conduction, and Cell Cycle in Mice Lacking miRNA-1-2. *Cell*. 2007;129:303–317.
203. Karakikes I, Chaanine AH, Kang S, Mukete BN, Jeong D, Zhang S, Hajjar RJ, Lebeche D. Therapeutic cardiac-targeted delivery of miR-1 reverses pressure overload-induced cardiac hypertrophy and attenuates pathological remodeling. *J Am Heart Assoc*. 2013;2(2):17–19.
204. Krenz M, Robbins J. Impact of beta-myosin heavy chain expression on cardiac function during stress. *J Am Coll Cardiol*. 2004;44(12):2390–2397.

205. van Rooij E, Sutherland LB, Qi X, Richardson JA, Hill J, Olson EN, van Rooij E. Control of stress-dependent cardiac growth and gene expression by a microRNA. *Science*. 2007;316(5824):575–579.
206. Montgomery RL, Hullinger TG, Semus HM, Dickinson BA, Seto AG, Lynch JM, Stack C, Latimer PA, Olson EN, van Rooij E. Therapeutic inhibition of miR-208a improves cardiac function and survival during heart failure. *Circulation*. 2011;124(14):1537–1547.
207. Kakimoto Y, Tanaka M, Kamiguchi H, Hayashi H, Ochiai E, Osawa M. MicroRNA deep sequencing reveals chamber-specific miR-208 family expression patterns in the human heart. *Int J Cardiol*. 2016;211:43–48.
208. Dirkx E, Gladka MM, Philippen LE, et al. Nfat and miR-25 cooperate to reactivate the transcription factor Hand2 in heart failure. *Nat Cell Biol*. 2013;15(11):1282–1293.
209. Wahlquist C, Jeong D, Rojas-Muñoz A, Kho C, Lee A, Mitsuyama S, van Mil A, Park WJ, Sluijter JPG, Doevendans P a F, Hajjar RJ, Mercola M. Inhibition of miR-25 improves cardiac contractility in the failing heart. *Nature*. 2014;508(7497):531–535.
210. Bush EW, van Rooij E. miR-25 in heart failure. *Circ Res*. 2014;115(7):610–612.
211. Mitchell PS, Parkin RK, Kroh EM, et al. Circulating microRNAs as stable blood-based markers for cancer detection. *Proc Natl Acad Sci U S A*. 2008;105(30):10513–10518.
212. Arroyo JD, Chevillet JR, Kroh EM, Ruf IK, Pritchard CC, Gibson DF, Mitchell PS, Bennett CF, Pogosova-Agadjanyan EL, Stirewalt DL, Tait JF, Tewari M. Argonaute2 complexes carry a population of circulating microRNAs independent of vesicles in human plasma. *Proc Natl Acad Sci U S A*. 2011;108(12):5003–5008.
213. Vickers KC, Palmisano BT, Shoucri BM, Shamburek RD, Remaley AT. MicroRNAs are transported in plasma and delivered to recipient cells by high-density lipoproteins. *Nat Cell Biol*. 2011;13(4):423–433.
214. Turchinovich A, Weiz L, Langheinz A, Burwinkel B. Characterization of extracellular circulating microRNA. *Nucleic Acids Res*. 2011;39(16):7223–7233.
215. Mcmanus DD, Freedman JE. MicroRNAs in platelet function and cardiovascular disease. *Nat Rev Cardiol*. 2015;12(12):1–7.
216. Creemers EE, Tijsen AJ, Pinto YM. Circulating MicroRNAs: Novel biomarkers and extracellular communicators in cardiovascular disease? *Circ Res*. 2012;110(3):483–495.
217. Kaudewitz D, Skroblin P, Bender LH, et al. Association of microRNAs and yRNAs with platelet function. *Circ Res*. 2016;118(3):420–432.
218. Mayr M, Zampetaki A, Willeit P, Willeit J, Kiechl S. MicroRNAs within the continuum of postgenomics biomarker discovery. *Arterioscler Thromb Vasc Biol*. 2013;33(2):206–214.
219. Willeit P, Zampetaki A, Dudek K, et al. Circulating microRNAs as novel biomarkers for platelet activation. *Circ Res*. 2013;112(4):595–600.
220. Denis MM, Tolley ND, Bunting M, et al. Escaping the nuclear confines: signal-dependent pre-mRNA splicing in anucleate platelets. *Cell*. 2005;122(3):379–391.
221. Booyse FM, Hoveke TP, Rafelson ME. Studies on human platelets. II. Protein synthetic activity of various platelet populations. *Biochim Biophys Acta*. 1968;157(3):660–663.
222. Warshaw AL, Laster L, Shulman NR. Protein synthesis by human

platelets. *J Biol Chem*. 1967;242(9):2094–2097.
223. Landry P, Plante I, Ouellet DL, Perron MP, Rousseau G, Provost P. Existence of a microRNA pathway in anucleate platelets. *Nat Struct Mol Biol*. 2009;16(9):961–966.
224. Plé H, Landry P, Benham A, Coarfa C, Gunaratne PH, Provost P. The repertoire and features of human platelet microRNAs. *PLoS One*. 2012;7(12):e50746.
225. Bray PF, McKenzie SE, Edelstein LC, Nagalla S, Delgrosso K, Ertel A, Kupper J, Jing Y, Londin E, Loher P, Chen H-W, Fortina P, Rigoutsos I. The complex transcriptional landscape of the anucleate human platelet. *BMC Genomics*. 2013;14(1):1.
226. Stratz C, Nührenberg TG, Binder H, Valina CM, Trenk D, Hochholzer W, Neumann FJ, Fiebich BL. Micro-array profiling exhibits remarkable intra-individual stability of human platelet micro-RNA. *Thromb Haemost*. 2012;107(4):634–641.
227. Gidlöf O, van der Brug M, Ohman J, Gilje P, Olde B, Wahlestedt C, Erlinge D. Platelets activated during myocardial infarction release functional miRNA, which can be taken up by endothelial cells and regulate ICAM1 expression. *Blood*. 2013;121(19):3908–17, S1-26.
228. Elgheznawy A, Shi L, Hu J, Wittig I, Laban H, Pircher J, Mann A, Provost P, Randriamboavonjy V, Fleming I. Dicer cleavage by calpain determines platelet microRNA levels and function in diabetes. *Circ Res*. 2015;117(2):157–165.
229. Opalinska JB, Bersenev A, Zhang Z, Schmaier AA, Choi J, Yao Y, D'Souza J, Tong W, Weiss MJ. MicroRNA expression in maturing murine megakaryocytes. *Blood*. 2010;116(23):e128-138.
230. Risitano A, Beaulieu LM, Vitseva O, Freedman JE. Platelets and platelet-like particles mediate intercellular RNA transfer. *Blood*. 2012;119(26):6288–6295.
231. Clancy L, Beaulieu LM, Tanriverdi K, Freedman JE. The role of RNA uptake in platelet heterogeneity. *Thromb Haemost*. 2017;117(5):948–961.
232. Zampetaki A, Kiechl S, Drozdov I, Willeit P, Mayr U, Prokopi M, Mayr A, Weger S, Oberhollenzer F, Bonora E, Shah A, Willeit J, Mayr M. Plasma microRNA profiling reveals loss of endothelial miR-126 and other microRNAs in type 2 diabetes. *Circ Res*. 2010;107(6):810–817.
233. Zampetaki A, Willeit P, Tilling L, et al. Prospective study on circulating MicroRNAs and risk of myocardial infarction. *J Am Coll Cardiol*. 2012;60(4):290–299.
234. Schulte C, Molz S, Appelbaum S, Karakas M, Ojeda F, Lau DM, Hartmann T, Lackner KJ, Westermann D, Schnabel RB, Blankenberg S, Zeller T. miRNA-197 and miRNA-223 Predict Cardiovascular Death in a Cohort of Patients with Symptomatic Coronary Artery Disease. *PLoS One*. 2015;10(12):e0145930.
235. Yu X-Y, Chen J-Y, Zheng Z-W, Wu H, Li L-W, Zhang Z-W, Chen Z-H, Lin Q-X, Han Y-L, Zhong S-L. Plasma miR-126 as a potential marker predicting major adverse cardiac events in dual antiplatelet-treated patients after percutaneous coronary intervention. *EuroIntervention*. 2013;9(5):546–554.
236. Kondkar AA, Bray MS, Leal SM, Nagalla S, Liu DJ, Jin Y, Dong JF, Ren Q, Whiteheart SW, Shaw C, Bray PF. VAMP8/endobrevin is overexpressed in hyperreactive human platelets: suggested role for

platelet microRNA. *J Thromb Haemost*. 2010;8(2):369–378.
237. Edelstein LC, Simon LM, Montoya RT, Holinstat M, Chen ES, Bergeron A, Kong X, Nagalla S, Mohandas N, Cohen DE, Dong J, Shaw C, Bray PF. Racial differences in human platelet PAR4 reactivity reflect expression of PCTP and miR-376c. *Nat Med*. 2013;19(12):1609–1616.
238. Leierseder S, Petzold T, Zhang L, Loyer X, Massberg S, Engelhardt S. MiR-223 is dispensable for platelet production and function in mice. *Thromb Haemost*. 2013;110(6):1207–1214.
239. AJ A, Colburn WA, DeGruttola VG, DeMets DL, Downing GJ, Hoth DF, Oates JA, Peck CC, Schooley RT, Spilker BA, Woodcock J, Zeger SL. Biomarkers and surrogate endpoints: Preferred definitions and conceptual framework. *Clin Pharmacol Ther*. 2001;69(3):89–95.
240. Wang G-K, Zhu J-Q, Zhang J-T, Li Q, Li Y, He J, Qin Y-W, Jing Q. Circulating microRNA: a novel potential biomarker for early diagnosis of acute myocardial infarction in humans. *Eur Heart J*. 2010;31(6):659–666.
241. Widera C, Gupta SK, Lorenzen JM, Bang C, Bauersachs J, Bethmann K, Kempf T, Wollert KC, Thum T. Diagnostic and prognostic impact of six circulating microRNAs in acute coronary syndrome. *J Mol Cell Cardiol*. 2011;51(5):872–875.
242. Karakas M, Schulte C, Appelbaum S, Ojeda F, Lackner KJ, Münzel T, Schnabel RB, Blankenberg S, Zeller T. Circulating microRNAs strongly predict cardiovascular death in patients with coronary artery disease-results from the large AtheroGene study. *Eur Heart J*. 2016:ehw250.
243. Bye A, Røsjø H, Nauman J, Silva GJJ, Follestad T, Omland T, Wisløff U. Circulating microRNAs predict future fatal myocardial infarction in healthy individuals - The HUNT study. *J Mol Cell Cardiol*. 2016;97:162–168.
244. Roncarati R, Viviani Anselmi C, Losi MA, et al. Circulating miR-29a, among other up-regulated microRNAs, is the only biomarker for both hypertrophy and fibrosis in patients with hypertrophic cardiomyopathy. *J Am Coll Cardiol*. 2014;63(9):920–927.
245. Zile MR, Mehurg SM, Arroyo JE, Stroud RE, DeSantis SM, Spinale FG. Relationship between the temporal profile of plasma microRNA and left ventricular remodeling in patients after myocardial infarction. *Circ Cardiovasc Genet*. 2011;4(6):614–619.
246. Stammet P, Goretti E, Vausort M, Zhang L, Wagner DR, Devaux Y. Circulating microRNAs after cardiac arrest. *Crit Care Med*. 2012;40(12):3209–3214.
247. Darabi F, Aghaei M, Movahedian A, Pourmoghadas A, Sarrafzadegan N. The role of serum levels of microRNA-21 and matrix metalloproteinase-9 in patients with acute coronary syndrome. *Mol Cell Biochem*. 2016;422(1–2):51–60.
248. Zhang Y, Liu Y-J, Liu T, Zhang H, Yang S-J. Plasma microRNA-21 is a potential diagnostic biomarker of acute myocardial infarction. *Eur Rev Med Pharmacol Sci*. 2016;20(2):323–329.
249. Liebetrau C, Möllmann H, Dörr O, Szardien S, Troidl C, Willmer M, Voss S, Gaede L, Rixe J, Rolf A, Hamm C, Nef H. Release kinetics of circulating muscle-enriched microRNAs in patients undergoing transcoronary ablation of septal hypertrophy. *J Am Coll Cardiol*. 2013;62(11):992–998.
250. Liu X, Dong Y, Chen S, Zhang G, Zhang M, Gong Y, Li X. Circulating

MicroRNA-146a and MicroRNA-21 Predict Left Ventricular Remodeling after ST-Elevation Myocardial Infarction. *Cardiology*. 2015;132(4):233–241.
251. Fang L, Ellims AH, Moore X, White DA, Taylor AJ, Chin-Dusting J, Dart AM. Circulating microRNAs as biomarkers for diffuse myocardial fibrosis in patients with hypertrophic cardiomyopathy. *J Transl Med*. 2015;13:314.
252. van Rooij E, Olson EN. MicroRNA therapeutics for cardiovascular disease: opportunities and obstacles. *Nat Rev Drug Discov*. 2012;11(11):860–872.
253. Sen CK, Roy S. MicroRNA 21 in tissue injury and inflammation. *Cardiovasc Res*. 2012;96(2):230–233.
254. Flierl U, Nero TL, Lim B, et al. Phosphorothioate backbone modifications of nucleotide-based drugs are potent platelet activators. *J Exp Med*. 2015;212(2):129–137.
255. Ganesan J, Ramanujam D, Sassi Y, Ahles A, Jentzsch C, Werfel S, Leierseder S, Loyer X, Giacca M, Zentilin L, Thum T, Laggerbauer B, Engelhardt S. MiR-378 controls cardiac hypertrophy by combined repression of mitogen-activated protein kinase pathway factors. *Circulation*. 2013;127(21):2097–2106.
256. Borel F, Kay MA, Mueller C. Recombinant AAV as a platform for translating the therapeutic potential of RNA interference. *Mol Ther*. 2014;22(4):692–701.
257. Rupaimoole R, Slack FJ. MicroRNA therapeutics: Towards a new era for the management of cancer and other diseases. *Nat Rev Drug Discov*. 2017;16(3):203–221.
258. Lucas T, Schäfer F, Müller P, Eming SA, Heckel A, Dimmeler S. Light-inducible antimiR-92a as a therapeutic strategy to promote skin repair in healing-impaired diabetic mice. *Nat Commun*. 2017;8(May):15162.
259. Janssen HL a, Reesink HW, Lawitz EJ, et al. Treatment of HCV infection by targeting microRNA. *N Engl J Med*. 2013;368(18):1685–1694.
260. Dalpke A, Helm M. RNA mediated Toll-like receptor stimulation in health and disease. *RNA Biol*. 2012;9(6):828–842.
261. Gomez IG, MacKenna DA, Johnson BG, et al. Anti-microRNA-21 oligonucleotides prevent Alport nephropathy progression by stimulating metabolic pathways. *J Clin Invest*. 2015;125(1):141–156.
262. Gross O, Kashtan CE, Rheault MN, et al. Advances and unmet needs in genetic, basic and clinical science in Alport syndrome: report from the 2015 International Workshop on Alport Syndrome. *Nephrol Dial Transplant*. 2017;32(6):916–924.
263. Gross O, Licht C, Anders HJ, et al. Early angiotensin-converting enzyme inhibition in Alport syndrome delays renal failure and improves life expectancy. *Kidney Int*. 2012;81(5):494–501.
264. Gross O, Schulze-Lohoff E, Koepke M-L, Beirowski B, Addicks K, Bloch W, Smyth N, Weber M. Antifibrotic, nephroprotective potential of ACE inhibitor vs AT1 antagonist in a murine model of renal fibrosis. *Nephrol Dial Transplant*. 2004;19(7):1716–1723.
265. Keller A, Nesvizhskii AI, Kolker E, Aebersold R. Empirical statistical model to estimate the accuracy of peptide identifications made by MS/MS and database search. *Anal Chem*. 2002;74(20):5383–5392.
266. Nesvizhskii AI, Keller A, Kolker E, Aebersold R. A statistical model for

identifying proteins by tandem mass spectrometry. *Anal Chem*. 2003;75(17):4646–4658.
267. Livak KJ, Schmittgen TD. Analysis of relative gene expression data using real-time quantitative PCR and. *Methods*. 2001;25:402–408.
268. Xie F, Xiao P, Chen D, Xu L, Zhang B. miRDeepFinder: a miRNA analysis tool for deep sequencing of plant small RNAs. *Plant Mol Biol*. 2012;80(1):75–84.
269. Naba A, Clauser KR, Ding H, Whittaker CA, Carr SA, Hynes RO. The extracellular matrix: tools and insights for the “omics” era. *Matrix Biol*. 2016;49:10–24.
270. Kiechl S, Lorenz E, Reindl M, Wiedermann CJ, Oberhollenzer F, Bonora E, Willeit J, Schwartz DA. Toll-like receptor 4 polymorphisms and atherogenesis. *N Engl J Med*. 2002;347(3):185–192.
271. Kong F-MS, Zhao L, Wang L, Chen Y, Hu J, Fu X, Bai C, Wang L, Lawrence TS, Anscher MS, Dicker A, Okunieff P. Ensuring sample quality for blood biomarker studies in clinical trials: a multicenter international study for plasma and serum sample preparation. *Transl lung cancer Res*. 2017;6(6):625–634.
272. Tammen H, Schulte I, Hess R, Menzel C, Kellmann M, Mohring T, Schulz-Knappe P. Peptidomic analysis of human blood specimens: comparison between plasma specimens and serum by differential peptide display. *Proteomics*. 2005;5(13):3414–3422.
273. Brouwers J, Noviyanti R, Fijnheer R, de Groot PG, Trianty L, Mudaliana S, Roest M, Syafruddin D, van der Ven A, de Mast Q. Platelet activation determines angiopoietin-1 and VEGF levels in malaria: implications for their use as biomarkers. *PLoS One*. 2014;8(6):e64850.
274. Cheng HH, Yi HS, Kim Y, Kroh EM, Chien JW, Eaton KD, Goodman MT, Tait JF, Tewari M, Pritchard CC. Plasma processing conditions substantially influence circulating microRNA biomarker levels. *PLoS One*. 2013;8(6):e64795.
275. Mitchell AJ, Gray WD, Hayek SS, Ko Y-A, Thomas S, Rooney K, Awad M, Roback JD, Quyyumi A, Searles CD. Platelets confound the measurement of extracellular miRNA in archived plasma. *Sci Rep*. 2016;6:32651.
276. Wakefield LM, Letterio JJ, Chen T, Danielpour D, Allison RS, Pai LH, Denicoff AM, Noone MH, Cowan KH, O’Shaughnessy JA. Transforming growth factor-beta1 circulates in normal human plasma and is unchanged in advanced metastatic breast cancer. *Clin Cancer Res*. 1995;1(1):129–136.
277. Coupes BM, Williams S, Roberts IS, Short CD, Brenchley PE. Plasma transforming growth factor beta(1) and platelet activation: implications for studies in transplant recipients. *Nephrol Dial Transplant*. 2001;16(2):361–367.
278. Adcock Funk DM, Lippi G, Favaloro EJ. Quality standards for sample processing, transportation, and storage in hemostasis testing. *Semin Thromb Hemost*. 2012;38(6):576–85.
279. Pengo V, Tripodi A, Reber G, Rand JH, Ortel TL, Galli M, De Groot PG, Subcommittee on Lupus Anticoagulant/Antiphospholipid Antibody of the Scientific and Standardisation Committee of the International Society on Thrombosis and Haemostasis. Update of the guidelines for lupus anticoagulant detection. Subcommittee on Lupus

Anticoagulant/Antiphospholipid Antibody of the Scientific and Standardisation Committee of the International Society on Thrombosis and Haemostasis. *J Thromb Haemost*. 2009;7(10):1737–40.
280. Willeit P, Skroblin P, Moschen AR, et al. Circulating MicroRNA-122 Is Associated With the Risk of New-Onset Metabolic Syndrome and Type 2 Diabetes. *Diabetes*. 2017;66(2):347–357.
281. Zampetaki A, Attia R, Mayr U, et al. Role of miR-195 in aortic aneurysmal disease. *Circ Res*. 2014;115(10):857–866.
282. Maynard DM, Heijnen HFG, Horne MK, White JG, Gahl WA. Proteomic analysis of platelet alpha-granules using mass spectrometry. *J Thromb Haemost*. 2007;5(9):1945–1955.
283. Burkhart JM, Vaudel M, Gambaryan S, Radau S, Walter U, Martens L, Geiger J, Sickmann A, Zahedi RP. The first comprehensive and quantitative analysis of human platelet protein composition allows the comparative analysis of structural and functional pathways. *Blood*. 2012;120(15):e73-82.
284. Dweep H, Gretz N. miRWalk2.0: a comprehensive atlas of microRNA-target interactions. *Nat Methods*. 2015;12(8):697.
285. Huntley RP, Sitnikov D, Orlic-Milacic M, et al. Guidelines for the functional annotation of microRNAs using the Gene Ontology. *RNA*. 2016;22(5):667–76.
286. Rehmsmeier M, Steffen P, Hochsmann M, Giegerich R. Fast and effective prediction of microRNA/target duplexes. *RNA*. 2004;10(10):1507–1517.
287. Choi H, Kim S, Fermin D, Tsou C-C, Nesvizhskii AI. QPROT: Statistical method for testing differential expression using protein-level intensity data in label-free quantitative proteomics. *J Proteomics*. 2015;129:121–126.
288. Oka T, Xu J, Kaiser RA, Melendez J, Hambleton M, Sargent MA, Lorts A, Brunskill EW, Dorn GW, Conway SJ, Aronow BJ, Robbins J, Molkentin JD. Genetic manipulation of periostin expression reveals a role in cardiac hypertrophy and ventricular remodeling. *Circ Res*. 2007;101(3):313–321.
289. Kanisicak O, Khalil H, Ivey MJ, Karch J, Maliken BD, Correll RN, Brody MJ, J Lin S-C, Aronow BJ, Tallquist MD, Molkentin JD. Genetic lineage tracing defines myofibroblast origin and function in the injured heart. *Nat Commun*. 2016;7:12260.
290. Gonzalez C, Auw Yang KG, Schwab JH, Fitzsimmons JS, Reinholz MM, Resch ZT, Bale LK, Clemens VR, Conover CA, O'Driscoll SW, Reinholz GG. Transforming growth factor-beta1 modulates insulin-like growth factor binding protein-4 expression and proteolysis in cultured periosteal explants. *Growth Horm IGF Res*. 2010;20(2):81–86.
291. Cosme J, Guo H, Hadipour-Lakmehsari S, Emili A, Gramolini AO. Hypoxia-Induced Changes in the Fibroblast Secretome, Exosome, and Whole-Cell Proteome Using Cultured, Cardiac-Derived Cells Isolated from Neonatal Mice. *J Proteome Res*. 2017;16(8):2836–2847.
292. Kähäri VM, Larjava H, Uitto J. Differential regulation of extracellular matrix proteoglycan (PG) gene expression. *J Biol Chem*. 1991;266(16):10608–10615.
293. Barallobre-Barreiro J, Gupta SK, Zoccarato A, et al. Glycoproteomics reveals decorin peptides with anti-myostatin activity in human atrial fibrillation. *Circulation*. 2016;134(11):817–832.

294. Drozdov I, Didangelos A, Yin X, Zampetaki A, Abonnenc M, Murdoch C, Zhang M, Ouzounis CA, Mayr M, Tsoka S, Shah AM. Gene network and proteomic analyses of cardiac responses to pathological and physiological stress. *Circ Cardiovasc Genet*. 2013;6(6):588–597.
295. Herro R, Da Silva Antunes R, Aguilera AR, Tamada K, Croft M. Tumor necrosis factor superfamily 14 (LIGHT) controls thymic stromal lymphopoietin to drive pulmonary fibrosis. *J Allergy Clin Immunol*. 2015;136(3):757–768.
296. Zhang D, Contu R, Latronico MVG, et al. MTORC1 regulates cardiac function and myocyte survival through 4E-BP1 inhibition in mice. *J Clin Invest*. 2010;120(8):2805–2816.
297. Johnson KJ, Sage H, Briscoe G, Erickson HP. The compact conformation of fibronectin is determined by intramolecular ionic interactions. *J Biol Chem*. 1999;274(22):15473–15479.
298. Mosesson MW. Fibrinogen and fibrin structure and functions. *J Thromb Haemost*. 2005;3(8):1894–1904.
299. Asselta R, Duga S, Tenchini ML. The molecular basis of quantitative fibrinogen disorders. *J Thromb Haemost*. 2006;4(10):2115–2129.
300. Xiang B, Zhang G, Guo L, Li X-A, Morris AJ, Daugherty A, Whiteheart SW, Smyth SS, Li Z. Platelets protect from septic shock by inhibiting macrophage-dependent inflammation via the cyclooxygenase 1 signalling pathway. *Nat Commun*. 2013;4:2657.
301. Armstrong PCJ, Kirkby NS, Chan M, Finsterbusch M, Hogg N, Nourshargh S, Warner TD. Novel whole blood assay for phenotyping platelet reactivity in mice identifies ICAM-1 as a mediator of platelet-monocyte interaction. *Blood*. 2015;126(10):e11–e18.
302. Kraus T. Megakaryocyte (ID # 00060032). *Am Soc Hematol Image Bank*. 2015.
303. Kahounová Z, Kurfürstová D, Bouchal J, Kharaishvili G, Navrátil J, Remšík J, Šimečková Š, Študent V, Kozubík A, Souček K. The fibroblast surface markers FAP, anti-fibroblast, and FSP are expressed by cells of epithelial origin and may be altered during epithelial-to-mesenchymal transition. *Cytometry A*. 2017.
304. Cook-Mills JM, Marchese ME, Abdala-Valencia H. Vascular cell adhesion molecule-1 expression and signaling during disease: regulation by reactive oxygen species and antioxidants. *Antioxid Redox Signal*. 2011;15(6):1607–1638.
305. Cybulsky MI, Iiyama K, Li H, Zhu S, Chen M, Iiyama M, Davis V, Gutierrez-Ramos JC, Connelly PW, Milstone DS. A major role for VCAM-1, but not ICAM-1, in early atherosclerosis. *J Clin Invest*. 2001;107(10):1255–1262.
306. Yu Y, Schürpf T, Springer TA. How natalizumab binds and antagonizes α4 integrins. *J Biol Chem*. 2013;288(45):32314–32325.
307. Li H, Cybulsky MI, Gimbrone MA, Libby P. Inducible expression of vascular cell adhesion molecule-1 by vascular smooth muscle cells in vitro and within rabbit atheroma. *Am J Pathol*. 1993;143(6):1551–1559.
308. Chen K, Chen J, Liu Y, Xie J, Li D, Sawamura T, Hermonat PL, Mehta JL. Adhesion molecule expression in fibroblasts: alteration in fibroblast biology after transfection with LOX-1 plasmids. *Hypertens (Dallas, Tex 1979)*. 2005;46(3):622–627.
309. Agassandian M, Tedrow JR, Sembrat J, Kass DJ, Zhang Y, Goncharova EA, Kaminski N, Mallampalli RK, Vuga LJ. VCAM-1 is a

TGF-β1 inducible gene upregulated in idiopathic pulmonary fibrosis. *Cell Signal*. 2015;27(12):2467–2473.
310. Jin C, Zhao Y, Yu L, Xu S, Fu G. MicroRNA-21 mediates the rapamycin-induced suppression of endothelial proliferation and migration. *FEBS Lett*. 2013;587(4):378–385.
311. Di Bernardini E, Campagnolo P, Margariti A, Zampetaki A, Karamariti E, Hu Y, Xu Q. Endothelial Lineage differentiation from induced Pluripotent Stem Cells is regulated by MicroRNA-21 and transforming growth Factor β2 (TGF-β2) Pathways. *J Biol Chem*. 2014;289(6):3383–3393.
312. Sabatel C, Malvaux L, Bovy N, Deroanne C, Lambert V, Gonzalez M-LA, Colige A, Rakic J-M, Noël A, Martial JA, Struman I. MicroRNA-21 exhibits antiangiogenic function by targeting RhoB expression in endothelial cells. *PLoS One*. 2011;6(2):e16979.
313. Zhou J, Wang K-C, Wu W, Subramaniam S, Shyy JY-J, Chiu J-J, Li JY-S, Chien S. MicroRNA-21 targets peroxisome proliferators-activated receptor-alpha in an autoregulatory loop to modulate flow-induced endothelial inflammation. *Proc Natl Acad Sci U S A*. 2011;108(25):10355–10360.
314. Koths K, Taylor E, Halenbeck R, Casipit C, Wang A. Cloning and characterization of a human Mac-2-binding protein, a new member of the superfamily defined by the macrophage scavenger receptor cysteine-rich domain. *J Biol Chem*. 1993;268(19):14245–14249.
315. Sasaki T, Brakebusch C, Engel J, Timpl R. Mac-2 binding protein is a cell-adhesive protein of the extracellular matrix which self-assembles into ring-like structures and binds beta1 integrins, collagens and fibronectin. *EMBO J*. 1998;17(6):1606–1613.
316. DeRoo EP, Wrobleski SK, Shea EM, Al-Khalil RK, Hawley AE, Henke PK, Myers DD, Wakefield TW, Diaz JA. The role of galectin-3 and galectin-3-binding protein in venous thrombosis. *Blood*. 2015;125(11):1813–1821.
317. Langley SR, Willeit K, Didangelos A, et al. Extracellular matrix proteomics identifies molecular signature of symptomatic carotid plaques. *J Clin Invest*. 2017;127(4):1546–1560.
318. White MJ V, Roife D, Gomer RH. Galectin-3 Binding Protein Secreted by Breast Cancer Cells Inhibits Monocyte-Derived Fibrocyte Differentiation. *J Immunol*. 2015;195(4):1858–1867.
319. Meijers WC, van der Velde AR, Pascual-Figal DA, de Boer RA. Galectin-3 and post-myocardial infarction cardiac remodeling. *Eur J Pharmacol*. 2015;763(Pt A):115–121.
320. Pineda MA, Cuervo H, Fresno M, Soto M, Bonay P. Lack of Galectin-3 Prevents Cardiac Fibrosis and Effective Immune Responses in a Murine Model of Trypanosoma cruzi Infection. *J Infect Dis*. 2015;212(7):1160–1171.
321. Conover CA, Kiefer MC, Zapf J. Posttranslational regulation of insulin-like growth factor binding protein-4 in normal and transformed human fibroblasts. *J Clin Invest*. 1993;91(3):1129–1137.
322. Price WA. Regulation of insulin-like growth factor (IGF)-binding protein expression by growth factors and cytokines alters IGF-mediated proliferation of postnatal lung fibroblasts. *Exp Lung Res*. 2004;30(4):261–283.
323. Lawrence JB, Oxvig C, Overgaard MT, Sottrup-Jensen L, Gleich GJ,

Hays LG, Yates JR, Conover CA. The insulin-like growth factor (IGF)-dependent IGF binding protein-4 protease secreted by human fibroblasts is pregnancy-associated plasma protein-A. *Proc Natl Acad Sci U S A*. 1999;96(6):3149–3153.
324. Zazzi H, Nikoshkov A, Hall K, Luthman H. Structure and transcription regulation of the human insulin-like growth factor binding protein 4 gene (IGFBP4). *Genomics*. 1998;49(3):401–410.
325. Mohan S, Baylink DJ. IGF-binding proteins are multifunctional and act via IGF-dependent and -independent mechanisms. *J Endocrinol*. 2002;175(1):19–31.
326. Miyakoshi N, Richman C, Qin X, Baylink DJ, Mohan S. Effects of recombinant insulin-like growth factor-binding protein-4 on bone formation parameters in mice. *Endocrinology*. 1999;140(12):5719–5728.
327. Wang J, Niu W, Witte DP, Chernausek SD, Nikiforov YE, Clemens TL, Sharifi B, Strauch AR, Fagin JA. Overexpression of insulin-like growth factor-binding protein-4 (IGFBP-4) in smooth muscle cells of transgenic mice through a smooth muscle alpha-actin-IGFBP-4 fusion gene induces smooth muscle hypoplasia. *Endocrinology*. 1998;139(5):2605–2614.
328. Contois LW, Nugent DP, Caron JM, Cretu A, Tweedie E, Akalu A, Liebes L, Friesel R, Rosen C, Vary C, Brooks PC. Insulin-like growth factor binding protein-4 differentially inhibits growth factor-induced angiogenesis. *J Biol Chem*. 2012;287(3):1779–1789.
329. Gealekman O, Gurav K, Chouinard M, Straubhaar J, Thompson M, Malkani S, Hartigan C, Corvera S. Control of adipose tissue expandability in response to high fat diet by the insulin-like growth factor-binding protein-4. *J Biol Chem*. 2014;289(26):18327–18338.
330. Zhu W, Shiojima I, Ito Y, et al. IGFBP-4 is an inhibitor of canonical Wnt signalling required for cardiogenesis. *Nature*. 2008;454(7202):345–349.
331. Xue Y, Yan Y, Gong H, Fang B, Zhou Y, Ding Z, Yin P, Zhang G, Ye Y, Yang C, Ge J, Zou Y. Insulin-like growth factor binding protein 4 enhances cardiomyocytes induction in murine-induced pluripotent stem cells. *J Cell Biochem*. 2014;115(9):1495–1504.
332. Miyakoshi N, Qin X, Kasukawa Y, Richman C, Srivastava AK, Baylink DJ, Mohan S. Systemic administration of insulin-like growth factor (IGF)-binding protein-4 (IGFBP-4) increases bone formation parameters in mice by increasing IGF bioavailability via an IGFBP-4 protease-dependent mechanism. *Endocrinology*. 2001;142(6):2641–2648.
333. Cruts M, Gijselinck I, van der Zee J, et al. Null mutations in progranulin cause ubiquitin-positive frontotemporal dementia linked to chromosome 17q21. *Nature*. 2006;442(7105):920–924.
334. De Muynck L, Van Damme P. Cellular effects of progranulin in health and disease. *J Mol Neurosci*. 2011;45(3):549–560.
335. He Z, Ong CHP, Halper J, Bateman A. Progranulin is a mediator of the wound response. *Nat Med*. 2003;9(2):225–229.
336. Zhu J, Nathan C, Jin W, Sim D, Ashcroft GS, Wahl SM, Lacomis L, Erdjument-Bromage H, Tempst P, Wright CD, Ding A. Conversion of proepithelin to epithelins: roles of SLPI and elastase in host defense and wound repair. *Cell*. 2002;111(6):867–878.

337. Daniel R, He Z, Carmichael KP, Halper J, Bateman A. Cellular localization of gene expression for progranulin. *J Histochem Cytochem*. 2000;48(7):999–1009.
338. Kessenbrock K, Fröhlich L, Sixt M, Lämmermann T, Pfister H, Bateman A, Belaaouaj A, Ring J, Ollert M, Fässler R, Jenne DE. Proteinase 3 and neutrophil elastase enhance inflammation in mice by inactivating antiinflammatory progranulin. *J Clin Invest*. 2008;118(7):2438–2447.
339. Bashey RI, Martinez-Hernandez A, Jimenez SA. Isolation, characterization, and localization of cardiac collagen type VI. Associations with other extracellular matrix components. *Circ Res*. 1992;70(5):1006–1017.
340. Behrens DT, Villone D, Koch M, Brunner G, Sorokin L, Robenek H, Bruckner-Tuderman L, Bruckner P, Hansen U. The epidermal basement membrane is a composite of separate laminin- or collagen IV-containing networks connected by aggregated perlecan, but not by nidogens. *J Biol Chem*. 2012;287(22):18700–18709.
341. Wang L, Zhou L, Jiang P, Lu L, Chen X, Lan H, Guttridge DC, Sun H, Wang H. Loss of miR-29 in myoblasts contributes to dystrophic muscle pathogenesis. *Mol Ther*. 2012;20(6):1222–1233.
342. Schrickel JW, Brixius K, Herr C, et al. Enhanced heterogeneity of myocardial conduction and severe cardiac electrical instability in annexin A7-deficient mice. *Cardiovasc Res*. 2007;76(2):257–268.
343. Naugle JE, Olson ER, Zhang X, Mase SE, Pilati CF, Maron MB, Folkesson HG, Horne WI, Doane KJ, Meszaros JG. Type VI collagen induces cardiac myofibroblast differentiation: implications for postinfarction remodeling. *Am J Physiol Heart Circ Physiol*. 2006;290(1):H323-330.
344. Yu RZ, Grundy JS, Geary RS. Clinical pharmacokinetics of second generation antisense oligonucleotides. *Expert Opin Drug Metab Toxicol*. 2013;9(2):169–182.
345. Fleissner F, Jazbutyte V, Fiedler J, Gupta SK, Yin X, Xu Q, Galuppo P, Kneitz S, Mayr M, Ertl G, Bauersachs J, Thum T. Short communication: asymmetric dimethylarginine impairs angiogenic progenitor cell function in patients with coronary artery disease through a microRNA-21-dependent mechanism. *Circ Res*. 2010;107(1):138–143.
346. Gryshkova V, Fleming A, McGhan P, De Ron P, Fleurance R, Valentin J-P, Nogueira da Costa A. miR-21-5p as a potential biomarker of inflammatory infiltration in the heart upon acute drug-induced cardiac injury in rats. *Toxicol Lett*. 2018;286:31–38.
347. Dees C, Akhmetshina A, Zerr P, et al. Platelet-derived serotonin links vascular disease and tissue fibrosis. *J Exp Med*. 2011;208(5):961–972.
348. Liu Y, Gao X-M, Fang L, et al. Novel role of platelets in mediating inflammatory responses and ventricular rupture or remodeling following myocardial infarction. *Arterioscler Thromb Vasc Biol*. 2011;31(4):834–841.
349. Yang F, Dong A, Mueller P, Caicedo J, Sutton AM, Odetunde J, Barrick CJ, Klyachkin YM, Abdel-Latif A, Smyth SS. Coronary artery remodeling in a model of left ventricular pressure overload is influenced by platelets and inflammatory cells. *PLoS One*. 2012;7(8):e40196.
350. Verheugt FW, Lindenfeld J, Kirch DL, Steele PP. Left ventricular platelet deposition after acute myocardial infarction. An attempt at quantification using blood pool subtracted indium-111 platelet

scintigraphy. *Br Heart J*. 1984;52(5):490–496.
351. Chauhan A, Adams DH, Watson SP, Lalor PF. Platelets: No longer bystanders in liver disease. *Hepatology*. 2016;64(5):1774–1784.
352. Yoshida S, Ikenaga N, Liu SB, Peng Z-W, Chung J, Sverdlov DY, Miyamoto M, Kim YO, Ogawa S, Arch RH, Schuppan D, Popov Y. Extrahepatic platelet-derived growth factor-β, delivered by platelets, promotes activation of hepatic stellate cells and biliary fibrosis in mice. *Gastroenterology*. 2014;147(6):1378–1392.
353. Sheedy FJ. Turning 21: induction of miR-21 as a key switch in the inflammatory response. *Front Immunol*. 2015;6:19.
354. Hashimi ST, Fulcher JA, Chang MH, Gov L, Wang S, Lee B. MicroRNA profiling identifies miR-34a and miR-21 and their target genes JAG1 and WNT1 in the coordinate regulation of dendritic cell differentiation. *Blood*. 2009;114(2):404–414.
355. Kasashima K, Nakamura Y, Kozu T. Altered expression profiles of microRNAs during TPA-induced differentiation of HL-60 cells. *Biochem Biophys Res Commun*. 2004;322(2):403–410.
356. Cekaite L, Clancy T, Sioud M. Increased miR-21 expression during human monocyte differentiation into DCs. *Front Biosci (Elite Ed)*. 2010;2:818–828.
357. Tian T, Zhu Y-L, Zhou Y-Y, Liang G-F, Wang Y-Y, Hu F-H, Xiao Z-D. Exosome uptake through clathrin-mediated endocytosis and macropinocytosis and mediating miR-21 delivery. *J Biol Chem*. 2014;289(32):22258–22267.
358. Das A, Ganesh K, Khanna S, Sen CK, Roy S. Engulfment of apoptotic cells by macrophages: a role of microRNA-21 in the resolution of wound inflammation. *J Immunol*. 2014;192(3):1120–1129.
359. Graff JW, Dickson AM, Clay G, McCaffrey AP, Wilson ME. Identifying functional microRNAs in macrophages with polarized phenotypes. *J Biol Chem*. 2012;287(26):21816–21825.
360. Sheedy FJ, Palsson-McDermott E, Hennessy EJ, Martin C, O'Leary JJ, Ruan Q, Johnson DS, Chen Y, O'Neill L a J. Negative regulation of TLR4 via targeting of the proinflammatory tumor suppressor PDCD4 by the microRNA miR-21. *Nat Immunol*. 2010;11(2):141–147.
361. Yue S, Rao J, Zhu J, Busuttil RW, Kupiec-Weglinski JW, Lu L, Wang X, Zhai Y. Myeloid PTEN deficiency protects livers from ischemia reperfusion injury by facilitating M2 macrophage differentiation. *J Immunol*. 2014;192(11):5343–5353.
362. Martinez FO, Gordon S. The M1 and M2 paradigm of macrophage activation: time for reassessment. *F1000Prime Rep*. 2014;6:13.
363. Lu TX, Hartner J, Lim E-J, Fabry V, Mingler MK, Cole ET, Orkin SH, Aronow BJ, Rothenberg ME. MicroRNA-21 limits in vivo immune response-mediated activation of the IL-12/IFN-gamma pathway, Th1 polarization, and the severity of delayed-type hypersensitivity. *J Immunol*. 2011;187(6):3362–3373.
364. Sawant D V., Wu H, Kaplan MH, Dent AL. The Bcl6 target gene microRNA-21 promotes Th2 differentiation by a T cell intrinsic pathway. *Mol Immunol*. 2013;54(3–4):435–442.
365. Lu TX, Munitz A, Rothenberg ME. MicroRNA-21 is up-regulated in allergic airway inflammation and regulates IL-12p35 expression. *J Immunol*. 2009;182(8):4994–5002.
366. Guinea-Viniegra J, Jiménez M, Schonthaler HB, Navarro R, Delgado Y,

Concha-Garzón MJ, Tschachler E, Obad S, Daudén E, Wagner EF. Targeting miR-21 to treat psoriasis. *Sci Transl Med*. 2014;6(225):225re1.
367. Garchow BG, Bartulos Encinas O, Leung YT, Tsao PY, Eisenberg RA, Caricchio R, Obad S, Petri A, Kauppinen S, Kiriakidou M. Silencing of microRNA-21 in vivo ameliorates autoimmune splenomegaly in lupus mice. *EMBO Mol Med*. 2011;3(10):605–615.
368. Rachidi S, Metelli A, Riesenberg B, Wu BX, Nelson MH, Wallace C, Paulos CM, Rubinstein MP, Garrett-Mayer E, Hennig M, Bearden DW, Yang Y, Liu B, Li Z. Platelets subvert T cell immunity against cancer via GARP-TGFβ axis. *Sci Immunol*. 2017;2(11):eaai7911.
369. Werfel S, Leierseder S, Ruprecht B, Kuster B, Engelhardt S. Preferential microRNA targeting revealed by in vivo competitive binding and differential Argonaute immunoprecipitation. *Nucleic Acids Res*. 2017;45(17):10218–10228.
370. Yin X, Baig F, Haudebourg E, et al. Plasma proteomics for epidemiology: increasing throughput with standard-flow rates. *Circ Cardiovasc Genet*. 2017;10(6):e001808.
371. Assarsson E, Lundberg M, Holmquist G, et al. Homogenous 96-plex PEA immunoassay exhibiting high sensitivity, specificity, and excellent scalability. *PLoS One*. 2014;9(4):e95192.
372. Hsieh SY, Chen RK, Pan YH, Lee HL. Systematical evaluation of the effects of sample collection procedures on low-molecular-weight serum/plasma proteome profiling. *Proteomics*. 2006;6(10):3189–3198.
373. Shen Q, Björkesten J, Galli J, Ekman D, Broberg J, Nordberg N, Tillander A, Kamali-Moghaddam M, Tybring G, Landegren U. Strong impact on plasma protein profiles by precentrifugation delay but not by repeated freeze-thaw cycles, as analyzed using multiplex proximity extension assays. *Clin Chem Lab Med*. 2018;56(4):582–594.
374. Tran DQ, Andersson J, Wang R, Ramsey H, Unutmaz D, Shevach EM. GARP (LRRC32) is essential for the surface expression of latent TGF-beta on platelets and activated FOXP3+ regulatory T cells. *Proc Natl Acad Sci U S A*. 2009;106(32):13445–13450.
375. Cuende J, Liénart S, Dedobbeleer O, et al. Monoclonal antibodies against GARP/TGF-β1 complexes inhibit the immunosuppressive activity of human regulatory T cells in vivo. *Sci Transl Med*. 2015;7(284):284ra56.
376. Blakytny R, Ludlow A, Martin GEM, Ireland G, Lund LR, Ferguson MWJ, Brunner G. Latent TGF-b1 activation by platelets. *J Cell Physiol*. 2004;199(1):67–76.
377. Starkey Lewis PJ, Dear J, Platt V, Simpson KJ, Craig DGN, Antoine DJ, French NS, Dhaun N, Webb DJ, Costello EM, Neoptolemos JP, Moggs J, Goldring CE, Park BK. Circulating microRNAs as potential markers of human drug-induced liver injury. *Hepatology*. 2011;54(5):1767–1776.
378. Heneghan HM, Miller N, Lowery AJ, Sweeney KJ, Newell J, Kerin MJ. Circulating microRNAs as novel minimally invasive biomarkers for breast cancer. *Ann Surg*. 2010;251(3):499–505.
379. Bergmeier W, Rackebrandt K, Schröder W, Zirngibl H, Nieswandt B. Structural and functional characterization of the mouse von Willebrand factor receptor GPIb-IX with novel monoclonal antibodies. *Blood*. 2000;95(3):886–893.

380. Rowley JW, Chappaz S, Corduan A, et al. Dicer1-mediated miRNA processing shapes the mRNA profile and function of murine platelets. *Blood*. 2016;127(14):1743–1751.
381. Boilard E, Belleannée C. (Dicer)phering roles of microRNA in platelets. *Blood*. 2016;127(14):1733–4.
382. Sewing S, Roth AB, Winter M, Dieckmann A, Bertinetti-Lapatki C, Tessier Y, McGinnis C, Huber S, Koller E, Ploix C, Reed JC, Singer T, Rothfuss A. Assessing single-stranded oligonucleotide drug-induced effects in vitro reveals key risk factors for thrombocytopenia. *PLoS One*. 2017;12(11):e0187574.
383. Zhao L, Liu J, He C, et al. Protein kinase A determines platelet life span and survival by regulating apoptosis. *J Clin Invest*. 2017;127(12):4338–4351.
384. Chan M, Armstrong PCJ, Papalia F, Kirkby NS, Warner TD. Optical multichannel (optimul) platelet aggregometry in 96-well plates as an additional method of platelet reactivity testing. *Platelets*. 2011;22(7):485–494.
385. Lordkipanidzé M, Lowe GC, Kirkby NS, et al. Characterization of multiple platelet activation pathways in patients with bleeding as a high-throughput screening option: use of 96-well Optimul assay. *Blood*. 2014;123(8):e11-22.
386. McDonald B, Reep B, Lapetina EG, Molina y Vedia L. Glyceraldehyde-3-phosphate dehydrogenase is required for the transport of nitric oxide in platelets. *Proc Natl Acad Sci U S A*. 1993;90(23):11122–11126.
387. Senis YA, Mazharian A, Mori J. Src family kinases: at the forefront of platelet activation. *Blood*. 2014;124(13):2013–2024.
388. White JG. Ultrastructural studies of the gray platelet syndrome. *Am J Pathol*. 1979;95(2):445–462.
389. White JG. Interaction of membrane systems in blood platelets. *Am J Pathol*. 1972;66(2):295–312.
390. White GC, Rompietti R. Platelet secretion: indiscriminately spewed forth or highly orchestrated? *J Thromb Haemost*. 2007;5(10):2006–2008.
391. Yadav S, Storrie B. The cellular basis of platelet secretion: Emerging structure/function relationships. *Platelets*. 2017;28(2):108–118.
392. Ma L, Perini R, McKnight W, Dicay M, Klein A, Hollenberg MD, Wallace JL. Proteinase-activated receptors 1 and 4 counter-regulate endostatin and VEGF release from human platelets. *Proc Natl Acad Sci U S A*. 2005;102(1):216–220.
393. Italiano JE, Richardson JL, Patel-Hett S, Battinelli E, Zaslavsky A, Short S, Ryeom S, Folkman J, Klement GL. Angiogenesis is regulated by a novel mechanism: pro- and antiangiogenic proteins are organized into separate platelet alpha granules and differentially released. *Blood*. 2008;111(3):1227–1233.
394. Battinelli EM, Markens BA, Italiano JE. Release of angiogenesis regulatory proteins from platelet alpha granules: modulation of physiologic and pathologic angiogenesis. *Blood*. 2011;118(5):1359–1369.
395. Sehgal S, Storrie B. Evidence that differential packaging of the major platelet granule proteins von Willebrand factor and fibrinogen can support their differential release. *J Thromb Haemost*. 2007;5(10):2009–2016.

396. Peters CG, Michelson AD, Flaumenhaft R. Granule exocytosis is required for platelet spreading: differential sorting of α-granules expressing VAMP-7. *Blood*. 2012;120(1):199–206.
397. Thrasher AJ, Burns SO. WASP: a key immunological multitasker. *Nat Rev Immunol*. 2010;10(3):182–192.
398. Derry JM, Ochs HD, Francke U. Isolation of a novel gene mutated in Wiskott-Aldrich syndrome. *Cell*. 1994;78(4):635–644.
399. Falet H, Hoffmeister KM, Neujahr R, Hartwig JH. Normal Arp2/3 complex activation in platelets lacking WASp. *Blood*. 2002;100(6):2113–2122.
400. Torres E, Rosen MK. Contingent phosphorylation/dephosphorylation provides a mechanism of molecular memory in WASP. *Mol Cell*. 2003;11(5):1215–1227.
401. Gross BS, Wilde JI, Quek L, Chapel H, Nelson DL, Watson SP. Regulation and function of WASp in platelets by the collagen receptor, glycoprotein VI. *Blood*. 1999;94(12):4166–4176.
402. Oda A, Ikeda Y, Ochs HD, Druker BJ, Ozaki K, Handa M, Ariga T, Sakiyama Y, Witte ON, Wahl MI. Rapid tyrosine phosphorylation and activation of Bruton's tyrosine/Tec kinases in platelets induced by collagen binding or CD32 cross-linking. *Blood*. 2000;95(5):1663–1670.
403. Lutskiy MI, Shcherbina A, Bachli ET, Cooley J, Remold-O'Donnell E. WASP localizes to the membrane skeleton of platelets. *Br J Haematol*. 2007;139(1):98–105.
404. Lewis BP, Shih I, Jones-Rhoades MW, Bartel DP, Burge CB. Prediction of mammalian microRNA targets. *Cell*. 2003;115(7):787–798.
405. Nurden AT, Nurden P. The gray platelet syndrome: Clinical spectrum of the disease. *Blood Rev*. 2007;21(1):21–36.

Supplemental tables

1. Supplemental table 1. ECM proteins identified in CF conditioned media following miR-21 mimic or inhibitor (LNA-21) transfection.
2. Supplemental table 2. MiR-21 *null* cardiac gene expression analysis.
3. Supplemental table 3. MiR-21 *null* cardiac ECM protein analysis.
4. Supplemental table 4. Proteins identified in the releasate of washed murine platelets, isolated after antagomiR-21 or -control treatment.
5. Supplemental table 5. Predicted targets of miR-21 in the mouse genome using miRWALK 2.0.

Supplemental Table 1. ECM proteins identified in unstimulated or TGF-β1-stimulated murine CF secretome following miR-21 mimic or inhibitor (LNA-21) transfection. Secretome was analysed by gel LC-MS/MS analysis using an LTQ-Orbitrap XL. Values shown are mean±SEM of normalised spectral counts, based on four biological replicates for each condition. Differential expression was determined using a hierarchical Bayes estimation of generalized linear mixed effects model. FDR is calculated using an empirical Bayes method, with an FDR<0.05 considered significant. Proteins that yielded an FDR<0.05 for at least one condition are marked in bold.

				miR-21 mimic - Unstimulated cardiac fibroblasts				miR-21 mimic - TGF-β1-stimulated cardiac fibroblasts				miR-21 inhibitor (LNA) - Unstimulated cardiac fibroblasts				miR-21 inhibitor (LNA) - TGF-β1-stimulated cardiac fibroblasts			
				Mean ± SEM				Mean ± SEM				Mean ± SEM				Mean ± SEM			
Full protein name	**Accession ID**	**Gene**	**MW (kDa)**	**Control**	**miR-21**	**FDR**	**log2 FC**	**Control**	**miR-21**	**FDR**	**log2 FC**	**Control**	**miR-21**	**FDR**	**log2 FC**	**Control**	**miR-21**	**FDR**	**log2 FC**
Adipocyte enhancer-binding protein 1	AEBP1_MOUSE	Aebp1	128	10.3±1.4	8.0±2.5	0.90	-0.24	18.7±2.4	15.2±1.8	1.00	-0.24	6.5±1.4	4.9±3.4	0.99	-0.33	6.5±2.3	9.6±3.5	0.98	0.18
Agrin	AGRIN_MOUSE	Agrn	208	0.4±0.5	4.4±1.5	0.20	1.15	0.0±0.0	4.3±0.8	n.a.	n.a.	0.0±0.0	3.5±1.5	n.a.	n.a.	0.0±0.0	9.3±4.5	n.a.	n.a.
Annexin A2	ANXA2_MOUSE	Anxa2	39	6.5±2.5	3.6±1.2	0.62	-0.45	6.8±2.2	4.9±2.2	0.99	-0.28	3.1±2.2	2.8±2.8	n.a.	n.a.	2.9±1.8	6.2±3.5	0.97	0.55
Apolipoprotein E	APOE_MOUSE	Apoe	36	4.7±1.8	6.2±2.4	1.00	0.24	2.0±1.2	3.2±1.9	0.27	0.19	11.6±4.4	4.8±1.7	1.00	-0.76	0.6±0.6	1.6±1.0	n.a.	n.a.
A disintegrin and metalloproteinase with thrombospondin motifs 5	ATS5_MOUSE	Adamts5	102	10.6±2.6	12.7±3.2	1.00	0.28	1.5±0.9	1.4±0.5	0.73	-0.05	0.0±0.0	0.0±0.0	n.a.	n.a.	0.0±0.0	0.0±0.0	n.a.	n.a.
Bone morphogenetic protein 1	BMP1_MOUSE	Bmp1	112	15.2±3.7	26.0±6.8	0.62	0.58	19.7±2.4	27.1±3.4	0.14	0.21	1.8±1.8	2.6±2.6	n.a.	n.a.	19.1±12.1	18.9±9.1	0.99	0.03
Cathepsin B	CATB_MOUSE	Ctsb	37	14.2±1.6	16.9±1.4	0.78	0.15	11.6±0.9	10.8±1.4	1.00	-0.21	20.2±4.2	20.3±4.4	1.00	-0.16	21.6±4.4	24.3±4.2	0.98	0.17
Cathepsin D	CATD_MOUSE	Ctsd	45	19.6±3.8	22.2±4.8	1.00	0.08	30.1±5.1	22.9±6.1	1.00	-0.46	11.5±3.6	14.9±0.6	0.54	0.33	23.9±3.6	26.5±2.2	0.94	0.16
Cathepsin L1	**CATL1_MOUSE**	**Ctsl**	**38**	**5.2±3.1**	**6.5±1.3**	**1.00**	**0.18**	**5.2±2.1**	**11.1±0.8**	**0.01**	**0.59**	**14.8±4.6**	**20.8±3.4**	**0.66**	**0.46**	**25.4±2.0**	**27.4±2.8**	**0.99**	**0.09**
Cathepsin Z	CATZ_MOUSE	Ctsz	34	3.2±1.3	4.2±1.7	1.00	0.23	1.1±1.1	0.7±0.7	n.a.	n.a.	10.1±4.9	16.0±5.4	0.57	0.50	17.2±1.6	18.7±1.9	0.99	0.01
C-C motif chemokine 2	CCL2_MOUSE	Ccl2	16	2.6±1.0	0.8±0.5	0.70	-0.54	0.0±0.0	0.0±0.0	n.a.	n.a.	0.0±0.0	1.0±1.0	n.a.	n.a.	0.0±0.0	1.5±1.5	n.a.	n.a.
Collagen alpha-1(I) chain	CO1A1_MOUSE	Col1a1	138	728.9±67.5	821.2±87.5	1.00	0.01	643.2±42.3	782.7±17.9	0.76	-0.01	211.3±109.8	114.1±29.8	1.00	-0.15	227.1±55.7	184.8±39.2	0.98	0.13
Collagen alpha-2(I) chain	CO1A2_MOUSE	Col1a2	130	427.1±20.6	488.3±29.6	0.89	-0.12	404.1±10.3	433.7±16.1	0.31	0.06	85.5±22.7	77.1±5.8	0.93	0.04	110.6±27.5	89.7±18.3	1.00	-0.10
Collagen alpha-1(III) chain	CO3A1_MOUSE	Col3a1	139	407.3±34.4	489.7±53.2	1.00	0.07	318.8±21.1	359.1±13.0	0.31	0.07	335.3±130.3	250.7±63.7	1.00	-0.30	291.3±71.6	228.1±59.9	1.00	-0.12
Collagen alpha-1(IV) chain	CO4A1_MOUSE	Col4a1	161	52.0±2.0	47.1±4.2	0.81	-0.17	56.1±5.3	49.3±2.0	1.00	-0.19	24.2±7.7	9.2±6.0	0.30	-1.38	43.5±10.4	34.9±9.8	1.00	-0.36
Collagen alpha-2(IV) chain	CO4A2_MOUSE	Col4a2	167	86.1±3.6	87.0±12.3	1.00	0.02	99.4±6.0	83.4±9.0	1.00	-0.17	21.7±3.4	24.7±6.6	1.00	-0.17	27.0±7.2	26.2±6.6	1.00	-0.01
Collagen alpha-1(V) chain	CO5A1_MOUSE	Col5a1	184	31.3±2.7	28.6±1.3	0.65	-0.24	33.5±3.4	38.0±3.7	0.37	0.07	17.1±9.6	7.5±2.6	1.00	-0.50	29.6±9.2	18.3±8.5	1.00	-0.58
Collagen alpha-2(V) chain	CO5A2_MOUSE	Col5a2	145	149.7±8.4	159.4±7.5	1.00	0.00	176.0±13.0	194.3±13.5	0.34	0.07	33.6±25.4	12.8±8.3	1.00	-0.72	55.1±17.8	35.1±12.4	1.00	-0.39
Collagen alpha-1(VI) chain	CO6A1_MOUSE	Col6a1	108	45.0±1.9	57.7±5.6	0.61	0.23	36.2±4.4	30.8±3.2	1.00	-0.29	72.9±20.6	69.9±21.3	1.00	-0.24	66.2±19.0	56.9±17.6	1.00	-0.15
Collagen alpha-2(VI) chain	CO6A2_MOUSE	Col6a2	110	14.8±0.5	13.0±0.9	0.86	-0.13	9.6±0.7	6.1±0.8	0.18	-0.52	21.5±7.9	19.6±7.4	0.99	-0.23	16.5±7.3	9.5±3.9	1.00	-0.25
Collagen alpha-1(VIII) chain	CO8A1_MOUSE	Col8a1	74	2.1±0.8	3.5±0.5	0.58	0.33	0.0±0.0	0.0±0.0	n.a.	n.a.	0.0±0.0	0.0±0.0	n.a.	n.a.	4.3±2.6	2.6±1.7	1.00	-0.42
Collagen alpha-1(XI) chain	**COBA1_MOUSE**	**Col11a1**	**181**	**1.7±1.7**	**6.8±3.2**	**n.a.**	**n.a.**	**23.9±2.4**	**40.8±2.8**	**0.02**	**0.44**	**2.1±1.2**	**0.0±0.0**	**n.a.**	**n.a.**	**8.9±3.0**	**6.5±2.4**	**1.00**	**-0.22**
Collagen alpha-1(XII) chain	COCA1_MOUSE	Col12a1	340	27.4±3.3	33.7±6.3	1.00	0.07	48.6±7.4	58.7±6.0	0.35	0.09	26.2±15.5	17.2±8.6	0.99	-0.02	79.6±32.2	53.3±23.5	1.00	-0.15
Collagen alpha-1(XIV) chain	COEA1_MOUSE	Col14a1	193	0.6±0.6	4.0±1.5	n.a.	n.a.	1.1±1.1	0.9±0.9	n.a.	n.a.	3.6±1.5	3.0±1.2	0.99	-0.27	5.1±2.5	3.0±1.8	1.00	-0.32
Collagen alpha-1(XV) chain	COFA1_MOUSE	Col15a1	140	2.3±1.3	2.1±1.4	1.00	-0.03	2.2±0.8	3.6±1.7	0.50	0.11	2.7±1.6	1.4±1.4	n.a.	n.a.	5.9±2.2	5.1±2.0	1.00	-0.09
Macrophage colony-stimulating factor 1	CSF1_MOUSE	Csf1	61	8.3±0.6	8.9±1.7	1.00	0.10	15.4±2.3	15.7±3.2	0.99	-0.13	4.6±0.6	7.1±2.6	0.88	0.11	11.3±4.2	11.3±4.8	1.00	-0.10
Versican core protein	CSPG2_MOUSE	Vcan	367	2.0±2.0	4.9±1.7	n.a.	n.a.	2.0±1.2	3.6±1.3	0.27	0.20	1.5±1.5	3.5±2.3	n.a.	n.a.	8.5±3.4	0.0±0.0	n.a.	n.a.
Connective tissue growth factor	CTGF_MOUSE	Ctgf	38	14.1±0.4	9.0±1.6	0.50	-0.45	30.9±2.7	25.9±1.7	0.82	-0.33	9.8±1.4	12.8±2.7	0.94	0.05	43.7±4.3	59.6±7.8	0.71	0.30
Collagen triple helix repeat-containing protein 1	CTHR1_MOUSE	Cthrc1	26	1.9±1.2	3.6±1.5	0.92	0.33	3.5±1.4	5.8±1.8	0.28	0.28	2.1±1.3	0.6±0.6	n.a.	n.a.	3.1±1.1	3.2±1.1	0.99	0.08
Cytochrome c, somatic	CYC_MOUSE	Cycs	12	4.1±0.9	3.4±1.4	1.00	0.02	5.1±0.7	3.6±0.6	0.98	-0.38	6.0±2.5	4.0±2.4	0.99	-0.34	1.8±1.9	1.8±1.8	n.a.	n.a.
Cystatin-C	CYTC_MOUSE	Cst3	16	12.3±4.3	18.5±3.0	0.79	0.24	17.0±2.4	21.2±1.8	0.11	0.18	12.5±6.2	9.7±5.8	1.00	-0.39	8.1±4.7	3.0±1.8	1.00	-0.62
Dystroglycan	DAG1_MOUSE	Dag1	97	4.0±0.7	2.5±1.1	0.93	-0.22	2.5±1.0	1.1±1.1	1.00	-0.50	4.5±1.6	3.0±1.8	1.00	-0.27	5.9±2.3	6.9±2.3	0.98	0.15
Dermatopontin	DERM_MOUSE	Dpt	24	12.1±3.0	16.9±2.9	0.73	0.41	12.3±1.4	11.5±1.0	1.00	-0.14	23.3±6.6	16.3±6.8	0.99	-0.37	7.7±3.1	5.0±2.3	1.00	-0.33
Extracellular matrix protein 1	ECM1_MOUSE	Ecm1	63	37.3±2.3	48.6±2.6	0.74	0.21	27.0±2.9	33.4±1.9	0.11	0.20	70.8±18.3	59.8±14.7	1.00	-0.21	55.1±13.7	56.0±13.2	1.00	-0.02
EMILIN-1	EMIL1_MOUSE	Emilin1	108	2.4±1.4	5.9±1.6	0.60	0.54	3.1±1.2	3.1±1.1	0.93	-0.10	3.6±1.6	4.6±2.7	0.99	-0.03	6.0±2.6	5.7±2.1	0.99	0.03
Fibulin-1	FBLN1_MOUSE	Fbln1	78	12.0±2.4	12.6±2.2	1.00	0.15	5.8±1.3	2.5±1.6	1.00	-0.67	23.3±9.8	29.5±11.2	0.87	0.12	10.5±4.3	4.7±1.9	1.00	-0.52
Fibulin-2	FBLN2_MOUSE	Fbln2	132	226.8±18.1	239.1±19.1	1.00	0.00	215.5±7.5	220.6±8.7	0.37	0.06	307.7±45.1	309.2±46.9	0.77	0.09	291.1±44.8	283.0±37.2	0.99	0.02
EGF-containing fibulin-like extracellular matrix protein 1	FBLN3_MOUSE	Efemp1	55	21.0±2.2	35.8±2.5	0.24	0.45	1.3±0.9	3.4±2.0	0.21	0.45	51.8±17.7	43.8±14.8	1.00	-0.29	11.1±5.7	8.8±3.8	1.00	0.01
EGF-containing fibulin-like extracellular matrix protein 2	FBLN4_MOUSE	Efemp2	49	22.3±3.2	28.2±0.4	0.81	0.23	15.9±1.7	15.1±4.9	1.00	-0.33	27.2±8.3	29.4±7.9	0.93	0.13	23.2±7.8	25.7±7.1	0.99	0.28
Fibulin-5	FBLN5_MOUSE	Fbln5	50	24.4±2.0	22.4±2.3	0.85	-0.16	35.4±3.4	29.4±6.0	1.00	-0.29	0.0±0.0	1.7±1.0	n.a.	n.a.	12.1±7.0	9.2±6.7	1.00	-0.23
Fibrillin-1	FBN1_MOUSE	Fbn1	312	57.2±6.8	71.7±9.3	0.57	0.29	44.2±5.5	48.7±3.6	0.52	0.03	292.4±88.2	262.6±75.4	1.00	-0.07	258.2±65.1	243.1±68.4	1.00	-0.11
Fibronectin	FINC_MOUSE	Fn1	273	330.0±15.4	323.2±26.4	1.00	0.04	401.7±18.6	379.0±30.1	1.00	-0.10	232.4±68.4	239.6±66.9	0.88	0.09	247.6±61.7	237.2±84.9	1.00	-0.04
Fibromodulin	FMOD_MOUSE	Fmod	43	14.0±2.7	10.6±4.1	0.90	-0.26	8.1±1.3	7.4±3.0	1.00	-0.37	0.9±0.9	0.0±0.0	n.a.	n.a.	0.0±0.0	0.0±0.0	n.a.	n.a.
Follistatin-related protein 1	FSTL1_MOUSE	Fstl1	35	84.0±8.0	69.6±5.5	0.99	-0.08	85.7±3.4	84.8±3.3	0.51	0.02	50.5±7.0	54.5±9.4	1.00	-0.08	88.1±16.8	82.8±17.3	1.00	-0.08

Supplemental Table 1. (continued)

				miR-21 mimic - Unstimulated cardiac fibroblasts				miR-21 mimic - TGF-β1-stimulated cardiac fibroblasts				miR-21 inhibitor (LNA) - Unstimulated cardiac fibroblasts				miR-21 inhibitor (LNA) - TGF-β1-stimulated cardiac fibroblasts			
				Mean ± SEM				Mean ± SEM				Mean ± SEM				Mean ± SEM			
Full protein name	**Accession ID**	**Gene**	**MW (kDa)**	**Control**	**miR-21**	**FDR**	**log2 FC**	**Control**	**miR-21**	**FDR**	**log2 FC**	**Control**	**miR-21**	**FDR**	**log2 FC**	**Control**	**miR-21**	**FDR**	**log2 FC**
Gelsolin	GELS_MOUSE	Gsn	86	59.8±7.0	66.2±13.4	1.00	0.01	14.3±2.2	8.3±3.3	1.00	-0.50	87.0±29.8	75.9±26.3	1.00	-0.33	43.1±19.7	35.8±16.1	1.00	-0.19
Granulins	**GRN_MOUSE**	**Grn**	**63**	**3.7±1.3**	**11.2±2.0**	**2.8E-04**	**1.08**	**4.9±0.6**	**14.2±1.3**	**3.0E-06**	**0.89**	**2.1±1.3**	**3.2±2.0**	**0.87**	**0.26**	**0.7±0.8**	**10.8±2.2**	**0.03**	**1.87**
Insulin-like growth factor-binding protein 2	IBP2_MOUSE	Igfbp2	33	3.4±1.6	0.6±0.7	n.a.	n.a.	9.0±1.9	10.1±1.5	0.51	0.07	0.0±0.0	0.0±0.0	n.a.	n.a.	1.9±2.0	1.2±1.2	n.a.	n.a.
Insulin-like growth factor-binding protein 4	**IBP4_MOUSE**	**Igfbp4**	**28**	**7.8±2.3**	**21.8±2.0**	**8.1E-04**	**1.25**	**6.5±1.4**	**5.9±0.9**	**1.00**	**-0.17**	**6.8±4.0**	**5.5±3.3**	**1.00**	**-0.19**	**3.8±2.2**	**3.1±1.8**	**1.00**	**-0.26**
Insulin-like growth factor-binding protein 7	IBP7_MOUSE	Igfbp7	29	49.6±5.8	53.8±7.3	1.00	0.02	65.8±5.8	54.3±5.1	1.00	-0.26	31.1±5.6	33.3±2.4	0.97	0.02	50.9±5.2	43.0±6.7	1.00	-0.14
Plasma protease C1 inhibitor	IC1_MOUSE	Serping1	56	13.3±2.0	10.6±3.7	0.84	-0.30	8.5±1.3	13.2±3.1	0.25	0.14	32.3±13.2	47.1±12.1	0.58	0.40	20.2±9.1	28.6±8.1	0.71	0.66
Laminin subunit alpha-2	LAMA2_MOUSE	Lama2	344	10.4±1.7	12.2±1.0	0.99	0.23	15.2±3.3	24.9±2.1	0.06	0.46	15.8±6.7	12.5±6.2	1.00	-0.25	46.8±18.5	39.6±15.8	1.00	-0.03
Laminin subunit alpha-4	LAMA4_MOUSE	Lama4	202	67.3±5.7	60.7±5.4	0.85	-0.14	49.4±5.1	44.4±1.8	0.99	-0.17	70.2±23.7	61.8±19.9	1.00	-0.66	66.4±22.0	62.1±23.8	1.00	-0.09
Laminin subunit beta-1	LAMB1_MOUSE	Lamb1	197	21.0±4.2	18.7±4.1	1.00	-0.10	21.4±2.6	16.3±1.2	0.91	-0.39	15.1±6.5	18.2±9.2	0.98	0.00	30.0±11.0	26.0±11.0	1.00	-0.01
Laminin subunit beta-2	LAMB2_MOUSE	Lamb2	197	53.1±4.3	54.7±2.9	1.00	0.01	38.1±1.4	48.3±4.3	0.22	0.10	42.5±16.6	55.3±17.3	0.80	0.39	44.8±13.5	37.8±15.2	1.00	-0.21
Laminin subunit gamma-1	LAMC1_MOUSE	Lamc1	177	61.9±6.2	62.6±4.8	1.00	0.02	62.2±0.8	58.4±0.3	0.98	-0.07	57.7±18.6	84.2±27.3	0.74	0.27	86.7±17.4	85.0±23.0	0.98	0.11
Galectin-1	LEG1_MOUSE	Lgals1	15	7.5±1.8	7.0±0.9	1.00	0.03	5.3±1.0	5.9±1.4	0.65	0.01	5.1±2.4	5.4±2.5	1.00	-0.04	4.0±2.6	4.3±2.6	0.99	0.15
Galectin-3-binding protein	**LG3BP_MOUSE**	**Lgals3bp**	**64**	**20.2±4.4**	**31.8±8.1**	**0.69**	**0.41**	**17.1±3.7**	**22.4±5.0**	**0.23**	**0.22**	**11.2±6.2**	**54.5±15.7**	**3.0E-06**	**1.73**	**7.7±6.6**	**49.5±16.3**	**0.02**	**2.35**
Lysyl oxidase homolog 2	LOXL2_MOUSE	Loxl2	87	10.2±2.0	5.3±2.6	0.70	-0.60	10.9±3.4	14.0±0.8	0.11	0.38	0.0±0.0	0.0±0.0	n.a.	n.a.	1.2±1.2	1.3±0.8	n.a.	n.a.
Latent-transforming growth factor beta-binding protein 2	LTBP2_MOUSE	Ltbp2	196	0.0±0.0	0.0±0.0	n.a.	n.a.	0.7±0.7	6.5±1.9	n.a.	n.a.	0.0±0.0	0.0±0.0	n.a.	n.a.	18.7±5.7	15.6±6.0	1.00	-0.12
Latent-transforming growth factor beta-binding protein 4	LTBP4_MOUSE	Ltbp4	179	0.0±0.0	0.0±0.0	n.a.	n.a.	0.0±0.0	0.0±0.0	n.a.	n.a.	3.6±2.1	0.9±0.9	n.a.	n.a.	13.9±5.6	6.3±2.6	1.00	-0.53
Lumican	LUM_MOUSE	Lum	38	10.2±1.2	17.0±1.3	0.13	0.44	4.8±2.4	5.0±1.9	0.57	0.06	28.3±7.1	19.5±7.5	1.00	-0.49	16.2±3.4	8.7±4.1	1.00	-0.57
Protein-lysine 6-oxidase	LYOX_MOUSE	Lox	47	14.8±2.6	10.0±3.5	0.68	-0.48	15.8±3.9	13.6±3.3	1.00	-0.23	0.0±0.0	0.0±0.0	n.a.	n.a.	0.7±0.8	0.0±0.0	n.a.	n.a.
Matrilin-2	MATN2_MOUSE	Matn2	107	3.0±0.6	3.9±0.8	0.80	0.32	0.0±0.0	0.0±0.0	n.a.	n.a.	6.5±3.0	2.9±2.2	1.00	-0.75	0.0±0.0	2.0±1.2	n.a.	n.a.
72 kDa type IV collagenase	MMP2_MOUSE	Mmp2	74	15.2±3.1	12.5±4.3	0.98	-0.26	18.6±1.0	18.0±2.3	1.00	-0.13	5.1±2.7	4.6±3.5	1.00	-0.31	3.1±1.8	1.9±1.2	1.00	-0.31
Stromelysin-1	MMP3_MOUSE	Mmp3	54	19.5±6.1	37.0±8.0	0.35	0.67	21.3±6.4	34.6±11.9	0.16	0.43	10.9±3.9	12.2±3.1	0.96	0.06	1.2±1.3	4.2±1.9	n.a.	n.a.
Nidogen-1	NID1_MOUSE	Nid1	137	72.9±5.4	73.7±7.0	1.00	-0.03	72.3±4.1	64.7±3.9	1.00	-0.12	76.2±14.7	94.4±20.3	0.69	0.16	81.7±19.7	85.1±22.5	0.98	0.10
Nidogen-2	NID2_MOUSE	Nid2	154	12.6±1.6	9.3±1.5	0.55	-0.34	0.7±0.7	2.9±1.2	n.a.	n.a.	0.0±0.0	0.0±0.0	n.a.	n.a.	0.0±0.0	0.0±0.0	n.a.	n.a.
Plasminogen activator inhibitor 1	PAI1_MOUSE	Serpine1	45	108.6±3.8	89.8±5.8	0.96	-0.09	203.8±16.3	210.7±32.6	1.00	-0.15	47.3±4.1	57.7±4.8	0.75	0.14	201.9±17.1	193.5±20.6	1.00	0.00
Procollagen C-endopeptidase enhancer 1	PCOC1_MOUSE	Pcolce	50	55.1±8.1	85.0±10.1	0.37	0.47	55.1±4.9	60.3±6.3	0.38	0.06	47.3±11.9	50.6±15.3	1.00	-0.18	37.5±9.9	35.4±6.7	1.00	-0.03
Protein disulfide-isomerase A3	PDIA3_MOUSE	Pdia3	57	30.5±6.0	15.4±2.0	0.24	-0.64	25.0±3.2	14.6±1.2	0.28	-0.56	64.3±7.5	58.8±11.6	1.00	-0.19	53.4±7.3	49.3±7.8	0.99	0.11
Protein disulfide-isomerase A6	PDIA6_MOUSE	Pdia6	48	5.1±1.7	5.0±0.8	0.78	0.25	6.5±0.6	4.7±0.4	0.40	-0.48	8.4±3.0	5.9±2.5	0.99	-0.33	7.8±2.6	6.4±1.5	1.00	-0.16
Pigment epithelium-derived factor	PEDF_MOUSE	Serpinf1	46	68.8±5.1	72.9±12.8	1.00	-0.04	93.1±3.8	87.3±8.1	0.94	-0.05	105.6±16.0	125.4±19.9	0.28	0.25	139.3±17.8	146.9±13.2	0.93	0.20
Basement membrane-specific heparan sulfate proteoglycan core protein	PGBM_MOUSE	Hspg2	398	102.9±8.6	71.3±9.9	0.63	-0.33	81.0±18.0	95.3±8.6	0.24	0.15	20.1±6.6	19.3±6.1	1.00	-0.12	66.4±16.4	52.0±19.7	1.00	-0.40
Biglycan	PGS1_MOUSE	Bgn	42	95.8±7.1	86.7±15.5	0.97	-0.15	147.6±5.1	140.4±12.6	0.45	0.04	59.8±12.7	75.7±14.0	0.58	0.19	104.6±24.8	107.8±18.3	0.79	0.25
Decorin	PGS2_MOUSE	Dcn	40	61.0±6.5	55.8±2.3	0.99	-0.09	42.1±3.0	38.0±2.7	1.00	-0.22	110.9±22.1	93.7±18.4	1.00	-0.19	67.7±12.8	63.9±11.4	0.99	0.05
Procollagen-lysine,2-oxoglutarate 5-dioxygenase 1	PLOD1_MOUSE	Plod1	84	4.3±0.9	3.3±1.2	1.00	-0.06	2.2±1.4	3.8±1.9	n.a.	n.a.	0.0±0.0	0.0±0.0	n.a.	n.a.	0.0±0.0	2.0±1.2	n.a.	n.a.
Procollagen-lysine,2-oxoglutarate 5-dioxygenase 2	PLOD2_MOUSE	Plod2	84	4.7±0.8	3.1±0.6	0.84	-0.21	4.9±0.8	2.7±1.7	1.00	-0.40	0.0±0.0	0.0±0.0	n.a.	n.a.	1.4±1.4	0.0±0.0	n.a.	n.a.
Procollagen-lysine,2-oxoglutarate 5-dioxygenase 3	PLOD3_MOUSE	Plod3	85	5.8±0.6	7.6±1.7	0.67	0.30	6.2±1.0	10.1±1.4	0.13	0.27	2.7±0.9	6.2±2.8	0.30	0.55	11.9±4.3	12.3±4.4	0.99	0.11
Periostin	POSTN_MOUSE	Postn	93	27.4±5.6	30.0±7.0	1.00	0.05	81.0±7.4	100.0±10.5	0.16	0.17	12.3±7.2	17.2±9.5	0.95	0.18	92.2±33.2	78.6±28.8	1.00	-0.30
Peptidyl-prolyl cis-trans isomerase A	PPIA_MOUSE	Ppia	18	16.2±5.3	9.4±2.7	0.86	-0.38	8.9±2.6	8.2±1.0	0.81	-0.05	6.4±3.7	11.2±0.9	0.21	0.45	7.1±1.6	8.2±1.2	0.96	0.22
Peptidyl-prolyl cis-trans isomerase B	PPIB_MOUSE	Ppib	24	13.6±2.4	8.3±1.3	0.40	-0.48	10.9±2.0	7.6±1.4	0.79	-0.53	17.3±3.6	16.2±1.7	1.00	-0.11	10.7±3.3	17.0±2.0	0.71	0.52
Peroxiredoxin-1	PRDX1_MOUSE	Prdx1	22	17.7±3.9	17.1±3.2	1.00	0.05	15.7±4.3	11.2±2.5	1.00	-0.38	18.0±3.5	20.2±3.4	0.96	0.03	15.0±3.1	26.3±6.2	0.81	0.54
Peroxiredoxin-2	PRDX2_MOUSE	Prdx2	22	5.4±0.8	3.8±0.8	0.76	-0.29	3.6±1.0	3.4±0.6	0.86	-0.07	5.5±1.9	7.4±1.6	0.86	0.11	7.6±1.0	7.8±1.2	1.00	0.00
Peroxiredoxin-6	PRDX6_MOUSE	Prdx6	25	3.9±2.5	4.4±2.4	1.00	0.14	6.9±1.7	3.8±1.4	1.00	-0.58	6.2±1.1	8.2±2.9	0.99	-0.03	2.1±1.3	7.3±4.2	0.95	0.85
Prolargin	PRELP_MOUSE	Prelp	43	8.9±3.9	0.0±0.0	0.59	-8.26	3.4±1.3	2.0±1.2	1.00	-0.29	5.9±3.5	11.1±4.0	0.63	0.24	0.8±0.9	0.7±0.8	n.a.	n.a.
Pentraxin-related protein PTX3	PTX3_MOUSE	Ptx3	42	36.2±5.1	49.6±4.0	0.91	0.18	26.8±1.7	33.3±3.1	0.26	0.11	24.5±2.9	41.4±7.8	0.43	0.36	22.6±2.4	30.9±4.8	0.88	0.28
Extracellular superoxide dismutase [Cu-Zn]	SODE_MOUSE	Sod3	27	28.4±4.0	27.7±4.1	0.95	-0.17	27.3±2.6	24.9±3.0	1.00	-0.19	15.8±5.5	18.1±7.6	1.00	-0.11	22.8±6.1	23.2±5.9	0.99	0.05
Serine protease inhibitor A3N	SPA3N_MOUSE	Serpina3n	47	36.4±8.9	42.5±5.6	1.00	0.07	27.9±4.3	26.8±5.6	1.00	-0.14	40.6±11.3	57.3±16.7	0.91	0.13	39.7±11.9	25.5±7.7	1.00	-0.41
SPARC	SPRC_MOUSE	Sparc	34	92.7±5.4	98.8±12.7	0.94	0.12	117.7±11.2	106.6±7.4	1.00	-0.12	41.6±4.2	44.8±4.4	1.00	-0.10	58.6±3.3	54.5±2.7	1.00	0.00
Tenascin	TENA_MOUSE	Tnc	232	26.0±4.4	20.0±5.5	0.76	-0.44	35.8±4.9	35.1±5.4	1.00	-0.14	12.5±5.9	23.2±9.7	0.24	0.61	23.5±10.0	30.4±14.2	0.98	0.29
Tetranectin	TETN_MOUSE	Clec3b	22	3.0±1.0	2.5±0.9	0.96	-0.16	0.0±0.0	0.0±0.0	n.a.	n.a.	7.1±3.2	4.8±1.8	1.00	-0.22	0.0±0.0	0.0±0.0	n.a.	n.a.
Metalloproteinase inhibitor 1	TIMP1_MOUSE	Timp1	23	10.4±0.7	8.7±3.3	1.00	-0.09	20.1±4.9	26.4±3.9	0.24	0.21	9.6±4.6	6.9±5.6	1.00	-0.76	10.2±5.4	15.0±5.4	0.79	0.78
Metalloproteinase inhibitor 2	TIMP2_MOUSE	Timp2	24	9.5±3.2	12.6±2.0	0.96	0.21	12.3±1.7	13.5±1.2	0.36	0.10	11.3±4.6	6.9±2.6	0.99	-0.39	1.6±0.9	0.0±0.0	n.a.	n.a.
Thrombospondin-1	TSP1_MOUSE	Thbs1	130	7.1±1.2	4.4±0.7	0.79	-0.34	19.6±3.2	25.0±5.6	0.56	0.04	4.2±3.2	3.3±2.2	1.00	-0.22	9.8±2.4	10.1±2.1	0.99	0.07
Thrombospondin-2	TSP2_MOUSE	Thbs2	130	3.6±1.5	9.4±1.7	0.26	0.94	0.9±0.9	7.7±1.2	n.a.	n.a.	12.6±6.1	1.4±0.9	0.67	-1.47	3.1±1.1	3.3±2.1	0.99	0.12
Vascular cell adhesion protein 1	**VCAM1_MOUSE**	**Vcam1**	**81**	**8.8±2.0**	**7.6±1.1**	**1.00**	**-0.01**	**7.8±1.8**	**6.8±1.7**	**1.00**	**-0.28**	**1.6±1.0**	**16.3±1.3**	**<1.0E-06**	**1.50**	**2.2±0.9**	**10.8±1.9**	**3.5E-05**	**1.25**
Vinculin	VINC_MOUSE	Vcl	117	8.3±4.7	1.9±1.9	n.a.	n.a.	8.0±2.3	0.7±0.7	0.11	-1.41	13.0±3.3	14.3±4.3	1.00	-0.09	15.5±4.8	17.3±4.6	0.99	0.22

Supplemental table 2. MiR-21 *null* cardiac gene expression analysis. Analysis was performed in RNA extracted from the heart ventricle of miR-21 *null* mice or littermate controls (n=6 vs. 6). Relative quantities were calculated with the $2^{-\Delta\Delta Cq}$ method using *Actb* as the reference gene transcript. FDR-adjusted p-values (q-values) were calculated using the two-stage step-up method of Benjamini, Krieger and Yekutieli. Q for significant discovery was set to 5%.

Gene ID	miR-21$^{+/+}$	miR-21$^{-/-}$	p-value	q-value
Bgn	1±0.04	1.04±0.04	0.4873	0.8759
Col1a1	1±0.05	1.05±0.05	0.5336	0.8759
Col1a2	1±0.05	1.04±0.07	0.7007	0.8759
Col3a1	1±0.05	1.05±0.06	0.5887	0.8759
Col4a2	1±0.12	1.23±0.23	0.5050	0.8759
Col5a2	1±0.06	1.13±0.07	0.1725	0.7547
Col6a1	1±0.10	1.03±0.11	0.8754	0.9575
Dcn	1±0.06	0.95±0.03	0.5716	0.8759
Fbn1	1±0.04	1.15±0.10	0.2446	0.8759
Fn1	1±0.03	1.14±0.07	0.1106	0.6767
Fstl1	1±0.04	1.06±0.05	0.3253	0.8759
Grn	1±0.04	1.04±0.06	0.6047	0.8759
Hspg2	1±0.03	1.10±0.05	0.0814	0.6767
Igfbp4	1±0.03	0.97±0.02	0.4624	0.8759
Lama4	1±0.03	1.14±0.02	0.0040	0.1049
Lamc1	1±0.04	1.00±0.03	0.9880	>0.9999
Lgals3bp	1±0.03	1.12±0.06	0.1289	0.6767
Nid1	1±0.03	0.98±0.04	0.6828	0.8759
Pcolce	1±0.04	1.02±0.06	0.8677	0.9575
Postn	1±0.07	1.05±0.07	0.6280	0.8759
Serpine1	1±0.15	1.11±0.17	0.6601	0.8759
Serpinf1	1±0.04	1.02±0.05	0.7662	0.9143
Sparc	1±0.09	1.27±0.06	0.0217	0.2848
Tgfb1	1±0.04	1.03±0.04	0.6256	0.8759
Vcam1	1±0.04	1.05±0.06	0.5047	0.8759

miRNA ID	miR-21$^{+/+}$	miR-21$^{-/-}$	p-value	q-value
miR-1	1±0.05	0.98±0.07	0.7465	0.9482
miR-21	1±0.04	0.00±0.00	<0.0001	<0.0001
miR-29b	1±0.04	0.92±0.04	0.1697	0.3592
miR-30c	1±0.03	0.95±0.02	0.1842	0.3592
miR-31	1±0.05	0.89±0.06	0.1754	0.3592
miR-126	1±0.03	1.00±0.04	0.9499	0.9482
miR-133	1±0.04	1.00±0.04	0.9642	0.9482
miR-143	1±0.02	1.00±0.05	0.9726	0.9482
miR-145	1±0.03	0.99±0.06	0.8119	0.9482
miR-146a	1±0.08	1.08±0.09	0.5585	0.8470
miR-499	1±0.04	0.79±0.05	0.0085	0.0583

Supplemental table 3. MiR-21 *null* cardiac ECM protein analysis. Analysis was performed using the three-step extraction method, involving sequential incubation in NaCl, SDS and GuHCl to enrich for ECM proteins. Combined analysis of the NaCl and GuHCl fractions by LC-MS/MS was annotated using the Matrisome database for murine ECM and ECM-associated proteins. Values indicate normalised total precursor intensity. FDR-adjusted p-values (q-values) were calculated using the two-stage step-up method of Benjamini, Krieger and Yekutieli. Q for significant discovery was set to 5%.

Protein ID	Gene	miR-21$^{+/+}$	miR-21$^{-/-}$	p-value	q-value
CO1A1_MOUSE	Col1a1	2.5E+10	2.2E+10	0.6351	>0.9999
CO3A1_MOUSE	Col3a1	2.5E+10	2.2E+10	0.7349	>0.9999
CO1A2_MOUSE	Col1a2	1.4E+10	1.2E+10	0.6783	>0.9999
PGBM_MOUSE	Hspg2	1.4E+10	1.2E+10	0.3143	>0.9999
ANXA6_MOUSE	Anxa6	9.5E+09	9.2E+09	0.7367	>0.9999
NID1_MOUSE	Nid1	7.5E+09	6.7E+09	0.5165	>0.9999
A1AT2_MOUSE	Serpina1b	6.1E+09	6.8E+09	0.5223	>0.9999
LEG1_MOUSE	Lgals1	4.8E+09	5.0E+09	0.7817	>0.9999
ANXA5_MOUSE	Anxa5	3.9E+09	4.4E+09	0.1604	>0.9999
LAMA2_MOUSE	Lama2	3.5E+09	3.2E+09	0.6058	>0.9999
LAMC1_MOUSE	Lamc1	3.5E+09	3.1E+09	0.5586	>0.9999
PGS2_MOUSE	Dcn	3.1E+09	2.9E+09	0.7459	>0.9999
ANXA2_MOUSE	Anxa2	3.0E+09	3.3E+09	0.6398	>0.9999
SPA3K_MOUSE	Serpina3k	2.7E+09	2.8E+09	0.8040	>0.9999
TGM2_MOUSE	Tgm2	2.6E+09	2.7E+09	0.7984	>0.9999
CO6A1_MOUSE	Col6a1	2.2E+09	2.5E+09	0.5046	>0.9999
LAMB2_MOUSE	Lamb2	1.7E+09	1.7E+09	0.9022	>0.9999
LAMB1_MOUSE	Lamb1	1.6E+09	1.4E+09	0.3810	>0.9999
PZP_MOUSE	Pzp	1.6E+09	1.6E+09	0.9815	>0.9999
CO6A2_MOUSE	Col6a2	1.5E+09	1.6E+09	0.8764	>0.9999
MFAP5_MOUSE	Mfap5	1.3E+09	8.0E+08	0.2806	>0.9999
CO5A2_MOUSE	Col5a2	1.2E+09	1.2E+09	0.8809	>0.9999
SERPH_MOUSE	Serpinh1	1.2E+09	1.5E+09	0.3230	>0.9999
S10A1_MOUSE	S100a1	1.1E+09	1.1E+09	0.7563	>0.9999
COFA1_MOUSE	Col15a1	1.1E+09	1.1E+09	0.9553	>0.9999
HEMO_MOUSE	Hpx	1.0E+09	1.0E+09	0.9673	>0.9999
CATD_MOUSE	Ctsd	1.0E+09	9.7E+08	0.8106	>0.9999
NID2_MOUSE	Nid2	9.7E+08	7.9E+08	0.2888	>0.9999
CO4A1_MOUSE	Col4a1	9.2E+08	7.8E+08	0.7734	>0.9999
CO5A1_MOUSE	Col5a1	8.2E+08	8.4E+08	0.9057	>0.9999
CO4A2_MOUSE	Col4a2	7.8E+08	5.9E+08	0.5286	>0.9999
DERM_MOUSE	Dpt	7.2E+08	6.3E+08	0.4697	>0.9999
S10AA_MOUSE	S100a10	7.1E+08	8.3E+08	0.2888	>0.9999
ANT3_MOUSE	Serpinc1	5.5E+08	5.2E+08	0.8099	>0.9999
FBN1_MOUSE	Fbn1	5.5E+08	5.0E+08	0.8727	>0.9999
LUM_MOUSE	Lum	5.2E+08	6.0E+08	0.4485	>0.9999
KNG1_MOUSE	Kng1	5.1E+08	4.7E+08	0.7729	>0.9999
FINC_MOUSE	Fn1	4.4E+08	6.8E+08	0.3155	>0.9999
FIBB_MOUSE	Fgb	3.9E+08	5.1E+08	0.4691	>0.9999
LAMA4_MOUSE	Lama4	3.8E+08	4.2E+08	0.6975	>0.9999
ANXA7_MOUSE	Anxa7	3.5E+08	2.1E+08	0.0790	>0.9999
PGS1_MOUSE	Bgn	3.4E+08	3.0E+08	0.8318	>0.9999
ADIPO_MOUSE	Adipoq	3.0E+08	3.3E+08	0.3310	>0.9999
ANX11_MOUSE	Anxa11	2.7E+08	3.1E+08	0.4079	>0.9999
FIBA_MOUSE	Fga	2.7E+08	3.0E+08	0.8466	>0.9999
CATB_MOUSE	Ctsb	2.5E+08	1.9E+08	0.3092	>0.9999
PRELP_MOUSE	Prelp	2.3E+08	2.0E+08	0.5583	>0.9999
PPN_MOUSE	Papln	2.0E+08	2.1E+08	0.9080	>0.9999
FIBG_MOUSE	Fgg	1.7E+08	2.9E+08	0.4163	>0.9999
LAMA5_MOUSE	Lama5	1.4E+08	1.5E+08	0.8689	>0.9999
ANXA4_MOUSE	Anxa4	1.4E+08	1.3E+08	0.8081	>0.9999
TINAL_MOUSE	Tinagl1	1.3E+08	8.4E+07	0.2736	>0.9999
CO6A6_MOUSE	Col6a6	1.1E+08	4.5E+07	0.0244	>0.9999
AGRIN_MOUSE	Agrn	8.4E+07	6.7E+07	0.5389	>0.9999
VMA5A_MOUSE	Vwa5a	7.4E+07	9.6E+07	0.3572	>0.9999

Supplemental table 4. Proteins identified in the thrombin-induced releasate of washed platelets, isolated from mice treated with antagomiR-21 or -control. The platelet releasate was analysed by gel LC-MS/MS using an LTQ-Orbitrap XL. Values shown are mean±SEM of normalized spectral counts (NSpC), based on three biological replicates (each replicate consisting of pooled platelets from 4 mice) for each condition. Identified releasate proteins with an average NSpC >5 for at least one sample category are shown. FC reflect the ratio between the average NSpC in samples after antagomiR-21 treatment and after control-antagomiR with a t-test evaluating statistical significance.

Full protein name	Accession ID	Gene ID	MW (kDa)	Control (NSpC)	AntagomiR -21 (NSpC)	P-value	log 2 FC	Human releasate	a-granule (GO:0031091/3)	d-granule (GO:0031089)
14-3-3 protein zeta/delta	1433Z_MOUSE	Ywhaz	28	85.6±12.1	113.5±6.1	0.134	0.41	x		
6-phosphogluconate dehydrogenase, decarboxylating	6PGD_MOUSE	Pgd	53	16.6±8.6	22.5±2.4	0.574	0.43	x		
Alpha-1-antitrypsin 1-1	A1AT1_MOUSE	Serpina1a	46	61.8±19.1	64.4±5.9	0.908	0.06	x	x	
Alpha-2-macroglobulin	A2M_MOUSE	Pzp	166	40.3±34.8	46.8±5.9	0.870	0.22	x	x	
Alpha-actinin-1	ACTN1_MOUSE	Actn1	103	99.9±11.7	87.2±26.9	0.696	-0.20	x	x	
Fructose-bisphosphate aldolase A	ALDOA_MOUSE	Aldoa	39	79.2±10.1	86.1±7.4	0.613	0.12	x	x	
Antithrombin-III	ANT3_MOUSE	Serpinc1	52	5.6±2.3	1.3±1.3	0.187	-2.16			
Annexin A5	ANXA5_MOUSE	Anxa5	36	30.0±7.7	26.7±2.2	0.720	-0.17			
Adenylyl cyclase-associated protein 1	CAP1_MOUSE	Cap1	52	94.4±4.3	97.2±3.1	0.623	0.04	x		
Catalase	CATA_MOUSE	Cat	60	4.5±1.4	7.2±2.3	0.368	0.69	x		
Chloride intracellular channel protein 1	CLIC1_MOUSE	Clic1	27	15.4±3.2	16.3±1.6	0.826	0.08	x		
Cofilin-1	COF1_MOUSE	Cfl1	19	21.2±5.1	16.8±3.9	0.530	-0.34			
Coronin-1A	COR1A_MOUSE	Coro1a	51	84.7±7.0	87.4±9.2	0.829	0.04	x		
Coronin-1C	COR1C_MOUSE	Coro1c	53	7.3±4.4	4.7±2.4	0.630	-0.65			
Extracellular matrix protein 1	ECM1_MOUSE	Ecm1	63	8.4±4.3	0.8±0.8	0.216	-3.48			x
EMILIN-1	EMIL1_MOUSE	Emilin1	108	6.1±3.1	5.4±4.0	0.906	-0.16			
Alpha-enolase	ENOA_MOUSE	Eno1	47	61.8±11.0	69.2±8.5	0.622	0.16	x		
Endoplasmin	ENPL_MOUSE	Hsp90b1	92	24.2±4.5	17.7±8.7	0.554	-0.45	x		
Coagulation factor X	FA10_MOUSE	F10	54	10.4±2.1	6.3±2.7	0.300	-0.72			
Four and a half LIM domains protein 1	FHL1_MOUSE	Fhl1	32	13.1±3.8	5.7±4.7	0.291	-1.19	x		

Supplemental table 4 (continued)

Full protein name	Accession ID	Gene ID	MW (kDa)	Control (NSpC)	AntagomiR -21 (NSpC)	P-value	log 2 FC	Human released	a-granule (GO:00310	d-granule (GO:00310
Fibrinogen alpha chain	FIBA_MOUSE	Fga	87	154.7±44.1	55.4±14.3	0.143	-1.48	x	x	
Fibrinogen beta chain	FIBB_MOUSE	Fgb	55	111.5±35.5	44.2±9.8	0.192	-1.34	x	x	
Fibrinogen gamma chain	FIBG_MOUSE	Fgg	49	110.0±36.5	25.8±8.9	0.141	-2.09	x	x	
Fibronectin	**FINC_MOUSE**	**Fn1**	**273**	**9.4±1.7**	**2.1±1.0**	**0.030**	**-2.18**	**x**	**x**	
Glyceraldehyde-3-phosphate dehydrogenase	G3P_MOUSE	Gapdh	36	24.7±4.6	39.3±15.0	0.435	0.67	x		
Rab GDP dissociation inhibitor beta	GDIB_MOUSE	Gdi2	51	37.3±10.6	46.2±8.3	0.548	0.31	x		
Glia-derived nexin	GDN_MOUSE	Serpine2	44	28.8±10.0	15.7±2.9	0.321	-0.88		x	
Gelsolin	GELS_MOUSE	Gsn	86	38.5±6.4	21.5±11.4	0.280	-0.84	x		
Platelet glycoprotein Ib alpha chain	GP1BA_MOUSE	Gp1ba	80	67.8±7.7	61.2±1.4	0.483	-0.15	x		
Platelet glycoprotein V	GPV_MOUSE	Gp5	63	14.7±5.4	9.4±1.9	0.435	-0.65	x		
78 kDa glucose-regulated protein	GRP78_MOUSE	Hspa5	72	54.6±20.0	78.9±17.0	0.410	0.53	x		
Heparanase	HPSE_MOUSE	Hpse	60	8.6±3.3	4.6±2.4	0.390	-0.91			
Heat shock protein 105 kDa	HS105_MOUSE	Hsph1	96	7.1±3.6	3.5±3.5	0.520	-1.01			
Heat shock 70 kDa protein 4L	HS74L_MOUSE	Hspa4l	94	5.5±2.8	4.8±4.8	0.902	-0.21			
Heat shock protein HSP 90-alpha	HS90A_MOUSE	Hsp90aa1	85	28.3±6.4	19.1±4.2	0.304	-0.57	x		
Heat shock protein HSP 90-beta	HS90B_MOUSE	Hsp90ab1	83	19.9±10.1	3.3±3.3	0.237	-2.61	x		
Heat shock 70 kDa protein 4	HSP74_MOUSE	Hspa4	94	20.7±2.5	20.7±5.5	0.998	0.00			
Heat shock cognate 71 kDa protein	HSP7C_MOUSE	Hspa8	71	90.8±9.2	120.2±7.3	0.069	0.40	x		
Leukocyte elastase inhibitor A	ILEUA_MOUSE	Serpinb1a	43	35.5±8.1	30.8±3.2	0.637	-0.20	x		
Integrin-linked protein kinase	ILK_MOUSE	Ilk	51	18.1±12.6	4.6±4.1	0.402	-1.97			

Supplemental table 4 (continued)

Full protein name	Accession ID	Gene ID	MW (kDa)	Control (NSpC)	AntagomiR -21 (NSpC)	P-value	log 2 FC	Human releasate	a-granule (GO:00310	d-granule (GO:00310
Integrin alpha-IIb	ITA2B_MOUSE	Itga2b	113	6.7±2.4	0.8±0.8	0.127	-3.15	x	x	
Kininogen-1	KNG1_MOUSE	Kng1	73	11.5±3.1	11.8±4.2	0.962	0.03		x	
Pyruvate kinase PKM	KPYM_MOUSE	Pkm	58	53.7±10.7	32.4±0.9	0.183	-0.73	x		
Galectin-related protein	LEGL_MOUSE	Lgalsl	19	8.3±1.0	6.8±0.9	0.332	-0.29			
Latent-transforming growth factor beta-binding protein 1	LTBP1_MOUSE	Ltbp1	187	5.6±3.2	0.0±0.0	n.a.	n.a.	x		
Lysozyme C-2	LYZ2_MOUSE	Lyz2	17	31.2±5.9	26.1±6.9	0.606	-0.26	x		
Beta-parvin	PARVB_MOUSE	Parvb	42	15.7±6.2	5.7±1.0	0.244	-1.46			
Protein disulfide-isomerase A3	PDIA3_MOUSE	Pdia3	57	59.2±2.9	81.4±23.2	0.439	0.46	x		
Protein disulfide-isomerase A4	PDIA4_MOUSE	Pdia4	72	8.0±4.3	7.3±3.9	0.910	-0.13	x		
PDZ and LIM domain protein 1	PDLI1_MOUSE	Pdlim1	36	7.4±0.8	5.5±0.1	0.136	-0.45			
Pleckstrin	PLEK_MOUSE	Plek	40	46.9±8.7	52.4±0.6	0.587	0.16	x		
Platelet factor 4	PLF4_MOUSE	Pf4	11	28.4±12.0	8.8±8.8	0.264	-1.69	x	x	
Plasminogen	PLMN_MOUSE	Plg	91	26.5±6.2	5.5±3.8	0.055	-2.26	x	x	
Plastin-1	PLSI_MOUSE	Pls1	70	8.5±5.8	0.0±0.0	n.a.	n.a.			
Peptidyl-prolyl cis-trans isomerase A	PPIA_MOUSE	Ppia	18	43.1±5.7	42.5±4.9	0.940	-0.02	x		
Peptidyl-prolyl cis-trans isomerase B	PPIB_MOUSE	Ppib	24	20.4±4.4	15.3±6.3	0.542	-0.42	x		
Peroxiredoxin-1	PRDX1_MOUSE	Prdx1	22	13.3±1.8	13.2±4.0	0.985	-0.01			
Peroxiredoxin-6	PRDX6_MOUSE	Prdx6	25	17.3±0.9	17.5±3.2	0.957	0.02	x		
Profilin-1	PROF1_MOUSE	Pfn1	15	69.2±7.4	88.3±14.1	0.318	0.35	x		
Vitamin K-dependent protein S	PROS_MOUSE	Pros1	75	6.9±5.5	0.0±0.0	n.a.	n.a.	x	x	

Supplemental table 4 (continued)

Full protein name	Accession ID	Gene ID	MW (kDa)	Control (NSpC)	AntagomiR -21 (NSpC)	P-value	log 2 FC	Human relevant	a-granule (GO:00310	d-granule (GO:00310
Puromycin-sensitive aminopeptidase	PSA_MOUSE	Npepps	103	8.8±4.1	6.0±4.0	0.644	-0.57	x		
Proteasome subunit alpha type-6	PSA6_MOUSE	Psma6	27	7.7±1.0	6.7±1.2	0.555	-0.20			
Bifunctional purine biosynthesis protein PURH	PUR9_MOUSE	Atic	64	16.7±2.7	14.4±7.2	0.784	-0.22	x		
Sulfhydryl oxidase 1	QSOX1_MOUSE	Qsox1	83	16.8±7.7	6.4±4.8	0.327	-1.40	x	x	
Superoxide dismutase [Cu-Zn]	SODC_MOUSE	Sod1	16	13.2±2.7	18.3±2.5	0.234	0.47			
Serine protease inhibitor A3K	SPA3K_MOUSE	Serpina3k	47	24.0±13.4	24.3±5.4	0.982	0.02		x	
Serine protease inhibitor A3N	SPA3N_MOUSE	Serpina3n	47	5.5±2.8	8.9±4.4	0.556	0.70		x	
Neuronal proto-oncogene tyrosine-protein kinase Src	SRC_MOUSE	Src	61	7.4±0.8	13.0±4.4	0.329	0.82			
Serglycin	SRGN_MOUSE	Srgn	17	16.8±5.0	3.3±3.3	0.098	-2.36		x	
Transgelin-2	TAGL2_MOUSE	Tagln2	22	32.9±3.6	34.3±3.6	0.796	0.06	x		
Transitional endoplasmic reticulum ATPase	TERA_MOUSE	Vcp	89	47.1±5.3	41.7±9.6	0.654	-0.18	x		
Transforming growth factor beta-1	**TGFB1_MOUSE**	**Tgfb1**	**44**	**9.2±2.2**	**1.3±1.3**	**0.047**	**-2.86**	**x**		**x**
Triosephosphate isomerase	TPIS_MOUSE	Tpi1	32	22.0±3.0	22.5±1.1	0.901	0.03	x		
Thrombospondin-1	TSP1_MOUSE	Thbs1	130	421.9±54.4	289.4±31.2	0.120	-0.54	x	x	
Thymosin beta-4	TYB4_MOUSE	Tmsb4x	6	6.5±0.6	3.4±1.7	0.204	-0.94		x	
Fermitin family homolog 3	URP2_MOUSE	Fermt3	76	19.1±10.6	0.0±0.0	n.a.	n.a.		x	
von Willebrand factor	**VWF_MOUSE**	**Vwf**	**309**	**22.4±4.9**	**3.5±3.5**	**0.040**	**-2.67**	**x**	**x**	
WD repeat-containing protein 1	WDR1_MOUSE	Wdr1	66	66.8±5.7	66.7±3.5	0.991	0.00	x		
Zyxin	ZYX_MOUSE	Zyx	61	7.9±2.3	3.7±0.4	0.209	-1.08			

Supplemental table 5. Predicted targets of miR-21 in the mouse genome using miRWALK 2.0. The miRWALK score indicates the number of algorithms that predicted targeting miR-21 to occur. Included algorithms were miRWalk, Microt4, miRanda, mirbridge, miRDB, miRMap, miRNAMap, Pictar2, PITA, RNA22, RNAhybrid and Targetscan. As the full list includes 18332 predicted targets, the top-237 predicted targets are shown, complemented with the predicted targets that were annotated as experimentally validated targets in the amiGO Gene Ontology (GO) database. This indicates the high false-positive and false-negative rate, given that the majority of predicted targets have thus far not been validated, whilst most validated targets were not predicted by most algorithms (including the newly identified miR-21 target *Was*).

Rank	Gene	EntrezID	miRWALK score	Validated target (GO)
1	Tgfbi	21810	10	
2	**Reck**	**53614**	**10**	**X**
3	Aspn	66695	10	
4	Peli1	67245	10	
5	Wwp1	107568	10	
6	Zfp704	170753	10	
7	Glcci1	170772	10	
8	Chic1	12212	9	
9	Dvl2	13543	9	
10	Eif1a	13664	9	
11	Fem1b	14155	9	
12	Fhl4	14202	9	
13	Fut9	14348	9	
14	Hnf4a	15378	9	
15	**Smad7**	**17131**	**9**	**X**
16	Mybl1	17864	9	
17	Nfatc3	18021	9	
18	**Nfib**	**18028**	**9**	**X**
19	Pcm1	18536	9	
20	**Pdcd4**	**18569**	**9**	**X**
21	Prkci	18759	9	
22	Plxna2	18845	9	
23	Uimc1	20184	9	
24	Ccl22	20299	9	
25	Sim1	20464	9	
26	Ski	20481	9	
27	Stag2	20843	9	
28	Bhlhe40	20893	9	
29	Tbx2	21385	9	
30	Tnks	21951	9	
31	Vcl	22330	9	
32	Wisp1	22402	9	
33	Xk	22439	9	
34	Klf6	23849	9	
35	**Pcbp1**	**23983**	**9**	**X**
36	Sgcb	24051	9	
37	Slc35a1	24060	9	
38	**Spry1**	**24063**	**9**	**X**
39	Trp53bp1	27223	9	
40	Pcdh12	53601	9	
41	Zranb2	53861	9	
42	Rab11a	53869	9	
43	Socs5	56468	9	
44	Plag1	56711	9	
45	Rqcd1	58184	9	
46	Rsad2	58185	9	
47	Pvrl3	58998	9	
48	Il21	60505	9	
49	Zfp110	65020	9	
50	Ube2d3	66105	9	

Rank	Gene	EntrezID	miRWALK score	Validated target (GO)
51	Cdip1	66626	9	
52	Gid4	66771	9	
53	Pbrm1	66923	9	
54	Dnajb4	67035	9	
55	Smc6	67241	9	
56	Pigm	67556	9	
57	Elf2	69257	9	
58	Naa30	70646	9	
59	Zcchc8	70650	9	
60	Tmem68	72098	9	
61	Seh1l	72124	9	
62	Pan3	72587	9	
63	Appl1	72993	9	
64	Cpne4	74020	9	
65	Spata9	75571	9	
66	Mynn	80732	9	
67	Slmap	83997	9	
68	Aff4	93736	9	
69	Trim33	94093	9	
70	Srl	106393	9	
71	**Ccdc88a**	**108686**	**9**	**X**
72	Acat1	110446	9	
73	Sec63	140740	9	
74	Slc25a36	192287	9	
75	Cpeb3	208922	9	
76	Pank3	211347	9	
77	Rhbdd2	215160	9	
78	Alx1	216285	9	
79	Cep68	216543	9	
80	Tmem106a	217203	9	
81	Fgd4	224014	9	
82	Clic5	224796	9	
83	Fbxo11	225055	9	
84	Galnt12	230145	9	
85	Slc6a1	232333	9	
86	Klhl42	232539	9	
87	Sc5d	235293	9	
88	Fam63b	235461	9	
89	Akap6	238161	9	
90	Zfp367	238673	9	
91	Wdr78	242584	9	
92	Tmprss11f	243083	9	
93	Ppp1r3b	244416	9	
94	Dpy19l1	244745	9	
95	Pcmtd2	245867	9	
96	Caskin1	268932	9	
97	Cntn4	269784	9	
98	Magee2	272790	9	
99	Eml5	319670	9	
100	Tmem229a	319832	9	

Supplemental table 5 (continued)

Rank	Gene	EntrezID	miRWALK score	Validated target (GO)
101	Zdhhc17	320150	9	
102	Lrrc58	320184	9	
103	Fam154b	330577	9	
104	Dgkk	331374	9	
105	Fa2h	338521	9	
106	Atxn7l3b	382423	9	
107	Adk	11534	8	
108	Adra2b	11552	8	
109	Alx4	11695	8	
110	Aqp4	11829	8	
111	Opn1sw	12057	8	
112	Hrk	12123	8	
113	Bmpr1b	12167	8	
114	Zfp36l2	12193	8	
115	Cacna1e	12290	8	
116	Cacybp	12301	8	
117	Camk4	12326	8	
118	Cbx4	12418	8	
119	Ms4a1	12482	8	
120	Cd2ap	12488	8	
121	Entpd6	12497	8	
122	Arhgap31	12549	8	
123	Cfl2	12632	8	
124	Cnr1	12801	8	
125	Cr2	12902	8	
126	Dazl	13164	8	
127	Dsg1a	13510	8	
128	Epyc	13516	8	
129	Mapre1	13589	8	
130	Edar	13608	8	
131	Edil3	13612	8	
132	Egf	13645	8	
133	Ehd1	13660	8	
134	Fasl	14103	8	
135	Srsf10	14105	8	
136	Gnb4	14696	8	
137	Nr4a1	15370	8	
138	**Hpgd**	**15446**	**8**	**X**
139	Dnaja1	15502	8	
140	Htr4	15562	8	
141	Il2ra	16184	8	
142	Itgav	16410	8	
143	Kcna1	16485	8	
144	Lats1	16798	8	
145	Ltbp2	16997	8	
146	Mbd4	17193	8	
147	Cxcl9	17329	8	
148	Mknk1	17346	8	
149	Nedd4	17999	8	
150	Notch2	18129	8	

Rank	Gene	EntrezID	miRWALK score	Validated target (GO)
151	Ntf3	18205	8	
153	Dusp8	18218	8	
154	Ovol1	18426	8	
155	P4ha1	18451	8	
156	Pdha1	18597	8	
157	Padi2	18600	8	
158	Per2	18627	8	
159	Pip4k2a	18718	8	
160	Pitpna	18738	8	
161	Pitx2	18741	8	
162	Plp1	18823	8	
163	Pnp	18950	8	
164	**Rasgrp1**	**19419**	**8**	**X**
165	Rfx3	19726	8	
166	Rlim	19820	8	
167	Scnn1g	20278	8	
168	Ccl1	20290	8	
169	**Ccl20**	**20297**	**8**	**X**
170	Ccl3	20302	8	
171	Sel1l	20338	8	
172	Sema3a	20346	8	
173	Sema3e	20349	8	
174	Sema5a	20356	8	
175	Sftpa1	20387	8	
176	Slc34a2	20531	8	
177	Snn	20621	8	
178	Sntb2	20650	8	
179	Sox2	20674	8	
180	**Sox5**	**20678**	**8**	**X**
181	Sox6	20679	8	
182	Srpk2	20817	8	
183	Stat1	20846	8	
184	Stat3	20848	8	
185	Stc1	20855	8	
186	Cntn2	21367	8	
187	Tsc22d1	21807	8	
188	**Tgfbr2**	**21813**	**8**	**X**
189	Thrb	21834	8	
190	Tnfaip3	21929	8	
191	Tssk2	22115	8	
192	Ubr1	22222	8	
193	Vdr	22337	8	
194	**Vhl**	**22346**	**8**	**X**
195	Zik1	22775	8	
196	Bace1	23821	8	
197	Xcr1	23832	8	
198	Papss2	23972	8	
199	Ptpn21	24000	8	
200	**Spry2**	**24064**	**8**	**X**
201	**Map2k3**	**26397**	**8**	**X**

Supplemental table 5 (continued)

Rank	Gene	EntrezID	miRWALK score	Validated target (GO)
202	Map3k1	26401	8	
203	Map3k7	26409	8	
204	Mapk10	26414	8	
205	B3galt1	26877	8	
206	Mprip	26936	8	
207	Eif2ak4	27103	8	
208	Skp2	27401	8	
209	Peg12	27412	8	
210	Fam3c	27999	8	
211	Slco1a4	28250	8	
212	Postn	50706	8	
213	Fubp1	51886	8	
214	Rnf24	51902	8	
215	Kcnk6	52150	8	
216	Gpr123	52389	8	
217	Suz12	52615	8	
218	Pnrc2	52830	8	
219	Vamp4	53330	8	
220	Hpgds	54486	8	
221	Dfna5	54722	8	
222	Fmo2	55990	8	
223	Metap2	56307	8	
224	Ankrd49	56503	8	
225	Kcnd3	56543	8	
226	Gsk3b	56637	8	
227	Mbnl1	56758	8	
228	Dkk2	56811	8	
229	**Jmy**	**57748**	**8**	**X**
230	Kcne4	57814	8	
231	Prokr1	58182	8	
232	Trpm7	58800	8	
233	Xpo7	65246	8	
234	Tipin	66131	8	
235	Uggt2	66435	8	
236	Cmc2	66531	8	
237	Tbc1d15	66687	8	
242	**Mtap**	**66902**	**8**	**X**
249	**Rffl**	**67338**	**8**	**X**
445	**Btg2**	**12227**	**7**	**X**
452	**Cdc25a**	**12530**	**7**	**X**
494	**Jag1**	**16449**	**7**	**X**
503	**Mef2c**	**17260**	**7**	**X**
575	**Tiam1**	**21844**	**7**	**X**
577	**Timp3**	**21859**	**7**	**X**
1281	**Ccdc93**	**70829**	**6**	**X**
1653	**Col4a1**	**12826**	**5**	**X**
1728	**Lrrfip1**	**16978**	**5**	**X**
1771	**Ppara**	**19013**	**5**	**X**
1823	**Tgfbr3**	**21814**	**5**	**X**
2156	**Dock9**	**105445**	**5**	**X**

Rank	Gene	EntrezID	miRWALK score	Validated target (GO)
2477	**Adam22**	**11496**	**4**	**X**
2499	**Bmpr2**	**12168**	**4**	**X**
2771	**Sp1**	**20683**	**4**	**X**
2853	**Plod3**	**26433**	**4**	**X**
3052	**Rtn4**	**68585**	**4**	**X**
3059	**Dock5**	**68813**	**4**	**X**
3935	**Cdk2ap1**	**13445**	**3**	**X**
4004	**Gdf5**	**14563**	**3**	**X**
4112	**Marcks**	**17118**	**3**	**X**
4160	**Myd88**	**17874**	**3**	**X**
4254	**Pten**	**19211**	**3**	**X**
4695	**Dusp10**	**63953**	**3**	**X**
4750	**Spryd4**	**66701**	**3**	**X**
4832	**Derl1**	**67819**	**3**	**X**
5553	**Acsl6**	**216739**	**3**	**X**
5753	**Dock4**	**238130**	**3**	**X**
6161	**Apaf1**	**11783**	**2**	**X**
6238	**Cacna1c**	**12288**	**2**	**X**
6687	**Hnrnpk**	**15387**	**2**	**X**
6722	**Icam1**	**15894**	**2**	**X**
6746	**Irak1**	**16179**	**2**	**X**
7176	**Rxra**	**20181**	**2**	**X**
7237	**Smarca4**	**20586**	**2**	**X**
7342	**Tnf**	**21926**	**2**	**X**
7344	**Tnfrsf10b**	**21933**	**2**	**X**
7451	**Arih2**	**23807**	**2**	**X**
9528	**Mlxip**	**208104**	**2**	**X**
9569	**Dock10**	**210293**	**2**	**X**
10413	**Dock6**	**319899**	**2**	**X**
10509	**Dock1**	**330662**	**2**	**X**
10993	**Cacnb2**	**12296**	**1**	**X**
11202	**Cyp27b1**	**13115**	**1**	**X**
11211	**Daxx**	**13163**	**1**	**X**
11687	**Il1b**	**16176**	**1**	**X**
11964	**Msh6**	**17688**	**1**	**X**
12193	**Plat**	**18791**	**1**	**X**
12445	**Glg1**	**20340**	**1**	**X**
12535	**Sod3**	**20657**	**1**	**X**
12712	**Tpm1**	**22003**	**1**	**X**
12817	**Was**	**22376**	**1**	**X**
13247	**Ncapg**	**54392**	**1**	**X**
13957	**Dock7**	**67299**	**1**	**X**
14441	**Basp1**	**70350**	**1**	**X**
15145	**Dock11**	**75974**	**1**	**X**
15390	**Parp9**	**80285**	**1**	**X**
15732	**Ppif**	**105675**	**1**	**X**
15740	**Topors**	**106021**	**1**	**X**
16631	**Pias3**	**229615**	**1**	**X**
16683	**Cep104**	**230967**	**1**	**X**
17330	**Sybu**	**319613**	**1**	**X**

Curriculum vitae

Temo Barwari

Education

2014 - current **Interdisciplinary PhD in cardiovascular research**
British Heart Foundation (BHF) Centre of Research Excellence at King's College London

2010 **Arabic language**
Damascus University, Damascus and Saifi Institute, Beirut
▪ Levantine Arabic and Modern Standard Arabic

2005 - 2013 **Doctor of Medicine**
University of Amsterdam/Academic Medical Centre, Amsterdam
▪ Grade: 8.8/10 (*cum laude*)
▪ Clinical elective at the cardiology department of the Bahrain Defence Force and Royal Medical Services Hospital
▪ Honours Programme, 2006-2010: clinical research involvement, teaching and clinical shadowing
▪ Extracurricular modules: history and philosophy of science, psychiatry and Middle Eastern politics

2003 - 2004 **University of Leiden Advanced Pre-University Programme for Top students (LAPP-Top)**

Work experience

2017 - current **Postdoctoral research associate**
BHF Centre of Research Excellence at King's College London

2014 (3 months) **Volunteer medical officer in aid of Syrian refugees**
Syrian refugee camp 'Domiz', Kurdistan Region in Iraq

2010 - 2013 **Instructor in anatomy, embryology and physical examination**
Department of Anatomy, Embryology and Physiology, Academic Medical Centre, Amsterdam

2007 - 2010 **Clinical research assistant**
Departments of Internal Medicine (AMC) and Intensive Care Medicine (OLVG Hospital), Amsterdam

Further academic experience

2017 (4 months) **Postgraduate research consultant**
Computer Science and Informatics departments, King's College London

2012 - 2013 **Ombudsman in the liaison committee for the faculty of medicine ('CoRaad')**

2012 - current **Scientific journal reviewer**
▪ 'Cardiovascular Research'; 'Diabetes, Obesity & Metabolism'

Volunteering

- **Mentor for PADILEIA**, supporting Syrian refugees during English language courses, offered by King's College London through FutureLearn.
- **Instructor for cardiopulmonary resuscitation and basic life support** on behalf of the BHF.

Scholarships & Awards

- **Young Investigator Award** at Eurothrombosis, October 2018 in Barcelona, Spain, awarded by the European Society of Cardiology working group on Thrombosis
- **New Investigator Travel Award**, American Heart Association (AHA) Basic Cardiovascular Science (BCVS) Council, July 2018, San Antonio (TX), USA
- **Runner-up for best moderated poster presentation** at British Cardiovascular Society/British Atherosclerosis Society joint meeting, June 2018, Manchester
- **International Travel Grant**, AHA Council on Functional Genomics and Translational Biology (FGTB), November 2017, Anaheim (CA), USA
- **Best Poster Presentation Prize** by a first-year PhD student, Annual BHF Centre Postgraduate Symposium, May 2015, London
- **Dr I. Snapper Award**, Ruitinga van Swieten Foundation; awarded for contribution to research in the field of internal medicine, October 2010, Amsterdam
- **AMC Educational Scholarship**; awarded for presentation of a research project on health anxiety in medical students, January 2007, Amsterdam

Publications

Publications during this thesis

1. **Inhibition of Pro-Fibrotic MicroRNA-21 Affects Platelets and their Releasate.**
   Barwari T, Eminaga S, Mayr U, Lu R, Armstrong PC, Chan MV, Sahraei M, Fernández-Fuertes M, Moreau T, Barallobre-Barreiro J, Lynch M, Yin X, Schulte C, Baig F, Pechlaner R, Langley SR, Zampetaki A, Santer P, Weger M, Plasenzotti R, Schosserer M, Grillari J, Kiechl S, Willeit J, Shah AM, Ghevaert C, Warner TD, Fernández-Hernando C, Suárez Y, Mayr M. JCI Insight. 2018;3(21):e123335.
2. **The characterisation of circulating biomarkers before and after Cardiac Resynchronization Therapy and their role in predicting CRT response.**
   McAloon CJ, **Barwari T**, Hu J, Hamborg T, Nevill A, Hyndman S, Ansell V, Musa A, Jones J, Goodby J, Banerjee P, O'Hare P, Mayr M, Randeva H, Osman F. Open Heart. 2018;5(2):e000899.
3. **Role of ADAMTS-5 in Aortic Dilatation and Extracellular Matrix Remodeling.**
   Fava M, Barallobre-Barreiro J, Mayr U, Lu R, Didangelos A, Baig F, Lynch M, Catibog N, Joshi A, **Barwari T**, Yin X, Jahangiri M, Mayr M. Arterioscler Thromb Vasc Biol. 2018;38(7):1537-1548.
4. **MicroRNA-21 and the Vulnerability of Atherosclerotic Plaques.**
   Barwari T, Rienks M, Mayr M. Mol Ther. 2018;26(4):938-940.
5. **Reply: The Complex miRNAs-p53 Signaling Network in Cardiovascular Disease.**
   Barwari T, Joshi A, Mayr M. J Am Coll Cardiol. 2017;69(16):2100.
6. **Extracellular matrix proteomics identifies molecular signature of symptomatic carotid plaques.**
   Langley SR, Willeit K, Didangelos A, Matic LP, Skroblin P, Barallobre-Barreiro J, Lengquist M, Rungger G, Kapustin A, Kedenko L, Molenaar C, Lu R, **Barwari T**, Suna G, Yin X, Iglseder B, Paulweber B, Willeit P, Shalhoub J, Pasterkamp G, Davies AH, Monaco C, Hedin U, Shanahan CM, Willeit J, Kiechl S, Mayr M. J Clin Invest. 2017;127(4):1546-1560.
7. **Circulating MicroRNA-122 Is Associated With the Risk of New-Onset Metabolic Syndrome and Type 2 Diabetes.**
   Willeit P, Skroblin P, Moschen AR, Yin X, Kaudewitz D, Zampetaki A, **Barwari T**, Whitehead M, Ramírez CM, Goedeke L, Rotllan N, Bonora E, Hughes AD, Santer P, Fernández-Hernando C, Tilg H, Willeit J, Kiechl S, Mayr M. Diabetes**.** 2017;66(2):347-357.

8. **MicroRNA Biomarkers and Platelet Reactivity: The Clot Thickens.**
   Sunderland N, Skroblin P, **Barwari T**, Huntley RP, Lu R, Joshi A, Lovering RC, Mayr M. Circ Res. 2017;120(2):418-435.
9. **MicroRNAs in Cardiovascular Disease.**
   Barwari T, Joshi A, Mayr M. J Am Coll Cardiol. 2016;68(23):2577-2584.
10. **Extracellular matrix remodelling in response to venous hypertension: proteomics of human varicose veins.**
    Barallobre-Barreiro J, Oklu R, Lynch M, Fava M, Baig F, Yin X, **Barwari T**, Potier DN, Albadawi H, Jahangiri M, Porter KE, Watkins MT, Misra S, Stoughton J, Mayr M. Cardiovasc Res. 2016;110(3):419-430**.**
11. **When Sweet Turns Salty: Glucose-Induced Suppression of Atrial Natriuretic Peptide by MicroRNA-425.**
    Barwari T, Skroblin P, Mayr M. J Am Coll Cardiol. 2016;67(7):813-6.
12. ***Association of MicroRNAs and YRNAs With Platelet Function.***
    Kaudewitz D, Skroblin P, Bender LH, **Barwari T**, Willeit P, Pechlaner R, Sunderland NP, Willeit K, Morton AC, Armstrong PC, Chan MV, Lu R, Yin X, Gracio F, Dudek K, Langley SR, Zampetaki A, de Rinaldis E, Ye S, Warner TD, Saxena A, Kiechl S, Storey RF, Mayr M. Circ Res. 2016;118(3):420-432.

Publications from previous research

1. **Microcirculation and its relation to continuous subcutaneous glucose sensor accuracy in cardiac surgery patients in the intensive care unit.**
   Siegelaar SE, **Barwari T**, Hermanides J, van der Voort PH, Hoekstra JB, DeVries JH. J Thorac Cardiovasc Surg. 2013;146(5):1283-9.
2. **Accuracy and reliability of continuous glucose monitoring in the intensive care unit: a head-to-head comparison of two subcutaneous glucose sensors in cardiac surgery patients.**
   Siegelaar SE, **Barwari T**, Hermanides J, Stooker W, van der Voort PH, DeVries JH. Diabetes Care. 2011;34(3):e31.
3. **No relevant relationship between glucose variability and oxidative stress in well-regulated type 2 diabetes patients.**
   Siegelaar SE, **Barwari T**, Kulik W, Hoekstra JB, DeVries JH. J Diabetes Sci Technol. 2011;5(1):86-92.
4. **Cathepsin L, target in cancer treatment?**
   Lankelma JM, Voorend DM, **Barwari T**, Koetsveld J, Van der Spek AH, De Porto AP, Van Rooijen G, Van Noorden CJ. Life Sci. 2010;86(7-8):225-33.

Presentations at international scientific meetings

1. '**MicroRNA-21 Regulates TGF-β1 Release from Platelets'**
   - Poster presentation at the British Heart Foundation / Journal of Clinical Investigation meeting 'Advances in Heart Failure', London, January 2018
   - Poster presentation at American Heart Association Scientific Sessions in Anaheim (USA) 2017 and at AHA Basic Cardiovascular Sciences 2018 in San Antonio (USA).
   - Oral presentation and poster at international workshop 'Non-Coding RNA-Mediated Metabolic Regulation in Health and Disease' in Baeza (Spain), 2017
2. **'MicroRNA and Cardiovascular Disease: Biomarkers or Therapeutic Targets?'**
   - Presentation at Science Xpression meeting, La Coruña (Spain), 2017
3. **'Associations of plasma microRNAs with platelet proteins and platelet function'**
   - Poster at European Society of Cardiology annual meeting in London, 2015

Appendix

1. Collage of the Bruneck Study 2015 evaluation.

2. Published article: **Barwari T**, Joshi A, Mayr M. MicroRNAs in Cardiovascular Disease. *J Am Coll Cardiol*. 2016;68(23):2577–2584.

3. Published article: Sunderland N, Skroblin P, **Barwari T**, Huntley RP, Lu R, Joshi A, Lovering RC, Mayr M. MicroRNA Biomarkers and Platelet Reactivity: The Clot Thickens. *Circ Res*. 2017;120(2):418–435.

4. Published article: **Barwari T**, Rienks M, Mayr M. MicroRNA-21 and the Vulnerability of Atherosclerotic Plaques. *Mol Ther*. 2018;26(4):938-940.

5. Published article: **Barwari T**, Eminaga S, Mayr U, Lu R, Armstrong PC, Chan MV, Sahraei M, Fernández-Fuertes M, Moreau T, Barallobre-Barreiro J, Lynch M, Yin X, Schulte C, Baig F, Pechlaner R, Langley SR, Zampetaki A, Santer P, Weger M, Plasenzotti R, Schosserer M, Grillari J, Kiechl S, Willeit J, Shah AM, Ghevaert C, Warner TD, Fernández-Hernando C, Suárez Y, Mayr M. Inhibition of Pro-Fibrotic MicroRNA-21 Affects Platelets and their Releasate. *JCI Insight. 2018;3(21):e123335.*

Appendix 1: Bruneck Study 2015

For the year 2015 follow-up of the Bruneck Study, we transported a 'mobile laboratory' from King's College London to the north of Italy. In a bathroom of Bruneck Hospital, a research laboratory was set up for sampling in 330 participants as described in this thesis.

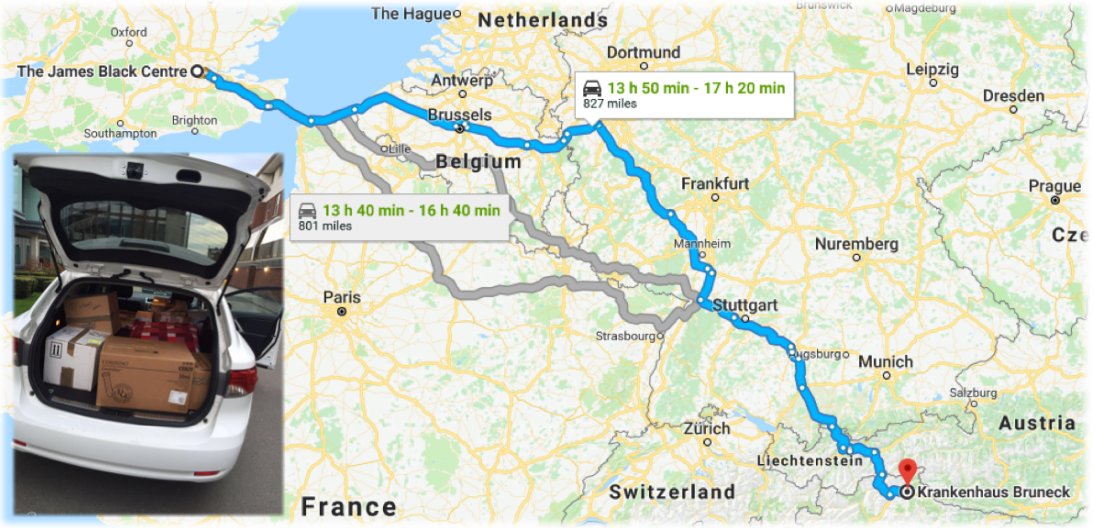

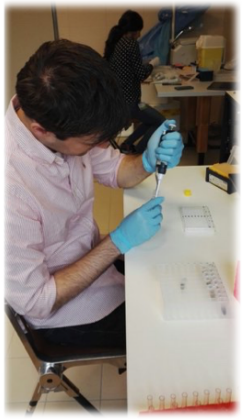

Appendix 2

Published article:

MicroRNAs in Cardiovascular Disease.

Barwari T, Joshi A, Mayr M.

J Am Coll Cardiol. 2016;68(23):2577–2584.

Accepted for publication: 16 September 2016

JOURNAL OF THE AMERICAN COLLEGE OF CARDIOLOGY
© 2016 BY THE AMERICAN COLLEGE OF CARDIOLOGY FOUNDATION
PUBLISHED BY ELSEVIER

VOL. 68, NO. 23, 2016
ISSN 0735-1097/$36.00
http://dx.doi.org/10.1016/j.jacc.2016.09.945

REVIEW TOPIC OF THE WEEK

MicroRNAs in Cardiovascular Disease

Temo Barwari, MD, Abhishek Joshi, BA, BMBCh, Manuel Mayr, MD, PhD

ABSTRACT

Micro-ribonucleic acids (miRNAs) are in the spotlight as post-transcriptional regulators of gene expression. More than 1,000 miRNAs are encoded in the human genome. In this review, we provide an introduction to miRNA biology and research methodology, and highlight advances in cardiovascular research to date. This includes the potential of miRNAs as therapeutic targets in cardiac and vascular disease, and their use as novel biomarkers. Although some miRNA therapies are already undergoing clinical evaluation, we stress the importance of integrating current knowledge of miRNA biology into a systemic context. Discovery studies focus on miRNA effects within one specific organ, whereas the expression of most miRNAs is not restricted to a single tissue. Because most miRNA-based therapies act systemically, this may preclude widespread clinical use. The development of more targeted interventions will bolster well-informed clinical applications, increasing the chances of success and minimizing the risk of setbacks for miRNA-based therapeutics. (J Am Coll Cardiol 2016;68:2577–84) © 2016 by the American College of Cardiology Foundation.

Only 1% of the human genome codes for genes that function in protein synthesis (1). The remaining 99% of deoxyribonucleic acid (DNA) was initially considered to be junk. It is now recognized that the majority of the genome may have biochemical functions, representing regulatory, noncoding ribonucleic acid (RNA). Several subcategories of noncoding RNAs exist, in particular, long noncoding RNAs and small noncoding RNAs. Among the latter, microRNAs (miRNAs/miRs) have thus far attracted most attention since their discovery in *Caenorhabditis elegans* (2). MiRNAs affect the production of proteins by interacting with transcribed messenger RNAs (mRNAs), thus silencing the expression of genes. Here, we aim to provide an overview of miRNA biology for clinicians, discussing their therapeutic and diagnostic potential, as well as their limitations.

BASIC BIOLOGY OF miRNAs

MiRNAs are short (~22 nucleotides), noncoding RNA molecules. They exert their function via the seed region, a sequence of 6 to 8 nucleotides that binds to messenger ribonucleic acid (mRNA), the so-called miRNA targets (3). MiRNA synthesis and silencing have both been extensively reviewed recently (4,5). The key biological concepts are summarized in the **Central Illustration**. Initially, a precursor transcript is produced and then forms double-stranded RNA. Later, the miRNA duplex undergoes unwinding, whereby only a single strand, the so-called guide strand, which is usually the functional unit, is loaded in the RNA-induced silencing complex (RISC). The other strand or passenger strand is often degraded, but may also function as a mature miRNA (6). In the RISC, the miRNA binds to its target mRNA, preventing its translation into a protein. Single miRNAs suppress more than 1 gene, and miRNAs with similar seed regions may suppress a similar, but nonidentical, set of genes, and to differing degrees. Gene suppression is usually partial, rather than total, and a single gene can have binding sites for multiple miRNAs. This organizational complexity, illustrated by a high false-positive rate of target prediction

Listen to this manuscript's audio summary by *JACC* Editor-in-Chief Dr. Valentin Fuster.

From the King's British Heart Foundation Centre, King's College London, London, United Kingdom. Dr. Barwari is an Interdisciplinary PhD student funded by the British Heart Foundation (BHF). Dr. Joshi has been awarded a BHF Clinical Research Training Fellowship. Dr. Mayr is a BHF Senior Research Fellow (FS/13/2/29892) and supported by the Fondation Leducq (MIRVAD; 13 CVD 02) and the NIHR Biomedical Research Center based at Guy's and St. Thomas' National Health Service Foundation Trust and King's College London, in partnership with King's College Hospital. King's College London and Prof. Mayr hold patents on microRNA biomarkers. All other authors have reported that they have no relationships relevant to the contents of this paper to disclose.

Manuscript received July 18, 2016; revised manuscript received September 12, 2016, accepted September 13, 2016.

ABBREVIATIONS AND ACRONYMS

anti-miRs = inhibitors of miRNAs

CVD = cardiovascular disease

ECM = extracellular matrix

MHC = myosin heavy chain

MI = myocardial infarction

miRNA/miR = micro-ribonucleic acid

mRNA = messenger ribonucleic acid

RISC = ribonucleic acid-induced silencing complex

SMC = smooth muscle cell

algorithms (7), presents challenges in both understanding the functions of miRNAs and manipulating their effects.

MEASUREMENT OF miRNAs

miRNAs are relatively stable, and can be reliably measured in tissues, as well as in biofluids (8). Several techniques have been developed to identify and quantify miRNAs. Benefits and disadvantages of different techniques have been summarized previously elsewhere (8). Here, we briefly discuss the most commonly used methods.

Real-time quantitative polymerase chain reaction has been the cornerstone for miRNA quantification and remains the most reliable technique for quantitative comparison of miRNA expression levels. This technique uses predefined primers to amplify and measure individual miRNAs in a sample. Microarrays use hybridization of miRNAs to specific primers, trading less accurate quantification for higher throughput and lower cost, and measuring hundreds of miRNAs in parallel. Because both of these techniques rely on predefined primer sequences, they are not able to discover previously uncharacterized miRNAs.

RNA sequencing techniques provide "hypothesis-free" identification of RNA species, allowing the discovery of new miRNAs and quantitative analysis of a comprehensive miRNA transcriptome. The use of computational solutions to resolve reads into miRNAs suffers from the risk of reporting putative sequences that do not have real-world correlates (9).

Without added spike-ins and standard curves, all techniques rely on relative rather than absolute quantification, meaning that differences in miRNAs are presented as a "fold change" between paired samples, and not as an absolute unit, requiring information on the context of abundance. Experimental work must show downstream effects of miRNA changes as readout for miRNA function, specifically by comparing the profiles of multiple miRNAs with differential expression of target proteins. Ideally, the miRNA/mRNA duplexes in the RISC are analyzed to prove direct interactions.

THERAPEUTIC MANIPULATION OF miRNAs

The central action of miRNAs is to suppress protein expression through binding and silencing specific target mRNAs, which, in turn, reduces protein synthesis. Therefore, miRNAs offer a tantalizing mechanism for manipulating protein synthesis; in most cases, overexpression of a miRNA will suppress its direct targets, whereas inhibiting an endogenous miRNA will de-repress their expression.

Unmodified RNA strands are degraded upon administration; thus, miRNA therapeutics require either efficient methods of cell type-specific delivery or modifications that enhance stability but preserve miRNA function. For now, clinical studies with miRNA therapeutics mainly use inhibitors of miRNAs (anti-miRs). Anti-miRs are synthetic single strands of RNA, consisting of complementary nucleotides to an endogenous miRNA. Various structural modifications have been designed to increase their half-life in the circulation, bypass degradation in tissues and enhance intracellular delivery (10). Cardiotropic adeno-associated viruses achieve efficient cardiomyocyte-specific miRNA delivery (11). The translational potential of adeno-associated virus-mediated oligonucleotide delivery has been reviewed elsewhere (12). Currently, overexpressing a miRNA is generally considered less safe than inhibiting an endogenous miRNA.

Miravirsen is an anti-miR targeting miR-122 for treatment of hepatitis C (13), which has completed a multicenter phase 2a trial (14) and is currently in a phase 2b trial. The choice of miR-122 as the first therapeutic target highlights the challenges when targeting cardiovascular disease (CVD). First, miR-122 shows exquisite tissue specificity, whereas most miRNAs identified as treatment targets for CVD are ubiquitously expressed, raising concerns for off-target effects. Second, anti-miRs predominantly accumulate in the liver and kidneys, circumventing the need for tissue-specific targeting (13). The latter is further illustrated by the evaluation of anti-miR-21 as a therapy for Alport nephropathy (15). These ongoing clinical trials will provide more insight into the practical use of miRNA therapeutics.

Targeting the heart or vasculature with systemic anti-miRs would require significantly higher dosing, and efficiency may be low. Animal models have shown nephrotoxicity at higher doses of some anti-miRs, although the clinical trial of Miravirsen did not find evidence for renal injury in humans (14). The human immune system has evolved to detect viral RNA. Toll-like receptors recognize both single- and double-stranded RNA (16). High doses of synthetic oligonucleotides may elicit an immune response that could compromise efficacy and safety. Thus, cardiovascular applications will require solutions for local or cell-type-specific delivery, and clinically detectable, reliable readouts to monitor successful target engagement.

miRNAs IN HEART FAILURE

At the cellular level, heart failure is caused by cardiomyocyte dysfunction and fibrosis due to accumulation of extracellular matrix (ECM). These processes remain almost entirely untreated by standard heart failure treatment regimens.

miR-133 is highly abundant in cardiomyocytes, but is reduced in animal models of hypertrophy and in patients with hypertrophic cardiomyopathy (17). In vitro and in vivo studies showed increased hypertrophy upon miR-133 inhibition, and preserved cardiac function upon miR-133 overexpression. Targeting of the beta-1 adrenergic receptor pathway, central to the progression and treatment of heart failure, was implicated as the underlying mechanism (18). In addition to the heart, miR-133 is also present in skeletal muscle, albeit at lower levels than in cardiomyocytes. Here, miR-133 inhibition again increases responsiveness to adrenergic stimuli and promotes differentiation to brown fat tissue (19). miR-133 manipulation also seems to affect the cardiac action potential (20).

MiR-1 is part of the same cluster as miR-133 and shares its abundance, as well as its lower expression in heart failure patients (21). Both increased (22) and reduced (23) expression of miR-1 lead to electrophysiological abnormalities. Interestingly, miR-1 targets insulin-like growth factor-1, which itself represses processing of the pre-miR-1 transcript (21). The insulin-like growth factor-1 pathway is an important contributor to cardiac hypertrophy and arrhythmias, and increasing miR-1 levels seems to improve cardiac function (24).

MiR-208 is also highly enriched in cardiomyocytes, and regulates the balance between the α- and β-myosin heavy chains (MHC). Induction of the β-MHC isotype is a known maladaptive response to cardiac stress and reduces contractility (25). MiR-208 knockout mice, and rats treated systemically with anti-miR-208, had preserved balance between both MHC isotypes in response to experimental cardiac stress, with better cardiac function (26). MiR-208 inhibition has therefore been suggested as a protective treatment in heart failure. However, β-MHC expression is not altered in normal hearts of miR-208 knockout mice, indicating that effects of this miRNA are either dependent on disease context or subject to parallel controls (27). Furthermore, recent deep sequencing data from human hearts suggest that miR-208 expression is relatively low compared with other cardiac miRNAs, such as miR-1 and miR-133 (28). Preclinical trials using miR-208 inhibition in heart failure were announced in 2011, but have not progressed further.

In 1 study, miR-25 expression was repressed in failing human hearts (29), but its expression was increased in another study (30). Where the former study described the targeting of deleterious embryonic gene programs that worsen cardiac function, the latter showed repression of the sarcoplasmic/endoplasmic reticulum calcium adenosine triphosphatase (SERCA), an important contributor to excitation-contraction coupling in cardiomyocytes, and subsequent improvement in cardiac function. Differences in timing and chemical properties of the anti-miR treatment, as well as the study duration, could explain these contradictory results. This highlights the formidable task of determining optimal anti-miR chemistry, given the combinatorial possibilities of modifications that can be introduced, even in small oligonucleotides. Different oligonucleotides targeting the same miRNA may not achieve the same therapeutic benefit.

miRNAs IN CARDIAC REGENERATION

MiRNAs have been proposed as an alternative to cell therapy for cardiac regeneration. Studies on neonatal rat cardiomyocyte proliferation highlighted miR-199a and miR-590 as capable of inducing mitosis (31). Injecting these miRNAs into rodent hearts after myocardial infarction (MI) preserved cardiac function. Along similar lines, inhibition of miR-34a improved cardiac function after MI in mice, attenuating cardiomyocyte apoptosis and telomere shortening (32). MiRNA-based therapies for cardiac regeneration and repair still require validation in models with greater translational potential. A miRNA that is pursued currently for therapeutic applications in CVD is miR-92a. Inhibition of miR-92a reduces endothelial inflammation (33) and promotes angiogenesis and functional recovery in ischemic myocardium (34). However, this miRNA is part of a cluster of miRNA genes (miR-17∼92), also known as oncomiR-1 because its members target cell-cycle regulation. This raises concerns about potential side effects of miR-92a therapeutics.

miRNAs IN CARDIAC FIBROSIS

Several miRNAs have been implicated in cardiac fibroblast survival and related signaling pathways. Although some miRNAs directly target genes coding for ECM proteins (35,36), others prevent cardiac fibroblasts from attaining an activated secretory phenotype (37,38). In addition to its role in cardiac hypertrophy, miR-133 is considered antifibrotic

CENTRAL ILLUSTRATION **miRNA Biogenesis and Function**

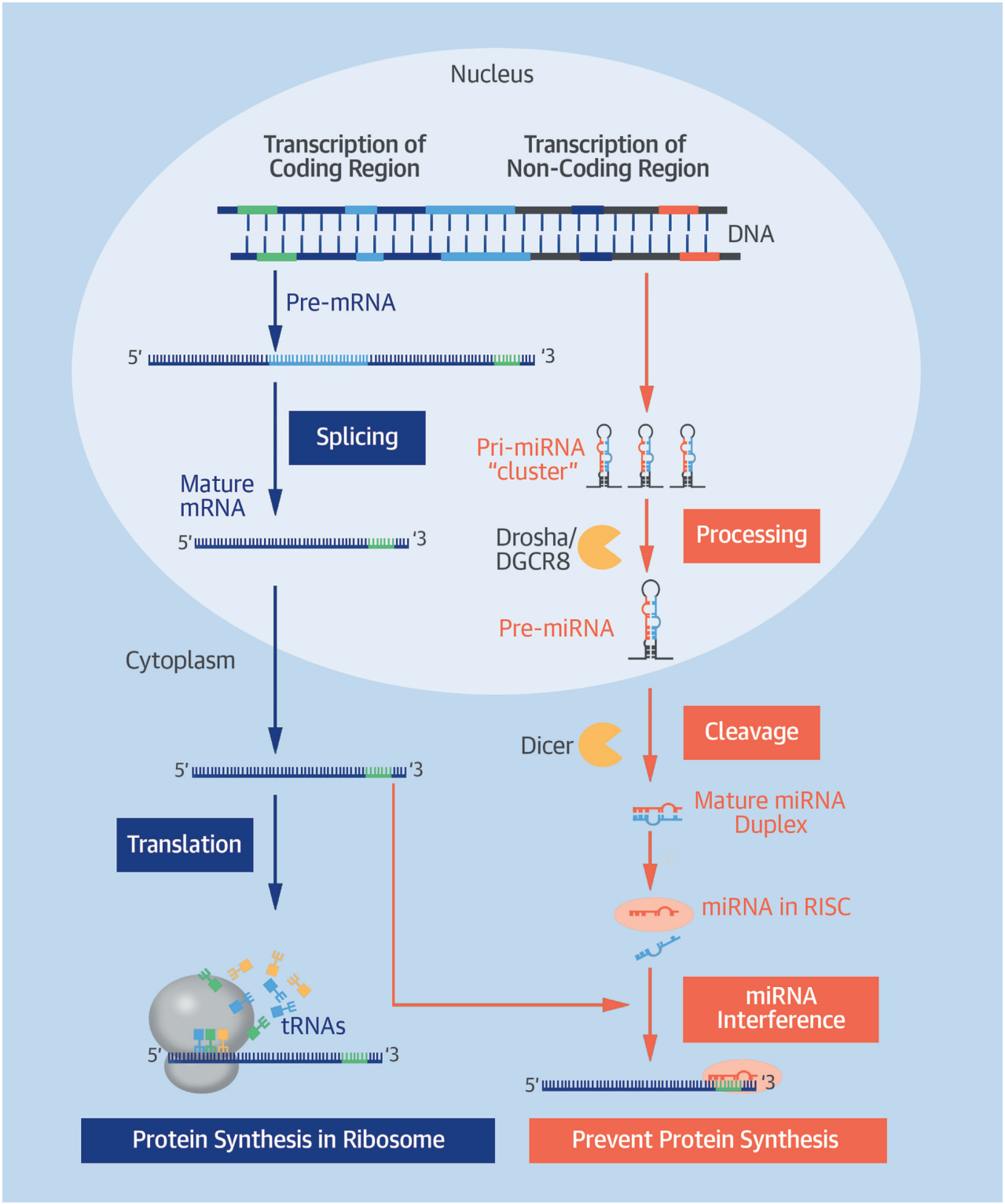

Barwari, T. et al. J Am Coll Cardiol. 2016;68(23):2577–84.

Continued on the next page

through targeting of connective tissue growth factor, a key regulator of the fibrotic process (37), as well as collagen I α-1, a main constituent of the cardiac ECM (39).

MiR-21 has been studied most extensively in the context of fibrosis. This miRNA is increased in heart failure patients and in cardiac fibroblasts of fibrotic mouse hearts (40), and promotes ECM deposition in mouse models of increased afterload (41) and myocardial ischemia (42). In vivo inhibition of miR-21 attenuates the fibrotic response and improves cardiac function in mouse models of heart failure (41). These results were not reproduced in a subsequent study using a different anti-miR, reiterating the importance of optimizing the anti-miR chemistry (43). MiR-21 also serves as an example of a miRNA where both the guide and passenger strands mediate function, with the passenger strand being transferred from fibroblasts to cardiomyocytes, where it exerts a pro-hypertrophic effect (6). This highlights another difficulty in translating findings from preclinical models to patients. If both strands mediate function, then inhibition of just 1 strand by anti-miR treatment may not recapitulate the phenotype observed in knockout mice, where both strands are deleted from the genome.

miRNAs IN NEOINTIMA FORMATION AND ATHEROSCLEROSIS

In addition to its profibrotic role, miR-21 enhances neointimal growth through pro-proliferative and antiapoptotic effects on vascular smooth muscle cells (SMCs) (44). Inhibition of miR-21 reduces in-stent restenosis in animals (45). The development of miRNA-eluting stents (46) could overcome one of the major challenges in miRNA therapies, because local delivery decreases the risk of off-target effects. The same can be argued for miR-29b, which represses ECM production by vascular SMCs (47), whereas inhibition slows abdominal aortic aneurysm progression (48) and promotes favorable plaque remodeling in atherosclerotic mice (49). Delivered locally, miR-29b antagonism could more subtly alter the ECM balance, if stents eluting anti-miR-29b were developed to inhibit aneurysm progression or to stabilize symptomatic atherosclerotic plaques.

Key events in atherosclerosis are endothelial injury and the switch of SMCs from a contractile to a synthetic phenotype. MiR-143 and miR-145 are transcribed together as a cluster and are highly abundant in SMCs, with a marked down-regulation seen in vessels with neointima formation (50,51). Together, these miRNAs regulate vascular SMC differentiation and, consequently, their loss contributes to SMC dedifferentiation and atherosclerosis (52). MiR-126 is highly enriched in endothelial cells (53). It indirectly enhances vascular endothelial growth factor signaling, and therefore has been studied in the context of angiogenesis and endothelial repair. Interestingly, the endothelial effects of this miRNA seem to be mediated by the passenger strand, rather than the guide strand (54). Although miR-126 has been described as endothelial cell-specific (53), this miRNA is expressed in megakaryocytes and may have a role in platelet function as mentioned elsewhere in this paper.

miRNAs IN LIPID METABOLISM

MiR-122 is highly abundant in the liver (55,56). Pharmacological strategies to lower miR-122 levels decreased plasma cholesterol levels (13,55). Unfortunately, initial optimism was dampened by subsequent studies that showed a simultaneous decrease in high-density lipoprotein cholesterol levels (57). Similar findings were obtained for miR-33, an miRNA that regulates cholesterol metabolism. Short-term inhibition was beneficial (58,59), but long-term inhibition in animals fed a high-fat diet had detrimental effects, such as hepatic steatosis (60). More recently, a study in human hepatic cells identified miR-148a as a regulator of the low-density lipoprotein cholesterol receptor (61). Systemic inhibition of miR-148a caused a significant reduction in plasma low-density lipoprotein cholesterol, but also increased high-density

CENTRAL ILLUSTRATION Continued

MicroRNAs (miRNAs) originate from primary transcripts (pri-miRNAs) that are derived from introns (the noncoding regions within a primary mRNA transcript) of protein-coding genes or from intergenic regions within the genome. Primary transcripts are processed in the nucleus to a hairpin-shaped pre-miRNA by the Drosha/DGCR8 complex, transported to the cytoplasm, and then processed to mature miRNA duplexes by the Dicer complex. To exert its function, the mature miRNA is incorporated into an RNA-induced silencing complex (RISC). This complex can then target mRNA through sequence complementarity: the sequence of the incorporated miRNA, with the 6 to 8 nucleotide-long seed sequence on the 5′ end in particular, binds to the targeted mRNA, usually to the untranslated region at the 3′ end. Depending on several factors, including the extent of sequence complementarity, this leads to cleavage or translation repression of the mRNA, preventing a protein from being assembled. mRNA = messenger RNA; RISC = ribonucleic acid-induced silencing complex; tRNA = transfer RNA.

lipoprotein cholesterol levels. Long-term side effects of miR-122 and miR-33 inhibition, combined with the advent of novel therapeutic options for dyslipidemia, may limit the clinical use of miRNAs to modulate lipid metabolism.

miRNAs AS BIOMARKERS

MiRNAs are present, stable, and detectable in the circulation (62), both in plasma or serum, where they are either bound to protein complexes or contained in microvesicles or lipoproteins. Microvesicle- and lipoprotein-borne miRNAs have been suggested to affect protein expression when delivered to cells (63–66). For example, miR-223 is relatively abundant in plasma, and may transduce an endocrine signal between blood cells and vascular cells (67). Because absolute levels of circulating miRNAs are low, it remains to be proven whether miRNA transfer is sufficient to achieve effective target repression in recipient cells.

Several cardiac miRNAs are detectable in blood early after MI, potentially reducing time to diagnosis (68). However, head-to-head comparisons with established biomarkers, such as high-sensitivity troponins, found that detection of miRNAs did not improve on the accuracy or usefulness of current methods (69). Furthermore, current miRNA detection techniques are time consuming and do not allow for the rapid diagnosis required in patients with MI. In the context of hypertrophic cardiomyopathy, higher levels of miR-29a correlate with both hypertrophy and fibrosis (70), but its clinical benefits beside current diagnostic tools remain unclear.

New biomarker searches should focus on unmet clinical needs, rather than areas where well-performing, established markers already exist. For example, current risk prediction models for MI could improve. Three studies, albeit with differing methodologies, have detected differentially expressed miRNAs in patients who went on to suffer acute MI (71–73). Karakas et al. (71) found a surprisingly strong correlation of single miRNAs with the risk of cardiovascular death, although this was in a highly selected population, and was not compared with traditional risk models. No single miRNA conferred a clinically significant change in risk of acute MI in either the study by Bye et al. (72) or by Zampetaki et al. (73), but the combined usefulness of an miRNA panel improved the predictive power of traditional Framingham risk models. The miRNAs selected by Zampetaki et al. (73) also predicted mortality in a cohort of patients with symptomatic coronary artery disease (74). Mechanistic links have been reported between 2 of these miRNAs and platelet function: miR-126 (75) and miR-223 (76). Circulating miRNAs can be derived from a range of cell types, but platelets contribute substantially (75,76). Levels of circulating miRNAs are affected by the administration of antiplatelet therapy (77), and correlate with existing platelet reactivity assays in patients post-MI (75). Platelet miRNAs have been linked to hyper-reactive platelets (78).

CONCLUSIONS

MiRNAs can regulate protein expression, and so are the subject of intense interest in understanding and treating CVD. Treatment strategies currently focus on systemic anti-miR delivery, which raises concerns for off-target effects, including platelet activation (79). Future efforts should be aimed at evaluating cell-type-specific strategies or local delivery. For the cardiovascular system, enhanced targeting could be achieved through the use of adeno-associated virus vectors for cell-type-specific miRNA delivery or nanoparticle-bound anti-miRs or miRNA mimics (80).

Preclinical research has focused mainly on identifying mechanisms within a single tissue or cell type. However, caution needs to be exercised to avoid moving toward clinical evaluation too quickly. MiRNA regulation of protein expression is highly dependent on context and cell type, and their ubiquitous expression makes side effects of miRNA therapies unpredictable. Targeting individual miRNAs therefore requires meticulous evaluation of systemic effects. A careful approach in advancing miRNA therapies may slow progression toward clinical application, but may spare miRNA therapeutics a setback similar to gene therapy. The great potential of miRNAs justifies the exercise of apprehension before large-scale clinical studies for CVD.

Circulating miRNAs are expressed differentially across disease phenotypes and are implicated as novel biomarkers. Their platelet origin could make circulating miRNAs particularly relevant in the context of CVD. Platelet reactivity may confer cardiovascular risk, but there is no single accepted biomarker. More mechanistic studies and validation in larger cohorts are required to establish the clinical utility of miRNA biomarkers.

REPRINT REQUESTS AND CORRESPONDENCE: Professor Manuel Mayr, King's British Heart Foundation Centre, King's College London, 125 Coldharbour Lane, London SE59NU, United Kingdom. E-mail: manuel.mayr@kcl.ac.uk.

REFERENCES

1. Venter JC, Adams MD, Myers EW, et al. The sequence of the human genome. Science 2001;291:1304–51.

2. Lee RC, Feinbaum RL, Ambros V. The C. elegans heterochronic gene lin-4 encodes small RNAs with antisense complementarity to lin-14. Cell 1993;75:843–54.

3. Condorelli G, Latronico MVG, Cavarretta E. microRNAs in cardiovascular diseases: current knowledge and the road ahead. J Am Coll Cardiol 2014;63:2177–87.

4. Ipsaro JJ, Joshua-Tor L. From guide to target: molecular insights into eukaryotic RNA-interference machinery. Nat Struct Mol Biol 2015;22:20–8.

5. Jonas S, Izaurralde E. Towards a molecular understanding of microRNA-mediated gene silencing. Nat Rev Genet 2015;16:421–33.

6. Bang C, Batkai S, Dangwal S, et al. Cardiac fibroblast-derived microRNA passenger strand-enriched exosomes mediate cardiomyocyte hypertrophy. J Clin Invest 2014;124:2136–46.

7. Zampetaki A, Mayr M. MicroRNAs in vascular and metabolic disease. Circ Res 2012;110:508–22.

8. Pritchard CC, Cheng HH, Tewari M. MicroRNA profiling: approaches and considerations. Nat Rev Genet 2012;13:358–69.

9. Wang Z, Gerstein M, Snyder M. RNA-Seq: a revolutionary tool for transcriptomics. Nat Rev Genet 2009;10:57–63.

10. van Rooij E, Olson EN. MicroRNA therapeutics for cardiovascular disease: opportunities and obstacles. Nat Rev Drug Discov 2012;11:860–72.

11. Ganesan J, Ramanujam D, Sassi Y, et al. MiR-378 controls cardiac hypertrophy by combined repression of mitogen-activated protein kinase pathway factors. Circulation 2013;127:2097–106.

12. Borel F, Kay MA, Mueller C. Recombinant AAV as a platform for translating the therapeutic potential of RNA interference. Mol Ther 2014;22:692–701.

13. Krützfeldt J, Rajewsky N, Braich R, et al. Silencing of microRNAs in vivo with 'antagomirs'. Nature 2005;438:685–9.

14. Janssen HLA, Reesink HW, Lawitz EJ, et al. Treatment of HCV infection by targeting microRNA. N Engl J Med 2013;368:1685–94.

15. Gomez IG, MacKenna DA, Johnson BG, et al. Anti-microRNA-21 oligonucleotides prevent Alport nephropathy progression by stimulating metabolic pathways. J Clin Invest 2015;125:141–56.

16. Dalpke A, Helm M. RNA mediated Toll-like receptor stimulation in health and disease. RNA Biol 2012;9:828–42.

17. Carè A, Catalucci D, Felicetti F, et al. MicroRNA-133 controls cardiac hypertrophy. Nat Med 2007;13:613–8.

18. Castaldi A, Zaglia T, Di Mauro V, et al. MicroRNA-133 modulates the β1-adrenergic receptor transduction cascade. Circ Res 2014;115:273–83.

19. Trajkovski M, Ahmed K, Esau CC, et al. MyomiR-133 regulates brown fat differentiation through Prdm16. Nat Cell Biol 2012;14:1330–5.

20. Matkovich SJ, Wang W, Tu Y, et al. MicroRNA-133a protects against myocardial fibrosis and modulates electrical repolarization without affecting hypertrophy in pressure-overloaded adult hearts. Circ Res 2010;106:166–75.

21. Elia L, Contu R, Quintavalle M, et al. Reciprocal regulation of microRNA-1 and insulin-like growth factor-1 signal transduction cascade in cardiac and skeletal muscle in physiological and pathological conditions. Circulation 2009;120:2377–85.

22. Yang B, Lin H, Xiao J, et al. The muscle-specific microRNA miR-1 regulates cardiac arrhythmogenic potential by targeting GJA1 and KCNJ2. Nat Med 2007;13:486–91.

23. Zhao Y, Ransom JF, Li A, et al. Dysregulation of cardiogenesis, cardiac conduction, and cell cycle in mice lacking miRNA-1-2. Cell 2007;129:303–17.

24. Karakikes I, Chaanine AH, Kang S, et al. Therapeutic cardiac-targeted delivery of miR-1 reverses pressure overload-induced cardiac hypertrophy and attenuates pathological remodeling. J Am Heart Assoc 2013;2:e000078.

25. Krenz M, Robbins J. Impact of beta-myosin heavy chain expression on cardiac function during stress. J Am Coll Cardiol 2004;44:2390–7.

26. van Rooij E, Sutherland LB, Qi X, et al. Control of stress-dependent cardiac growth and gene expression by a microRNA. Science 2007;316:575–9.

27. Montgomery RL, Hullinger TG, Semus HM, et al. Therapeutic inhibition of miR-208a improves cardiac function and survival during heart failure. Circulation 2011;124:1537–47.

28. Kakimoto Y, Tanaka M, Kamiguchi H, et al. MicroRNA deep sequencing reveals chamber-specific miR-208 family expression patterns in the human heart. Int J Cardiol 2016;211:43–8.

29. Dirkx E, Gladka MM, Philippen LE, et al. Nfat and miR-25 cooperate to reactivate the transcription factor Hand2 in heart failure. Nat Cell Biol 2013;15:1282–93.

30. Wahlquist C, Jeong D, Rojas-Muñoz A, et al. Inhibition of miR-25 improves cardiac contractility in the failing heart. Nature 2014;508:531–5.

31. Eulalio A, Mano M, Dal Ferro M, et al. Functional screening identifies miRNAs inducing cardiac regeneration. Nature 2012;492:376–81.

32. Boon RA, Iekushi K, Lechner S, et al. MicroRNA-34a regulates cardiac ageing and function. Nature 2013;495:107–10.

33. Loyer X, Potteaux S, Vion AC, et al. Inhibition of microRNA-92a prevents endothelial dysfunction and atherosclerosis in mice. Circ Res 2014;114:434–43.

34. Bonauer A, Carmona G, Iwasaki M, et al. MicroRNA-92a controls angiogenesis and functional recovery of ischemic tissues in mice. Science 2009;324:1710–3.

35. van Rooij E, Sutherland LB, Thatcher JE, et al. Dysregulation of microRNAs after myocardial infarction reveals a role of miR-29 in cardiac fibrosis. Proc Natl Acad Sci U S A 2008;105:13027–32.

36. Abonnenc M, Nabeebaccus AA, Mayr U, et al. Extracellular matrix secretion by cardiac fibroblasts: role of microRNA-29b and microRNA-30c. Circ Res 2013;113:1138–47.

37. Duisters RF, Tijsen AJ, Schroen B, et al. miR-133 and miR-30 regulate connective tissue growth factor: implications for a role of microRNAs in myocardial matrix remodeling. Circ Res 2009;104:170–8.

38. Tijsen AJ, van der Made I, van den Hoogenhof MM, et al. The microRNA-15 family inhibits the TGFβ-pathway in the heart. Cardiovasc Res 2014;104:61–71.

39. Castoldi G, di Gioia CRT, Bombardi C, et al. MiR-133a regulates collagen 1A1: potential role of miR-133a in myocardial fibrosis in angiotensin II-dependent hypertension. J Cell Physiol 2012;227:850–6.

40. van Rooij E, Sutherland LB, Liu N, et al. A signature pattern of stress-responsive microRNAs that can evoke cardiac hypertrophy and heart failure. Proc Natl Acad Sci U S A 2006;103:18255–60.

41. Thum T, Gross C, Fiedler J, et al. MicroRNA-21 contributes to myocardial disease by stimulating MAP kinase signalling in fibroblasts. Nature 2008;456:980–4.

42. Roy S, Khanna S, Hussain SRA, et al. MicroRNA expression in response to murine myocardial infarction: miR-21 regulates fibroblast metalloprotease-2 via phosphatase and tensin homologue. Cardiovasc Res 2009;82:21–9.

43. Patrick DM, Montgomery RL, Qi X, et al. Stress-dependent cardiac remodeling occurs in the absence of microRNA-21 in mice. J Clin Invest 2010;120:3912–6.

44. Ji R, Cheng Y, Yue J, et al. MicroRNA expression signature and antisense-mediated depletion reveal an essential role of microRNA in vascular neointimal lesion formation. Circ Res 2007;100:1579–88.

45. McDonald RA, Halliday CA, Miller AM, et al. Reducing in-stent restenosis: therapeutic manipulation of miRNA in vascular remodeling and inflammation. J Am Coll Cardiol 2015;65:2314–27.

46. Wang D, Deuse T, Stubbendorff M, et al. Local microRNA modulation using a novel anti-miR-21-eluting stent effectively prevents experimental in-stent restenosis. Arterioscler Thromb Vasc Biol 2015;35:1945–53.

47. Zampetaki A, Attia R, Mayr U, et al. Role of miR-195 in aortic aneurysmal disease. Circ Res 2014;115:857–66.

48. Maegdefessel L, Azuma J, Toh R, et al. Inhibition of microRNA-29b reduces murine abdominal aortic aneurysm development. J Clin Invest 2012;122:497–506.

49. Ulrich V, Rotllan N, Araldi E, et al. Chronic miR-29 antagonism promotes favorable plaque remodeling in atherosclerotic mice. EMBO Mol Med 2016;8:643–53.

50. Cheng Y, Liu X, Yang J, et al. MicroRNA-145, a novel smooth muscle cell phenotypic marker and modulator, controls vascular neointimal lesion formation. Circ Res 2009;105:158–66.

51. Cordes KR, Sheehy NT, White MP, et al. miR-145 and miR-143 regulate smooth muscle cell fate and plasticity. Nature 2009;460:705–10.

52. Lovren F, Pan Y, Quan A, et al. MicroRNA-145 targeted therapy reduces atherosclerosis. Circulation 2012;126:S81–90.

53. Wang S, Aurora AB, Johnson BA, et al. The endothelial-specific microRNA miR-126 governs vascular integrity and angiogenesis. Dev Cell 2008;15:261–71.

54. Schober A, Nazari-Jahantigh M, Wei Y, et al. MicroRNA-126-5p promotes endothelial proliferation and limits atherosclerosis by suppressing Dlk1. Nat Med 2014;20:368–76.

55. Esau C, Davis S, Murray SF, et al. miR-122 regulation of lipid metabolism revealed by in vivo antisense targeting. Cell Metab 2006;3:87–98.

56. Willeit P, Skroblin P, Kiechl S, et al. Liver microRNAs: potential mediators and biomarkers for metabolic and cardiovascular disease? Eur Heart J 2016 Apr 20 [E-pub ahead of print].

57. Elmén J, Lindow M, Schütz S, et al. LNA-mediated microRNA silencing in non-human primates. Nature 2008;452:896–9.

58. Rayner KJ, Suárez Y, Dávalos A, et al. MiR-33 contributes to the regulation of cholesterol homeostasis. Science 2010;328:1570–3.

59. Najafi-Shoushtari SH, Kristo F, Li Y, et al. MicroRNA-33 and the SREBP host genes cooperate to control cholesterol homeostasis. Science 2010;328:1566–9.

60. Horie T, Nishino T, Baba O, et al. MicroRNA-33 regulates sterol regulatory element-binding protein 1 expression in mice. Nat Commun 2013;4:2883.

61. Goedeke L, Rotllan N, Canfrán-Duque A, et al. MicroRNA-148a regulates LDL receptor and ABCA1 expression to control circulating lipoprotein levels. Nat Med 2015;21:1280–9.

62. Mitchell PS, Parkin RK, Kroh EM, et al. Circulating microRNAs as stable blood-based markers for cancer detection. Proc Natl Acad Sci U S A 2008;105:10513–8.

63. Vickers KC, Palmisano BT, Shoucri BM, et al. MicroRNAs are transported in plasma and delivered to recipient cells by high-density lipoproteins. Nat Cell Biol 2011;13:423–33.

64. Laffont B, Corduan A, Plé H, et al. Activated platelets can deliver mRNA regulatory Ago2·microRNA complexes to endothelial cells via microparticles. Blood 2013;122:253–61.

65. Gidlöf O, van der Brug M, Ohman J, et al. Platelets activated during myocardial infarction release functional miRNA, which can be taken up by endothelial cells and regulate ICAM1 expression. Blood 2013;121:3908–17, S1–26.

66. Tabet F, Vickers KC, Cuesta Torres LF, et al. HDL-transferred microRNA-223 regulates ICAM-1 expression in endothelial cells. Nat Commun 2014;5:3292.

67. Shan Z, Qin S, Li W, et al. An endocrine genetic signal between blood cells and vascular smooth muscle cells: role of microRNA-223 in smooth muscle function and atherogenesis. J Am Coll Cardiol 2015;65:2526–37.

68. Wang G-K, Zhu J-Q, Zhang J-T, et al. Circulating microRNA: a novel potential biomarker for early diagnosis of acute myocardial infarction in humans. Eur Heart J 2010;31:659–66.

69. Widera C, Gupta SK, Lorenzen JM, et al. Diagnostic and prognostic impact of six circulating microRNAs in acute coronary syndrome. J Mol Cell Cardiol 2011;51:872–5.

70. Roncarati R, Viviani Anselmi C, Losi MA, et al. Circulating miR-29a, among other up-regulated microRNAs, is the only biomarker for both hypertrophy and fibrosis in patients with hypertrophic cardiomyopathy. J Am Coll Cardiol 2014;63:920–7.

71. Karakas M, Schulte C, Appelbaum S, et al. Circulating microRNAs strongly predict cardiovascular death in patients with coronary artery disease—results from the large AtheroGene study. Eur Heart J 2016 Jun 29 [E-pub ahead of print].

72. Bye A, Røsjø H, Nauman J, et al. Circulating microRNAs predict future fatal myocardial infarction in healthy individuals – the HUNT study. J Mol Cell Cardiol 2016;97:162–8.

73. Zampetaki A, Willeit P, Tilling L, et al. Prospective study on circulating microRNAs and risk of myocardial infarction. J Am Coll Cardiol 2012;60:290–9.

74. Schulte C, Molz S, Appelbaum S, et al. miRNA-197 and miRNA-223 predict cardiovascular death in a cohort of patients with symptomatic coronary artery disease. PLoS One 2015;10:e0145930.

75. Kaudewitz D, Skroblin P, Bender LH, et al. Association of microRNAs and YRNAs with platelet function. Circ Res 2016;118:420–32.

76. Elgheznawy A, Shi L, Hu J, et al. Dicer cleavage by calpain determines platelet microRNA levels and function in diabetes. Circ Res 2015;117:157–65.

77. Willeit P, Zampetaki A, Dudek K, et al. Circulating microRNAs as novel biomarkers for platelet activation. Circ Res 2013;112:595–600.

78. Kondkar AA, Bray MS, Leal SM, et al. VAMP8/endobrevin is overexpressed in hyperreactive human platelets: suggested role for platelet microRNA. J Thromb Haemost 2010;8:369–78.

79. Flierl U, Nero TL, Lim B, et al. Phosphorothioate backbone modifications of nucleotide-based drugs are potent platelet activators. J Exp Med 2015;212:129–37.

80. Anand S, Majeti BK, Acevedo LM, et al. MicroRNA-132-mediated loss of p120RasGAP activates the endothelium to facilitate pathological angiogenesis. Nat Med 2010;16:909–14.

KEY WORDS biomarkers, genetic therapy, noncoding RNA, RNA therapeutic

Appendix 3

Published article:

MicroRNA Biomarkers and Platelet Reactivity: The Clot Thickens.

Sunderland N, Skroblin P, **Barwari T**, Huntley RP, Lu R, Joshi A, Lovering RC, Mayr M.

Circ Res. 2017;120(2):418–435.

Accepted for publication: 20 December 2016

MicroRNA Biomarkers and Platelet Reactivity

The Clot Thickens

Nicholas Sunderland, Philipp Skroblin, Temo Barwari, Rachael P. Huntley, Ruifang Lu, Abhishek Joshi, Ruth C. Lovering, Manuel Mayr

Abstract: **Over the last few years, several groups have evaluated the potential of microRNAs (miRNAs) as biomarkers for cardiometabolic disease. In this review, we discuss the emerging literature on the role of miRNAs and other small noncoding RNAs in platelets and in the circulation, and the potential use of miRNAs as biomarkers for platelet activation. Platelets are a major source of miRNAs, YRNAs, and circular RNAs. By harnessing multiomics approaches, we may gain valuable insights into their potential function. Because not all miRNAs are detectable in the circulation, we also created a gene ontology annotation for circulating miRNAs using the gene ontology term extracellular space as part of blood plasma. Finally, we share key insights for measuring circulating miRNAs. We propose ways to standardize miRNA measurements, in particular by using platelet-poor plasma to avoid confounding caused by residual platelets in plasma or by adding RNase inhibitors to serum to reduce degradation. This should enhance comparability of miRNA measurements across different cohorts. We provide recommendations for future miRNA biomarker studies, emphasizing the need for accurate interpretation within a biological and methodological context. (*Circ Res*. 2017;120:418-435. DOI: 10.1161/CIRCRESAHA.116.309303.)**

Key Words: acute coronary syndrome ■ biomarker ■ noncoding RNA ■ platelet ■ platelet inhibitor

Platelets play a key role in hemostasis, initiating and propagating thrombosis.[1] Dysregulation and inappropriate activation of platelets underpin a wide range of important diseases, including stroke and myocardial infarction, whereas impairment of platelet function results in bleeding disorders. Platelets are anucleate and were previously considered to be simple cytoplasmic fragments of megakaryocytes. We now know that platelets house an array of molecules, including proteins, RNA, and the subcellular machinery of de novo protein synthesis. Platelets can synthesize new proteins, such as the integrin alpha3 (glycoprotein-IIIa) protein and the fibrinogen receptor.[2,3] They contain messenger RNA (mRNA), which codes for around a third of human genes.[4,5] More recently, the discoveries that platelets are an abundant source of microRNAs (miRNA),[6] and that miRNA expression profiles within platelets correlate with platelet reactivity,[7] raised the exciting possibility of novel therapeutic targets and disease biomarkers.

Initial studies by Mitchell et al[8] revealed that not all miRNAs in the circulation are intracellular. This pool of extracellular circulating miRNA consists of miRNA within microvesicles, exosomes, or bound to proteins. The finding that miRNAs can also be measured in cell-free serum and plasma was surprising, given their high RNase activity. Compared with mRNAs, miRNAs remain relatively stable in the circulation through several protective mechanisms: association with RNA-binding proteins and lipoproteins, or housing in shed microvesicles, such as exosomes or microparticles (MPs).[9–12] Platelets release MPs, particularly during activation. These vesicles contain a host of proteins, inflammatory mediators, and noncoding RNAs.[13–15] Microvesicles might be taken up by other cells, introducing another layer of complexity in terms of intercellular signaling by potentially allowing direct regulation of the recipient cell's mRNA profile and gene expression.[16,17] Given this emerging role for circulating miRNAs, plasma and serum miRNA profiles may find use in clinical practice as novel markers of disease, organ function, and prognosis.[18]

In this review, we bring together nearly a decade's experience with circulating noncoding RNAs, with particular focus on platelet-derived and associated miRNAs, YRNAs, long noncoding RNAs (lncRNAs), and circular RNAs (circRNAs). We conducted a literature search in PubMed as queried on November 23, 2016, using the search terms "platelet* AND (miRNA [MeSH Terms] OR micro RNA [MeSH Terms] OR micro-RNA OR microRNA)". Four hundred and thirty-four results were retrieved, of which 75 were relevant primary research papers and 39 were relevant literature reviews. From the literature to date, we collate the known platelet repertoire of noncoding RNAs and contemplate their physiological significance. We also examine their disease associations and

Original received October 4, 2016; revision received December 20, 2016; accepted December 20, 2016.

From the King's British Heart Foundation Centre, King's College London, United Kingdom (N.S., P.S., T.B., R.L., A.J., M.M.); and Centre for Cardiovascular Genetics, Institute of Cardiovascular Science, University College London, United Kingdom (R.P.H., R.C.L.).

Correspondence to Manuel Mayr, King's British Heart Foundation Centre, King's College London, 125 Coldharbour Ln, London SE5 9NU, United Kingdom. E-mail manuel.mayr@kcl.ac.uk

Nonstandard Abbreviations and Acronyms	
circRNAs	circular RNAs
Ct	cycle threshold
GO	gene ontology
lncRNAs	long noncoding RNAs
miRNA	microRNA
MP	microparticle
mRNA	messenger RNA
NGS	next-generation sequencing
PCPT	phosphatidylcholine transfer protein
PPP	platelet-poor plasma
PRP	platelet-rich plasma
qPCR	quantitative polymerase chain reaction
rRNA	ribosomal RNA

potential clinical applications. Finally, we discuss the practical challenges in measuring and comparing miRNA levels, highlighting obstacles that will need to be overcome for this relatively new field to come of age.

Noncoding RNAs in Platelets and the Circulation

Different noncoding RNAs have been described (Figure 1).

miRNAs

The human genome codes for small (≈22 nucleotide) regulatory RNA molecules, termed miRNAs or miRs. Since miRNAs were first discovered in 1993, over 2500 have been defined.[19,20] They are highly evolutionarily conserved and important in the posttranscriptional regulation of protein expression—about one third to half of the human genes are estimated to be regulated by miRNAs.[21–23] MiRNAs act by imperfect Watson–Crick base pairing to the 3′untranslated region (UTR) of target mRNA to affect translation or induce degradation.[24,25] MiRNAs can be expressed as stand-alone scripts or alongside the parent gene mRNA. In either case, the primary miRNA transcript is processed by the nuclear microprocessor complex consisting of the endoribonuclease Drosha and the double-stranded RNA-binding protein Pasha/DGCR8.[26,27] The resultant hairpin pre-miRNA is then transferred to the cytoplasm by the nuclear membrane protein exportin-5 and further processed by the endoribonuclease Dicer.[28] The resulting mature miRNA duplex associates with an Argonaute (Ago) protein, which unwinds the double strand and incorporates one of the 2 complementary miRNA strands, forming the RNA-induced silencing complex.[29] The RNA-induced silencing complex stabilizes the miRNA strand and guides it to its target mRNA. Because platelets do not have a nucleus and thus cannot transcribe miRNAs, it is currently thought that they inherit their miRNA content during the shedding process from megakaryocytes.[30] Thus, the platelet miRNAome in the circulation may provide insights into megakaryocyte function in the bone marrow.

There are many more miRNAs encoded in the human genome than there are detectable in the circulation.[31] For example, we detected >200 miRNAs using next-generation sequencing (NGS) in plasma samples.[32] Detectable miRNAs greatly vary in abundance. Not all miRNAs that are present in the circulation can be consistently quantified with cycle threshold (Ct) values of <32 by quantitative polymerase chain reaction (qPCR), even after preamplification. Another striking observation is the high correlation among the abundant circulating miRNAs.[33] This may be because of their common platelet origin: in response to antiplatelet drugs, circulating levels of many miRNAs are reduced in platelet-poor plasma (PPP).[34] Research into miRNAs is hampered by the current lack of functional miRNA data in bioinformatics resources. Access to cataloged experimental data is crucial to enable simple questions to be asked, such as, Which miRNAs are present in the circulation?, as well as the ability to perform sophisticated pathway and network analyses.[35] This lack of freely accessible data is being addressed by the addition of gene ontology (GO) annotations for cardiovascular-related miRNAs.[36,37] To answer the question of circulatory miRNAs, we have created GO annotations for those miRNAs identified as being present in human plasma from our previous study.[32] In the parlance of GO, the annotations were created using the GO term extracellular space (GO:0005615) with the addition of contextual information describing the extracellular space as part of blood plasma (using the Uber Ontology term Uberon:0001969). A large number of miRNAs were identified in PPP and platelet-rich plasma (PRP).[32] For those with marked enrichment in PRP, as well as significantly increased levels in a platelet spike-in experiment, we were additionally able to include in the annotation that the miRNAs present in the extracellular space are likely to have originated from platelets (using the cell ontology term CL:0000233). In total, we have identified 230 human miRNAs as present in the circulation, and the annotations providing this information are available in the GO database.[38] Inclusion of functional annotations such as these into public databases will enable researchers to find and analyze miRNA data more easily, allowing for faster progression of their research.

YRNAs

In our most recent study, we have also identified YRNAs as another species of circulating noncoding RNAs that is platelet-derived.[32] YRNAs are small noncoding RNAs, ≈100 nucleotides in length, that originate from 4 human genes (*RNY1*, *RNY3*, *RNY4*, and *RNY5* and ≈900 pseudogenes).[39,40] Using NGS in PPP and PRP, we observed a dominant peak at sequences of 32 to 33 nucleotides long, which was mapped to YRNA genes (Figure 2A).[32] The full-length YRNAs have cytoplasmic or nuclear localization and are involved in the initiation of DNA replication, as well as in ribosomal RNA quality control.[41,42] They are components of Ro ribonucleoproteins, which constitute important autoantigens in autoimmune diseases, such as systemic lupus erythematosus and Sjögren's syndrome.[43] YRNA fragments are present in the circulation, with 5′ fragments being much more abundant than 3′ fragments for the majority of RNY genes.[32,44] YRNA fragments are generated during cell stress or apoptosis. Given that YRNA fragments are abundant in platelets, and strongly correlate to platelet-derived proteins in the circulation (Figure 2B),[32] we speculate that the

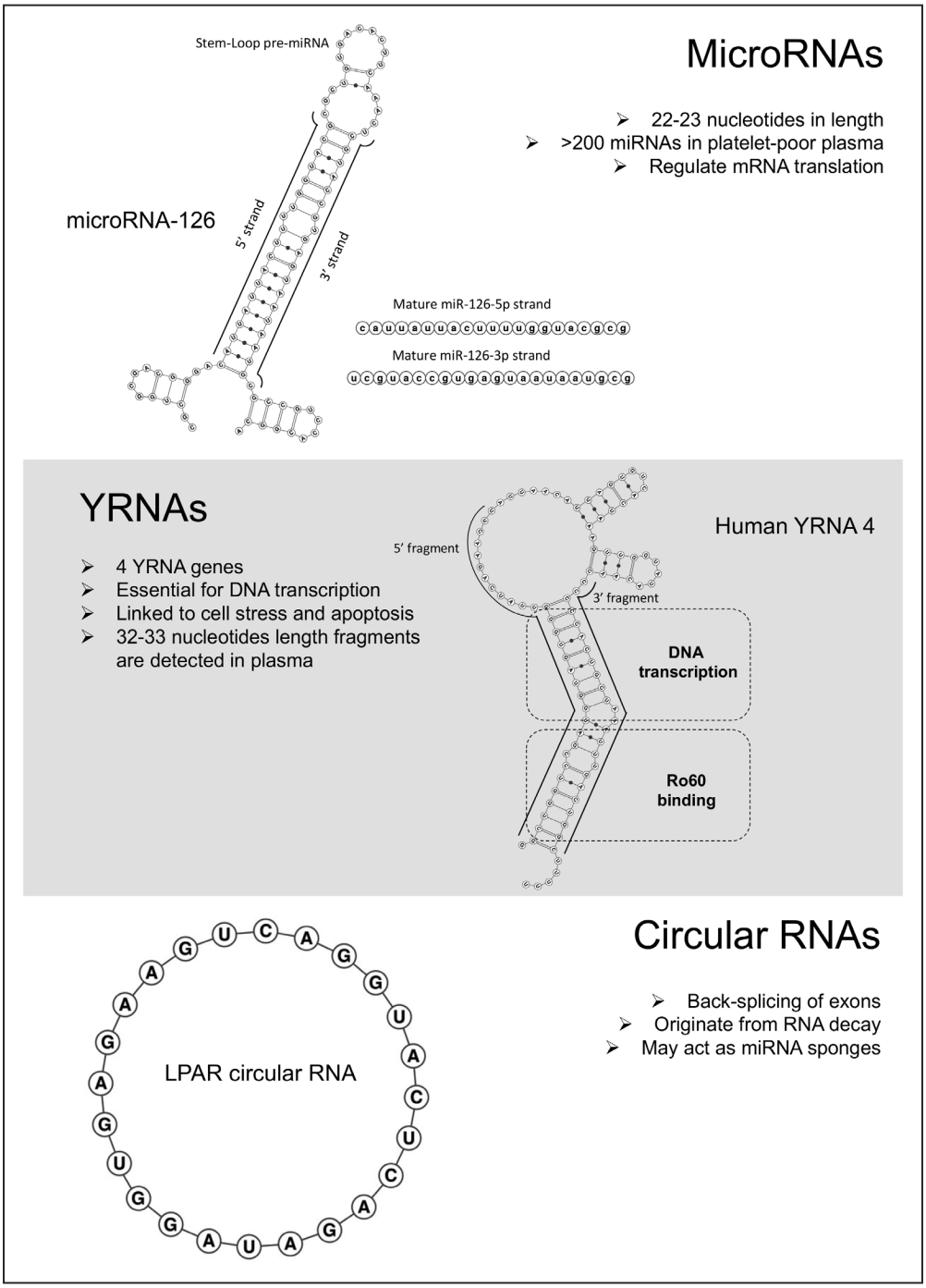

Figure 1. Overview of noncoding RNAs in platelets. Although platelets are anucleate, they contain genetic material in the form of noncoding RNAs. These include small noncoding RNAs, such as microRNAs (miRNAs) and YRNA fragments, as well as long noncoding RNAs, such as circular RNAs (circRNAs). Secondary structures of RNA sequences were predicted using RTips (http://rtips.dna.bio.keio.ac.jp).

YRNA fragments are formed during the budding of platelets from megakaryocytes. In contrast to the processing of mature miRNAs from precursor miRNAs, YRNA fragments are generated by a Dicer-independent mechanism.[45] Unlike miRNAs, we also failed to detect YRNAs in Ago2 complexes of MEG-01 cells, a human megakaryoblastic cell line.[32] The predominant platelet origin of YRNA fragments in human plasma is further supported by the results from platelet spike-in experiments.[32]

Ribosomal RNA

Ribosomal RNA is a key regulator of intracellular protein synthesis and is also detected in the circulation. Tissue damage and unregulated cell death result in significant quantities of ribosomal RNA shifting into the extracellular compartment.[46,47] As reviewed recently,[48] extracellular ribosomal RNA may have several important pathophysiological roles in atherosclerotic plaques, including promotion of vascular hyperpermeability, initiation of coagulation and thrombus

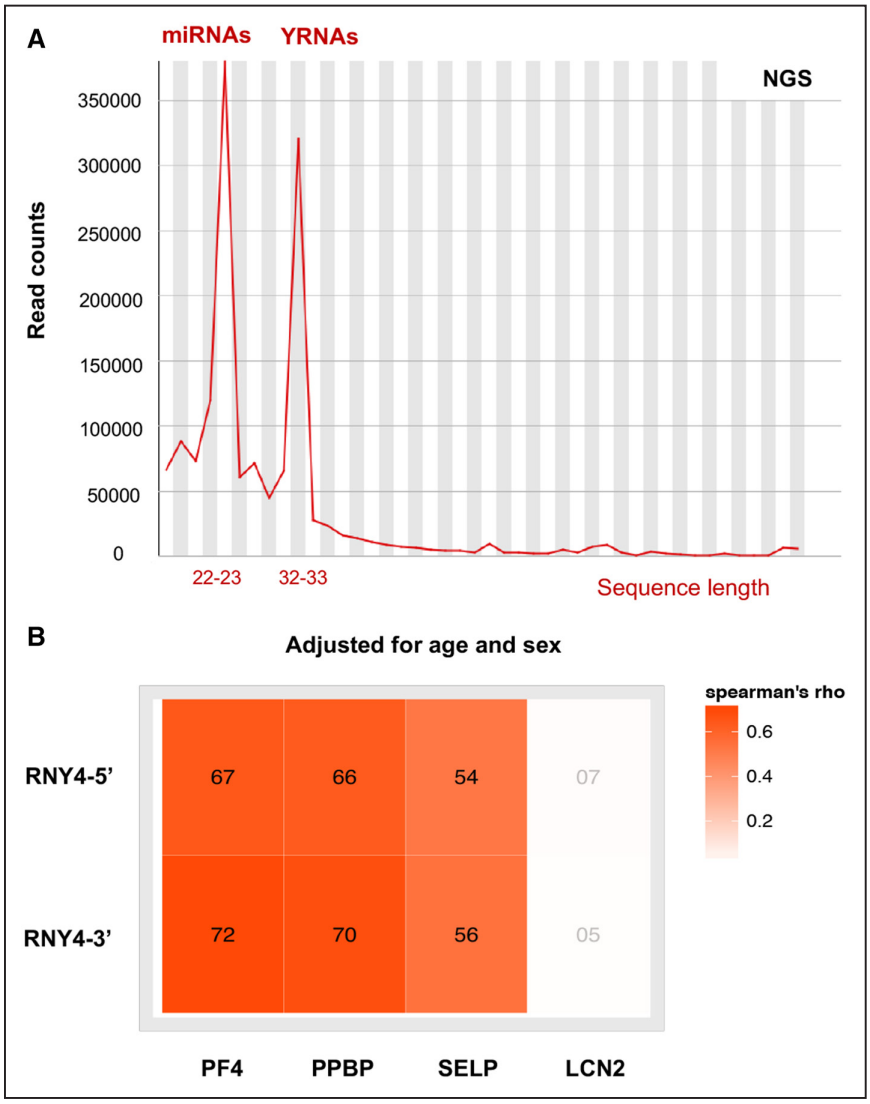

Figure 2. Small noncoding RNAs in plasma. A, Two peaks corresponding to miRNAs and YRNAs were observed by small RNA sequencing in plasma. **B**, Correlation of YRNA fragments to plasma levels of platelet factor 4 (PF4), proplatelet basic protein (PPBP), and P-selectin (SELP). Lipocalin 2 (LCN2) was used as control. N=667. NGS indicates next generation sequencing.

formation, recruitment of leukocytes, promotion of a proinflammatory phenotype of monocytes/macrophages, and promotion of cardiomyocyte death.

Long Noncoding RNAs

Recently, attention has shifted from small noncoding to lncRNAs. Unlike miRNAs and YRNA fragments, which are mainly found in the cytosol, lncRNAs are predominantly retained in the nucleus.[49] This nuclear localization has important implications for their release mechanism. Although miRNAs and YRNA fragments are secreted as part of any budding process of microvesicles with cytoplasmic components, even in the absence of injury, the secretion of lncRNAs may be dependent on cellular damage that is sufficient to release nuclear material. On release, the lncRNAs require protection from RNase degradation. In general, lncRNAs may be more susceptible to RNase activity than small noncoding RNAs because the longer sequence is more vulnerable to cleavage and not as easily complexed and protected by RNA-binding proteins. Although lncRNAs are readily detected in whole blood, levels in plasma or serum tend to be low, at least in healthy individuals without tissue injury. The release of mitochondria-associated lncRNAs has been described in patients with myocardial infarction.[50] It is possible that mitochondrial lncRNAs are protected from RNase degradation. Further, because cardiomyocytes are particularly rich in mitochondria, these lncRNAs may indeed be cardiac-derived. However, unlike troponins, lncRNAs are not cardiac muscle-specific, so contributions from other cell types cannot be excluded.[51] Because platelets are anuclear and have a low mitochondrial content, most lncRNAs may not be detectable in platelets, with the notable exception of circRNAs.

Circular RNAs

Recent evidence suggests that platelets are relatively abundant in circRNAs,[52] an emerging class of noncoding RNAs that had been described as early as 1976.[53] Development of advanced NGS techniques led to their recent rediscovery,[54] showing ubiquitous expression in both humans and mice.[55] Several pathways exist to generate circRNAs.[56] Most commonly, they are derived from exons of protein-coding genes through back-splicing, whereas some arise from intronic or intergenic regions via alternative splicing. circRNAs are generally localized in the cytoplasm, but how they are exported from the nucleus remains unknown. RNA-binding proteins

like Quaking and Muscleblind are thought to affect the abundance of circRNAs in human cells through binding of the specific RNA-binding proteins to flanking intronic sequence motifs. Interaction between the RNA-binding proteins on each end approximates both ends of the exon and facilitates the formation of a circle. Quaking regulates human circRNA biogenesis, and knockdown of Quaking decreases the expression of abundant circRNAs.[57] CircRNAs were found to be enriched in platelets, where they are generated by exon back-splicing.[52] Using RNase R to selectively remove linear transcripts, several distinct circRNAs were identified in platelets. Although the majority of circRNAs are not cell type-specific, human platelets and erythrocytes were found to be highly enriched for circRNAs compared with nucleated cell types. Several circRNAs were expressed at much higher levels than the linear form of the RNA in platelets and erythrocytes. Interestingly, the relative proportion of circRNAs in cultured megakaryocytes is much lower compared with mature platelets. Combined with the finding that circRNA decays at a significantly slower rate than linear RNA, and platelets lose >90% of their progenitor mRNA, the enrichment of circRNA in platelets might be the result of linear RNA degradation.[52] This process has a profound effect on the composition of RNA because anucleate platelets cannot transcribe new RNA. Recent reports demonstrated that circRNAs can serve as miRNA sponges, which are believed to negatively regulate miRNAs by sequestering miRNA molecules.[58] This raises questions of how circRNAs interact with miRNAs and mRNAs in platelets and how circRNA transcripts are formed in platelets. With their enrichment being a signature of mRNA decay, platelet circRNAs may reflect platelet function or ageing.

miRNA Repertoire of Platelets

Landry et al[6] first reported a large number of platelet miRNAs by using locked nucleic acid–based microarray profiling. NGS has enabled the discovery of novel miRNA species. Plé et al[59] identified nearly 500 species, with the let-7 family of miRNAs comprising nearly 50% of the total. Since then, Bray et al[4] have identified many more, bringing the total of recognized platelet miRNAs to ≈750. The variation in reported platelet miRNA expression is not solely because of interindividual differences, such as sex and age.[60] Sample preparation, storage, normalization procedures, and measurement platforms play an important role. Studies aimed at defining the platelet miRNA profile use a variety of techniques, including microarrays, qPCR-based methods, and NGS. For example, Wang et al[61] demonstrated platform-associated amplification differences in miR-107, which showed much higher amplification with locked nucleic acid–based assays compared with TaqMan assays. In clinical laboratory conditions, Yu et al[62] showed upregulation of several apoptosis-related platelet miRNAs after prolonged blood bank storage of platelets. As platelet preparation from whole blood can lead to contamination with leukocytes and erythrocytes, themselves abundant sources of miRNAs, controlling cellular contamination of platelet preparations is essential.[61] Variation in preparation and storage conditions can drastically affect platelet miRNA expression, which may explain why interstudy miRNA expression ranks are highly variable. Based on the current literature, a combined interstudy miRNA expression rank list is presented in Figure 3.

Association of Platelet miRNAs With Disease

Antiplatelet drugs reduce the risk of cardiovascular events, but patients on antiplatelet therapy still suffer thrombotic events. Ever more potent antiplatelet strategies carry the risk of bleeding complications. Ideally, a so-called "sweet spot" could be defined for each patient, which offers maximum platelet inhibition with minimal bleeding risk.[63] For optimal platelet inhibition, platelet turnover is important: with a life span of 7 to 9 days, 10% to 15% of the platelet pool must be replenished every day, equivalent to 10^{10} to 10^{11} platelets per day.[64] The platelet turnover rate may be important for the efficiency of drugs like aspirin with a short half-life. Aspirin irreversibly binds cyclooxygenase, so is effective for the full life span of the platelet. However, increased platelet turnover can lead to budding of new platelets without inactive cyclooxygenase between doses. Furthermore, newly formed platelets are larger, more reticulated, more reactive, and more prone to participate in thrombus formation compared with older platelets. They also contain a higher amount of RNA and are more able to produce proteins, in particular, alpha granule proteins. Counting the subset of reticulated platelets may be a parameter for platelet turnover. However, the intrinsic properties of platelets could be even more important for platelet reactivity than their turnover rate.[65] In light of the enrichment of miRNAs and circRNAs, and the described effects of mRNA degradation during the lifetime of platelets, the noncoding RNA content of platelets may better reflect their intrinsic properties.

Platelet miRNA expression profiles in healthy volunteers remain stable over the life-span of a platelet.[66] This expression profile is significantly altered in various disease states, including myocardial infarction,[67,68] diabetes mellitus,[69] and cancer.[70] There is, therefore, the opportunity to find new biomarkers or therapeutic targets and increase our understanding of the pathophysiological mechanisms of these diseases. Anucleate platelets lack transcriptional control, so differences in miRNA signatures during platelet-activating disease states have been ascribed to several mechanisms: shedding of MPs,[71] synthesis of mature miRNA from precursor miRNAs,[69] and posttranscriptional modifications.[59] We undertook the first systematic analysis of circulating miRNAs in a large population-based study (the Bruneck study) and revealed a loss of miRNAs in type 2 diabetes mellitus.[72] Subsequent studies indicated that this loss may be attributed to activation of calpain, which can affect platelet levels of Dicer.[73] Because this endoribonuclease is key in the processing of precursor miRNAs to mature miRNAs, its loss resulted in decreased levels of several platelet-enriched miRNAs.[69,74] These findings are in line with studies showing that circulating miRNA changes in cardiovascular risk can be attributed to platelets.[32,34] Additionally, we demonstrated that a combination of miRNAs may predict future cardiovascular events.[75] This has been confirmed by other investigators.[76] In continuation of our work on circulating miRNAs in diabetes mellitus,[72] we have identified 2 angiogenic miRNAs as biomarkers for diabetic retinopathy.[77]

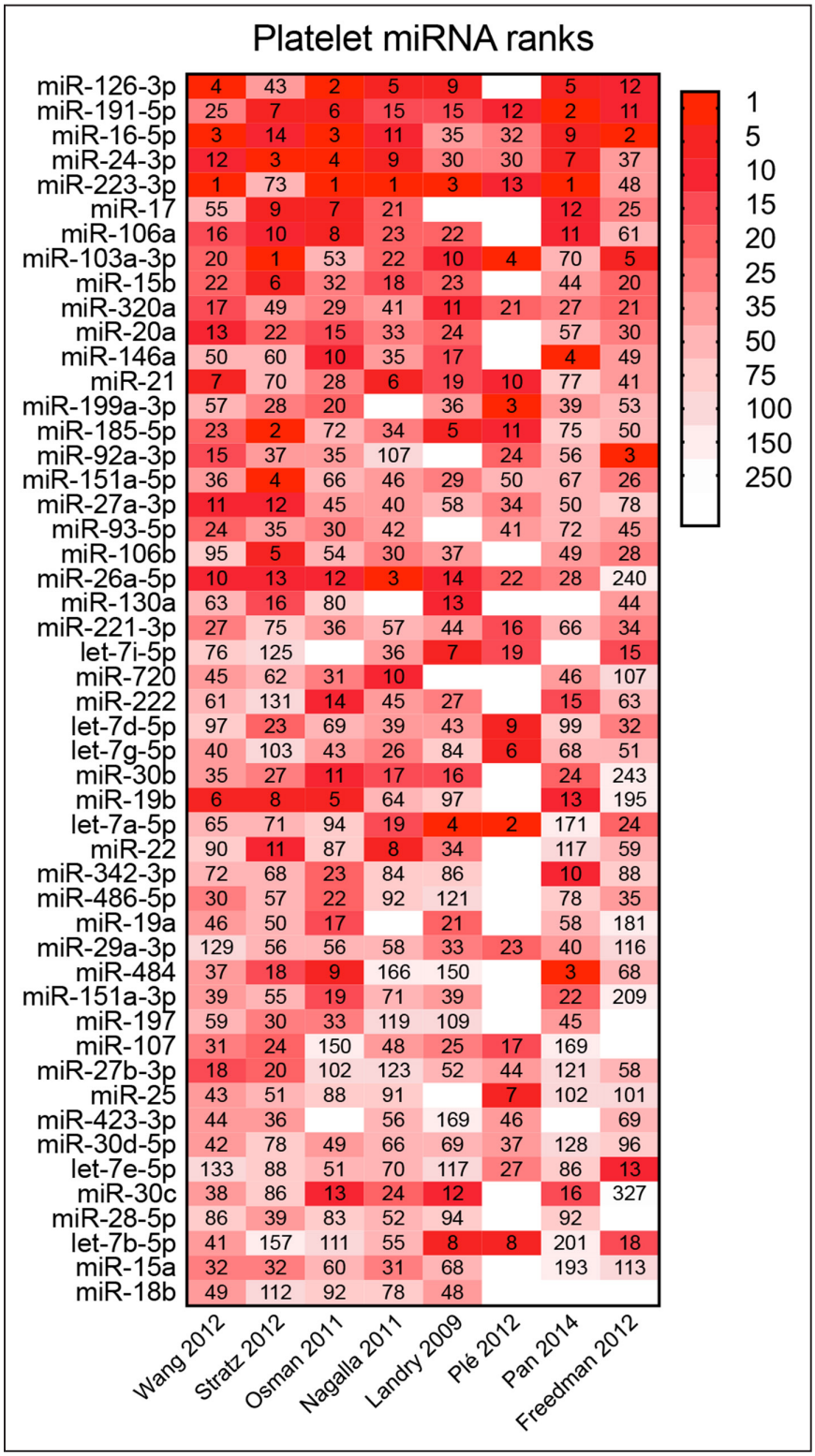

Figure 3. Platelet miRNA levels. Relative abundance of miRNAs in platelets was reported in 8 studies (indicated by first author and year of publication). The 50 highest ranking on average are presented here, indicating marked variation between different studies for the miRNAs beyond the top-10.

Findings by other investigators and our group suggest that platelet miRNAs might not only reflect but also affect platelet function.

miR-96 and Vesicle-Associated Membrane Protein 8

In 2010, Kondkar et al[78] reported a role for miR-96 in platelet reactivity. They showed that miR-96 may act through regulation of vesicle-associated membrane protein 8 (VAMP8), an important SNARE protein involved in platelet degranulation. Healthy volunteers' platelets were categorized as either hyper- or hyporeactive. mRNA profiling revealed differential expression of a range of scripts, including VAMP8 mRNA (4.8-fold decrease in the hyporeactive versus hyper-reactive platelets). This translated to a 2.5-fold lower VAMP8 protein expression in the hyporeactive

platelets. miR-96 levels were upregulated in the hyporeactive platelets (2.6-fold higher). Transfection of VAMP8-expressing human colorectal cancer cells with miR-96 was associated with dose-dependent reductions in VAMP8 mRNA and protein levels; a similar finding was reported in cells of a megakaryocyte lineage. miR-96 was predicted to bind the 3′UTR of VAMP8. In contrast with this study, Shi et al[79] reported no association between platelet response to clopidogrel and miR-96 expression, and miR-96 was not among the most highly expressed miRNAs found in human platelets. Although this does not discredit a role for miR-96 in regulating platelet reactivity, these findings need to be validated and explained in a larger study.

MiR-376c, miR-599, and Platelet Phosphatidylcholine Transfer Protein

There is a racial disparity in survival in coronary heart disease between patients with Caucasian and Afro-Caribbean background, even after adjusting for all known factors. Edelstein et al[80] investigated whether racial differences in platelet function underpin an increased thrombotic risk. One hundred and fifty-four healthy black and white volunteers were recruited, and platelet reactivity to thrombin was measured. Higher aggregation and platelet calcium responses to PAR4-AP (thrombin receptor 4 activating peptide) in Afro-Caribbean individuals were found. PCTP (phosphatidylcholine transfer protein)–encoding mRNA was found to be upregulated in Afro-Caribbeans. After profiling platelet miRNA signatures, 178 miRNAs, including miR-376c, were predicted to target PCTP mRNA. miR-376c levels inversely correlated with PCTP mRNA levels, PCTP protein levels, and PAR4 reactivity. miR-376c is part of a cluster of miRNAs differentially expressed by ethnic origin, which may underpin differences in platelet function. Interestingly, a statistical cluster of 24 miRNAs all mapped to chromosome 14q32.2. Among other differentially expressed miRNAs were some of the most abundant platelet miRNAs: miR-223, miR-21, miR-23b, miR-107, and let-7c. Plé et al[81] also found evidence of miRNA regulation of PCTP. Their analysis predicted miR-599 targeting of the 3′UTR of PCTP mRNA and showed downregulation of a reporter gene containing the PCTP 3′UTR in HEK293 (human embryonic kidney) cells transfected with pre-miR-599.

miR-223 and $P2Y_{12}$ Receptor Expression

miR-223 is highly expressed in platelets and megakaryocytes, where it is thought to regulate thrombopoiesis. One of the most interesting features of miR-223 is its ability to bind to the 3′UTR of human $P2Y_{12}$ receptor mRNA.[6] The $P2Y_{12}$ receptor mediates important platelet functions, including aggregation and granule secretion, and is activated by ADP, the physiological agonist of this Gi_2 protein-coupled receptor. Landry et al[6] showed that platelet $P2Y_{12}$ receptor mRNA coprecipitates with Ago2, suggesting that miR-223 could regulate receptor levels and, thereby, platelet function. Platelet response to ADP antagonists is clinically relevant given the widespread use of drugs such as clopidogrel, prasugrel, and ticagrelor in the treatment of myocardial infarction and ischemic stroke.

Because of the proposed regulation of $P2Y_{12}$ receptor function, miR-223 has been the focus of many clinically orientated studies. In particular, there is great interest in relation to platelet responsiveness to clopidogrel, a prodrug that requires hepatic cytochrome P450 enzymes to become active. Shi et al[79] reported decreased levels of platelet miR-223 in association with high platelet reactivity, despite treatment with clopidogrel. They looked at patients presenting with non–ST-elevation acute coronary syndrome, in terms of their platelet reactivity index, who were treated with aspirin and clopidogrel. In patients who had a reduced response to clopidogrel, platelet miR-223 was significantly downregulated, whereas miR-96 was unchanged. Platelet miR-223 also inversely correlated with the platelet reactivity index. Of note, neither miR-223 nor miR-96 were significantly different between normal and low responders when ADP-induced platelet aggregometry was used. These results suggest that platelet miR-223 may be a predictor of normal and low responders to clopidogrel. This is supported by the fact that $P2Y_{12}$ mRNA can be found in Ago2 immunoprecipitates.[6]

In a preliminary report including 21 males presenting with non–ST-elevation acute coronary syndrome, Chyrchel et al[82] studied miR-223 plasma levels. Patients were treated with aspirin plus either clopidogrel, prasugrel, or ticagrelor. Although there were no differences in plasma miR-223 levels between drug types, when all the data were pooled, miR-223 positively correlated with the level of platelet inhibition.[82] These results seem in line with those of Shi et al[79] who found that high platelet miR-223 levels predicted efficacious platelet inhibition with clopidogrel. Similarly, Zhang et al[83] report decreased plasma miR-223 to be associated with clopidogrel low responders. In this study of 62 patients with unstable angina, miR-223 was found to be the only independent predictor of low responders to clopidogrel and was higher with greater degrees of platelet inhibition.

miR-223 is also expressed in mouse platelets. In response to high agonist concentrations, miR-223 knockout mice do not show any detectable alteration in aggregation, speed of clot retraction, platelet adhesion, or bleeding time. $P2Y_{12}$ mRNA expression levels are also unchanged.[84] This is probably because of mouse $P2Y_{12}$ mRNA lacking the specific binding site for miR-223, rendering mouse models difficult to interpret in this context. Nonetheless, Elgheznawy et al[69] subsequently demonstrated that miR-223 deletion in mice did result in modestly higher platelet activation at lower agonist concentrations. Proteomic analysis revealed differential expression of kindlin-3 and coagulation factor XIII-A in platelets from miR-223-deficient mice.

Zampetaki et al[75] found that serum miR-223 levels are inversely associated with risk of future myocardial infarction and showed a stronger association with fatal than nonfatal events. Badrnya et al[85] showed reduced platelet microvesicle miR-223 in smokers. These findings are potentially complementary to those relating low platelet miR-223 level to increased $P2Y_{12}$ activity in humans and to those showing higher platelet reactivity in response to miR-223 deletion in mice. Subsequent clinical studies have investigated platelet miR-223, including in a small cohort of patients who suffered an ischemic stroke. Duan et al[86] report that platelet miR-223 and miR-146a were lower in stroke patients with diabetes mellitus versus controls. Platelet miR-223 and miR-146a levels significantly correlated with platelet reactivity as measured by P-selectin expression and also correlated to plasma levels, suggesting that platelets are a major source of circulating miR-223.

In summary, miR-223 targets the 3′UTR of the human $P2Y_{12}$ platelet receptor mRNA. The $P2Y_{12}$ receptor is important in platelet activation and is the target of many drugs used to inhibit platelet function. Lower levels of platelet miR-223, therefore, may result in more $P2Y_{12}$ receptor activity and, thus, higher platelet reactivity. In this way, lower platelet miR-223 levels may increase the risk of thrombotic disease, such as myocardial infarction. This also may underpin the observation that lower platelet miR-223 levels are associated with reduced efficacy of $P2Y_{12}$ receptor antagonists, such as clopidogrel. Mice lack the specific miR-223-binding site on the $P2Y_{12}$ mRNA, and so comparisons to human data is difficult. Nonetheless, miR-223-deficient mice do seem to have altered platelet function, perhaps through regulation of other proteins.

miR-126 and ADAM9 (A Disintegrin and Metalloproteinase Domain-Containing Protein 9)

Early studies, including one from our group,[72] stated that miR-126 is endothelial specific. Although miR-126 is enriched in endothelial cells and supports endothelial integrity, its circulating levels cannot be attributed solely to endothelial cells. In fact, megakaryocytes and endothelial cells both express miR-126, and circulating miR-126 levels seem to be predominantly platelet derived.[34,77]

de Boer et al[87] investigated the effects of aspirin on the platelet contribution of circulating miR-126 in patients with type 2 diabetes mellitus. PRP from subjects was treated with either arachidonic acid (a platelet activator) or arachidonic acid plus aspirin. Once the PRP had been treated, it was centrifuged to separate the platelets from the now PPP. Platelet activation resulted in a considerable transfer of miR-126 to the PPP fraction, and this could be rescued with the addition of aspirin. miR-223, miR-16, and miR-423 showed a similar pattern, suggesting that they are all released from platelets on activation and that aspirin attenuates this release. miR-126 levels also correlated with platelet activation as measured by soluble P-selectin. As part of another clinical trial involving patients with type 2 diabetes mellitus, the platelet activation state (measured via P-selectin expression) was assessed in 40 patients treated with increasing doses of aspirin. Platelet activation positively correlated with plasma miR-126 and aspirin reduced circulating levels of miRNA-126. Arguing against an endothelial origin of miR-126, the authors point out that aspirin primarily inhibits platelet-enriched COX-1, whereas the endothelium predominantly expresses COX-2. They also demonstrated no change in circulating von Willebrand factor.[87] Taken together, these findings suggest that aspirin has the potential to significantly alter the miRNA signature of plasma, and careful consideration should be given when designing clinical studies in pursuit of novel biomarkers.

In our experiments, we demonstrated that plasma miR-126 levels (1) correlate to platelet MPs, (2) are reduced on platelet inhibition, and (3) are associated with markers of platelet activation in the general population.[32] These associations were further substantiated by genetic evidence. The single nucleotide polymorphism rs4636297 is located in the primary transcript-encoding region of miR-126 and affects its processing to mature miR-126. The minor allele is associated with increased processing of the primary miRNA to mature miR-126. In a population-based study, carriers of the minor allele had higher levels of miR-126 in plasma and in serum.[32] The increase in circulating miR-126 was associated with a rise in platelet activation markers, such as platelet factor 4 and proplatelet basic protein. The genetic data on miR-126 and platelet function were in line with findings in the Bruneck cohort, in which miR-126 serum levels were positively associated with risk of myocardial infarction after adjustment for miR-223 and miR-197, again with platelets being identified as the most probable source.[75] A study by Yu et al[88] showed that higher plasma miR-126 predicted major adverse cardiac events in 491 patients after a percutaneous coronary intervention, while on dual antiplatelet therapy.

In mice, inhibition of miR-126 by antagomiRs (synthetic inhibitors of miRNAs) decreased thromboxane A2-dependent platelet aggregation. This effect is likely because of megakaryocyte miR-126, but because antagomiRs are administered systemically, the contribution of other cell types, in particular endothelial cells, cannot be excluded. However, inhibition of miR-126 expression in endothelial cells would be expected to result in endothelial dysfunction and increased platelet activation. Similarly, if the effects of the single nucleotide polymorphism rs4636297 were limited to endothelial cells, one might expect that higher miR-126 levels are protective for endothelial cells and, thus, reduce platelet activity. The opposite was observed in mice and men. In MEG-01 cells, ADAM9 was confirmed as a direct miR-126 target that attenuates the adhesion of platelets to collagen. Inhibition of miR-126 by antagomiRs also had indirect effects on $P2Y_{12}$ expression levels, at least in mice. Thus, in addition to endothelial cells, miR-126 affects megakaryocytes. It remains to be seen whether platelet-specific deletion of miR-126 can recapitulate the accelerated atherosclerosis phenotype seen in miR-126-deficient mice.[89]

In summary, higher plasma or serum levels of miR-126 are associated with an increased risk of myocardial infarction and other major adverse cardiac events. This may, at least in part, occur via increased platelet activation. Inhibition of miR-126 with antagomiR-126 reduces platelet activation in mice, which may be explained by blocking of ADAM9's negative effect on platelet:collagen adhesion or via indirectly affecting platelet $P2Y_{12}$ expression levels.

Cellular Crosstalk Via miRNAs?

Several studies suggest that secreted miRNAs may act as paracrine mediators. The concept is appealing, but most evidence is currently limited to in vitro studies. By overexpressing a miRNA in one cell type, harvesting microvesicles from the conditioned media, and adding these microvesicles to recipient cells, miRNA transfer and downregulation of miRNA targets is detectable, suggesting that the miRNA uptake has biological function. There are several caveats to these in vitro studies:

1. MiRNAs are not abundant in the circulation, and preamplification is usually required for all but the most abundant miRNAs for reliable detection by

qPCR. It is difficult to envisage how the few copies of miRNAs would have a potent effect on target gene expression. The amount of circulating miRNAs is several orders of magnitude below the cellular miRNA content, and exogenous miRNAs would have to compete with the endogenous miRNAs in the recipient cells for loading into the RNA-induced silencing complex. Unless there is a receptor that recognizes miRNAs and initiates a downstream signaling cascade, it is difficult to envisage how uptake of exogenous miRNAs could mediate biological effects.

2. MPs and exosomes are rich in proteins. The protein content of microvesicles may be functionally more important than their miRNA load. RNase treatment does not unambiguously prove that the observed biological effect is because of miRNAs. Protein degradation may also occur during the RNase digestion step.
3. In situ hybridization studies for a particular miRNA tend to reveal a characteristic staining pattern. For example, staining for miR-126 is confined to endothelial cells, whereas staining for miR-143 and miR-145 is observed in vascular smooth muscle cells. If miRNA transfer was a common phenomenon, such specificity would not be detected, and a more homogenous staining pattern would be expected.
4. Importantly, the tissue architecture, including basement membranes and extracellular matrix, should act as a physical barrier for the exchange of microvesicles.
5. Routine cell culture uses fetal calf serum, which is a source of bovine microvesicles.

Thus, we currently lack convincing evidence that the exchange of miRNAs is more than an in vitro phenomenon. In uninjured tissues, cellular miRNA exchange might be low. It is conceivable that miRNA transfer could occur under pathological conditions, such as platelet activation and clearance by inflammatory cells. Several experiments shed light on the role of platelet miRNA as a putative paracrine regulator of cellular function via regulation of other cells' mRNA and protein expression. For abundant platelet miRNAs, such as miR-223, target genes have been described, many of which are associated with inflammation. This miRNA is also expressed in leukocytes, further indicating a potential role. Given that platelets are already heavily implicated in several disease processes with an inflammatory basis, an interplay between endothelial cells, leukocytes, monocytes, and other cell types by endogenous and transferred miRNA seems plausible and an important area for further investigation.

Jansen et al[90] sought to define the miRNA content of circulating microvesicles and vesicle-free plasma in 176 patients with stable coronary artery disease undergoing coronary angiography. Over 6 years follow-up, microvesicle miR-126 and miR-199a levels above the median were associated with significantly fewer major adverse cardiac events and percutaneous coronary interventions. There was no association between miRNAs from PPP and cardiovascular events. Microvesicle miR-126 was significantly reduced, and miR-199a trended toward reduction, in coronary artery disease patients versus age-matched controls. Again, no such difference was found in the PPP. Through microvesicle typing of surface markers, they established that miR-126 expression is highest in $CD31^+/CD42b^-$ microvesicles (ie, endothelial), consistent with known expression patterns in endothelial cells, and miR-199a is highest in $CD31^+/CD42b^+$ microvesicles (ie, megakaryocyte-derived). These results are in contrast to results for circulating miR-126 levels. However, this study by Jansen et al[90] looked specifically at the microvesicular compartment, making cross-study comparisons difficult.

Laffont et al[17] showed that activated platelets can deliver regulatory Ago2–miRNA complexes to endothelial cells and that this occurs via MPs. First, they confirmed that activated platelets release substantially more MPs than quiescent platelets. Profiling the miRNA content of the MPs showed that the miR-223 content was greatly increased after platelet activation, suggesting selective packaging of miRNAs into platelet MPs. They then showed that the MPs contain functional Ago2:miR-223 complexes, which could cleave a complementary miR-223 RNA sensor, suggesting that these complexes are functionally relevant. Next, they used fluorescently labeled MPs to demonstrate internalization by human umbilical vein endothelial cells. Endothelial miR-223 levels increased 22-fold after incubation with MPs for 1 hour, an effect that persisted for 48 hours. Again addressing functional relevance, endothelial cells demonstrated a 44% reduction in a transfected reporter gene under miR-223 control when incubated with MPs. Significant downregulation of endogenous RNA levels occurred within 6 hours of exposure to platelet MPs, an effect that was rescued with the addition of an miR-223-neutralizing sponge.[17]

Pan et al[91] also showed increased MP release and MP miRNA enrichment after platelet activation. In the apolipoprotein E-null mouse model of atherosclerosis, MP miR-223 content was higher than in controls. This finding was also tested in a small selection of humans, in whom miR-223 expression was found to be higher in platelets and MPs of patients with inflammatory diseases compared with healthy controls. The authors demonstrated that endothelial cells take up MPs in an ATP-dependent manner, and endothelial miR-223 levels increase without an increase in pre-miR-223, suggesting that the increase was not because of de novo synthesis in recipient cells. Both an miR-223 mimic and incubation with MPs were shown to reduce insulin-like growth factor 1 receptor protein levels. This effect was blocked by anti-miR-223. miR-223 delivery increased advanced glycation end products–induced apoptosis, potentially via reduced levels of the insulin-like growth factor 1 receptor.[91]

Finally, Gidlöf et al[67] showed that patients with ST-segment–elevation myocardial infarction had reduced levels of miR-22, miR-185, miR-320b, and miR-423-5p in platelets compared with controls and an even greater reduction in aspirated coronary artery thrombus. The authors concluded that this is because of platelet activation and miRNA release. In vitro, they demonstrated miR-22, miR-185, miR-320b, and miR-423-5p release into the supernatant after thrombin-induced platelet activation. Using platelets transfected with a scrambled, fluorescently labeled miRNA, they showed effective transfer to endothelial cells when incubated with activated platelets. Furthermore, this was shown to be MP-dependent because the addition of brefeldin A (a vesicle formation

inhibitor) prevented miRNA transfer. Overexpression of miR-22 and miR-320b in endothelial cells suggested that these miRNAs were involved in the regulation of intercellular adhesion molecule 1. When endothelial cells were incubated with platelet releasate, intercellular adhesion molecule 1 expression was downregulated by 30%. Knockdown of endogenous endothelial miR-22 and miR-320b caused an increase in intercellular adhesion molecule 1 expression, confirming that the effect was because of MP miR-22 or miR-320b. Interestingly, this could be rescued by incubating the cells with platelet releasate.

In summary, there is now good evidence that (1) platelets transfer miRNAs and (2) that this is mediated by MPs.[92,93] However, it is less certain whether this transfer is functionally relevant at physiological concentrations in vivo and to what extent the observed effects are mediated by the miRNA content rather than the protein content of the platelet MP material. Although most studies have focused on platelet transfer of miRNA to endothelial cells, Risitano et al[71] showed that RNA transfer can occur between circulating platelets and monocytes.

Guidance on How to Measure Circulating miRNAs

Research on circulating miRNAs is attracting increasing attention because noncoding RNAs may constitute an entirely new entity of biomarkers. A prerequisite for advances in this area is the generation of comparative data by independent groups. To help this, we have suggested a set of minimum-reporting standards and recommended methods for circulating miRNA data (Table).

Plasma or Serum?

A fundamental question is the choice of plasma or serum for measuring miRNAs (Figure 4). The origin of miRNAs in plasma and serum may not be the same because platelets are activated during clotting and may contribute a larger proportion of miRNAs to serum compared with plasma. In plasma, the cells are removed by centrifugation in the presence of an anticoagulant. Citrate and EDTA are the preferred anticoagulants. Heparin plasma, for the reasons outlined below, is less suitable for miRNA measurements. Platelet activation during plasma centrifugation is another concern. Serum, on the other hand, is obtained by clotting blood at room temperature for 30 minutes to 1 hour. The clotting process involves the activation of thrombin, which cleaves fibrinogen to fibrin. Thrombin is a protease and its substrate specificity is not restricted to fibrinogen. The coagulation cascade involves a series of proteases, which may degrade carrier proteins of miRNAs. This might result in a loss of miRNAs, which can be mitigated by adding RNase inhibitors.[94] If platelets release miRNAs on activation, then findings in plasma and serum might give opposite results: plasma miRNAs may reflect the platelet release prior to blood sampling, whereas serum miRNAs may reflect the extracellular and platelet miRNA content combined—the more the release, the less the content. Thus, for our most recent studies, we used PPP to link miRNAs to in vivo platelet activation.[32,34]

Platelets, Microvesicles, and Exosomes

An understanding of which specific fraction of the circulation is being measured is of the utmost importance for reproducibility and adequate interstudy comparison. Ideally, one would be able to easily separate different circulating compartments: the cellular compartments (erythrocytes, leukocytes, and platelets), the microvesicle compartment, the exosome compartment, and the particle-free compartment devoid of membrane-bound vesicles or cells. Although isolating erythrocytes and leukocytes is relatively easy based on their size and density, isolating the smaller and less dense compartments poses a greater challenge. Isolating platelets from PRP is done routinely but requires care to avoid activating the platelets during the early centrifugation steps. As platelets release microvesicles on activation, this could affect the measured miRNAs in platelets, as well as plasma.

Table. Minimum Reporting Standards and Methodological Recommendations for the Analysis of Circulating miRNAs

Minimum Reporting Standards	Recommendations
1.Phlebotomy protocol	Sample venous blood using butterfly or regular blood collection needle; standardize relevant preanalytical variables (eg, fasting, smoking, exercise).
2.Anticoagulant used	Use citrate or EDTA; avoid heparin because of interference with qPCR.
3.Time until processing	Start sample processing immediately or soon after sampling to minimize variability and degradation.
4.Sample processing	Perform an initial soft spin to collect plasma, followed by a faster platelet depletion spin with added inhibitors of platelet activation, standardize clotting time for serum.
5.Sample storage	Store samples at −80°C, avoiding freeze-thaw cycles prior to analysis.
6.RNA protocol	Use a validated miRNA or total RNA extraction kit; use a carrier (MS2 RNA or glycogen); avoid potential batch effects by coisolating RNA from across compared groups.
7.miRNA measurement platform	Avoid batch effects of different technical lots for used laboratory material and equipment.
8.Average Ct levels for each assay	Assays with an average Ct value >32 (when using a 40-cycle protocol) should be avoided. Report average Ct values to facilitate adequate interpretation of presented fold changes.
9.Variability of the normalization reference	Across-sample variability of quality control markers such as an exogenous spike-in miRNA should not exceed 1 PCR cycle.
10.Normalization method(s)	Normalize to the average Ct value of multiple assays or to an exogenous spike-in control.

Ct indicates cycle threshold; miRNA, microRNA; and qPCR, quantitative polymerase chain reaction.

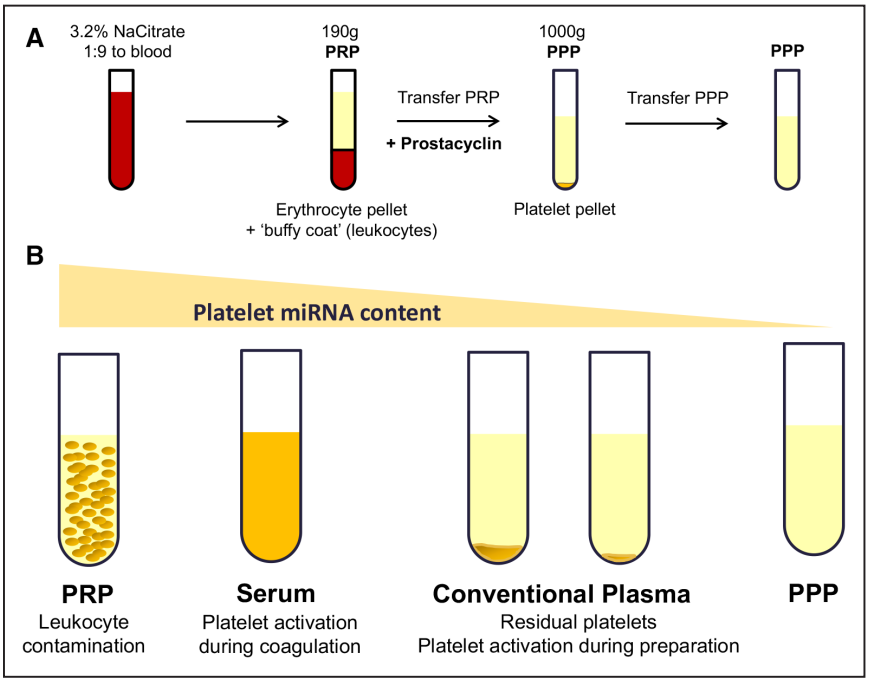

Figure 4. Choice of samples. **A**, Workflow for the preparation of platelet-poor plasma (PPP) from platelet-rich plasma (PRP). Addition of prostacyclin inhibits platelet activation during centrifugation. **B**, Concerns with regards to miRNA measurements in the different samples range from a contamination with leukocytes in PRP, proteolytic activity in serum to residual platelets in plasma. PRP and serum should reflect platelet miRNA content; PPP platelet miRNA release; plasma samples will reflect extracellular miRNA content but may additionally reflect either, platelet miRNA content or release. This depends on the amount of residual platelets in the plasma samples or platelet activation during plasma preparation, in particular during centrifugation.

Residual Platelets

Platelets contain a substantial amount of miRNAs and are likely to be major contributors to the circulating miRNA pool, as discussed earlier.[34] This further complicates sample preparation for miRNA analysis: differences in plasma preparation, centrifugation speed, duration of coagulation, and the residual platelet content will have an impact on multiple miRNAs.[95,96] In RNA extracts from plasma samples, the detection of the platelet- and megakaryocyte-specific transcript integrin α-IIb can be used to assess platelet content. Notably, the expression of integrin α-IIb correlates with the expression of abundant platelet-derived plasma miRNAs (miR-24, miR-126, miR-191, and miR-223). If plasma samples have a high residual platelet content, their miRNA profile may be more similar to that of serum and reflect predominantly platelet miRNA content rather than platelet miRNA release. Plasma platelet content must be uniform to allow comparisons between samples because residual platelets may introduce confounding. When plasma samples have already been collected, an additional centrifugation prior to RNA extraction may reduce the platelet content.[95] However, centrifugation of plasma after freezing is still subject to the risk of contamination from platelets lysed during the freeze/thaw cycle. Ideally, a method for the preparation of PPP prior to storage should be used to minimize the effect of residual platelets on miRNA measurements.

Hemolysis

Erythrocytes are the most abundant cell type in blood. The rupture of erythrocytes can occur because of high shear forces in the needle during blood collection or improper handling during sample processing. Because hemolytic samples contain a high amount of red blood cell–derived miRNAs, the levels of multiple miRNAs are altered in hemolytic samples.[97] Hemolysis can be assessed in plasma and serum by measuring hemoglobin spectrophotometrically or in the respective RNA extracts by analyzing miRNAs known to be affected by hemolysis, such as miR-451.[98] It is advisable to exclude hemolytic samples from further analyses. Alternatively, such compromised samples can only be used for miRNAs of interest that are unaffected by hemolysis.[99]

Leukocyte Contamination

Cells shed miRNAs via MPs and exosomes into the extracellular space. The miRNA content of the MPs and exosomes differs depending on the stimulus of the parent cells. However, the intracellular concentration of miRNAs is much higher than that in plasma or serum. Considering the low concentration of extracellular, circulating miRNAs, any contamination of plasma or serum samples with cellular material, for example, leukocytes, will greatly affect the miRNA profile. Thus, studies reporting a surprisingly large number of circulating miRNAs compared with other publications may have analyzed samples that were contaminated with cellular material.

Batch Effects

Batch effects can occur when analyzing the expression of miRNAs on multiple qPCR plates. To minimize their effect, several precautions should be taken to obtain reliable data: (1) to correct for variability between plates, a calibrator sample should be included across all plates. (2) The same batch of plasticware and reagents, such as PCR Mastermix, primers, and probes should be used for the entire study cohort. We have previously observed lot-to-lot-variability for miRNA reagents, even from leading manufacturers. (3) Reagents should be aliquoted because freeze-thaw cycles affect their quality and performance. (4) Samples from different groups should be distributed equally across all batches. These precautions minimize the effect of batch effects and help to obtain more reliable data.

Endogenous Normalization Controls

Normalization procedures should eliminate technical and experimental variation across samples to more reliably identify biological differences. In qPCR analysis, normalization controls are used to correct for variability in RNA extraction, reverse transcription, and PCR. Ideally, a normalization control is stably expressed and not affected by experimental conditions or clinical parameters. For the analysis of miRNAs in cells or tissue, small nucleolar RNAs are routinely used to normalize data. In general, they accurately reflect the small RNA content of a sample, although there are limitations and drawbacks. For example, small nucleolar RNAs can correlate with cancer pathology and prognosis, which can introduce bias when they are used as normalization controls for cancer samples.[100] For circulating miRNAs, however, there is no generally accepted endogenous control. Small nucleolar RNAs are intracellular RNA molecules, and their levels in the circulation are very low. U6 RNA has been used as a normalization control in plasma and serum samples but circulating levels of U6 display interindividual variability and are affected by inflammatory processes, reducing its reliability.[101] Single miRNAs or panels of miRNAs have been used or suggested as endogenous controls: miRNAs that have been used as normalizers include miR-16, miR-21, miR-93, miR-103, miR-191, miR-192, miR-423, and miR-425. These miRNAs, however, may well be affected by other uninvestigated diseases or medications. Antiplatelet therapy, for example, has been demonstrated to lower the circulating levels of plasma-derived miRNAs, including miR-21 and miR-191.[34] Alternatively, data can be normalized to the average Ct of multiple or all analyzed miRNAs.[102] Generally, combinations of miRNAs may be a more robust approach, based on the assumption that overall miRNA expression is stable and not affected by disease to the same degree as individual miRNAs. The more miRNAs that are combined, the more robust the control should be. However, this normalization method can be problematic when several of the miRNAs used to normalize are dysregulated in a similar direction, potentially causing false-positive or false-negative findings. Nonetheless, accepting that no better alternatives exist, a combination of miRNAs represents the most stringent endogenous normalization control.

Exogenous Normalization Controls

The most commonly used exogenous normalization method for circulating miRNA analysis is the use of a spike-in control. For this purpose, synthetic oligonucleotides of miRNA sequences from other species are used, typically from the nematode *Caenorhabditis elegans* (eg, cel-miR-39). Such spike-in controls are added in equal amounts to each sample during RNA extraction or reverse transcription. A spike-in control added at the RNA extraction step can normalize for differences in extraction efficiency, reverse transcription, or qPCR efficiency, which may be caused by the presence of inhibitors in the sample or pipetting errors. Spike-in controls generally reflect miRNA quantities in different samples, but we have observed that RNA samples display a lower quantity of cel-miR-39 when they were stored at −80°C for a longer period of time, impairing analysis in older samples. Moreover, heparin medication can affect cel-miR-39, as well as the measurement of miRNAs, depending on their origin.[103,104] The cel-miR-39 measurements across samples must be stable. Variability exceeding 0.5 to 1 Ct values should be cause for concern.

MiRNA Measurements

The gold standard for miRNA measurements is qPCR. It provides independent and robust amplification and quantitative detection of minute RNA amounts across the wide dynamic range of miRNA expression levels. Among the drawbacks of the technology is the fact that its high-throughput capabilities are limited. We have previously compared commercial qPCR assays and obtained good agreement between assays from 2 suppliers, for individual Taqman miRNA assays and customized qPCR plates from Exiqon. For customized qPCR plates, however, there is the possibility that variations in the manufacturing process remain undetected. This is less likely to occur in standard miRNA assays because multiple users will rapidly detect manufacturing problems. Thus, it is important to know the expected measurement range for miRNAs of interest when using customized qPCR plates and to compare the results from each batch of customized qPCR plates with individual qPCR assays.

We and others have noted difficulties comparing miRNA measurements from different technologies. In particular, there is poor agreement between microarrays and qPCRs when assessing quantitative changes. Microarray-based technologies use hybridization and are suitable for detecting the presence of miRNA species, but have limited quantitative accuracy and dynamic range. Similarly, NGS has several drawbacks, in particular, requiring much larger sample volumes than qPCR analysis and the introduction of amplification bias for certain miRNAs during library preparation. For example, in our study, we obtained most reads for miR-486, a miRNA that is present in the circulation but has a relatively high Ct value by qPCR, suggesting that it is much less abundant than other circulating miRNAs. Thus, miRNAs with more sequencing reads are not necessarily more abundant (Figure 5). Quantitative comparison must only be made by comparing sequencing reads for the same miRNAs.

Freedman et al used high-throughput microfluidic quantitative PCR to analyze the miRNA signature in blood (whole blood, platelets, mononuclear cells, plasma, and serum) collected from 5 healthy individuals. They screened for 852 miRNAs in 83 patients undergoing diagnostic coronary angiography and categorized their patients into 2 groups: with coronary artery stenosis ≥70% (n=34) and without (n=49). Increased plasma levels of miR-494, miR-769-3p, and miR-490-3p were associated with ≥70% coronary stenosis, and logistic regression analysis found that antihypertensive therapy, smoking, and miR-769-3p were significantly associated with coronary status.[105] In this study, few of the commonly reported highly expressed miRNAs were amongst the top 10 ranking miRNAs in platelets (Figure 3). It is likely that there are similar discrepancies with plasma and serum miRNA measurements. One cause for this difference may be the high-throughput BioMark Real-Time Fluidigm PCR system used in this study to increase the number of miRNA measurements

that can be performed simultaneously; no direct comparison with conventional qPCR was provided.

Potential for Clinical Translation

The miRNA biomarker field is currently nascent. Although there is much to link the expression of miRNAs to various diseases, the clinical utility or validity of miRNA detection has not been demonstrated. Currently, miRNAs are manually extracted, presenting the largest obstacle to increasing throughput. If new technological platforms provide the opportunity for faster miRNA extraction or direct analysis of miRNAs without the need for miRNA extraction, they will significantly improve the ease-of-use in clinical settings. Increasing throughput, however, must not compromise the quantitative accuracy of the analysis for both low- and high-abundance miRNAs. Ideally, miRNA measurements need to be able to outperform current diagnostic methods to reach the clinical mainstream.

In addition to current practical limitations, miRNA biomarkers will also need to be presented in the context of related miRNAs to be adequately interpreted. There are relatively few tissue-specific miRNAs, with miR-122 being an exception given its exquisite liver specificity.[106] We have recently shown that high circulating miR-122 levels are associated with an adverse lipid profile and predict development of metabolic syndrome and diabetes mellitus type 2.[107] However, most circulating miRNAs are ubiquitously expressed, and numerous cell types can release miRNAs. This complicates the clinical application because levels of individual miRNAs can greatly vary between patients, without any pathological significance. Therefore, it is crucial to represent relative expression levels of a miRNA in relation to a network of several other miRNAs. The use of a so-called miRNA signature can greatly strengthen the predictive and diagnostic value.

Because the origin of many plasma miRNAs is unknown, De Rosa et al[108] investigated transcoronary gradients of various miRNAs in patients with acute coronary syndrome in a bid to define coronary-specific changes in the setting of myocardial damage. Samples were taken from the aorta and coronary sinus. They found an upregulation of the muscle-enriched miR-499, miR-133a, and miR-208a in acute coronary syndrome patients, of which miR-499 correlated with troponin levels, an established clinical marker of myocardial damage. Contrary to their predictions, miR-126 decreased across the coronary circulation, despite its high expression in endothelial cells. They also described a negative trend for miR-223 across the coronary circulation in the acute coronary syndrome group but not in the stable coronary artery disease group; however, this did not reach statistical significance.[108] An alternative explanation for the reduction in miR-126 and miR-223 across the

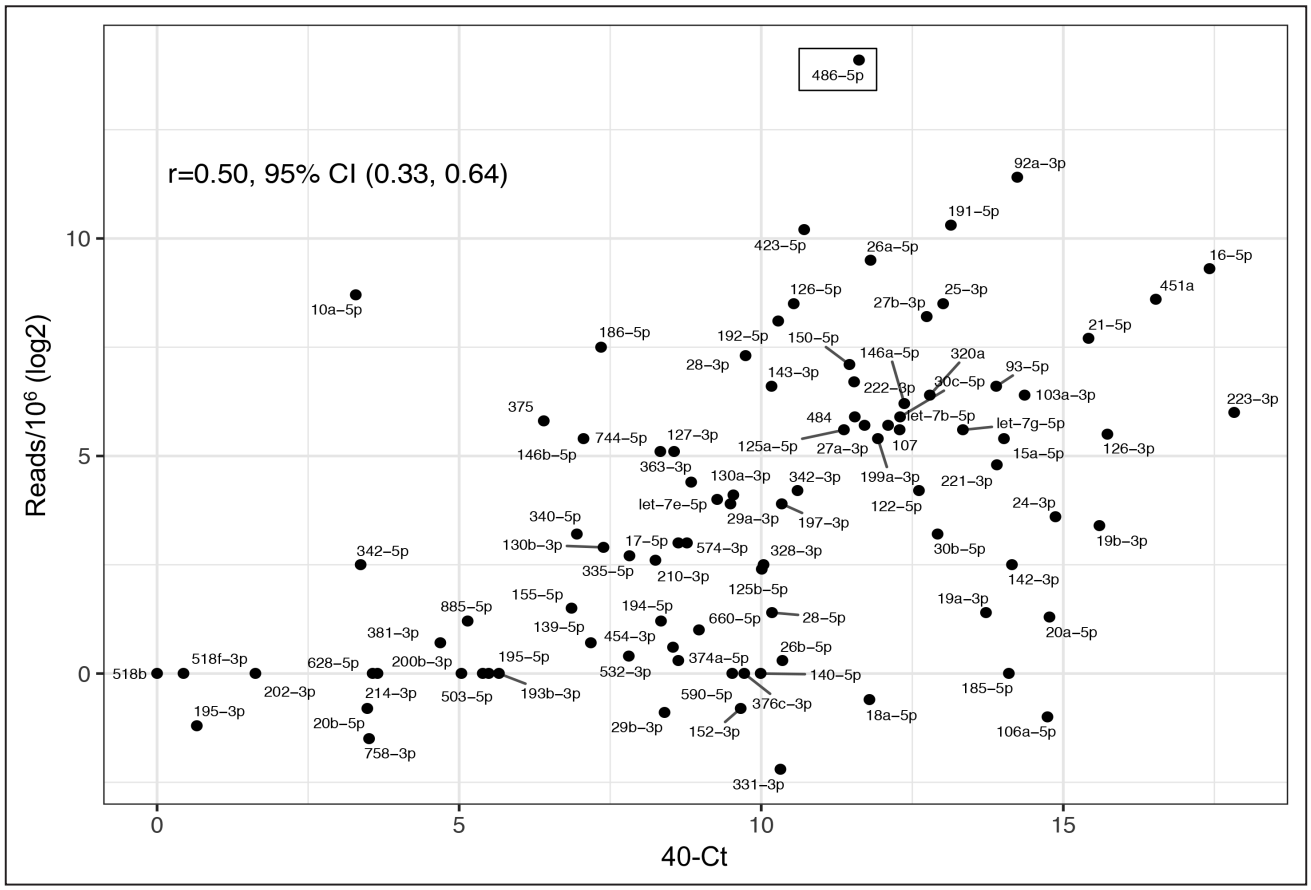

Figure 5. Discrepancy between miRNA quantification by reverse transcriptase quantitative polymerase chain reaction (RT-qPCR) and RNA sequencing. Average expression of 92 miRNAs was assessed in platelet-poor plasma (PPP) from healthy subjects (n=12), using custom-made Exiqon locked nucleic acid (LNA) qPCR plates. Cycle-to-threshold (Ct) values are shown as 40-Ct (*x* axis). Small RNA sequencing was performed with PPP from healthy subjects (n=2). miR-486-5p is highlighted, showing high sequencing reads (*y* axis), despite inferred midrange abundance by qPCR. CI indicates confidence interval.

coronary circulation is the retention of platelets and platelet MPs in the affected myocardium or differential activation of platelets in venous and arterial settings.

Pharmacological inhibitors can be used to identify the cellular origins of miRNAs. By comparing plasma miRNA levels in the same individuals before and after initiation of antiplatelet therapy, we identified a set of plasma miRNAs that is responsive to antiplatelet therapy.[34] The miRNA candidates were abundant in platelets, but they were not platelet-specific. Moreover, not every abundant platelet miRNA was equally affected by antiplatelet medication. Some miRNAs, despite their abundance in platelets, may be expressed at higher levels in other cell types. Consequently, their plasma levels may be less dependent on platelets. Given the platelet origin of many abundant circulating miRNAs, it is not surprising that the same miRNAs are dysregulated in multiple diseases. The question, however, remains whether the circulating miRNA changes are cause or consequence. In cancer, for example, many of the circulating miRNA alterations may be because of platelet activation or inflammation, rather than the release of miRNAs from tumor tissue.

Early studies compared platelet samples from different individuals. Longitudinal sampling eliminates interindividual variability. For example, using serial measurements before and after antiplatelet medication, we investigated the effect of 10 mg prasugrel followed by the addition of an escalating aspirin dose regimen (75 mg daily in week 2 and 300 mg daily in week 3) on the PPP miRNA signature of healthy young volunteers. Using custom-made miRNA qPCR plates, 92 targets were measured at 4 different time points. Antiplatelet therapy was associated with a reduction in plasma miR-223, miR-126, miR-15, miR-191, miR-20b, miR-21, and miR-24. The findings were replicated in plasma of patients with recent symptomatic carotid atherosclerosis who had begun treatment with dipyridamole or clopidogrel, in addition to aspirin. These patients showed a reduction in miR-223, miR-126, miR-150, and miR-191.[34] The effect was less pronounced, presumably because the symptomatic patients were on aspirin medication at baseline and the follow-up measurement was only taken after 48 hours. The reduction in platelet miRNAs on platelet inhibition complements previous findings by Zampetaki et al[75] in an ischemia/reperfusion injury model by thigh cuff inflation, in which plasma miRNAs increased on platelet activation.

The clinical use of platelet function tests is limited at present, despite clear differences in response to pharmacological platelet inhibition. In the case of clopidogrel, a prodrug, a large percentage of this variation can be attributed to different cytochrome P450 isoforms involved in its bioactivation.[109] However, this in itself does not explain all of the variation in efficacy. Measurements of platelet activity by light transmission aggregometry are considered the gold standard, but this test is performed ex vivo and not well standardized between laboratories. Vasodilator-stimulated phosphoprotein (VASP) phosphorylation and VerifyNow $P2Y_{12}$ assays measure platelet activation in full blood but only in response to a single pathway, ADP stimulation. Platelet miRNAs may offer an opportunity to obtain an alternative read-out for platelet activation in vivo that integrates activation by multiple agonists rather than just ADP (Figure 6). Platelet miRNA measurements, however, will only be useful if they provide diagnostic advantages. They also must be easy to perform and capable of discriminating the degree of interindividual variability in platelet inhibition or platelet turnover.

Conclusions

Initially, circulating miRNAs were thought to originate from tissue injury. This is indeed the case for cardiac miRNAs that are released after myocardial infarction akin to troponins. For basal miRNA levels, however, the importance of circulating cells is now apparent, and the contribution from anucleate cells such as erythrocytes and platelets must not be underestimated. Several challenges face the accurate detection and use of plasma and serum miRNAs:

1. Variability in samples' cell composition affect miRNA profiles. This includes anuclear cells such as erythrocytes and residual platelets. Preanalytic variation in sample preparation or handling must be minimized to avoid alterations of results. Given the platelet origin of many abundant circulating miRNAs, the use of PPP would seem to be an appropriate substrate for miRNA measurements. In conventional plasma samples, the number of residual platelets can vary. Also, without inhibitors, platelet activation may occur during centrifugation. In serum, the stability of miRNAs may be affected, and miRNAs may get trapped in the clot. This could introduce bias that affects results, in particular, if the clotting time varies between sampling.
2. The concentration of extracellularly circulating miRNAs is low, and the miRNA yield of plasma and serum is insufficient for conventional quality control methods, such as optical densitometry or Bioanalyzer. Generally, equal volumes of plasma or serum are used for extraction. No correction is performed for RNA content. This approach of normalizing by volume is, however, analogous to protein measurements. In both cases, the total RNA or total protein amount of plasma or serum would not be a suitable normalization control for the miRNA or protein biomarker of interest.
3. Currently, there is no endogenous control for the normalization of circulating miRNAs. Instead, exogenous spike-in controls are used for normalizing the extraction procedure. The values of spike-in controls such as cel-miR-39 relate entirely to the consistency of the isolation procedure, not to the starting RNA quantity. By measuring a broader panel of unrelated miRNAs, the mean Ct value can be used for normalization.
4. Circulating miRNAs are highly correlated. Assessing individual miRNAs without integration into a wider miRNA network is of limited utility. Relative changes in miRNAs to one another (so-called miRNA signatures) can be more informative than the changes of individual miRNAs.

These points will need to be addressed in future publications on miRNA biomarkers to facilitate comparability between studies, something that has been difficult with variations between measurement platforms and lack of guidelines for standardization. Standardized miRNA measurement platforms are currently under development, which could reduce measurement variability,

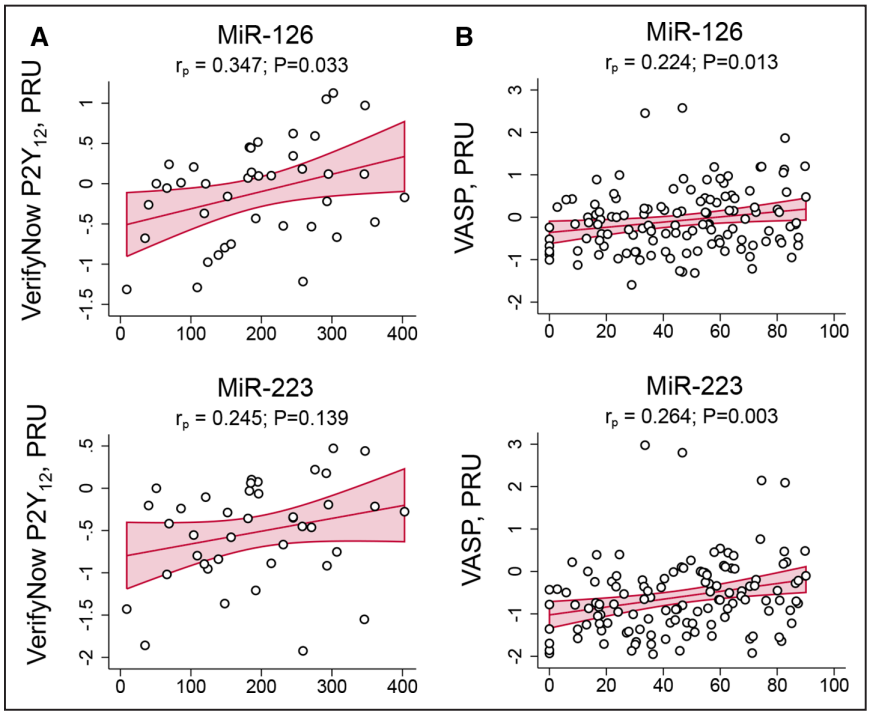

Figure 6. MiRNAs and platelet reactivity. Association of miR-126 and miR-223 levels in platelet-poor plasma (PPP) to the VerifyNow $P2Y_{12}$ aggregation test (**A**) and the vasodilator-stimulated phosphoprotein (VASP) phosphorylation assay (**B**) in patients on dual antiplatelet therapy for 30 days postacute coronary syndrome. Note that fewer samples were measured with the VerifyNow (n=39) compared with the VASP assay (n=123). PRU denotes $P2Y_{12}$ reaction units (*x* axis). Higher PRU values reflect higher $P2Y_{12}$-mediated platelet reactivity.

while facilitating cross-study comparisons. In addition to the need for consensus on sample preparation and analytic procedures, future research will need to move on from reporting on single miRNAs and focus more on miRNA signatures and integration with predicted target genes.[77,107,110] These issues are not insurmountable, and once addressed, future studies can further evaluate the potential of miRNA biomarkers for clinical use and whether miRNA assays will outperform existing clinical measurements.

Acknowledgments

We thank Dr Raimund Pechlaner and Dr Peter Willeit from the Department of Neurology, Medical University of Innsbruck, Austria, for providing figures.

Sources of Funding

M. Mayr is a Senior fellow of the British Heart Foundation (BHF, FS/13/2/29892) and supported by the Fondation Leducq (MIRVAD; 13 CVD 02) and the NIHR Biomedical Research Center based at Guy's and St. Thomas' National Health Service Foundation Trust and King's College London, in partnership with King's College Hospital. T. Barwari is an Interdisciplinary PhD student funded by the BHF. A. Joshi has been awarded a BHF Clinical Research Training Fellowship. R.P. Huntley and R.C. Lovering are supported by funding from a British Heart Foundation grant (RG/13/5/30112) and the National Institute for Health Research University College London Hospitals Biomedical Research Centre.

Disclosures

M. Mayr is named inventor on patents that detail claims related to circulating miRNAs as biomarkers. M. Mayr has received a research grant from Astra Zeneca for investigating the effects of antiplatelets on circulating miRNAs. The other authors report no conflicts.

References

1. Gurbel PA, Jeong YH, Navarese EP, Tantry US. Platelet-mediated thrombosis: from bench to bedside. *Circ Res*. 2016;118:1380–1391. doi: 10.1161/CIRCRESAHA.115.307016.
2. Kieffer N, Guichard J, Farcet JP, Vainchenker W, Breton-Gorius J. Biosynthesis of major platelet proteins in human blood platelets. *Eur J Biochem*. 1987;164:189–195.
3. Warshaw AL, Laster L, Shulman NR. Protein synthesis by human platelets. *J Biol Chem*. 1967;242:2094–2097.
4. Bray PF, McKenzie SE, Edelstein LC, Nagalla S, Delgrosso K, Ertel A, Kupper J, Jing Y, Londin E, Loher P, Chen HW, Fortina P, Rigoutsos I. The complex transcriptional landscape of the anucleate human platelet. *BMC Genomics*. 2013;14:1. doi: 10.1186/1471-2164-14-1.
5. Rowley JW, Oler AJ, Tolley ND, Hunter BN, Low EN, Nix DA, Yost CC, Zimmerman GA, Weyrich AS. Genome-wide RNA-seq analysis of human and mouse platelet transcriptomes. *Blood*. 2011;118:e101–e111. doi: 10.1182/blood-2011-03-339705.
6. Landry P, Plante I, Ouellet DL, Perron MP, Rousseau G, Provost P. Existence of a microRNA pathway in anucleate platelets. *Nat Struct Mol Biol*. 2009;16:961–966. doi: 10.1038/nsmb.1651.
7. Nagalla S, Shaw C, Kong X, Kondkar AA, Edelstein LC, Ma L, Chen J, McKnight GS, López JA, Yang L, Jin Y, Bray MS, Leal SM, Dong JF, Bray PF. Platelet microRNA-mRNA coexpression profiles correlate with platelet reactivity. *Blood*. 2011;117:5189–5197. doi: 10.1182/blood-2010-09-299719.
8. Mitchell PS, Parkin RK, Kroh EM, et al. Circulating microRNAs as stable blood-based markers for cancer detection. *Proc Natl Acad Sci U S A*. 2008;105:10513–10518. doi: 10.1073/pnas.0804549105.
9. Arroyo JD, Chevillet JR, Kroh EM, Ruf IK, Pritchard CC, Gibson DF, Mitchell PS, Bennett CF, Pogosova-Agadjanyan EL, Stirewalt DL, Tait JF, Tewari M. Argonaute2 complexes carry a population of circulating microRNAs independent of vesicles in human plasma. *Proc Natl Acad Sci U S A*. 2011;108:5003–5008. doi: 10.1073/pnas.1019055108.
10. Vickers KC, Palmisano BT, Shoucri BM, Shamburek RD, Remaley AT. MicroRNAs are transported in plasma and delivered to recipient cells by high-density lipoproteins. *Nat Cell Biol*. 2011;13:423–433. doi: 10.1038/ncb2210.
11. Turchinovich A, Weiz L, Langheinz A, Burwinkel B. Characterization of extracellular circulating microRNA. *Nucleic Acids Res*. 2011;39:7223–7233. doi: 10.1093/nar/gkr254.
12. Hunter MP, Ismail N, Zhang X, Aguda BD, Lee EJ, Yu L, Xiao T, Schafer J, Lee ML, Schmittgen TD, Nana-Sinkam SP, Jarjoura D, Marsh CB. Detection of microRNA expression in human peripheral blood microvesicles. *PLoS One*. 2008;3:e3694. doi: 10.1371/journal.pone.0003694.
13. Flaumenhaft R, Dilks JR, Richardson J, Alden E, Patel-Hett SR, Battinelli E, Klement GL, Sola-Visner M, Italiano JE Jr. Megakaryocyte-derived microparticles: direct visualization and distinction from

platelet-derived microparticles. *Blood*. 2009;113:1112–1121. doi: 10.1182/blood-2008-06-163832.
14. Burnouf T, Goubran HA, Chou ML, Devos D, Radosevic M. Platelet microparticles: detection and assessment of their paradoxical functional roles in disease and regenerative medicine. *Blood Rev*. 2014;28:155–166. doi: 10.1016/j.blre.2014.04.002.
15. Italiano JE Jr, Mairuhu AT, Flaumenhaft R. Clinical relevance of microparticles from platelets and megakaryocytes. *Curr Opin Hematol*. 2010;17:578–584. doi: 10.1097/MOH.0b013e32833e77ee.
16. Valadi H, Ekström K, Bossios A, Sjöstrand M, Lee JJ, Lötvall JO. Exosome-mediated transfer of mRNAs and microRNAs is a novel mechanism of genetic exchange between cells. *Nat Cell Biol*. 2007;9:654–659. doi: 10.1038/ncb1596.
17. Laffont B, Corduan A, Plé H, Duchez AC, Cloutier N, Boilard E, Provost P. Activated platelets can deliver mRNA regulatory Ago2•microRNA complexes to endothelial cells via microparticles. *Blood*. 2013;122:253–261. doi: 10.1182/blood-2013-03-492801.
18. McManus DD, Freedman JE. MicroRNAs in platelet function and cardiovascular disease. *Nat Rev Cardiol*. 2015;12:711–717. doi: 10.1038/nrcardio.2015.101.
19. Kozomara A, Griffiths-Jones S. miRBase: annotating high confidence microRNAs using deep sequencing data. *Nucleic Acids Res*. 2014;42:D68–D73. doi: 10.1093/nar/gkt1181.
20. Bartel DP. MicroRNAs: target recognition and regulatory functions. *Cell*. 2009;136:215–233. doi: 10.1016/j.cell.2009.01.002.
21. Friedman RC, Farh KK, Burge CB, Bartel DP. Most mammalian mRNAs are conserved targets of microRNAs. *Genome Res*. 2009;19:92–105. doi: 10.1101/gr.082701.108.
22. Selbach M, Schwanhäusser B, Thierfelder N, Fang Z, Khanin R, Rajewsky N. Widespread changes in protein synthesis induced by microRNAs. *Nature*. 2008;455:58–63. doi: 10.1038/nature07228.
23. Barwari T, Joshi A, Mayr M. MicroRNAs in cardiovascular disease. *J Am Coll Cardiol*. 2016;68:2577–2584. doi: 10.1016/j.jacc.2016.09.945.
24. Ipsaro JJ, Joshua-Tor L. From guide to target: molecular insights into eukaryotic RNA-interference machinery. *Nat Struct Mol Biol*. 2015;22:20–28. doi: 10.1038/nsmb.2931.
25. Jonas S, Izaurralde E. Towards a molecular understanding of microRNA-mediated gene silencing. *Nat Rev Genet*. 2015;16:421–433. doi: 10.1038/nrg3965.
26. Denli AM, Tops BB, Plasterk RH, Ketting RF, Hannon GJ. Processing of primary microRNAs by the Microprocessor complex. *Nature*. 2004;432:231–235. doi: 10.1038/nature03049.
27. Gregory RI, Yan KP, Amuthan G, Chendrimada T, Doratotaj B, Cooch N, Shiekhattar R. The Microprocessor complex mediates the genesis of microRNAs. *Nature*. 2004;432:235–240. doi: 10.1038/nature03120.
28. Chendrimada TP, Gregory RI, Kumaraswamy E, Norman J, Cooch N, Nishikura K, Shiekhattar R. TRBP recruits the Dicer complex to Ago2 for microRNA processing and gene silencing. *Nature*. 2005;436:740–744. doi: 10.1038/nature03868.
29. Rana TM. Illuminating the silence: understanding the structure and function of small RNAs. *Nat Rev Mol Cell Biol*. 2007;8:23–36. doi: 10.1038/nrm2085.
30. Opalinska JB, Bersenev A, Zhang Z, Schmaier AA, Choi J, Yao Y, D'Souza J, Tong W, Weiss MJ. MicroRNA expression in maturing murine megakaryocytes. *Blood*. 2010;116:e128–e138. doi: 10.1182/blood-2010-06-292920.
31. Creemers EE, Tijsen AJ, Pinto YM. Circulating microRNAs: novel biomarkers and extracellular communicators in cardiovascular disease? *Circ Res*. 2012;110:483–495. doi: 10.1161/CIRCRESAHA.111.247452.
32. Kaudewitz D, Skroblin P, Bender LH, et al. Association of microRNAs and YRNAs with platelet function. *Circ Res*. 2016;118:420–432. doi: 10.1161/CIRCRESAHA.114.305663.
33. Mayr M, Zampetaki A, Willeit P, Willeit J, Kiechl S. MicroRNAs within the continuum of postgenomics biomarker discovery. *Arterioscler Thromb Vasc Biol*. 2013;33:206–214. doi: 10.1161/ATVBAHA.112.300141.
34. Willeit P, Zampetaki A, Dudek K, et al. Circulating microRNAs as novel biomarkers for platelet activation. *Circ Res*. 2013;112:595–600. doi: 10.1161/CIRCRESAHA.111.300539.
35. Bleazard T, Lamb JA, Griffiths-Jones S. Bias in microRNA functional enrichment analysis. *Bioinformatics*. 2015;31:1592–1598. doi: 10.1093/bioinformatics/btv023.
36. Huntley RP, Sitnikov D, Orlic-Milacic M, et al. Guidelines for the functional annotation of microRNAs using the gene ontology. *RNA*. 2016;22:667–676. doi: 10.1261/rna.055301.115.
37. Gene Ontology microRNAs. Available at https://www.ucl.ac.uk/functional-gene-annotation/cardiovascular/projects/tabs/gene-ontology-mirnas. Accessed November 23, 2016.
38. AmiGO2; Kaudewitz *et al*. Available at http://amigo.geneontology.org/amigo/reference/PMID:26646931. Accessed November 23, 2016.
39. Wolin SL, Steitz JA. Genes for two small cytoplasmic Ro RNAs are adjacent and appear to be single-copy in the human genome. *Cell*. 1983;32:735–744.
40. Perreault J, Perreault JP, Boire G. Ro-associated Y RNAs in metazoans: evolution and diversification. *Mol Biol Evol*. 2007;24:1678–1689. doi: 10.1093/molbev/msm084.
41. Christov CP, Gardiner TJ, Szüts D, Krude T. Functional requirement of noncoding Y RNAs for human chromosomal DNA replication. *Mol Cell Biol*. 2006;26:6993–7004. doi: 10.1128/MCB.01060-06.
42. Hogg JR, Collins K. Human Y5 RNA specializes a Ro ribonucleoprotein for 5S ribosomal RNA quality control. *Genes Dev*. 2007;21:3067–3072. doi: 10.1101/gad.1603907.
43. Chen X, Wolin SL. The Ro 60 kDa autoantigen: insights into cellular function and role in autoimmunity. *J Mol Med (Berl)*. 2004;82:232–239.
44. Dhahbi JM, Spindler SR, Atamna H, Boffelli D, Mote P, Martin DI. 5'-YRNA fragments derived by processing of transcripts from specific YRNA genes and pseudogenes are abundant in human serum and plasma. *Physiol Genomics*. 2013;45:990–998. doi: 10.1152/physiolgenomics.00129.2013.
45. Nicolas FE, Hall AE, Csorba T, Turnbull C, Dalmay T. Biogenesis of Y RNA-derived small RNAs is independent of the microRNA pathway. *FEBS Lett*. 2012;586:1226–1230. doi: 10.1016/j.febslet.2012.03.026.
46. Böttcher K, Wenzel A, Warnecke JM. Investigation of the origin of extracellular RNA in human cell culture. *Ann N Y Acad Sci*. 2006;1075:50–56. doi: 10.1196/annals.1368.006.
47. Cabrera-Fuentes HA, Ruiz-Meana M, Simsekyilmaz S, et al. RNase1 prevents the damaging interplay between extracellular RNA and tumour necrosis factor-α in cardiac ischaemia/reperfusion injury. *Thromb Haemost*. 2014;112:1110–1119. doi: 10.1160/TH14-08-0703.
48. Zernecke A, Preissner KT. Extracellular ribonucleic acids (RNA) enter the stage in cardiovascular disease. *Circ Res*. 2016;118:469–479. doi: 10.1161/CIRCRESAHA.115.307961.
49. Derrien T, Johnson R, Bussotti G, et al. The GENCODE v7 catalog of human long noncoding RNAs: analysis of their gene structure, evolution, and expression. *Genome Res*. 2012;22:1775–1789. doi: 10.1101/gr.132159.111.
50. Kumarswamy R, Bauters C, Volkmann I, Maury F, Fetisch J, Holzmann A, Lemesle G, de Groote P, Pinet F, Thum T. Circulating long noncoding RNA, LIPCAR, predicts survival in patients with heart failure. *Circ Res*. 2014;114:1569–1575. doi: 10.1161/CIRCRESAHA.114.303915.
51. Skroblin P, Mayr M. "Going long": long non-coding RNAs as biomarkers. *Circ Res*. 2014;115:607–609. doi: 10.1161/CIRCRESAHA.114.304839.
52. Alhasan AA, Izuogu OG, Al-Balool HH, Steyn JS, Evans A, Colzani M, Ghevaert C, Mountford JC, Marenah L, Elliott DJ, Santibanez-Koref M, Jackson MS. Circular RNA enrichment in platelets is a signature of transcriptome degradation. *Blood*. 2016;127:e1–e11. doi: 10.1182/blood-2015-06-649434.
53. Sanger HL, Klotz G, Riesner D, Gross HJ, Kleinschmidt AK. Viroids are single-stranded covalently closed circular RNA molecules existing as highly base-paired rod-like structures. *Proc Natl Acad Sci U S A*. 1976;73:3852–3856.
54. Salzman J, Gawad C, Wang PL, Lacayo N, Brown PO. Circular RNAs are the predominant transcript isoform from hundreds of human genes in diverse cell types. *PLoS One*. 2012;7:e30733. doi: 10.1371/journal.pone.0030733.
55. Memczak S, Jens M, Elefsinioti A, et al. Circular RNAs are a large class of animal RNAs with regulatory potency. *Nature*. 2013;495:333–338. doi: 10.1038/nature11928.
56. Chen LL. The biogenesis and emerging roles of circular RNAs. *Nat Rev Mol Cell Biol*. 2016;17:205–211. doi: 10.1038/nrm.2015.32.
57. Conn SJ, Pillman KA, Toubia J, Conn VM, Salmanidis M, Phillips CA, Roslan S, Schreiber AW, Gregory PA, Goodall GJ. The RNA binding protein quaking regulates formation of circRNAs. *Cell*. 2015;160:1125–1134. doi: 10.1016/j.cell.2015.02.014.
58. Hansen TB, Jensen TI, Clausen BH, Bramsen JB, Finsen B, Damgaard CK, Kjems J. Natural RNA circles function as efficient microRNA sponges. *Nature*. 2013;495:384–388. doi: 10.1038/nature11993.
59. Plé H, Landry P, Benham A, Coarfa C, Gunaratne PH, Provost P. The repertoire and features of human platelet microRNAs. *PLoS ONE*. 2012;7:e50746. doi: 10.1371/journal.pone.0050746.

60. Simon LM, Edelstein LC, Nagalla S, Woodley AB, Chen ES, Kong X, Ma L, Fortina P, Kunapuli S, Holinstat M, McKenzie SE, Dong JF, Shaw CA, Bray PF. Human platelet microRNA-mRNA networks associated with age and gender revealed by integrated plateletomics. *Blood*. 2014;123:e37–e45. doi: 10.1182/blood-2013-12-544692.
61. Wang K, Yuan Y, Cho JH, McClarty S, Baxter D, Galas DJ. Comparing the MicroRNA spectrum between serum and plasma. *PLoS One*. 2012;7:e41561. doi: 10.1371/journal.pone.0041561.
62. Yu S, Deng G, Qian D, Xie Z, Sun H, Huang D, Li Q. Detection of apoptosis-associated microRNA in human apheresis platelets during storage by quantitative real-time polymerase chain reaction analysis. *Blood Transfus*. 2014;12:541–547. doi: 10.2450/2014.0291-13.
63. Ferreiro JL, Sibbing D, Angiolillo DJ. Platelet function testing and risk of bleeding complications. *Thromb Haemost*. 2010;103:1128–1135. doi: 10.1160/TH09-11-0799.
64. Capodanno D, Patel A, Dharmashankar K, Ferreiro JL, Ueno M, Kodali M, Tomasello SD, Capranzano P, Seecheran N, Darlington A, Tello-Montoliu A, Desai B, Bass TA, Angiolillo DJ. Pharmacodynamic effects of different aspirin dosing regimens in type 2 diabetes mellitus patients with coronary artery disease. *Circ Cardiovasc Interv*. 2011;4:180–187. doi: 10.1161/CIRCINTERVENTIONS.110.960187.
65. Bernlochner I, Goedel A, Plischke C, Schüpke S, Haller B, Schulz C, Mayer K, Morath T, Braun S, Schunkert H, Siess W, Kastrati A, Laugwitz KL. Impact of immature platelets on platelet response to ticagrelor and prasugrel in patients with acute coronary syndrome. *Eur Heart J*. 2015;36:3202–3210. doi: 10.1093/eurheartj/ehv326.
66. Stratz C, Nührenberg TG, Binder H, Valina CM, Trenk D, Hochholzer W, Neumann FJ, Fiebich BL. Micro-array profiling exhibits remarkable intra-individual stability of human platelet micro-RNA. *Thromb Haemost*. 2012;107:634–641. doi: 10.1160/TH11-10-0742.
67. Gidlöf O, van der Brug M, Ohman J, Gilje P, Olde B, Wahlestedt C, Erlinge D. Platelets activated during myocardial infarction release functional miRNA, which can be taken up by endothelial cells and regulate ICAM1 expression. *Blood*. 2013;121:3908–3917, S1. doi: 10.1182/blood-2012-10-461798.
68. Ward JA, Esa N, Pidikiti R, Freedman JE, Keaney JF, Tanriverdi K, Vitseva O, Ambros V, Lee R, McManus DD. Circulating cell and plasma microRNA profiles differ between Non-ST-segment and ST-segment-elevation myocardial infarction. *Fam Med Med Sci Res*. 2013;2:108. doi: 10.4172/2327-4972.1000108.
69. Elgheznawy A, Shi L, Hu J, Wittig I, Laban H, Pircher J, Mann A, Provost P, Randriamboavonjy V, Fleming I. Dicer cleavage by calpain determines platelet microRNA levels and function in diabetes. *Circ Res*. 2015;117:157–165. doi: 10.1161/CIRCRESAHA.117.305784.
70. Liang H, Yan X, Pan Y, Wang Y, Wang N, Li L, Liu Y, Chen X, Zhang CY, Gu H, Zen K. MicroRNA-223 delivered by platelet-derived microvesicles promotes lung cancer cell invasion via targeting tumor suppressor EPB41L3. *Mol Cancer*. 2015;14:58. doi: 10.1186/s12943-015-0327-z.
71. Risitano A, Beaulieu LM, Vitseva O, Freedman JE. Platelets and platelet-like particles mediate intercellular RNA transfer. *Blood*. 2012;119:6288–6295. doi: 10.1182/blood-2011-12-396440.
72. Zampetaki A, Kiechl S, Drozdov I, Willeit P, Mayr U, Prokopi M, Mayr A, Weger S, Oberhollenzer F, Bonora E, Shah A, Willeit J, Mayr M. Plasma microRNA profiling reveals loss of endothelial miR-126 and other microRNAs in type 2 diabetes. *Circ Res*. 2010;107:810–817. doi: 10.1161/CIRCRESAHA.110.226357.
73. Randriamboavonjy V, Isaak J, Elgheznawy A, Pistrosch F, Frömel T, Yin X, Badenhoop K, Heide H, Mayr M, Fleming I. Calpain inhibition stabilizes the platelet proteome and reactivity in diabetes. *Blood*. 2012;120:415–423. doi: 10.1182/blood-2011-12-399980.
74. Zampetaki A, Mayr M. Sweet dicer: impairment of micro-RNA processing by diabetes. *Circ Res*. 2015;117:116–118. doi: 10.1161/CIRCRESAHA.117.306817.
75. Zampetaki A, Willeit P, Tilling L, Drozdov I, Prokopi M, Renard JM, Mayr A, Weger S, Schett G, Shah A, Boulanger CM, Willeit J, Chowienczyk PJ, Kiechl S, Mayr M. Prospective study on circulating MicroRNAs and risk of myocardial infarction. *J Am Coll Cardiol*. 2012;60:290–299. doi: 10.1016/j.jacc.2012.03.056.
76. Schulte C, Molz S, Appelbaum S, Karakas M, Ojeda F, Lau DM, Hartmann T, Lackner KJ, Westermann D, Schnabel RB, Blankenberg S, Zeller T. miRNA-197 and miRNA-223 predict cardiovascular death in a cohort of patients with symptomatic coronary artery disease. *PLoS One*. 2015;10:e0145930. doi: 10.1371/journal.pone.0145930.
77. Zampetaki A, Willeit P, Burr S, Yin X, Langley SR, Kiechl S, Klein R, Rossing P, Chaturvedi N, Mayr M. Angiogenic microRNAs linked to incidence and progression of diabetic retinopathy in type 1 diabetes. *Diabetes*. 2016;65:216–227. doi: 10.2337/db15-0389.
78. Kondkar AA, Bray MS, Leal SM, Nagalla S, Liu DJ, Jin Y, Dong JF, Ren Q, Whiteheart SW, Shaw C, Bray PF. VAMP8/endobrevin is overexpressed in hyperreactive human platelets: suggested role for platelet microRNA. *J Thromb Haemost*. 2010;8:369–378. doi: 10.1111/j.1538-7836.2009.03700.x.
79. Shi R, Ge L, Zhou X, Ji WJ, Lu RY, Zhang YY, Zeng S, Liu X, Zhao JH, Zhang WC, Jiang TM, Li YM. Decreased platelet miR-223 expression is associated with high on-clopidogrel platelet reactivity. *Thromb Res*. 2013;131:508–513. doi: 10.1016/j.thromres.2013.02.015.
80. Edelstein LC, Simon LM, Montoya RT, Holinstat M, Chen ES, Bergeron A, Kong X, Nagalla S, Mohandas N, Cohen DE, Dong JF, Shaw C, Bray PF. Racial differences in human platelet PAR4 reactivity reflect expression of PCTP and miR-376c. *Nat Med*. 2013;19:1609–1616. doi: 10.1038/nm.3385.
81. Plé H, Maltais M, Corduan A, Rousseau G, Madore F, Provost P. Alteration of the platelet transcriptome in chronic kidney disease. *Thromb Haemost*. 2012;108:605–615. doi: 10.1160/TH12-03-0153.
82. Chyrchel B, Totoń-Żurańska J, Kruszelnicka O, Chyrchel M, Mielecki W, Kołton-Wróż M, Wołkow P, Surdacki A. Association of plasma miR-223 and platelet reactivity in patients with coronary artery disease on dual antiplatelet therapy: A preliminary report. *Platelets*. 2015;26:593–597. doi: 10.3109/09537104.2014.974527.
83. Zhang YY, Zhou X, Ji WJ, Shi R, Lu RY, Li JL, Yang GH, Luo T, Zhang JQ, Zhao JH, Jiang TM, Li YM. Decreased circulating microRNA-223 level predicts high on-treatment platelet reactivity in patients with troponin-negative non-ST elevation acute coronary syndrome. *J Thromb Thrombolysis*. 2014;38:65–72. doi: 10.1007/s11239-013-1022-9.
84. Leierseder S, Petzold T, Zhang L, Loyer X, Massberg S, Engelhardt S. MiR-223 is dispensable for platelet production and function in mice. *Thromb Haemost*. 2013;110:1207–1214. doi: 10.1160/TH13-07-0623.
85. Badrnya S, Baumgartner R, Assinger A. Smoking alters circulating plasma microvesicle pattern and microRNA signatures. *Thromb Haemost*. 2014;112:128–136. doi: 10.1160/TH13-11-0977.
86. Duan X, Zhan Q, Song B, Zeng S, Zhou J, Long Y, Lu J, Li Z, Yuan M, Chen X, Yang Q, Xia J. Detection of platelet microRNA expression in patients with diabetes mellitus with or without ischemic stroke. *J Diabetes Complications*. 2014;28:705–710. doi: 10.1016/j.jdiacomp.2014.04.012.
87. de Boer HC, van Solingen C, Prins J, Duijs JM, Huisman MV, Rabelink TJ, van Zonneveld AJ. Aspirin treatment hampers the use of plasma microRNA-126 as a biomarker for the progression of vascular disease. *Eur Heart J*. 2013;34:3451–3457. doi: 10.1093/eurheartj/eht007.
88. Yu XY, Chen JY, Zheng ZW, Wu H, Li LW, Zhang ZW, Chen ZH, Lin QX, Han YL, Zhong SL. Plasma miR-126 as a potential marker predicting major adverse cardiac events in dual antiplatelet-treated patients after percutaneous coronary intervention. *EuroIntervention*. 2013;9:546–554. doi: 10.4244/EIJV9I5A90.
89. Schober A, Nazari-Jahantigh M, Wei Y, Bidzhekov K, Gremse F, Grommes J, Megens RT, Heyll K, Noels H, Hristov M, Wang S, Kiessling F, Olson EN, Weber C. MicroRNA-126-5p promotes endothelial proliferation and limits atherosclerosis by suppressing Dlk1. *Nat Med*. 2014;20:368–376. doi: 10.1038/nm.3487.
90. Jansen F, Yang X, Proebsting S, Hoelscher M, Przybilla D, Baumann K, Schmitz T, Dolf A, Endl E, Franklin BS, Sinning JM, Vasa-Nicotera M, Nickenig G, Werner N. MicroRNA expression in circulating microvesicles predicts cardiovascular events in patients with coronary artery disease. *J Am Heart Assoc*. 2014;3:e001249. doi: 10.1161/JAHA.114.001249.
91. Pan Y, Liang H, Liu H, Li D, Chen X, Li L, Zhang CY, Zen K. Platelet-secreted microRNA-223 promotes endothelial cell apoptosis induced by advanced glycation end products via targeting the insulin-like growth factor 1 receptor. *J Immunol*. 2014;192:437–446. doi: 10.4049/jimmunol.1301790.
92. Prokopi M, Mayr M. Proteomics: a reality-check for putative stem cells. *Circ Res*. 2011;108:499–511. doi: 10.1161/CIRCRESAHA.110.226902.
93. Prokopi M, Pula G, Mayr U, Devue C, Gallagher J, Xiao Q, Boulanger CM, Westwood N, Urbich C, Willeit J, Steiner M, Breuss J, Xu Q, Kiechl S, Mayr M. Proteomic analysis reveals presence of platelet microparticles in endothelial progenitor cell cultures. *Blood*. 2009;114:723–732. doi: 10.1182/blood-2009-02-205930.
94. Köberle V, Pleli T, Schmithals C, Augusto Alonso E, Haupenthal J, Bönig H, Peveling-Oberhag J, Biondi RM, Zeuzem S, Kronenberger B, Waidmann O, Piiper A. Differential stability of cell-free circulating microRNAs: implications for their utilization as biomarkers. *PLoS One*. 2013;8:e75184. doi: 10.1371/journal.pone.0075184.
95. Cheng HH, Yi HS, Kim Y, Kroh EM, Chien JW, Eaton KD, Goodman MT, Tait JF, Tewari M, Pritchard CC. Plasma processing conditions

substantially influence circulating microRNA biomarker levels. *PLoS One*. 2013;8:e64795. doi: 10.1371/journal.pone.0064795.
96. Mitchell AJ, Gray WD, Hayek SS, Ko YA, Thomas S, Rooney K, Awad M, Roback JD, Quyyumi A, Searles CD. Platelets confound the measurement of extracellular miRNA in archived plasma. *Sci Rep*. 2016;6:32651. doi: 10.1038/srep32651.
97. Pritchard CC, Kroh E, Wood B, Arroyo JD, Dougherty KJ, Miyaji MM, Tait JF, Tewari M. Blood cell origin of circulating microRNAs: a cautionary note for cancer biomarker studies. *Cancer Prev Res (Phila)*. 2012;5:492–497. doi: 10.1158/1940-6207.CAPR-11-0370.
98. Blondal T, Jensby Nielsen S, Baker A, Andreasen D, Mouritzen P, Wrang Teilum M, Dahlsveen IK. Assessing sample and miRNA profile quality in serum and plasma or other biofluids. *Methods*. 2013;59:S1–S6. doi: 10.1016/j.ymeth.2012.09.015.
99. Kirschner MB, van Zandwijk N, Reid G. Cell-free microRNAs: potential biomarkers in need of standardized reporting. *Front Genet*. 2013;4:56. doi: 10.3389/fgene.2013.00056.
100. Gee HE, Buffa FM, Camps C, Ramachandran A, Leek R, Taylor M, Patil M, Sheldon H, Betts G, Homer J, West C, Ragoussis J, Harris AL. The small-nucleolar RNAs commonly used for microRNA normalisation correlate with tumour pathology and prognosis. *Br J Cancer*. 2011;104:1168–1177. doi: 10.1038/sj.bjc.6606076.
101. Benz F, Roderburg C, Vargas Cardenas D, Vucur M, Gautheron J, Koch A, Zimmermann H, Janssen J, Nieuwenhuijsen L, Luedde M, Frey N, Tacke F, Trautwein C, Luedde T. U6 is unsuitable for normalization of serum miRNA levels in patients with sepsis or liver fibrosis. *Exp Mol Med*. 2013;45:e42. doi: 10.1038/emm.2013.81.
102. Mestdagh P, Van Vlierberghe P, De Weer A, Muth D, Westermann F, Speleman F, Vandesompele J. A novel and universal method for microRNA RT-qPCR data normalization. *Genome Biol*. 2009;10:R64. doi: 10.1186/gb-2009-10-6-r64.
103. Boeckel JN, Thomé CE, Leistner D, Zeiher AM, Fichtlscherer S, Dimmeler S. Heparin selectively affects the quantification of microRNAs in human blood samples. *Clin Chem*. 2013;59:1125–1127. doi: 10.1373/clinchem.2012.199505.
104. Kaudewitz D, Lee R, Willeit P, McGregor R, Markus HS, Kiechl S, Zampetaki A, Storey RF, Channon KM, Mayr M. Impact of intravenous heparin on quantification of circulating microRNAs in patients with coronary artery disease. *Thromb Haemost*. 2013;110:609–615. doi: 10.1160/TH13-05-0368.
105. Freedman JE, Ercan B, Morin KM, Liu CT, Tamer L, Ayaz L, Kanadasi M, Cicek D, Seyhan AI, Akilli RE, Camci C, Cengiz B, Oztuzcu S, Tanriverdi K. The distribution of circulating microRNA and their relation to coronary disease. *F1000Res*. 2012;1:50. doi: 10.12688/f1000research.1-50.v1.
106. Willeit P, Skroblin P, Kiechl S, Fernández-Hernando C, Mayr M. Liver microRNAs: potential mediators and biomarkers for metabolic and cardiovascular disease? *Eur Heart J*. 2016;37:3260–3266. doi: 10.1093/eurheartj/ehw146.
107. Willeit P, Skroblin P, Moschen AR, et al. Circulating microRNA-122 is associated with the risk of new-onset metabolic syndrome and type-2-diabetes [published online ahead of print November 29, 2016]. *Diabetes*. doi: 10.2337/db16-0731. http://diabetes.diabetesjournals.org/content/early/2016/11/22/db16-0731.long.
108. De Rosa S, Fichtlscherer S, Lehmann R, Assmus B, Dimmeler S, Zeiher AM. Transcoronary concentration gradients of circulating microRNAs. *Circulation*. 2011;124:1936–1944. doi: 10.1161/CIRCULATIONAHA.111.037572.
109. Varenhorst C, James S, Erlinge D, Brandt JT, Braun OO, Man M, Siegbahn A, Walker J, Wallentin L, Winters KJ, Close SL. Genetic variation of CYP2C19 affects both pharmacokinetic and pharmacodynamic responses to clopidogrel but not prasugrel in aspirin-treated patients with coronary artery disease. *Eur Heart J*. 2009;30:1744–1752. doi: 10.1093/eurheartj/ehp157.
110. Osman A, Fälker K. Characterization of human platelet microRNA by quantitative PCR coupled with an annotation network for predicted target genes. *Platelets*. 2011;22:433–441. doi: 10.3109/09537104.2011.560305.

Appendix 4

Published article:

MicroRNA-21 and the Vulnerability of Atherosclerotic Plaques.

Barwari T, Rienks M, Mayr M.

Mol Ther. 2018;26(4):938-940.

Accepted for publication: 25 February 2018

Please cite this article in press as: Barwari et al., MicroRNA-21 and the Vulnerability of Atherosclerotic Plaques, Molecular Therapy (2018), https://doi.org/10.1016/j.ymthe.2018.03.005

Molecular Therapy
Commentary

MicroRNA-21 and the Vulnerability of Atherosclerotic Plaques

Temo Barwari,[1] Marieke Rienks,[1] and Manuel Mayr[1]

https://doi.org/10.1016/j.ymthe.2018.03.005

Stabilizing atherosclerotic lesions and preventing plaque ruptures can be seen as the Holy Grail in vascular medicine. In this issue of *Molecular Therapy*, Jin et al.[1] suggest the local delivery of microRNA-21 (miR-21) mimics as a potential therapeutic strategy to reduce plaque vulnerability. Interestingly, inhibition of this microRNA has also been proposed as a therapeutic approach for in-stent restenosis, where the application of anti-miR-21 oligonucleotides on stents improved vessel patency.[2]

Atherosclerosis is a chronic inflammatory disease resulting from the build-up of lipid deposits in the innermost layer of an artery. Apart from lipids, atherosclerotic plaques comprise mainly smooth muscle cells (SMCs), macrophages, calcium, and fibrous connective tissue. Upon rupture or erosion of vulnerable atherosclerotic plaques, platelet aggregation results in thrombus formation that can occlude the vessel lumen. Stents are metallic scaffolds placed into the occluded segment of a diseased artery to hold it open. Current drug-eluting stents (DESs) are designed to inhibit vascular SMC proliferation to reduce neo-intima formation within the stent lumen. While greatly enhancing stent patency in coronary arteries, these anti-proliferative agents also inhibit the proliferation of endothelial cells, thus delaying re-endothelialization and arterial healing. After DES implantation, dual antiplatelet therapy is therefore required to prevent the inherent risk of thrombosis and stent occlusion. Alternatives to current DESs that would inhibit SMC proliferation without delaying re-endothelialization should result in less thrombogenicity.

In the vasculature, miR-21 has previously been implicated as a determinant of SMC proliferation.[3–6] For example, pharmacological and genetic miR-21 inhibition markedly decreased neo-intima formation in vein grafts[5,6] and balloon-injured carotid arteries.[3] These findings led to the exploration of local therapeutic strategies by coating stents with miR-21 inhibitors. When deployed in denuded arteries in rats, this approach prevented SMC-mediated in-stent restenosis without delaying re-endothelialization.[2]

Conversely, SMC proliferation can also be beneficial in stabilizing the vessel wall and atherosclerotic plaques. For example, the proliferative effects of miR-21 mimics in SMCs reduced the expansion of abdominal aortic aneurysms.[7] The results presented by Jin et al.[1] in this issue propose the use of miR-21 mimics to enhance plaque stability. Unstable human plaques and atherosclerotic lesions in apolipoprotein E (apoE)-deficient mice ($Apoe^{-/-}$) exhibit lower miR-21 levels. Based on *in situ* hybridization and immunohistochemistry, this expression pattern was ascribed to SMCs. The authors further show that plaques in *Apoe/miR-21* double-deficient mice ($Apoe^{-/-}miR\text{-}21^{-/-}$) were more prone to rupture. Additionally, the unstable plaques were shown to harbor lower levels of the RE1-silencing transcription factor (REST). REST has been identified as a regulator of miR-21 while also being a direct target of miR-21. Subsequent *in vitro* analysis of SMCs revealed an anti-proliferative effect of REST, confirming the proliferative role of miR-21. Finally, local delivery of miR-21 mimics to carotid plaques using ultrasound-targeted microbubble destruction enhanced plaque stability. These findings suggest that, by increasing SMC proliferation, miR-21 mimics could stabilize the SMC-rich fibrous cap that shields the lipid-filled core of atherosclerotic plaques.

As is the case for most miRNAs, miR-21 is ubiquitously expressed.[8] It is particularly abundant in circulating hematopoietic cells, where it appears to act as an "emergency brake" on inflammation. In macrophages, miR-21 directly targets the pro-inflammatory programmed cell death protein 4 (PDCD4), thereby increasing the secretion of anti-inflammatory interleukin-10 (IL-10).[9] miR-21 also directly targets phosphatase and tensin homolog (PTEN), steering macrophages toward a reparative phenotype that promotes resolution of inflammation and tissue recovery.[10] Thus, miR-21 may also modulate tissue inflammation, in part, through monocyte differentiation toward an anti-inflammatory macrophage phenotype.

A recent study by Canfrán-Duque et al.[11] also focused on miR-21 in the context of atherosclerosis. miR-21 accumulated in murine atherosclerotic plaques along with CD68, a macrophage marker. Deficiency of miR-21 in bone marrow cells promoted vascular inflammation and plaque necrosis in low-density lipoprotein receptor (LDLr) *null* mice. Compared to wild-type bone marrow, transplantation of $miR\text{-}21^{-/-}$ bone marrow into $Ldlr^{-/-}$ mice resulted in larger and less stable atherosclerotic plaques due to increased inflammatory cell infiltration. Thus, miR-21 expression in murine hematopoietic cells attenuates vascular inflammation. The findings of Jin et al.[1] also highlight the impact of miR-21 on the influx of macrophages. $Apoe^{-/-}miR\text{-}21^{-/-}$ mice displayed more advanced plaque formation at an early age, with a concomitant increase of macrophage infiltration and foam cell formation. In line with the recent findings of Canfrán-Duque et al.,[11] miR-21 *null* peritoneal macrophages displayed an increase in oxidized LDL uptake and foam cell formation through enhanced nuclear factor κB (NF-κB) signaling. Notably, secreted factors from $Apoe^{-/-}miR\text{-}21^{-/-}$ macrophages could suppress SMC proliferation *in vitro*.

[1]King's British Heart Foundation Centre, King's College London, London, UK

Correspondence: Manuel Mayr, King's British Heart Foundation Centre, King's College London, 125 Coldharbour Lane, London SE5 9NU, UK.
E-mail: manuel.mayr@kcl.ac.uk

Please cite this article in press as: Barwari et al., MicroRNA-21 and the Vulnerability of Atherosclerotic Plaques, Molecular Therapy (2018), https://doi.org/10.1016/j.ymthe.2018.03.005

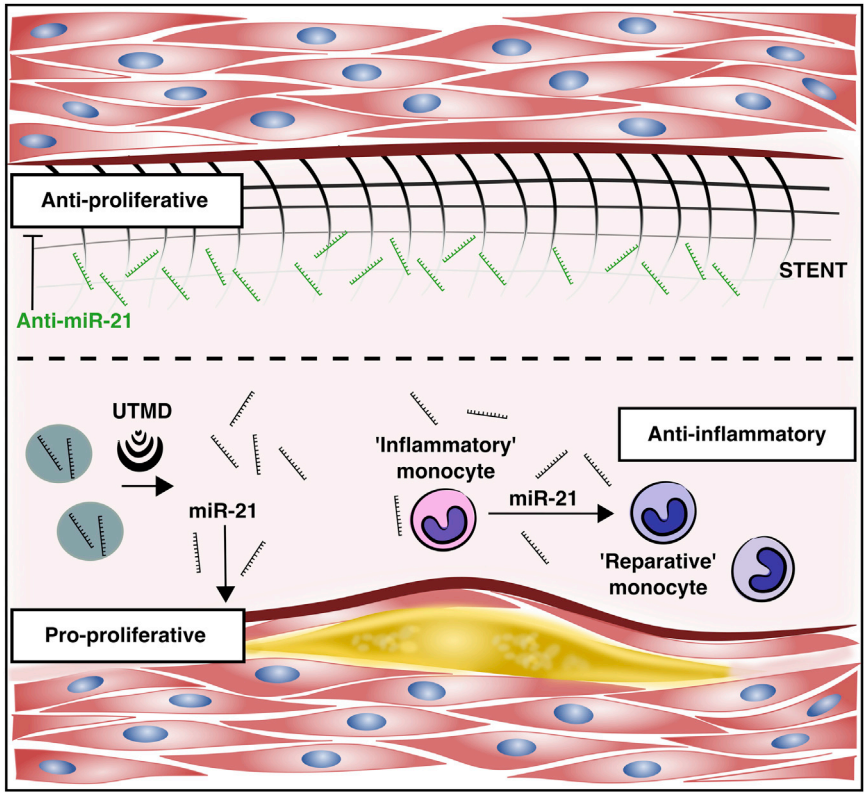

Figure 1. MicroRNA-21-Based Therapy for Plaque Vulnerability and In-Stent Restenosis
Delivery of microRNA-21 (miR-21) mimic to atherosclerotic plaques by ultrasound-targeted microbubble destruction (UTMD) enhances smooth muscle cell proliferation while also steering monocytes toward a reparative, anti-inflammatory phenotype. Conversely, stents coated with miR-21 inhibitor (anti-miR-21) prevent in-stent restenosis through their anti-proliferative effect on smooth muscle cells.

A common challenge in miRNA research is to identify the cell types that are responsible for the observed therapeutic benefits. Although the present study confirms a mechanistic link between miR-21 and SMC proliferation, it remains unclear whether the beneficial effect relies predominantly on SMCs, macrophages, or other cell types (Figure 1). Using a multi-omics approach, we recently identified a protein signature of symptomatic atherosclerotic plaques that implied a shared involvement of immune cells and SMCs.[12] Also, the plasticity of SMCs is currently under debate, with lineage tracing experiments suggesting a potential SMC origin of macrophage-like cell types.[13,14] Finally, apoE mediates the reverse cholesterol transport,[15] and atherosclerosis is known to differ between man and apoE *null* mice.[16]

Despite these notes of caution, the study by Jin et al.[1] advances our insight into the role of miR-21 in vascular biology. This is a timely contribution as miRNA-based therapies progress to clinical application. Clinical trials are currently underway in patients with Alport syndrome, where systemic miR-21 inhibition is evaluated for the treatment of renal fibrosis. A better understanding of the effects of miR-21 in the context of other diseases is therefore highly relevant. The findings of Jin et al.[1] implicate that local therapy with miR-21 may indeed achieve higher drug concentrations at the target site and could minimize the risk of systemic side effects from miRNA therapeutics. Nevertheless, even local therapy for ubiquitously expressed miRNAs could have potential systemic effects, for example, by affecting circulating cells in the blood stream.

ACKNOWLEDGMENTS

T.B. is funded by an Interdisciplinary Studentship of the King's British Heart Foundation Centre. M.M. is a British Heart Foundation (BHF) Chair Holder (CH/16/3/32406) with BHF programme grant support (RG/16/14/32397) and member of a network on "MicroRNA-based Therapeutic Strategies in Vascular Disease" funded by the Fondation Leducq. He is also supported by an excellent initiative (Competence Centers for Excellent Technologies [COMET]) of the FFG (Austrian Research Promotion Agency): Research Center of Excellence in Vascular Ageing-Tyrol, VASCage (K- Project No. 843536) funded by BMVIT (Federal Ministry for Transport, Innovation and Technology), BMWFW (federal Ministry of Science, Research and Economy), the Wirtschaftsagentur Wien, and Standortagentur Tirol.

REFERENCES

1. Jin, H., Li, D.Y., Chernogubova, E., Sun, C., Busch, A., Eken, S.M., Saliba-Gustafsson, P., Winter, H., Winski, G., Raaz, U., et al. (2018). Local Delivery of miR-21 Stabilizes Fibrous Caps in Vulnerable Atherosclerotic Lesions. Mol Ther. *26*, Published online April 4, 2018. https://doi.org/10.1016/j.ymthe.2018.01.011.
2. Wang, D., Deuse, T., Stubbendorff, M., Chernogubova, E., Erben, R.G., Eken, S.M., Jin, H., Li, Y., Busch, A., Heeger, C.-H., et al. (2015). Local microRNA modulation using a novel anti-miR-21-eluting stent effectively prevents experimental in-stent restenosis. Arterioscler. Thromb. Vasc. Biol. *35*, 1945–1953.
3. Ji, R., Cheng, Y., Yue, J., Yang, J., Liu, X., Chen, H., Dean, D.B., and Zhang, C. (2007). MicroRNA expression signature and antisense-mediated depletion reveal an essential role of MicroRNA in vascular neointimal lesion formation. Circ. Res. *100*, 1579–1588.
4. Wang, M., Li, W., Chang, G.-Q., Ye, C.-S., Ou, J.-S., Li, X.-X., Liu, Y., Cheang, T.-Y., Huang, X.-L., and Wang, S.-M. (2011). MicroRNA-21 regulates vascular smooth muscle cell function via targeting tropomyosin 1 in arteriosclerosis obliterans of lower extremities. Arterioscler. Thromb. Vasc. Biol. *31*, 2044–2053.
5. McDonald, R.A., Halliday, C.A., Miller, A.M., Diver, L.A., Dakin, R.S., Montgomery, J., McBride, M.W., Kennedy, S., McClure, J.D., Robertson, K.E., et al. (2015). Reducing in-stent restenosis: Therapeutic manipulation of miRNA in vascular remodeling and inflammation. J. Am. Coll. Cardiol. *65*, 2314–2327.
6. McDonald, R.A., White, K.M., Wu, J., Cooley, B.C., Robertson, K.E., Halliday, C.A., McClure, J.D., Francis, S., Lu, R., Kennedy, S., et al. (2013). miRNA-21 is dysregulated in response to vein grafting in multiple models and genetic ablation in mice attenuates neointima formation. Eur. Heart J. *34*, 1636–1643.
7. Maegdefessel, L., Azuma, J., Toh, R., Deng, A., Merk, D.R., Raiesdana, A., Leeper, N.J., Raaz, U.,

Schoelmerich, A.M., McConnell, M.V., et al. (2012). MicroRNA-21 blocks abdominal aortic aneurysm development and nicotine-augmented expansion. Sci. Transl. Med. *4*, 122ra22.

8. Barwari, T., Joshi, A., and Mayr, M. (2016). MicroRNAs in cardiovascular disease. J. Am. Coll. Cardiol. *68*, 2577–2584.

9. Sheedy, F.J., Palsson-McDermott, E., Hennessy, E.J., Martin, C., O'Leary, J.J., Ruan, Q., Johnson, D.S., Chen, Y., and O'Neill, L.A. (2010). Negative regulation of TLR4 via targeting of the proinflammatory tumor suppressor PDCD4 by the microRNA miR-21. Nat. Immunol. *11*, 141–147.

10. Das, A., Ganesh, K., Khanna, S., Sen, C.K., and Roy, S. (2014). Engulfment of apoptotic cells by macrophages: a role of microRNA-21 in the resolution of wound inflammation. J. Immunol. *192*, 1120–1129.

11. Canfrán-Duque, A., Rotllan, N., Zhang, X., Fernández-Fuertes, M., Ramírez-Hidalgo, C., Araldi, E., Daimiel, L., Busto, R., Fernández-Hernando, C., and Suárez, Y. (2017). Macrophage deficiency of miR-21 promotes apoptosis, plaque necrosis, and vascular inflammation during atherogenesis. EMBO Mol. Med. *9*, 1244–1262.

12. Langley, S.R., Willeit, K., Didangelos, A., Matic, L.P., Skroblin, P., Barallobre-Barreiro, J., Lengquist, M., Rungger, G., Kapustin, A., Kedenko, L., et al. (2017). Extracellular matrix proteomics identifies molecular signature of symptomatic carotid plaques. J. Clin. Invest. *127*, 1546–1560.

13. Shankman, L.S., Gomez, D., Cherepanova, O.A., Salmon, M., Alencar, G.F., Haskins, R.M., Swiatlowska, P., Newman, A.A.C., Greene, E.S., Straub, A.C., et al. (2015). KLF4-dependent phenotypic modulation of smooth muscle cells has a key role in atherosclerotic plaque pathogenesis. Nat. Med. *21*, 628–637.

14. Bennett, M.R., Sinha, S., and Owens, G.K. (2016). Vascular smooth muscle cells in atherosclerosis. Circ. Res. *118*, 692–702.

15. Zanotti, I., Pedrelli, M., Potì, F., Stomeo, G., Gomaraschi, M., Calabresi, L., and Bernini, F. (2011). Macrophage, but not systemic, apolipoprotein E is necessary for macrophage reverse cholesterol transport in vivo. Arterioscler. Thromb. Vasc. Biol. *31*, 74–80.

16. Allahverdian, S., Pannu, P.S., and Francis, G.A. (2012). Contribution of monocyte-derived macrophages and smooth muscle cells to arterial foam cell formation. Cardiovasc. Res. *95*, 165–172.

Appendix 5

Published article:

Inhibition of profibrotic microRNA-21 affects platelets and their releasate.

Barwari T, Eminaga S, Mayr U, Lu R, Armstrong PC, Chan MV, Sahraei M, Fernández-Fuertes M, Moreau T, Barallobre-Barreiro J, Lynch M, Yin X, Schulte C, Baig F, Pechlaner R, Langley SR, Zampetaki A, Santer P, Weger M, Plasenzotti R, Schosserer M, Grillari J, Kiechl S, Willeit J, Shah AM, Ghevaert C, Warner TD, Fernández-Hernando C, Suárez Y, Mayr M.

JCI Insight. 2018;3(21):e123335

Accepted for publication: 26 September 2018

JCI insight

RESEARCH ARTICLE

Inhibition of profibrotic microRNA-21 affects platelets and their releasate

Temo Barwari,[1] Seda Eminaga,[1] Ursula Mayr,[1] Ruifang Lu,[1] Paul C. Armstrong,[2] Melissa V. Chan,[2] Mahnaz Sahraei,[3] Marta Fernández-Fuertes,[3] Thomas Moreau,[4] Javier Barallobre-Barreiro,[1] Marc Lynch,[1] Xiaoke Yin,[1] Christian Schulte,[1] Ferheen Baig,[1] Raimund Pechlaner,[5] Sarah R. Langley,[6,7] Anna Zampetaki,[1] Peter Santer,[8] Martin Weger,[9] Roberto Plasenzotti,[10] Markus Schosserer,[11] Johannes Grillari,[11] Stefan Kiechl,[5] Johann Willeit,[5] Ajay M. Shah,[1] Cedric Ghevaert,[4] Timothy D. Warner,[2] Carlos Fernández-Hernando,[3] Yajaira Suárez,[3] and Manuel Mayr[1]

[1]King's British Heart Foundation Centre, King's College London, London, United Kingdom. [2]Blizard Institute, Barts and The London School of Medicine and Dentistry, Queen Mary University of London, London, United Kingdom. [3]Department of Comparative Medicine and Vascular Biology and Therapeutics Program, Yale University School of Medicine, New Haven, Connecticut, USA. [4]Department of Haematology, University of Cambridge, National Health Blood Service Centre, Cambridge, United Kingdom. [5]Department of Neurology, Medical University Innsbruck, Innsbruck, Austria. [6]Duke-NUS Medical School, Singapore. [7]National Heart Centre Singapore, Singapore. [8]Department of Laboratory Medicine and [9]Department of Internal Medicine, Bruneck Hospital, Bruneck, Italy. [10]Medical University of Vienna, Institute of Biomedical Research, Vienna, Austria. [11]Christian Doppler Laboratory on Biotechnology of Skin Aging, Department of Biotechnology, BOKU – University of Natural Resources and Life Sciences, Vienna, Austria.

Fibrosis is a major contributor to organ disease for which no specific therapy is available. MicroRNA-21 (miR-21) has been implicated in the fibrogenetic response, and inhibitors of miR-21 are currently undergoing clinical trials. Here, we explore how miR-21 inhibition may attenuate fibrosis using a proteomics approach. Transfection of miR-21 mimic or inhibitor in murine cardiac fibroblasts revealed limited effects on extracellular matrix (ECM) protein secretion. Similarly, miR-21–null mouse hearts showed an unaltered ECM composition. Thus, we searched for additional explanations as to how miR-21 might regulate fibrosis. In plasma samples from the community-based Bruneck Study, we found a marked correlation of miR-21 levels with several platelet-derived profibrotic factors, including TGF-β1. Pharmacological miR-21 inhibition with an antagomiR reduced the platelet release of TGF-β1 in mice. Mechanistically, Wiskott-Aldrich syndrome protein, a negative regulator of platelet TGF-β1 secretion, was identified as a direct target of miR-21. miR-21–null mice had lower platelet and leukocyte counts compared with littermate controls but higher megakaryocyte numbers in the bone marrow. Thus, to our knowledge this study reports a previously unrecognized effect of miR-21 inhibition on platelets. The effect of antagomiR-21 treatment on platelet TGF-β1 release, in particular, may contribute to the antifibrotic effects of miR-21 inhibitors.

Conflict of interest: SK, JW, and MM are named inventors on patents for miRNA biomarkers (EP15193448.6, EP2776580 B1, DE112013006129T5, GB2524692A, EP2576826 B, JP2013-513740). JG is cofounder of TAmiRNA and Evercyte.

Submitted: July 6, 2018
Accepted: September 26, 2018
Published: November 2, 2018

Reference information:
JCI Insight. 2018;3(21):e123335. https://doi.org/10.1172/jci.insight.123335.

Introduction

MicroRNAs (miRNAs) have been linked to cardiac remodeling, with miR-21 being implicated in cardiac fibrosis (1). Using different models of tissue injury, several, but not all (2), studies reported a reduction of cardiac fibrosis with systemic miR-21 inhibition (3–5). miR-21 is ubiquitously expressed in mammalian cell types. Besides myocardial fibrosis (3–6), it has been linked to fibrotic kidney (7, 8) and lung disease (9), in-stent restenosis and vein graft failure (10–12), and aortic aneurysmal disease (13). As a mechanistic explanation, studies of miR-21 have suggested an effect on cardiac fibroblast (CF) survival and proliferation that may contribute to fibrosis (2–6). miR-21 may also enhance fibrosis through modulating fibroblast senescence (14). Surprisingly, miR-21–null mice did not show a difference in cardiac function at baseline or with cardiac injury (2). Using a proteomics approach, we have previously reported the first detailed characterization of the CF secretome, identifying numerous targets of miR-29b among extracellular matrix (ECM) proteins (15). We pursued a similar approach to investigate the role of miR-21.

The "master switch" in fibrosis is widely regarded to be TGF-β1. In the heart, TGF-β1 expression is induced by an array of factors, including angiotensin II and mechanical stretch (16). In addition to cardiomyocytes and CFs, high TGF-β1 levels are also found in blood platelets, where its release is controlled by Wiskott-Aldrich syndrome protein (WASp) (17). The platelet releasate is supposed to be a key driver of the inflammatory response in cardiac remodeling (18). It has been suggested that extravasated platelets are a major source of TGF-β1 in the myocardium upon cardiac injury (16). Using megakaryocyte-specific TGF-β1–knockout mice, platelet TGF-β1 has indeed been implicated in the development of cardiac hypertrophy and fibrosis in several models of cardiac remodeling (19–21). We have previously established that many of the abundant circulating miRNAs are of platelet origin (22). Moreover, there is accumulating evidence that abundant platelet miRNAs, such as miR-223 and miR-126, also affect platelet function (23–25).

In this study, we demonstrate that genetic ablation of miR-21 reduces the number of circulating platelets, while pharmacological inhibition attenuates platelet release of TGF-β1 through miR-21–mediated targeting of WASp. In contrast, changes in miR-21 levels alter CF proliferation but have no major effect on the secretion of ECM proteins. Furthermore, we show that plasma concentrations of TGF-β1 are dependent on platelets and correlate strongly with miR-21 levels. Thus, in addition to directly acting on fibroblasts, miR-21 may contribute to fibrosis indirectly through its effects on platelets.

Results

Mimics and inhibitors of miR-21 affect murine CF proliferation. Previous studies have reported a role of miR-21 in cardiac ECM remodeling, predominantly ascribing the attenuation of fibrosis upon miR-21 inhibition to the nonmyocyte or CF niche of the cardiac cell population (3, 4, 6, 26). To study the direct effects of miR-21 on this cell type using proteomics, CFs were isolated from hearts of 8- to 10-week-old male C57BL/6 mice as previously described (15). Cultured cells were transfected (Supplemental Figure 1) with a miR-21 mimic or inhibitor (locked nucleic acid 21 [LNA-21]) and respective controls (n = 4 per group). qPCR analysis of miR-21 levels confirmed a significant and specific effect of the transfections (Figure 1A and Supplemental Figure 2). To assess CF proliferation, cells were plated and monitored using an electrical impedance-based assay (xCELLigence). Real-time recording revealed an increase in proliferation within 24 hours after miR-21 mimic transfection, which was in line with previous findings (3). A concomitant reduction in proliferation was seen after miR-21 inhibitor transfection (Supplemental Figure 3).

Mimics and inhibitors of miR-21 have a limited effect on ECM protein secretion. To study the effects of miR-21 on the secretion of ECM proteins, isolated CFs were transfected, followed by stimulation with recombinant TGF-β1 or a vehicle control. After 48 hours of culturing in serum-free conditions, conditioned media were collected and processed for secretome analysis (Supplemental Figure 4). As expected, TGF-β1 markedly increased secretion of periostin (fold change [FC] = 4.5 and 10.3, P = 0.008 and 0.008 for miR-21 mimic and LNA-21–transfected cells, respectively) and biglycan (FC = 3.5 and 7.0, P = 0.016 and 0.008, respectively). No significant differences were observed for decorin and laminin γ1 (Figure 1B and Supplemental Figure 5).

Next, the secretome was analyzed using proteomics. Normalized spectral counts of ECM proteins identified by liquid chromatography tandem mass spectrometry (LC-MS/MS) are provided in Supplemental Table 3. Consistent with the immunoblotting results, periostin levels were markedly increased by TGF-β1 stimulation (Supplemental Figure 6A). Importantly, secretome levels for the 20 proteins with the highest number of identified spectra, which includes periostin, did not significantly differ after miR-21 mimic or inhibitor transfection (Figure 1C). Overall, a marginal effect of miR-21 on ECM secretion was observed (Supplemental Figure 7). After miR-21 mimic transfection, only insulin-like growth factor–binding protein 4 (IBP4) and granulin (GRN) showed a significant upregulation in unstimulated CFs, whereas higher levels of GRN, cathepsin L (CATL1), and the α-1 chain of collagen 11 (COBA1) were seen in TGF-β1–stimulated cells. Upon miR-21 inhibition, GRN showed a significant increase only in TGF-β1–stimulated cells, whereas galectin-3 binding protein (LG3BP) and VCAM-1 were increased in both unstimulated and TGF-β1–stimulated CFs (Supplemental Figure 8).

To complement the proteomic findings, changes in gene expression were determined. In response to TGF-β1, expression of commonly used markers of the myofibroblast-like phenotype (Supplemental Figure 6B), such as α smooth muscle actin (*Acta2*; FC = 1.6, P < 0.0001), periostin (*Postn*; FC = 3.2, P = 0.0001), and TGF-β1 itself (*Tgfb1*; FC = 1.3, P < 0.0001), was increased. Evaluation of transcripts corresponding to the 20 proteins with the highest number of identified spectra (Supplemental Figure 9) and those significantly changing in the secretome (Supplemental Figure 10) showed a trend toward higher expression of periostin and the

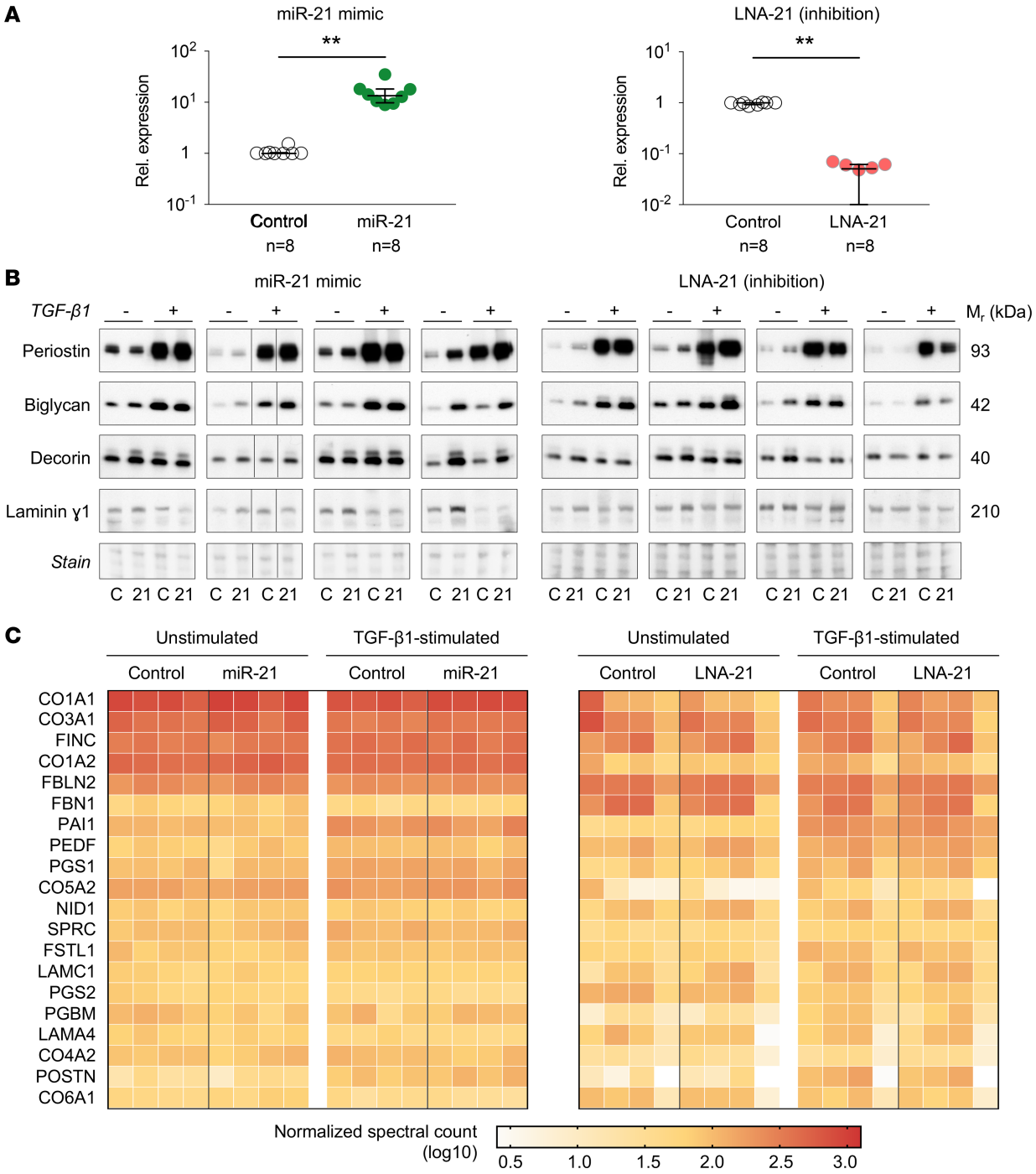

Figure 1. Transfections of cardiac fibroblasts with miR-21 mimic and inhibitor. (**A**) Cardiac fibroblasts (CFs) were isolated from wild-type mice and transfected with miR-21 mimic or LNA-21 (inhibitor), followed by stimulation with TGF-β1 or control treatment. Overexpression and inhibition were confirmed by qPCR (n = 8 for each transfection condition; Wilcoxon matched-pairs signed-rank test; lines and error bars represent median [IQR]; note that in 3 samples miR-21 was undetectable after transfection with LNA-21). (**B**) Immunoblotting for several extracellular matrix (ECM) proteins showed effects of TGF-β1 treatment but not of miR-21 mimic or inhibitor transfection (n = 4 for each condition). Ponceau S staining was used as loading control. C, control mimic/LNA; 21, miR-21 mimic/LNA-21; M_r, relative mass. TGF-β1 +/– indicates treatment 48 hours prior to conditioned media collection. (**C**) Proteomic analysis of the CF secretome after transfections with miR-21 mimic or inhibitor identified no significant changes in the 20 most abundant ECM proteins. Four biological replicates were analyzed for each transfection type in the presence or absence of TGF-β1 treatment. No statistically significant difference was seen between miR-21 mimic or inhibitor and its respective control for any of the shown proteins, using a FDR < 0.05, calculated with the Empirical Bayes method.

transcript encoding LG3BP (*Lgals3bp*) after miR-21 mimic and inhibitor transfection, respectively. However, none of the changes in expression upon miR-21 overexpression or inhibition reached statistical significance. In summary, miR-21 had no major effect on the expression and secretion of ECM proteins by CFs in vitro.

The cardiac ECM is unaffected in miR-21–null mice. In contrast to the profound effects of pharmacological miR-21 inhibition on the fibrotic phenotype, previous analysis of miR-21–null mice reported a normal cardiac morphology and contractility (2). Since no comprehensive analysis of their cardiac ECM has been performed to date, we evaluated the ECM of ventricular cardiac tissue from miR-21–null mice and littermate controls (n = 6 per group). qPCR analysis confirmed undetectable levels of miR-21, whereas no differences were found for other abundant cardiac miRNAs (Figure 2A, top). Cardiac expression levels of genes encoding various ECM constituents were unaltered in miR-21–null mice (Figure 2A, bottom).

Next, a comprehensive proteomics analysis of the cardiac ECM was performed using our established 3-step sequential enrichment protocol (27, 28). FDR-corrected comparisons between both genotypes revealed no difference in abundance for any of the identified proteins (Figure 2B and Supplemental Table 4) (29). Thus, consistent with our in vitro results, a combined transcriptomic and proteomic analysis of the cardiac ECM revealed no major change upon genetic miR-21 deletion.

miR-21 correlates with levels of platelet-derived profibrotic factors in the circulation. Given the limited effects on ECM secretion by CFs, we explored additional explanations for the observed profibrotic role of miR-21. Previous studies have shown that miR-21 is abundant in hematopoietic cells and the circulation (23, 25, 30). We therefore measured 228 proteins in plasma from the community-based Bruneck Study (year 2000 evaluation, n = 660), using proximity extension assays, LC-MS/MS, and ELISA. These protein measurements were then correlated to circulating miR-21 levels, as determined by qPCR (Figure 3A). A significant correlation was seen between miR-21 and the latency-associated peptide of TGF-β1 (LAP-TGF-β1; r = 0.65, P < 0.0001; Figure 3B) as well as several other profibrotic factors, such as PDGF subunit β (PDGFβ; r = 0.73, P < 0.0001), suggesting a common origin. Furthermore, miR-21 levels were significantly correlated with those of markers of platelet activity, such as proplatelet basic protein (PPBP) and platelet factor 4 (PF4), as also indicated by gene ontology (GO) analysis for the terms "platelet activation" and "platelet degranulation." These findings are in line with our previous report indicating that circulating miR-21 levels are dependent on platelets (23). The correlation between circulating miR-21 and mature TGF-β1 was confirmed by qPCR and ELISA analysis, respectively, in platelet-poor plasma (PPP) collected during the 2015 follow-up (n = 332) of the Bruneck Study (Figure 3C). Our previous studies have also identified miR-21 as a major platelet miRNA (23, 31). To confirm enrichment of this miRNA in megakaryocytes, argonaute 2 (Ago2) immunoprecipitation was performed in a human megakaryoblastic leukemia cell line (MEG-01). Here, enrichment of miR-21 in the Ago2 complex was found, along with 2 previously identified platelet-enriched miRNAs (Figure 3D) (25). This suggests a functional role for miR-21 in megakaryocytes and platelets. Altogether, analyses in a community-based cohort study and in MEG-01 cells imply a role of miR-21 in platelets.

TGF-β1 is enriched in megakaryocytes, and plasma levels are dependent on platelets. Colocalization of TGF-β1 with PF4 was demonstrated by immunofluorescence staining of the murine bone marrow (Figure 4A). Further magnification of TGF-β1/PF4–positive cells showed large and lobulated nuclei characteristic of megakaryocyte morphology (Figure 4B). TGF-β1 staining beyond the areas of colocalization with PF4 was negligible, demonstrating that megakaryocytes are the major source for TGF-β1 in the bone marrow.

To study the dependency of plasma TGF-β1 levels on platelets, we used an antibody-mediated thrombocytopenia model in wild-type mice (Figure 4C) (32). Successful platelet depletion was confirmed by a significant reduction of platelet-specific gene transcripts (Figure 4D) in whole blood as well as by reduced levels of PF4 in PPP (Figure 4E). *Ptprc*, an abundant transcript in leukocytes encoding the cluster of differentiation 45 (CD45), was not affected. Importantly, levels of TGF-β1 in PPP were significantly decreased (median [interquartile range], 1.9 [1.6–2.1] and 0.78 [0.73–0.84] ng/ml after control or depletion, respectively; P = 0.0025; Figure 4F). These findings confirm platelets as the major source of TGF-β1 in the circulation.

miR-21 affects the release of TGF-β1 from platelets. Next, we assessed the effect of miR-21 inhibition on platelets using antagomiR-21 treatment in mice (Figure 5A). First, platelet counts were determined by flow cytometry using allophycocyanin-CD41 staining (Supplemental Figure 11). No significant difference in platelet numbers was found between mice treated with antagomiR-21 or control (Figure 5B). miRNAs have previously been shown to alter platelet function (22, 24, 25). To determine whether miR-21 inhibition altered platelet activation, we measured the aggregation response to various agonists using a similar approach as that previously described for miR-126 (25). Unlike miR-126, pharmacological inhibition of

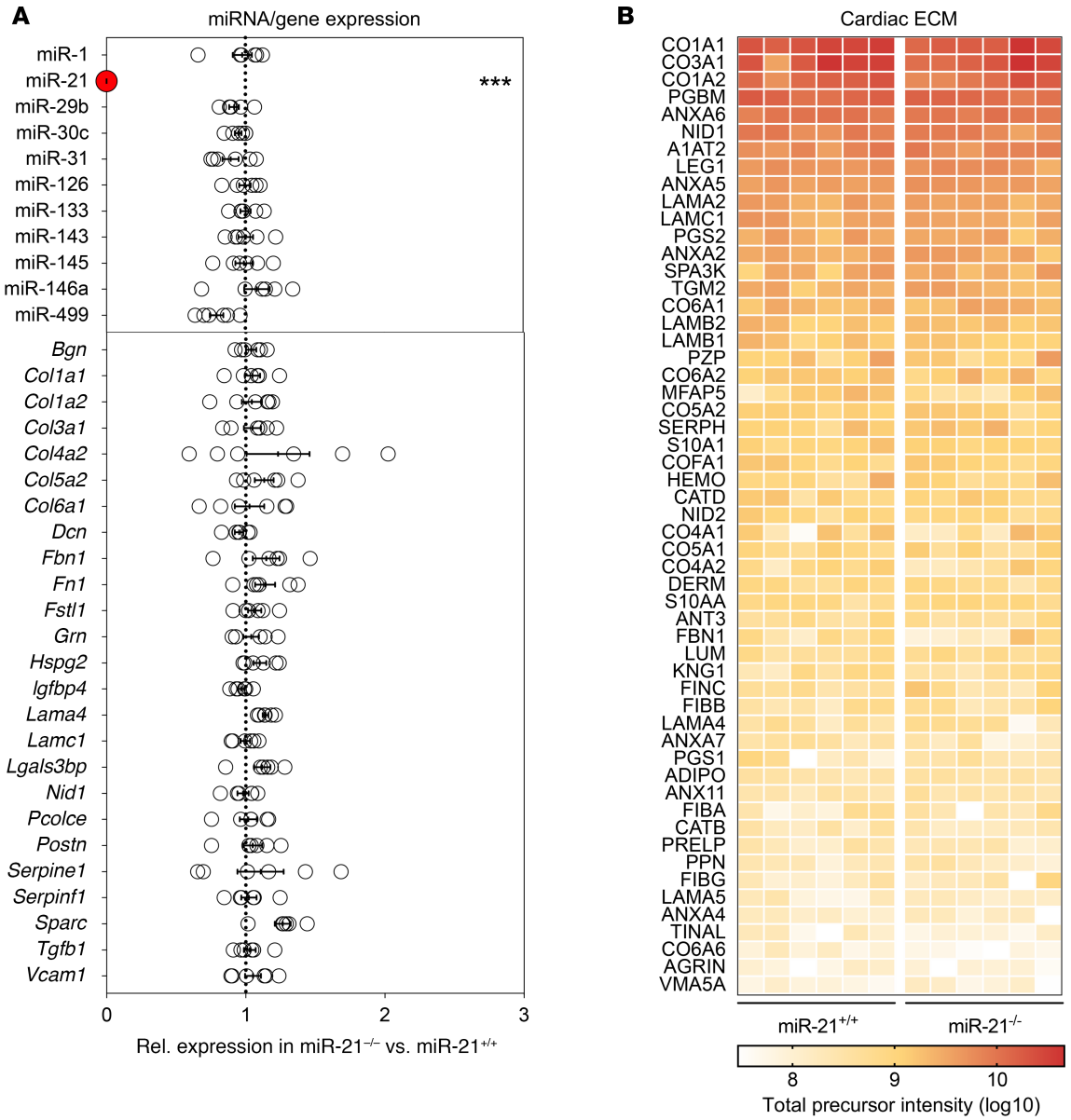

Figure 2. The cardiac ECM of miR-21–null mice. (**A**) Hearts from miR-21–null mice and littermate wild-type controls were used for RNA isolation. Expression levels of miRNAs (top) and selected ECM genes based on the CF transfection experiments (bottom) were determined by qPCR. Expression levels of *U6* and *Actb* were used as reference transcripts, respectively. (**B**) The same hearts were used for proteomics by combining our sequential ECM extraction procedure with analysis by mass spectrometry. Using normalized precursor intensities, no significant differences were observed between hearts from miR-21–null mice and littermate controls. An FDR-based approach was used for all 3 analyses using a $q < 0.05$ for statistical significance. For all 3 analyses, n = 6 miR-21-null mice vs. n = 6 control mice.

miR-21 did not affect the platelet aggregation response to arachidonic acid, protease-activated receptor 4 (PAR4) amide, or collagen (Figure 5C). In light of the correlation between miR-21 and TGF-β1 levels in human plasma, we evaluated whether plasma levels and platelet release of TGF-β1 were affected by antagomiR-21 (Figure 5D). Interestingly, platelet TGF-β1 release was significantly reduced in response to PAR4 amide ($P = 0.003$) and collagen ($P = 0.011$). The release of PF4, a marker of platelet activation, was less affected. No differences were seen for levels of either protein in PPP.

WASp is a direct target of miR-21. Several platelet-derived factors, including TGF-β1, have previously been implicated in cardiac remodeling (19, 33). We therefore determined the effects of pharmacological miR-21 inhibition on the platelet protein releasate in mice. Platelets were isolated from mice treated with antagomiR-21 or control, aggregation was induced with thrombin, and the platelet releasate was used for proteomic analysis (Figure 6A). In agreement with the findings presented in Figure 5D, TGF-β1 was

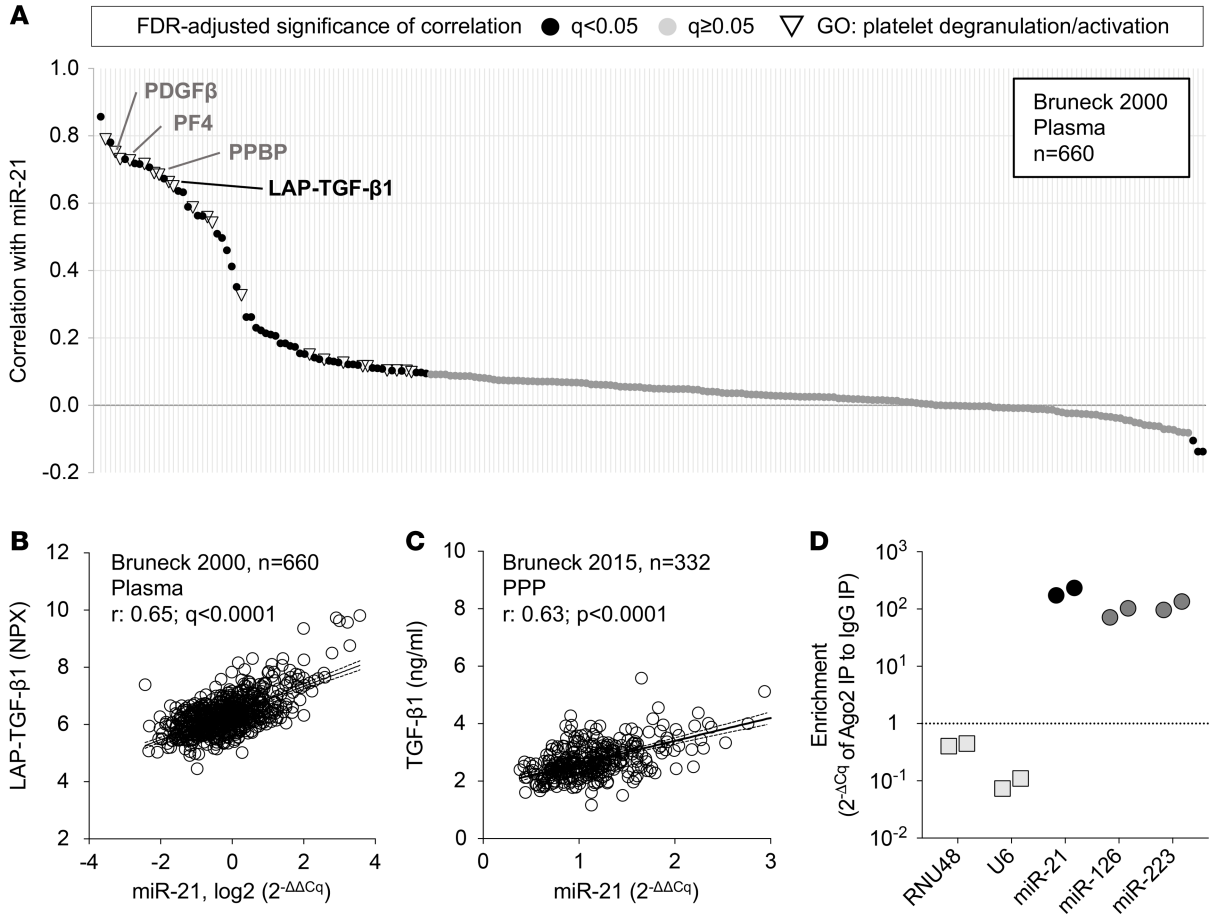

Figure 3. Plasma levels of miR-21 and TGF-β1. (**A**) Plasma miR-21 levels were measured using qPCR in samples from the year 2000 follow-up of the community-based Bruneck Study (n = 660). Pearson coefficients for the correlation of miR-21 with circulating proteins associated with cardiovascular disease and inflammation were calculated based on measurements by a combination of proximity extension assays, mass spectrometry, and ELISA. Each point indicates an individual protein, with its corresponding correlation coefficient on the y axis. PF4, platelet factor 4; PPBP, proplatelet basic protein; LAP-TGF-β1, latency-associated peptide of TGF-β1. Black points indicate FDR-adjusted significance < 0.05, with inverted triangles indicating significantly correlating proteins that were annotated with the "platelet degranulation" and "platelet activation" gene ontology (GO) terms. (**B**) The correlation of miR-21 and LAP-TGF-β1 in plasma of the Bruneck study, year 2000 follow-up. Solid and dashed lines indicate linear regression and 95% confidence interval, respectively. NPX, normalized protein expression. q, FDR-corrected P value for Pearson correlation. (**C**) The correlation of miR-21 and mature TGF-β1, as measured by ELISA, using platelet-poor plasma (PPP) from the 2015 evaluation of the Bruneck Study (n = 332). r, Pearson correlation coefficient; P value for Pearson correlation. (**D**) Argonaute 2 (Ago2) immunoprecipitation was performed in lysates from a human megakaryoblastic leukemia cell line (MEG-01) to isolate coprecipitated RNA. Analysis by qPCR showed enrichment for miR-21, along with miR-126 and -223 (25), suggesting a functional relevance for these miRNAs in megakaryocytes. *U6* and *RNU48* were used as control RNAs. n = 2 for each measurement.

among the differentially regulated proteins after miR-21 inhibition ($\log_2$ FC = –2.86, P = 0.047). Other differentially regulated proteins were von Willebrand factor (VWF; $\log_2$ FC = –2.67, P = 0.040) and fibronectin (FINC; $\log_2$ FC = –2.18, P = 0.030). GO annotation identified all 3 proteins with presence in the α-granule lumen. Several other proteins with this GO term showed a similar trend of reduced release after antagomiR-21 treatment (Supplemental Table 5).

Platelet TGF-β1 release has previously been shown to be curtailed by WASp (17), an actin assembly protein selectively expressed in cells of hematopoietic origin (34). To evaluate levels of TGF-β1 and WASp by immunoblotting, platelets were isolated and lysed after antagomiR-21 or control treatment. While platelet levels of TGF-β1 (FC = 0.98, P = 0.909) and PF4 (FC = 1.05, P = 0.473) were unaltered upon pharmacological miR-21 inhibition, levels of WASp (FC = 1.90, P = 0.047) were significantly increased (Figure 6B and Supplemental Figure 12). Analysis of WASp phosphorylation at tyrosine 293 (Y293; p-WASp), which constitutes the active form of WASp that restricts platelet TGF-β1 release (17), showed a similar trend (FC = 1.49, P = 0.056). Phosphorylation did not differ after normalization for total WASp levels (Figure 6B and Supplemental Figure 12C). The effect on total WASp levels was confirmed by qPCR in the bone marrow of antagomiR-21–treated mice, showing increased *Was* gene expression levels (FC = 1.08; P < 0.001) (Figure 6C). Target prediction

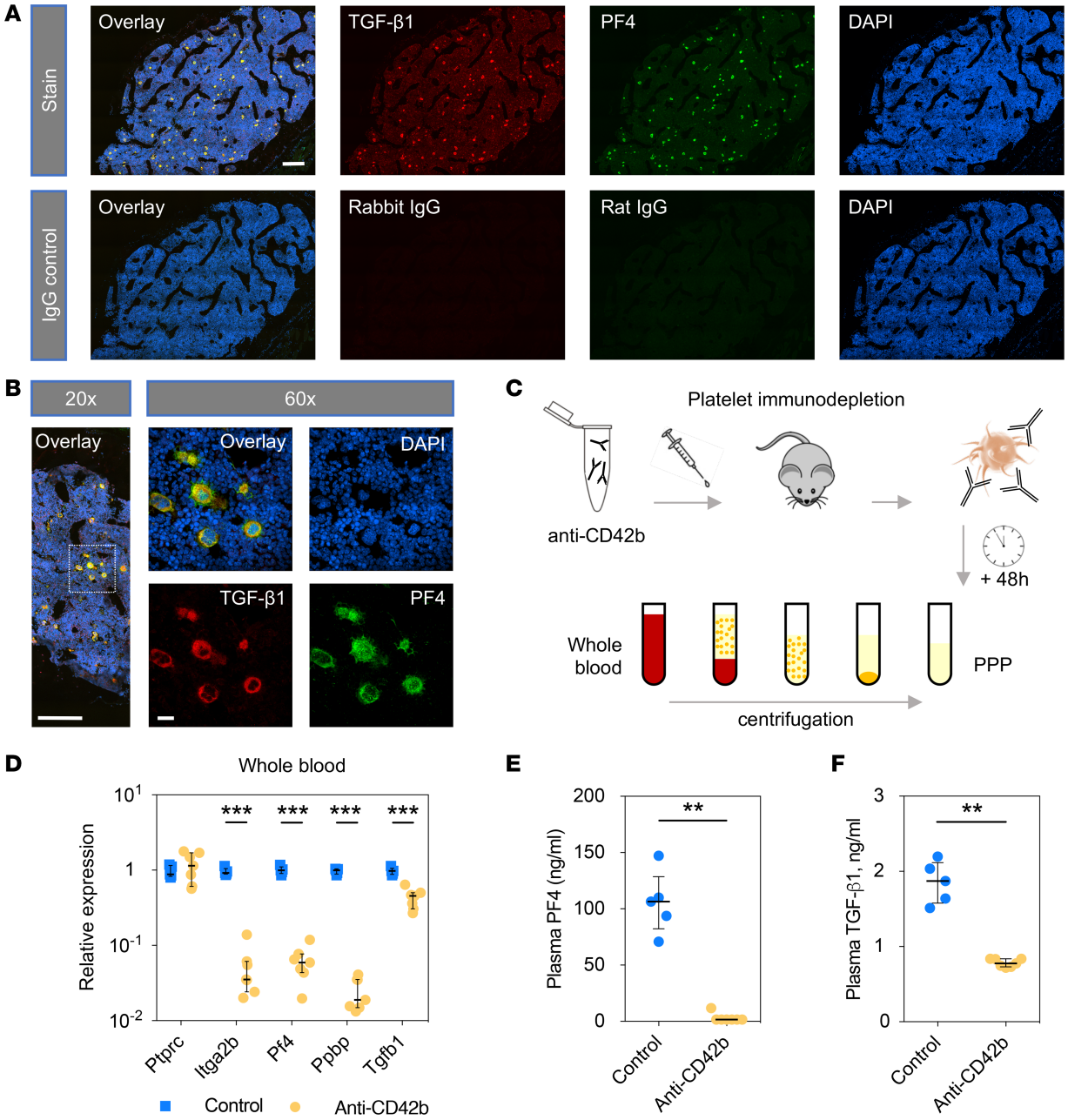

Figure 4. TGF-β1 in the bone marrow and circulation. (**A**) Transverse femoral sections from wild-type mice were used for immunohistochemical analysis of the bone marrow (n = 7; representative images shown). Sections were stained for TGF-β1 (red) and PF4 (green). DAPI was used as a nuclear counterstain (blue). Scale bar: 200 μm. (**B**) Images (original magnification, ×60) identifying the cellular and lobulated nuclear morphology characteristic of megakaryocytes. Scale bar: 200 μm and 20 μm for ×20 and ×60, respectively.(**C**) Wild-type mice were treated with a monoclonal antibody directed against GPIbα (anti-CD42b; 4 mg/kg intraperitoneally) to deplete platelets. Whole blood and platelet-poor plasma (PPP) were collected 48 hours after injection. (**D**) Expression levels of several platelet genes, as well as *Tgfb1*, were significantly lower in whole blood after platelet depletion. Expression of *Ptprc*, widely expressed in leukocytes, was not altered. *Gapdh* was used as reference gene transcript. Lines and error bars represent median (IQR). Statistical analysis was performed with Mann-Whitney test; n = 5 (control) versus 7 (anti-CD42b). (**E** and **F**) Effect of platelet depletion in mice on PPP levels of TGF-β1 and PF4 (Mann-Whitney test, n = 5 for control, n = 7 for anti-CD42b antibody-treated mice). Lines and error bars represent median (IQR).

algorithms have a high false-positive rate (35), with a combination of commonly used algorithms yielding over 14,000 putative genes for canonical miR-21 targeting (36). A luciferase reporter assay was therefore used to evaluate targeting of *Was* by miR-21. This indeed suggested direct targeting (FC = 0.71; P = 0.003) (Figure 6D). To assess whether miR-21 inhibition can affect the expression of *WAS* in human megakaryocytes, forward-programmed human pluripotent stem cell–derived (hPSC-derived) megakaryocytes (FoP-MKs) were used (37). Two independent lines with >95% megakaryocyte purity (Supplemental Figure 13A) were transfected with a

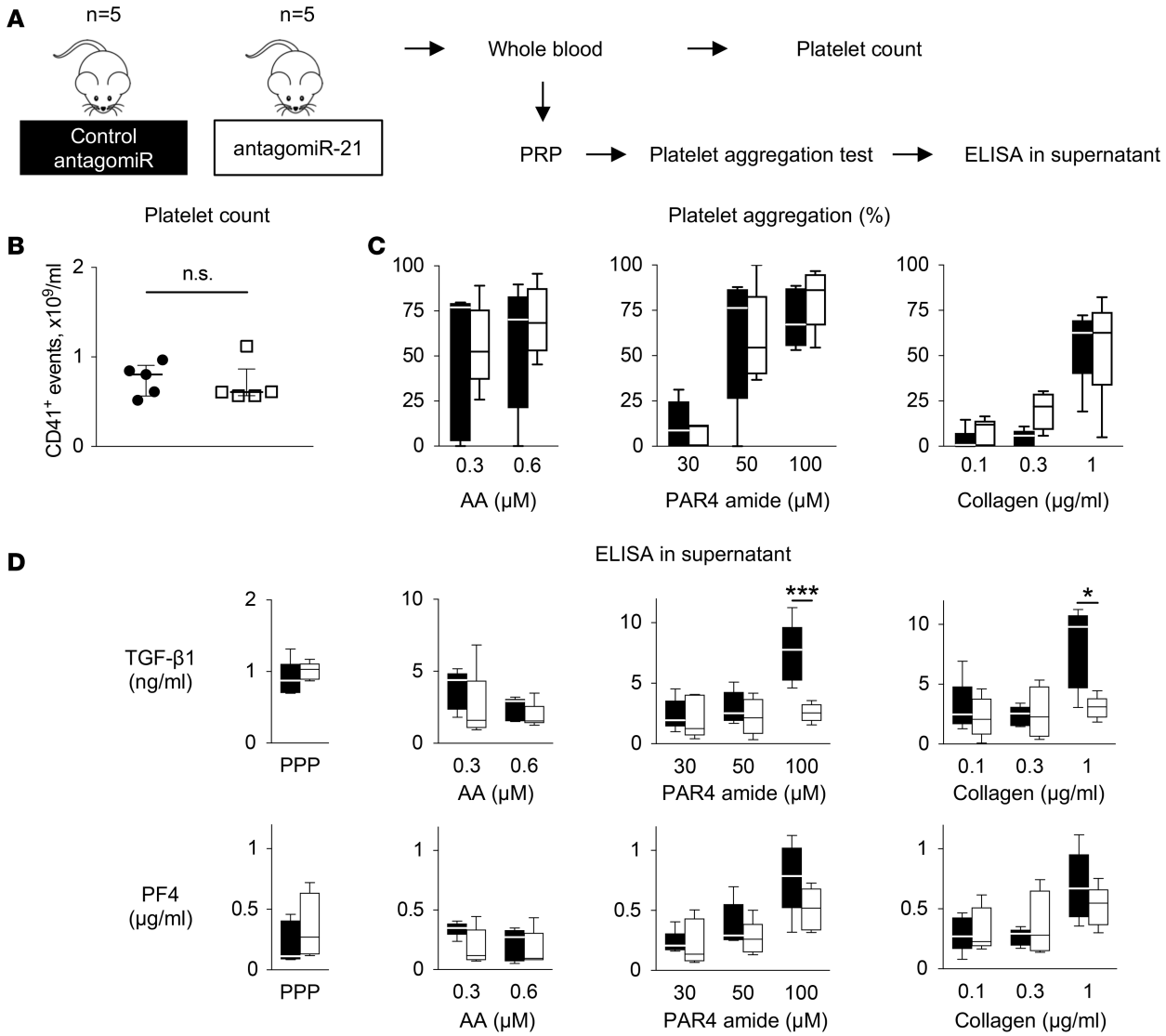

Figure 5. Pharmacological inhibition of miR-21 decreases platelet TGF-β1 release. (**A**) Platelet counts and their aggregation response were assessed in whole blood and platelet-rich plasma (PRP), respectively, isolated from mice treated with antagomiR-21 or control antagomiR. ELISAs were subsequently performed in the supernatant of aggregated platelets. (**B**) Platelet counts were assessed by flow cytometry using a CD41-allophycocyanin antibody on gated platelets. Statistical analysis was performed with Mann-Whitney test; *n* = 5 antagomiR-21–treated mice vs. *n* = 5 control antagomiR-treated mice. Lines and error bars represent median (IQR).(**C**) Platelet aggregation in response to arachidonic acid (AA), protease activated receptor 4 (PAR4) amide, or collagen did not show a significant difference after antagomiR-21 treatment (2-way ANOVA with post hoc Šidák's test; *n* = 5 for each treatment type). (**D**) TGF-β1 release from platelets in response to collagen and PAR4 amide was reduced after treatment with antagomiR-21. PF4 was less affected. TGF-β1 levels in platelet-poor plasma (PPP) were unchanged. Statistical analysis was performed with 2-way ANOVA for agonists and Mann-Whitney test for PPP; *n* = 5 antagomiR-21–treated mice vs. *n* = 5 control antagomiR-treated mice for each condition; **P* < 0.05; ****P* < 0.001.

nontargeting control or a miR-21 inhibitor, resulting in a significant decrease of miR-21 levels (Figure 6E). In line with our findings in murine bone marrow and platelets, as well as the luciferase assay for the murine *Was* 3′ UTR, inhibition of miR-21 resulted in a concomitant increase of *WAS* expression levels (Figure 6F). No significant effect was seen on megakaryocyte purity or maturity (Supplemental Figure 13, B–D). Thus, our findings indicate that pharmacological miR-21 inhibition leads to derepression of WASp, which has previously been shown to affect the release of TGF-β1 from platelets (17).

miR-21–null mice have a reduced number of circulating platelets. Previous studies into miR-21 and cardiac fibrosis have highlighted a discrepancy between pharmacological and genetic inhibition of this miRNA (2, 3). miR-21–null mice were reported to develop fibrosis in response to myocardial infarction or pressure overload that is equivalent to that of wild-type mice. ELISA measurements for TGF-β1 and PF4 in PPP showed no significant difference between wild-type and miR-21–null mice. Similarly, platelet levels of WASp and TGF-β1 were also

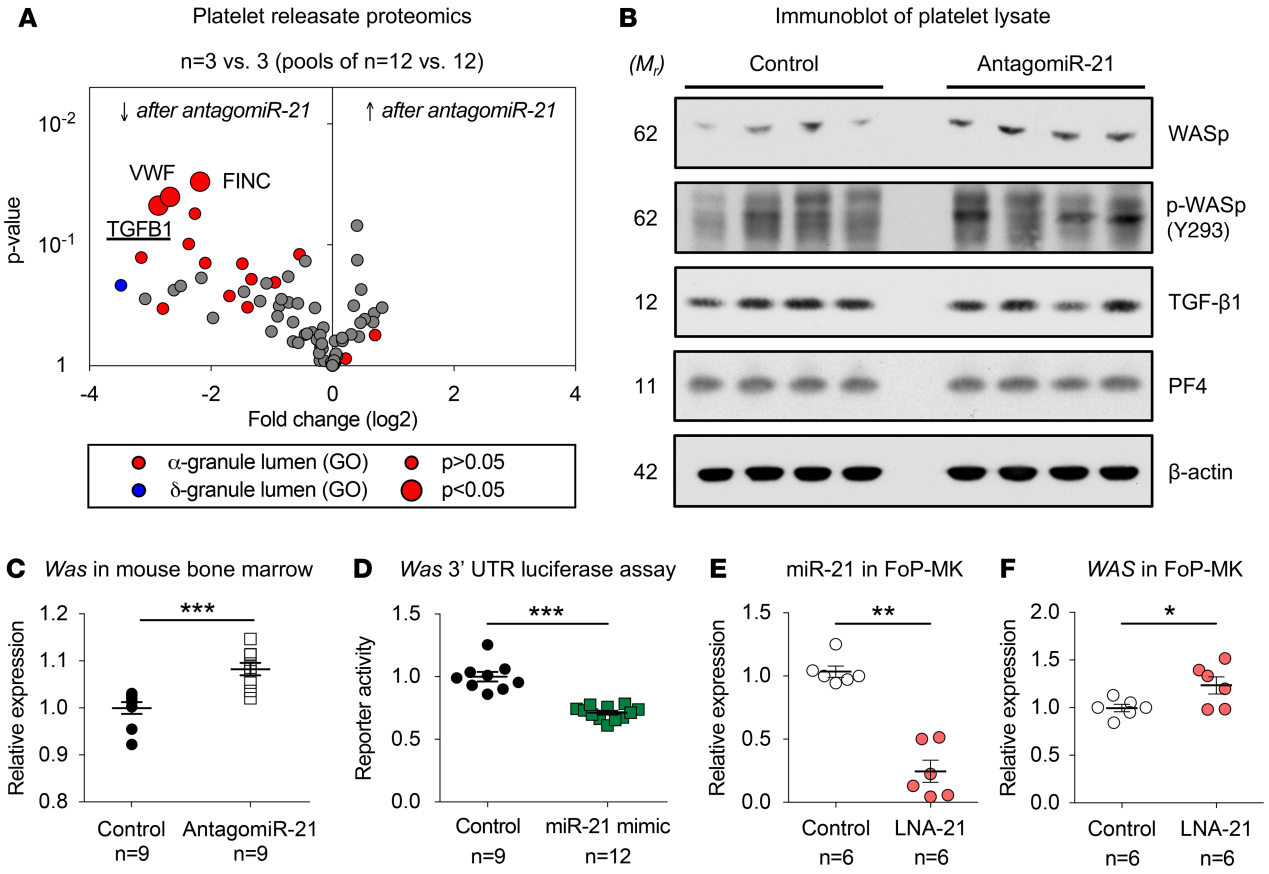

Figure 6. Pharmacological inhibition of miR-21 affects platelet TGF-β1 release through targeting Wiskott-Aldrich syndrome protein. (**A**) The platelet releasate was obtained by thrombin-mediated activation of washed platelets collected from antagomiR-21– or control-treated mice. Proteomics analysis uncovered an attenuated release of TGF-β1 and 2 other α-granule proteins, von Willebrand factor (VWF) and fibronectin (FINC), from platelets isolated after antagomiR-21 treatment. Statistical analysis was performed using Welch's *t* test (*n* = 3 vs. 3 biological replicates; pooled from *n* = 12 antagomiR-21–treated mice and *n* = 12 control antagomiR–treated mice). (**B**) Platelets were isolated from mice after miR-21 inhibition. Immunoblots showed higher levels of Wiskott-Aldrich syndrome protein (WASp), while TGF-β1 content was unchanged (*n* = 4 antagomiR-21–treated mice vs. 4 control antagomiR–treated mice; statistical comparisons of densitometry using Welch's *t* test). Similarly, WASp phosphorylation at tyrosine 293 (p-WASp; Y293) was unaffected.(**C**) Gene expression of *Was* in murine bone marrow after antagomiR-21 treatment was assessed by qPCR (*n* = 9 antagomiR-21–treated mice vs. 9 antagomiR control–treated mice; Welch's *t* test). *Actb* was used as a normalization control. (**D**) Transfection of HEK293T cells with miR-21 mimic significantly suppressed luciferase reporter activity using vectors harboring the 3′ untranslated region of *Was* (3 independent experiments in triplicates [control] or quadruplicates [miR-21 mimic]; paired *t* test used for statistical comparison). (**E** and **F**) Megakaryocytes were produced by forward programming (FoP-MK) of human pluripotent stem cells (hPSCs). Upon transfection with a miR-21 inhibitor (LNA-21), miR-21 levels were markedly reduced. The inhibition of miR-21 was accompanied by increased gene expression levels of *WAS* (*n* = 6 LNA-control transfections vs. 6 LNA-21 transfections; Welch's *t* test). **P* < 0.05, ***P* < 0.01, ****P* < 0.001. M_r, relative mass.

unaffected (Supplemental Figure 14). To assess other potential changes in platelets from miR-21–null mice, we performed a whole-blood platelet count using a Hemavet hematology analyzer. In contrast to short-term pharmacological inhibition of miR-21, blood from miR-21–null mice showed significantly lower platelet counts compared with wild-type littermates (Figure 7A). Lymphocyte and monocyte numbers were also reduced but still fell within the normal reference range. To determine the megakaryocyte response to the lower platelet count, immunohistological staining of the bone marrow was performed in decalcified femoral sections (Figure 7B). A significant increase in megakaryocyte numbers was seen in miR-21–null bone marrow, with a median (interquartile range) count per mm^2 of 84.7 (78.0–90.0) and 106.3 (99.5–121.2) for wild-type and miR-21–null mice, respectively ($P = 0.003$ for Mann-Whitney test) (Figure 7C). We next studied gene expression levels in the bone marrow of these mice (Figure 7D). No significant differences were seen for expression of *Tgfb1*, *Ptprc* (CD45), or *Was*. However, transcript levels of several megakaryocyte-specific genes were significantly higher (FC = 1.70 [$P = 0.005$] for *Itga2b*, 1.72 [$P = 0.026$] for *Pf4,* 1.90 [$P = 0.030$] for *Ppbp*). Furthermore, there was a trend toward higher expression levels for *Tgfbr2* (FC = 1.32, $P = 0.055$), a previously described direct target of miR-21 (38). Altogether, platelet and megakaryocyte numbers are altered in miR-21–null mice.

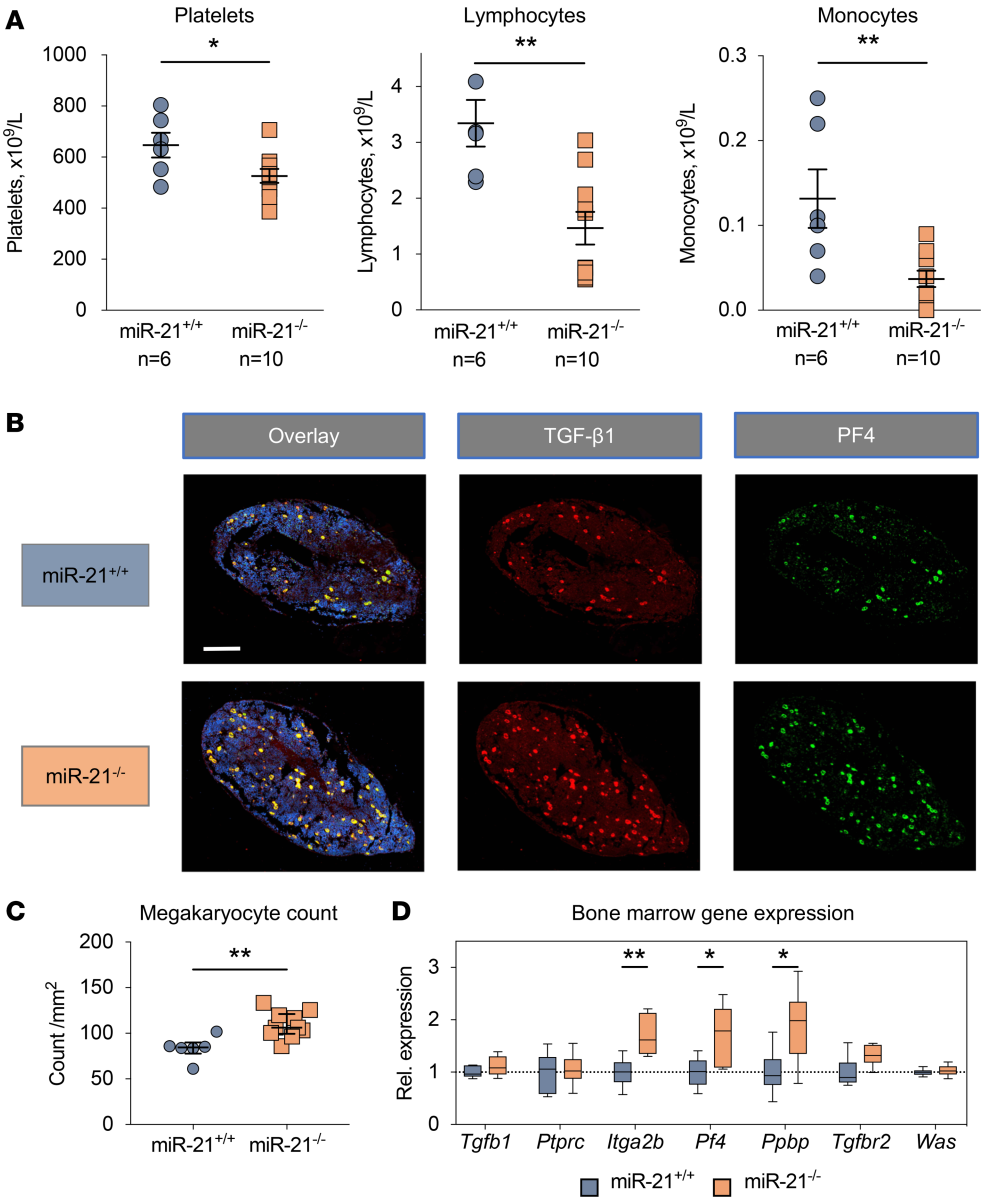

Figure 7. miR-21–null mice display lower platelet and leukocyte numbers but higher numbers of megakaryocytes. (**A**) Using Hemavet blood cell counting, significantly lower numbers of platelets, lymphocytes, and monocytes were found in miR-21–null mice (n = 6) compared with those in wild-type littermates (n = 10) (Welch's t test). (**B**) Immunohistochemical analysis was performed for TGF-β1 (red), PF4 (green), and a nuclear counterstain (DAPI, blue), using femoral bone marrow sections of miR-21–null mice (n = 10). Representative images are shown. (**C**) Examination of bone marrow sections from miR-21–null mice revealed increased megakaryocyte numbers, as identified based on morphology and PF4 positivity. Statistical comparison was performed using the Mann-Whitney test; n = 6 vs. 10 for littermate control and miR-21–null mice, respectively. Lines and error bars represent median (IQR). (**D**) qPCR analysis revealed increased expression levels of megakaryocyte-specific genes *Itga2b*, *Pf4*, and *Ppbp* in bone marrow cells isolated from miR-21–null and littermate control mice. Transcript levels of *Tgfb1*, *Was*, and *Ptprc* (CD45) were not affected. Statistical comparisons using Welch's t test; n = 6 vs. 6. $^*P < 0.05$, $^{**}P < 0.01$.

Discussion

In this study, we identify a potential novel mechanism for the antifibrotic effects of miR-21–targeted therapy: notably, miR-21 minimally affects ECM protein secretion by CFs in vitro and in miR-21–null mice. Instead, miR-21 levels correlate with several platelet-derived profibrotic factors in the circulation, and its genetic ablation decreases platelet counts. Short-term pharmacological miR-21 inhibition attenuates the release of TGF-β1 from platelets. This suggests that pharmacological inhibition of miR-21 acts systemically in addition to its effects on CF proliferation. On the other hand, genetic deletion of miR-21 reduces platelet numbers and stimulates megakaryocyte proliferation. These findings may have implications for miR-21–based therapeutics, in particular with regard to local versus systemic delivery.

Direct effects of miR-21 in the heart. There is strong evidence for the contribution of miR-21 in fibrosis. Systemic inhibition could prevent and even reverse cardiac fibrosis in a pressure-overload model (3), which was confirmed in most (4, 5), but not all (2), studies. Fibroblasts are the primary contributors to fibrosis (39, 40), with the TGF-β pathway playing a central role in fibroblast activation. Despite enhancing CF proliferation, miR-21 had no major effect on cardiac ECM protein secretion. These findings are in stark contrast with previous studies that revealed major changes in ECM protein secretion using a similar approach for miR-29b (15) and hypoxia (41). Experiments in CFs were performed based on equal cell numbers prior to transfection and

TGF-β1 treatment. Hence, it can be stated that, despite enhancing proliferation, this antiproliferative effect of miR-21 inhibition was insufficient to cause detectable changes in total ECM protein secretion. Previous discrepancies between studies on miR-21 and cardiac fibrosis have been ascribed to differences between pharmacological and genetic miR-21 inhibition (42). In line with our in vitro findings and with functional cardiac analysis by others (2), the composition of the cardiac ECM did not significantly differ in miR-21–null mice. A recent study by Ramanujam et al. used viral vectors with different tropism to distinguish effects of miR-21 inhibition in different cardiac cell types (26). While cardiomyocyte inhibition of miR-21 aggravated fibrosis, nonmyocyte targeting attenuated remodeling in a mouse model of cardiac overload. Importantly, effects of miR-21 on cardiac fibrosis are observed only in the presence of tissue injury (3–6).

miR-21 as a modulator of the bone marrow. miR-21 is ubiquitously expressed and has been implicated in fibrosis in different organs (7–9). Furthermore, miR-21 is highly abundant in circulating cells, such as monocytes and platelets (43). Recent studies on atherosclerosis identified an immunomodulatory role of miR-21 in mononuclear cells (12, 30, 44). Leukocytes and platelets are major contributors to the tissue injury response (45). Thus, the widely reported induction of miR-21 upon injury may be secondary to an immune cell infiltration or platelet deposition rather than induction of miR-21 expression in resident cells (46). In addition, expression and processing of the miR-21 precursor is enhanced by TGF-β signaling (47). A platelet contribution may explain why miR-21 inhibition has no effect on fibrosis in the absence of tissue injury. Tissue injury induces platelet activation. In addition to local fibroblast activation, platelet-derived proteins (33), including TGF-β1 (19), contribute to the onset and progression of fibrosis. Platelet inhibition or depletion attenuates cardiac remodeling after myocardial infarction (48, 49) or in response to pressure overload (18, 33). We have previously demonstrated that miR-21 is abundant in platelets and miR-21 plasma levels are decreased by antiplatelet therapy (23). Ago2 immunoprecipitation showed marked enrichment of miR-21 in a human megakaryoblastic leukemia cell line. Bone marrow cells are more readily affected by antagomiR treatment compared with cardiac tissue (50). This is in contrast with the absence of miR-21 across tissues upon genetic ablation in mice. In miR-21–null mice, we found no major effect on cardiac ECM proteins, but we observed significantly lower platelet and leukocyte counts, accompanied by a marked increase in megakaryocyte numbers. Altogether, these findings imply that miR-21 inhibition alters the bone marrow.

Pharmacological miR-21 inhibition affects the platelet releasate. Platelets constitute a major source of circulating TGF-β1 (19). This is reflected in the strong correlation between plasma levels of miR-21 and TGF-β1 in the Bruneck cohort and by the reduction in TGF-β1 plasma levels upon platelet depletion in mice. In the bone marrow of mice, we observed a striking colocalization of TGF-β1 with megakaryocytes. Pharmacological inhibition of miR-21 did not alter the platelet count or their aggregation response but significantly decreased the release of several α-granule proteins. Our observation of miR-21 inhibition affecting platelet TGF-β1 release suggests a feed-forward mechanism, where TGF-β1 induces miR-21 expression in megakaryocytes, which subsequently enhances platelet TGF-β1 release through inhibiting WASp. WASp has been described as a regulator of actin polymerization in neutrophils, macrophages, and lymphocytes (51), being expressed solely in hematopoietic cells (34). While WASp is present in platelets, it is not required for platelet spreading, despite the importance of cytoskeletal F-actin polymerization in this process (52). This indicates redundancy in the mechanisms that regulate actin polymerization in platelets. Consequently, miR-21–mediated titration of WASp levels may be a refined way of interfering with TGF-β signaling. Previous approaches of TGF-β1–targeting therapy have thus far failed due to major side effects (53). Altering the platelet release of profibrotic factors may provide a more targeted approach, as platelet activation occurs at sites of tissue injury. In summary, our findings provide evidence that the reported antifibrotic effects upon miR-21 inhibition may, at least in part, occur through decreasing platelet release of TGF-β1.

Study limitations. The culture of CFs for secretome analysis was performed in serum-free medium. This may have suppressed some of the effects of miR-21 in these cells. In addition, ECM proteins were assessed only in miR-21–null mice without cardiac injury to promote fibrosis. Correlations between miR-21 and markers of platelet activation or profibrotic factors do not rule out potential confounding by contaminating leukocyte subtypes. For TGF-β1, however, the immunohistochemistry results from the bone marrow indicate a high degree of specificity for megakaryocytes. Our findings suggest that antagomiR-21 treatment may reduce TGF-β1 release through derepressing WASp. While direct targeting was indicated by a luciferase reporter assay and by miR-21 inhibition in hPSC-derived megakaryocytes, in vivo evidence for this interaction is correlative. In addition, as suggested by the proteomic analysis of the platelet releasate, antagomiR-21 treatment may affect release of other α-granule proteins as well. Further studies are needed

to determine whether miR-21 has effects on the release of other constituents of platelets and on leukocytes, given that WASp is predominantly expressed in hematopoietic cells and Wiskott-Aldrich syndrome is characterized by immune deficiency as well as thrombocytopenia (34).

Conclusions. This study is a timely contribution, given that miR-21–based therapies are progressing to clinical trials for Alport syndrome (7). The current assumption that miR-21 inhibition attenuates fibrosis predominantly through direct effects on fibroblasts is challenged by the marginal changes in ECM protein composition and secretion. Our findings after pharmacological and genetic miR-21 inhibition in mice indicate that other cell types, in particular bone marrow–derived cells, may also contribute. While local delivery of miRNA therapeutics may decrease the likelihood for off-target effects (10), it could also limit therapeutic efficacy if the benefit is not solely mediated by local cells. A broad appraisal of the multifaceted systemic response of targeting ubiquitously expressed miRNAs will aid the success of miRNA-based therapeutics in clinical trials.

Methods

Detailed methods are provided in the Supplemental Methods.

RNA isolation, reverse transcription, and PCRs. RNA isolation, reverse transcription (RT), and preamplification as well as individual quantitative real-time PCR (qPCR) for miRNA and gene expression were performed as described previously (25). A comprehensive list of assays is provided in Supplemental Table 1.

CF isolation and transfection for secretome analysis. Primary mouse CFs were isolated from the hearts of male (8- to 10-week-old; n = 8) C57BL/6 mice (Charles River) by collagenase II–based digestion as described previously (15). Cells from different animals were maintained as separate biological replicates. Cells at passage 3 were used in all experiments. Transfections of miR-21 mimic (Dharmacon) or miR-21 inhibitor (LNA-21; Exiqon A/S) were each carried out, with corresponding controls in parallel using 4 separate biological replicates. Lipofectamine RNAiMAX (Life Technologies) was used in reduced serum medium (Opti-MEM, Life Technologies) at a final concentration of 50 nmol/l for transfection of all 4 sequences. After 24 hours, CFs were stimulated with 10 ng/ml recombinant TGF-β1 (Peprotech) in serum-free medium. After 48 hours, conditioned medium and cells were harvested for analysis. Samples were processed for qPCR analysis, immunoblotting, or proteomic analysis as described previously (15) and in the Supplemental Methods. See complete unedited blots in the supplemental material.

Proliferation assay in transfected CFs. A proliferation assay was performed using the xCELLigence RTCA DP Instrument (ACEA Biosciences). CFs were isolated and transfected using the same methods and concentrations as above. After 24 hours, cells (5×10^3 cells/well; 4 biological replicates per condition, in duplicate) were seeded in an E-Plate VIEW 16 (ACEA Biosciences) in complete DMEM medium. Following plating, cells were allowed to attach while at room temperature for 30 minutes before placing the plate in the incubator at 37°C. Two wells per plate were loaded with media only to assess background levels. Cell index values were recorded by 150 sweeps per interval every 30 minutes using proprietary software, with the baseline recording reset at 4 hours. Data were analyzed using the difference (Δ) in cell index according to the manufacturer's instructions with the baseline recording reset at 4 hours.

ECM extraction and analysis. ECM protein enrichment was performed on hearts from female miR-21–null mice or littermate controls, aged 14–16 weeks, using our previously published 3-step extraction method (28, 54). Generation of the miR-21–null mice has previously been described (2). Proteins in the sodium chloride and guanidine hydrochloride extracts were enzymatically deglycosylated, followed by denaturation, reduction, alkylation, and tryptic digestion. Peptides were purified using a C18 spin plate (Harvard Apparatus) and analyzed by LC-MS/MS. Identified proteins were annotated using the Matrisome database (29).

Bruneck cohort. The Bruneck Study is a community-based, prospective survey of the epidemiology and pathogenesis of atherosclerosis and cardiovascular disease (25, 55). At the 1990 baseline evaluation, the study population comprised an age- and sex-stratified random sample of all inhabitants of Bruneck (125 men and 125 women from each of the fifth through eighth decades of age, all White). In the present study, citrate plasma samples from the 2000 (n = 660) and 2015 (n = 332) follow-up were analyzed. These samples were drawn after an overnight fast and 12 hours of abstinence from smoking. During the 2000 follow-up, citrate plasma was prepared by single centrifugation and aliquots were immediately stored at –80°C. For the 2015 follow-up, platelet-rich plasma (PRP) was first isolated by centrifugation at 175 g for 15 minutes with slow brake. An aliquot of PRP was then supplemented with prostacyclin (PGI_2, epoprostenol, 2 μg/ml; Tocris Bioscience) and centrifuged at 1,000 g for 10 minutes to obtain PPP. Samples were immediately stored at –80°C. Levels of miR-21 and a panel of 228 proteins were measured by RT-qPCR (25) and a combination

of Olink Proseek Proximity Extension Assays (Proseek Multiplex CVD I and Inflammation panels, Olink) (55, 56) and mass spectrometry–based assays (PlasmaDive, Biognosys AG) (57), respectively, as described previously (25). In addition, TGF-β1 (DY240, R&D Systems), PF4 (DY795, R&D Systems), and PPBP (DY393, R&D Systems) levels were measured using DuoSet ELISA Development kits and DuoSet Ancillary Reagent Kits 1 and 2 (R&D Systems) according to the manufacturer's instructions. Absorbance at 450 nm was measured on a plate reader (Tecan Infinite 200 Pro) using 570 nm as a reference wavelength. Results were calculated using a 4-parameter logistic fit.

Platelet immunodepletion in mice. Male C57BL/6J mice (Charles River) were treated with a rat anti-mouse GPIbα antibody (4 mg/kg, Emfret Analytics) or sterile PBS via intraperitoneal injection. Blood was collected after 48 hours into acid-citrate-dextrose buffer by cardiac puncture, followed by preparation of PRP and PPP using serial centrifugation at 100 *g* and 1,000 *g* for 10 minutes at room temperature, respectively. Samples were divided into aliquots, blinded, randomized, and immediately stored at –80°C. RNA isolated from whole blood was used for qPCR analysis. TGF-β1 (DY1679) and PF4 (DY595) levels were measured in PPP using DuoSet ELISA Development kits (R&D Systems) according to the manufacturer's instructions.

Ago2 immunoprecipitation. Immunoprecipitation of ribonucleoprotein was carried out in MEG-01 cells (ATCC, CRL-2021), as previously described (25, 58). Briefly, 50–100 million cells were lysed in 500 μl ice-cold polysome lysis buffer (5 mM $MgCl_2$, 100 mM KCl, 10 mM HEPES, pH 7.0, 0.5% Nonidet P-40), with freshly added 1 mM DTT, 100 U/ml RNase inhibitor (Life Technologies) and 1× protease inhibitor (cOmplete Mini, ethylenediaminetetraacetic acid–free [EDTA-free], Roche) for 15 minutes. Centrifugation was performed at 14,000 *g* at 4 °C for 10 minutes. The supernatant was mixed with 500 μl ice-cold NT2 buffer (50 mM Tris, pH 7.4, 150 mM NaCl, 1 mM $MgCl_2$, 0.05% Nonidet P-40) containing freshly added 200 U/ml RNase inhibitor, 0.5% vanadyl ribonucleoside, 1 mM DTT, 15 mM EDTA, and 50 μl mouse anti-human Ago2-coated (Abcam) sepharose G beads (Life Technologies). Incubation was carried out overnight at 4°C on a rocking platform. The following day, beads were washed 5 times with ice-cold NT2 buffer and used for RNA isolation.

Murine platelet and bone marrow analysis. For pharmacological miR-21 inhibition, male C57BL/6J mice, aged 10–12 weeks (Charles River), were injected intraperitoneally with cholesterol-conjugated antagomiR constructs (Fidelity Systems) targeting miR-21 or using a nontargeting sequence, as previously described (25). Sequences were designed to target miR-21 (5′-U*C*AACAUCAGUCUGAUAAG*C*U*A*-Chol*T-3′) or to serve as nontargeting control (5′-A*A*GGCAAGCUGACCCUGAA*G*U*U*-Chol*T-3′), with the asterisks denoting phosphorothioate backbone modification and "Chol" indicating cholesterol conjugation. Constructs were reconstituted in sterile PBS, and intraperitoneal injections of 500 μl were performed on day 0, 1, and 2 in a dose of 25 mg/kg for the platelet releasate isolation and 40 mg/kg for the aggregometry experiments and the ELISA measurements in plasma. Treatment with both constructs was performed in parallel. On day 7, mice were anesthetized using pentobarbital for blood and tissue collection. Upon sample collection, samples were blinded and randomized prior to analysis. Blood and bone marrow samples were obtained from equal numbers of male and female miR-21–null mice (Mir21atm1Yoli/J, Jax 016856; The Jackson Laboratory) and littermate controls, aged 8–12 weeks. Mice were kept under constant temperature and humidity in a 12-hour-controlled dark/light cycle.

A Hemavet (Drew Scientific) blood cell counter was used for analysis of miR-21–null blood samples. Platelet counting after antagomiR-21 treatment was performed on diluted whole blood incubated with an allophycocyanin-labeled anti-mouse CD41 antibody (BioLegend), using an Accuri C6 flow cytometer (BD Biosciences). Light transmission aggregometry was performed with PRP as described previously (25). Platelets were isolated by blood collection into acid-citrate-dextrose buffer, followed by 2-step centrifugation and washing in modified Tyrode-HEPES buffer supplemented with prostaglandin E_1. PPP was isolated by 2-step centrifugation, obtaining PRP followed by a second spin to obtain PPP. TGF-β1 and PF4 levels were measured in PPP and light transmission aggregometry supernatants using DuoSet ELISA Development kits (R&D Systems) according to the manufacturer's instructions. Releasate was obtained by thrombin-induced platelet aggregation in platelets obtained from blood pooled from 4 mice, followed by gel-based LC-MS/MS analysis. Bone marrow cells were isolated from femora and filtered using a 100-μm cell strainer (Corning), followed by red blood cell lysis and subsequent RNA isolation for qPCR analysis. For immunohistochemistry, femora were fixed in 4% formaldehyde and then decalcified in a 0.38 mol/l EDTA solution at 4°C for 3 weeks. Bones were paraffin embedded and sectioned for staining. After primary antibody incubation (TGF-β1 and PF4; see Supplemental Table 2) overnight, sections were incubated with fluorescently labeled species-specific

secondary antibodies. Staining was visualized using an inverted spinning disc confocal microscope (Nikon Ti-Eclipse, teamed with a Yokogawa CSU-X1 Andor Spinning Disc with iXon EM-CCD camera). Imaging was performed with a 1.70 NA ×20 or 1.40 NA ×60 magnification objective lens.

Transfection of miR-21 inhibitor in human megakaryocytes. Human megakaryocytes were obtained by forward programming of hPSCs as previously described (37). Transfections of miR-21 inhibitor or a nontargeting control (PowerLNA, Qiagen) were carried out in triplicate in 2 independent megakaryocyte lines. Conjugation to TurboFect reagent (Thermo Scientific) was used to enhance the transfection efficiency. A final concentration of 25 nmol/l was used for both oligonucleotides. After 48 hours, cells were collected for RNA isolation by centrifugation at 120 *g* and washed once in sterile PBS. Prior to transfection and during collection, an aliquot of cells was incubated with anti-CD41a-APC-H7 and anti-CD42a-APC (BD Pharmingen) to assess megakaryocyte purity and maturity, respectively, using a Gallios flow cytometer (Beckman Coulter).

Statistics. Gel-based MS data were quantified using normalized spectral counts. Qspec (59) was used to detect differential expression in the CF secretome analysis. Qspec utilizes a hierarchical Bayes estimation of a generalized linear mixed-effects model to share information across proteins, which increases the power to detect differential expression. The FDR was calculated using an Empirical Bayes method, and FDR < 5% was considered significant. All other statistical analyses were performed with Microsoft Excel (version 15.41) and GraphPad Prism (version 7.0d). Distribution of data was analyzed using the Shapiro-Wilk normality test, where $P > 0.05$ was considered to indicate normal distribution. When at least 1 sample group within an experiment showed nonnormal distribution, nonparametric tests were used for the analysis. For unpaired data, 2-tailed Welch's *t* test or Mann-Whitney rank tests were performed for parametric and nonparametric distribution, respectively. For paired data, paired *t* tests or Wilcoxon's matched-pairs signed-ranks tests were used, respectively. Where appropriate, a 2-way ANOVA was used, with post hoc analysis of individual effects by Šidák's test. Time course data of the CF proliferation assay were analyzed using the nonparametric Friedman test with post hoc analysis of differences between each targeting and nontargeting transfection type using Dunn's multiple comparisons test. Comparison of gene expression and ECM protein abundance between miR-21–null or wild-type mice was performed using an FDR approach with the 2-stage step-up method of Benjamini, Krieger, and Yekutieli, with an FDR for significant discovery set to 5%. Relationships between the concentrations of plasma proteins and the relative quantities of miRNAs were investigated using Pearson correlations with *P* value adjustment (producing *q* values) using FDR adjustment according to Benjamini, Krieger, and Yekutieli. Data are shown as mean ± SEM unless stated otherwise. Where box-and-whisker plots are shown, the line indicates the median, bounds of boxes indicate quartiles, and whiskers indicate the range. $P < 0.05$ or $q < 0.05$ was considered significant.

Study approval. The Bruneck study protocol was reviewed and approved by the ethics committees of Verona and Bolzano, Italy, and all participants provided written informed consent before entering the study. All animal studies were performed under protocols in strict accordance with the UK Animals (Scientific Procedures) Act 1986 or the Institutional Animal Care Use Committee of Yale University School of Medicine.

Author contributions

TB was involved with the study design, performed and analyzed CF and miR-21–null sample experiments; collected and analyzed samples for the Bruneck 2015 evaluation; designed and analyzed samples from antagomiR treatment and platelet depletion experiments in mice; performed statistical analysis; and drafted the manuscript. SE designed and performed experiments in CFs for secretome and proliferation analysis. UM and ML performed antagomiR and platelet depletion experiments in mice. RL performed immunohistological staining and analysis and the Ago2 immunoprecipitation experiment. PCA and MVC performed functional analysis in murine platelets and supported the Bruneck 2015 evaluation sample collection. MS, MFF, and YS collected and analyzed blood and bone marrow samples from miR-21–null mice. TM and TB performed experiments in FoP-MKs. JBB supported the design and immunoblot experiments of CF secretome analysis and provided ECM expertise. ML and CS performed ECM and qPCR analysis in miR-21–null samples, respectively. XY and FB performed LC-MS/MS analysis. RP and SRL performed statistical analysis. AZ supported the experimental design and performed the luciferase reporter experiment. PS, MW, SK, and JW were involved in the design and running of the Bruneck study. RP, MS, and JG provided support in the miR-21–null mouse heart analysis. AMS, CG, TDW, and CFH secured funding and supported interpretation of the study. MM conceived and designed the analysis, secured funding, and edited the manuscript.

Acknowledgments

TB is funded by a British Heart Foundation (BHF) Interdisciplinary PhD studentship. SE (FS/16/21/31860) and AZ (FS/13/18/30207) are Intermediate Fellows of the BHF. PCA and MVC are supported by BHF project grants PG/15/79/31777 and PG/15/47/31591, respectively. TM is funded through an award of the National Health Service (NHS) Blood and Transplant. CS is the recipient of a research fellowship by the Deutsche Forschungsgemeinschaft (SCHU 2983/1-1). JG gratefully acknowledges funding by the Austrian Science Fund FWF (I2514) as well as by FP7 EU projects Frailomics and Sybil. The YS laboratory is supported by grants from the National Institutes of Health (R01HL105945 and R01HL135012) and the American Heart Association (16GRNT26420047). MM is a BHF Chair Holder (CH/16/3/32406), with BHF program grant support (RG/16/14/32397), and was awarded a BHF Special Project grant to participate in the ERA-CVD Transnational Grant "MacroERA: Noncoding RNAs in cardiac macrophages and their role in heart failure." MM and CFH are members of a network on "MicroRNA-based Therapeutic Strategies in Vascular Disease" funded by the Fondation Leducq. The research was supported by the National Institute of Health Research Biomedical Research Centre based at Guy's and St Thomas' NHS Foundation Trust and King's College London in partnership with King's College Hospital and by the BHF UK Cardiovascular Regenerative Medicine Centre (RE/13/2/30182). RP, JW, SK, and MM are supported by an excellence initiative (Competence Centers for Excellent Technologies) of the Austrian Research Promotion Agency FFG, "Research Center of Excellence in Vascular Ageing – Tyrol, VASCage" (K-Project 843536), funded by the Bundesministerium für Verkehr, Innovation und Technologie, Bundesministerium für Wissenschaft, Forschung und Wirtschaft, the Wirtschaftsagentur Wien, and the Standortagentur Tirol. We thank Christian Cassel for assistance with histological analysis of murine bone marrow samples, Irina Zalivina for assistance with in vitro proliferation assays, and Philipp Skroblin for assistance with analysis of the Bruneck study, year 2000 follow-up. We thank the Wohl Cellular Imaging Centre at King's College London for help with light microscopy. miR-21–null mice used for cardiac ECM analysis were a gift from Eric Olson, UT Southwestern, Dallas, Texas, USA.

Address correspondence to: Manuel Mayr, King's British Heart Foundation Centre, King's College London, 125 Coldharbour Lane, London SE5 9NU, United Kingdom. Phone: 44.20.7848.5446; Email: manuel.mayr@kcl.ac.uk.

1. Barwari T, Joshi A, Mayr M. MicroRNAs in cardiovascular disease. *J Am Coll Cardiol.* 2016;68(23):2577–2584.
2. Patrick DM, et al. Stress-dependent cardiac remodeling occurs in the absence of microRNA-21 in mice. *J Clin Invest*. 2010;120(11):3912–3916.
3. Thum T, et al. MicroRNA-21 contributes to myocardial disease by stimulating MAP kinase signalling in fibroblasts. *Nature*. 2008;456(7224):980–984.
4. Roy S, et al. MicroRNA expression in response to murine myocardial infarction: miR-21 regulates fibroblast metalloprotease-2 via phosphatase and tensin homologue. *Cardiovasc Res*. 2009;82(1):21–29.
5. Adam O, et al. Role of miR-21 in the pathogenesis of atrial fibrosis. *Basic Res Cardiol*. 2012;107(5):278.
6. Reddy S, et al. miR-21 is associated with fibrosis and right ventricular failure. *JCI Insight*. 2017;2(9):91625.
7. Gomez IG, et al. Anti-microRNA-21 oligonucleotides prevent Alport nephropathy progression by stimulating metabolic pathways. *J Clin Invest*. 2015;125(1):141–156.
8. McClelland AD, et al. miR-21 promotes renal fibrosis in diabetic nephropathy by targeting PTEN and SMAD7. *Clin Sci*. 2015;129(12):1237–1249.
9. Liu G, et al. miR-21 mediates fibrogenic activation of pulmonary fibroblasts and lung fibrosis. *J Exp Med*. 2010;207(8):1589–1597.
10. Wang D, et al. Local MicroRNA modulation using a novel anti-miR-21-eluting stent effectively prevents experimental in-stent restenosis. *Arterioscler Thromb Vasc Biol*. 2015;35(9):1945–1953.
11. McDonald RA, et al. Reducing in-stent restenosis: therapeutic manipulation of miRNA in vascular remodeling and inflammation. *J Am Coll Cardiol*. 2015;65(21):2314–2327.
12. Jin H, et al. Local delivery of miR-21 stabilizes fibrous caps in vulnerable atherosclerotic lesions. *Mol Ther*. 2018;26(4):1040–1055.
13. Maegdefessel L, et al. MicroRNA-21 blocks abdominal aortic aneurysm development and nicotine-augmented expansion. *Sci Transl Med*. 2012;4(122):122ra22.
14. Dellago H, et al. High levels of oncomiR-21 contribute to the senescence-induced growth arrest in normal human cells and its knock-down increases the replicative lifespan. *Aging Cell*. 2013;12(3):446–458.
15. Abonnenc M, et al. Extracellular matrix secretion by cardiac fibroblasts: role of microRNA-29b and microRNA-30c. *Circ Res*. 2013;113(10):1138–1147.
16. Bujak M, Frangogiannis NG. The role of TGF-β signaling in myocardial infarction and cardiac remodeling. *Cardiovasc Res*. 2007;74(2):184–195.
17. Kim H, Falet H, Hoffmeister KM, Hartwig JH. Wiskott-Aldrich syndrome protein (WASp) controls the delivery of platelet

transforming growth factor-β1. *J Biol Chem*. 2013;288(48):34352–34363.
18. Wu L, et al. P2y12 receptor promotes pressure overload-induced cardiac remodeling via platelet-driven inflammation in mice. *Hypertension*. 2017;70(4):759–769.
19. Meyer A, et al. Platelet TGF-β1 contributions to plasma TGF-β1, cardiac fibrosis, and systolic dysfunction in a mouse model of pressure overload. *Blood*. 2012;119(4):1064–1074.
20. Ahamed J, Terry H, Choi ME, Laurence J. Transforming growth factor-β1-mediated cardiac fibrosis: potential role in HIV and HIV/antiretroviral therapy-linked cardiovascular disease. *AIDS*. 2016;30(4):535–542.
21. Laurence J, et al. HIV protease inhibitor-induced cardiac dysfunction and fibrosis is mediated by platelet-derived TGF-β1 and can be suppressed by exogenous carbon monoxide. *PLoS One*. 2017;12(10):e0187185.
22. Sunderland N, et al. MicroRNA biomarkers and platelet reactivity: the clot thickens. *Circ Res*. 2017;120(2):418–435.
23. Willeit P, et al. Circulating microRNAs as novel biomarkers for platelet activation. *Circ Res*. 2013;112(4):595–600.
24. Elgheznawy A, et al. Dicer cleavage by calpain determines platelet microRNA levels and function in diabetes. *Circ Res*. 2015;117(2):157–165.
25. Kaudewitz D, et al. Association of MicroRNAs and YRNAs with platelet function. *Circ Res*. 2016;118(3):420–432.
26. Ramanujam D, Sassi Y, Laggerbauer B, Engelhardt S. Viral vector-based targeting of miR-21 in cardiac nonmyocyte cells reduces pathologic remodeling of the heart. *Mol Ther*. 2016;24(11):1939–1948.
27. Drozdov I, et al. Gene network and proteomic analyses of cardiac responses to pathological and physiological stress. *Circ Cardiovasc Genet*. 2013;6(6):588–597.
28. Barallobre-Barreiro J, et al. Glycoproteomics reveals decorin peptides with anti-myostatin activity in human atrial fibrillation. *Circulation*. 2016;134(11):817–832.
29. Naba A, Clauser KR, Ding H, Whittaker CA, Carr SA, Hynes RO. The extracellular matrix: tools and insights for the "omics" era. *Matrix Biol*. 2016;49:10–24.
30. Canfrán-Duque A, et al. Macrophage deficiency of miR-21 promotes apoptosis, plaque necrosis, and vascular inflammation during atherogenesis. *EMBO Mol Med*. 2017;9(9):1244–1262.
31. Zampetaki A, et al. Prospective study on circulating MicroRNAs and risk of myocardial infarction. *J Am Coll Cardiol*. 2012;60(4):290–299.
32. Xiang B, et al. Platelets protect from septic shock by inhibiting macrophage-dependent inflammation via the cyclooxygenase 1 signalling pathway. *Nat Commun*. 2013;4:2657.
33. Jia LX, et al. Inhibition of platelet activation by clopidogrel prevents hypertension-induced cardiac inflammation and fibrosis. *Cardiovasc Drugs Ther*. 2013;27(6):521–530.
34. Derry JM, Ochs HD, Francke U. Isolation of a novel gene mutated in Wiskott-Aldrich syndrome. *Cell*. 1994;78(4):635–644.
35. Pinzón N, et al. microRNA target prediction programs predict many false positives. *Genome Res*. 2017;27(2):234–245.
36. Dweep H, Gretz N. miRWalk2.0: a comprehensive atlas of microRNA-target interactions. *Nat Methods*. 2015;12(8):697.
37. Moreau T, et al. Large-scale production of megakaryocytes from human pluripotent stem cells by chemically defined forward programming. *Nat Commun*. 2016;7:11208.
38. Kim YJ, Hwang SJ, Bae YC, Jung JS. MiR-21 regulates adipogenic differentiation through the modulation of TGF-beta signaling in mesenchymal stem cells derived from human adipose tissue. *Stem Cells*. 2009;27(12):3093–3102.
39. Moore-Morris T, et al. Resident fibroblast lineages mediate pressure overload-induced cardiac fibrosis. *J Clin Invest*. 2014;124(7):2921–2934.
40. Rog-Zielinska EA, Norris RA, Kohl P, Markwald R. The living scar — cardiac fibroblasts and the injured heart. *Trends Mol Med*. 2016;22(2):99–114.
41. Cosme J, Guo H, Hadipour-Lakmehsari S, Emili A, Gramolini AO. Hypoxia-induced changes in the fibroblast secretome, exosome, and whole-cell proteome using cultured, cardiac-derived cells isolated from neonatal mice. *J Proteome Res*. 2017;16(8):2836–2847.
42. Sen CK, Roy S. MicroRNA 21 in tissue injury and inflammation. *Cardiovasc Res*. 2012;96(2):230–233.
43. Sheedy FJ. Turning 21: Induction of miR-21 as a key switch in the inflammatory response. *Front Immunol*. 2015;6:19.
44. Barwari T, Rienks M, Mayr M. MicroRNA-21 and the vulnerability of atherosclerotic plaques. *Mol Ther*. 2018;26(4):938–940.
45. Golebiewska EM, Poole AW. Platelet secretion: From haemostasis to wound healing and beyond. *Blood Rev*. 2015;29(3):153–162.
46. Gryshkova V, et al. miR-21-5p as a potential biomarker of inflammatory infiltration in the heart upon acute drug-induced cardiac injury in rats. *Toxicol Lett*. 2018;286:31–38.
47. Davis BN, Hilyard AC, Lagna G, Hata A. SMAD proteins control DROSHA-mediated microRNA maturation. *Nature*. 2008;454(7200):56–61.
48. Liu Y, et al. Novel role of platelets in mediating inflammatory responses and ventricular rupture or remodeling following myocardial infarction. *Arterioscler Thromb Vasc Biol*. 2011;31(4):834–841.
49. Kalkman EA, van Suylen RJ, van Dijk JP, Saxena PR, Schoemaker RG. Chronic aspirin treatment affects collagen deposition in non-infarcted myocardium during remodeling after coronary artery ligation in the rat. *J Mol Cell Cardiol*. 1995;27(11):2483–2494.
50. Krützfeldt J, et al. Silencing of microRNAs in vivo with 'antagomirs'. *Nature*. 2005;438(7068):685–689.
51. Thrasher AJ, Burns SO. WASP: a key immunological multitasker. *Nat Rev Immunol*. 2010;10(3):182–192.
52. Falet H, Hoffmeister KM, Neujahr R, Hartwig JH. Normal Arp2/3 complex activation in platelets lacking WASp. *Blood*. 2002;100(6):2113–2122.
53. Frantz S, et al. Transforming growth factor beta inhibition increases mortality and left ventricular dilatation after myocardial infarction. *Basic Res Cardiol*. 2008;103(5):485–492.
54. Barallobre-Barreiro J, Lynch M, Yin X, Mayr M. Systems biology-opportunities and challenges: the application of proteomics to study the cardiovascular extracellular matrix. *Cardiovasc Res*. 2016;112(3):626–636.
55. Langley SR, et al. Extracellular matrix proteomics identifies molecular signature of symptomatic carotid plaques. *J Clin Invest*. 2017;127(4):1546–1560.
56. Assarsson E, et al. Homogenous 96-plex PEA immunoassay exhibiting high sensitivity, specificity, and excellent scalability. *PLoS One*. 2014;9(4):e95192.

57. Yin X, et al. Plasma proteomics for epidemiology: increasing throughput with standard-flow rates. *Circ Cardiovasc Genet*. 2017;10(6):e001808.
58. Keene JD, Komisarow JM, Friedersdorf MB. RIP-Chip: the isolation and identification of mRNAs, microRNAs and protein components of ribonucleoprotein complexes from cell extracts. *Nat Protoc*. 2006;1(1):302–307.
59. Choi H, Kim S, Fermin D, Tsou CC, Nesvizhskii AI. QPROT: Statistical method for testing differential expression using protein-level intensity data in label-free quantitative proteomics. *J Proteomics*. 2015;129:121–126.